Univerza v Ljubljani
Fakulteta za elektrotehniko

Samo Mahnič-Kalamiza

Effects of electrical and thermal pre-treatment on mass transport in biological tissue

DOCTORAL DISSERTATION

Ljubljana, 2015

Univerza v Ljubljani
Fakulteta za elektrotehniko

Samo Mahnič-Kalamiza

Effects of electrical and thermal pre-treatment on mass transport in biological tissue

DOCTORAL DISSERTATION

Supervisors

prof. Eugène Vorobiev

prof. Damijan Miklavčič

Ljubljana, 2015

“Science is a way of thinking much more than it is a body of knowledge.”

CARL SAGAN

To my wife.
À mon épouse.
Moji ženi.

Samo Mahnič-Kalamiza, December / Décembre / Gruden 2015

Preface

This thesis has been prepared in co-supervision (Fr. thèse en cotutelle) between the University of Ljubljana, Ljubljana, Slovenia, and the Université de Technologie de Compiègne, Compiègne, France. The modalities of co-supervision are specified in full detail in the *Agreement of supervision* between the two universities. The thesis has been jointly co-supervised by prof. Damijan Miklavčič from University of Ljubljana, Faculty of Electrical Engineering, where the thesis has been registered in the disciplinary field of *Electrical Engineering*; and by prof. Eugène Vorobiev from the Université de Technologie de Compiègne, where the thesis has been registered in the disciplinary field of *Industrial Process Engineering and Sustainable Development*.

Acknowledgements

I am grateful to my thesis supervisors and mentors prof. Damijan Miklavčič and prof. Eugène Vorobiev for their guidance and support in my doctoral studies and research work performed throughout the course of preparation of this doctorate.

I also wish to acknowledge the financial support attributed to me by the French Ministry of Higher Education and Research that has enabled me to stay in France and do research work at the Université de Technologie de Compiègne during the period of October 2012 to July 2015.

Last but by no means least I acknowledge the support of my friends and family, especially that of my wife Tina who has been with me throughout my (our) stay in Compiègne.

Samo Mahnič-Kalamiza

Abstract

An electric field of sufficient strength can cause an increase of conductivity and permeability of cell membrane. Effect is known as electroporation and is attributed to creation of aqueous pathways in the membrane.

Quantifying mass transport in connection with electroporation of biological tissues is an important goal. The ability to fully comprehend transport processes has ramifications in improved juice extraction and improved selective extraction of compounds from plant cells, improved drug delivery, and solutions to environmental challenges.

While electroporation is intensively investigated, there is a lack of models that can be used to model mass transport in complex structures such as biological tissues with relation to electroporation. This thesis presents an attempt at constructing a theoretical mathematical description – a model, for studying mass (and heat) transfer in electroporated tissue.

The model was developed employing conservation and transport laws and enables coupling effects of electroporation to the membrane of individual cells with the resulting mass transport or heat transfer in tissue. An analytical solution has been found though the model can be extended with additional dependencies to account for the phenomenon of electroporation, and solved numerically.

Thesis comprises five peer-reviewed papers describing electroporation in the food industry, model creation for the problem of diffusion, translation of the model to the mathematically-related case of juice expression, model validation, as well as suggestions for possible future development, extension, and generalization. An additional chapter is dedicated to transfer of heat in tissue.

Keywords: electroporation; mathematical modelling; mass transport; plant tissue; diffusion, filtration-consolidation; electric field strength; mechanistic model; cell membrane; electropores

Titre en français : *Effets de prétraitement électrique et thermique sur le transport de la matière dans les tissus biologiques*

Résumé

Le champ électrique d'une puissance suffisante peut provoquer une augmentation de conductivité et perméabilité de la membrane cellulaire. L'effet est connu comme l'électroporation, attribuée à la création de voies aqueuses dans la membrane.

Quantifier le transport de la matière dans le cadre d'électroporation est un objectif important. Comprendre ces processus a des ramifications dans l'extraction du jus ou l'extraction sélective des composés de cellules végétales, l'amélioration de l'administration de médicaments, et des solutions aux défis environnementaux.

Il y a un manque de modèles qui pourraient être utilisés pour modéliser le transport de la matière dans les structures complexes (tissus biologiques) par rapport à l'électroporation. Cette thèse présente une description mathématique théorique (un modèle) pour étudier le transport de la matière et le transfert de la chaleur dans tissu traité par l'électroporation.

Le modèle a été développé en utilisant les lois de conservation et de transport et permet le couplage des effets de l'électroporation sur la membrane des cellules individuelles au transport de la matière ou la chaleur dans le tissu. Une solution analytique a été trouvée par une simplification, mais le modèle peut être étendu avec des dépendances fonctionnelles supplémentaires et résolu numériquement.

La thèse comprend cinq articles sur l'électroporation dans l'industrie alimentaire, la création de modèle pour le problème de diffusion, la traduction du modèle au problème lié à l'expression de jus, validation du modèle, ainsi que des suggestions pour une élaboration future du modèle. Un chapitre supplémentaire est dédié au transfert de la chaleur dans tissu.

Mots-clés: électroporation; modélisation mathématique; transfert de la matière; tissu végétal; diffusion, filtration-consolidation; intensité du champ électrique; modèle mécaniste; membrane cellulaire; électropores

Naslov v slovenskem jeziku: *Učinki električne in toplotne obdelave na transport snovi v biološkem tkivu*

Povzetek

Električno polje dovoljšne jakosti lahko povzroči znatno povečanje električne prevodnosti in prepustnosti celične membrane. Pojav je poznan kot elektroporacija in je pripisan vzpostavitvi vodnih kanalov v lipidnem dvosloju imenovanih pore.

Elektroporacija je bila in je še vedno predmet intenzivnih raziskav na številnih področjih, kot so biomedicina (za gensko transfekcijo, elektrokemoterapijo, vnos zdravil preko kože, in ablacijo mehkih tkiv, npr. tumorjev); v predelavi hrane in kemijskem inženirstvu (za povečanje količine ekstrakta pri pridobivanju sokov ali dragocenih snovi, izboljšanju kakovosti pridobljenih snovi, ali konzervacijo hrane); prav tako pa tudi v okolijskih znanostih (pri predelavi odpadnih voda, pridobivanju lipidov iz mikroorganizmov, ali stimulaciji rasti rastlin). Skoraj na vseh teh področjih nas zanima izboljšanje vnosa snovi v biološke celice ali pa pridobivanja snovi iz bioloških celic.

Razumevanje in kvantifikacija transporta snovi v povezavi z elektroporacijo sta pomembna cilja pri raziskavah elektroporacije. Sposobnost dobrega razumevanja procesov transporta snovi ima pomembne posledice za, na primer, nadaljnje izboljšanje selektivnega pridobivanja snovi ali sokov iz rastlinskih celic, za izboljšanje dostave zdravil v ciljna tkiva oziroma celice, in za uspešno reševanje trenutnih okolijskih izzivov.

Pri elektroporaciji med dovajanjem električnih pulzov skozi obdelovano tkivo teče električni tok, kar lahko do določene mere tkivo tudi segreje. To je še posebej pomembno v industrijskih aplikacijah, kjer so lahko dovedene energije zaradi visoke amplitude in števila pulzov tudi zelo velike. Zato je pomembno poznati poleg transporta snovi tudi toplotne razmere v tkivu pri elektroporaciji, ter kakšen vpliv ima povišana temperatura na transport snovi v elektroporiranem tkivu.

Čeprav so elektroporacija in z njo povezani pojavi predmet intenzivnih raziskav, je občutiti pomanjkanje kompleksnejših oziroma popolnejših modelov, ki bi se lahko uporabljali za modeliranje transporta snovi v kompleksnih strukturah, kakršna so biološka tkiva, še posebej v povezavi z elektroporacijo. Pričujoča dizertacija predstavlja poskus izgradnje teoretičnega matematičnega opisa – tj. modela – za proučevanje transporta snovi v elektroporiranem tkivu.

Model, poimenovan model dvojne poroznosti, je osnovan na podlagi obstoječe teoretične analize tlačnih razmer (hidrodinamike) v prsteh, sedimentih, prodnih nanosih ter lomljenih

kamninah. Med temi sistemi ter strukturo bioloških tkiv obstaja analogija, ki je izkoriščena za vzpostavitev ekvivalentne matematične obravnave bioloških tkiv z že obstoječimi metodami in pristopi, ki so bili prvotno razviti v geoloških znanostih, so pa bili že uporabljeni tudi v povezavi z biološkimi materiali, denimo pri obravnavi procesa prešanja z oljem bogatih semen.

Model dvojne poroznosti je bil razvit upoštevaje zakone o ohranitvi mase in zakone masnega transporta (termodinamika sistemov v neravnovesju), in omogoča sklapljanje efektov elektroporacije na membrano posameznih celic z rezultirajočim transportom snovi preko membrane in v izvenceličnem prostoru. Slednje predstavlja tudi poglavitni izvirni prispevek znanosti, saj model dvojne poroznosti še ni bil zapisan za difuzijo in v preteklih delih ni predstavljen v povezavi z elektroporacijo. Predstavljena je tudi poučna analitična rešitev modela, ki dovoljuje fizikalno interpretacijo, model pa se lahko enostavno nadgradi z dodatnimi odvisnostmi in s tem modelira učinke elektroporacije, ter nato reši numerično.

Dizertacijo sestavlja pet znanstvenih člankov. Prvi podaja pregled nad aplikacijami elektroporacije v industriji predelave hrane ter biorafineriji. Drugi znanstveni članek zajema konstrukcijo modela dvojne poroznosti za problem difuzije topljenca v elektroporiranem tkivu po elektroporaciji. V tretjem članku je zajeta prilagoditev oz. predelava modela dvojne poroznosti za difuzijski problem (koncentracijske razmere) v formo primerno za obravnav problema iztiskanja soka iz elektroporiranega tkiva oz. problem konsolidacije elektroporiranega vzorca rastlinskega tkiva (tlačne razmere). Četrti članek združuje oba modela, model difuzije ter konsolidacije, ter dodaja potrebno validacijo modela prek primerjave eksperimentalno pridobljenih podatkov z rezultati pridobljenimi prek simulacij na modelu. Sledi poglavje posvečeno modeliranju prenosa toplote v biološkem tkivu in povezavi med modelom porazdelitve temperature ter modeli transporta snovi. Sklepno poglavje podaja še kratek oris najnovejših rezultatov v smeri izboljšav modela z vključitvijo drugih pomembnih dejavnikov v model kot so izguba turgorja in elektroosmoza, ter predloge za možne prihodnje nadgradnje modela, njegovo razširitev in posplošitev.

Ključne besede: elektroporacija; matematično modeliranje; transport snovi; rastlinsko tkivo; difuzija, filtracija-konsolidacija; električna poljska jakost; mehanistični model; celična membrana; elektro-pore

Table of contents

1 Extended abstracts in French and Slovene

1.1 Résumé substantiel en français

1.1.1 Introduction

Comme le montrent les expériences sur des bicouches lipidiques, les cellules et les tissus biologiques, le champ électrique d'une intensité suffisante peut provoquer une augmentation significative de la conductivité et de la perméabilité de la membrane lipidique. L'effet est connu comme l'électroporation ou l'électroperméabilisation, et comme il est réalisé par exposition de tissue à des impulsions électriques, il est également connu sous le nom de « traitement à champ électrique pulsé ». L'électroporation est décrite comme la création de voies aqueuses, c'est-à-dire les pores, dans la bicouche lipidique.

En fonction de la durée de l'exposition de la cellule au champ électrique, l'intensité locale du champ (c'est-à-dire le facteur limitant l'énergie électrique maximale qui est potentiellement livrable à la membrane par l'intermédiaire du champ électrique imposée de l'extérieur), et le taux de récupération de la membrane, il y a trois résultats possibles de l'application d'un champ électrique. Si l'intensité du champ et le temps d'exposition ne sont pas suffisantes, il n'y a pas d'électroporation, et la perméabilité de la membrane de cellule ainsi que la viabilité des cellules ne sont pas affectées. Si l'intensité du champ dépasse ce qui est connu comme l'intensité du seuil et l'exposition est d'une durée suffisante, l'électroporation dite réversible se produit; la membrane est perméabilisée et reste dans un état de plus grande perméabilité pour une période de temps, mais est finalement en mesure de revenir à son état d'origine par des moyens de refermeture de la membrane, un processus dans lequel les pores se ferment et la membrane cellulaire restaure son état normal, ça veut dire la perméabilité sélective qui est seulement possible si les conditions environnementales restent favorables pour la survie et la fonction des cellules. Si l'intensité du champ et la quantité d'énergie délivrée sont trop élevés, l'électroporation irréversible se produit résultant en une perte de l'homéostasie cellulaire (et éventuellement une rupture de la membrane cellulaire), effectivement tuer la cellule.

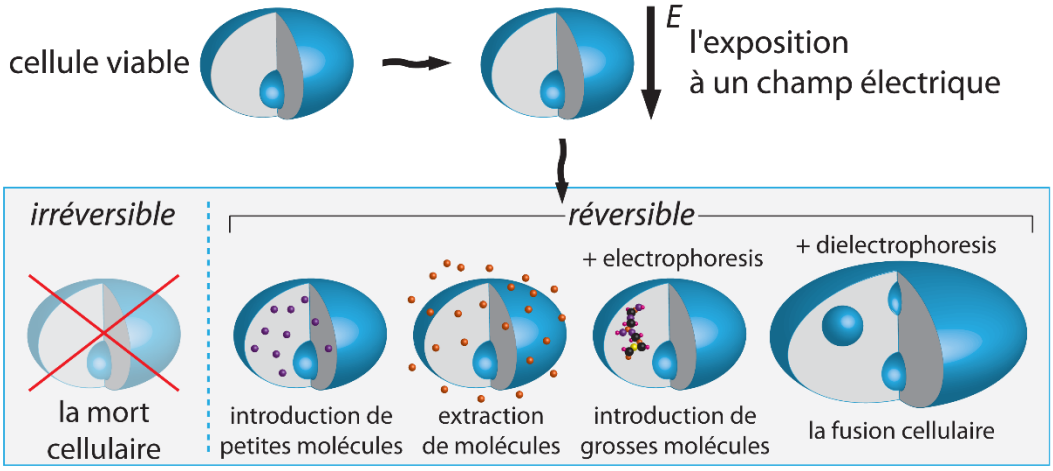

Figure 1.1: Applications d'électroporation, avec les résultats possibles de l'application du traitement.

Les deux, l'électroporation réversible et irréversible, ont trouvé leurs applications dans des domaines tels que la biomédecine, la transformation des aliments, la biotechnologie et les sciences de l'environnement. Dans la biomédecine, l'électroporation réversible est utilisé pour introduire des médicaments cytotoxiques dans des cellules tumorales dans un processus connu sous le nom d'électrochimiothérapie, pour l'administration des médicaments et des matériels génétiques par la voie transdermique, pour la fusion cellulaire, ainsi que pour l'insertion des protéines dans la membrane plasmique, tandis que l'électroporation irréversible est utilisé comme un moyen d'ablation de tissu pour l'ablation de tissus mous, y compris le traitement du cancer.

Dans la transformation des aliments et de la biotechnologie, l'électroporation a montré des résultats prometteurs pour l'extraction de jus de fruits et d'autres composés intéressants de tissus végétaux et de micro-organismes, tels que les microalgues, la déshydratation des tissus, et la conservation non thermique et la stérilisation par l'inactivation microbienne. Électroporation réversible peut également aider à créer de nouvelles méthodes de cryoconservation de tissus biologiques, et la stimulation de métabolisme de la plante. Parmi les applications environnementales, nous trouvons le traitement des eaux usées et la production de biocarburants, les deux toujours en cours de recherche et développements intensifs comme les applications d'électroporation prometteurs.

Tout au long des divers domaines de la recherche et les applications de l'électroporation, la compréhension et être en mesure de quantifier le transport de la matière dans le cadre d'électroporation de tissus biologiques est un objectif important, puisque dans la majorité de ses applications, nous sommes à la recherche de moyens pour soit introduire la matière (solutés ou solution) dans les cellules, ou d'extraire le jus intracellulaire et des composés intracellulaires hors

des cellules. La capacité de comprendre pleinement ces processus de transport a des ramifications dans, par exemple, l'amélioration d'extraction sélective des composés de cellules végétales, réduisant ainsi les coûts de raffinage, l'amélioration de l'administration de médicaments conduisant à des modalités de traitement plus efficaces ou nouveaux pour lutter contre les maladies, et des solutions pour les défis environnementaux actuels tels que la disponibilité de sources d'énergie propres.

Alors que les phénomènes d'électroporation et connexes continuent d'être des recherches intensives, il y a un manque de modèles intégrales qui pourraient être utilisés pour modéliser le transport de la matière dans les structures complexes telles que sont les tissus biologiques, en particulier par rapport à l'électroporation. Cette thèse présente une tentative de construire une description mathématique théorique, ça veut dire un modèle, pour étudier le transport de la matière dans le tissu traité par l'électroporation.

Le modèle a été développé en utilisant les lois de conservation (de la matière et/ou de l'énergie) et de transport de la matière, et permet le couplage des effets de l'électroporation à la membrane des cellules individuelles au transport de la matière transmembranaire ainsi que extracellulaire résultantes. Une solution analytique instructive pour le modèle a été trouvée par une simplification, mais le modèle peut être étendu avec des dépendances fonctionnelles supplémentaires pour mieux prendre en compte des phénomènes de l'électroporation, et puis résolu numériquement.

Puisque les effets thermiques dans les tissus pendant l'électroporation parfois ne peuvent pas être négligés (dans certains applications, le chauffage associé à électroporation est une composante majeure de la modalité de traitement), cette thèse explore également théoriquement en bref de quelle importance sont les relations thermiques au transport de la matière dans le tissu traité (ou pas) par l'électroporation. À cette fin, un analogue thermique au modèle à double porosité est présenté pour le transfert de chaleur dans les tissus traités par l'électroporation, par une étude paramétrique utilisant les modèles de transport de la matière (diffusion et expression). Ces modèles sont couplés avec le modèle de distribution de la chaleur, à laquelle une section plus courte de cette thèse est consacrée afin d'introduire des moyens par lesquels on pourrait, dans une simulation simple par ordinateur, évaluer l'effet d'augmentation de la température dans le tissu suivant l'électroporation à des processus de transport de la matière. Le modèle de transfert de chaleur et son couplage avec les modèles de transport de la matière représentent un travail en cours de réalisation qui reste à être validée.

Cette thèse comprend cinq articles publiés, décrivant les applications d'électroporation dans l'industrie alimentaire, la création de modèle pour le problème de la diffusion, la traduction du problème au problème mathématiquement lié à l'expression de jus, validation du modèle, une

section sur son extension à un modèle décrivant les relations thermiques, ainsi que des suggestions pour le développement futur possible du modèle, son extension, et sa généralisation.

1.1.2 Matériels et méthodes

Cette section donne des détails que sur les matériaux physiques et les méthodes utilisées dans les expériences sur deux tissus modèles qui ont été menées afin de valider le modèle à double porosité nouvellement développé. Le modèle à double porosité représente le résultat principal et la majeure partie des efforts entrepris dans le cadre de cette thèse, et sa construction est présenté dans la section suivante avec toutes les dérivations théoriques.

1.1.2.1 Les essais de diffusion

Les expériences de diffusion qui sont décrits dans l'Article II et l'Article IV ont été réalisées selon le même protocole. L'Article III concerne les expériences du pressage uniquement, et par conséquent, les expériences décrites ici ne le concernent pas.

Selon le protocole d'expériences de diffusion, des échantillons cylindriques (disques) de la racine de betterave à sucre et des pommes (sans la peau) ont été obtenus à partir des tranches de 5 mm d'épaisseur prises de la racine de la betterave à sucre ou de pommes (dans le texte continue désignés comme le tissu de betterave à sucre ou le tissu de pomme, respectivement). Tous les échantillons ont mesuré 25 mm de diamètre. Chaque échantillon a été soumis premièrement à un traitement d'électroporation par l'application de 150, 200, 300, ou 400 V entre deux électrodes à plaques parallèles en acier inoxydable de 5 mm distance inter-électrodes (égal à l'épaisseur de l'échantillon). L'intention était de soumettre le tissu traité au champ de l'intensité de 300, 400, 600, et 800 V/cm, respectivement (à noter l'épaisseur de 5 mm des échantillons). L'intensité du champ électrique souhaitée n'a pas été atteinte de façon homogène dans le tissu, car il ne s'agit pas d'un matériau homogène, et de plus en raison de dimensions d'électrodes finis l'intensité atteint sa valeur maximale (souhaitée) que dans la zone centrale loin de bords de l'électrode (voir les figures 1 et 5 dans l'Article V pour une illustration). Impulsions rectangulaires de polarité alternée (voir Figure 1.4 dans la section 1.1.2.3) ont été livrés en deux trains de 8 impulsions, où chaque impulsion était de 100 μs en durée et la fréquence de répétition des impulsions dans le train était 1 kHz. Deux de ces trains ont été livrés avec une pause d'une seconde entre les deux trains. Ce protocole est considéré comme le protocole du traitement A. Les impulsions ont été fournis par un générateur d'impulsions fait sur mesure avec un courant de sortie maximal de 38 A à la tension

maximale possible de 400 V, assemblé par le Service Electronique UTC, Compiègne, France (voir la section 1.1.2.4 ci-dessous).

Ensuite, les échantillons ont été retirés de la chambre de traitement électrique après le traitement d'électroporation, après quoi les surfaces des disques d'échantillons ont été mises en contact avec du papier absorbant et ainsi les surfaces ont été séchées pour éliminer le liquide sucré accumulé au niveau des surfaces. Ce liquide est présent à cause du coupage (en petites quantités) et, éventuellement, en raison des effets électroosmotiques ou des effets de changement de pression (perte de turgescence) qui se produisent pendant l'application du traitement d'électroporation (une plus grande mesure). N'avaient pas les surfaces été séchées, le jus sur la surface provoquerait une augmentation immédiate de la concentration en sucre dans la solution au début de l'expérience de diffusion, ce qui entraîne une cinétique également connu sous le nom « étape de lavage » du processus (voir section 2.2.3.3 de la revue de la littérature). Cet effet n'est pas capturée par le modèle ni facile à soustraire du cinétiques enregistrées en raison de la différence de concentration de sucre dans le jus et la quantité de ce liquide de surface qui varie entre les échantillons. Les échantillons de surface séchés ont été placés dans un ballon équipé d'un agitateur magnétique. Ce mélange d'échantillon liquide a été constamment agité et échantillonné à intervalles réguliers; la concentration des solides solubles totales (principalement le sucre) a été analysée avec un réfractomètre numérique (détails donnés dans la section 1.1.2.5 ci-dessous). Le rapport liquide-solide était de 2:1 dans toutes les expériences.

La quantité mesurée par le réfractomètre numérique est la concentration de sucre (pour être précis – la concentration de solides solubles totaux) en liquide et est affiché en unités degrés Brix (°Bx), où un degré Brix est de 1 gramme de saccharose dans 100 grammes de solution et représente la concentration de la solution sous forme de pourcentage en poids (% p/p). La teneur initiale en sucre de la solution aqueuse $°Bx_0$ est connu et normalement égale à zéro, et durant l'expérience, la teneur actuel en sucre °Bx(t) est mesurée. Mesures connectés tracent la courbe de la cinétique d'extraction, et la concentration finale de sucre $°Bx_d$ peut être déterminée séparément. Théoriquement, $°Bx_d$ est la concentration des solutés totaux en solution dans des conditions idéales de tissu complètement perméabilisée et après un temps infini de la diffusion. Dans la pratique, il peut facilement être obtenu en mesurant la concentration des solutés dans le fruit pur / jus de racine, et la mise à l'échelle de mesures en fonction du rapport massique liquide / jus (également connu comme étant le rapport solide-liquide). Puisque les concentrations initiales ainsi que maximales sont connus, le *degré Brix normalisé* au temps t – c'est-à-dire $B(t)$, peut être exprimé et calculé comme

$$B(t) = \frac{°\mathrm{Bx}(t) - °\mathrm{Bx}_0}{°\mathrm{Bx}_d - °\mathrm{Bx}_0}$$

Brix normalisé est utilisé dans les travaux décrits dans le présent mémoire en tant qu'une mesure de la quantité de soluté (par exemple sucre) qui a diffusé hors de l'échantillon de tissu à partir de l'instant t_0 jusqu'à l'instant t. Elle prend des valeurs de l'intervalle $0 \leq B(t) \leq 1$, et est sans dimension. Elle peut être calculée selon l'équation donnée ci-dessus à partir des mesures obtenues avec le réfractomètre. La représentation schématique de l'expérience de diffusion est donnée par la Figure 1.2.

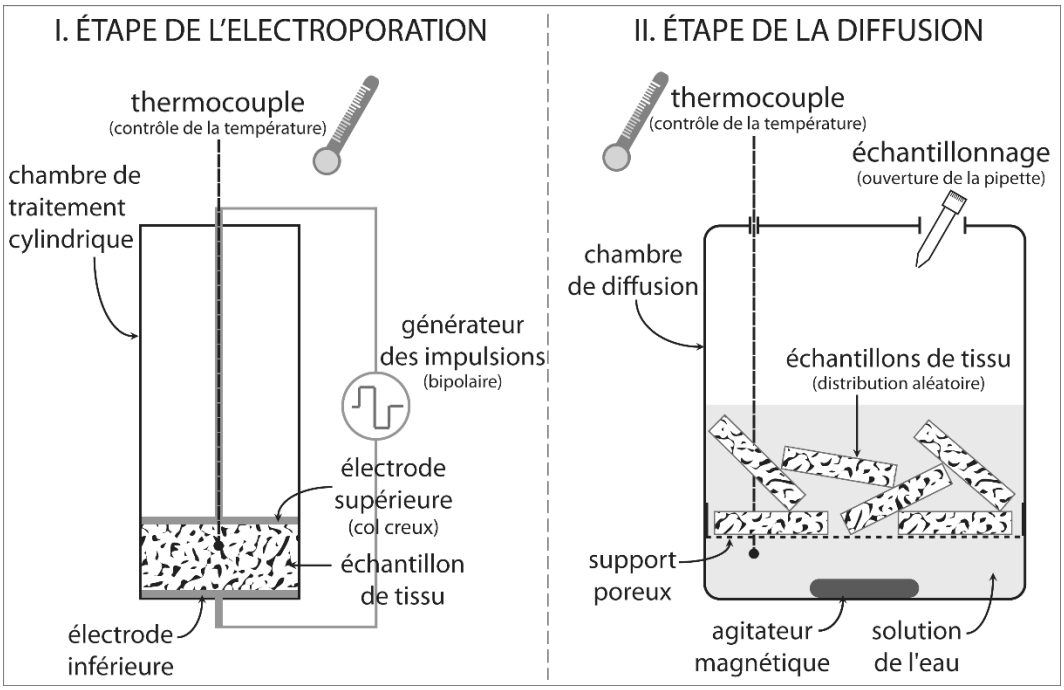

Figure 1.2: Représentation schématique de la configuration d'expérience de diffusion - le traitement d'électroporation (à gauche) et l'étape de diffusion ultérieure (à droite).

1.1.2.2 Les essais de pressage

Comme dans les expériences de diffusion, des échantillons cylindriques de betterave à sucre et de pomme ont été utilisés, 25 mm de diamètre et de 5 mm d'épaisseur. Les échantillons ont été placés entre deux électrodes à plaques parallèles en acier inoxydable, et des impulsions d'électroporation ont été appliquées en utilisant trois protocoles différents (voir la Figure 1.4). Protocole A: On a fait varier la tension, à l'aide de 150 V, 200 V, 300 V, 350 V ou 400 V appliquée aux électrodes. Impulsions de polarité alternée ont été livrés en deux trains de 8 impulsions par train, avec une fréquence de répétition de 1 kHz dans le train, 1 seconde de pause entre les deux trains, et 100 μs durée de chaque impulsion. Protocole B: La tension a été modifiée de même

manière que dans le protocole A, cependant, seulement deux impulsions unipolaires ont été livrés de 800 ms chacune, et avec un temps de retard de 1 s entre les deux impulsions. Protocole C: La tension a été modifiée que dans le protocole A et B, sauf que 8 impulsions monopolaires (de même polarité) ont été livrés, 100 μs de durée à chaque seconde (c'est-à-dire la fréquence de répétition des impulsions était de 1 Hz). Ce protocole est aussi connu comme l'un des protocoles standards pour l'électrochimiothérapie. Notez que le t_t – temps de traitement total (produit de la durée d'une impulsion t_p, nombre d'impulsions n_p, et le nombre de trains n_t) – calculé à partir du protocole de l'électroporation, était le même pour les protocoles A et B (t_t = 1,6 ms), et était inférieur de 50% dans le cas du protocole C (t_t = 0,8 ms) par rapport aux deux autres protocoles. L'énergie délivrée dans la configuration calculée sur la base du courant électrique mesuré a variée entre 6 J/kg (minimum atteint pour la betterave à sucre, le protocole C, à 150 V) et 250 J/kg (maximum atteint pour les pommes, Protocole B, à 400 V). En termes de distribution d'énergie et la durée du traitement, ces protocoles de traitement ne sont généralement pas rencontrés dans le domaine de la transformation des aliments, où les énergies de l'ordre de plusieurs kJ/kg sont généralement livrées aux tissus. L'énergie total maximum délivrée de l'ordre de 0,25 kJ/kg entraîne, dans le pire des cas et ne prenant pas en compte de toute dissipation de la chaleur par l'intermédiaire d'électrodes ou surfaces de la chambre de traitement, une augmentation négligeable de la température d'échantillon inférieure à 0,1 K. Cette estimation est fondée sur la capacité thermique des tissus de pomme, et de l'énergie maximale connue qui a été livré. Les raisons et les conséquences de ce choix particulier du traitement de faible intensité, ça veut dire des protocoles de traitement « douces », sont données et discutées dans la section « Résultats et discussion » du Article III et Article IV.

Dans tous les cas, quel que soit le protocole d'électroporation, le traitement électrique est suivi par le pressage. Échantillons traités par l'électroporation ont été immédiatement placés dans une chambre de traitement spécialement fabriqué et soumis à une charge de 300 N – c'est-à-dire d'environ 580 kPa (betterave à sucre), ou 150 N – environ 290 kPa (pomme), en utilisant un texturomètre (analyseur de texture, détails dans la section 1.1.2.5). Le déplacement du piston a été enregistré par le texturomètre sous pression (force) constante lors de l'application d'une heure.

Le déplacement du piston est égal à la déformation de l'échantillon le long de l'axe de l'application de pression. Cette déformation d'échantillon est théoriquement liée à la perte de pression du liquide dans le tissu par le premier modèle présenté dans l'Article III. Cela permet la comparaison des résultats expérimentaux et modèles. La représentation schématique de l'expérience de pressage est donnée par la Figure 1.3.

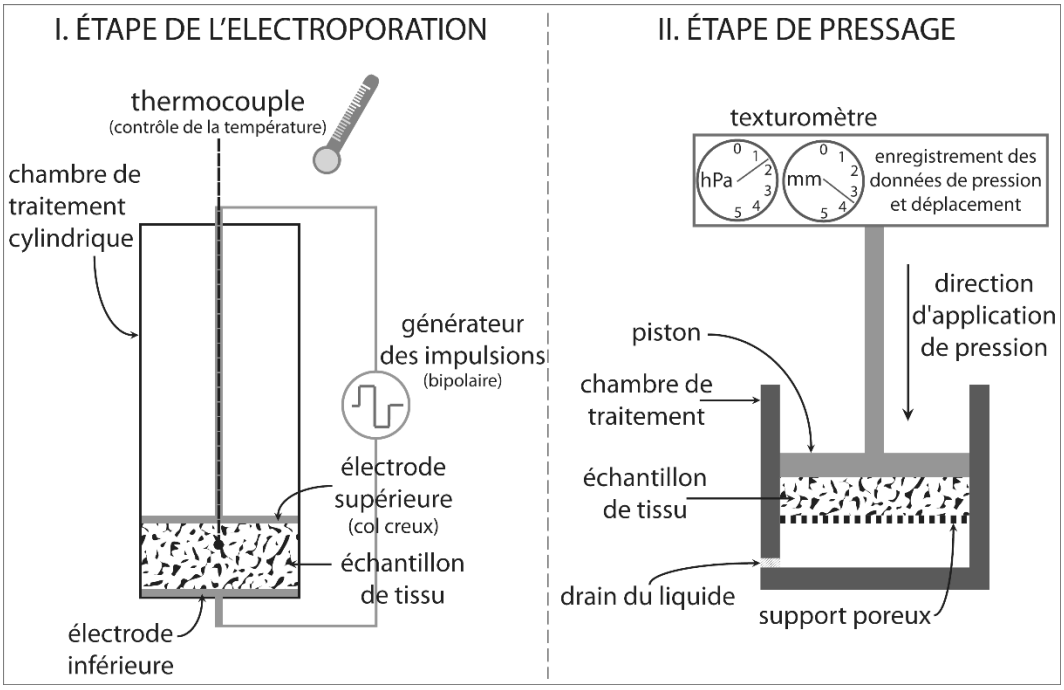

Figure 1.3: Représentation schématique de l'installation de l'expérience de pressage – le traitement d'électroporation (à gauche) et l'étape suivante de pressage (à droite).

1.1.2.3 Les protocoles de traitement utilisés

Trois protocoles de traitement d'électroporation différents ont été utilisés pour obtenir les résultats présentés dans les articles II-IV. Les protocoles sont précisés en détail dans l'Article IV, section 2.3, et illustrés au moyen d'une figure donnée dans l'Article IV, Figure 3.2 (reproduite ci-dessous comme la Figure 1.4 pour référence). Trois protocoles de traitement différents ont été utilisés dans le but d'examiner s'il y a une différence détectable dans la façon dont les différents protocoles de traitement influencent la formation et l'évolution des pores dans les membranes cellulaires, ce qui pourrait se refléter dans la cinétique de la consolidation du tissu, et ensuite modélisé par le modèle à double porosité. Résultats de la comparaison sont donnés dans la section appropriée de l'Article IV.

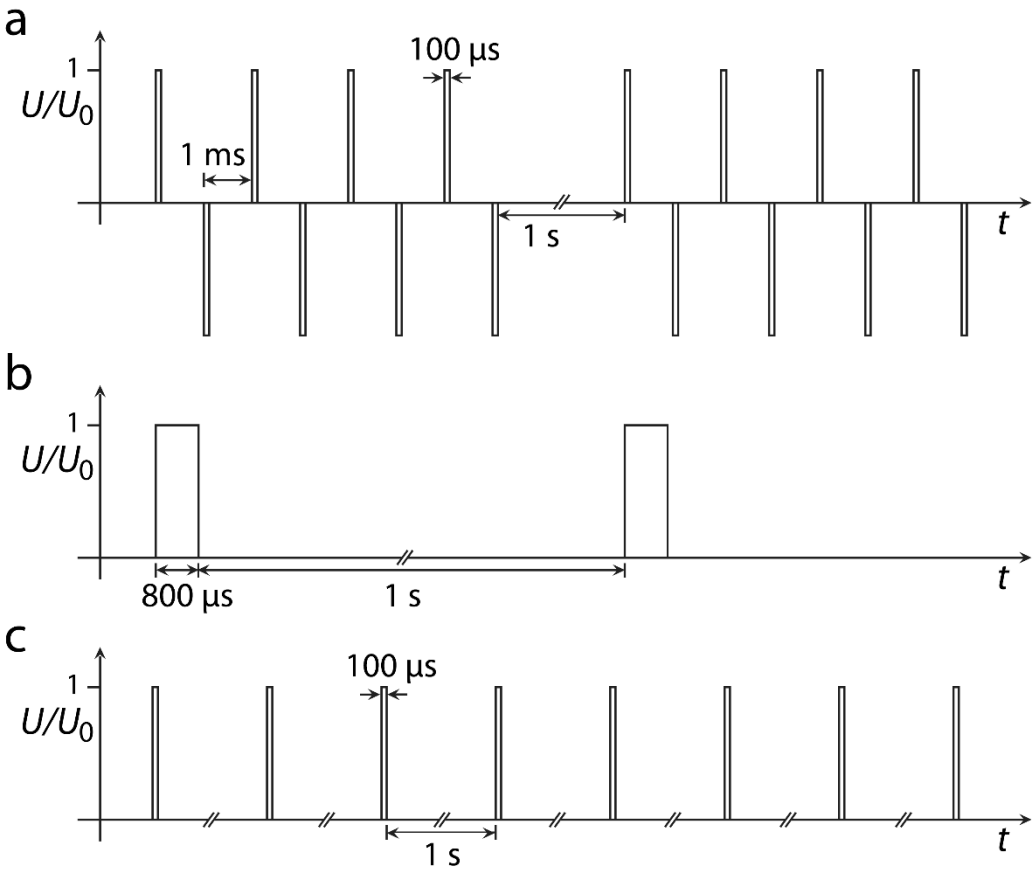

Figure 1.4: Une représentation graphique des trois protocoles d'application d'impulsions: Protocole A (a), protocole B (b), et le protocole C (c). Des durées d'impulsions et les distances sont à l'échelle, sauf si désigné autrement – le signe « // » indique une discontinuité dans l'axe (c'est-à-dire qu'il y a une pause d'une seconde entre tous les deux impulsions entre lesquelles la discontinuité est indiqué).

1.1.2.4 Générateurs

Pour réaliser les expériences rapportées ou mentionnés dans cette mémoire, trois générateurs différents ont été utilisés pour provoquer l'électroporation dans le tissu traité; deux générateurs à l'échelle laboratoire et un à l'échelle pilote industriel. Toutefois, un seul générateur a été utilisé pour obtenir les résultats présentés dans les articles II-IV qui constituent le corps principal du travail rapporté dans cette mémoire. Le générateur utilisé pour traiter la betterave à sucre et tissu de pommes utilisé dans les expériences de validation pour le modèle à double porosité a été fabriqué par le Service Electronique de l'Université de Technologie de Compiègne (UTC). Il est capable de délivrer une tension maximale de 400 V et son courant maximal est de 38 A. Le générateur produit des impulsions exclusivement bipolaires de forme quasi-rectangulaire (temps de montée / descente de l'ordre de quelques µs).

Les deux autres générateurs ont été utilisés dans les travaux ultérieurs sur la relaxation de turgescence et l'effet d'électroosmose qui sont brièvement référé dans le dernier chapitre de cette mémoire. Les deux produisent des impulsions exclusivement unipolaires, et sont capables de délivrer des impulsions électriques rectangulaires à des tensions supérieures à 400 V. Comme il est souhaitable que des tensions supérieures à 400 V sont appliquées dans des expériences de relaxation de turgescence (pour des intensités de champ électrique plus élevés), et des impulsions unipolaires résultent en courant monodirectionnel et il est considéré comme nécessaire de désassocier les effets de l'électroosmose et les autres, la tension de 400 V maximale de générateur d'impulsions bipolaires ne convenait pas à ces deux séries d'expériences. Parce qu'aucune discussion détaillée n'est pas donnée sur la perte de turgescence et les expériences d'électroosmose et leurs résultats dans cette mémoire, les spécifications des deux générateurs d'impulsions unipolaires sont hors de portée de la thèse et sont par conséquent omis de cette section.

1.1.2.5 D'autres équipements

Afin d'obtenir la cinétique d'expression, une pression faible constante a été appliquée à des échantillons de tissus en utilisant un texturomètre (un analyseur de texture) de haute précision, fabriqué par Stable Micro Systems, modèle « TA.XT *plus* ». La force maximale laquelle cet analyseur de texture peut exercer sur un échantillon est de 50 kg (500 N), avec une résolution de 1 N. Le texturomètre a été utilisé dans le mode de fonctionnement à force constante, ce qui signifie qu'une force choisie a été appliquée sur les échantillons du tissu par le piston du texturomètre pour une période de temps spécifié et le déplacement a été mesuré et enregistré à haute résolution de 0,001 mm avec une précision de ± 0,001 mm.

Afin de mesurer la concentration totale de solutés solubles dans les expériences avec la betterave à sucre et tissu de pomme, deux réfractomètres numériques ont été utilisés. Les résultats rapportés dans l'Article II ont été obtenus en utilisant le réfractomètre numérique ATAGO PR-32α (alpha), et les nouveaux résultats rapportés dans l'Article IV avec l'aide de réfractomètre numérique ATAGO PR-101α (alpha). Tous les deux ont une résolution de 0,1 % Brix, ainsi qu'une précision de mesure de 0,1 % Brix, cependant la plage de mesure du modèle PR-32α est de 0,0 % Brix à 32,0 % Brix, tandis que pour le modèle de PR-101α l'intervalle respectif est de 0,0 % Brix à 45,0 % Brix. Les deux réfractomètres ont été étalonnés avant l'utilisation par l'eau distillée et une solution de référence (mélangé sur place) de saccharose et de l'eau distillée.

1.1.3 Résultats et discussion

1.1.3.1 Le modèle à double porosité

Le modèle à double porosité tel que est présenté dans cette mémoire a des analogies avec les modèles développés dans la mécanique des roches pour les relations de l'eau dans les sols et les roches fracturées, ainsi que les modèles de la thermodynamique de non-équilibre. Pour une revue de la littérature et des informations plus amples, voir la section 2.2.4.2 et sections d'introduction dans les articles II - IV.

L'idée de base derrière la construction du modèle à double porosité suit à partir de la nécessité d’associer les effets d'électroporation sur les membranes cellulaires avec soit flux de diffusion dans le tissu ou le comportement filtration-consolidation (ça veut dire l’expression liquide) du tissu. Pour modéliser les effets de l'électroporation dans un modèle de transport de la matière dans les tissus, il faut d'abord introduire un nouveau niveau de complexité dans le concept d'un bloc de matériau de l'échantillon. Nous suivons la théorie développée pour l'écoulement de liquide dans les matériaux poreux tels que les sols et les roches fracturées, où le concept de médias de porosité multiples a été intensivement étudié.

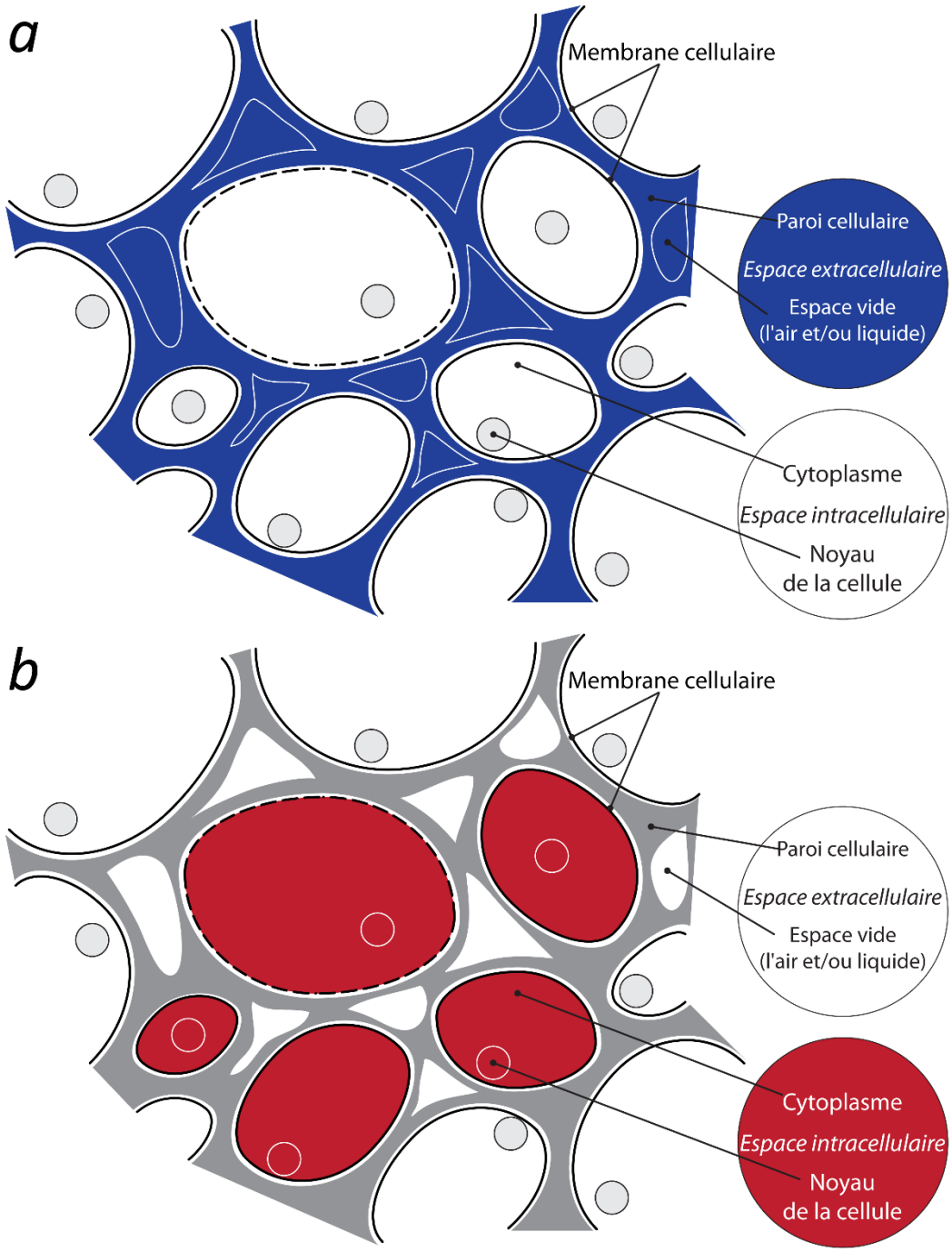

Figure 1.5: Une représentation schématique (simplifiée) de tissu végétal avec des phases identifiés: (a) l'extracellulaire; et (b) l'intracellulaire.

Tissu biologique, si on le compare à une suspension simple (des solutés, des cellules, etc.), est morphologiquement plus complexe et ne peut pas être représenté comme matériau homogène et non plus comme comprenant que des solides et des liquides (voir la Figure 1.5); plutôt, il est constitué d'au minimum deux phases ou deux espaces – l'espace intracellulaire et l'espace extracellulaire. Chacune de ces espaces est ensuite composée de solides et de liquide contenant le soluté. L'interface qui sépare les deux phases est la membrane cellulaire semi-perméable, la

perméabilité de laquelle est une fonction du traitement de l'électroporation. Ce concept de base est commun au problème de diffusion ainsi qu'au problème de consolidation car il concerne la modélisation d'une propriété inhérente de la structure du matériau cible. Cependant, lorsqu'on commence à discuter le transport de la matière, les principes fondamentaux commencent à différer et il est nécessaire de prendre des approches différentes (même s'elles sont mathématiquement similaires ou bien équivalentes).

1.1.3.2 Le modèle à double porosité pour le problème de diffusion

Les équations fondamentales du modèle pour la concentration dans l'espace extracellulaire et intracellulaire sont, respectivement,

$$\frac{\partial c_e(z,t)}{\partial t} - D_{s,e}\frac{\partial^2 c_e(z,t)}{\partial z^2} - \frac{1-\varepsilon}{\varepsilon}k\cdot\left[c_i(z,t)-c_e(z,t)\right]=0 \tag{1.1.1}$$

$$\frac{\partial c_i(z,t)}{\partial t} + k\cdot\left[c_i(z,t)-c_e(z,t)\right]=0 \tag{1.1.2}$$

où c_e et c_i sont des concentrations de soluté extracellulaires et intracellulaires, respectivement, $D_{s,e}$ est le coefficient de diffusion intrinsèque du soluté espèce s dans l'espace extracellulaire, ε est la porosité du tissu (la fraction du volume extracellulaire, soit $\varepsilon = 1 - F$, où F est la fraction volumique de cellules), et k est le coefficient d'écoulement transmembranaire défini par éq. 1.1.14.

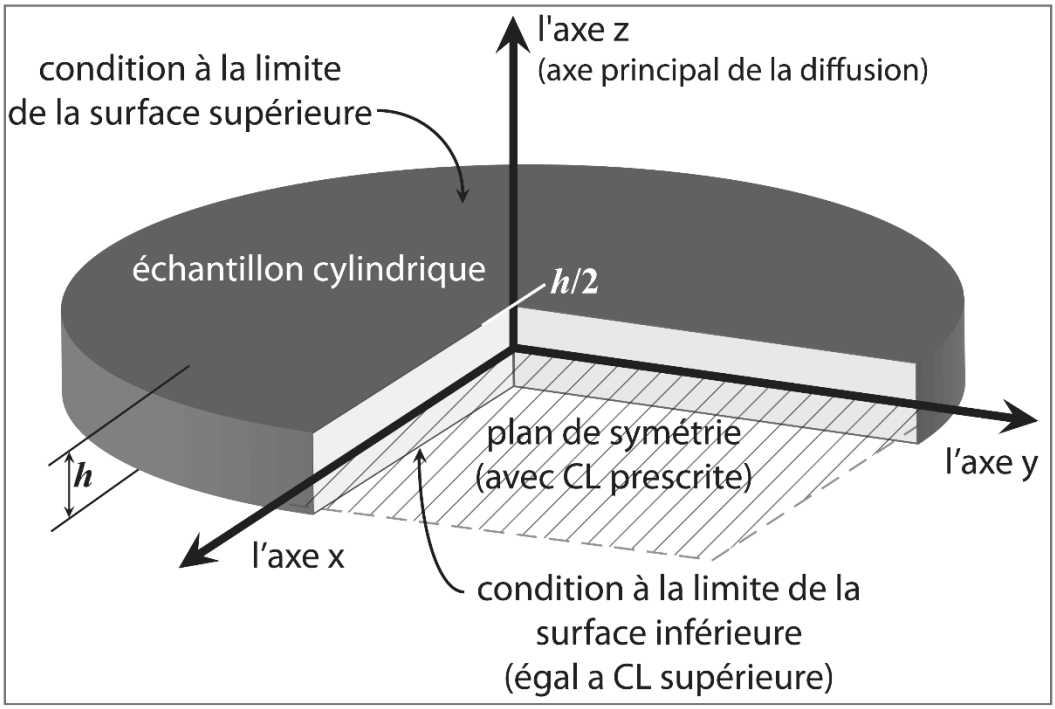

Figure 1.6: Une représentation schématique d'un échantillon de tissu utilisé dans les expériences

de diffusion – la géométrie du modèle, le système de coordonnées et les conditions aux limites (CL).

Pour déterminer les conditions aux limites, il faut examiner la représentation schématique d'un échantillon de tissu qui est l'objet de modélisation (reportez-vous à la configuration des expériences de diffusion comme le montre la Figure 1.2). Car on a seulement besoin de modéliser la moitié d'un échantillon de tissu cylindrique, les conditions aux limites sont les suivantes

$$c_e(t)\big|_{z=h/2} = 0 \tag{1.1.3}$$

$$c_i(t)\big|_{z=h/2} = c_{i0}e^{-kt} \tag{1.1.4}$$

$$\left.\frac{\partial c_e(t)}{\partial z}\right|_{z=0} = 0 \tag{1.1.5}$$

$$\left.\frac{\partial c_i(t)}{\partial z}\right|_{z=0} = 0 \tag{1.1.6}$$

Pour déterminer les conditions initiales, une répartition homogène de la concentration initiale du soluté à travers l'échantillon est supposée. Les concentrations initiales ne sont pas nécessairement égales dans l'espace extracellulaire et intracellulaire, ce qui est une hypothèse valable pour le tissu intact ou mal perméabilisé où soluté reste intracellulaire. Constantes c_{e0} et c_{i0} sont définis comme

$$c_e(z,0) = c_{e0} \tag{1.1.7}$$

$$c_i(z,0) = c_{i0} \tag{1.1.8}$$

La solution du système d'équations aux dérivées partielles (éq. 1.1.1–1.1.2) pour les conditions aux limites et les conditions initiales (éq. 1.1.3–1.1.8) est

$$c_e(z,t) = \frac{4c_{i0}}{\pi}\sum_{n=0}^{\infty}\frac{(-1)^n}{2n+1}\cos(\lambda_n z)\left(C_{n,1}e^{\gamma_{n,1}t}\left(\frac{\gamma_{n,1}}{k}+1\right)+C_{n,2}e^{\gamma_{n,2}t}\left(\frac{\gamma_{n,2}}{k}+1\right)\right), \tag{1.1.9}$$

$$c_i(z,t) = \frac{4c_{i0}}{\pi}\sum_{n=0}^{\infty}\frac{(-1)^n}{2n+1}\cos(\lambda_n z)\left(C_{n,1}e^{\gamma_{n,1}t}+C_{n,2}e^{\gamma_{n,2}t}-e^{-kt}\right)+c_{i0}e^{-kt}, \tag{1.1.10}$$

où

$$C_{n,1} = \frac{\left(\frac{c_{e0}}{c_{i0}} - 1\right)k - \gamma_{n,2}}{\gamma_{n,1} - \gamma_{n,2}}, \tag{1.1.11}$$

$$C_{n,2} = \frac{\left(1 - \frac{c_{e0}}{c_{i0}}\right)k + \gamma_{n,1}}{\gamma_{n,1} - \gamma_{n,2}}, \tag{1.1.12}$$

et

$$\gamma_{n_{1,2}} = \frac{-\left((\delta+1)k + \lambda_n{}^2 D_{s,e}\right) \pm \sqrt{\left((\delta+1)k + \lambda_n{}^2 D_{s,e}\right)^2 - 4k\lambda_n{}^2 D_{s,e}}}{2}, \tag{1.1.13}$$

où, pour simplifier l'algèbre, on a mis $\delta = (1 - \varepsilon)/\varepsilon$. Les valeurs propres λ_n sont égales à $\lambda_n = (2n+1) \cdot \pi/h$.

Le coefficient d'écoulement transmembranaire (aussi appelé le coefficient de transfert de la matière) k est le constituant essentiel du modèle qui décrit l'électroporation de la membrane cellulaire. Si les cellules peuvent être modélisés comme des sphères parfaites de rayon R et de la membrane d'épaisseur d_m, $D_{s,0}$ est la constante de diffusion du soluté dans l'eau à une température donnée, y_s est le coefficient d'empêchement de diffusion à travers les pores et f_p est la fraction de surface des pores stables ($f_p = N_p \cdot A_p/A_0$, où N_p est le nombre de pores par cellule, A_p la zone de pores moyenne unique et A_0 la zone de la cellule égalant $4\pi R^2$), on peut exprimer et déterminer k comme

$$k = \frac{3D_{s,0}y_s f_p}{d_m R} \tag{1.1.14}$$

L'électroporation affecte la fraction de surface des pores f_p ainsi que le coefficient d'empêchement y_s, en supposant que le rayon moyen d'un pore stable est dépendant de paramètres de traitement. Pour plus de détails sur les coefficients k et y_s, voir l'Article II.

1.1.3.3 Le modèle à double porosité pour le problème de filtration-consolidation sous la pression extérieure

Il y a une analogie évidente de point de vue de la mathématique et physique entre la loi de diffusion de Fick et de la loi de Darcy d'écoulement du liquide dans les milieux poreux. Le modèle à double porosité donnée par éq. 1.1.1–1.1.2 peut donc également être écrit pour décrire le comportement de filtration-consolidation du tissu sous la pression appliquée. La formulation du modèle reste la même, sauf pour certains remplacements, omissions, et quelques détails mineurs à changer. À savoir, le coefficient de diffusion $D_{s,e}$ est remplacé par la perméabilité hydraulique k_e

du tissu divisé par la viscosité μ, c'est-à-dire par k_e/μ, et le coefficient de transport de la matière k est remplacé par le coefficient de proportionnalité α divisé par la viscosité μ, c'est-à-dire par α/μ. La porosité initiale ε du tissu est déjà pris en compte par la perméabilité k_e et le module de compressibilité $G_{\varepsilon,e}$ qui ne sont pas des paramètres intrinsèque, mais plutôt des quantités moyennes en volume entier de l'échantillon du tissu, et il est donc possible d'omettre le facteur $(1 - \varepsilon)/\varepsilon$. Enfin, les gradients de concentration sont remplacées, comme les forces d'entraînement des processus de transport, par les gradients de pression de liquide, et donc les concentrations c_e et c_i sont remplacés par des pressions de liquide p_e et p_i, respectivement. En conséquence, comme analogues aux équations de diffusion fondamentaux du modèle (éq 1.1.1–1.1.2.), on obtient les équations suivantes

$$\frac{1}{G_{\varepsilon,e}}\frac{\partial p_e}{\partial t} - \frac{\partial}{\partial z}\left(\frac{k_e}{\mu}\frac{\partial p_e}{\partial z}\right) - \frac{\alpha}{\mu}\left(p_i - p_e\right) = 0 \tag{1.1.15}$$

$$\frac{1}{G_{\varepsilon,i}}\frac{\partial p_i}{\partial t} + \frac{\alpha}{\mu}\left(p_i - p_e\right) = 0 \tag{1.1.16}$$

Ces équations sont, même comme dans le problème de la diffusion, dérivée de la loi de conservation de la matière. Cependant, par opposition à la concentration du soluté, qui est à la fois la quantité mesurée et la quantité observé ainsi que (par l'intermédiaire de son gradient) la force originaire du flux de soluté par la diffusion, la pression du liquide, si une force motrice, n'est pas elle-même un objet de la loi de conservation de la matière. Elle doit être liée à la densité conservée et, par conséquent, la porosité des espaces respectifs par les modules de compressibilité. Le module d'élasticité ou de compressibilité est traditionnellement défini comme une variation relative de volume en réponse à un changement de pression donnée. Si le rapport de vide e désigne le rapport entre le vide (liquide) et une phase solide au sein de l'espace intra- ou extracellulaire, des modules de compressibilité peuvent être déterminées à partir des équations

$$\frac{\partial e_e}{\partial t} = -\frac{\partial p_e}{\partial t}\cdot\frac{\partial e_e}{\partial p_{e,S}} = \frac{1}{G_e}\frac{\partial p_e}{\partial t} \tag{1.1.17}$$

$$\frac{\partial e_i}{\partial t} = -\frac{\partial p_i}{\partial t}\cdot\frac{\partial e_i}{\partial p_{i,S}} = \frac{1}{G_i}\frac{\partial p_i}{\partial t} \tag{1.1.18}$$

Les modules de compressibilité G_e et G_i concernent le changement de rapport de vide avec la perte de pression du liquide. Dans les expériences, le déplacement du piston est mesurée, et par le déplacement, la déformation de l'échantillon de tissu. La déformation mesurée est plus étroitement liée à la porosité ε (rapport de vide total du volume) plutôt qu'au rapport de vide e. Pour cette raison, les modules de compressibilité ont été redéfinies via la porosité moyenne de chaque espace, de sorte que

$$\bar{G}_{\varepsilon,e} = G_e\left(1+\bar{e}_e\right)^2 \tag{1.1.19}$$

$$\bar{G}_{\varepsilon,i} = G_i\left(1+\bar{e}_i\right)^2 \tag{1.1.20}$$

Notez que dans toutes les équations sauf éq. 1.1.19–1.1.20, la notation des valeurs moyennes a été omise. Cette définition rend des estimations initiales pour les modules faciles à obtenir à partir de points de la déformation totale ou finale atteint dans les expériences. Cependant, il y a un compromis. Le rapport de vide moyenne, une fonction à la fois de l'espace et du temps, et qu'on suppose soit constante, rétrécit l'applicabilité générale du modèle. Il est maintenant valide pour un segment particulier de l'espace des paramètres qui exige le déplacement du piston soit faible par rapport à l'épaisseur de la totalité de l'échantillon. Cette condition est remplie si le tissu n'est pas gravement endommagé par le traitement appliqué, quelque chose à garder à l'esprit au moment d'interpréter les résultats des modèles. Une approche plus générale en omettant ces simplifications est très exigeante en termes mathématiques et difficile en termes du traitement analytique.

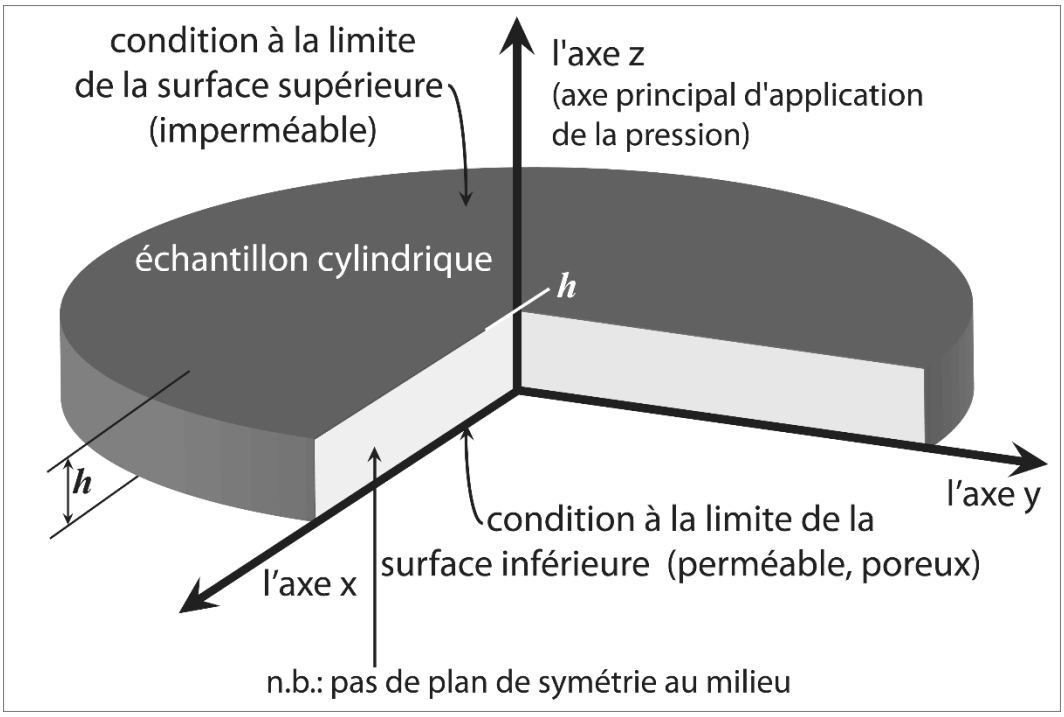

Figure 1.7: Une représentation schématique d'un échantillon de tissu utilisé dans les expériences du pressage – la géométrie du modèle, le système de coordonnées et les conditions aux limites (CL).

Pour résoudre le système d'éq. 1.1.15–1.1.16, les conditions aux limites et conditions initiales appropriées sont nécessaires. Les conditions initiales peuvent être réécrites à partir des éq. 1.1.7–1.1.8 par un remplacement simple de la concentration avec la pression du liquide, on obtient

$$p_e(z,0) = p_{e0} \tag{1.1.21}$$

$$p_i(z,0) = p_{i0} \tag{1.1.22}$$

D'autre part, les conditions aux limites sont un peu différentes, car il n'y a pas de plan central de symétrie dans la section médiane de l'échantillon de tissu (voir la Figure 1.7). Au lieu de cela, il y a une limite de non-flux à la surface de contact du échantillon–piston, exigeant que

$$\left.\frac{\partial p_e}{\partial z}\right|_{z=h} = \left.\frac{\partial p_i}{\partial z}\right|_{z=h} = 0 \tag{1.1.23}$$

et la libre circulation de liquide à la surface de contact de l'échantillon–support poreux

$$p_e\big|_{z=0} = 0 \tag{1.1.24}$$

tandis que le calcul de condition limite de la pression liquide intracellulaire sur cette surface suit la même logique que pour le problème de la diffusion, donnant

$$p_i\big|_{z=0} = p_{i0} e^{-\frac{\alpha G_{\varepsilon,i}}{\mu} t} \tag{1.1.25}$$

La solution des éq. 1.1.15–1.1.16 sous conditions initiales et aux limites éq. 1.1.21–1.1.25 est analogue à celle pour le problème de diffusion, avec les seules exceptions de sinus remplacer le cosinus dans la série de Fourier et de modifications mineures aux valeurs propres en raison des différentes conditions aux limites, produisant

$$p_e(z,t) = \frac{4p_{i0}}{\pi} \sum_{n=0}^{\infty} \frac{1}{2n+1} \left(\left(\gamma_{n,1}\tau + 1\right) C_1 e^{\gamma_{n,1} t} + \left(\gamma_{n,2}\tau + 1\right) C_2 e^{\gamma_{n,2} t} \right) \sin\left(\frac{(2n+1)\pi}{2h} z \right) \tag{1.1.26}$$

$$p_i(z,t) = \frac{4p_{i0}}{\pi} \sum_{n=0}^{\infty} \frac{1}{2n+1} \left(C_1 e^{\gamma_{n,1} t} + C_2 e^{\gamma_{n,2} t} - e^{-\tau^{-1} t} \right) \sin\left(\frac{(2n+1)\pi}{2h} z \right) + p_{i0} e^{-\tau^{-1} t} \tag{1.1.27}$$

où

$$C_1 = \frac{\left(\frac{p_{e0}}{p_{i0}} - 1 \right) \tau^{-1} - \gamma_{n,2}}{\gamma_{n,1} - \gamma_{n,2}} \tag{1.1.28}$$

$$C_2 = \frac{\left(1 - \frac{p_{e0}}{p_{i0}} \right) \tau^{-1} + \gamma_{n,1}}{\gamma_{n,1} - \gamma_{n,2}} \tag{1.1.29}$$

et

$$\gamma_{n_{1,2}} = \frac{-\left(\tau^{-1}\delta + {\lambda_n}^2 \nu\right) \pm \sqrt{\left(\tau^{-1}\delta + {\lambda_n}^2 \nu\right)^2 - 4{\lambda_n}^2 \nu \tau^{-1}}}{2} \tag{1.1.30}$$

Pour simplifier l'algèbre, les remplacements suivants ont été réalisés

$$\nu = \frac{k_e G_{\varepsilon,e}}{\mu};\ \tau^{-1} = \frac{\alpha G_{\varepsilon,i}}{\mu};\ \delta = \left(1 + \frac{G_{\varepsilon,e}}{G_{\varepsilon,i}}\right) \tag{1.1.31}$$

et les valeurs propres λ_n sont égales à $\lambda_n = (2n+1) \cdot \pi/2h$.

Une fois que des pressions de liquide sont connues, éq. 1.1.17–1.1.20 peut être utilisées pour calculer la déformation de l'échantillon. S'y on utilise les déformations sans dimension $s_\varepsilon(t)$ normalisées par rapport à la hauteur de l'échantillon initial, la formule est

$$s_\varepsilon(t) = \frac{S_\varepsilon(t)}{h} = \frac{1}{G_{\varepsilon,e}} \int_0^1 \int_{p_e(z,t)}^{p_e(z,0)} dp_e \cdot dz + \frac{1}{G_{\varepsilon,i}} \int_0^1 \int_{p_i(z,t)}^{p_i(z,0)} dp_i \cdot dz \tag{1.1.32}$$

Le paramètre restant dans le besoin de quelques explications est le facteur sans dimension α, qui représente l'influence du traitement d'électroporation sur la perméabilité hydraulique de la membrane cellulaire. Selon la théorie présentée dans l'Article III, pour une cellule sphérique de rayon R, avec une fraction de surface de pores stable f_p consistant en N_p pores d'un rayon moyenne r_p, il peut être écrit sous la forme

$$\alpha = \frac{9 f_p r_p^2}{8R^2} \tag{1.1.33}$$

où $k_p = r_p^2/8$ est la perméabilité hydraulique d'un seul pore.

1.1.3.4 Validation du modèle et une démonstration de son application

Les matériels et méthodes, sections 1.1.2.1 – 1.1.2.3, décrivent les expériences de la diffusion et du pressage qui ont été menées pour tester et valider le modèle à double porosité. Cette section donne des rapports sur les résultats de ces expériences (des cinétiques mesurées) et une comparaison des mesures avec les cinétiques simulées obtenues en utilisant le modèle à double porosité. Les résultats combinés sont représentés graphiquement à la Figure 1.8 ci-dessous et brièvement discuté. Les résultats reproduits ici ont été obtenues exclusivement par l'application du traitement électrique selon le protocole de traitement A des échantillons de tissus. Le lecteur intéressé est référée à la section « Résultats et discussion », à voir la Figure 10 de l'Article IV pour plus de résultats avec d'autres protocoles de traitement.

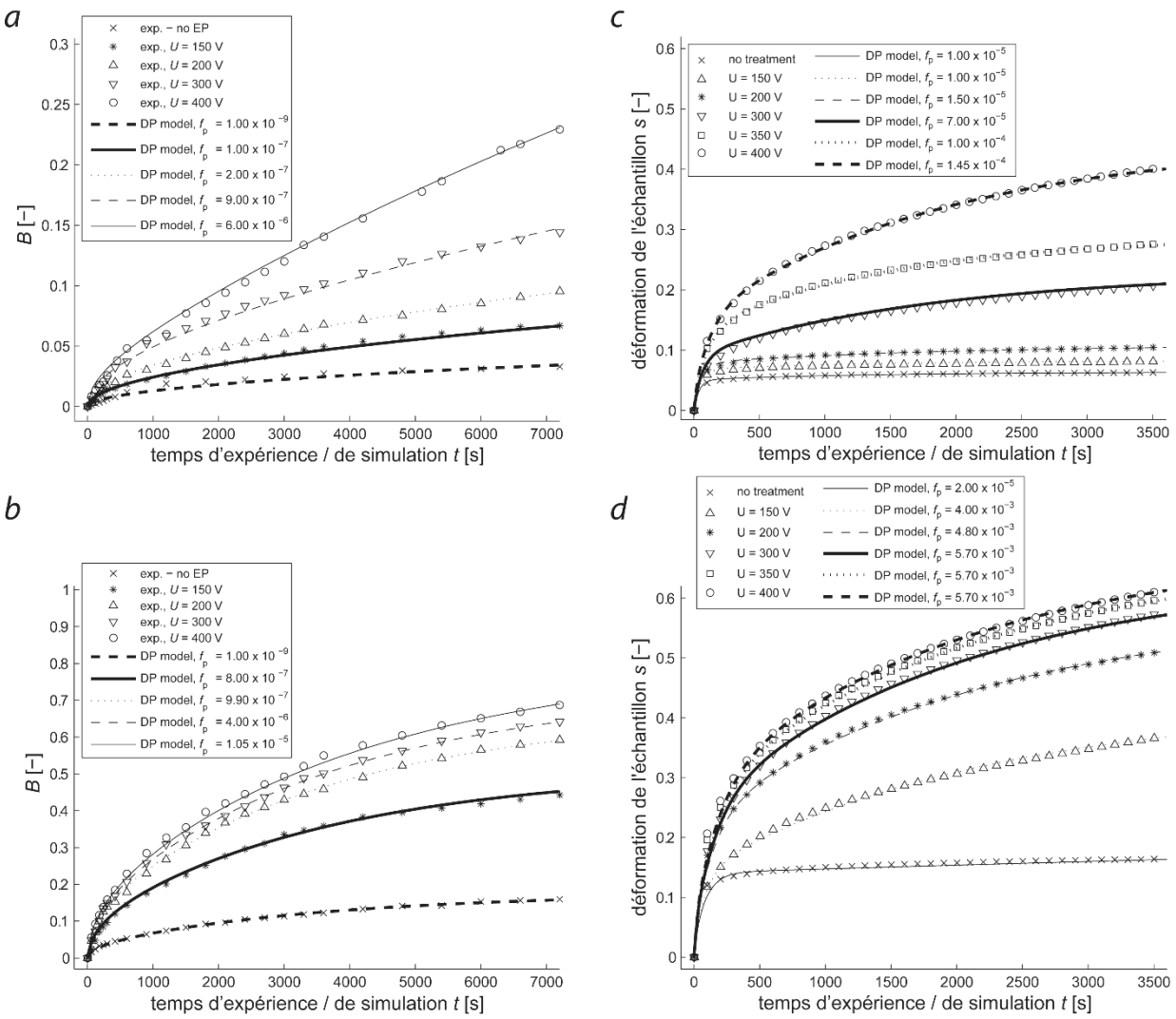

Figure 1.8: Résultats des expériences de diffusion (a – b) et de pressage (c – d) effectuées selon la méthodologie expérimentale décrite, et les cinétiques d'extraction obtenues par des simulations du modèle avec les tissus de la betterave à sucre (a, c) et de la pomme (b, d).

Comme la Figure 1.8 le montre, le modèle à double porosité est capable de modéliser les cinétiques obtenues expérimentalement avec une grande précision. Etant donné un ensemble varié et large de réponses à l'électroporation et l'extraction ultérieure de soluté ou de jus, les paramètres du modèle peuvent être ajustés en conséquence pour obtenir une bonne correspondance entre les simulations et les expérimentations. Néanmoins, plusieurs questions peuvent être soulevées lors de l'examen des valeurs des paramètres qui ont été émis par la procédure d'optimisation de simulation utilisé pour trouver leurs valeurs optimales. Les valeurs de ces paramètres semblent indiquer que la fraction de surface de pores n'est pas le seul paramètre important, et d'autres paramètres doivent impérativement faire varier pour obtenir un bon ajustement du modèle aux cinétiques expérimentales. Ce doit être mis en conformité avec la théorie de l'électroporation, ou le modèle doit encore être améliorée et sa sensibilité aux différents paramètres évaluée

indépendamment pour chaque paramètre. Il serait également souhaitable de réduire le nombre de degrés de liberté qui sont représentés par le grand nombre de paramètres qui influencent la cinétique finale de la même manière, ça veut dire ils présentent une tendance commune. Le lecteur est invité à ce point de se référer à la section « Résultats et discussion » de l'Article IV pour une discussion très détaillée des résultats reproduit ici dans la Figure 1.8, et une critique d'accompagnement plus rigoureuse sur les points forts de modèle et ses rétractions.

La figure suivante (Figure 1.9) illustre l'idée fondamentale et principale du modèle à double porosité. Cette représentation est présenté ensemble avec les résultats de la Figure 1.8, car elle donne les profils de pression de liquide dans la phase intra- et extracellulaire, tels que ceux qui ont ensuite été intégrés pour obtenir la cinétique de l'expression du liquide, comme présentée sur la Figure 1.8 (c – d). Cette figure démontre clairement l'effet de retard de chute de pression (ou la concentration dans le problème de diffusion) intracellulaire en raison de la perméabilité de la membrane qui est inférieur par rapport à la perméabilité de la phase extracellulaire.

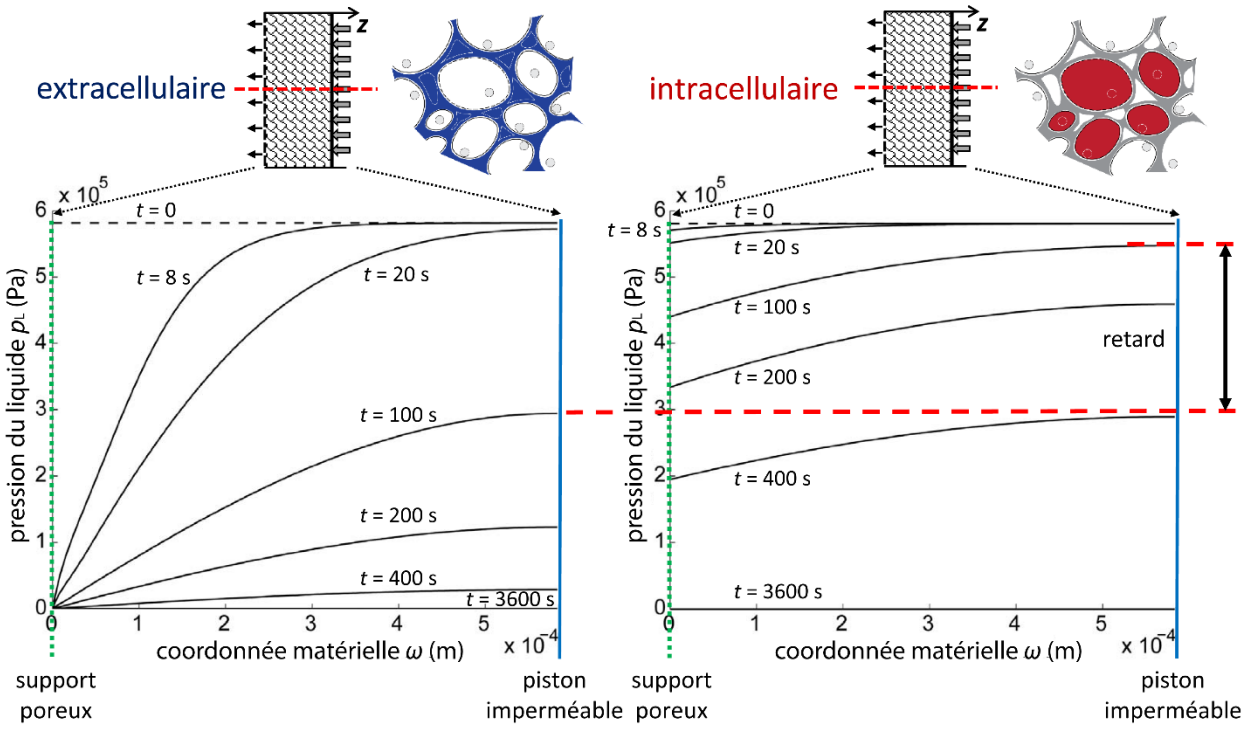

Figure 1.9: Les profils de pression le long de la coupe transversale de l'échantillon de tissu pour différents moments de l'expérience simulée. Notez que sur l'abscisse les coordonnées matérielles sont utilisées car ces profils simulés de pression ont été obtenus en utilisant un modèle à double porosité amélioré, plus complexe et résolu numériquement pour le problème de filtration/consolidation du tissu traité par l'électroporation. Ce modèle n'est pas élaboré dans cette thèse (manuscrit sous rédaction).

1.1.3.5 Relations thermiques dans le tissu – analyse par le modèle à double porosité et les relations entre la distribution de température et le transfert de la matière

Par analogie de la loi de la diffusion de Fick et la loi de Darcy pour l'écoulement de liquide, le modèle à double porosité de diffusion a été traduit au problème de filtration-consolidation d'un tissu biologique lors du pressage (comparer l'Article II et l'Article III, ou se référer à l'Article IV). Par une analogie physiquement et mathématiquement équivalente de la loi de Fourier de transfert de la chaleur, et en utilisant les relations de base de la thermodynamique de non-équilibre, on peut postuler qu'un modèle à double porosité peut être écrit aussi pour décrire les relations thermiques dans les tissus biologiques, ce qui devrait, en principe, être applicable si le tissu est traité par l'électroporation ou non.

Les équations du modèle thermique pour le cas de flux thermique le long d'un axe principal, dans l'espace extracellulaire et intracellulaire sont, respectivement

$$\frac{\partial T_e}{\partial t} - \frac{k_e}{\rho c_p}\frac{\partial^2 T_e}{\partial z^2} - \frac{f_v h_v}{\rho c_p}\left(T_i - T_e\right) = 0 \tag{1.1.34}$$

$$\frac{\partial T_i}{\partial t} - \frac{k_i}{\rho c_p}\frac{\partial^2 T_i}{\partial z^2} + \frac{h_v}{\rho c_p}\left(T_i - T_e\right) = 0 \tag{1.1.35}$$

Dans l'éq. 1.1.34, le nouveau paramètre – le rapport volumétrique f_v – est un facteur multiplicatif qui représente le déséquilibre de la distribution volumétrique de l'espace (intra- et extracellulaire) et est égal à $F/(1 - F)$. D'autres quantités sont les suivantes: T_e et T_i sont la température extracellulaire et intracellulaire en [K], respectivement; k_e et k_i sont les conductivités thermiques dans l'espace extracellulaire et intracellulaire en [W/(m.K)], respectivement; z est la coordonnée d'espace et t celle du temps; c_p est la capacité thermique de tissu [J/(kg.K)]; ρ la densité de tissu [kg / m3]; h_v est le coefficient de transfert de chaleur volumétrique en [W/(m^3.K)]. Le coefficient h_v reflète la conductivité thermique de la membrane plasmique et la géométrie particulière d'interface d'échange de chaleur, et une dépendance spatio-temporelle de ce paramètre en fonction de l'électroporation peut être postulée pour maintenir une généralité complète du modèle à ce stade. Si une telle dépendance existe ou non doit être théoriquement et expérimentalement évalué.

Une remarque sur la différence entre les équations 1.1.34 ou 1.1.35 et les équations correspondantes pour le problème de la diffusion/du pressage. Dans les deux cas, ceux de la diffusion ainsi que dans la version du modèle à double porosité pour l'étude de la consolidation-filtration sous pression, la porosité intracellulaire et les gradients de la concentration ou de pression associés ont été négligés, ce qui simplifie l'équation de l'espace intracellulaire. Cette simplification a été basée sur l'hypothèse que le facteur limitant dans le transport de solutés ou de l'écoulement

du liquide est la perméabilité limitée de la membrane cellulaire, qui a été supposé être des ordres de grandeur plus faible par rapport à la diffusivité ou de la perméabilité hydraulique correspondant dans l'espace extracellulaire. Toutefois, le problème thermique, si l'on compare les conductivités thermiques de cytoplasme, de membrane de plasma et de liquide extracellulaire, elles ne sont pas différentes dans des ordres de grandeur. Par conséquent, une simplification en omettant le flux thermique intracellulaire ne peut pas être justifiée, et ce terme doit être gardé dans l'équation, ce qui complique substantiellement la solution analytique pour le cas général où $k_e \neq k_i$, et seulement une allusion est faite à la solution de ce type du problème général dans l'annexe au chapitre 5.

Pour le cas moins général, où $k_e = k_i$, il est possible de trouver facilement une solution analytique pour T_e et T_i, égalant

$$T_i(z,t) = \frac{4}{\pi}\left(\frac{f_v T_{i0} + T_{e0}}{f_v + 1} + \frac{T_{i0} - T_{e0}}{f_v + 1} e^{-\beta(1+f_v)t}\right)\sum_{n=0}^{\infty}\frac{(-1)^n}{2n+1}\cos(\lambda_n z)e^{-\lambda_n{}^2\alpha t} \tag{1.1.36}$$

$$T_e(z,t) = \frac{4}{\pi}\left(\frac{f_v T_{i0} + T_{e0}}{f_v + 1} - \frac{f_v(T_{i0} - T_{e0})}{f_v + 1} e^{-\beta(1+f_v)t}\right)\sum_{n=0}^{\infty}\frac{(-1)^n}{2n+1}\cos(\lambda_n z)e^{-\lambda_n{}^2\alpha t} \tag{1.1.37}$$

où $\alpha = k/\rho c_p$ et $\beta = h_v/\rho c_p$. Cette solution est également présentée au paragraphe 5.1.2 du chapitre 5 du mémoire de cette thèse. Les simulations donnent, pour différentes valeurs du paramètre h_v (le coefficient volumétrique de transfert de chaleur transmembranaire) et la géométrie du modèle typique utilisée dans les études de transport de masse, résultats présentés dans la Figure 1.10. Notez qu'en raison de l'équivalence $k_e = k_i$, une perturbation initiale dans le système est nécessaire (faite ici par la mise en $T_{e0} \neq T_{i0}$) afin de montrer une différence entre la température de l'espace intra- et extracellulaire. Il est évident d'après ces résultats simulés que la valeur du paramètre h_v doit se situer entre 10^4 $Wm^{-3}K^{-1}$ et 10^5 $Wm^{-3}K^{-1}$ pour que la différence de température initiale puisse produire une réponse non-instantanée du système sur l'échelle de temps de quelques secondes.

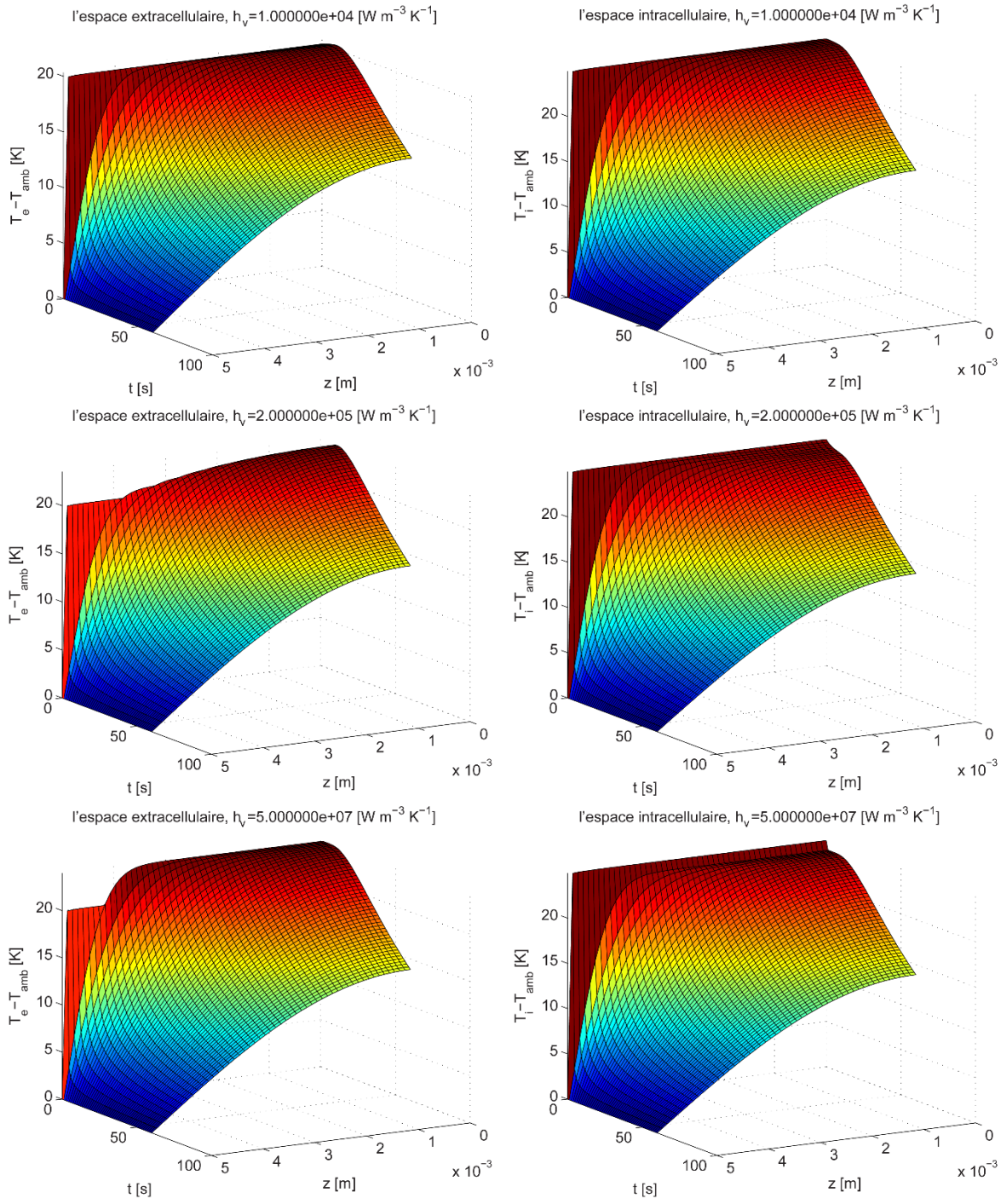

Figure 1.10: Les profils spatio-temporels de la température (intrinsèque) dans l'espace intra- et extracellulaire pour trois valeurs différentes du coefficient volumétrique de transfert de chaleur transmembranaire h_v. Les températures initiales supérieures à la température d'ambiante T_{amb} ont été T_{i0} = 25 °C et T_{e0} = 20 °C dans tous les cas.

Le traitement théorique des relations thermiques dans les tissus avec l'utilisation d'une approche à double porosité est poursuivi par l'élaboration d'une solution numérique plus générale où la situation $k_e \neq k_i$ peut être modélisée, avec des résultats (omis ici pour la brièveté) pointant à nouveau sur l'importance du coefficient de transfert de chaleur de membrane h_v. Si ce coefficient

est grand, l'échange de chaleur transmembranaire est trop rapide, et il n'y a aucune différence détectable entre les profils de température intra- et extracellulaires. Cela confirme l'importance du paramètre h_v dans l'approche à double porosité et cette approche est montrée comme raisonnable pour l'étude des relations thermiques dans les tissus en ordre du temps de quelques secondes. Une analyse théorique sur l'estimation réaliste de paramètre h_v pour le tissu modèle de pomme est présentée dans la continuation du chapitre 5 (voir section/paragraphe 5.1.4).

Selon l'analyse présentée dans la section 5.1.4, le coefficient de transfert de chaleur volumétrique h_v est égal à

$$h_v = \frac{3k_i}{2R^2} = \frac{3 \cdot 0.559}{2\left(100 \cdot 10^{-6}\right)^2} = 8.385 \cdot 10^7 \, \frac{\mathrm{W}}{\mathrm{m}^3\mathrm{K}}, \tag{1.1.38}$$

une estimation réaliste en vue que la conductivité thermique finie de le cytoplasme cellulaire et celle de l'espace extracellulaire ont été pris en compte. Cependant, la valeur est encore plus grande que la plus grande valeur utilisée dans des simulations à l'aide de la solution analytique (voir Figure 1.10). La conclusion qui peut être tirée de cela, sur la base du comportement observé pour les températures dans la Figure 1.10 pour les valeurs de h_v supérieures à 10^6, est que tout gradient thermique transmembranaire qui résulterait d'inhomogénéités du champ électrique local ou de sa distribution actuelle, serait instantanément (c'est-à-dire sur une échelle de temps de moins qu'une seconde) équilibrée en raison du transfert thermique rapide à travers la membrane.

Cette constatation ne doit pas conduire à la conclusion que le modèle thermique à double porosité est inutilement compliquée avec le terme source, car l'analyse est instructive, et toutes les dérivations mathématiques présentées dans la section 5.1 peuvent être utilisées pour faire progresser l'état de connaissance des analogues du modèle à double porosité sur le transport de la matière. En outre, la solution numérique, c'est-à-dire la solution qui permet que la conductivité thermique intra- et extracellulaire soient différentes, pourrait encore être pertinent pour l'étude des relations thermiques dans les tissus, que ce soit traité par électroporation ou pas, si les conductivités thermique de chaque phase/espace sont significativement différentes.

Le reste du chapitre 5 est consacré à l'étude des effets de la température sur les processus de transport de la matière par l'intermédiaire de paramètres dépendant de la température dans les modèles de transport de la matière, tels que le coefficient de diffusion et la viscosité. Solutions numériques des modèles à double porosité de transport de la matière par diffusion et pendant le pressage ont été trouvés afin de tenir compte de l'effet de la température et de la dépendance spatio-temporelle de ces coefficients de transport ($D_{s,0}(T(z, t)) = D_{s,0}(z, t)$ and $\eta(T(z, t)) = \eta(z, t)$) dans l'étude de la cinétique de transport de la matière. Les résultats d'une étude paramétrique sont donnés sur la Figure 1.11 et semblent indiquer que, étant donné la température ambiante fixe de

20 °C, même une augmentation substantielle de la température des tissus initialement au début de la diffusion ou de l'étape de pressage ne conduit pas à une augmentation substantielle de la vitesse de diffusion ou de l'expression du jus. Cela est dû à une dissipation relativement rapide de la chaleur du tissu dans le milieu environnant. Notez que ces résultats simulés ont été obtenus pour des échantillons minces de 5 mm d'épaisseur et la supposition sur l'état de la température ambiante restant constante est valable uniquement dans des conditions spécifiques, telle que développée dans le paragraphe/section 5.2.2. D'autres travaux pris en charge par la validation expérimentale seront nécessaires pour élucider ce sujet, cependant, ce qu'il est malheureusement hors de portée de cette thèse.

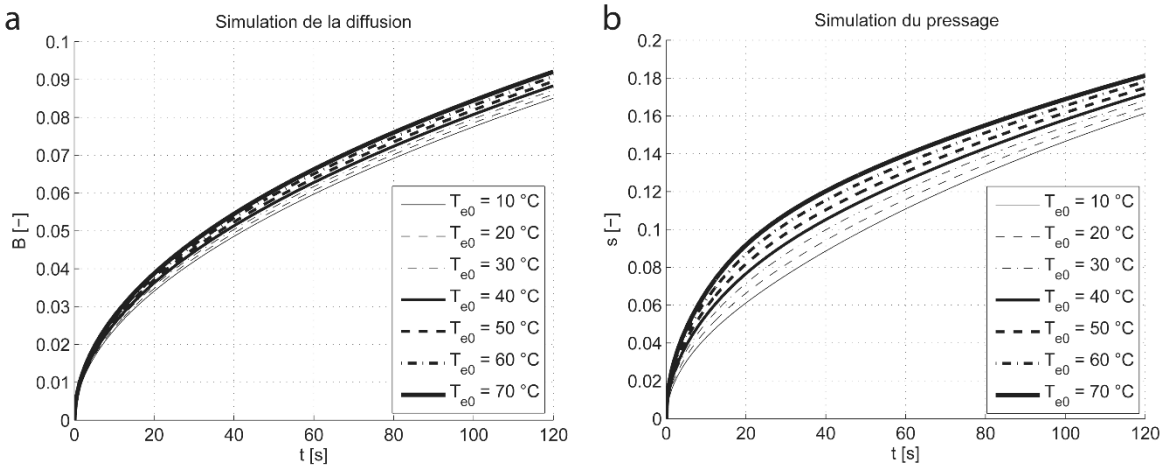

Figure 1.11: L'étude paramétrique pour les tissus traité par l'électroporation avec les modèles à double porosité de diffusion de soluté et pressage, illustrant l'effet de paramètres de ces modèles dépendant de la température (coefficient de diffusion, viscosité). Seul le coefficient de diffusion et / ou la viscosité étaient variés afin d'obtenir des cinétiques différentes, et ceux-ci étaient dépendants de l'augmentation de la température initiale (le paramètre varié).

1.1.4 Contributions à la science et conclusion

La contribution originale principale à la science de cette thèse est le modèle à double porosité nouvellement développé pour l'étude des processus de transport de la matière liés à l'électroporation dans les tissus, plus spécifiquement, de la diffusion de soluté et de la consolidation du tissu ou la filtration (expression) du jus.

La thèse démontre (voir les articles II – IV) le modèle est capable de modéliser avec haute précision les cinétiques d'extraction obtenus par diffusion ainsi que par les expériences de pressage. Lors de la construction du modèle, un paramètre de modèle, la fraction de surface des pores, a été identifié comme le paramètre le plus important qui est une fonction de paramètres de

traitement d'électroporation – pour rappel, ce sont l'intensité locale du champ électrique, le nombre d'impulsions, et la durée d'une impulsion. Une méthode d'analyse de l'estimation de l'importance de ce paramètre pour le transport transmembranaire a été développée, et couplée au flux diffusif transmembranaire dans le problème de la diffusion, ainsi qu'au flux du liquide transmembranaire dans le problème de l'écoulement de liquide lors de l'étape de consolidation (pressage). Dans le travail le plus récent qui est présenté dans cette thèse sur la validation des modèles, d'autres facteurs importants ont été identifiés (surtout changements de perméabilité et de compressibilité des tissus en raison de modifications structurelles) qui reflètent la nature complexe des effets de champ électrique sur la texture et le transport de la matière dans le tissu traité par l'électroporation.

Pour développer davantage le modèle, les travaux futurs auront très probablement besoin de se concentrer sur l'évaluation et la description mathématique de l'influence d'autres effets importants, pour arriver à un modèle plus généralisé, dont la solution sera capable de prédire la cinétique d'extraction en fonction des paramètres de traitement et des caractéristiques des matériaux qui peut être obtenu soit à partir de la littérature ou estimés par des expériences indépendantes.

Les travaux préliminaires déjà effectués au-delà de la portée de cette thèse indiquent que des mécanismes tels que la perte de pression de turgescence (applicable uniquement dans les tissus comportant des parois cellulaires) ainsi que l'électro-osmose pourraient jouer un rôle important dans le transport de la matière et doivent être évaluées indépendamment, puis incorporé dans le modèle à double porosité. Les progrès récents dans les méthodes de détection et d'imagerie de la force du champ électrique dans les tissus offrent de nouvelles possibilités intéressantes pour coupler les modèles de distribution de champ électrique avec des modèles d'évolution des pores et le modèle à double porosité. Le modèle résultant, un modèle spatio-temporelle fortement couplé, pourrait être complété par l'ensemble d'équations de Nernst-Stokes pour électrodiffusion, tiendrait compte des effets de l'électro-osmose, et représenterait une traduction bien nécessaire de connaissances et de savoirs acquis au niveau de l'électroporation d'une seule cellule au niveau beaucoup plus complexe tel que des tissus biologiques réels.

Néanmoins, l'auteur est convaincu que le modèle à double porosité peut déjà être appliquée avec succès pour évaluer l'efficacité du traitement par l'électroporation par rapport au transport de la matière, qu'il peut être utilisé pour l'optimisation des paramètres de traitement avec la prévision des résultats du traitement, et que la poursuite de son développement permettra aider à comprendre les phénomènes liés à transport de la matière et propriétés texturales de matériel biologique traité par l'électroporation.

1.2 Razširjeni povzetek v slovenščini

1.2.1 Uvod

Kot je bilo pokazano s poskusi na lipidnih dvoslojih, celicah in bioloških tkivih, lahko električno polje dovoljšne jakosti povzroči znatno povečanje prevodnosti in prepustnosti lipidne membrane. Učinek je znan kot elektroporacija, elektropermeabilizacija, in ker je dosežen s pomočjo izpostavitve električnim pulzom, tudi kot obdelava s pulzirajočim električni poljem. Elektroporacijo opišemo kot ustvarjanje vodnih poti, tako imenovanih por, v lipidnem dvosloju.

Glede na čas trajanja izpostavitve celice električnemu polju, lokalno porazdelitev električne poljske jakosti (le ta je omejujoči dejavnik za največjo možno dovedeno električno energijo, ki jo potencialno lahko membrani preda zunanje električno polje), ter glede na hitrost in sposobnost celjenja membrane, obstajajo trije možni izidi apliciranja električnega polja. Če je poljska jakost premajhna in/ali čas izpostavljenosti premajhen, do elektroporacije ne pride, in propustnost celične membrane ter sposobnost preživetja celice ostaneta nespremenjena. Če električna poljska jakost preseže prag, znan kot reverzibilni (tj. povratni) prag in je izpostavljenost celične membrane polju dovolj dolgo trajajoča, pride do tako imenovane reverzibilne elektroporacije; membrane je permeabilizirana in ostane v stanju zvišane propustnosti za neko obdobje, a se po določenem času propustnost membrane zniža na normalno v procesu celjenja celične membrane. Tokom tega procesa se pore v membrani zapro in celična membrana vzpostavi normalno, tj. selektivno propustnost, kar pa je možno le, če so pogoji v okolju ugodni za preživetje in funkcioniranje celice. Če je poljska jakost ali količina dovedene energije prevelika, pride do ireverzibilne elektroporacije, kar rezultira v izgubi celične homeostaze (in morda tudi v popolnem razpadu plazma membrane), kar efektivno povzroči celično smrt.

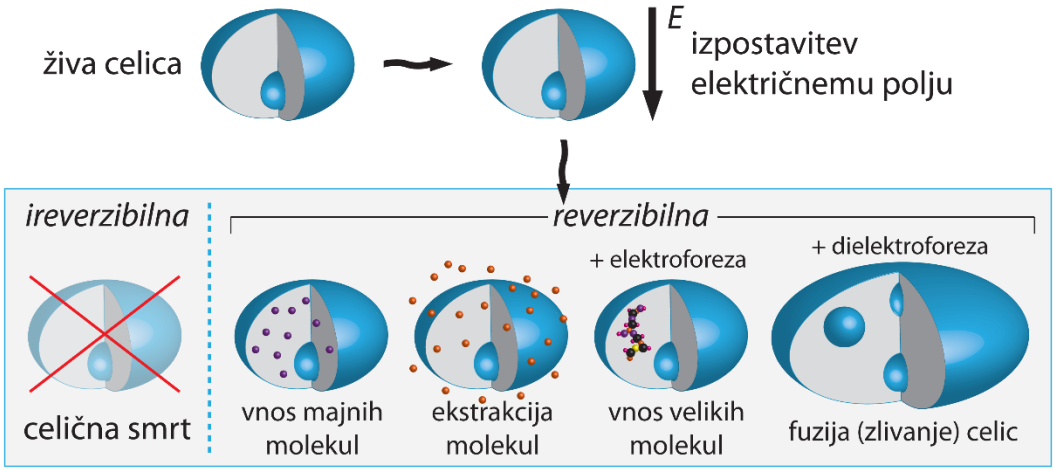

Slika 1.12: Različne opcije uporabe elektroporacije z možnimi izidi.

Tako reverzibilna kot ireverzibilna elektroporacija sta našli svoje mesto uporabe na področjih kot so biomedicine, predelava hrane, biotehnologija, in v okolijskih znanostih. V biomedicini se reverzibilna elektroporacija uporablja za vnos citotoksičnih zdravil v tumorske celice v procesu poznanem kot elektrokemoterapija, za vnos genov in transdermalni (tj. preko kože) vnos zdravil, fuzijo celic, in za vnos proteinov v celično membrano, medtem ko se ireverzibilna elektroporacije uporablja kot metoda ablacije tkiva, vključno z mehkimi tkivi pri zdravljenju raka.

Na področju obdelavi ali predelavi hrane in biotehnologije, kaže elektroporacija obetavne rezultate pri ekstrakciji sokov in drugih dragocenih snovi iz rastlinskih tkiv in mikroorganizmov kot so mikroalge, pri dehidraciji tkiv, in ne-termični konzervaciji in sterilizaciji prek inaktivacije mikrobov. Reverzibilna elektroporacija pa lahko pomaga pri ustvarjanju novih metod krioprezervacije bioloških tkiv in pri stimulaciji rastlinskega metabolizma. Med okolijskimi aplikacijami najdemo predelavo odpadnih voda in proizvodnjo biogoriv, obe področji sta trenutno predmet intenzivnih raziskav in razvoja kot obetavni aplikaciji elektroporacije.

Skozi celoten raznolik nabor raziskovalnih področij možnosti uporabe elektroporacije, je pomemben cilj zmožnost razumeti in ovrednotiti transport snovi v povezavi z elektroporacijo bioloških tkiv, saj pri večini aplikacije elektroporacije skušamo z njeno pomočjo najti nov ali izboljšati obstoječ način, kako v celico ali vnesti snov (topljenca/-e ali raztopino), ali pa iz celice pridobiti znotrajcelične sokove ali druge snovi. Zmožnost popolnega razumevanja transportnih procesov snovi ima pomembne posledice, na primer, za morebitno izboljšanje selektivnega pridobivanja snovi iz rastlinskih celic, kar znižuje stroške poznejše rafinerije, ali pa denimo za izboljšanje vnosa zdravil v ciljna tkiva, kar rezultira v novih ali bolj učinkovitih metodah zdravljenja in spopadanja z boleznimi. Na področju okolijskih znanosti nam lahko elektroporacija morda pomaga nasloviti trenutno pereče okolijske izzive, kot je dostopnost čistih virov energije.

Čeprav so elektroporacija in z njo povezani pojavi še naprej predmet intenzivnih raziskav, pa ostaja pomanjkanje popolnih modelov, ki bi jih bilo mogoče uporabiti pri modeliranju transporta snovi v kompleksnih strukturah kakršna so biološka tkiva, še posebej v povezavi z elektroporacijo. Ta dizertacija predstavlja poskus kreiranja teoretičnega matematičnega opisa, tj. modela, za proučevanje transporta snovi v elektroporiranem tkivu.

Ker v določenih primerih rabe elektroporacije ni mogoče zanemariti spremljajočih toplotnih učinkov oziroma pojavov v tkivu (pri nekaterih rabah elektroporacije je segrevanje povezano z elektroporacijo celo ena poglavitnih komponent obdelave), dizertacija na kratko teoretično obravnava tudi vpliv termičnih razmer v tkivu na transport snovi. Predstavljen je toplotni analog modelu dvojne poroznosti, ki opisuje prenos toplote v elektroporiranem tkivu, skupaj s parametrično študijo na modelih transporta snovi (difuzija in iztiskanje). Ta dva modela sta

povezana z modelom prenosa in razporeditve toplote, čemur je posvečen krajši del dizertacije, katerega namen je predstaviti enega od možnih pristopov k ovrednotenju (s pomočjo preproste računalniške simulacije) učinka dviga temperature v tkivu po elektroporaciji na transport snovi. Podan model prenosa toplote v povezavi z modeli transporta snovi je delo v procesu razvoja, ki ga je potrebno še validirati.

Model je bil razvit na podlagi zakonov o ohranitvi mase in zakonitosti transporta snovi, ter omogoča spojitev učinkov elektroporacije na membrano posamezne celice z rezultirajočim transportom prek membrane ter izvenceličnim transportom snovi. Prek poenostavitev je bila poiskana tudi poučna analitična rešitev modela, kljub temu pa se model lahko razširi z dodatnimi funkcijskimi odvisnostmi, ki opredeljujejo pojave elektroporacije, in reši numerično.

Dizertacija obsega pet objavljenih znanstvenih člankov, ki zajemajo opis aplikacij elektroporacije v industriji predelave hrane ter s tem umeščajo delo v širši kontekst področja, postopek ustvarjanja modela za problem difuzije snovi v elektroporiranem tkivu, prevod problema difuzije na matematično-ekvivalenten problem iztiskanja sokov, validacijo modela, ter predloge za mogoče prihodnje nadgradnje, razvoj, in posplošitve modela.

1.2.2 Materiali in metode

To poglavje podaja podrobnosti le o fizikalnih materialih in metodah, ki so bili uporabljeni v eksperimentih na dveh vzorčnih tkivih z namenom validirati novo-razviti model dvojne poroznosti. Model predstavlja glavni rezultat ter večino predstavljenega dela opravljenega in opisanega v tej dizertaciji, zato je njegov razvoj opisan v sledečem poglavju skupaj z vsemi teoretičnimi izpeljavami.

1.2.2.1 Difuzijski eksperimenti

Difuzijski eksperimenti, ki so opisani v člankih II in IV, so bili opravljeni po enakem protokolu. Članek III pa zadeva izključno poskuse z iztiskanjem, zato na tem mestu opisana metodologija teh poskusov ne zadeva (namesto tega, glej sledeče poglavje 1.2.2.2).

Po protokolu za poskuse z difuzijo, so bili iz gomolja sladkorne pese ter sadeža jabolka (brez kože) najprej pridobljeni (izrezani) 5 mm debeli cilindrični koščki tkiva. V nadaljevanju se na ti dve vrsti tkiv sklicujemo kot na tkivo sladkorne pese in jabolka. Vsi vzorci so merili 25 mm v premer. Vsak izmed vzorcev je bil najprej izpostavljen elektroporaciji prek aplikacije 150, 200, 300, ali 400 V napetosti na vzporednih jeklenih ploščatih elektrodah, ki sta bili fiksirani na razdaljo 5 mm druga od druge, z vzorcem tkiva med elektrodama. Namen takšne konfiguracije je v

izpostavitvi tkiva električnim poljskim jakostim 300, 400, 600 in 800 V/cm (izračunano po približni formuli *poljska jakost = napetost / razdalja med elektrodama,* zato 5 mm razdalja med elektrodama). Želena poljska jakost ni bila dosežena homogeno v tkivu, saj tkivo ni električno homogen material (dielektričnost, prevodnost, idr.), poleg tega so elektrode končnih dimenzij in polje doseže maksimalno (ciljno) vrednost le v centralnem delu dovolj daleč od robov elektrod (glej slike 1 in 5 v članku V za ilustracijo). Pravokotni pulzi izmenjujoče polaritete (glej Sliko 1.15 v poglavju 1.2.2.3) so bili aplicirani v dveh vlakih po 8 pulzov, kjer je bil vsak pulz dolg 100 μs, s frekvenco ponavljanja pulzov 1 kHz. Dva taka vlaka sta bila dovedena z medsebojnim časovnim razmakom ene sekunde. Ta elektroporacijski protokol je poimenovan Protokol A. Pulzi so bili dovedeni s pomočjo po meri narejenega pulznega generatorja z maksimalnim izhodnim tokom 38 A ter maksimalno dosegljivo napetostjo 400 V na elektrodah. Generator je bil izdelan oz. prirejen v Service Electronique UTC, Compiègne, France (več o generatorju v poglavju 1.2.2.4).

Po elektroporaciji so bili vzorci tkiva odstranjeni iz obdelovalne komore, nato pa so bile površine vzorcev za kratek čas v kontaktu z vpojnim papirjem, zato da so se osušile in je bil na ta način s površine odstranjen sladek sok, ki se je pojavil na površini vzorcev po elektroporaciji. Ta tekočina je prisotna na površini v določeni manjši meri zaradi rezanja vzorcev, predvsem (v večji meri) pa zaradi elektroosmotskih ter tlačnih razmer v tkivu med in po elektroporaciji (izguba turgorja). V kolikor površine vzorcev ne bi bile osušene, bi sok nabran na površini povzročil takojšen dvig koncentracije sladkorja v raztopini že takoj na začetku difuzijskega poskusa, kar bi rezultiralo v izmerjeni kinetiki difuzije poznani kot »faza izpiranja« (glej poglavje 2.2.3.3 v pregledu literature). Tega pojava model dvojne poroznosti ne zajema, in njegov doprinos k izmerjeni koncentraciji je težko odšteti od izmerjene kinetike zaradi različne vsebnosti sladkorja ter količine tekočine na površinah, ki se razlikujeta med posameznimi vzorci. Tako osušeni (le površine) vzorci so bili dani v bučko skupaj z magnetnim mešalom ter destilirano vodo. Tako pripravljena vzorčna mešanica je bila konstantno mešana s pomočjo magnetnega mešala na nizki frekvenci vrtenja. Vzorci tekočine so bili odvzeti v vnaprej določenih intervalih, pri čemer je bila z digitalnim analizatorjem koncentracije vodotopnih snovi – refraktometrom (podrobnosti v poglavju 1.2.2.5 spodaj), izmerjena koncentracija vseh topnih snovi, med katerimi prevladujejo sladkorji. Ves čas je bilo razmerje med tekočino ter skupnim volumnom vzorcev tkiva 2 proti 1, v vseh poskusih z difuzijo.

Veličina, katero meri digitalni refraktometer, je koncentracija sladkorja (natančneje – koncentracija vseh vodotopnih snovi) v tekočini, in je podana v enotah stopinje Brix-a (°Bx), kjer je ena stopinja Brix-a enaka 1 gramu raztopljene saharoze v 100 gramih tekočine in predstavlja koncentracijo snovi v raztopini kot razmerje v teži topljenca proti raztopini. Začetna koncentracija

sladkorja v vodni raztopini °Bx_0 je znana in običajno enaka nič, med poskusom pa merimo vsebnost oz. koncentracijo sladkorja, s čemer dobimo funkcijsko odvisnost °Bx(t). Ta odvisnost predstavlja ekstrakcijsko kinetiko (kinetiko izvlečenja) sladkorja iz vzorčnega tkiva. Končno koncentracijo sladkorja v raztopini označeno kot °Bx_d lahko izmerimo posebej. Teoretično je °Bx_d koncentracija topljencev v raztopini v idealnih pogojih popolnoma permeabiliziranega tkiva in po neskončno dolgem času za difuzijo. V praksi lahko °Bx_d ocenimo enostavno prek meritve koncentracije topljencev (sladkorjev) v čistem sadnem soku oz. soku pridobljenem mehansko iz gomolja. Nato je potrebno dobljeno koncentracijo v soku le sorazmerno povečati ali zmanjšati glede na v poskusih uporabljeno razmerje med masnim deležem tkiva ter raztopine (vode). Ker sta začetna ter končna ali maksimalna koncentracija znani, lahko vpeljemo tako imenovano *normalizirano stopnjo Brix-a* v času t, tj. $B(t)$, ki jo lahko izrazimo in izračunamo po formuli

$$B(t) = \frac{°\mathrm{Bx}(t) - °\mathrm{Bx}_0}{°\mathrm{Bx}_d - °\mathrm{Bx}_0}$$

Normalizirana stopnja Brix-a B se uporablja v vseh delih predstavljenih v tej dizertaciji, ki zadevajo difuzijske poskuse. B se uporablja kot mera za množino topljenca (tj. sladkorja), ki je difundiral iz vzorcev tkiva od časa t_0 do t. Vrednosti B so vedno z intervala $0 \leq B(t) \leq 1$, in mera je brez enot. Računamo jo po zgornji enačbi iz izmerjenih vrednosti z refraktometrom ob znanih °Bx_d ter °Bx_0. Shematična ilustracija difuzijskih poskusov je podana na sliki 1.13.

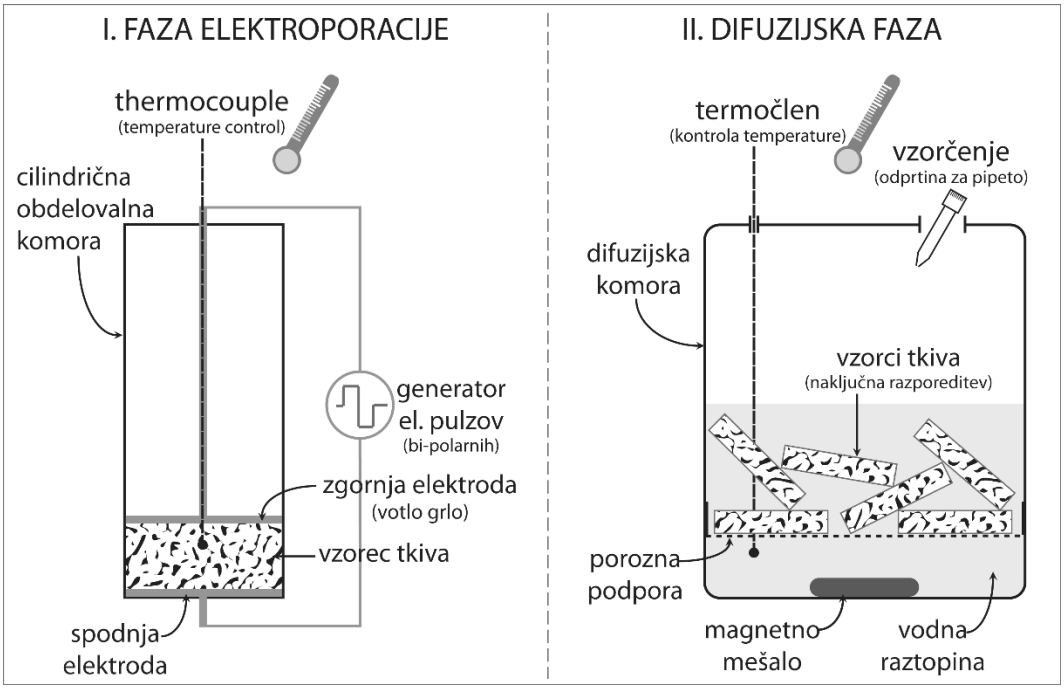

Slika 1.13: Shematična predstavitev konfiguracije difuzijskih poskusov – faza elektroporacije (levo) ter sledeča faza difuzije (desno).

1.2.2.2 Tlačni eksperimenti / Eksperimenti z iztiskanjem

Kot pri poskusih z difuzijo, so bili pri poskusih z iztiskanjem uporabljeni cilindrični vzorci tkiva sladkorne pese ter jabolk premera 25 mm in debeline 5 mm. Vzorci so bili dani med dve vzporedni ploščati elektrodi iz nerjavečega jekla, nakar so bili dovedeni elektroporacijski pulzi glede na tri različne protokole (glej sliko 1.15). Protokol A: Napetost se je med poskusi spreminjala, in je bila 150 V, 200 V, 300 V, 350 V, ali 400 V na elektrodah. Pulzi spreminjajoče polaritete so bili dovedeni v dveh vlakih po 8 pulzov na vlak, s frekvenco ponavljaja pulzov znotraj posameznega vlaka 1 kHz, eno-sekundno pavzo med prvim ter drugim vlakom, širina posameznega pulza v vlaku je bila 100 μs. Protokol B: Napetost je bila ponovno variabilna kot pri Protokoli A, le da so bili tokrat dovedeni unipolarni pulzi dolžine 800 μs vsak, s časovnim zamikom 1 sekunde med obema pulzoma. Protokol C: Napetost je bila variabilna kot v primeru protokolov A in B, dovedenih pa je bilo 8 unipolarnih pulzov dolžine 100 μs vsako sekundo, torej s frekvenco ponavljanja 1 Hz. Ta protokol je znan tudi kot eden od *standardnih protokolov za elektrokemoterapijo*. Celotni čas obdelave t_t (produkt dolžine pulza t_p, števila pulzov n_p ter števila vlakov n_t) izračunan glede na elektroporacijski protokol je bil enak za protokola A in B (t_t = 1.6 ms), medtem ko je 50 % krajši v primeru protokola C (t_t = 0.8 ms) glede na preostala dva protokola. Dovedena električna energija v opisanih poskusih, izračunana s pomočjo meritev toka, je bila med 6 J/kg (minimum dosežen pri sladkorni pesi, protokol C, 150 V) ter 250 J/kg (maksimum dosežen za jabolko, protokol B, 400 V). S stališča dovedene energije ter časa obdelave, so ti protokoli neobičajni za področje predelave ali obdelave hrane z elektroporacijo, kjer so običajnejše energije dovedene tkivu reda nekaj kJ/kg. Maksimalna celotna dovedena energija okrog 0.25 kJ/kg rezultira – v najslabšem primeru, torej ne upoštevaje prehajanje toplote s tkiva na elektrode ali površine obdelovalne komore – v zanemarljivem dvigu temperature vzorca za vsega manj kot 0.1 K. Ta ocena je osnovana na toplotni kapaciteti tkiva jabolka, ter znani maksimalni količini energije. Razlogi za izbiro in implikacije izbire prav teh, »nežnejših« protokolov elektroporacije, so podrobneje navedeni ter komentirani v poglavju Rezultati pri člankih III in IV.

V vseh primerih, ne glede na elektroporacijski protokol, je električni obdelavi sledilo iztiskanje (apliciranje tlaka). Elektroporirani vzorci so bili nemudoma po elektroporaciji vstavljeni v posebej za te na namen izdelano obdelovalno komoro ter izpostavljeni obremenitvi 150 N – približno 580 kPa (jabolko), oziroma 300 N – približno 290 kPa (sladkorna pesa) s pomočjo analizatorja teksture (podrobnosti v podpoglavju 1.2.2.5). Analizator teksture je med obremenitvijo vzorca s konstantno silo beležil premik bata v obdobju ene ure.

Premik bata je enak deformaciji vzorca vzdolž iste osi, v smeri katere na vzorec deluje sila analizatorja teksture. Ta deformacija vzorca je teoretično povezana z izgubo tlaka tekočine v tkivu

(model je prvič predstavljen v članku III). To omogoča primerjavo eksperimentalnih rezultatov z rezultati modela (simulacijami). Shematično predstavlja poskuse z iztiskanjem Slika 1.14.

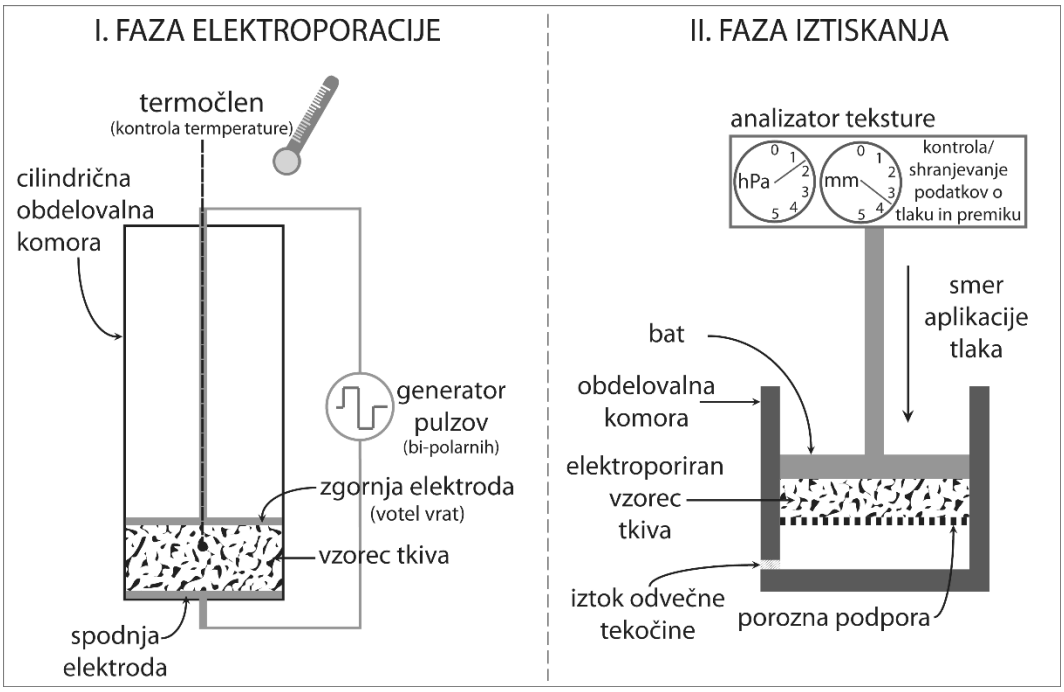

Slika 1.14: Shematična predstavitev konfiguracije poskusov z iztiskanjem – faza elektroporacije (levo), ter sledeča faza iztiskanja soka z analizatorjem teksture (desno).

1.2.2.3 Uporabljeni protokoli obdelave z električnim poljem

Trije različni elektroporacijski protokoli so bili uporabljeni v postopku pridobivanja eksperimentalnih rezultatov, predstavljenih v člankih II-IV (v članku II samo protokol A). Protokoli so specificirani podrobneje v članku IV, podpoglavje 2.3, in ilustrirani s pomočjo shematičnega prikaza na sliki 3.2, ki je bila prvič objavljena v članku IV (slika je reproducirana spodaj kot slika 1.15 v pomoč bralcu). Trije različni protokoli so bili uporabljeni z namenom poskusiti ugotoviti ali obstaja zaznavna razlika med vplivom različnih protokolov elektroporacije na snovanje por v celični membrani ter njihov razvoj, kar bi lahko odražale konsolidacijske krivulje (tj. deformacija vzorca kot funkcija časa) in kar bi posledično lahko modeliral model dvojne poroznosti. Rezultati primerjave so dani v ustreznih poglavjih v članku IV.

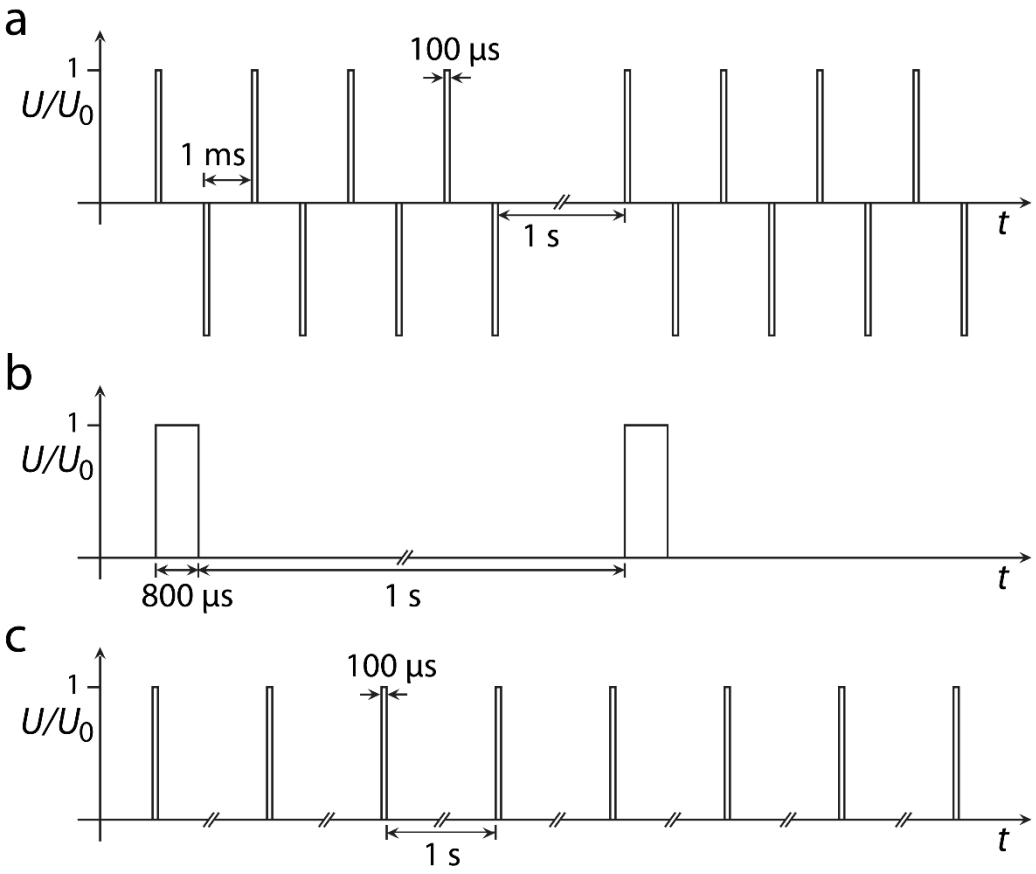

Slika 1.15: Grafična predstavitev treh protokolov elektroporacije: Protokol A (a), Protokol B (b), in Protokol C (c). Dolžine pulzov in razdalje so v razmerjih, razen tam, kjer je to označeno z uporabo znaka '//', ki označuje prelom na osi (znak označuje eno sekundo trajajoč premor med pulzi povsod, kjer je vrisan na os).

1.2.2.4 Generatorji

V poskusih omenjenih ali opisanih v tej dizertaciji so bili uporabljeni trije različni generatorji za dosego elektroporacije v obdelovanem tkivu; dva laboratorijska ter en industrijski / pilotni generator. Kljub temu pa je bil za pridobitev eksperimentalnih rezultatov predstavljenih v člankih II-IV, ki predstavljajo glavnino dela opisanega v tej dizertaciji, uporabljen samo eden od teh generatorjev. Generator, uporabljen za elektroporacijo gomolja sladkorne pese ter sadeža jabolka pri validacijskih eksperimentih za potrditev modela dvojne poroznosti, je bil izdelan oziroma prirejen s strani službe UTC Service Electronique (Elektrotehnični oddelek na Université de Technologie de Compiègne), in je sposoben dovesti maksimalno napetost pulza 400 V ter maksimalni tok 38 A, ter proizvaja izključno bipolarne pulze skoraj kvadratne oblike (čas vzpona/padca napetosti je reda nekaj µs).

Druga dva generatorja sta bila uporabljena v poznejših poskusih na temo izgube turgorja ter elektroosmoze, katere na kratko opisuje sklepno poglavje te dizertacije. Oba generatorja proizvajata izključno le unipolarne pulze, in sta sposobna dovesti pravokotne pulze pri napetostih višjih od 400 V. Ker je bilo pri omenjenih poskusih z izgubo turgorja zaželeno, da napetosti presežejo 400 V (za višje električne poljske jakosti), in pa ker so unipolarni pulzi potrebni za enosmerni električni tok, ki bi naj bil potreben za dosego zaznavnih učinkov elektroosmoze v tkivu, za tovrstne poskuse ni bil primeren prvi generator, ki dovaja bipolarne pulze pri maksimalni napetosti 400 V. Ker dizertacija ne podaja podrobnih informacij ali diskusije o poskusih s turgorjem ali elektroosmotskih poskusih in rezultatih teh poskusov, so specifikacije obeh unipolarnih generatorjev zunaj okvirja pričujoče dizertacije in so zato izpuščene iz tega podpoglavja.

1.2.2.5 Druga oprema

Pri meritvah, ki tvorijo konsolidacijske krivulje (gl. 1.2.2.2), je bil apliciran konstanten tlak na vzorce tkiva, in sicer s pomočjo analizatorja teksture nizke moči in visoke natančnosti proizvajalca Stable Micro Systems, model "TA.XT *plus*". Maksimalna sila, s katero ta analizator teksture lahko pritiska na vzorec je 50 kg (500 N), z ločljivostjo sile 1 N. Analizator teksture je bil uporabljan izključno v načinu delovanja s *konstantno silo* (angl. *constant force*), kar pomeni, da je bila želena sila pritisnjena na vzorce tkiva prek bata analizatorja za želeno časovno obdobje, v tem času pa je analizator meril ter beležil premik bata z visoko natančnostjo 0.001 mm in točnostjo meritve ± 0.001 mm.

Za meritve koncentracije vseh vodotopnih snovi pri poskusih s tkivom gomolja sladkorne pese in sadeža jabolka sta bila uporabljena dva digitalna refraktometra. Rezultati, objavljeni v članku II so bili pridobljeni s pomočjo digitalnega refraktometra ATAGO PR-32α (alfa), medtem ko so bili novi rezultati difuzijskih poskusov, predstavljeni v članku IV, pridobljeni s pomočjo digitalnega refraktometra ATAGO PR-101α (alfa). Oba sta natančna do 0.1 % Brix, in imata merilno točnost 0.1 % Brix. Razlikujeta se merilni območji; merilno območje modela PR-32α je od 0.0 % Brix do 32.0 % Brix, medtem ko je to območje pri modelu PR-101α nekoliko večje, od 0.0 % Brix do 45.0 % Brix. Oba refraktometra sta bila pred uporabo kalibrirana z uporabo destilirane vode ter referenčne raztopine (pripravljene v laboratoriju) saharoze in destilirane vode.

1.2.3 Rezultati in razprava

1.2.3.1 Model dvojne poroznosti

Model dvojne poroznosti, predstavljen v tej dizertaciji, ima analogijo z modeli razvitimi v mehaniki kamnin za vodne razmere v lomljenih kamninah, sedimentih in prsteh, ter je osnovan na osnovnih zakonitostih termodinamike sistemov v neravnovesju. Za pregled literature ter več informacij, glej podpoglavje 2.2.4.2 ter uvodna poglavja v člankih II – IV.

Osnovna ideja modela dvojne poroznosti izhaja iz potrebe po sklopitvi učinkov elektroporacije na celične membrane s transmembranskim difuzijskim fluksom v tkivu ali filtracijsko-konsolidacijskim obnašanjem tkiva pod tlakom (iztiskanje tekočine). Da bi lahko modelirali učinke elektroporacije v modelu transporta snovi v tkivu, je potrebno najprej vpeljati nov nivo kompleksnosti v koncept vzorčnega volumna materiala. Pri tem sledimo teoriji, razviti za pretok tekočine v poroznih materialih kot so prsti ali lomljene kamnine, kjer je koncept multiplih poroznosti dobro raziskan, poznan in uporabljan.

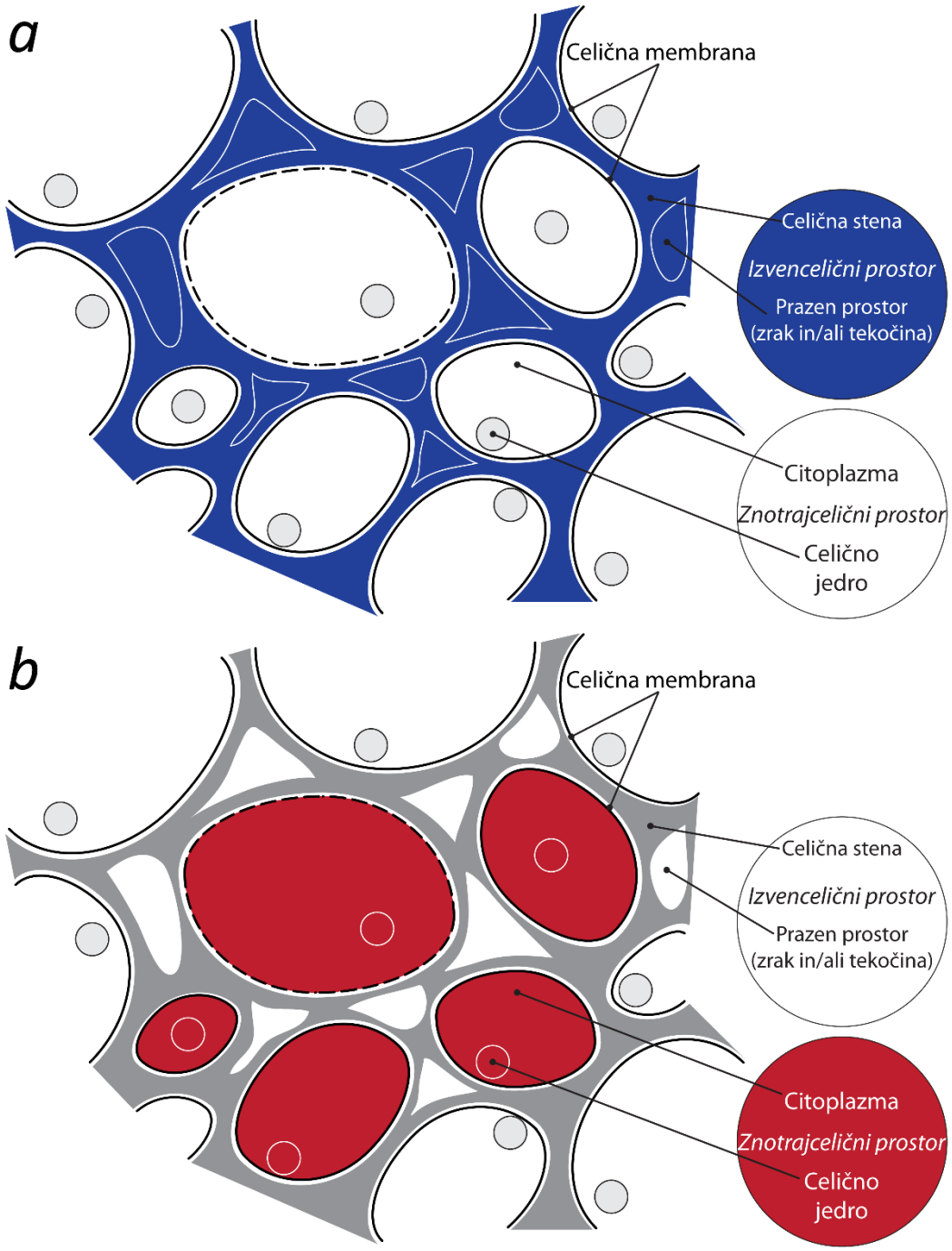

Figure 1.16: Poenostavljen shematični prikaz strukture rastlinskega tkiva z identificiranimi prostori: (a) izvencelični prostor; ter (b) znotrajcelični prostor.

Biološko tkivo je, v primerjavi z mnogo preprostejšimi suspenzijami (topljencev, celic, idr.), morfološko mnogo bolj kompleksen, in ga ni moč predstaviti kot homogen material ali material sestavljen le iz trdnih snovi in tekočine (glej sliko 1.16). Namesto tega ga predstavimo kot sestavljenega iz vsaj dveh prostorov ali faz – znotrajceličnega ter izvenceličnega prostora. Vsak prostor je nato dalje sestavljen iz trdnih snovi ter tekočine, v kateri so topljenci ter netopne »trdne« snovi. Stik med obema prostoroma, ki ju ločuje, je polpropustna celična membrana, katere

propustnost se spreminja zaradi elektroporacije. Ta osnovni koncept je skupen tako difuzijskemu kot konsolidacijskemu problemu, saj zadeva modeliranje inherentne lastnosti ciljne snovne strukture materiala. Osnovni principi pa se prično razlikovati, ko govorimo o transportu snovi. Pristop pri obravnavi transporta snovi je v smislu nastopa veličin pri obravnavi povsem različen, vendar so matematično gledano rešitve lahko povsem ekvivalentne, saj gre za analogne zakonitosti iz termodinamike neravnovesja.

1.2.3.2 Model dvojne poroznosti za difuzijski problem

Osnovne enačbe modela dvojne poroznosti za koncentracijo v izvenceličnem ter znotrajceličnem prostoru so

$$\frac{\partial c_e(z,t)}{\partial t} - D_{s,e}\frac{\partial^2 c_e(z,t)}{\partial z^2} - \frac{1-\varepsilon}{\varepsilon}k\cdot\left[c_i(z,t)-c_e(z,t)\right]=0 \tag{1.2.1}$$

$$\frac{\partial c_i(z,t)}{\partial t} + k\cdot\left[c_i(z,t)-c_e(z,t)\right]=0 \tag{1.2.2}$$

kjer sta c_e in c_i izvencelična ter znotrajcelična koncentracija topljenca, $D_{s,e}$ je intrinzični difuzijski koeficient topljenca vrste s v izvenceličnem prostoru, ε je poroznost tkiva (volumetrični delež izvenceličnega prostora v tkivu, torej $\varepsilon = 1 - F$, kjer je F volumetrični delež celic), in k je koeficient transmembranskega difuzijskega pretoka topljenca, ki je definiran z enačbo 1.2.14.

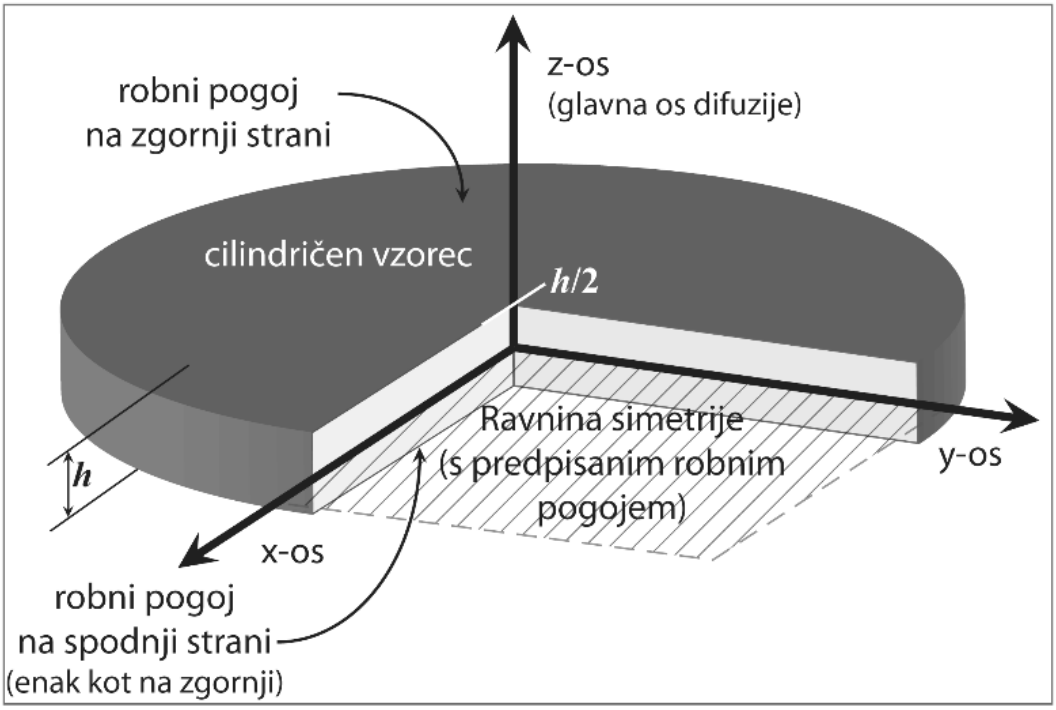

Slika 1.17: Shematična predstavitev vzorca tkiva, kakršen je bil uporabljen v poskusih z difuzijo – geometrija modela, koordinatni sistem in robni pogoji.

Robne pogoje določata narava procesa ter specifična konfiguracija difuzijskega poskusa (glej shematični prikaz difuzijskega eksperimenta kot je prikazan na sliki 1.13). Ker je potrebno modelirati samo eno polovico cilindričnega vzorca tkiva (glej sliko 1.17), so robni pogoji enaki

$$c_e(t)\big|_{z=h/2} = 0 \tag{1.2.3}$$

$$c_i(t)\big|_{z=h/2} = c_{i0}e^{-kt} \tag{1.2.4}$$

$$\left.\frac{\partial c_e(t)}{\partial z}\right|_{z=0} = 0 \tag{1.2.5}$$

$$\left.\frac{\partial c_i(t)}{\partial z}\right|_{z=0} = 0 \tag{1.2.6}$$

Za začetne pogoje je predpostavljena homogena začetna razporeditev koncentracije topljenca čez celoten vzorec tkiva. Začetna koncentracija naj v splošnem ne bodo enake tako v izvenceličnem kot znotrajceličnem prostoru, kar je utemeljena predpostavka za nepoškodovano ali le rahlo elektroporirano tkivo, kjer topljenec lahko ostane v znotrajceličnem prostoru. Konstanti c_{e0} in c_{i0} sta definirani kot

$$c_e(z,0) = c_{e0} \tag{1.2.7}$$

$$c_i(z,0) = c_{i0} \tag{1.2.8}$$

Analitična rešitev sistema parcialnih diferencialnih enačb (en. 1.2.1–1.2.2) za robne ter začetne pogoje (en. 1.2.3–1.2.8) je

$$c_e(z,t) = \frac{4c_{i0}}{\pi}\sum_{n=0}^{\infty}\frac{(-1)^n}{2n+1}\cos(\lambda_n z)\left(C_{n,1}e^{\gamma_{n,1}t}\left(\frac{\gamma_{n,1}}{k}+1\right)+C_{n,2}e^{\gamma_{n,2}t}\left(\frac{\gamma_{n,2}}{k}+1\right)\right), \tag{1.2.9}$$

$$c_i(z,t) = \frac{4c_{i0}}{\pi}\sum_{n=0}^{\infty}\frac{(-1)^n}{2n+1}\cos(\lambda_n z)\left(C_{n,1}e^{\gamma_{n,1}t}+C_{n,2}e^{\gamma_{n,2}t}-e^{-kt}\right)+c_{i0}e^{-kt}, \tag{1.2.10}$$

kjer so

$$C_{n,1} = \frac{\left(\frac{c_{e0}}{c_{i0}}-1\right)k-\gamma_{n,2}}{\gamma_{n,1}-\gamma_{n,2}}, \tag{1.2.11}$$

$$C_{n,2} = \frac{\left(1-\frac{c_{e0}}{c_{i0}}\right)k+\gamma_{n,1}}{\gamma_{n,1}-\gamma_{n,2}}, \tag{1.2.12}$$

in

$$\gamma_{n_{1,2}} = \frac{-\left((\delta+1)k+\lambda_n{}^2 D_{s,e}\right) \pm \sqrt{\left((\delta+1)k+\lambda_n{}^2 D_{s,e}\right)^2 - 4k\lambda_n{}^2 D_{s,e}}}{2}, \tag{1.2.13}$$

kjer je bila zavoljo lažjega zapisa vpeljana nova konstanta $\delta = (1 - \varepsilon)/\varepsilon$, lastne vrednosti λ_n pa so enake $\lambda_n = (2n+1) \cdot \pi/h$.

Koeficient transmembranskega difuzijskega toka (poimenovan tudi koeficient transporta snovi) k je ključni sestavni del modela, ki zajema učinke elektroporacije na celično membrano v relaciji s transmembranskim transportom snovi, in kvalitativno opisuje učinke elektroporacije na propustnost celične membrane. Če je moč celico modelirati kot popolnoma sferičen objekt radija R in debeline membrane d_m, $D_{s,0}$ je difuzijski koeficient za topljenec vrste s v vodi pri dani temperaturi, y_s je koeficient oviranja difuzije v pori, in f_p površinski delež stabilnih por ($f_p = N_p \cdot A_p/A_0$, kjer je N_p število por na celico, A_p je povprečna površina posamezne povprečne pore ter A_0 površina celice enaka $4\pi R^2$), lahko k izrazimo kot

$$k = \frac{3D_{s,0}y_s f_p}{d_m R} \tag{1.2.14}$$

Elektroporacija učinkuje na površinski delež pore f_p, prav tako pa tudi na koeficient oviranja difuzije v pori y_s ob predpostavki, da je radij povprečne stabilne pore odvisen od parametrov elektroporacije. Za več podrobnosti glede koeficientov y_s ter k, glej članek II.

1.2.3.3 Model dvojne poroznosti za filtracijsko-konsolidacijski problem

Z vidika fizike in matematike obstaja očitna analogija med Fickovim zakonom difuzije ter Darcyjevim zakonom, ki narekuje hidrodinamične razmere v poroznih materialih. Model dvojne poroznosti, kot ga podajajo enačbe 1.2.1–1.2.2, je torej moč zapisati tudi za opis filtracijsko-konsolidacijskega obnašanja tkiva pod pritiskom, pri čemer matematično gledano ostaja formulacija enaka z izjemo nekaterih zamenjav, opustitev ali dodanih podrobnosti. Difuzijski koeficient $D_{s,e}$ namreč v primeru konsolidacijskega modela zamenja hidravlična propustnost tkiva k_e deljena z viskoznostjo μ, tj. k_e/μ, in koeficient transporta snovi k podoben proporcionalnostni koeficient α, ponovno tudi ta ulomljen z viskoznostjo, tj. α/μ. Začetna poroznost tkiva ε je že zajeta v koeficientu k_e ter s stisljivostnim modulom $G_{\varepsilon,e}$, ki nista intrinzični, temveč prostorsko-povprečeni veličini na celoten vzorec tkiva, in zato je moč opustiti faktor $(1 - \varepsilon)/\varepsilon$. Zamenjani so tudi koncentracijski gradienti, in sicer z gradienti tlaka tekočine, saj so pri iztiskanju pod tlakom slednji primarno odgovorni za transport snovi, ki je v tem primeru tekočina skupaj z raztopljenimi snovmi. Posledično so koncentracije c_e in c_i nadomeščene s tlaki tekočin p_e in p_i. Kot rezultat sta,

analogno osnovnim enačbam za difuzijski problem (en. 1.2.1 – 1.2.2), pridobljeni sledeči dve osnovni enačbi

$$\frac{1}{G_{\varepsilon,e}}\frac{\partial p_e}{\partial t}-\frac{\partial}{\partial z}\left(\frac{k_e}{\mu}\frac{\partial p_e}{\partial z}\right)-\frac{\alpha}{\mu}\left(p_i-p_e\right)=0 \tag{1.2.15}$$

$$\frac{1}{G_{\varepsilon,i}}\frac{\partial p_i}{\partial t}+\frac{\alpha}{\mu}\left(p_i-p_e\right)=0 \tag{1.2.16}$$

Ti dve enačbi tako kot njun difuzijski analog izhajata iz zakonov o ohranitvi mase. Vendar pa, v nasprotju s koncentracijo topljenca, ki je tako merjena/opazovana veličina kot (preko svojega gradienta) tudi izvorna gonilna sila procesa transporta snovi, je tlak tekočine v konsolidacijskem problemu sicer izvorna sila in promotor transporta, ni pa tudi direktno merjena ali opazovana veličina in ni predmet zakona o ohranitvi mase. Tlak mora zato biti povezan z maso ali volumnom tekočine, ki se ohranjata, in posledično s poroznostjo posameznega prostora v tkivu, kar je v modelu doseženo z vpeljavo tako imenovanih stisljivostnih modulov (angl. *compressibility moduli*). Stisljivostni modul ali njegova obratna vrednost, stisljivost (angl. *bulk modulus*), je običajno definiran kot razmerje med relativno spremembo v volumnu (tako imenovano razmerje prostega volumna – angl. *void ratio*), ki jo povzroči dana sprememba tlaka, in to tlačno spremembo. Če razmerje prostega volumna e označuje razmerje med prostim volumnom (tekočino) ter trdnimi snovmi v znotraj- in izvenceličnem prostoru, sta lahko stisljivostna modula določena iz relacij

$$\frac{\partial e_e}{\partial t}=-\frac{\partial p_e}{\partial t}\cdot\frac{\partial e_e}{\partial p_{e,S}}=\frac{1}{G_e}\frac{\partial p_e}{\partial t} \tag{1.2.17}$$

$$\frac{\partial e_i}{\partial t}=-\frac{\partial p_i}{\partial t}\cdot\frac{\partial e_i}{\partial p_{i,S}}=\frac{1}{G_i}\frac{\partial p_i}{\partial t} \tag{1.2.18}$$

Stisljivostna modula G_e in G_i povezujeta spremembo v razmerju prostega volumna z izgubo tlaka tekočine. V poskusih je merjen premik bata, ki ustvarja v sistemu pritisk, s čimer postane poznana deformacija vzorca tkiva, ki je tesneje povezana s poroznostjo (razmerje med prostim volumnom ter celotnim volumnom tkiva) kot pa z razmerjem prostega volumna, ki podaja, kot že rečeno, razmerje med volumnom tekočine in volumnom trdnih snovi. Zato so stisljivostni moduli ponovno definirani prek povprečne poroznosti obeh prostorov, tako da velja

$$\bar{G}_{\varepsilon,e}=G_e\left(1+\bar{e}_e\right)^2 \tag{1.2.19}$$

$$\bar{G}_{\varepsilon,i}=G_i\left(1+\bar{e}_i\right)^2 \tag{1.2.20}$$

Povsod, razen v enačbah 1.2.19–1.2.20, je notacija, ki označuje povprečne vrednosti izpuščena, čeprav implicitno vsebovana. Ta definicija omogoča enostavno pridobitev začetnih ocen za

stisljivostne module na podlagi končne deformacije tkiva, ki je dobljena eksperimentalno. Vendar gre pri tem za kompromis. Povprečenje razmerja prostega volumna *e*, ki je v splošnem tako prostorska kot časovna funkcija, ki pa se pri poenostavitvi smatra za konstanto, močno zoži splošno uporabnost modela. Tako poenostavljen je namreč veljaven za točno določen segment v parametričnem prostoru, ki zahteva, da so premiki bata majhni v primerjavi z debelino celotnega vzorca tkiva, torej je model veljaven za majhne deformacije. Ta pogoj je izpolnjen samo, če je tkivo relativno nepoškodovano s strani dovedene obdelave (tj. ne intenzivno elektroporirano), kar zahteva pozornost pri interpretaciji rezultatov. Bolj splošen pristop, ki ne vključuje tovrstnih poenostavitev je mnogo bolj matematično zahteven ter neprimeren za analitično obravnavo.

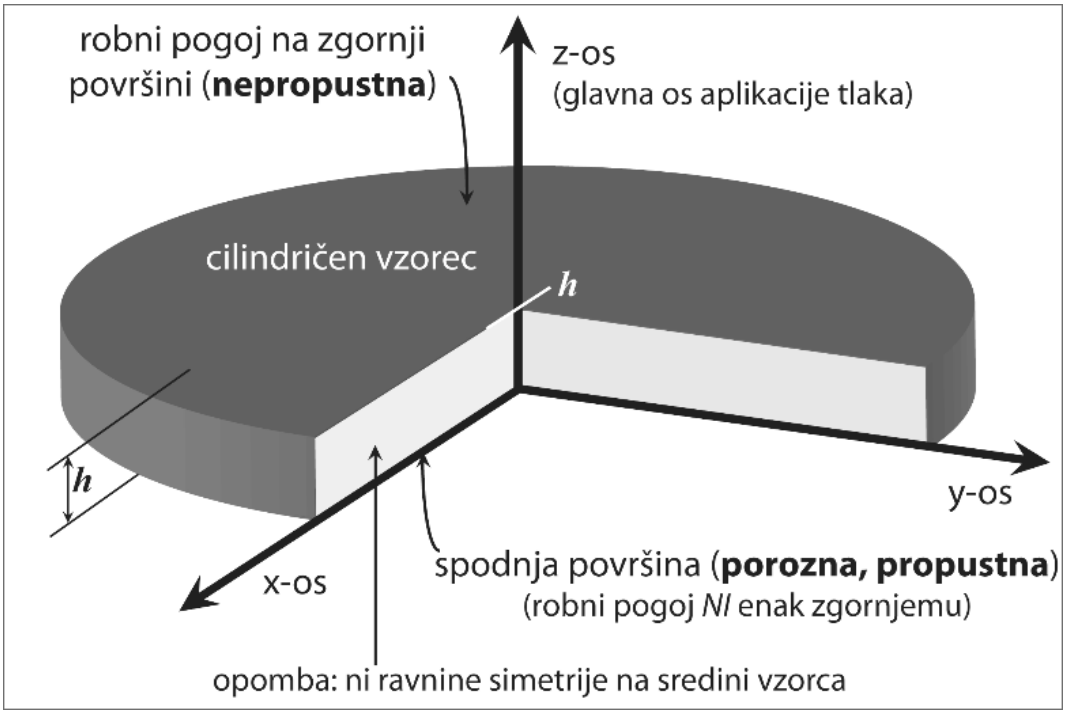

Slika 1.18: Shematična predstavitev vzorca tkiva, kakršen je bil uporabljen v poskusih z iztiskanjem – geometrija modela, koordinatni sistem in robni pogoji.

Da bi bilo moč najti rešitev sistema enačb 1.2.15–1.2.16, so potrebni tudi primerni robni ter začetni pogoji. Začetne pogoje je moč ponovno zapisati glede na enačbi 1.2.7–1.2.8 s preprosto zamenjavo koncentracij s tlakom tekočine, kar da

$$p_e(z,0) = p_{e0} \tag{1.2.21}$$

$$p_i(z,0) = p_{i0} \tag{1.2.22}$$

Po drugi strani pa so pri robnih pogojih razlike. Pri iztiskanju v konfiguraciji kakršno prikazuje slika 1.14 ni ravnine simetrije na sredini vzorca (glej sliko 1.18). Namesto centralne simetrije je v

tem primeru popolna zapora za pretok tekočine na kontaktu med batom in vzorcem, kar za robni pogoj pomeni, da je

$$\left.\frac{\partial p_e}{\partial z}\right|_{z=h} = \left.\frac{\partial p_i}{\partial z}\right|_{z=h} = 0\,, \tag{1.2.23}$$

medtem ko tekočina na spodnji kontaktni površini prosto zapušča vzorec tkiva čez zunajcelični prostor in je tukaj njen tlak enak nič, torej

$$p_e\big|_{z=0} = 0 \tag{1.2.24}$$

medtem ko izračun poteka znotrajceličnega tlaka tekočine za ta robni pogoj sledi enaki logiki kot pri difuzijskem problemu, kar da

$$p_i\big|_{z=0} = p_{i0}e^{-\frac{\alpha G_{\varepsilon,i}}{\mu}t} \tag{1.2.25}$$

Rešitev en. 1.2.15–1.2.16 z začetnimi ter robnimi pogoji (en. 1.2.21–1.2.25) je povsem analogna rešitvi difuzijskega problema, z edino razliko, da sinus v Fourierjevi vrsti zamenja kosinus, prav tako pa se zaradi robnih pogojev rahlo spremenijo tudi lastne vrednosti, in končna analitična rešitev je

$$p_e(z,t) = \frac{4p_{i0}}{\pi}\sum_{n=0}^{\infty}\frac{1}{2n+1}\left(\left(\gamma_{n,1}\tau+1\right)C_1e^{\gamma_{n,1}t} + \left(\gamma_{n,2}\tau+1\right)C_2e^{\gamma_{n,2}t}\right)\sin\left(\frac{(2n+1)\pi}{2h}z\right) \tag{1.2.26}$$

$$p_i(z,t) = \frac{4p_{i0}}{\pi}\sum_{n=0}^{\infty}\frac{1}{2n+1}\left(C_1e^{\gamma_{n,1}t} + C_2e^{\gamma_{n,2}t} - e^{-\tau^{-1}t}\right)\sin\left(\frac{(2n+1)\pi}{2h}z\right) + p_{i0}e^{-\tau^{-1}t} \tag{1.2.27}$$

kjer so

$$C_1 = \frac{\left(\frac{p_{e0}}{p_{i0}}-1\right)\tau^{-1}-\gamma_{n,2}}{\gamma_{n,1}-\gamma_{n,2}} \tag{1.2.28}$$

$$C_2 = \frac{\left(1-\frac{p_{e0}}{p_{i0}}\right)\tau^{-1}+\gamma_{n,1}}{\gamma_{n,1}-\gamma_{n,2}} \tag{1.2.29}$$

in

$$\gamma_{n_{1,2}} = \frac{-\left(\tau^{-1}\delta+\lambda_n{}^2\nu\right)\pm\sqrt{\left(\tau^{-1}\delta+\lambda_n{}^2\nu\right)^2-4\lambda_n{}^2\nu\tau^{-1}}}{2} \tag{1.2.30}$$

Zavoljo lažjega zapisa, so bile narejene sledeče zamenjave

$$\nu = \frac{k_eG_{\varepsilon,e}}{\mu};\ \tau^{-1} = \frac{\alpha G_{\varepsilon,i}}{\mu};\ \delta = \left(1+\frac{G_{\varepsilon,e}}{G_{\varepsilon,i}}\right) \tag{1.2.31}$$

in lastne vrednosti λ_n so enake $\lambda_n = (2n+1)\cdot\pi/2h$.

Ko sta tlak tekočine v znotraj- in izvenceličnem prostoru znana, je moč uporabiti enačbi 1.2.17–1.2.20 za izračun deformacije vzorca. Po zapisu za brezdimenzijsko deformacijo $s_\varepsilon(t)$, ki je normalizirana na začetno debelino vzorca, je izračun deformacije iz znanih tlakov sledeč

$$s_\varepsilon(t) = \frac{S_\varepsilon(t)}{h} = \frac{1}{G_{\varepsilon,e}} \int_0^1 \int_{p_e(z,t)}^{p_e(z,0)} dp_e \cdot dz + \frac{1}{G_{\varepsilon,i}} \int_0^1 \int_{p_i(z,t)}^{p_i(z,0)} dp_i \cdot dz \tag{1.2.32}$$

Zadnji parameter, ki zahteva obravnavo, je brezdimenzijski faktor α, ki povezuje vpliv elektroporacije na hidravlično propustnost celične membrane. Glede na teorijo, predstavljeno v članku III, velja za sferično celico radija R s površinskim deležem stabilne populacije por f_p, ki jo sestavlja N_p por povprečnega radija r_p, relacija

$$\alpha = \frac{9 f_p r_p^2}{8R^2} \tag{1.2.33}$$

kjer je $k_p = r_p^2/8$ hidravlična propustnost posamezne pore.

1.2.3.4 Validacija modela in demonstracija njegove uporabe

Podpoglavja v Materiali in metode 1.2.2.1 – 1.2.2.3 opisujejo difuzijske in tlačne / konsolidacijske eksperimente, ki so bili izvedeni z namenom testiranja in validacije modela dvojne poroznosti. To poglavje podaja glavne rezultate teh poskusov (izmerjene časovne profile difuzije in konsolidacije – tj. kinetike) in primerjavo meritev s simuliranimi časovnimi poteki, pridobljenimi z modelom dvojne poroznosti. Združeni rezultati so grafično prikazani na sliki 1.19 spodaj in na kratko komentirani. Tu predstavljeni rezultati so bili dobljeni izključno z uporabo elektroporacijskega protokola A, po katerem so bili vzorci tkiva elektroporirani. Bolj poglobljeno diskusijo rezultatov ter interpretacijo, prav tako pa rezultate za druge protokole obdelave, je moč najti v ustreznem poglavju v članku IV.

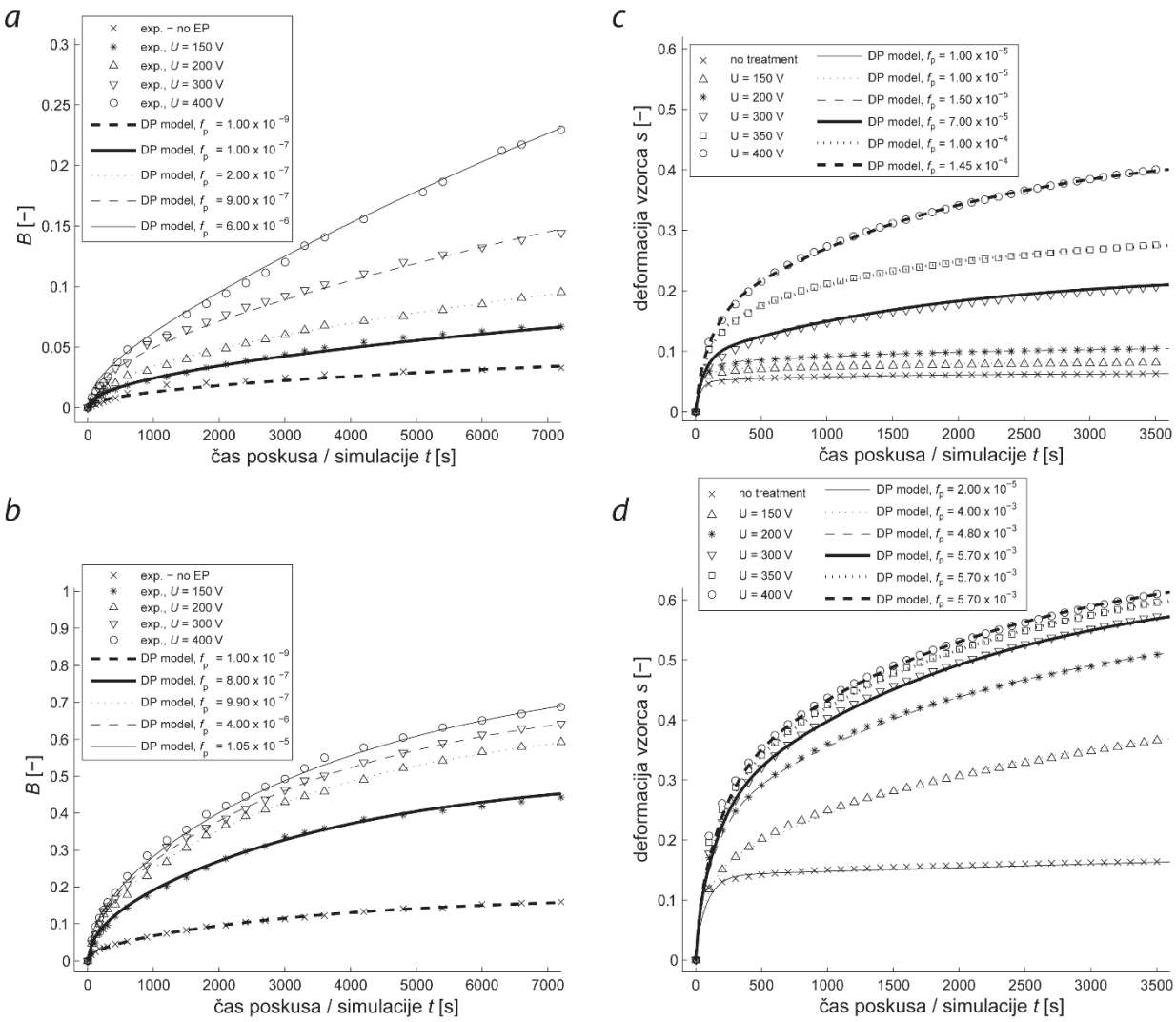

Slika 1.19: Rezultati poskusov z difuzijo v vodni raztopini (a – b) in iztiskanjem/prešanjem vzorcev tkiva (c – d). Poskusi so bili izvedeni v skladu s predstavljeno eksperimentalno metodologijo na vzorcih tkiva sladkorne pese (a, c) in jabolk (b, d). Rezultati predstavljajo kinetiko, pridobljeno eksperimentalno ter prek simulacij na modelu.

Kot prikazuje slika 1.19, je model dvojne poroznosti zmožen modelirati eksperimentalno-pridobljene podatke z visoko natančnostjo. Glede na raznolik in širok spekter možnih odzivov tkiva na elektroporacijo v povezavi s posledičnim transportom snovi, je moč parametre modela ustrezno prilagoditi, da je doseženo dobro ujemanje med simulacijo in eksperimenti. Na tem mestu je glede na vrednosti parametrov, ki so rezultat optimizacije modela, da dobro modelira eksperimentalne podatke, potrebnega nekaj komentarja. Vrednosti parametrov namreč indicirajo, da delež površine por f_p ni edini pomembni parameter, ki odraža elektroporacijo, temveč morajo tudi nekateri drugi parametri nujno variirati, da bi bilo doseženo dobro ujemanje med modelom in eksperimentom. To je potrebno razložiti v okviru teorije elektroporacije, ali pa mora biti model še izboljšan ter njegova občutljivost ocenjena neodvisno od drugih parametrov za vsak posamezen

parameter. Prav tako bi bilo zaželeno oziroma potrebno zmanjšati število prostostnih stopenj modela, ki jih vnašajo številni parametri modela, ki vplivajo na rezultate simulacije istosmiselno, tj. izkazujejo istosmiseln vpliv na končni rezultat. Bolj podrobna analiza omenjene problematike je predstavljena v poglavju »Results and discussion« v članku IV, in vključuje bolj rigorozno kritiko modela, njegovih prednosti ter slabosti.

Sledeča slika 1.20 ilustrira poglavitno in temeljno idejo modela dvojne poroznosti. Prikazana je na tem mestu skupaj z rezultati (slika 1.19) zato, ker podaja tlačne profile tekočine v znotraj- in zunajceličnem prostoru. Ti profili so bili integrirani (glej npr. en. 1.2.32) v postopku izračuna simuliranih kinetik iztiska tekočine, kot jih podaja slika 1.19 (c – d). Ta slika jasno prikazuje učinek zakasnjenega padca tlaka tekočine (ali koncentracije pri analognem problemu difuzije) v znotrajceličnem prostoru glede na zunajceličnega, do katerega pride zaradi nižje propustnosti membrane v primerjavi s propustnostjo zunajceličnega prostora.

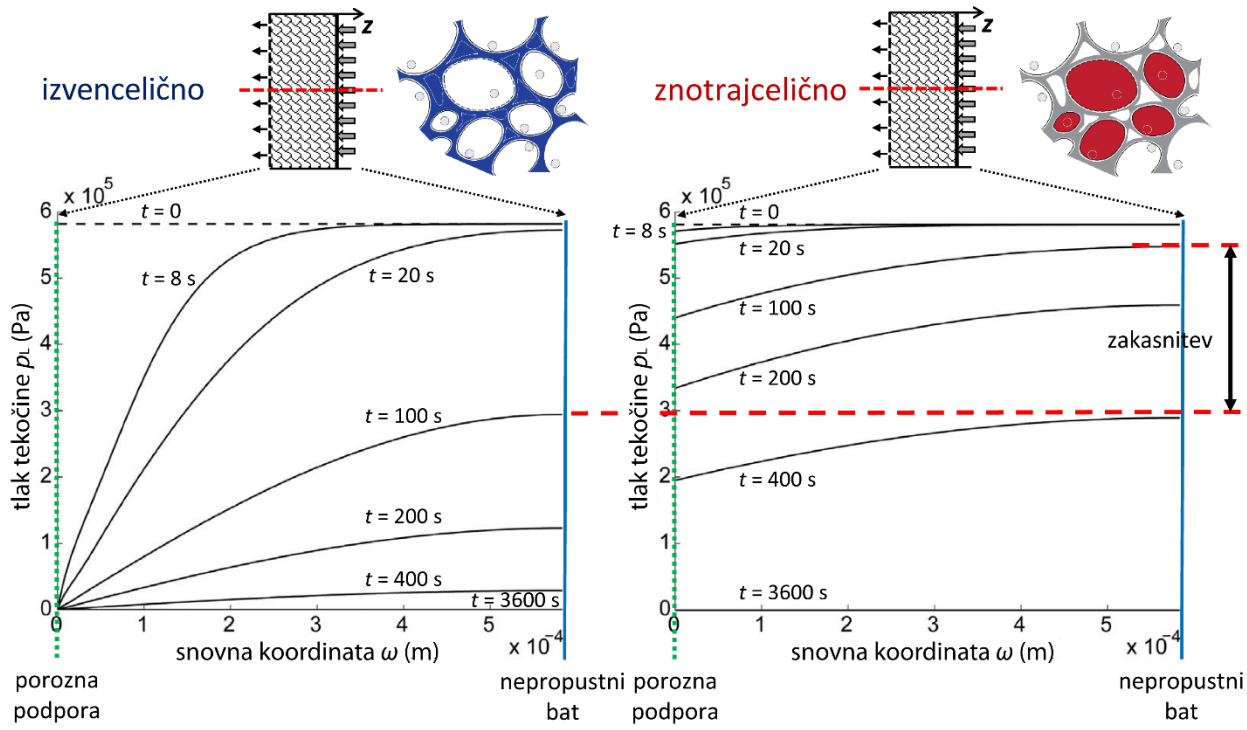

Slika 1.20: Profili tlaka vzdolž prečnega prereza vzorca tkiva za različne trenutke tekom simuliranega poskusa z iztiskanjem. Ker so bili ti profili pridobljeni s pomočjo nadgrajenega, kompleksnejšega ter numerično rešljivega (ter rešenega) modela dvojne poroznosti za opis filtracijsko-konsolidacijskih lastnosti elektroporiranega tkiva, je na abscisi navedena snovna koordinata ω namesto realne fizične koordinate z, ki sicer odraža dejanske dimenzije vzorca. Pretvorba prostorske koordinate z v snovno koordinato ω sicer ni opisana v tej dizertaciji (znanstveni članek v pripravi).

1.2.3.5 Toplotne razmere v tkivu – analiza z modelom dvojne poroznosti in relacija med distribucijo temperature v tkivu ter transportom snovi

S pomočjo analogije med Fickovim zakonom difuzije ter Darcyjevim zakonom o pretoku tekočine, je bil model dvojne poroznosti za difuzijski problem preveden in prilagojen za uporabo pri proučevanju filtracijsko-konsolidacijskega obnašanja elektroporiranega tkiva med iztiskanjem s pomočjo zunanje apliciranega tlaka (primerjaj teorijo v članku II ter članku III, ali pa glej članek IV). Prek fizikalno in matematično enake analogije zakonov s Fourierjevim zakonom prenosa toplote s kondukcijo (angl. *thermal conduction*), ter upoštevaje osnovne zakonitosti iz termodinamike neravnovesnih stanj, lahko postuliramo, da je moč model dvojne poroznosti zapisati tudi za opis toplotnih razmer v bioloških tkivih, kar bi moralo v principu veljati če je tkivo elektroporirano ali ne.

Enačbe toplotnega modela za primer toplotnega fluksa vzdolž ene glave osi prevajanja toplote, se za izven- ter znotrajcelični prostor glasijo

$$\frac{\partial T_e}{\partial t} - \frac{k_e}{\rho c_p}\frac{\partial^2 T_e}{\partial z^2} - \frac{f_v h_v}{\rho c_p}\left(T_i - T_e\right) = 0 \tag{1.2.34}$$

$$\frac{\partial T_i}{\partial t} - \frac{k_i}{\rho c_p}\frac{\partial^2 T_i}{\partial z^2} + \frac{h_v}{\rho c_p}\left(T_i - T_e\right) = 0 \tag{1.2.35}$$

V enačbi 1.2.34 nastopa nov parameter, volumsko razmerje f_v; ta multiplikativni parameter omogoča upoštevanje prostorskega (volumskega) deleža celic v celotnem volumnu tkiva in je enak $F/(1–F)$. Ostale veličine so sledeče: T_e in T_i sta temperaturi v izven- in znotrajceličnem prostoru [K]; k_e in k_i sta izven- ter znotrajcelični toplotni prevodnosti [W/(m.K)]; z je prostorska in t časovna koordinata; c_p je specifična toplotna kapaciteta tkiva [J/(kg.K)]; ρ gostota tkiva [kg/m^3]; in h_v volumski koeficient prenosa toplote [W/(m^3.K)]. Koeficient h_v odraža toplotno prevodnost celične membrane in značilne geometrije sistema izmenjave toplote. Na tej točki lahko privzamemo, da je koeficient funkcija tako prostora kot časa v odvisnosti od elektroporacije, pri čemer ohranimo popolno splošnost obravnave problema. Ali takšna prostorsko/časovna odvisnost od elektroporacije obstaja ali ne, pa je potrebno še teoretično oceniti in eksperimentalno preveriti, v kolikor je to mogoče.

Opomba k razliki med enačbama 1.2.35 ali 1.2.34 ter ustrezajočimi enačbami za difuzijski / tlačni problem. Tako pri difuzijskem modelu dvojne poroznosti kot pri modelu dvojne poroznosti za opis filtracijsko-konsolidacijskega obnašanja elektroporiranega tkiva, je vpliv končne znotrajcelična poroznost ter z njo povezanih koncentracijskih ali tlačnih gradientov zanemarjen., kar poenostavi ravnovesno enačbo za znotrajcelični prostor. Ta poenostavitev je osnovana na predpostavki, da je nizka transmembranska propustnost za difuzijo topljenca ali iztok

znotrajcelične tekočine omejujoč dejavnik pri transportu snovi, in je ta propustnost membrane nekaj velikostnih razredov manjša od difuzijske konstante v izvenceličnem prostoru oz. hidravlične prepustnosti izvenceličnega prostora.. Pri toplotnem problemu (gl. en. 1.2.34–1.2.35) pa se toplotne prevodnosti citoplazme, celične membrane ter izvenceličnega prostora bistveno ne razlikujejo. Zato neupoštevanje znotrajceličnega toplotnega toka ne more biti upravičeno, in člen v enačbi, ki opisuje prevajanje toplote prek znotrajceličnega prostora, mora ostati prisoten v enačbi energijskega ravnovesja v znotrajceličnem prostoru (en. 1.2.35), kar znatno zaplete postopek razvoja analitične rešitve za splošen primer, pri katerem je $k_e \neq k_i$. Zato je v pričujočem delu analitična rešitev splošno zastavljenega problema samo orisana v dodatnem podpoglavju k poglavju 5.

Za manj splošen primer, ko velja $k_e = k_i$, je moč najti analitično rešitev za T_e in T_i, ki je enaka

$$T_i(z,t) = \frac{4}{\pi}\left(\frac{f_v T_{i0} + T_{e0}}{f_v + 1} + \frac{T_{i0} - T_{e0}}{f_v + 1} e^{-\beta(1+f_v)t} \right) \sum_{n=0}^{\infty} \frac{(-1)^n}{2n+1} \cos(\lambda_n z) e^{-\lambda_n^2 \alpha t} \tag{1.2.36}$$

$$T_e(z,t) = \frac{4}{\pi}\left(\frac{f_v T_{i0} + T_{e0}}{f_v + 1} - \frac{f_v (T_{i0} - T_{e0})}{f_v + 1} e^{-\beta(1+f_v)t} \right) \sum_{n=0}^{\infty} \frac{(-1)^n}{2n+1} \cos(\lambda_n z) e^{-\lambda_n^2 \alpha t} \tag{1.2.37}$$

in je podana v podpoglavju 5.1.2 poglavja 5, pri čemer je $\alpha = k/\rho c_p$ in $\beta = h_v/\rho c_p$. Simulacija z modelom da, za različne vrednosti parametra h_v (transmembranski prostorninski/volumski koeficient prenosa toplote) in tipično geometrijo problema, kot je že bila uporabljena pri študijah transporta snovi, rezultate podane na sliki 1.21. Ker je $k_e = k_i$, je potrebno v sistem vnesti začetno neravnovesje (perturbacijo), ki je v tem primeru izvedena prek izbire različnih začetnih vrednosti temperature ($T_{e0} \neq T_{i0}$), zato da se razlika med znotraj- in zunajcelično temperaturo sploh pojavi v sistemu. Iz simuliranih rezultatov je razvidno, da mora biti vrednost parametra h_v nekje med 10^4 $Wm^{-3}K^{-1}$ in 10^5 $Wm^{-3}K^{-1}$, da bi začetna razlika v temperaturah povzročila prehoden odziv sistema, ki bi ga bilo moč opazovati tekom časovnega obdobja nekaj sekund.

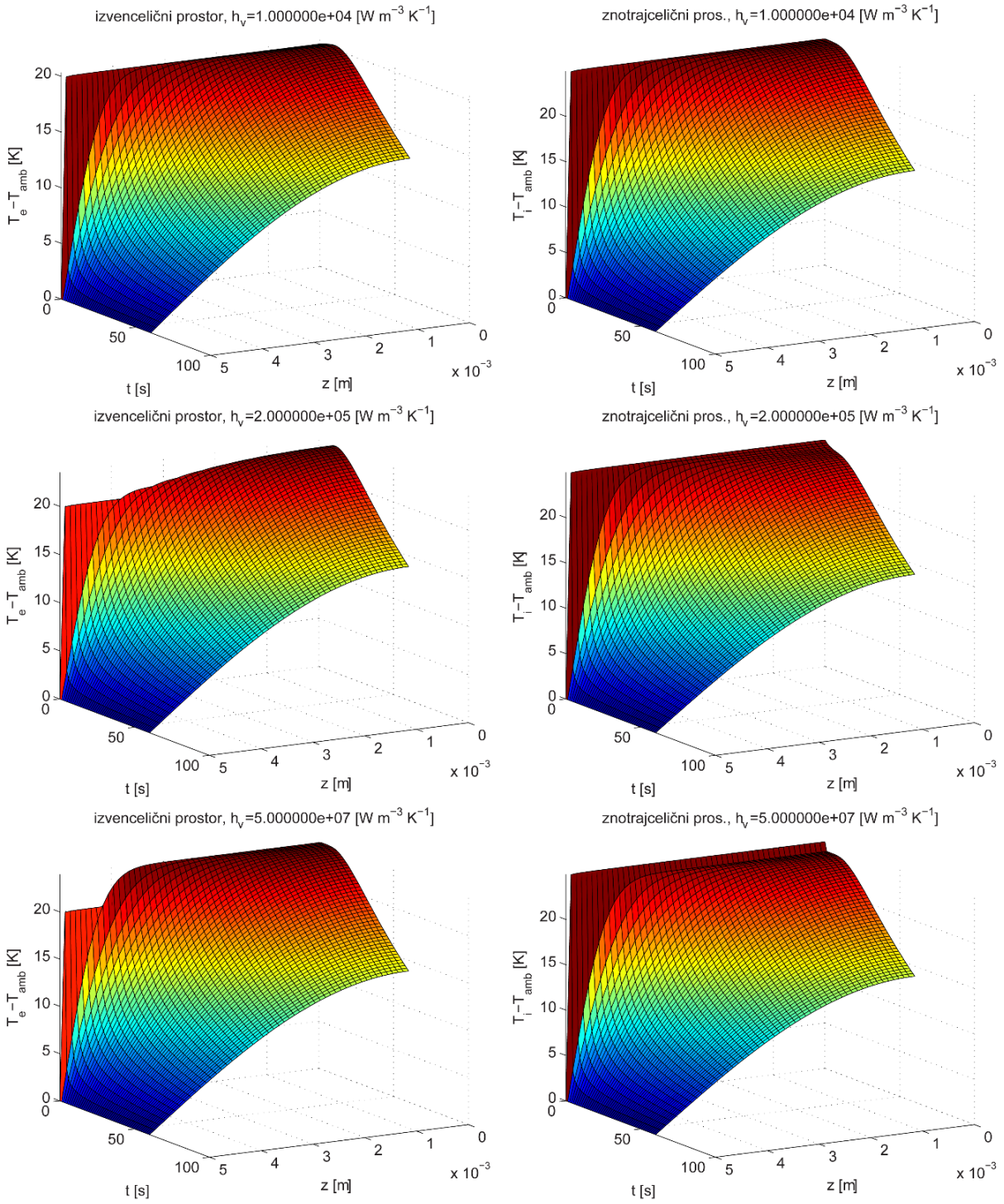

Slika 1.21: Prostorsko-časovni profili intrinzične temperature v znotraj- ter izvenceličnem prostoru za tri različne vrednosti transmembranskega volumskega koeficienta prenosa toplote h_v. Začetni nadtemperaturi nad temperaturo okolice T_{amb} sta bili T_{i0} = 25 °C in T_{e0} = 20 °C v vseh primerih.

Teoretična obravnava toplotnih razmer v tkivu s pomočjo modela dvojne poroznosti se v tem doktorskem delu nadaljuje z razvojem splošnejše numerične rešitve, s katero se lahko modelira situacija, ko je $k_e \neq k_i$. Rezultati (na tem mestu izpuščeni zaradi jedrnatosti) ponovno kažejo na

pomen transmembranskega volumskega koeficienta prenosa toplote (h_v). Če je ta koeficient velik, je izmenjava toplote prek membrane prehitra, in v obdobju opazovanja dolgem nekaj sekund ni zaznavne razlike med znotraj- in zunajcelični temperaturnim profilom. To potrjuje pomen parametra h_v pri odgovoru na vprašanje, ali je pristop z modelom dvojne poroznosti sploh smiseln pri proučevanju toplotnih razmer v tkivu. Da bi dokončno lahko odgovorili na to vprašanje, je v nadaljevanju podana teoretična analiza za realistično oceno vrednosti tega parametra za vzorčni tip rastlinskega tkiva (jabolko). Analiza je predstavljena v podpoglavju 5.1.4.

Glede na zgoraj omenjeno teoretično analizo, je transmembranski volumski koeficient prenosa toplote h_v enak

$$h_v = \frac{3k_i}{2R^2} = \frac{3 \cdot 0.559}{2\left(100 \cdot 10^{-6}\right)^2} = 8.385 \cdot 10^7 \, \frac{\mathrm{W}}{\mathrm{m}^3\mathrm{K}} \tag{1.2.38}$$

kar je realistična ocena upoštevaje končno toplotno prevodnost citoplazme ter izvenceličnega prostora. Vrednost, dobljena z enačbo 1.2.38, je kljub konzervativni realistični oceni (v idealiziranem primeru je vrednost še večja) še vedno večja, kot največja vrednost uporabljena v simulacijah z analitično obliko modela (gl. sliko 1.21). Zaključek, ki ga je moč narediti na podlagi te analize opirajoč se na temperaturne profile s slike 1.21 in vrednosti h_v večje od 10^6 je, da so kakršnikoli transmembranski gradienti temperature, ki bi se pojavili zaradi nehomogenosti v lokalni porazdelitvi električne poljske jakosti ali toka, praktično takoj (tj. v časovnem obdobju krajšem od ene sekunde) uravnovešeni in izničeni zaradi hitrega prenosa toplote prek membrane.

Ta ugotovitev pa ne pomeni, da je model dvojne poroznosti za toplotne razmere po nepotrebnem kompleksen, saj je analiza problema zelo poučna, in vso matematično analizo, predstavljeno v podpoglavju 5.1, je moč uporabiti za nadaljnje izboljšave in razvoj sorodnih oblik modela dvojne poroznosti za primer transporta snovi z difuzijo ali zaradi gradientov tlaka tekočine (iztiskanje). Poleg tega numerična rešitev omogoča, da se znotraj- ter zunajcelični toplotni prevodnosti razlikujeta, kar se še lahko v prihodnje izkaže kot uporabno in relevantno pri proučevanju toplotnih razmer v tkivu, če je le to elektroporirano ali ne, pod pogojem, da se toplotni prevodnosti znatno razlikujeta.

Preostanek poglavja 5 je posvečen proučevanju vpliva temperature na procese transporta snovi prek temperaturno odvisnih parametrov v modelih dvojne poroznosti za problem transporta snovi. Primer takšnih parametrov sta difuzijski koeficient topljenca $D_{s,0}$ ter viskoznost tekočine (soka) μ. Razvite so bile numerične rešitve modelov dvojne poroznosti za transport snovi z difuzijo in iztiskanjem/prešanjem, zato da je moč upoštevati lokalno in časovno porazdelitev temperature v tkivu in torej prostorsko-časovne funkcijske odvisnosti parametrov $D_{s,0}$ ter μ od temperature, torej velja $D_{s,0}(T(z,\ t)) = D_{s,0}(z,\ t)$ in $\eta(T(z,\ t)) = \eta(z,\ t)$ pri simulacijah transporta snovi. Rezultati

parametrične študije so podani na sliki 1.22 in kažejo, da v kolikor temperatura okolice ostane enaka 20 °C, celo znaten prehodni dveh temperature tkiva v začetku simuliranega eksperimenta na začetku difuzijske faze ali faze iztiskanja ne rezultira v znatnem dvigu hitrosti difuzije ali pospešeni konsolidaciji tkiva oz. pospešenem iztiskanju tekočine iz vzorca. Vzrok temu gre pripisati relativno hitremu odvajanju toplotne energije iz tkiva v okoliški medij (raztopina oz. elektrode/bat). Seveda analiza velja za tanke vzorce tkiva debeline 5 mm in stalno temperaturo okolice, kar sta pogoja, veljavna le v posebnih pogojih, kateri so podrobneje opredeljeni v podpoglavju 5.2.2. Potrebno je nadaljnje delo na validaciji modela in predpostavk z eksperimenti, da bi bilo moč bolje osvetliti to problematiko, vendar pa je takšna poglobljena analiza izven obsega tega doktorskega dela.

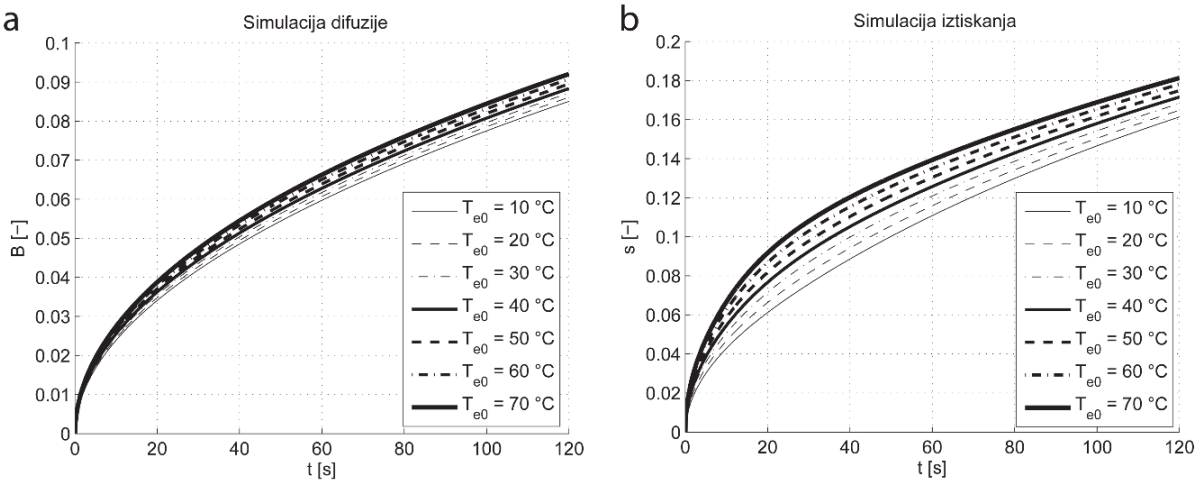

Slika 1.22: Parametrična študija elektroporiranega tkiva z modelom dvojne poroznosti za difuzijski problem in problem iztiskanja/tlačne deformacije tkiva, ki ilustrira vpliv temperaturne odvisnosti nekaterih parametrov v teh modelih (difuzijski koeficient, viskoznost). Samo vrednosti difuzijskega koeficienta in/ali viskoznosti so variirale glede na začetno nadtemperaturo (variabilni parameter) v procesu simulacije za izračun predstavljenih krivulj ekstrakcije/tlačne deformacije.

1.2.4 Prispevki znanosti in zaključek

Glavni izvirni prispevek znanosti te dizertacije je novo-razviti model dvojne poroznosti za proučevanje z elektroporacijo povezanih pojavov transporta snovi v tkivih, oziroma bolj natančno, povezanih s pojavi difuzije topljenca in konsolidacijsko-filtracijskega obnašanja elektroporiranega tkiva pod pritiskom (iztiskanje sokov).

Kot je prikazano v pričujoči dizertaciji (znanstveni članki II – IV), je odlika modela natančna in verna reprodukcija kinetike ekstrakcije snovi iz tkiva s pomočjo difuzije ali mehanskega

tlačnega iztiskanja. Tokom konstrukcije modela je bil en parameter, površinski delež por, identificiran kot najpomembnejši parameter, ki je funkcija elektroporacijskih parametrov – električne poljske jakosti, števila pulzov, in dolžine pulzov. Bila je poiskana analitična metoda za pridobitev ocene pomembnosti parametra, ki je odgovoren za iznos transmembranskega transporta, in sklopljena s transmembranskim difuzijskim tokom v difuzijskem problemu, prav tako pa z transmembranskim tokom tekočine v konsolidacijskem (tlačnem) problemu. V najnovejšem delu, ki je predstavljeno v dizertaciji, je podana študija validacije modela, tokom katere so bili prepoznani tudi drugi pomembni dejavniki (poleg površinskega deleža por na membrani), ki jih je potrebno upoštevati pri modeliranju transporta snovi v elektroporiranem tkivu. Med najpomembnejšimi dejavniki so spremembe v propustnosti in kompresibilnosti tkiva zaradi strukturnih sprememb, povzročenih z elektroporacijo ali apliciranjem tlaka. Ti dodatni vplivni dejavniki odražajo kompleksno naravo učinkov električnih polj na teksturo ter masni transport v elektroporiranem tkivu.

Da bi bilo moč model nadalje nadgraditi in dopolniti, bo prihodnje delo verjetno osredotočeno na ovrednotenje in matematični opis vpliva drugih pomembnih dejavnikov na transport snovi v tkivu (elektroosmoza, relaksacija turgorja, ipd.), da bi se model razvil v bolj splošno različico, katere rešitev bi posedovala odliko zmožnosti predvidevanja (predikcije) na podlagi danih parametrov elektroporacije ter znanih snovno-fizikalnih lastnosti obdelovanega tkiva, katere je moč pridobiti iz obstoječe literature ali oceniti s pomočjo neodvisnih eksperimentalnih metod.

Uvodno delo na področju nadaljnjih raziskav, ki so izven obsega te dizertacije, nakazuje, da mehanizmi kot so izguba turgorja (primerno izključno v tkivih, kjer so prisotni gradienti tlaka – npr. rastlinska tkiva s celično steno in hiperosmotskimi razmerami), in pa elektroosmotski pojavi, lahko igrajo pomembno vlogo v transportu snovi in kličejo po neodvisnem ovrednotenju, ter eventualni vključitvi matematičnega opisa teh pojavov v obstoječ model dvojne poroznosti. Nedavni napredek pri metodah detekcije in zanimive nove možnosti za združevanje modelov razporeditve električne poljske jakosti z modeli evolucije por ter modelom dvojne poroznosti. Rezultirajoč, v visoki meri sklopljen prostorsko-časovni model bi bilo moč dopolniti tudi z Nernst-Stokesovim setom enačb za elektrodifuzijo, ki opisuje učinke elektroosmoze ter elektroforeze, kar bi predstavljalo prepotrebno translacijo znanja in uvida pridobljenega v poskusih na posameznih celicah na mnogo bolj kompleksno raven realističnih bioloških tkiv.

Kljub vsemu napisanemu glede možnosti nadgradnje modela v prihodnje, pa je avtor prepričanja, da je moč model dvojne poroznosti že uspešno uporabiti za ovrednotenje učinkovitosti elektroporacije v odnosu do transporta snovi, da ga je moč uporabiti za optimizacijo parametrov obdelave za predvidevanje rezultatov obdelave pri danih parametrih, ter da bo njegov nadaljnji

razvoj prinesel doprinos k boljšemu razumevanju pojavov, ki so povezani s transportom snovi ter teksturnimi lastnostmi elektroporiranega biološkega materiala.

2 Introduction

2.1 Paper I: A review article “Electroporation in Food Processing and Biorefinery”

The following paper introduces the process of electroporation and presents a review of current applications of this phenomenon and related technologies in the food processing and biorefinery sectors of industry. It also highlights the state of the art and contains a brief overview of some of the challenges encountered and the approaches taken to overcome them that have been recently reported on in literature.

The article was conceived as an introductory work intended for a broad audience of researchers interested in electroporation and its applications in the food processing and biorefinery industries. A more narrowly focused review of literature pertinent to the problems of mass transport in electroporated tissus is given in the section following the review article, i.e. section 2.2 entitled “A literature review on mass transport in electroporated biological tissue”.

J Membrane Biol (2014) 247:1279–1304
DOI 10.1007/s00232-014-9737-x

Electroporation in Food Processing and Biorefinery

Samo Mahnič-Kalamiza · Eugène Vorobiev · Damijan Miklavčič

Received: 5 June 2014 / Accepted: 25 September 2014 / Published online: 7 October 2014

Abstract Electroporation is a method of treatment of plant tissue that due to its nonthermal nature enables preservation of the natural quality, colour and vitamin composition of food products. The range of processes where electroporation was shown to preserve quality, increase extract yield or optimize energy input into the process is overwhelming, though not exhausted; e.g. extraction of valuable compounds and juices, dehydration, cryopreservation, etc. Electroporation is—due to its antimicrobial action—a subject of research as one stage of the pasteurization or sterilization process, as well as a method of plant metabolism stimulation. This paper provides an overview of electroporation as applied to plant materials and electroporation applications in food processing, a quick summary of the basic technical aspects on the topic, and a brief discussion on perspectives for future research and development in the field. The paper is a review in the very broadest sense of the word, written with the purpose of orienting the interested newcomer to the field of electroporation applications in food technology towards the pertinent, highly relevant and more in-depth literature from the respective subdomains of electroporation research.

S. Mahnič-Kalamiza · E. Vorobiev
Centre de Recherches de Royallieu, University of Technology of Compiègne, BP 20529, 60205 Compiègne Cedex, France
e-mail: samo.mahnic@gmail.com; samo.mahnic@utc.fr; samo.mahnic-kalamiza@fe.uni-lj.si

S. Mahnič-Kalamiza · D. Miklavčič (✉)
Laboratory of Biocybernetics, Faculty of Electrical Engineering, University of Ljubljana, Tržaška Cesta 25, 1000 Ljubljana, Slovenia
e-mail: damijan.miklavcic@fe.uni-lj.si

Keywords Electroporation · Pulsed electric fields · Extraction · Microbial inactivation · Biorefinery · Food processing

Introduction

The Electroporation Phenomenon

Electroporation (also termed electropermeabilization or pulsed electric field treatment) is a process in which induced transmembrane potential by means of an externally applied electric field of sufficient strength causes an increase in cell's plasma membrane conductivity and permeability. This increase is attributed to creation of aqueous pathways i.e. pores in the lipid bilayer and has been demonstrated by experiment on lipid bilayers, cells in suspension, monolayers and biological tissues. See e.g. (Krassowska and Filev 2007a; Neu and Neu 2009; Kotnik et al. 2012a) as essential reading in fundamentals of electroporation. Although other terminology is also in use, such as electropermeabilization and PEF treatment, we will continue to refer to the process in the remainder of this paper as electroporation.

Depending on the duration of cell's exposure to the electric field, the local field strength (i.e. the maximum amount of energy deliverable to the membrane via the external electric field), and the rate of membrane recovery, there are three possible outcomes of electric field application. If the field strength and exposure time are insufficient, there is no electroporation, and cell's permeability and viability remain unaffected. See (Kotnik et al. 2012a) for the basic principles of the electroporation phenomena. If the field strength exceeds what is known as reversible threshold and exposure is of sufficient duration, so-called

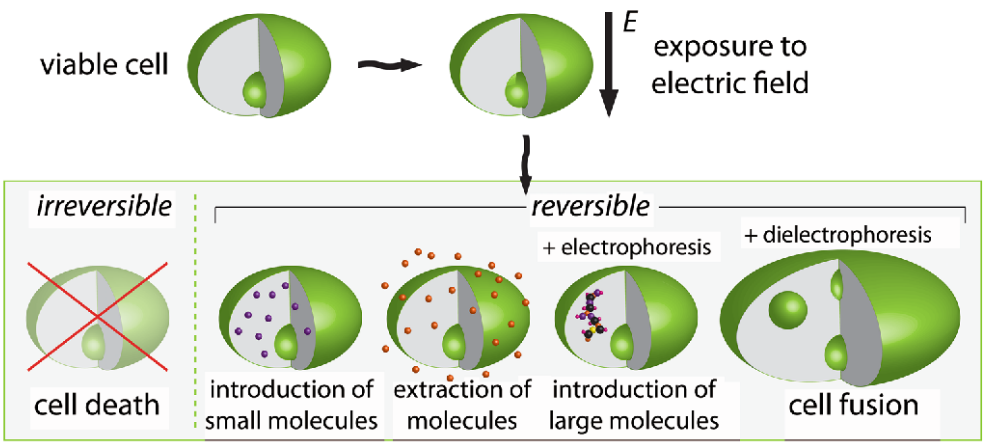

Fig. 1 A schematic representation of cell electroporation with possible outcomes depending on the pulsing protocol (amplitude, shape, duration of pulses) and additional cell manipulation techniques, e.g. (di)electrophoresis. Schema redrawn based on Fig. 16.1 in (Rebersek and Miklavcic 2010)

reversible electroporation occurs (Rols and Teissié 1990; Phoon et al. 2008; Čorović et al. 2012); the membrane is permeabilized and remains in a state of higher permeability for a period of time, but is eventually able to spontaneously return to its original state by means of membrane resealing, a process in which the pores close and the cell restores its normal transmembrane potential. We should point out that this is only possible provided the environmental conditions stay favourable for cell survival and function. If the field strength and amount of delivered energy are too high, however, irreversible electroporation occurs (Davalos et al. 2005; Al-Sakere et al. 2007), resulting in loss of cell homeostasis (and possibly in a complete breakdown of the plasma membrane), effectively killing the cell. Figure 1 is a schematic representation of some of electroporation applications depending on the outcome of the treatment and on whether additional low-voltage electric fields are used in combination with electroporation facilitating other phenomena, such as electrophoresis and dielectrophoresis (Kanduser et al. 2009; Usaj et al. 2010; Hu et al. 2013; Rems et al. 2013).

Both reversible and irreversible electroporation have found their applications in fields such as biomedicine, biotechnology and the environmental sciences (Haberl et al. 2013; Yarmush et al. 2014). In biomedicine, reversible electroporation is used in electrochemotherapy to introduce cytotoxic drugs into tumour cells in a process known as electrochemotherapy (Miklavcic et al. 2012; Mali et al. 2013), for gene and transdermal drug delivery (Gehl 2003; Denet et al. 2004; Pavselj and Miklavcic 2008; Chiarella et al. 2013), cell fusion (Hu et al. 2013; Rems et al. 2013), as well as inserting proteins into the plasma membrane (Raffy et al. 2004), while non-thermal irreversible electroporation (NTIRE—non-thermal irreversible electroporation) is being used as a means of tissue ablation for cancer treatment (Davalos et al. 2005; Garcia et al. 2011).

In food processing, electroporation has shown promising results for extraction of juices and other valuable compounds from plant tissue and microorganisms, such as microalgae (Fincan et al. 2004; Vorobiev and Lebovka 2008; Donsi et al. 2010; Puertolas et al. 2012; Vanthoor-Koopmans et al. 2013), tissue dehydration (Ade-Omowaye et al. 2001; Lebovka et al. 2007b; Shynkaryk et al. 2008; Jaeger et al. 2012) and nonthermal preservation and sterilization by microbial inactivation (Qin et al. 1996; Jayaram 2000; Yeom et al. 2002; Wesierska and Trziszka 2007; Mosqueda-Melgar et al. 2012; Bermudez-Aguirre et al. 2012; Marsellés-Fontanet et al. 2012). Reversible electroporation may also help in creating new methods for cryopreservation of biological tissues (Phoon et al. 2008; Shayanfar et al. 2013), and plant metabolism stimulation (Sabri et al. 1996; Ye et al. 2004; Saw et al. 2012; Dymek et al. 2012; Straessner et al. 2013). Among the environmental applications, we find wastewater treatment (Rieder et al. 2008; Gusbeth et al. 2009; Junfeng et al. 2013) and biofuel production (Vanthoor-Koopmans et al. 2013; Zbinden et al. 2013; Eing et al. 2013; Grimi et al. 2014), both currently under intensive research and development as promising electroporation applications.

This paper focuses on the applications of electroporation in the field of food processing and valuable compounds recovery (biorefinery). We first give a brief overview of potential electroporation applications in the food processing industry, followed by a more detailed review of the current state–of-the-art within the scope of each of the applications. We then present some of the problems encountered and common challenges facing researchers in the field. Thereon, we continue by describing approaches taken when transferring theoretical knowledge to practical implementations and conclude with electroporation in food processing and environmental technologies in light of perspectives for future research and development. For more comprehensive reviews on electroporation as an emerging

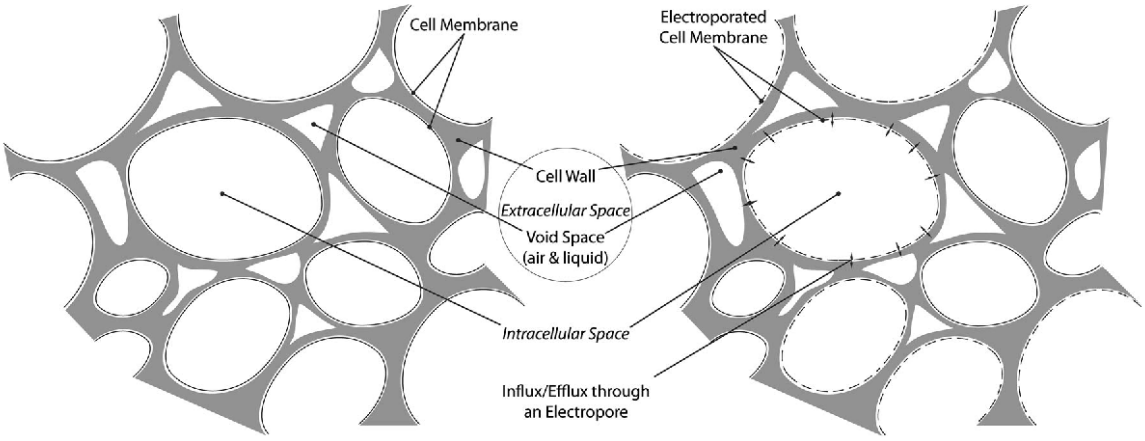

Fig. 2 A schematic representation of plant tissue before (*left*) and after electroporation (*right*). The pores created in the plasma membrane facilitate influx and/or efflux of water and solutes into the cells from the extracellular space or from the cells into the extracellular space. Redrawn based on Fig. 17 in (Halder et al. 2011)

technology in food processing, see e.g. (Vorobiev and Lebovka 2010; Knorr et al. 2011).

Overview of Fundamentals and Applications of Electroporation in Food Processing

As shown by the schematic representation of plant tissue in Fig. 2 (left-hand part) in plant tissue cells are embedded into a structure formed by the extracellular matrix—the cell wall. The cell wall provides support to the plasma membrane, enabling it to withstand enormous pressure differences across the membrane due to turgor and gives shape to the cell. The cell wall is a selective filter that allows water and ions to diffuse freely, but is a limiting factor in diffusion or convective flux of large molecules of more than 20 kDa in size. However, molecules of up to 10 kDa can pass between cells of some higher plants through structures known as plasmodesmata, i.e. specialized cell–cell junctions that extend through the cell wall (Lodish et al. 2008). Note that these junctions are not shown in Fig. 2. Although in intact plant tissue the plasma membrane is the structure providing the largest resistance to intercellular (i.e. cell-to-cell) transport, as well as to transport between intracellular and extracellular space, we must bear in mind also the hindrance and filtering behaviour of the cell wall when considering mass transport in plant tissues (Buttersack and Basler 1991), as opposed to animal tissues where cells are not embedded in a porous extracellular structure akin to the cell wall. The cell wall thus presents an additional complexity and must be considered when studying electroporation and related mass transport phenomena in plants (Janositz and Knorr 2010; Janositz et al. 2011).

Figure 2 (right-hand part) gives a simplified schematic representation of plant tissue that has been electroporated. The plasma membrane has increased permeability due to electroporation (depicted by the dashed line representing the permeabilized membrane) and has lost the ability to selectively control influx and efflux of water and of those solutes that are, depending on their hydrodynamic size, able to pass through the membrane. According to current knowledge, see e.g. (Galindo et al. 2008; Ganeva et al. 2014; Stirke et al. 2014), electroporation may also affect the cell wall and either decrease or increase its permeability (results of recent studies seem to be rather contradictory, and further studies are needed). The effect of electroporation on cell wall appears to depend on cell configuration (cells in suspension, monolayers or tissues), species of organism (yeast, plants) and treatment protocol. However, the increase in permeability and conductivity of electroporation-treated plant tissue is by general consensus attributed predominantly to the increased permeability of the cell membrane. As mentioned in "The Electroporation Phenomenon" section, electroporation may cause the cell membrane to break down completely (irreversible electroporation), in which case the cytosol, parts of disintegrated membrane, and the intracellular material remain trapped in the extracellular matrix.

The described phenomenon of plant cell membrane increased permeability or destruction via electroporation opens up a plethora of interesting possibilities from the food processing point of view. The mass transport facilitated by the disrupted plasma membrane and promoted by concentration gradients (diffusion) or pressure gradients (process is often referred to as *expression*), is of interest in many applications in food industry. In Table 1, we list applications where the interest is predominantly in mass transport enhancement by electroporation, also identifying the primary mechanism or objective of processing improved by electroporation, as well as the required field strength and specific energy consumption per unit mass of the treated material.

Table 1 Electroporation applications to food materials with focus on improving mass transport

Application	Electric field strength[a] (kV/cm)	Energy consumption[a] (kJ/kg)	Primary mechanism of action	Typically studied (model) materials
Juice extraction	0.1–5	1–15	Extraction of intracellular water with solutes	Apple, carrot, potato, sugarbeet
Valuable compounds recovery	0.1–10	0.5–90	Extraction of intracellular compounds e.g. phenols	Apple, carrot, chicory, rapeseed, red beetroot, sugarbeet
Wine quality enhancement	2–10	0.4–10	Release of polyphenols into grape juice	Cabernet sauvignon, Riesling, Aglianico, and other local varieties
Dehydration	0.1–3	0.5–25	Extraction of water	Apple, carrot, mango, pepper, potato, strawberry, green biomass
Biorefinery[b]	1.5–50	10–60	Lipid, protein extraction, release of other extractives	Microalgae, yeast, alfalfa, grapes, rapeseed
Cryopreservation[c]	App. 0.5	n/a	Reversible electroporation, infusion of cryopreservant	Spinach leafs
Meat processing (meat curing)[d]	2–3	10	Infusion of curing agent (e.g. salts)	Pork (ham, sausages, minced meat)

Consolidated from data given in (Donsi et al. 2010), except where otherwise indicated

[a] A range of averages is given to consolidate findings from most of the reviewed studies. See reference(s) for details

[b] See e.g. (Gachovska et al. 2006; Liu et al. 2012, 2013; Grimi et al. 2014)

[c] See e.g. (Phoon et al. 2008)

[d] See e.g. (Toepfl 2006; Toepfl and Heinz 2008)

In case of water or solute introduction into or extraction out of tissue, we are applying the electric treatment via a series of trains of electric pulses of moderate field strength[1] (MEF—moderate electric field), i.e. several 100 V/cm up to 1–2 kV/cm (see Table 1; Puertolas et al. 2012). However, the augmenting effect of electroporation to mass transport has also been observed in applications of low intensity electric fields to the biological material, on the order of less than 100 V/cm (Asavasanti et al. 2010). If the applied electric pulses are of high intensity (HPEF—high pulsed electric field), on the order of about 5–50 kV/cm, they may cause irreversible damage to cells of bacteria, yeasts and moulds, and can therefore be used to preserve material through inactivation and destruction of these microorganisms; the objective in this case is to pasteurize or sterilize the biological liquids: foods or sludge (Álvarez et al. 2006; Mosqueda-Melgar et al. 2008a, 2008b; Guerrero-Beltran et al. 2010; Bermudez-Aguirre et al. 2012). This is often achieved through a combination of electroporation treatment and other traditional techniques of food preservation—e.g. thermal, chemical or pressure based (Martín-Belloso and Sobrino-López 2011)—as many of the harmful microorganisms, such as bacterial spores, prove to be hard to destroy by pulsed electric fields alone (Shin et al. 2010; Bermudez-Aguirre et al. 2012) and are considered as one of the hurdles in pasteurization and sterilization processes. Table 2 summarizes the applications where electroporation is employed primarily with intent to inhibit microbial activity in the treated liquid. Additional information in terms of the required field strengths and energy consumption is also given. By comparing data in Table 2 with data presented in Table 1, note the higher field requirements and specific energy consumption in microbial inactivation applications. To understand why microbial inactivation generally requires significantly higher field strengths and energy consumption in comparison with e.g. extraction applications, it is important to understand the mechanisms of action of electroporation and related phenomena. The process of exposing a viable cell to an external electric field can be divided into several stages (Saulis 2010). First, the transmembrane potential increases with time due to charging of the plasma membrane by the electric field. The amplitude of the transmembrane potential reached is determined by cell size and shape, membrane and medium conductivities (intra and extracellular) and pulse parameters (shape, duration, field strength). A critical transmembrane potential is required in order for pore initiation stage to begin, when a population of small metastable hydrophilic pores appears in the plasma membrane. This population evolves in time, during which the number of pores as well as their sizes change. Following the electric treatment, in the post-treatment stage lasting

[1] Though no formal definition exists, the electric field strengths are often referred to in the literature as per the defined ranges or abbreviations, and these designations do not necessarily represent the actual local electric field strength the cells are exposed to.

Table 2 Electroporation applications with focus on microbial inactivation

Application	Electric field strength[a] (kV/cm)	Energy consumption[a] (kJ/kg)	Reference(s)
Juice preservation	2–30	5–250	(Toepfl 2011)
Solid and semisolid food products preservation[b]	Comparatively higher than in juice preservation	Comparatively higher than in juice preservation	(Gudmundsson and Hafsteinsson 2005)
Enzyme deactivation	10–90	100–2500	(Mañas and Vercet 2006; Buckow et al. 2013)
Sludge disintegration (wastewater treatment)	10–20	50–200	(Toepfl et al. 2006)

Typical field strengths and energy consumption

[a] A range of averages is given to consolidate findings from most of the reviewed studies. See reference(s) for details

[b] The subject of electroporation-assisted microorganism deactivation in solid products lacks reliable studies. It has been found that high field strengths required for inactivation (higher than for juices) have a detrimental effect on texture and structure, rendering the treatment application to these materials for preservation unrealistic (Gudmundsson and Hafsteinsson 2005)

from milliseconds to hours, leakage of intracellular compounds, entrance of substances present in the extracellular space into the cell and ultimately pore resealing or cell death as well as other processes, occur. The result of electroporation treatment, either a viable or a dead cell, is thus determined by conditions and processes that are occurring during all stages of electroporation treatment. These conditions can vary considerably for different applications. Considering an exemplary microorganism—a pathogenic bacterial species for example—as a typical prokaryotic organism only several micrometres in length, the induced transmembrane voltage is calculated to be an order of magnitude lower at the same external electric field strength, as compared to a small eukaryotic cell several tens of micrometres in diameter. The presence (and structure) of cell wall should also be considered (Aronsson et al. 2005; Golberg et al. 2012). For a more thorough and in-depth treatment of microbial inactivation from the point of view of electroporation theory, see for instance (Saulis 2010). We also give further references in discussions of pasteurization and sterilization by electroporation, found within "Inactivation and Destruction of Microbial Contaminants, Parameters Influencing the Success of Electroporation Treatment Application and Methods of Evaluating Their Importance, and Pasteurization and Sterilization of Liquid Foods: A New Arms Race?" sections.

In addition to the described enhanced mass transport or membrane destruction and applications based on these effects of electroporation, pulsed electric fields may also be used at low intensities (less than 100 V/cm) for induction of stress response in plant and yeast cells (Ye et al. 2004; Dymek et al. 2012; Straessner et al. 2013). Though a very limited body of research is available in this field of electroporation, we will briefly discuss the subject in the succeeding chapter, in which we examine the state of the art of electroporation research in food processing.

Figure 3 gives a schematic representation of exposure of a biological cell to an external electric field and applications of electroporation in food, biomaterials and wastewater processing.

Electroporation in Food Processing

Extraction of Juices

Juice is the liquid naturally contained in cells of fruits and vegetables and is generally extracted from tissue via application of one or several pre-treatment procedures, followed by pressing or passive diffusion. The pre-treatment processes, such as mechanical, thermal, chemical, enzymatic, etc. (Lebovka et al. 2011), are designed to damage the biological tissue (cells and the extracellular matrix), and are followed by application of pressure, which further facilitates the release of the liquid phase of cell interior by exerting force causing cell membrane breakdown. The pre-treatment may also be followed by suspending tissue in a solvent (e.g. water), thus facilitating extraction via diffusion that occurs due to the concentration gradient which is established as tissue with high concentration of solutes in juice is submerged into the solvent of higher purity (Bouzrara and Vorobiev 2003; Bazhal et al. 2003; Lopez et al. 2009).

For the food industry, optimizations in juice yield, quality and energy consumption have traditionally been at the forefront of interest. Since juices are often consumed for their favourable organoleptic properties and perceived benefits to health, it is highly undesirable that these properties should be lost during the pre-treatment and extraction processes (Puertolas et al. 2012). Enhancing hydraulic pressing efficiency, diffusion rate and increasing the yield in production of fruit and vegetable juices through

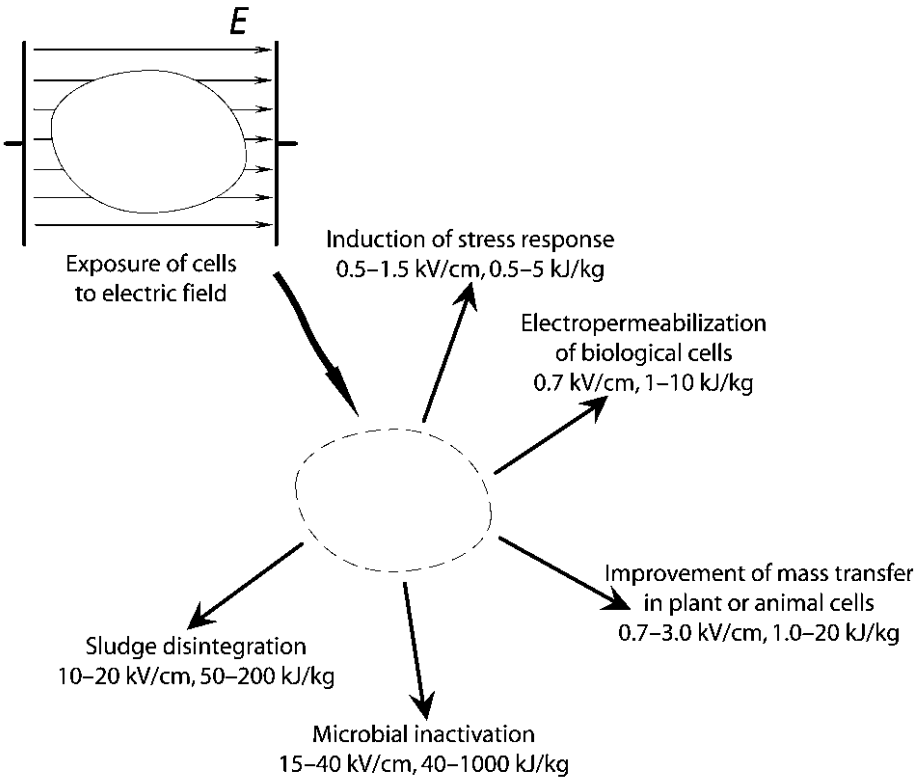

Fig. 3 A schematic representation of the exposure of a biological cell to an external electric field and resulting applications of electroporation in food, biomaterials and wastewater processing. Reproduction based on a figure given in (Toepfl et al. 2005)

membrane electroporation and damage are some of the beneficial effects of applying electroporation to plant tissues as a pre-treatment.

Initial attempts at electroporating plant tissue for improving juice extraction suffered from uncontrolled increase of food temperature and thus product quality deterioration due to high-intensity electric fields applied. In recent years, however, effective electroporation of plant cell membranes has been demonstrated at moderate electric pulse amplitude, avoiding excessive temperature increase and opening possibilities for numerous applications for juice extraction enhancement.

Some of the products for which efficiency of electroporation has been shown are alfalfa, apples, carrots, peppers, potatoes and sugar beet (Gachovska et al. 2006; Donsi et al. 2010; Vorobiev and Lebovka 2010). Electroporation-assisted extraction was shown to give increased juice yields of up to 70 % when applied as the sole pre-treatment technique, improving the quality of juice in terms of purity (as compared to thermal treatment), while also increasing concentration of valuable juice solutes such as proteins, minerals, β-carotene and others up to 60 %. In sugar beet, a 100 % increase in total soluble solids in juice was obtained with electroporation followed by pressing (Mhemdi et al. 2012). Synergistic effects between electroporation and ohmic heating have also been demonstrated, giving juice extraction yields up to 85 % higher as compared to traditional thermal or enzymatic pre-treatments. See e.g. (Vorobiev and Lebovka 2008, 2010; Puertolas et al. 2012) for a comprehensive review of the studies in electroporation-assisted juice extraction.

Recovery of Valuable Compounds

Extraction of several valuable metabolites that may be found in plant cells and inside cell organelles such as vacuoles is of great commercial interest. Electroporation in this context has been studied as means to enhance extraction of colourants (pigments), antioxidants (e.g. polyphenols), flavonoids and other secondary metabolites, sugars and lipids (e.g. oils) from plants and microalgae.

According to recent reviews in (Donsi et al. 2010; Vorobiev and Lebovka 2010; Puertolas et al. 2012), it has been demonstrated that applying electroporation treatment prior to extraction enhances the release of chlorophylls, carotenoids, betalains and flavonoids, especially anthocyanins. In a study with microalgae of species *Chlorella vulgaris* for instance, improvement in chlorophyll and carotenoids extraction by 80 and 52 %, respectively, was obtained after application of electric pulses. In a similar study with betanin extraction from red beetroot, 90 % of total red colourant was extracted from electroporated sample, in comparison with less than 5 % from the untreated control. Since these organic compounds are normally sensitive to light, temperature and oxidation, traditional extraction techniques are mild in nature (mild

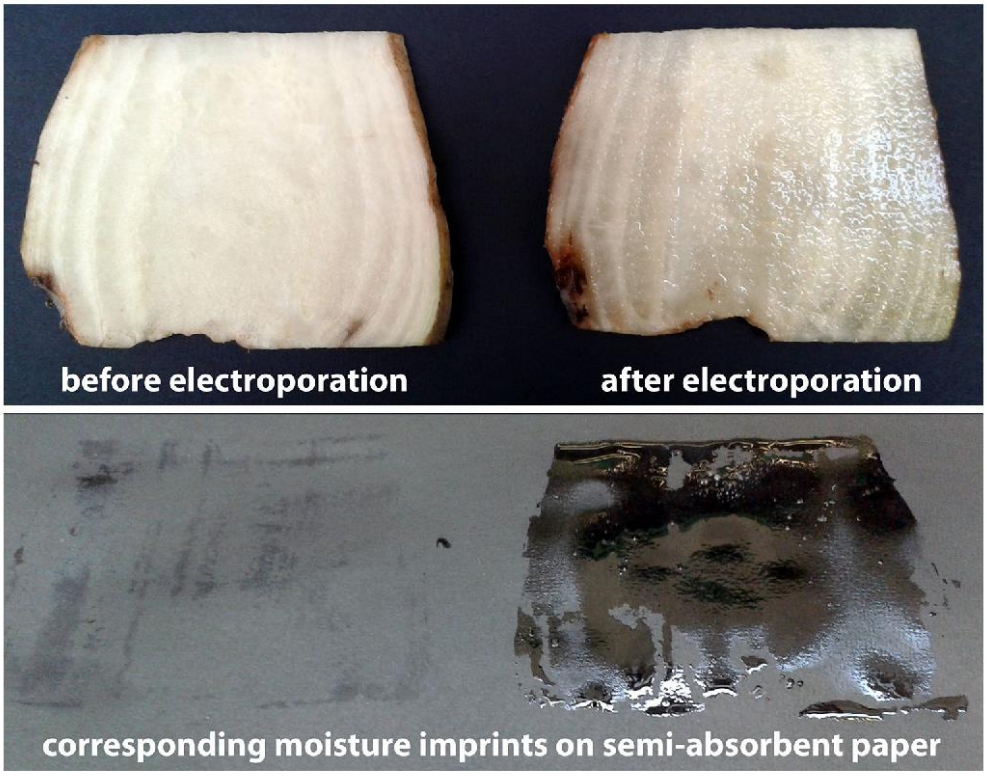

Fig. 4 *Upper half* Two slices of sugar beet before (*left*) and after (*right*) treatment with electroporation. *Lower half* The moisture imprints left on the semi-absorbent paper by the sugar beet slices (shown above), illustrating increased spontaneous (i.e. no pressure or mechanical treatment) release of sugar beet juice from the electroporated sugar beet slice. (Source: authors' own photograph)

thermal or pressing), and their efficiency can be greatly increased through combination with electroporation pretreatment.

In sugar from sugar beet extraction, traditional process involves slicing the roots into cossettes (beet cuts) followed by extraction by diffusion in hot water at 70–75 °C. This unfortunately leads to release of pectin into the juice, which requires complicated and costly purification. The combination of lower temperature and electroporation allows obtaining comparable results in terms of sugar yield, but at a much higher juice purity and hence lower energy and material costs for purification (Bouzrara and Vorobiev 2000; Eshtiaghi and Knorr 2002; Bluhm and Sack 2009). Figure 4 shows a cut through sugar beets before and after treatment by electroporation together with the corresponding moisture imprints left by the samples on a semi-absorbent sheet of coloured paper. The yield of juice obtained by cold pressing of electroporated sugar beet is considerably higher as compared to the control, i.e. non-treated sugar beet tissue. In addition to increased yield of juice, higher transparency of juice indicating higher purity has also been observed (Bluhm and Sack 2009).

Market-driven development of foods with health benefits promotes interest of the food and pharmaceutical industries in extraction of health-protecting compounds such as polyphenols, well known for their antioxidant, anti-inflammatory and anti-tumour properties. Since these bioactive compounds are sensitive to thermal and/or chemical processing, electroporation has been studied in relation with enhancement of polyphenols extraction. At high amounts of energy delivered during electroporation by the electric pulses, some deterioration and degradation of valuable compounds was observed, however, in general, electroporation treatment results in only a marginal reduction of bioactive compounds available for extraction and presents a promising method of increasing food quality with respect to health (Donsi et al. 2010). Recently, there has been an increase in scientific interest in recovery of valuable compounds from grape seeds and skins, waste by-products of the winemaking process, via the application of high-intensity electric fields, and even electric discharges, in order to extract the polyphenols from waste grape material (Boussetta et al. 2011).

Electroporation treatment has also been studied for enhancement of oil extraction from maize, olive, soybeans and rapeseed tissues. According to some studies, to achieve an observable benefit of electroporation application to oil yield, longer, high-energy pulses must be used with total energy delivered reaching as high as 90 kJ/kg. Even at these energies, however, the benefit to yield is only

marginal, while the treatment does, however, seem to improve the composition profile of the extracted oils; an increase in content of phytosterols and isoflavonoids in extracted oil after electroporation has been observed (Guderjan et al. 2005, 2007; Donsi et al. 2010). Other studies, summarized in (Puertolas et al. 2012) indicate an up to 30 % increase in oil yield from maize, and an increment of 55 % in the extraction yield in rapeseed oil production, as well as higher concentrations of tocopherols, polyphenols, antioxidants and phytosterols in oils produced using electroporation.

Electroporation in Winemaking

The potential of electroporation use for improvements in the wine making industry depends strongly on whether the treatment is applied in production of white or red wines. In white wine production, wine is made by fermenting the must obtained from crushing the white grapes. High-quality white wine is obtained from must with a low content of solid particles, low concentration of colour pigments and with reduced pressing time which limits the activity of enzymes that catalyse polyphenol oxidation causing must browning. Electroporation may be used to increase the yield of extracted grape juice of higher purity but with higher polyphenol content as opposed to juice obtained by traditional pressing method. Results of first laboratory-scale studies are promising, but need to be evaluated on the pilot plant scale (Praporscic et al. 2007; Luengo et al. 2012).

In red winemaking, however, wine is produced by fermenting must of red grapes together with grape skins. This step of the process is known as maceration. During maceration, polyphenolic compounds are extracted from grape skin and enhance the quality of the red wine by affecting the colour, flavour and ageing. Additionally, polyphenols are, as mentioned in the preceding section, associated with beneficial effects on health. Recently, a review giving sources to the essential reading material in the field of electroporation-enhanced polyphenol extraction in red winemaking was presented in (Luengo et al. 2012). The results of the studies reviewed indicate an up to 62 % increase in colour intensity, up to 43 % increase in anthocyanins content, and up to 45 % increase in total polyphenols during maceration as compared to the control samples, if the grape skins underwent electroporation prior to the start of the maceration process. When up-scaled from laboratory to a continuous-flow industrial-scale environment, studies show a 48-h decrease in maceration time and a higher content of polyphenols at the end of fermentation as compared to the control. From the sensory point of view, the wine produced by means of electroporation did not exhibit any unusual flavours or changes in taste. These results also come at a low energy cost (0.4–6.7 kJ/kg) and processing time (less than one second). For other recent studies on red grapes, see for instance (Delsart et al. 2014; Cholet et al. 2014).

As briefly mentioned in "Recovery of Valuable Compounds" section, electroporation-assisted extraction of polyphenols is also interesting in light of reuse of waste or by-products of winemaking industry. These by-products represent a vast and cheap source of polyphenols, and several authors have investigated the potential in harvesting these valuable compounds from biological waste. The energy requirements, however, appear to be higher in recovery of compounds from grape by-products as compared to those in applications for increasing polyphenol richness of must during maceration or fermentation (El Darra et al. 2013). The field of harvesting biological waste for valuable compounds is in its early research stages, and much more insight needs to be gained to evaluate its full industrial potential (Luengo et al. 2012).

Dehydration of Plant Material

The intact cell membranes in food materials represent a highly limiting factor (barrier) to water transport during drying of food matrices. Electroporation can, through increasing cell membrane permeability, enhance the mass transport and thus enable faster and more energy-efficient process of tissue dehydration. As shown in the Introduction in Fig. 2, cells and cell walls in plant tissue form the structure of a porous medium. Electroporation of cell membranes can thus greatly increase the porosity of tissue, increasing its hydrodynamic permeability as well as mass and heat transfer rates (Shynkaryk et al. 2008; Donsi et al. 2010; Jaeger et al. 2012; Mahnič-Kalamiza et al. 2014).

Drying of foods in the food industry is mostly accomplished through thermal or hot-air dehydration. Since these processes come at a high energy cost and affect the organoleptic properties of food material, osmotic dehydration has been proposed as an alternative solution. In osmotic dehydration, food material is introduced into a hypertonic solution, causing water to leave the material through osmosis and solute from the solution is introduced by diffusion into the biological tissue. This is, however, a slow process and not without negative effects to properties of dehydrated food (Amami et al. 2006; Puertolas et al. 2012). Several studies have been conducted where conventional thermal drying or osmotic dehydration were combined with electroporation. Recent reviews and summaries of the findings of these studies are found in (Donsi et al. 2010; Vorobiev and Lebovka 2010; Puertolas et al. 2012; Jaeger et al. 2012). In summary, products that were studied and positively responded to electroporation treatment with an increase in mass transport and thus drying rate includes

potatoes, carrots, bell pepper, okra, raisins, red beet, mangoes, strawberries, coconuts and apples. In conventional dehydration, electroporation decreased drying time by up to 30 % while not exceeding the drying temperature of 60 °C. In osmotic dehydration, an up to 30–50 % increase in water release as well as improved dehydration kinetics in samples pre-treated with electroporation were observed. Regarding the final product quality, in conventional thermal dehydration quality is enhanced due to lower drying temperature, while the results appear to be inconclusive for osmotic dehydration due to increased water release causing a proportional decrease in content of metabolites of interest, e.g. vitamin C.

Cryopreservation

Freezing is a fairly widespread method of food preservation. Formation of crystals during freezing and recrystallization after freezing often result in deterioration of frozen food characteristics such as texture and flavour. For this reason, attempts have been made to improve the resistance of raw food products to freezing damage through cryopreservation. This method involves infusing tissue with cryoprotectants, a group of substances that prevent formation of crystals during freezing. Sugars or other cryoprotectants (e.g. sugar alcohols such as mannitol) can be forced into the tissue via osmotic dehydration in hypertonic solution or by vacuum impregnation (Velickova et al. 2013). In intact tissue, however, these processes have limited effect since the intact plasma membrane is poorly permeable. The cryoprotectant is withheld mainly in the extracellular matrix and does not reach the intracellular space, which allows crystals to form during freezing (Phoon et al. 2008). Reversible electroporation, due to its transient increase in membrane permeabilization, enables introduction of ions and molecules into biological cells. This enables the cryoprotectant to efficiently permeate into the cells, protecting them from damage that would otherwise be incurred during freezing. Promising studies have been conducted on laboratory scale in recent years demonstrating the effectiveness of combining cryoprotectant with permeabilizing effects of pulsed electric fields for cryopreservation. Quality (texture, firmness, colour, etc.) of spinach leaves and potato strips was retained by impregnating the material with trehalose (Phoon et al. 2008; Shayanfar et al. 2013) or calcium chloride (Shayanfar et al. 2013).

Inactivation and Destruction of Microbial Contaminants

The most effective method of preserving food quality and assuring microbial safety of raw materials during production and processing is preventing contamination with microorganisms. Unfortunately, it is also the most difficult, if not impossible to achieve in industrial practice. The objective in food industry is thus to attempt and control the activity of microorganisms once the contamination has taken place (Álvarez et al. 2006), by either deactivating them temporarily (heating/cooling/freezing, addition of preservatives, changes in pH, changes in atmospheric composition, etc.) or destroying them completely. The idea of using electricity in food preservation has a long history, and application of pulsed electric fields for microbial inactivation has been studied for over 50 years (Barbosa-Canovas et al. 1997; Toepfl et al. 2007; Sobrino-Lopez and Martin-Belloso 2010; Saulis 2010; Knorr et al. 2011; Morales-de la Pena et al. 2011). During the last couple of decades, the potentials and aspects of electroporation in food preservation have been thoroughly studied, and a variety of microorganisms have effectively been inactivated in various aqueous solutions, e.g. juice, apple cider, milk, yakju, whole egg, pea soup, nutrient broths, model beer, algae extracts and miscellaneous model buffer solutions. In addition, synergistic effects between electroporation and other methods, e.g. nisin, acid treatment, mild heating, low temperature and high pressure, have been demonstrated (Toepfl et al. 2006; Saulis 2010).

The success of electroporation treatment of microorganisms strongly depends on a number of critical factors. Among others, these include processing parameters (e.g. treatment time, electric field strength, pulse number and duration), treatment medium characteristics (e.g. conductivity), as well as microbial characteristics (e.g. shape, size, cell wall structure and composition). The main process parameters that determine efficiency of treatment include electric field strength, shape and duration of the pulses, treatment time, pulse repetition frequency, energy delivered and temperature. Of these, field strength, treatment time and—on these two dependent—amount of energy delivered, are the most critical. Microbial characteristics of greatest importance were shown to be the type of microorganism, cell size and shape, and growth conditions. While yeast and bacterial cells are susceptible to high-energy electroporation treatment, bacterial spores seem to be largely resistant to electrical treatment. Therefore, the focus of studies and efforts in electroporation application for microbial inactivation can be found in pasteurization rather than sterilization (Álvarez et al. 2006).

Electric field strengths required for efficient inactivation of microbes in vegetable juices are within the range of 15–40 kV/cm, and energy requirements fall into the range between 50 and 1,000 kJ/kg (see Fig. 3). Treatment at these parameters causes electroporation of not only microbial, but also animal and plant cells, causing destruction of tissue integrity and structure, which are

highly undesirable in food processing industry. Thus, it appears that the technique is mostly applicable for achieving pasteurization of liquid foods, e.g. preservation of vegetable juice, milk, eggs, etc. (Toepfl et al. 2006).

The main strength of electroporation application in food industry for microbial inactivation seems to be in its ability to affect less and thus better preserve the nutritional and sensory properties of food material as compared to thermal treatment (Odriozola-Serrano et al. 2013). Also important are the observed synergistic effects of electroporation when combined with existing treatments (thermal for instance). There are also several other effects of electroporation that were noticed and might benefit its future widespread use in food industry and its acceptance with the consumers, such as sulphur dioxide and pesticide reduction in treated juices (Marsellés-Fontanet et al. 2012).

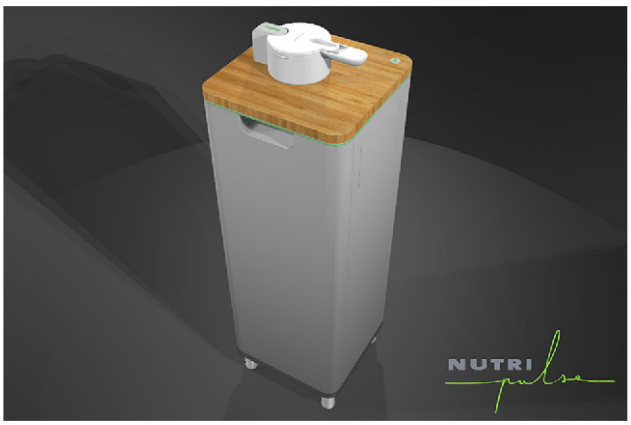

Fig. 5 NutriPulse® by IXL Netherlands B.V., an appliance marketed under claims of "cooking with the help of pulsed electric fields" (IXL Netherlands B.V. 2014)

Other Food Processing Applications and the Effect of Electroporation on Enzymes and Food Constituents

In addition to the applications of electroporation for food processing described in the preceding subsections, several other applications have been proposed, particularly in recent years. Inactivation capability of pulsed electric fields has been extended to attempts at controlling enzyme activity and metabolism activity with applications in food preservation (Mañas and Vercet 2006) and organism growth stimulation (Jaeger et al. 2008; Frey et al. 2011). The required pulse amplitudes for enzyme inactivation are even higher than for microbial inactivation due to higher resistance to treatment of enzymes as compared to microorganisms, and such treatment was not possible until introduction of powerful-enough generators. Since plant and fungi growth stimulation (metabolism control) requires low-energy fields as it is undesirable to negatively influence the organism's viability, pulses on the order of nanoseconds in duration and strengths of up to 50 kV/cm were used in some of the preliminary studies (Frey et al. 2011). Reversible electroporation has only recently gained interest among researchers as a stressing mechanism to promote production (biosynthesis) of metabolites, enabling large amounts of phytochemicals to be produced in bioreactors by stressing selected plant species using low-energy-pulsed electric fields (Jaeger et al. 2008; Mattar et al. 2013).

Several applications in preparation, curing and cooking of meat and vegetable products have also been proposed. While very limited literature exists on the subject, there is growing interest in the potential of electroporation application for meat and fish products. For instance, a weight increase of brine-marinated cod fillets has been observed following treatment by electroporation, and treatment impact on chicken muscle as well as salmon meat has been investigated. Electroporation has also been shown to accelerate fermentation of sausages by improving the availability of intracellular liquid for fermenting cultures (Toepfl et al. 2006). Although no mechanisms of action of electroporation on proteins have yet been proposed (Toepfl et al. 2006) and the subject invites further elucidation, a commercial "cooking" device, whose manufacturer advertises as capable of preparing food with help of electroporation (literally: "pulsed electric fields"), is in the testing phase (see Fig. 5, courtesy of IXL Netherlands B.V. 2014). Additionally, electroporation was shown to enhance peeling of some fruits (e.g. tomato, prune, mango), equalling the ease of skin removal to that of steam treatment, at the energy cost of an applied electroporation treatment of 1–7 kJ/kg (Toepfl 2012). Interesting changes in texture and viscoelastic properties of the treated tissues, presumably caused by the loss of turgor pressure during and following electroporation, were also observed (Grimi et al. 2009; Leong et al. 2014). These changes may facilitate easier handling of produce and more efficient processing (reduction in cutting force and wear of cutting implements).

Biorefinery (integrated biomass conversion processing) of microalgae for food, feed, chemicals and pharmaceuticals is a digression from existing and established attempts in environmental engineering to harvest microalgae for biofuel. Biofuel production, though facilitated by energy-efficient electroporation, is currently not in itself economically feasible (de Boer et al. 2012; Vanthoor-Koopmans et al. 2013). This is due to high energy demands required for mixing, concentrating and finally cracking the tough cell wall of the microalgae to obtain their products. Nevertheless, the application is interesting since harvesting microalgae constituents with high market value might, in combination with optimization of energy use, make

production and harvesting of these microorganisms economically viable. For this application, electroporation is investigated as a mild and effective mechanism of cell disruption, facilitating extraction of unaltered constituents at low energy costs (Vanthoor-Koopmans et al. 2013; Grimi et al. 2014; Flisar et al. 2014).

Valuables produced by microalgae include lipids, pigments, unsaturated fatty acids, proteins and polysaccharides. These compounds are stored intracellularly and a cell disintegration method has to be applied in order to extract this valuable material from within the algae (Goettel et al. 2013; Coustets et al. 2013). Up to now, different cell disruption methods have been investigated, including chemical, mechanical, thermal and enzymatic methods. These methods are, however, normally unable to preserve all of the valuable fractions in the obtained algae extract. This is due to the fact they are mostly focused on harvesting one of the valuable compounds, while inadvertently damaging the rest. Within this context, electroporation presents itself as an interesting mild or gentle extraction technique, preserving all extracted fractions and making them available for further biorefinery. Electroporation treatment thus enables an industrial-scale harvesting of the complete potential of microalgae (Vanthoor-Koopmans et al. 2013). Several studies have demonstrated that although electroporation treatment does not seem to cause a spontaneous increase in release of lipids, it does greatly enhance solvent extraction of lipids (Zbinden et al. 2013; Eing et al. 2013; Goettel et al. 2013). Use of electroporation is therefore envisioned as a part of a multi-stage process, where electric treatment would be used first as a cell disruption method, followed by two stages of biorefinery. During the first stage, high-value water-soluble compounds are extracted and dispatched for further processing. In the second stage, using an environmentally friendly organic solvent such as ethanol, the lipids and other compounds insoluble in water are extracted. This can be done with high efficiency in terms of both yield and energy, as the wet extraction of lipids during second stage of biorefinery does not require the conventional energy-consuming drying of biomass (Eing et al. 2013).

The number of technologies and applications harvesting the power of electroporation applied to biological material seems to be growing at an ever increasing rate. New ideas are constantly being put to the test as industrial processing is studied and optimized in every detail in light of what electroporation-based treatments can offer to the industry and the market. The task of reviewing the massive amount of knowledge accumulated in the field and the numerous applications currently under consideration is a difficult one, as we are continually surprised by the expanding field of electroporation applications in the food industry.

Challenges and Approaches to Problems Solving

This section is an attempt at giving a brief review of some of the more technical aspects of electroporation in food processing. We begin by presenting an established method of assessing changes in biological tissue due to electroporation, and continue with a brief overview of some of the parameters that determine success of electroporation application. Following, this is a short introduction to modelling in electroporation-assisted food processing, and we conclude the section with a glance at industrial equipment design and implementation, a major research domain within the field of electroporation.

Assessing the Degree of Electroporation in Biological Tissues

Commonly used methods for detecting cell membrane permeabilization range from microscopic observations of cells and tissues, often entailing the use of dyes, to macroscopic observations such as measuring release of liquid or the electrical conductivity of the released liquid, analysing the textural properties of treated tissues or measuring the electrical impedance of the tissues. The latter of these methods seems particularly suitable for quick, on-line and in-process evaluation of effects of electroporation in tissues and is the least invasive. A recent addition to this list of conventional methods is based on the nuclear magnetic resonance (NMR) technology, which is, due to its nature, a non-invasive technique of analysis.

Vorobiev and Lebovka (2008) defined the so-called damage degree P as the ratio of damaged (meaning electroporated) cells to the total number of cells in tissue. Studies have shown a possibility of estimating, approximately, the damage or electroporation degree P via measurements of effective diffusion coefficients of known solutes in biological materials (Jemai and Vorobiev 2002). In this case, P is approximated as $P \approx (D - D_\mathrm{i})/(D_\mathrm{d} - D_\mathrm{i})$, where D is the measured effective diffusion coefficient, and indices d and i refer to totally destroyed and intact cellular material, respectively. The effective diffusion coefficient D is measured via diffusion or drying experiments; however, these methods are indirect and invasive. Moreover, the measured effective diffusion coefficient captures not only the effect of membrane electroporation, but also the effect of electroporation of cells to the rate of solute diffusion through extracellular pathways in tissue (hence the coefficient is termed "effective"). As it is not easy to decouple these effects using a single measured parameter, this measure of tissue electroporation must, therefore, be considered as a rough estimate, but is nevertheless particularly useful for comparison of different treatment parameters and species of diffusing solute. A more practical measurement in terms of

invasiveness and speed of assessment is via the more conventionally used conductivity measurements. A *conductivity disintegration index* Z can be defined as $Z = (\sigma - \sigma_i)/(\sigma_d - \sigma_i)$, where σ is the electrical conductivity (the real component of complex admittance, measured at low frequency of about 1–5 kHz) and indices d and i refer to totally destroyed and intact cellular material, respectively (Lebovka et al. 2000). Thus, the defined index gives $Z = 1$ for completely electroporated tissue and $Z = 0$ for intact tissue. Although this method is useful, fast and relatively simple to use, it requires supplementary measurements to determine the conductivity of completely damaged tissue, using either freeze-thawed tissue samples or samples of electroporated tissue using very high electric field strengths and/or treatment times (Lebovka et al. 2007a). The connection between Z and P has not yet been explained theoretically. A phenomenological, experimentally determined empirical Archie's equation giving $Z \approx P^m$ has been proposed, with coefficient m determined experimentally for some food produce, e.g. potatoes, carrots and apples (Lebovka et al. 2002).

A more direct approach of assessing changes caused by electroporation in plant tissues in situ was proposed by Fincan and Dejmek (2002) and involves samples of tissue between electrodes arranged in a setup suitable for microscopy with the ability to record and analyse, post-experiment, the images during or after application of electroporation. In light of difficulties presented by preparing samples of quality suitable for microscopy, onion epidermis tissue presents a clear advantage in ease of sample preparation and was used in the cited study, with neutral red (NR) as the staining agent used to visually detect electropermeabilization of the cell membrane. Direct observation of NR-stained tissue was found useful in supporting previous permeabilization estimates based on conductivity measurements (index Z), as well as allowed for the detection and observation of individual permeabilized cells. Studies with microscopy and ion leakage measurements with electrically damaged plant tissues (particularly onions) and plant cells (e.g. tobacco), have recently experienced a renewal in interest from the scientific community (Asavasanti et al. 2010; Ersus and Barrett 2010; Janositz and Knorr 2010). The findings of these studies highlight and point at the complex behaviour of cells in biological tissues under exposure to electroporative pulses, in particular in relation to the structural inhomogeneity (e.g. variable cell size, shape, etc.) which is affecting the degree of cell membrane permeabilization. Ion leakage, alliin lyase enzyme activity, and textural property measurements were also used to determine critical field strengths required to reversibly and/or irreversibly electroporate cells in onion tissue (Asavasanti et al. 2010). A recent work with tobacco cells with and without cell walls studied under the microscope has shed more light on the impact of cell wall on the efficacy of electroporation of plant cells, evaluating sensitivity of cells to electric pulses with and without cell wall and measuring the resulting changes in cell size (Janositz and Knorr 2010). In a more recent study (Cholet et al. 2014), authors combined histocytological observations with a study of levels of polysaccharide fractions and total amounts of tannins in treated red grape skins to determine that a specific electroporation treatment substantially and profoundly modified the organization and composition of the skin cell walls. In another recent study, authors evaluated the suitability of NMR imaging for assessing cell membrane integrity in electroporated samples (Ersus et al. 2010).

Parameters Influencing the Success of Electroporation Treatment Application and Methods of Evaluating Their Importance

Parameters determining membrane permeabilization and thus the success of application of electroporation in treatment of food materials are related with all aspects of the produce and processing. This means that in addition to the physicochemical and electrical properties of the treated material (medium and cytosol conductivities, membrane composition, presence or absence of an exterior envelope, etc.), also the electrical treatment parameters used during electroporation (pulse shape, pulse amplitude, pulse duration, pulse repetition frequency, etc.), as well as other processing parameters (pH, temperature, etc.), all play an important role and determine the outcome of treatment (Barbosa-Canovas et al. 1997; Raso and Heinz 2010; Puertolas et al. 2012). For a review of the influences of various parameters on success of microbial inactivation by electroporation, see e.g. (Barbosa-Canovas et al. 1997; Álvarez et al. 2006; Sobrino-Lopez and Martin-Belloso 2010; Saulis 2010; Knorr et al. 2011). In the field of juice and valuable compounds extraction from plant materials or osmotic dehydration of vegetable tissues, work has been focused predominantly towards characterizing the damage degree index Z (as a relative measure of treatment performance) in relation to different parameters of the applied electric field (pulse duration, number, amplitude), various species and varieties of treated plants (e.g. potatoes, apples, carrots,…) and the combined effects of electroporation and other treatments, applied either concurrently or in succession. The treatments, often researched for their potential synergistic action with electroporation to enhance diffusion of solutes in tissue or expression of juices, are heat processing (temperature increase), pressure processing (pressing) and chemical processing (addition of enzymes, lime, lye, etc.). For relevant reviews and a listing of pertinent literature, see e.g. (Vorobiev and Lebovka 2008;

Donsi et al. 2010). For a recent study of pulse parameter effects on extraction from microalgae, see (Goettel et al. 2013).

To successfully electropermeabilize the membrane, the field strength experienced by the cell exposed to the electroporating pulses must achieve a certain minimum value, termed the *threshold of electroporation*, *critical field strength* or *reversible electroporation threshold* (Kotnik and Miklavcic 2000; Fincan and Dejmek 2002; Asavasanti et al. 2010), in order to induce the critical transmembrane voltage across the membrane required for the onset of increased permeability. Recent works, already mentioned in the preceding subsection on assessing the degree of electroporation, describe studies performed using onion tissue or tobacco cells as model materials (Asavasanti et al. 2010; Ersus and Barrett 2010; Janositz and Knorr 2010). Their findings indicate that the electroporation threshold or field strength required to reversibly permeabilize the membrane depends on the externally applied electric field strength, and on the method employed to detect permeabilization. The field strength reported as required for permeabilization falls in the range of 50–500 V/cm, with duration of treatment (treatment duration being an integral quantity given as the product of pulse duration and number of pulses) in range of 100–10,000 μs (Puertolas et al. 2012). When using pulses of shorter duration and/or shorter total treatment time (<100 μs), higher electric field strengths are required to permeabilize the membrane (Lopez et al. 2009). This is consistent with observations of Pucihar et al. (Pucihar et al. 2011a). Experiments with onion tissues reported by Asavasanti et al. indicate that higher electric field strengths are required also in order to permeabilize the tonoplast (membrane of the vacuole, an intracellular organelle), the permeabilization of which is necessary to release the solutes of interest, often contained within the cell's organelles (Asavasanti et al. 2010). The importance of cell wall presence has also been evaluated by microscopy (Janositz and Knorr 2010). These results suggest that the well-established descriptions of pulse protocol that are based on reporting only the total specific energy delivered to the material, as established by Knorr and Angersbach (Knorr and Angersbach 1998), might be insufficient to adequately describe the electrical treatment parameters. This consideration seems to be of greater importance in applications where the objective is the achievement of selective or reversible permeabilization of target cells, i.e. in applications of what could be referred to as 'gentle electroporation treatment'. A lot of insight on this subject is available in the biomedical field of electroporation research, which we will now briefly discuss.

A massive body of work done on eukaryotic cells is available in the biomedical domain of electroporation applications, where the primary interests most often lie in either molecule delivery, i.e. drug or gene delivery (Gehl 2003; Denet et al. 2004; Miklavcic et al. 2012; Mali et al. 2013; Chiarella et al. 2013; Zorec et al. 2013; Miklavčič et al. 2014), or in irreversibly permeabilizing cells causing tissue ablation (Davalos et al. 2005; Garcia et al. 2011). We illustrate this by citing two examples.

In a recent study of Pucihar et al., equivalent pulse parameters for achieving electroporation were sought for (Pucihar et al. 2011b). A calcium-sensitive dye was used to detect electroporation, and the relations between the amplitude and duration/number of pulses resulting in the same fraction of electroporated cells were determined. Pulse duration was varied between 150 ns and 100 ms, and number of pulses from 1 to 128. To achieve the same fraction of electroporated cells, the field strength had to be adjusted within range of 100 and 10,000 V/cm. These ranges with respect to pulse number, duration and electric field strength, are sufficient to capture conditions and parameters in many if not all electroporation applications for food processing, the most obvious exception being microbial inactivation, whose primary targets are predominantly prokaryotic cells susceptible only to high-intensity electric fields (Álvarez et al. 2006). The insights gained by the study should thus be applicable to materials and conditions encountered in food processing applications, e.g. in juice and valuable compounds extraction, tissue dehydration, cryopreservation, growth stimulation and others. The findings, if indeed applicable to plant materials, indicate that even when using different values of treatment parameters (pulse duration, pulse length, pulse number), if these values are carefully controlled and adjusted in relation to each other, we can arrive at the same degree of electropermeabilization. However, the relationship between pulse amplitude and pulse duration as well as the relationship between pulse amplitude and number of pulses were found to be highly nonlinear and best described using two-parameter power or three-parameter exponential functions. This implies that even though the energy input during treatment may be very high (for instance in using low-field-strength, long-duration pulses), it might not be as effective in permeabilizing the cells as a treatment protocol of same specific energy input, but using very high-intensity fields of shorter duration.

In a different, modelling and simulation study (Miklavcic and Towhidi 2010), the authors developed a chemical-kinetics and trapezium barrier models, supplemented with a molecular transport model across a permeabilized membrane to study the effects of varying pulse shape parameters (e.g. unipolar rectangular pulses with different rise/fall times, triangular, sinusoidal, unipolar rectangular modulated pulses, etc.). Their results show that rectangular pulses are more effective than sinusoidal or triangular pulses, but more importantly, that the rise and fall times of

unipolar rectangular pulses do not significantly affect the uptake of molecules by the cells. The work is significant because it provides a possible framework for evaluating effects of different pulse shapes and effects related with transitional effects in electric field generation in relation with cross-membrane mass transport, an issue which has not been theoretically studied in the field of electroporation applications for the food processing in much detail.

Additional insight may also be gained by experimenting with molecular dynamics (MD) simulations, whose feasibility has increased due to rapid progression in computing power especially over the last decade. In an MD simulation, a segment of the lipid bilayer representing the membrane of a biological cell is simulated in detail, meaning that physical interaction between its individual constituents (atoms and molecules) is described as an N-body problem using classical Newtonian physics. In addition to simulating occurrence, evolution and disappearance of pores in lipid bilayers induced by mechanical stress (Leontiadou et al. 2004), the influence of an externally superimposed field and the associated electrical stress can be also be accounted for in this manner. Recently, MD simulations on lipid bilayers were performed in order to, in example, evaluate the role of water in pore formation and evolution (Ho et al. 2013b), to examine pore conductance of monovalent salts—note the connection between membrane conductance and tissue electrical conductivity—(Ho et al. 2013a), and to determine electroporation thresholds with respect to the lipid bilayer composition (Polak et al. 2013). Although the segments of the simulated bilayer are (over)simplified and as of yet far from being complete digitized atom-by-atom replicas of living biological membranes, careful interpretation of results reported by the cited and related studies can significantly aid in corroborating or explaining experimentally obtained evidence, observed at the microscopic (macroscopic as compared to the scale of MD simulations) level (Delemotte and Tarek 2012).

Mathematical Modelling of Electroporation-Related Phenomena in Food Processing Assisted by Electroporation

Within the domain of electroporation in food processing, we can identify several directions in the published literature. A typical example would be modelling of a treatment chamber for purposes of thermal monitoring and control, optimizing treatment parameters or energy efficiency. Another purpose is to gain theoretical insight into the process-governing phenomena, but using food products as model materials. A good example of this is a through-pore solute diffusion model—the industrially relevant implications may be hinted at, but its main purpose lies in advancing knowledge in basic principles of phenomena and theoretically evaluating the importance of variations in parameters. These variations may result from either biological variability of material or differences in process or electrical treatment parameters.

With respect to the *method* of model construction, we encounter applications of purely phenomenological and empirically derived models, sometimes transferred to the field due to similarities in process physics from an unrelated scientific or engineering field. As an example, consider the empirical Archie's equation, briefly discussed in "Assessing the Degree of Electroporation in Biological Tissues" section. These models can be very useful, in particular if the purpose of their construction is of an engineering nature (optimization). Their drawback is that they are only valid within the range of parameters for which they were validated and may completely fail outside of this range. Also, their coefficients need to be experimentally determined directly or estimated based on comparable experiments. On the other hand, a model can be constructed using a combination of basic laws of thermodynamics (e.g. conservation of mass, energy, etc.), laws of classical electrodynamics (Maxwell's equations), some phenomenologically derived transport laws (e.g. Darcy's, Fourier's, Fick's, etc.), models of electroporation (the background of most of which are the thermodynamics of lipid bilayers) and if needed, biological laws (e.g. cell survival models). For examples, see works such as (Krassowska and Filev 2007b; Pucihar et al. 2008; Rauh et al. 2010; Golberg and Rubinsky 2010; Kotnik et al. 2010; Li and Lin 2011; Salengke et al. 2012; Kotnik et al. 2012b; Rems et al. 2013; Mahnič-Kalamiza et al. 2014).

These models can reach a high degree of complexity, are usually difficult to validate using experimental methods, and are seemingly not as attractive for use in industrial applications as are empirical models. In the electroporation-assisted food processing domain, these models have, however, gained a foothold in the subject of treatment chamber analysis and design, predominantly in the field of microbial inactivation research. They have yet to appear in problems of valuable compounds and juices extraction and dehydration (on the level of biological tissue) and microbial inactivation (on the level of cells).

As described in the applications review ("Electroporation in Food Processing" section), electroporation is being studied as a method of non-thermal food preservation, i.e. microbial inactivation, either as a single treatment or in combination with other processing techniques (e.g. thermal or high pressure) to achieve pasteurization or sterilization of liquid foods. During treatment, material as a liquid passes through a treatment chamber equipped with electrodes via which pulses are delivered. The flow of fluid can be described as a fluid dynamics flow field, with the

electrodes creating an electric field. The ohmic dissipation of energy within the fluid field, resulting from the application of electric pulses to conductive media, establishes also a thermal field (Joule heating). The challenge with utilization of these treatment chambers is in their optimal design and use of treatment parameters. This is in order to ensure that there are no dielectric breakdowns and under-treatment (electric field highs or lows) or overheating of the material (temperature highs), and that the treatment is efficient in addition to being effective (Rauh et al. 2010; Salengke et al. 2012). Numerical methods and models are used to describe the fluid, electric and thermal fields in the treatment chamber in order to facilitate design and parameter optimization. For a recent review on the coupled modelling approach, see e.g. (Gerlach et al. 2008), as well as individual studies for electric field and temperature distribution (Salengke et al. 2012) and differentiation between the electric and thermal field effects in the continuous-flow treatment chamber (Jaeger et al. 2010). For modelling of high pressure processing (HPP) in combination with electroporation and thermal effects, see for instance works of Rauh et al. (2010).

Saulis (2010) in his review on fundamentals of electroporation applications in food processing, focused predominantly on food pasteurization and sterilization, includes a listing with relevant sources of some of the often used models of the inactivation process by electroporation. As some of the most frequently employed models in order to describe the dependencies of the efficiency of inactivation on the different process variables, he cites the Weibull distribution, logarithmic, sigmoid, polynomial as well as other miscellaneous functions, adapted to approximate descriptions of experimental results. For more engineering perspectives and a more detailed review of models of microbial and enzymatic inactivation, see (Morales-de la Pena et al. 2011).

In the field of electroporation application for enhancing mass transport in treated material (valuable compounds and juices extraction, dehydration, winemaking, etc.), the models concern the effect of applied electroporative pulses on the diffusion rate of solutes, the transport rate of water molecules, or to the hydraulic permeability of cells and tissues if pressing is the chosen mode of intracellular compounds extraction. The mass transport models used in these cases to describe solute diffusion are often simple, analytically derived and based on known solutions of diffusion problems. For a comprehensive review of these models in electroporation-assisted extraction, see (Pataro et al. 2011).

The models used in analysing mass transport phenomena in electroporated biological tissues are based on either analytical solutions, or they are to some degree (or even completely) phenomenological in nature. As an example, see for instance (El-Belghiti et al. 2005) for an approach to a model study of two-stage solute extraction by diffusion, or (Lebovka et al. 2003) for a problem description with juice extraction from treated biological tissue. The phenomenological models of filtration–consolidation found in literature that describe juice extraction, are based on poro-mechanics approaches, found in theory of fractured rocks and soils. Their application to expression from biological material was already proposed by Lanoiselle et al. (1996) and can be found used in e.g. (Grimi et al. 2010). The diffusion models described above are considering material as homogeneous, i.e. not comprising cellular structure. Recently, some new or modified models were proposed (Petryk and Vorobiev 2013); Mahnič-Kalamiza et al. 2014; Mahnič-Kalamiza and Vorobiev 2014), rooted in the theory of porous media, introducing the cell membrane into the mass transport model. This allows the authors to couple the effects of electrical treatment to the cell membrane, thus offering an opportunity to theoretically study mass transport in relation to electroporation parameters. The importance and influence of these parameters have already been studied to a large degree not only in the food processing, but mainly in the biomedical field of electroporation applications. We believe it is necessary, in order to advance insights on the impact of electroporation treatment to mass transport in biological material, to couple a mass transport model with a model of pore evolution, e.g. (Krassowska and Filev 2007a). Furthermore, we should account for the effects of tissue as a packed multicellular structure (Essone Mezeme et al. 2012), material property discontinuities and inhomogeneity (Becker 2012), cell wall (Janositz and Knorr 2010), tissue electrical conductivity (Neal et al. 2012), effect of electrical field thresholds and conductivity changes (Sel et al. 2005; Corovic et al. 2013), pulse duration and number (Pucihar et al. 2011b) and electrokinetic effects such as electrophoresis (Li and Lin 2011; Li et al. 2013) and electroosmosis (Movahed and Li 2012).

Industrial Equipment Design, Implementation and Commercial Applications

An important aspect of an emerging processing technology is its integration and acceptance into the industrial environment. Ever since electroporation was first proposed as an application of relevance to the food industry in the 1960s, the fields of industrial equipment design for applying electroporation to food materials, as well as the implementation of this technology, have experienced interest from the scientific community and also several attempts from the industry to commercialize the process (Toepfl 2012). Historically, the major hurdles in implementation were posed by the poor reliability and performance of pulsed power switches required for continuous

delivery of high amounts of electrical energy and high electric field strengths required for industrial-scale applications. The scaling up from laboratory to industrial-level processing requires a corresponding scale-up from several kW to more than 100 kW in terms of power requirements (Toepfl 2011). The first commercial application in Europe was, therefore, introduced only relatively recently, in 2009, in the form of a juice preservation line (microbial inactivation) with processing capacity of 1,500 l/h. Encouraging results were obtained on an industrial pilot of 4.5 t/h for cider production (Turk et al. 2012a) and with a pilot for grape mash treatment (Sack et al. 2010a). This was followed in 2010 with the first industrial system for processing vegetables with capacity of 50 tons/h (Toepfl 2012). Recently, an industrial pilot for sugar beet processing (sucrose extraction and purification) was setup with the capacity of 10 tons/h (Vidal 2014).

Electroporation systems for food industry typically comprise a pulse power supply and a treatment chamber (Bluhm 2006; Sack et al. 2010b). Up to the last decade of the past century, spark gaps and vacuum tubes were predominantly employed for achieving power switching, but these systems were poorly reliable and of short lifetime. Recently, advances in high-performance semiconductor industry have provided interesting possibilities for the power switching applications on industrial scale with high-performance thyristors and transistors, though the implementation at present continues to pose challenges due to high power requirements. For this reason, recent designs are predominantly modular configurations allowing use of standard components, both for reasons of scalability, as well as for providing reliability and lower maintenance costs. An important issue that needs to be considered in the design is regulations that need to be followed, and demands pertaining to hygienic standards and operational safety in the industry, that need to be met (Toepfl 2012).

The selection or design of a suitable pulse generator is broadly determined by four parameters: the peak voltage required, which is highly dependent on the desired application (microbial inactivation vs. extraction in example, see Fig. 3); the peak current, determined by the product maximum conductivity and the geometry of the treatment chamber; the average power required, dependent on the desired processing capacity (tons, litres per hour); and the pulse waveform, which is typically either rectangular or exponentially decaying. Common generator designs comprise either setups of pulse transformers or semiconductor-based Marx generators. The typical average power these setups are capable of delivering falls within range of 30–400 kW. Although it is the average power level that determines the maximum treatment capacity, the peak power has been shown to present a greater challenge, since when using treatment chambers of large cross sections, required peak power can range up to several hundred MW (Toepfl 2012). At these extremely high currents and current densities, electrode erosion was studied as a possible concern. However, provided that stainless steel or in extreme cases titanium electrodes are used, electrochemical reactions and metal release to the product do not exceed acceptable limits (Morren et al. 2003; Roodenburg et al. 2005).

The other key component in addition to the power supply in a typical treatment system is the treatment chamber, the part in which electric pulses are delivered to the biological material. As opposed to the laboratory scale, in industrial-scale implementation setups capable of continuous processing are highly desirable. For batch or continuous processing, different chamber designs were proposed throughout the years, see e.g. (Huang and Wang 2009) for a review in treatment chamber designs as used for microbial inactivation. Broadly speaking, the parallel-plate, co-axial and co-linear designs are the most prevalent types. These different chamber designs present various advantages and drawbacks, mainly in relation to the homogeneity of the field to which the passing material is exposed, accessibility for cleaning and maintenance, and the average load resistance. The electric field distribution homogeneity is important in order to achieve uniform treatment of the product. This is especially important in microbial inactivation (in areas of field strength below critical the treatment may fail to achieve the necessary reduction in microorganism activity) and treatment of temperature-sensitive food materials (problem of local hotspots and overheating). The average load resistance is important because it determines, at a fixed peak pulse voltage, the maximum power (current) the power generator must be capable of delivering. In general, the low load resistance in parallel-plate configuration requires more powerful generators, but provides good field homogeneity, while co-linear and co-axial designs are easier to clean and have higher load resistance, thus lowering the current necessary to establish the required electric field strength (Morales-de la Pena et al. 2011). Researchers are working on improving the design of co-linear and co-axial chambers in terms of optimizing the homogeneity of electric field strength. For example, introduction of grids in the chamber as mechanic obstacles to the hydrodynamic flow of the particle suspension or juice, homogenizes the flow in the area where the electric field is applied, thus homogenizing the application of the treatment to the material. This prevents undesired overheating or insufficient treatment effects (Jaeger et al. 2009).

For applications where the material cannot be pumped (solid products treatment), a different design is required. For this purpose, belt or rotating systems were developed. Products are submerged in water (water is used as an

electrolyte, "extending" the electrodes to the product, delivering the energy to the target tissue) and conveyed through an electrode chamber by a belt. Parallel-plate electrodes apply the electroporating pulses, which are generally larger in comparison to those in tubular chamber designs for liquid food. Since the chamber has also a higher cross-section, resulting power consumption for equivalent field strength is thus significantly higher (as compared to tubular designs). Currently, systems with capacity up to 50 tons/h are available (Toepfl 2012). A special chamber with an added device for compaction of sliced particles and treatment of compacted slices without addition of liquid was recently patented (Vidal and Vorobiev 2011) and successfully tested in the sugar industry (Vidal 2014). Such a chamber permits electroporation of plant materials with no addition of liquid, thus significantly decreasing the energy consumption.

For additional reviews and more information on basic principles in designing generators of electric pulses and equipment used for electroporation, see for example (Bluhm 2006; Maged and Amer Eissa 2012; Rebersek et al. 2014), as well as (Sack et al. 2005, 2010a; Turk et al. 2012a, b) for some examples in implementation of electroporation devices on the industrial scale.

Perspectives for Future Research and Development

In this section, we indicate, in short, which direction the latest research and development into applications of electroporation for food processing seem to be pointing in. Along with these indications reflected in some of the more recent publications and some potential hurdles awaiting researchers in the long term, we also give a personal opinion on where we are currently at, and what we will most likely be reading about in the future in the field of electroporation-assisted food processing and biorefinery.

Modelling Electroporation-Related Phenomena in Electroporation of Food Materials and Environmental Applications

Comparing recent developments in modelling of electroporation-related phenomena in the biomedical domain with those in the field of food processing, we can roughly discern two modelling paradigms: the more theoretical, phenomenon-driven approach in biomedicine, focusing on modelling the effects of treatment protocol on biological material from the basics of the electroporation phenomena point of view, and the industry and engineering-oriented phenomenological and empirical models, prevalent in the food processing domain and used for more direct comparison or optimization of treatment parameter variations to the efficiency of the electroporation application. While empirical models may without argument present an invaluable source of information on the treatment efficacy and efficiency for the industry trying to implement this new technology into its processing lines, they may be—as already discussed (see "Mathematical Modelling of Electroporation-Related Phenomena in Food Processing Assisted by Electroporation" section)—reliably applied only within the ranges of parameters for which they were experimentally derived and validated. Moreover, if they are not based on the physics of the process, optimization must be performed on data obtained at the laboratory scale and transferred to the scale of operation and the applied treatment parameters, and this transfer and validation are normally performed through construction of and experimentation with setups at the level of pilot plants. More efforts need to be directed towards interdisciplinary collaboration, thus connecting researchers from disparate electroporation application domains working on modelling electroporation-related phenomena.

Modelling the phenomena of electroporation on the cell membrane, cell, and tissue levels, while including the mass transport, will allow for determination of necessary and/or optimal pulse parameters. From there, we can then derive what electrode chamber (providing local electric field) and finally what pulse generator is needed for a particular application. We can thus expect multi-scale models which incorporate electric, mass, temperature, and eventually chemical reactions models. This kind of models can then be directly coupled with electronics design software used in pulse generators design.

The Future of Electroporation in Valuable Compounds Recovery and Juice Extraction

As shown in the preceding sections of this paper, electroporation application for valuable compounds recovery and juice extraction has been extensively studied from the engineering and industrial points of view. There remains, however, some lack of understanding of basic principles of interaction of electric pulses, particularly of longer duration (order of ms) and high intensity (several kV/cm), with plant cells, tissues, and the bioactive compounds contained therein that are targeted for extraction.

Several recent works have shed more light on the subject, whilst opening a plethora of new questions into electroporation effects on cell structure. For instance, it was demonstrated that electric pulses of a given (sufficient) strength and duration modify not only the cell membrane, but also the cell wall and the internal membranes (of vacuoles and organelles). Electroporation can also modify molecular connections of intracellular components, thus modifying the properties of extracted components (Delsart et al. 2014; Cholet et al. 2014).

Another subject that beckons further elucidation is the influence of the pulse application frequency, particularly in the very high frequency range (nanosecond-scale pulses), a subject under intensive development in the biomedical field of electroporation applications, but poorly researched and understood in relation to food products and constituents under electric field treatment. Conversely, the low frequency, long pulse duration spectrum of potential effects and applications seem almost completely unexplored, i.e. there is a lack of research on electrokinetic effects in relation to mass transport (electroosmosis, electrophoresis). To again give analogy with biomedicine, use of electrophoretic low-voltage and long pulses post-permeabilization (after application of high-voltage, short-duration pulses) is an established method of increasing post-electroporation mass transport in transdermal drug and gene delivery (Satkauskas et al. 2002; Kanduser et al. 2009; Zorec et al. 2013). Given that enhanced mass transport in the electroporated material is the main objective of extraction applications, these augmenting effects of electrically driven transport must be evaluated also for the food processing applications.

Last but not least, following the trends in food processing applications of the recent decade or so, there is an increased interest and focus towards combining different treatments to food materials for achieving the given objective. In example, the combined (synergistic) effects of electroporation and heating (so-called thermo-electroporation) or of electroporation in combination with heating and high pressure treatment (so-called mano-thermo-electroporation) seem to be the directions of recent trends in research of electroporation for valuable compounds recovery and juice extraction, though they have traditionally been present for a much longer time in electroporation applications for microbial inactivation and sterilization.

Microalgae: A (Re)discovery of Bioreactors

Microalgae have been considered as a potential source of proteins, lipids as well as other valuable compounds (Becker 2007; Gouveia and Oliveira 2009; Wijffels et al. 2010; Chacon-Lee and Gonzalez-Marino 2010). They are considered to be extremely promising organisms for our sustainable future, as they can be grown on non-arable land and have high growth rate (Dismukes et al. 2008). In particular, microalgae can serve as a potential source of energy (Hannon et al. 2010), food (Draaisma et al. 2013), feed (Skrede et al. 2011; Kiron et al. 2012), cosmetics and pharmaceuticals (Pulz and Gross 2004; Gong and Jiang 2011), owing to their high photosynthetic efficiency, higher biomass production and faster growth compared to other energy crops (Widjaja et al. 2009). On the other hand, algae are already a relevant model for wastewater treatment and CO_2 sequestration, which is connected to solution of global environmental problems (Lam et al. 2012). Aquatic microalgae are among the fastest growing photosynthetic organisms, having carbon fixation rates an order of magnitude higher than those of land plants, as microalgae utilize CO_2 as one of the main building blocks for their biomass. Concerning energy, microalgae can be converted directly into energy sources, such as biodiesel, and therefore it appears to be a promising source of renewable energy (Gouveia and Oliveira 2009). Moreover, microalgae cultivation allows for the production of biomass containing a variety of valuable products that generate revenues contributing to the return of the investment (Olaizola 2003; Spolaore et al. 2006). Concerning food, microalgae are an attractive food and food supplement source, since they are rich in proteins, peptides, carbohydrates, lipids, polyunsaturated fatty acids, trace elements and other essential nutrients with protective and detoxifying roles (vitamins, minerals, pigments) (Gong and Jiang 2011).

The main problems are digestibility and availability. Various extraction techniques have been proposed with limited success (Wiyarno et al. 2011; Adam et al. 2012; McMillan et al. 2013; Biller et al. 2013). There are few reports at this stage on use of electroporation as an extraction technique in microalgae for water-soluble proteins (Coustets et al. 2013; Grimi et al. 2014), where the authors report selective extraction by means of electroporation and an increased, but limited success has been reported so far in extraction of lipids (Goettel et al. 2013). Suitable choice of pulse parameters and combination with other extraction techniques may place electroporation on the stage also in microalgae research (Coustets et al. 2013; Flisar et al. 2014).

Pasteurization and Sterilization of Liquid Foods: A New Arms Race?

As discussed in the preceding sections, microbial inactivation by electroporation presents interesting new possibilities for extending the shelf-life of food products to the processing industry. However, as we are constantly and consistently reminded on all open fronts against microorganisms, evolution is an inescapable and tireless process, opening a new arms race with every new method applied for an attempted control of microorganism proliferation. For example, the widespread use of antibiotics for agricultural purposes has rendered much of the antibiotics arsenal useless against selected resistant strains of pathogens, harmful not only to livestock, but also to humans, creating an arms race between research into finding new antibiotics on one side and the adaptation of pathogens on the other (Mathew et al. 2007). As demonstrated in a recent study by Sagarzazu et al. (Sagarzazu et al. 2013),

application of electroporation for inactivation of microorganisms raises similar concerns. The authors of the study report of an acquisition of resistance to electroporation treatment in a *Salmonella* serovar (specifically in *S. typhimurium* SL1344). They consistently observed an increased resistance to electric treatment after repeated rounds of electroporation and outgrowth of survivors. In addition to the acquired resistance to the electric treatment, higher tolerance to acidic pH, hydrogen peroxide and ethanol were also found. It is possible to assume—based on the results of the cited study—that significant risks could be taken in case of wide-scale application of the technology. The risk is that microorganisms, exhibiting increased tolerance to electric treatment, could be released into the uncontrolled natural environment. This suggests that more research is needed in future to insure the long-term efficacy and safety of applying electroporation technology for microorganism inactivation in large scale industrial deployments (as opposed to controlled laboratory-scale experiments). Isolation of "resistant" strains on the other hand could provide valuable insight in exact mechanisms of microbial inactivation mechanisms, providing us with leverage to engineer more efficient treatments.

The Future of Technology Transfer from Research to Industrial-Scale Processing

Final remarks and conclusions in relevant modern literature on industrial scale-up of electroporation-assisted food processing (see "Industrial Equipment Design, Implementation and Commercial Applications" section) almost invariably contain two bottom-line observations: primarily, that electroporation applications for food treatment, as evaluated based on research and pilot plant scale experimental setups, show promising prospects for application; and secondly, there are still major hurdles that need to be dealt with before electroporation will be accepted and firmly established in the food industry. Namely, highly resistant spores of many pathogenic microorganisms are problematic. Their inactivation calls for treatment parameters that considerably increase energy and equipment costs. The most commonly identified obstacles from the technical or economic point of view are the high initial cost of the systems that need to be introduced into an existing processing line; the availability of such systems, specifically in terms of commercial units available on the market; the lack of research on reliability and optimization of processing parameters in the industrial environment; and the lack of standards and regulative in this field of an emerging novel technology, which is related both with the industrial and consumer acceptance. On the other hand, the identified benefits of the technology that will help establish it in the industry are low energy requirements and processing costs; easy implementation and suitability for continuous operation; and the many advantages of electroporation in processing of high value-added foods (Sack et al. 2010b; Morales-de la Pena et al. 2011; Toepfl 2012). Structural changes of food material in particular (meat, fruit and vegetables, juice extraction, etc.) seem to have a bright future in the industry.

Concerning legislation and regulations, electroporation in food processing as a novel technology must be authorized by regulatory bodies, in order to certify the technology and its application to food materials as safe and effective. Two major concerns are raised in this respect: the efficacy of electroporation for food pasteurization and sterilization as compared to the traditional and well-established (e.g. thermal) treatment; and the possible interactions between the treated product and electroporation processing equipment with possible undesired effects and changes to the material (e.g. electrode erosion, electrochemical effects, etc.). In the U.S., the adoption of technology into the food processing industry is subject to the regulations of the Food and Drugs Administration (FDA), and in EU, it falls under the Novel Foods Regulation (EC) 258/97 (European Commission Regulation 258/97 1997; Góngora-Nieto et al. 2002; Jaeger et al. 2008).

Knowledge Transfer Within the Field of Electroporation Research and with the Industry

In July 2012, a European project COST[2] Action TD1104—*EP4Bio²Med* was launched (Miklavcic 2012), bringing up until now together more than 500 researchers coming from 35 countries and over 180 institutions and enterprises throughout the world, with one common denominator—they are all working with or are interested in electroporation. The Action's purpose is to facilitate better exchange of knowledge and collaboration among researchers working with electroporation in different domains of its applications; this ranges from the biomedical field to food processing and environmental applications. The member institutions, individual researchers and industrial partners connected through their participation and involvement in the project, are divided into five working groups. One of these groups is dedicated to those primarily interested in basic mechanisms and the theory of electroporation, one each to the fields of biomedical, food processing and environmental applications, and the fifth to the aspects of technology development and transfer. The ultimate goal is to establish lines of communication and transfer of knowledge and people within and between these groups, so

[2] COST stands for European Cooperation in Science and Technology.

that every research field as well as the industry may benefit to a greater extent from the current state-of-the-art in the related, but up to now evolving virtually in parallel domains of research. One of the principal purposes of putting this Action into place is to prevent duplication of research efforts on the European and also global scale, so that the national and European research funds can be spent more efficiently and findings from, in example biomedicine, need not be arrived at independently also by those focused on food processing. The underlying premise is that, among these diverse fields where electroporation has found its place, the basic principles and mechanisms of its action on biological material remain similar, if not the same.

Within the scope of the TD1104 Action, the international School on Electroporation-based Technologies and Treatments or EBTT was and will be organized in the years 2012–2015 (for more information on the upcoming School, visit 2014.ebtt.org or simply ebtt.org). The School has been organized biennially since 2003 in Ljubljana, Slovenia and annually since 2011. The purpose of the EBTT School is to provide all those interested in basic principles and techniques in electroporation-related applications with a quick and intensive course, transmitting knowledge gained by the last 30 years or so of electroporation research by means of lectures given by faculty members and invited lecturers, supplemented by practical hands-on laboratory work and an e-learning session. Traditionally, it was focused towards electroporation in biomedicine, but has recently (since it is being supported by the Action) expanded in scope towards food processing applications, covering also some topics on the design of industrial equipment for electroporation.

In January 2014, the first international School on Applications of Pulsed Electric Fields for Food Processing (PEFSchool) was organized at the Faculty of Veterinary Medicine of University of Zaragoza in Zaragoza, Spain (Raso et al. 2014a, b). Co-organized by COST TD1104, it was dedicated to applications of electroporation in the food processing industry and research and aimed at everyone academically or professionally interested in basic concepts of using electroporation for food materials manipulation. The School is planned to become an annually organized event, with venues selected every year in a different Action member institutions, one that is capable of organizing and hosting the School. The next edition is scheduled to be held on February 8–12, 2015, organized jointly by the ProdAl S.c.a.r.l. consortium and the University of Salerno, Fisciano, Italy.

Conclusions

In this paper, we gave a quick introduction to important concepts in electroporation of biological cells and tissues, followed by a brief review of some of the well investigated and promising applications of electroporation in food processing. Among these, we find applications with many different objectives, such as extraction of juices and other valuable compounds, e.g. anthocyanins, proteins, lipids; tissue dehydration and impregnation (cryopreservation); microbial inhibition and inactivation for pasteurization and/or sterilization; enhancing organoleptic properties of food materials (e.g. winemaking); growth stimulation; and even "cooking" by electroporation. We conclude by a general overview of some important methods for assessing effects of electroporation in plant materials; of factors that influence the success of electric treatment of food materials; of contemporary approaches in the field using modelling techniques and of considerations in industrial-scale equipment design and implementation. The final section on perspectives for future research and development highlights more issues related with transferring the knowledge from research into the industrial environment; possible future applications where electroporation may prove to be the treatment of choice for effective and efficient harvesting of valuable compounds, thus solving some of the pressing economic and environmental problems, and a seemingly hidden caveat of applying the technology to treatment of microorganisms. This paper is a review in the broadest sense of the word, written with the purpose of orienting the interested newcomer to the field of electroporation applications in food technology towards the pertinent, highly relevant and more in-depth literature from the respective subdomains of electroporation research.

In conclusion, the field of research into applications and phenomena related with electroporation of food products and raw materials is well established and its growth is gaining momentum with alimentation and energy sources becoming ever greater global issues. With increasing market demands for calories and nutrients that are safe and of high quality motivated by the evolving educated and conscientious consumer on the one hand, and pressing demands by the food industry to cut on processing costs predominantly due to globalization of production on the other, electroporation might present a large step in arriving at the next optimal equilibrium state between these two competing forces.

Acknowledgments This paper was in part made possible due to the networking activities of the COST ("*European Cooperation in Science and Technology*") Action (project) TD1104 – *EP4Bio²Med* (www.electroporation.net), as well as the financial support from the Slovenian Research Agency (ARRS – "*Javna agencija za raziskovalno dejavnost Republike Slovenije*") and the French Ministry of Higher Education and Research (MESR – "*Ministère de l'Enseignement supérieur et de la Recherche*"). The paper was written within the scope of the European Associated Laboratory on Applications of Pulsed Electric Fields in Biology and Medicine (LEA EBAM). The authors also wish to acknowledge Matej Reberšek as the

author of the original image with diagram representation of electroporation applications, the idea of which was adopted by the authors in preparing Fig. 1.

References

Adam F, Abert-Vian M, Peltier G, Chemat F (2012) "Solvent-free" ultrasound-assisted extraction of lipids from fresh microalgae cells: a green, clean and scalable process. Bioresour Technol 114:457–465. doi:10.1016/j.biortech.2012.02.096

Ade-Omowaye BIO, Angersbach A, Taiwo KA, Knorr D (2001) Use of pulsed electric field pre-treatment to improve dehydration characteristics of plant based foods. Trends Food Sci Technol 12:285–295. doi:10.1016/S0924-2244(01)00095-4

Al-Sakere B, André F, Bernat C et al (2007) Tumor ablation with irreversible electroporation. PLoS One 2:e1135. doi:10.1371/journal.pone.0001135

Álvarez I, Condón S, Raso J (2006) Microbial Inactivation By Pulsed Electric Fields. In: Raso J, Heinz V (eds) Pulsed electric fields technology for the food industry. Springer, New York, pp 97–129

Amami E, Vorobiev E, Kechaou N (2006) Modelling of mass transfer during osmotic dehydration of apple tissue pre-treated by pulsed electric field. LWT Food Sci Technol 39:1014–1021. doi:10.1016/j.lwt.2006.02.017

Aronsson K, Rönner U, Borch E (2005) Inactivation of *Escherichia coli*, *Listeria innocua* and *Saccharomyces cerevisiae* in relation to membrane permeabilization and subsequent leakage of intracellular compounds due to pulsed electric field processing. Int J Food Microbiol 99:19–32. doi:10.1016/j.ijfoodmicro.2004.07.012

Asavasanti S, Ersus S, Ristenpart W et al (2010) Critical electric field strengths of onion tissues treated by pulsed electric fields. J Food Sci 75:E433–E443. doi:10.1111/j.1750-3841.2010.01768.x

Barbosa-Canovas GV, Pothakamury UR, Palou E, Swanson BG (1997) Nonthermal preservation of foods. CRC Press, Boca Raton

Bazhal M, Lebovka N, Vorobiev E (2003) Optimisation of pulsed electric field strength for electroplasmolysis of vegetable tissues. Biosyst Eng 86:339–345. doi:10.1016/S1537-5110(03)00139-9

Becker EW (2007) Micro-algae as a source of protein. Biotechnol Adv 25:207–210. doi:10.1016/j.biotechadv.2006.11.002

Becker S (2012) Transport modeling of skin electroporation and the thermal behavior of the stratum corneum. Int J Therm Sci 54:48–61. doi:10.1016/j.ijthermalsci.2011.10.022

Bermudez-Aguirre D, Dunne CP, Barbosa-Canovas GV (2012) Effect of processing parameters on inactivation of *Bacillus cereus* spores in milk using pulsed electric fields. Int Dairy J 24:13–21. doi:10.1016/j.idairyj.2011.11.003

Biller P, Friedman C, Ross AB (2013) Hydrothermal microwave processing of microalgae as a pre-treatment and extraction technique for bio-fuels and bio-products. Bioresour Technol 136:188–195. doi:10.1016/j.biortech.2013.02.088

Bluhm H (2006) Examples of pulsed-power generators. Pulsed power systems. Springer, Berlin, pp 203–210

Bluhm H, Sack M (2009) Industrial-scale treatment of biological tissues with pulsed electric fields. Electrotechnologies for extraction from food plants and biomaterials. Springer, New York, pp 237–269

Boussetta N, Vorobiev E, Deloison V et al (2011) Valorisation of grape pomace by the extraction of phenolic antioxidants: application of high voltage electrical discharges. Food Chem 128:364–370. doi:10.1016/j.foodchem.2011.03.035

Bouzrara H, Vorobiev E (2000) Beet juice extraction by pressing and pulsed electric fields. Int Sugar J 102:194–200

Bouzrara H, Vorobiev E (2003) Solid–liquid expression of cellular materials enhanced by pulsed electric field. Chem Eng Process 42:249–257. doi:10.1016/S0255-2701(02)00010-7

Buckow R, Ng S, Toepfl S (2013) Pulsed electric field processing of orange juice: a review on microbial, enzymatic, nutritional, and sensory quality and stability. Compr Rev Food Sci Food Saf 12:455–467. doi:10.1111/1541-4337.12026

Buttersack C, Basler W (1991) Hydraulic conductivity of cell-walls in sugar-beet tissue. Plant Sci 76:229–237. doi:10.1016/0168-9452(91)90145-X

Chacon-Lee TL, Gonzalez-Marino GE (2010) Microalgae for "Healthy" foods-possibilities and challenges. Compr Rev Food Sci Food Saf 9:655–675. doi:10.1111/j.1541-4337.2010.00132.x

Chiarella P, Fazio VM, Signori E (2013) Electroporation in DNA vaccination protocols against cancer. Curr Drug Metab 14:291–299

Cholet C, Delsart C, Petrel M et al (2014) Structural and biochemical changes induced by pulsed electric field treatments on Cabernet Sauvignon grape berry skins: impact on cell wall total tannins and polysaccharides. J Agric Food Chem 62:2925–2934. doi:10.1021/jf404804d

Corovic S, Lackovic I, Sustaric P et al (2013) Modeling of electric field distribution in tissues during electroporation. Biomed Eng Online 12:16. doi:10.1186/1475-925X-12-16

Čorović S, Mir LM, Miklavčič D (2012) In vivo muscle electroporation threshold determination: realistic numerical models and in vivo experiments. J Membr Biol 245:509–520. doi:10.1007/s00232-012-9432-8

Coustets M, Al-Karablieh N, Thomsen C, Teissié J (2013) Flow process for electroextraction of total proteins from microalgae. J Membr Biol 246:751–760. doi:10.1007/s00232-013-9542-y

Davalos RV, Mir ILM, Rubinsky B (2005) Tissue ablation with irreversible electroporation. Ann Biomed Eng 33:223–231

de Boer K, Moheimani NR, Borowitzka MA, Bahri PA (2012) Extraction and conversion pathways for microalgae to biodiesel: a review focused on energy consumption. J Appl Phycol 24:1681–1698. doi:10.1007/s10811-012-9835-z

Delemotte L, Tarek M (2012) Molecular dynamics simulations of lipid membrane electroporation. J Membr Biol 245:531–543. doi:10.1007/s00232-012-9434-6

Delsart C, Cholet C, Ghidossi R et al (2014) Effects of pulsed electric fields on Cabernet Sauvignon grape berries and on the characteristics of wines. Food Bioprocess Technol 7:424–436. doi:10.1007/s11947-012-1039-7

Denet AR, Vanbever R, Preat V (2004) Skin electroporation for transdermal and topical delivery. Adv Drug Deliv Rev 56:659–674. doi:10.1016/j.addr.2003.10.027

Dismukes GC, Carrieri D, Bennette N et al (2008) Aquatic phototrophs: efficient alternatives to land-based crops for biofuels. Curr Opin Biotechnol 19:235–240. doi:10.1016/j.copbio.2008.05.007

Donsi F, Ferrari G, Pataro G (2010) Applications of pulsed electric field treatments for the enhancement of mass transfer from vegetable tissue. Food Eng Rev 2:109–130. doi:10.1007/s12393-010-9015-3

Draaisma RB, Wijffels RH, Slegers PM et al (2013) Food commodities from microalgae. Curr Opin Biotechnol 24:169–177. doi:10.1016/j.copbio.2012.09.012

Dymek K, Dejmek P, Panarese V et al (2012) Effect of pulsed electric field on the germination of barley seeds. LWT Food Sci Technol 47:161–166. doi:10.1016/j.lwt.2011.12.019

Eing C, Goettel M, Straessner R et al (2013) Pulsed electric field treatment of microalgae-benefits for microalgae biomass

processing. IEEE Trans Plasma Sci 41:2901–2907. doi:10.1109/TPS.2013.2274805

El Darra N, Grimi N, Maroun RG et al (2013) Pulsed electric field, ultrasound, and thermal pretreatments for better phenolic extraction during red fermentation. Eur Food Res Technol 236:47–56. doi:10.1007/s00217-012-1858-9

El-Belghiti K, Rabhi Z, Vorobiev E (2005) Kinetic model of sugar diffusion from sugar beet tissue treated by pulsed electric field. J Sci Food Agric 85:213–218. doi:10.1002/jsfa.1944

Ersus S, Barrett DM (2010) Determination of membrane integrity in onion tissues treated by pulsed electric fields: use of microscopic images and ion leakage measurements. Innov Food Sci Emerg Technol 11:598–603. doi:10.1016/j.ifset.2010.08.001

Ersus S, Oztop MH, McCarthy MJ, Barrett DM (2010) Disintegration efficiency of pulsed electric field induced effects on onion (*Allium cepa* L.) Tissues as a function of pulse protocol and determination of cell integrity by 1H-NMR relaxometry. J Food Sci 75:E444–E452. doi:10.1111/j.1750-3841.2010.01769.x

Eshtiaghi MN, Knorr D (2002) High electric field pulse pretreatment: potential for sugar beet processing. J Food Eng 52:265–272. doi:10.1016/S0260-8774(01)00114-5

Essone Mezeme M, Pucihar G, Pavlin M et al (2012) A numerical analysis of multicellular environment for modeling tissue electroporation. Appl Phys Lett 100:143701–143704. doi:10.1063/1.3700727

European Commission Regulation 258/97 (1997) EUROPA-Food Safety-Biotechnology-Novel Foods: Review of Regulation (EC) 258/97. In: ec.europa.eu. http://ec.europa.eu/food/food/biotechnology/novelfood/initiatives_en.htm. Accessed 30 May 2014

Fincan M, Dejmek P (2002) In situ visualization of the effect of a pulsed electric field on plant tissue. J Food Eng 55:223–230. doi:10.1016/S0260-8774(02)00079-1

Fincan M, DeVito F, Dejmek P (2004) Pulsed electric field treatment for solid–liquid extraction of red beetroot pigment. J Food Eng 64:381–388. doi:10.1016/j.jfoodeng.2003.11.006

Flisar K, Meglic SH, Morelj J et al (2014) Testing a prototype pulse generator for a continuous flow system and its use for *E. coli* inactivation and microalgae lipid extraction. Bioelectrochemistry. doi:10.1016/j.bioelechem.2014.03.008

Frey W, Flickinger B, Berghoefer T et al (2011) Electropermeabilization versus nsPEF-stimulation: pulsed electric fields can stimulate the growth of plants and fungi. European Bioelectromagnetics Association, ISBN 978-88-8286-231-2

Gachovska T, Ngadi M, Raghavan V (2006) Pulsed electric field assisted juice extraction from alfalfa. Can Biosyst Eng 48:33–37

Galindo FG, Vernier PT, Dejmek P et al (2008) Pulsed electric field reduces the permeability of potato cell wall. Bioelectromagnetics 29:296–301. doi:10.1002/bem.20394

Ganeva V, Galutzov B, Teissie J (2014) Evidence that pulsed electric field treatment enhances the cell wall porosity of yeast cells. Appl Biochem Biotechnol 172:1540–1552. doi:10.1007/s12010-013-0628-x

Garcia PA, Rossmeisl JH, Neal RE et al (2011) A parametric study delineating irreversible electroporation from thermal damage based on a minimally invasive intracranial procedure. Biomed Eng Online 10:34. doi:10.1186/1475-925X-10-34

Gehl J (2003) Electroporation: theory and methods, perspectives for drug delivery, gene therapy and research. Acta Physiol Scand 177:437–447. doi:10.1046/j.1365-201X.2003.01093.x

Gerlach D, Alleborn N, Baars A et al (2008) Numerical simulations of pulsed electric fields for food preservation: a review. Innov Food Sci Emerg Technol 9:408–417. doi:10.1016/j.ifset.2008.02.001

Goettel M, Eing C, Gusbeth C et al (2013) Pulsed electric field assisted extraction of intracellular valuables from microalgae. Algal Res 2:401–408. doi:10.1016/j.algal.2013.07.004

Golberg A, Rubinsky B (2010) A statistical model for multidimensional irreversible electroporation cell death in tissue. Biomed Eng Online 9:13. doi:10.1186/1475-925X-9-13

Golberg A, Rae CS, Rubinsky B (2012) Listeria monocytogenes cell wall constituents exert a charge effect on electroporation threshold. Biochim Biophys Acta Biomembr 1818:689–694. doi:10.1016/j.bbamem.2011.11.003

Gong Y, Jiang M (2011) Biodiesel production with microalgae as feedstock: from strains to biodiesel. Biotechnol Lett 33:1269–1284. doi:10.1007/s10529-011-0574-z

Góngora-Nieto MM, Sepúlveda DR, Pedrow P et al (2002) Food processing by pulsed electric fields: treatment delivery, inactivation level, and regulatory aspects. LWT Food Sci Technol 35:375–388. doi:10.1006/fstl.2001.0880

Gouveia L, Oliveira AC (2009) Microalgae as a raw material for biofuels production. J Ind Microbiol Biotechnol 36:269–274. doi:10.1007/s10295-008-0495-6

Grimi N, Lebovka N, Vorobiev E, Vaxelaire J (2009) Compressing behavior and texture evaluation for potatoes pretreated by pulsed electric field. J Texture Stud 40:208–224. doi:10.1111/j.1745-4603.2009.00177.x

Grimi N, Vorobiev E, Lebovka N, Vaxelaire J (2010) Solid–liquid expression from denaturated plant tissue: filtration–consolidation behaviour. J Food Eng 96:29–36. doi:10.1016/j.jfoodeng.2009.06.039

Grimi N, Dubois A, Marchal L et al (2014) Selective extraction from microalgae *Nannochloropsis* sp. using different methods of cell disruption. Bioresour Technol 153:254–259. doi:10.1016/j.biortech.2013.12.011

Guderjan M, Topfl S, Angersbach A, Knorr D (2005) Impact of pulsed electric field treatment on the recovery and quality of plant oils. J Food Eng 67:281–287. doi:10.1016/j.jfoodeng.2004.04.029

Guderjan M, Elez-Martinez P, Knorr D (2007) Application of pulsed electric fields at oil yield and content of functional food ingredients at the production of rapeseed oil. Innov Food Sci Emerg Technol 8:55–62. doi:10.1016/j.ifset.2006.07.001

Gudmundsson M, Hafsteinsson H (2005) Effect of high intensity electric field pulses on solid foods. Emerging technologies for food processing. Elsevier, Amsterdam, pp 141–153

Guerrero-Beltran JA, Sepulveda DR, Gongora-Nieto MM et al (2010) Milk thermization by pulsed electric fields (PEF) and electrically induced heat. J Food Eng 100:56–60. doi:10.1016/j.jfoodeng.2010.03.027

Gusbeth C, Frey W, Volkmann H et al (2009) Pulsed electric field treatment for bacteria reduction and its impact on hospital wastewater. Chemosphere 75:228–233. doi:10.1016/j.chemosphere.2008.11.066

Haberl S, Miklavcic D, Sersa G et al (2013) Cell membrane electroporation-part 2: the applications. IEEE Electr Insul Mag 29:29–37. doi:10.1109/MEI.2013.6410537

Halder A, Datta AK, Spanswick RM (2011) Water transport in cellular tissues during thermal processing. AIChE J 57:2574–2588. doi:10.1002/aic.12465

Hannon M, Gimpel J, Tran M et al (2010) Biofuels from algae: challenges and potential. Biofuels 1:763–784

Ho M-C, Casciola M, Levine ZA, Vernier PT (2013a) Molecular dynamics simulations of ion conductance in field-stabilized nanoscale lipid electropores. J Phys Chem B 117:11633–11640. doi:10.1021/jp401722g

Ho M-C, Levine ZA, Vernier PT (2013b) Nanoscale, electric field-driven water bridges in vacuum gaps and lipid bilayers. J Membr Biol 246:793–801. doi:10.1007/s00232-013-9549-4

Hu N, Yang J, Joo SW et al (2013) Cell electrofusion in microfluidic devices: a review. Sens Actuator B Chem 178:63–85. doi:10.1016/j.snb.2012.12.034

Huang K, Wang J (2009) Designs of pulsed electric fields treatment chambers for liquid foods pasteurization process: a review. J Food Eng 95:227–239. doi:10.1016/j.jfoodeng.2009.06.013

IXL Netherlands B.V. (2014) Nutri-Pulse®: IXL Netherlands B.V. In: The Nutri-Pulse® "cooks" with electric pulses. http://www.innovation-xl.com/en/nutripulse.html. Accessed 11 Feb 2014

Jaeger H, Balasa A, Knorr D (2008) Food industry applications for pulsed electric fields. Electrotechnologies for extraction from food plants and biomaterials. Springer, New York, pp 181–216

Jaeger H, Meneses N, Knorr D (2009) Impact of PEF treatment inhomogeneity such as electric field distribution, flow characteristics and temperature effects on the inactivation of *E. coli* and milk alkaline phosphatase. Innov Food Sci Emerg Technol 10:470–480. doi:10.1016/j.ifset.2009.03.001

Jaeger H, Meneses N, Moritz J, Knorr D (2010) Model for the differentiation of temperature and electric field effects during thermal assisted PEF processing. J Food Eng 100:109–118. doi:10.1016/j.jfoodeng.2010.03.034

Jaeger H, Buechner C, Knorr D (2012) PEF enhanced drying of plant based products. Stewart Postharvest Rev 8:1–7. doi:10.2212/spr.2012.2.1

Janositz A, Knorr D (2010) Microscopic visualization of pulsed electric field induced changes on plant cellular level. Innov Food Sci Emerg Technol 11:592–597. doi:10.1016/j.ifset.2010.07.004

Janositz A, Noack A-K, Knorr D (2011) Pulsed electric fields and their impact on the diffusion characteristics of potato slices. LWT Food Sci Technol 44:1939–1945. doi:10.1016/j.lwt.2011.04.006

Jayaram SH (2000) Sterilization of liquid foods by pulsed electric fields. IEEE Electr Insul Mag 16:17–25. doi:10.1109/57.887601

Jemai AB, Vorobiev E (2002) Effect of moderate electric field pulses on the diffusion coefficient of soluble substances from apple slices. Int J Food Sci Technol 37:73–86. doi:10.1046/j.1365-2621.2002.00516.x

Junfeng Z, Leping X, Daolun F et al (2013) Study on inactivation of microalgae in ship ballast water by pulsed electric field and heat treatment. In: Xu QJ, Ju YH, Ge HH (eds) Progress in environmental science and engineering, Pts 1-4. Trans Tech Publications Ltd., Stafa-Zurich, pp 3163–3166

Kanduser M, Miklavcic D, Pavlin M (2009) Mechanisms involved in gene electrotransfer using high- and low-voltage pulses: an in vitro study. Bioelectrochemistry 74:265–271. doi:10.1016/j.bioelechem.2008.09.002

Kiron V, Phromkunthong W, Huntley M et al (2012) Marine microalgae from biorefinery as a potential feed protein source for Atlantic salmon, common carp and whiteleg shrimp. Aquac Nutr 18:521–531. doi:10.1111/j.1365-2095.2011.00923.x

Knorr D, Angersbach A (1998) Impact of high-intensity electric field pulses on plant membrane permeabilization. Trends Food Sci Technol 9:185–191. doi:10.1016/S0924-2244(98)00040-5

Knorr D, Froehling A, Jaeger H et al (2011) Emerging technologies in food processing. Annu Rev Food Sci Technol 2:203–235. doi:10.1146/annurev.food.102308.124129

Kotnik T, Miklavcic D (2000) Analytical description of transmembrane voltage induced by electric fields on spheroidal cells. Biophys J 79:670–679. doi:10.1016/S0006-3495(00)76325-9

Kotnik T, Pucihar G, Miklavcic D (2010) Induced transmembrane voltage and its correlation with electroporation-mediated molecular transport. J Membr Biol 236:3–13. doi:10.1007/s00232-010-9279-9

Kotnik T, Kramar P, Pucihar G et al (2012) Cell membrane electroporation-part 1: the phenomenon. IEEE Electr Insul Mag 28:14–23. doi:10.1109/MEI.2012.6268438

Krassowska W, Filev PD (2007) Modeling electroporation in a single cell. Biophys J 92:404–417. doi:10.1529/biophysj.106.094235

Lam MK, Lee KT, Mohamed AR (2012) Current status and challenges on microalgae-based carbon capture. Int J Greenh Gas Con 10:456–469. doi:10.1016/j.ijggc.2012.07.010

Lanoiselle JL, Vorobyov EI, Bouvier JM, Piar G (1996) Modeling of solid/liquid expression for cellular materials. AIChE J 42:2057–2068. doi:10.1002/aic.690420726

Lebovka NI, Bazhal MI, Vorobiev E (2000) Simulation and experimental investigation of food material breakage using pulsed electric field treatment. J Food Eng 44:213–223. doi:10.1016/S0260-8774(00)00029-7

Lebovka NI, Bazhal MI, Vorobiev E (2002) Estimation of characteristic damage time of food materials in pulsed-electric fields. J Food Eng 54:337–346. doi:10.1016/S0260-8774(01)00220-5

Lebovka NI, Praporscic I, Vorobiev E (2003) Enhanced expression of juice from soft vegetable tissues by pulsed electric fields: consolidation stages analysis. J Food Eng 59:309–317. doi:10.1016/S0260-8774(02)00472-7

Lebovka NI, Shynkaryk MV, El-Belghiti K et al (2007a) Plasmolysis of sugarbeet: pulsed electric fields and thermal treatment. J Food Eng 80:639–644. doi:10.1016/j.jfoodeng.2006.06.020

Lebovka NI, Shynkaryk NV, Vorobiev E (2007b) Pulsed electric field enhanced drying of potato tissue. J Food Eng 78:606–613. doi:10.1016/j.jfoodeng.2005.10.032

Lebovka N, Vorobiev E, Chemat F (2011) Enhancing extraction processes in the food industry. CRC Press, Boca Raton

Leong SY, Richter L-K, Knorr D, Oey I (2014) Feasibility of using pulsed electric field processing to inactivate enzymes and reduce the cutting force of carrot (Daucus carota var. Nantes). Innov Food Sci Emerg Technol. doi:10.1016/j.ifset.2014.04.004

Leontiadou H, Mark AE, Marrink SJ (2004) Molecular dynamics simulations of hydrophilic pores in lipid bilayers. Biophys J 86:2156–2164

Li J, Lin H (2011) Numerical simulation of molecular uptake via electroporation. Bioelectrochemistry 82:10–21. doi:10.1016/j.bioelechem.2011.04.006

Li J, Tan W, Yu M, Lin H (2013) The effect of extracellular conductivity on electroporation-mediated molecular delivery. Biochim Biophys Acta. doi:10.1016/j.bbamem.2012.08.014

Liu M, Zhang M, Lin S et al (2012) Optimization of extraction parameters for protein from beer waste brewing yeast treated by pulsed electric fields (PEF). Afr J Microbiol Res 6:4739–4746. doi:10.5897/AJMR12.117

Liu D, Lebovka NI, Vorobiev E (2013) Impact of electric pulse treatment on selective extraction of intracellular compounds from saccharomyces cerevisiae yeasts. Food Bioprocess Technol 6:576–584. doi:10.1007/s11947-011-0703-7

Lodish HF, Berk A, Kaiser CA et al (2008) Molecular cell biology. W.H. Freeman, New York

Lopez N, Puertolas E, Condon S et al (2009) Enhancement of the solid–liquid extraction of sucrose from sugar beet (Beta vulgaris) by pulsed electric fields. LWT Food Sci Technol 42:1674–1680. doi:10.1016/j.lwt.2009.05.015

Luengo E, Puértolas AE, López BN et al (2012) Potential applications of pulsed electric fields in wineries. Stewart Postharvest Rev 8:1–6. doi:10.2212/spr.2012.2.2

Maged EAM, Amer Eissa AH (2012) Pulsed electric fields for food processing technology. Struct Funct Food Eng

Mahnič-Kalamiza S, Miklavčič D, Vorobiev E (2014) Dual-porosity model of solute diffusion in biological tissue modified by electroporation. Biochim Biophys Acta 1838:1950–1966. doi:10.1016/j.bbamem.2014.03.004

Mahnič-Kalamiza S, Vorobiev E (2014) Dual-porosity model of liquid extraction by pressing from biological tissue modified by electroporation. J Food Eng 137:76–87. doi:10.1016/j.jfoodeng.2014.03.035

Mali B, Miklavcic D, Campana LG et al (2013) Tumor size and effectiveness of electrochemotherapy. Radiol Oncol. doi:10.2478/raon-2013-0002

Mañas P, Vercet A (2006) Effect of PEF on enzymes and food constituents. In: Raso J, Heinz V (eds) Pulsed electric fields technology for the food industry. Springer, New York, pp 131–151

Marsellés-Fontanet AR, Elez-Martínez P, Martín-Belloso O (2012) Juice preservation by pulsed electric fields. Stewart Postharvest Rev 8:1–4. doi:10.2212/spr.2012.2.3

Martín-Belloso O, Sobrino-López A (2011) Combination of pulsed electric fields with other preservation techniques. Food Bioprocess Technol 4:954–968. doi:10.1007/s11947-011-0512-z

Mathew AG, Cissell R, Liamthong S (2007) Antibiotic resistance in bacteria associated with food animals: a United States perspective of livestock production. Foodborne Pathog Dis 4:115–133. doi:10.1089/fpd.2006.0066

Mattar J, Turk M, Nonus M et al (2013) Electro-stimulation of *Saccharomyces cerevisiae* wine yeasts by pulsed electric field and its effect on fermentation performance. arXiv:1304.5681 [physics, q-bio]

McMillan JR, Watson IA, Ali M, Jaafar W (2013) Evaluation and comparison of algal cell disruption methods: microwave, waterbath, blender, ultrasonic and laser treatment. Appl Energy 103:128–134. doi:10.1016/j.apenergy.2012.09.020

Mhemdi H, Bals O, Grimi N, Vorobiev E (2012) Filtration diffusivity and expression behaviour of thermally and electrically pretreated sugar beet tissue and press-cake. Sep Purif Technol 95:118–125. doi:10.1016/j.seppur.2012.04.031

Miklavcic D (2012) Network for development of electroporation-based technologies and treatments: cOST TD1104. J Membr Biol 245:591–598. doi:10.1007/s00232-012-9493-8

Miklavcic D, Towhidi L (2010) Numerical study of the electroporation pulse shape effect on molecular uptake of biological cells. Radiol Oncol 44:34–41. doi:10.2478/v10019-010-0002-3

Miklavcic D, Sersa G, Brecelj E et al (2012) Electrochemotherapy: technological advancements for efficient electroporation-based treatment of internal tumors. Med Biol Eng Comput 50:1213–1225. doi:10.1007/s11517-012-0991-8

Miklavčič D, Mali B, Kos B et al (2014) Electrochemotherapy: from the drawing board into medical practice. Biomed Eng Online 13:29. doi:10.1186/1475-925X-13-29

Morales-de la Pena M, Elez-Martinez P, Martin-Belloso O (2011) Food preservation by pulsed electric fields: an engineering perspective. Food Eng Rev 3:94–107. doi:10.1007/s12393-011-9035-7

Morren J, Roodenburg B, de Haan SWH (2003) Electrochemical reactions and electrode corrosion in pulsed electric field (PEF) treatment chambers. Innov Food Sci Emerg Technol 4:285–295. doi:10.1016/S1466-8564(03)00041-9

Mosqueda-Melgar J, Raybaudi-Massilia RM, Martin-Belloso O (2008a) Non-thermal pasteurization of fruit juices by combining high-intensity pulsed electric fields with natural antimicrobials. Innov Food Sci Emerg Technol 9:328–340. doi:10.1016/j.ifset.2007.09.003

Mosqueda-Melgar J, Raybaudi-Massilia RM, Martin-Belloso O (2008b) Combination of high-intensity pulsed electric fields with natural antimicrobials to inactivate pathogenic microorganisms and extend the shelf-life of melon and watermelon juices. Food Microbiol 25:479–491. doi:10.1016/j.fm.2008.01.002

Mosqueda-Melgar J, Raybaudi-Massilia RM, Martin-Belloso O (2012) Microbiological shelf life and sensory evaluation of fruit juices treated by high-intensity pulsed electric fields and antimicrobials. Food Bioprod Process 90:205–214. doi:10.1016/j.fbp.2011.03.004

Movahed S, Li D (2012) Electrokinetic transport through the nanopores in cell membrane during electroporation. J Colloid Interface Sci 369:442–452. doi:10.1016/j.jcis.2011.12.039

Neal RE 2nd, Garcia PA, Robertson JL, Davalos RV (2012) Experimental characterization and numerical modeling of tissue electrical conductivity during pulsed electric fields for irreversible electroporation treatment planning. IEEE Trans Biomed Eng 59:1076–1085. doi:10.1109/TBME.2012.2182994

Neu WK, Neu JC (2009) Theory of electroporation. In: Cardiac bioelectric therapy: mechanisms and practical implications. Springer, New York

Odriozola-Serrano I, Aguiló-Aguayo I, Soliva-Fortuny R, Martín-Belloso O (2013) Pulsed electric fields processing effects on quality and health-related constituents of plant-based foods. Trends Food Sci Technol 29:98–107. doi:10.1016/j.tifs.2011.10.003

Olaizola M (2003) Commercial development of microalgal biotechnology: from the test tube to the marketplace. Biomol Eng 20:459–466. doi:10.1016/S1389-0344(03)00076-5

Pataro G, Ferrari G, Donsi F (2011) Mass transfer enhancement by means of electroporation. In: Markoš J (ed) Mass transfer in chemical engineering processes. http://www.intechopen.com/books/mass-transfer-in-chemical-engineeringprocesses/mass-transfer-enhancement-by-means-of-electroporation

Pavselj N, Miklavcic D (2008) Numerical models of skin electropermeabilization taking into account conductivity changes and the presence of local transport regions. IEEE Trans Plasma Sci 36:1650–1658. doi:10.1109/TPS.2009.928715

Petryk M, Vorobiev E (2013) Numerical and analytical modeling of solid–liquid expression from soft plant materials. AIChE J 59:4762–4771. doi:10.1002/aic.14213

Phoon PY, Galindo FG, Vicente A, Deimek P (2008) Pulsed electric field in combination with vacuum impregnation with trehalose improves the freezing tolerance of spinach leaves. J Food Eng 88:144–148. doi:10.1016/j.jfoodeng.2007.12.016

Polak A, Bonhenry D, Dehez F et al (2013) On the electroporation thresholds of lipid bilayers: molecular dynamics simulation investigations. J Membr Biol 246:843–850. doi:10.1007/s00232-013-9570-7

Praporscic I, Lebovka N, Vorobiev E, Mietton-Peuchot M (2007) Pulsed electric field enhanced expression and juice quality of white grapes. Sep Purif Technol 52:520–526. doi:10.1016/j.seppur.2006.06.007

Pucihar G, Kotnik T, Miklavcic D, Teissie J (2008) Kinetics of transmembrane transport of small molecules into electropermeabilized cells. Biophys J 95:2837–2848. doi:10.1529/biophysj.108.135541

Pucihar G, Krmelj J, Reberšek M et al (2011) Equivalent pulse parameters for electroporation. IEEE Trans Biomed Eng 58:3279–3288. doi:10.1109/TBME.2011.2167232

Puertolas E, Luengo E, Alvarez I, Raso J (2012) Improving mass transfer to soften tissues by pulsed electric fields: fundamentals and applications. In: Doyle MP, Klaenhammer TR (eds) Annual review of food science and technology, vol 3. Annual Reviews, Palo Alto, pp 263–282

Pulz O, Gross W (2004) Valuable products from biotechnology of microalgae. Appl Microbiol Biotechnol 65:635–648. doi:10.1007/s00253-004-1647-x

Qin BL, Pothakamury UR, BarbosaCanovas GV, Swanson BG (1996) Nonthermal pasteurization of liquid foods using high-intensity pulsed electric fields. Crit Rev Food Sci Nutr 36:603–627

Raffy S, Lazdunski C, Teissie J (2004) Electroinsertion and activation of the C-terminal domain of colicin A, a voltage gated bacterial toxin, into mammalian cell membranes. Mol Membr Biol 21:237–246. doi:10.1080/09687680410001711632

Raso J, Heinz V (2010) Pulsed electric fields technology for the food industry: fundamentals and applications. Springer, New York

Raso J, Alvarez I, Condon S et al (2014a) PEFSchool Homepage. http://pefschool.unizar.es/. Accessed 25 Feb 2014

Raso J, Miklavčič D, Marjanovič I, Mahnič-Kalamiza S (2014b) COST TD1104 March 2014 Newsletter. In: electroporation.net: the official COST TD1104 Website. http://electroporation.net/News/March-2014. Accessed 25 Feb 2014

Rauh C, Krauss J, Ertunc O, Delgado A (2010) Numerical simulation of non-thermal food preservation. In: Psihoyios G, Tsitouras C (eds) Numerical analysis and applied mathematics, vol I–III. American Institute Physics, Melville, pp 1692–1695

Rebersek M, Miklavcic D (2010) Concepts of electroporation pulse generation and overview of electric pulse generators for cell and tissue electroporation. Advanced electroporation techniques in biology and medicine. CRC Press, Boca Raton, pp 323–339

Rebersek M, Miklavcic D, Bertacchini C, Sack M (2014) Cell membrane electroporation—part 3: the equipment. IEEE Electr Insul Mag 30:8–18. doi:10.1109/MEI.2014.6804737

Rems L, Ušaj M, Kandušer M et al (2013) Cell electrofusion using nanosecond electric pulses. Sci Rep. doi:10.1038/srep03382

Rieder A, Schwartz T, Schoen-Hoelz K et al (2008) Molecular monitoring of inactivation efficiencies of bacteria during pulsed electric field treatment of clinical wastewater. J Appl Microbiol 105:2035–2045. doi:10.1111/j.1365-2672.2008.03972.x

Rols MP, Teissié J (1990) Electropermeabilization of mammalian cells. Quantitative analysis of the phenomenon. Biophys J 58:1089–1098. doi:10.1016/S0006-3495(90)82451-6

Roodenburg B, Morren J, Berg HE, de Haan SWH (2005) Metal release in a stainless steel pulsed electric field (PEF) system: part II. The treatment of orange juice; related to legislation and treatment chamber lifetime. Innov Food Sci Emerg Technol 6:337–345. doi:10.1016/j.ifset.2005.04.004

Sabri N, Pelissier B, Teissié J (1996) Electropermeabilization of intact maize cells induces an oxidative stress. Eur J Biochem 238:737–743

Sack M, Schultheiss C, Bluhm H (2005) Triggered Marx generators for the industrial-scale electroporation of sugar beets. IEEE Trans Ind Appl 41:707–714. doi:10.1109/TIA.2005.847307

Sack M, Sigler J, Eing C et al (2010a) Operation of an electroporation device for grape mash. IEEE Trans Plasma Sci 38:1928–1934. doi:10.1109/TPS.2010.2050073

Sack M, Sigler J, Frenzel S et al (2010b) Research on industrial-scale electroporation devices fostering the extraction of substances from biological tissue. Food Eng Rev 2:147–156. doi:10.1007/s12393-010-9017-1

Sagarzazu N, Cebrián G, Pagán R et al (2013) Emergence of pulsed electric fields resistance in *Salmonella enterica* serovar Typhimurium SL1344. Int J Food Microbiol 166:219–225. doi:10.1016/j.ijfoodmicro.2013.07.001

Salengke S, Sastry SK, Zhang HQ (2012) Pulsed electric field technology: modeling of electric field and temperature distributions within continuous flow PEF treatment chamber. Int Food Res J 19:1137–1144

Satkauskas S, Bureau MF, Puc M et al (2002) Mechanisms of in vivo DNA electrotransfer: respective contributions of cell electropermeabilization and DNA electrophoresis. Mol Ther 5:133–140. doi:10.1006/mthe.2002.0526

Saulis G (2010) Electroporation of cell membranes: the fundamental effects of pulsed electric fields in food processing. Food Eng Rev 2:52–73. doi:10.1007/s12393-010-9023-3

Saw NMMT, Riedel H, Cai Z et al (2012) Stimulation of anthocyanin synthesis in grape (*Vitis vinifera*) cell cultures by pulsed electric fields and ethephon. Plant Cell Tissue Organ Cult 108:47–54. doi:10.1007/s11240-011-0010-z

Sel D, Cukjati D, Batiuskaite D et al (2005) Sequential finite element model of tissue electropermeabilization. IEEE Trans Biomed Eng 52:816–827. doi:10.1109/TBME.2005.845212

Shayanfar S, Chauhan OP, Toepfl S, Heinz V (2013) The interaction of pulsed electric fields and texturizing: antifreezing agents in quality retention of defrosted potato strips. Int J Food Sci Technol 48:1289–1295. doi:10.1111/ijfs.12089

Shin JK, Lee SJ, Cho HY et al (2010) Germination and subsequent inactivation of *Bacillus subtilis* spores by pulsed electric field treatment. J Food Process Preserv 34:43–54. doi:10.1111/j.1745-4549.2008.00321.x

Shynkaryk MV, Lebovka NI, Vorobiev E (2008) Pulsed electric fields and temperature effects on drying and rehydration of red beetroots. Dry Technol 26:695–704. doi:10.1080/07373930802046260

Skrede A, Mydland LT, Ahlstrom O et al (2011) Evaluation of microalgae as sources of digestible nutrients for monogastric animals. J Anim Feed Sci 20:131–142

Sobrino-Lopez A, Martin-Belloso O (2010) Review: potential of high-intensity pulsed electric field technology for milk processing. Food Eng Rev 2:17–27. doi:10.1007/s12393-009-9011-7

Spolaore P, Joannis-Cassan C, Duran E, Isambert A (2006) Commercial applications of microalgae. J Biosci Bioeng 101:87–96. doi:10.1263/jbb.101.87

Stirke A, Zimkus A, Ramanaviciene A et al (2014) Electric field-induced effects on yeast cell wall permeabilization. Bioelectromagnetics 35:136–144. doi:10.1002/bem.21824

Straessner R, Eing C, Goettel M et al (2013) Monitoring of pulsed electric field-induced abiotic stress on microalgae by chlorophyll fluorescence diagnostic. IEEE Trans Plasma Sci 41:2951–2958. doi:10.1109/TPS.2013.2281082

Toepfl S (2006) Pulsed electric fields (PEF) for permeabilization of cell membranes in food-and bioprocessing: applications, process and equipment design and cost analysis. University of Technology, Berlin

Toepfl S (2011) Pulsed electric field food treatment: scale up from lab to industrial scale. Proc Food Sci 1:776–779. doi:10.1016/j.profoo.2011.09.117

Toepfl S (2012) Pulsed electric field food processing–industrial equipment design and commercial applications. Stewart Postharvest Rev 8:1–7. doi:10.2212/spr.2012.2.4

Toepfl S, Heinz V (2008) The stability of uncooked cured products use of pulsed electric fields to accelerate mass transport operations in uncooked cured products. Fleischwirtschaft 88:127–130

Toepfl S, Heinz V, Knorr D (2005) Overview of pulsed electric field processing for food. In: Sun D-W (ed) Emerging technologies for food processing. Academic Press, London, pp 69–97

Toepfl S, Heinz V, Knorr D (2006) Applications of pulsed electric fields technology for the food industry. In: Raso J, Heinz V (eds) Pulsed electric fields technology for the food industry. Springer, New York, pp 197–221

Toepfl S, Heinz V, Knorr D (2007) History of pulsed electric field treatment. In: Lelieveld HLM, Notermans S, de Haan SWH (eds) Food Preservation by pulsed electric fields. Woodhead Publishing, Cambridge, pp 9–39

Turk MF, Billaud C, Vorobiev E, Baron A (2012a) Continuous pulsed electric field treatment of French cider apple and juice expression on the pilot scale belt press. Innov Food Sci Emerg Technol 14:61–69. doi:10.1016/j.ifset.2012.02.001

Turk MF, Vorobiev E, Baron A (2012b) Improving apple juice expression and quality by pulsed electric field on an industrial scale. LWT Food Sci Technol 49:245–250. doi:10.1016/j.lwt.2012.07.024

Usaj M, Trontelj K, Miklavcic D, Kanduser M (2010) Cell–cell electrofusion: optimization of electric field amplitude and

hypotonic treatment for mouse melanoma (B16-F1) and Chinese Hamster ovary (CHO) cells. J Membr Biol 236:107–116. doi:10.1007/s00232-010-9272-3

Vanthoor-Koopmans M, Wijffels RH, Barbosa MJ, Eppink MHM (2013) Biorefinery of microalgae for food and fuel. Bioresour Technol 135:142–149. doi:10.1016/j.biortech.2012.10.135

Velickova E, Tylewicz U, Dalla Rosa M et al (2013) Effect of vacuum infused cryoprotectants on the freezing tolerance of strawberry tissues. LWT Food Sci Technol 52:146–150. doi:10.1016/j.lwt.2011.09.013

Vidal O (2014) First pulsed electric field (PEF) application at industrial scale in beet sugar industry. Sugar Ind 139:37–39

Vidal OP, Vorobiev E (2011) Procédé et installation de traitement des tissus végétaux pour en extraire une substance végétale, notamment un jus. International Patent No 138248

Vorobiev E, Lebovka N (2008) Pulsed-electric-fields-induced effects in plant tissues: fundamental aspects and perspectives of applications. Electrotechnologies for extraction from food plants and biomaterials. Springer, New York, pp 39–81

Vorobiev E, Lebovka N (2010) Enhanced extraction from solid foods and biosuspensions by pulsed electrical energy. Food Eng Rev 2:95–108. doi:10.1007/s12393-010-9021-5

Wesierska E, Trziszka T (2007) Evaluation of the use of pulsed electrical field as a factor with antimicrobial activity. J Food Eng 78:1320–1325. doi:10.1016/j.foodeng.2006.01.002

Widjaja A, Chien C-C, Ju Y-H (2009) Study of increasing lipid production from fresh water microalgae *Chlorella vulgaris*. J Taiwan Inst Chem Eng 40:13–20. doi:10.1016/j.jtice.2008.07.007

Wijffels RH, Barbosa MJ, Eppink MHM (2010) Microalgae for the production of bulk chemicals and biofuels. Biofuels Bioprod Biorefining 4:287–295. doi:10.1002/bbb.215

Wiyarno B, Yunus RM, Mel M (2011) Extraction of algae oil from *Nannocloropsis* sp.: a study of soxhlet and ultrasonic-assisted extractions. J Appl Sci 11:3607–3612. doi:10.3923/jas.2011.3607.3612

Yarmush ML, Golberg A, Serša G et al (2014) Electroporation-based technologies for medicine: principles, applications, and challenges. Annu Rev Biomed Eng 16:295–320. doi:10.1146/annurev-bioeng-071813-104622

Ye H, Huang L-L, Chen S-D, Zhong J-J (2004) Pulsed electric field stimulates plant secondary metabolism in suspension cultures of *Taxus chinensis*. Biotechnol Bioeng 88:788–795. doi:10.1002/bit.20266

Yeom HW, McCann KT, Streaker CB, Zhang QH (2002) Pulsed electric field processing of high acid liquid foods: a review. Adv Food Nutr Res 44:1–32

Zbinden MDA, Sturm BSM, Nord RD et al (2013) Pulsed electric field (PEF) as an intensification pretreatment for greener solvent lipid extraction from microalgae. Biotechnol Bioeng 110:1605–1615. doi:10.1002/bit.24829

Zorec B, Préat V, Miklavčič D, Pavšelj N (2013) Active enhancement methods for intra- and transdermal drug delivery: a review. Slov Med J. doi:10.6016/1889

2.2 A literature review on mass transport and thermal relations in electroporated biological tissue

Mass transport in electroporation is a complex phenomenon or rather a set of multiple physical phenomena, the understanding of which is crucial for a sound understanding and evaluation of electroporation effects on treated material. This literature review is a brief overview of the current published works on the subject, summarizing the main results and conclusions as well as methodology, where the main purpose is to present approaches to elucidate this important aspect of electroporation and the applications based on this treatment.

2.2.1 Introduction

Electroporation or pulsed electric field application, as introduced in the 2.1 section of this thesis, is a method using the electric field, established in the treated medium or material using one or a series of electrical impulses of high voltage, ultimately resulting in changes of the cell membrane properties of biological cells. These changes then facilitate mass transport into or out of the cell across the membrane [1], [2], which would normally inhibit or prohibit this transport as cell membrane normally possesses a quality of the so-called *selective permeability*.

Electroporation is used in a multitude of different applications from various domains of research, clinics, and industry. In biomedicine, we find applications for cancer treatment [3], [4], gene transfection [5], [6], transdermal transport of drugs and genes [7], [8]. In the food processing industry, electroporation is more commonly referred to as pulse electric field treatment and used as means of vegetable or animal tissue pre-treatment for enhancing extraction of juices or valuable compounds [9]–[11], pasteurization and / or sterilization [12]–[14], tissue impregnation [15], [16] and even cooking [17]. There are also intensively researched environmental applications e.g. wastewater treatment [18] and harvesting biocompounds from bioreactors such as algae [13], [19]. With a number of these applications, the principal objective is the insertion of a solute or solution into the biological cell, or their extraction. This is especially the case with biomedical applications and food processing applications, where transport of either genes or drugs, or of valuable intracellular juices and compounds is the principal objective of electroporation application.

To be able to evaluate and possibly quantify mass transport from the extracellular medium into the cell, or in the opposite direction, and to be able to determine the optimal parameters of the electroporation protocol for reaching our objective, one should be capable of evaluating and characterizing the processes governing mass transport and the factors influencing the extent of this transport. To this end, numerous studies have been and still are being conducted in research

laboratories worldwide. These studies comprise advances in development of theoretical models of electroporation and mass transport, mathematical modelling techniques of the basic principles (e.g. modelling pore formation and evolution) as well as macroscopic level (e.g. modelling kinetics), computer-aided simulations (e.g. calculating field distribution in tissue, simulated extraction kinetics), and on the other hand, these theoretical advances and models are supplemented by or validated by conducting in vitro, ex vivo and in vivo experiments for model validation and further improvement, as well as trials in pilot plants and industrial implementations for evaluations of treatment economic feasibility.

The purpose of this literature review is to give a short overview over the results of some of the more recent studies in this domain, and to evaluate the current state of the art in the field of electroporation research and knowledge on related mass transport processes. This should also point the reader in the direction of further reading on the advances and future heading of electroporation research.

2.2.2 Analysis of processes and physio-chemical models

2.2.2.1 Modelling mass transport in aqueous solutions

The medium of a biological cell both extra- and intracellularly is an aqueous solution. These solutions contain, alongside the substances of interest, also a varying quantity of small ions. If these ionic concentrations are high in comparison to concentrations of solutes of interest, we can exclude the contribution of these small ions to mass transport from further analysis. This is important since many models already exist that consider the electrolyte-cell system and the related phenomena are extensively studied and understood [20], [21].

When the externally-imposed electric field is present in the medium, the charged particles are subject to an electric force. This results in an additional mass transport (electrophoresis) or the transport of the medium together with the solutes (electroosmosis). These two contributions are superimposed to the effect of passive thermodynamic diffusion. Diffusion is the transport of solute particles due to a difference in the solute concentration, i.e. the presence of a concentration gradient and the thermic energy of the particles. We can consider the resulting (i.e. sum of the electrokinetic effects and diffusion) net mass transport as electrodiffusion with a current density (of electrodiffusion). The electrodiffusion current is related via a continuity equation with a local change in solute concentration. The result is a differential equation with temporal and spatial derivatives, whose analytical solution cannot be obtained, in general for a 4-D space (3-D plus time). This is why we find, in [20], a simplification to a single dimension, and a discretization of the 1-D space. The final result is a non-linear model for the current of electrodiffusion that can be

used to analyse the influence of solute concentration and the electro-thermic potential to mass transport in discrete spatial units called compartments. Studies using this model incorporate a local quantification of the final solute concentration due to electrodiffusion, and permit the characterization of the stationary state (at the impermeable barriers), the velocity of electrodiffusion, etc. This model is of potential importance since it forms a theoretical basis for coupling a model of mass transport with existing models of electric field distribution in aqueous solutions and an electroporation (pore evolution) model. This is an important modelling paradigm that the present thesis aims to further support by presenting a similar model, given in the section 4 of the thesis (Paper II), but built for application to study of tissues rather than aqueous suspensions of cells.

2.2.2.2 Modelling mass transport in and out of a single cell

When reviewing literature presenting studies on mass transport in or out of individual cells (i.e. cells not forming tissue nor embedded into an extracellular matrix) that have been subjected to electroporation, several different approaches can be identified. Since the subject of study is transmembrane transport through via the supposed defects (termed pores) in the cell membrane, problem treatment usually begins with a model of electroporation. Such a model solves the electrical problem (field strength and energy delivered to the membrane) and the thermodynamic problem (a statistical description of the stochastic pore formation, evolution and annihilation processes) for the cell membrane during pulse application. In a sense, the model attempts to link a description of pore (population) formation and evolution with the electroporation treatment parameters (field orientation, pulse length, shape, amplitude, and number, pulse repetition frequency, etc.) and material properties (conductivity, solution composition, membrane composition, cell size and spatial distributions).

One of the first models describing mass transport between a cell and its exterior medium is presented in [22] and constructed as a two-compartment pharmacokinetic model. Its parameters are tuned in the sense that allows the model to give a good approximation of the Lucifer Yellow (LY) dye into DC-3F cells for various electroporation protocols. Thus, it models mass transport in experiments *in vitro* using small molecules such as those of the LY dye. Since it is a pharmacokinetic model, it gives no information on the contributions of individual components of the transport to the total observed transport, i.e. it cannot be used to differentiate between the net effects of electrophoresis, electroosmosis and free solute diffusion. In this respect it is an empirical model.

Contrary to the model just presented, an important reference in the field is described in [23], whose authors report on results of an *in vitro* study of propidium iodide (PI) uptake by CHO cells during and after electroporation, and compare the observed experimental results with the mathematical Nernst-Planck model of transport by electrodiffusion, which is also found used by many other sources (see e.g. [20], [20], [24]–[26]). Important conclusions of the study presented therein seem to indicate that transport of small molecules such as PI starts during the electroporation pulse, however, not immediately after the electric field is established. The delay depends on the parameters of the electric pulses applied. The authors noticed a slower uptake of PI molecules following pulse application, which was explained by the lack of the electrophoretic component that is no longer driving transport since there is no externally imposed electric field present. The resulting transport is governed by free solute diffusion, which is significantly slower than electrophoresis, and is eventually quenched by the resealing of the membrane and the re-establishing of the normal selective permeability of the membrane (provided that the membrane can recover). Taking into consideration the dominant contribution of electrophoresis during pulse application and of diffusion afterwards, the Nernst-Planck set of equations successfully approximated the experimental data with high fidelity. The main conclusion of the cited study is, that the bulk of the PI molecule transport takes place after the electric pulse, and should therefore be attributed to diffusion. This analysis applies to relatively small molecules of PI whose transport was studied. By contrast, we find in e.g. [27], a report on a study with introduction of very large molecules (DNA) into target cells, where electrophoresis has been identified as the necessary component to transmembrane transport and diffusion to be of negligible significance.

One of the more recent works from the field of modelling mass transport in single cells is described in [24], heavily references the previously described work presented in [23], and directly compares simulation results with results of *in vitro* experiments reported on in [28]. In [24], the model is a based on a temporal and spatial description of free ion and small molecule concentrations (PI, some drugs of size smaller than several kDa, etc.), and uses the Nernst-Planck set of equations with addition of equations describing a drain or source of solutes due to chemical reactions and equations accounting for the electrokinetic mechanism known as FASS (i.e. Field Amplified Sample Stacking, see [29]). As a model of electroporation (statistics on pore size, number, etc.), the authors employ the Asymptotic Smoluchowski Equation (ASE) [30], [31], which represents one of the possible thermodynamics-based models of electroporation. Coupled to this model is a modified system of Nernst-Planck equations for electrodiffusive current, where additionally the effect of chemical reactions is also considered. These chemical reactions contribute to the solute distribution with local drains or sources of the solute that enters as a reagent

or is produced in a chemical reaction. Results of simulations with this model lead to several interesting conclusions. The mechanism of field amplified sample stacking, caused by the spatial gradient in particle velocity in electrophoretic drag during the pulse, can significantly (by a factor greater than 10) increase the intracellular concentration of the observed solute as compared to its extracellular concentration. Under ideal conditions, the FASS mechanism is the factor limiting the maximal attainable intracellular concentration, which would, under these ideal conditions, be proportional to the ratio between the extra- and intracellular electric conductivity. The results also give evidence of the robustness of this mechanism, since a change in two orders of magnitude in the degree of simulated permeabilization (indicative of the number and size of the pores) did not cause a significant difference in final extra- and intracellular concentrations of the studied solute. We could consequentially draw a conclusion that post-electroporation diffusion has a negligible effect to final solute concentration, however, this would be irreconcilable with results presented in [23]. The authors thus do admit, that the effect of FASS needs to be evaluated on a model membrane with a realistic estimate of its permeability, and that the used ASE model of electroporation probably overestimates the velocity of pore resealing and transmembrane transport inhibition by the membrane in recovery. Parameters of electroporation such as the amplitude, number and duration of the pulse are also thought to play an important role [32], as well as the species of the ions or molecules under study. In order to compare simulation results with those of experiments using PI dye *in vitro*, these parameters would most likely have to be more closely matched for a direct comparison and evaluation. The latter finding indicates a strong need for future research in this direction.

The significance of electrokinetic phenomena – electrophoresis and electroosmosis – is also highlighted in [26]. In this study, the authors focused on the problem of extremely low pore dimensions on the nanometre scale (called nanopores) that appear as a result of electric pulse application. These small dimensions are problematic since they can cause classic models of electrokinetics to fail to describe the phenomena at this scale. One issue in example is the electric field which is established in such a nano-channel by the surface charges and the local ionic distribution. Taking the transmembrane voltage into account and the electric potential due to the external electric field, the authors write the Poisson equation to calculate the electric potential distribution in the nano-channel (nano-pore). For three spaces or compartments – the extracellular compartment in the immediate vicinity of the pore, the pore itself, and the intracellular compartment in the immediate vicinity of the pore – they give the Nernst-Planck equations for the electroosmotic, electrophoretic, and diffusive influence on the ionic concentrations, as well as the continuity equation and the Navier-Stokes equations for liquid flow (pressure, velocity). The

complete system of these highly coupled equations represents a complex numerical model of mass transport through a narrow nano-channel in the cell membrane. Model results (simulated) indicate that there is a significantly high electric field present in the pore, which strongly influences the electrophoretic effects. During the pulse, this field and its effects render the influence of free solute diffusion insignificant. Also, the contribution of electroosmosis, which has been largely overlooked or neglected and whose influence on transport is poorly understood in the field of electroporation, seems to increase if the radius of the pore increases, with respect to the contribution of electrophoresis. In the discussion, the authors compare their results with the experimental study presented in [23]. The conclusion of this comparison is that although diffusion during the electric pulse is about a thousand times slower and insignificantly contributes to the net transport of the solutes, it is on the other hand a thousand times longer after the pulse application when there is no longer an external field present and the electrokinetic mechanisms are negligible. The effect of diffusion in electroporation is therefore not negligible, however, it can be neglected for the short period of time of several micro- to milliseconds during pulse application (note that "classical" electroporation with pulses of micro- to millisecond duration has been considered and not "nano-electroporation" using extremely short pulses of higher intensity). These observations and deductions confirm the experimental results reported on in [23] and explains the importance of free solute diffusion. Among the other important results of this study is also the observed difference between the "front" and the "back" side of the cell (respective of the electric field orientation), between which there is a significant difference in mass transport (in terms of solute flux intensity).

In recent years, there has been an ever increasing interest in the scientific community working with electric fields and biological material in electroporation using extremely short pulses, termed nanopulses. The work presented in [33] attempts to introduce a model to estimate the mass transport before vs. after application using nanopulses. The model is based on the Nernst-Planck equation for electrodiffusion, modified by an addition of a factor accounting for the interaction between the solute and the pore due to comparable sizes of the two, and for the effect of the charges on the solute and those on the surface of the lipid pore during transport. The conclusions of the analysis using model simulations indicate that the majority of the transport facilitated by nanopulses occurs after the pulse application, while the transport during the pulse is insignificant due to the extremely low pulse duration (~ns). The primary consequence of the nanopulses is therefore most probably establishing and/or maintaining a large population of small pores in the membrane that facilitate diffusion of small ions after the pulse application, when the electrokinetic components of transport are no longer a factor.

2.2.2.3 Modelling mass transport in dense suspensions, monolayers, and tissues

As compared to studies of mass transport in idealised model suspensions of cells or isolated cells in suspensions, for which there exists already a substantial body of literature, only few sources exist presenting approaches for studying more realistic situations, where cells are not spherical, but attached to the bottom of a dish and of irregular shapes, or connected into a 3-D structure forming tissue. One study, presented in [34], concerns itself with the connection between the induced transmembrane voltage on molecule transport in cells of various shapes, in monolayers and in tissues. The findings indicate that mass transport in electroporation is limited for both cells of regular as well as of irregular shapes to the surface areas of the cells where the induced transmembrane voltage is the highest. The theoretical models were found to reflect well the conditions in real isolated cells, while for clusters of cells, additional information is required about the electrical properties of the contacts between the cells. In other words, knowledge is required as to whether the cells are electrically interconnected (coupled) or not. The answer to this question is not necessarily invariable, since the response of the cells in clusters predominantly depends on the electric field strength of the field to which the cells are exposed. At field strengths that are sufficient for electroporation, the cells respond as electrically isolated, while at lower fields, they behave as electrically connected. These results indicate that high electric field strengths influence the intercellular channels, thus changing the response of the cells as compared to an electrically unexcited state or normal conditions.

2.2.3 Specific approaches by domain of application

2.2.3.1 Enhancing drug transport by electroporation

Since electroporation has become an important technique in medicine, as it is used in e.g. gene therapy and electrochemotherapy, one must be able to predict or quantify the resulting mass transport during and after electroporation. In [35] we find an account of the development of a macroscopic-level mathematical model intended for analysis of mass transport in cells in tissue electroporation. The model combines a macroscopic model of the electric field distribution in tissue in the vicinity of the inserted needle electrodes, with the model of mass transport on the cellular level and the tissue level. It was designed to model a typical setup in electrochemotherapy, where we attempt to use reversible electroporation to introduce the chemotherapeutic drug bleomycin in cells of cancer tissue.

The model is based on a model published in [30], [31], that describes pore evolution in electroporation. To this model, the Fick's law of diffusion is added (coupled), relating the diffusive flux with the transmembrane concentration gradient, the diffusion constant and the membrane thickness. To this system, an additional equation is added describing extracellular diffusion. The model provides for two very long, parallel, thin needle electrodes inserted into tissue, which renders the problem two-dimensional.

The main result of the model is a spatio-temporal drug (bleomycin) distribution in cells comprising cancerous tissue, indicating, where there is a sufficient permeation of the drug into the cells and how long the process takes to complete (i.e. achieve sufficient levels of intracellular drug concentration).

Since electroporation is a complex phenomenon, dependent on a large number of parameters, a simple model as described in [35] gives a valuable framework for modelling phenomena in electrochemotherapy and is a promising invitation for further development of more complex and reliable models.

2.2.3.2 Skin applications

The skin is an important subject of interest in electroporation research, since electroporation can facilitate the transport of drugs into the organism via the skin – i.e. the transdermal transport, but also for DNA vaccination [8]. The layer of skin that represents the greatest barrier to the transdermal introduction of drugs is its top layer, called the stratum corneum. In [7] (see also [36]), a model of skin electroporation is presented, accounting for the physiological skin structure and the thermos-physical behaviour of the stratum corneum. The results of previous works indicate to the existence of microscopic aqueous pores or defects in the stratum corneum, whose creation can be attributed to the effects of electroporation. These defects improve the otherwise poor permeability of the stratum corneum layer for mass transport. These defects also result in a substantial decrease in the electrical resistance of the skin, and facilitate secondary effects that were observed such as electrophoresis and heating. All of these effects have been identified as important factors influencing transdermal drug delivery, and are analysed in [7]. The analysis presented is based on the model of heat distribution and a mass transport model. The influence of changes or variations in parameters are evaluated with the aid of observing the so-called Local Transport Regions or LTRs, regions of highly increased conductivity (electrical, ionic, etc.). The analysis involves a study of the development and properties of these transport regions and of the resulting mass transport via these regions. The conclusions of the study indicate that the transport itself and the local transport regions are heavily dependent on the parameters that are influencing

the electric field distribution in the stratum corneum, and additionally, the changes in the electrical conductivity of the stratum corneum have a stronger effect on the mass transport through the skin as compared to changes in permeability to a specific substance (i.e. so-called "molecular permeability"). Moreover, for charged molecules of high molecular weight (e.g. DNA), the electrophoretic forces dominate in importance over diffusion. The final conclusion of this study indicates that electroporation-facilitated transdermal transport is more sensitive to parameters influencing the electrical conductivity, than to parameters that influence the transport coefficients.

Problems, similar to the ones facing researchers in studying transdermal transport, are in treating highly heterogeneous tissues in plants, such as leaves. These also can be coated on the surface with material or substances that in their permeability for molecules and electrical properties closely resemble skin. While models of electric field distribution have recently been proposed [37] in these plant tissues, there is a lack of models of mass transport that would complement this knowledge and help elucidate the phenomena in valuable compounds recovery from various leafs and stems of plants.

2.2.3.3 Modelling mass transport in the field of food processing applications of electroporation

Electroporation or pulsed electric field treatment is often used as a method of pre-treating the raw material to enhance drying, juice extraction, etc. (see the introductory section 2.1 (Paper I) for a comprehensive review of applications).

The basic mathematical model in studying mass transport in food processing applications is often the so-called *two-exponential* model, as described in e.g. [38]–[41]. The model describes the two-stage kinetics of either solute diffusion or juice extraction by pressing post-electroporation. If studying solute transport only (without pressing), the first stage or the first kinetic is governed by and modelled as the contribution of washing – the convective component. Due to the loss of turgor pressure, juice is usually expressed out of the electroporated tissue without any external pressure application and collects at or near the surface of the sample. During the initial stage of diffusion, this solute-rich juice is mixed with the solute (water) into which the samples are submerged, and results in a rapid increase in the measured solute concentration in the surrounding liquid. This kinetic normally follows a rapidly decreasing exponential function. The second component, also following an exponentially decreasing function, albeit a slower one, models the much slower transport due to diffusion of solute out of the tissue sample, which occurs due to the difference between the concentration of solute in the cellular juices and the liquid used to "wash" the sample.

The described two-exponential model provides a good correspondence between simulated and experimentally observed kinetics of solute extraction, and is relevant to industrial processes. Its deficiency is that it is fundamentally an empirically-obtained phenomenological model, whose parameters are difficult or possibly impossible to couple to existing models of electroporation, electric field distribution, etc. This difficulty to upgrade or extend the model stems from the fact that it essentially treats electroporated tissue as completely homogeneous material, and there are no parameters reflecting the phenomena at the interfaces (such as the cellular membrane) in the model that could be used to couple these models of mass transport with other models. These models are also not applicable in any other field of electroporation application, and cannot help in understanding e.g. transdermal transport or transport of drugs/genes in electrochemotherapy/gene therapy.

2.2.4 Other literature relevant to problems of mass transport in biological material

2.2.4.1 Vascular permeability and the blood brain barrier

Electroporation has been shown to have important effects with beneficial consequences when studied in applications to complex biological tissues. In particular, several effects on the vascular system and the blood-brain barrier (BBB) have been observed and studied in the field of biomedical applications of electroporation.

Electroporation of living animal tissue is known to result in a state known as vascular lock [42], [43] with important consequences for electrochemotherapy (ECT), as it results in a prolonged retention of the chemotherapeutic drug that is administered intratumorally in the region of the tumour following electroporation. This in turn, due to higher extracellular concentrations of the drug in the tumour region, improves delivery of the chemotherapeutic into the cell by diffusion across the permeabilized cell membrane. The effect of vascular lock has been studied more closely and generally to characterize the effects of electroporation on the vascular structures and system, and it has been determined, that electroporation also increases the permeability of the vascular endothelium that under normal conditions controls the transport of plasma contents across the blood vessel wall. Electroporation has been shown to increase the permeability of the blood vessel wall for macromolecules, which normally do not extravasate from blood into skin interstitium in homeostatic conditions. A study presented in [44] combines mathematical modelling with *in vivo* measurements to study extravasation of two molecules of different sizes (comparable to antibodies and plasmid DNA) to evaluate the effect of electroporation on the ability of these molecules to extravasate from blood into the skin interstitium. The authors have calculated the apparent diffusion coefficients for both types of molecules by comparing the model with experimental

studies, which represents an important step in development of realistic mathematical models for prediction of extravasation and mass transport for therapeutic molecules of different sizes in electroporated animal tissues with a vascular structure.

Similarly, electroporation has been shown to have an effect on the blood brain barrier (BBB). The poor permeation of therapeutic drugs administered peripherally for treatment of brain pathologies across the blood brain barrier is one of the main reasons for inefficiency of such treatment. Reversible electroporation was found to have a disruptive effect on the blood brain barrier. Irreversible electroporation is a treatment modality for tissue ablation used, among other, in treatment of brain tumours. A recent study presented in [45] on rats demonstrates the feasibility of both reversible and irreversible electroporation for transient blood brain barrier disruption or permanent damage, respectively, and highlights the importance of determining the appropriate electrode positioning (see Paper V presented in this thesis) and characterization of the disruptive effects of reversible electroporation to the blood brain barrier, which is, in other words, the improved mass transport between the vascular system of the brain and brain tissue.

2.2.4.2 Modelling the consolidation-filtration behaviour of biological solid-liquid mixtures – i.e. water transport relations in biological tissues

Processes involving dehydration (drying) of biological tissue, mechanical extraction of juices or oils from fresh roots, fruit, or oil seeds and oleaginous fruits, are common in the food processing industry. In these applications, the considerable complexity of the structure of the source material presents a challenge to the understanding of mass transport processes. This is especially the case when thermal, mechanical, electrical, or chemical treatment is used to alter the cellular and extracellular structures to facilitate improved mass transport, thus increasing quality or yield and decreasing processing time and costs.

Purely phenomenological and kinetics models such as presented in section 2.2.3.3 are commonly found addressing the challenge of modelling mass transport in the above-described cases, however, a number of publications have been published over the past couple of decades presenting a more mechanistic approach based on a combination of empirically-supported understanding of tissue structure and physiology under altered conditions (treatment) on the one hand, and of mathematical models of water evaporation and/or liquid flow in porous materials on the other. The latter theory is largely based, in physical and mathematical terms, on the theory of water relations in sediments, soils, and fractured rocks, where liquid flow in a network of matrixes and fissures is mathematically described [46].

In [47], the authors describe the concept of extracellular, extraparticle, and intracellular space when modelling solid/liquid expression for cellular materials. They propose a complex model based on mass conservation laws in the three compartments or phases that are comprising the sample volume of material from which, by means of mechanical force (pressing), liquid is expressed. The model has since been extended and generalised [48], [49], however, none of the accounts written on the multiple-porosity modelling paradigm try to link the phenomenological relations of mass transport in biological material (i.e. the equations of non-equilibrium thermodynamics) with the effects of electrical treatment.

2.2.4.3 Thermal relations in electroporated tissue

Tissue electroporation and related thermal effects represent a vast and diversified field of research that deserves a substantial review of the subject area such as is presented for electroporation applications in food processing and biorefinery (see Paper I). Since this work is only marginally concerned with thermal effects on mass transport, only some of the most recent and essential works that are important for understanding the theory presented in section 5 on thermal relations with mass transport in electroporated tissue are mentioned and briefly discussed in this section.

As mentioned, thermal relations in biological material treated with electromagnetic fields have been studied extensively across a range of applications and on different scales by using various approaches, ranging from molecular dynamics studies to theoretical non-equilibrium thermodynamics models to *in vivo* studies on model animal tissues. An early consideration of the effects of Joule heating associated with electroporation is presented in [50]. The authors present an account of model development, whereby a theoretical model was developed to estimate the power dissipation in individual cells during electroporation. They concluded that although heating that may be considered as insignificant at the macroscopic level of a cell suspension or tissue, may actually be substantial on the level of the cell membrane. This supposed rise in temperature could be responsible for a lowering of the threshold required for electroporation, as thermal energy is additionally raising the energy level of the bilayer. This has recently been re-evaluated and examined in a study presenting an analytical model for calculating the cell membrane temperature gradient [51]. The authors of the study show that electric field generates cell membrane temperature gradients, particularly during sequential pulsing over a sustained period of time. They conjecture that thermal gradients may contribute to electroporation through induced transmembrane voltages.

A recent study in molecular dynamics simulations [52] shed light on the heat conduction characteristics of the cell membrane, by studying heat conduction characteristics of a DPPC lipid bilayer. Thermal conductivity of the lipid bilayer that was evaluated in this molecular dynamics simulation was found to be anisotropic, and lower than that of bulk water. This is thought to be mainly due to the lipid constituents at the centre of the bilayer, where acyl chains of lipid molecules face each other due to a loss of the covalent-bond and low number density, and thermal conductivity is the lowest. Even lower than thermal conductivity across the bilayer was found to be the thermal conductivity along the bilayer, and thus the bilayer was found to exhibit strong anisotropic behaviour in terms of heat conduction.

Thermal effects associated with electromagnetic fields are of high importance in biomedical applications, such as electrochemotherapy and tissue ablation by irreversible electroporation [53]–[55] or radiofrequency ablation [56]. In these applications, much attention is dedicated to ensuring that the damage to healthy tissue that should not be harmed by the treatment is under control and kept at the lowest possible extent, and various modelling techniques have been employed to evaluate Joule heating and subsequent thermal accumulation and dissipation. Numerical finite element models are often employed due to the complexity of the system (tissue heterogeneities and anisotropy) and the relatively complex form of the Pennes bioheat equation [57] that is normally used to describe thermal relations in perfused tissues.

Another field of electroporation applications that has seen considerable efforts in studying and modelling thermal effects with and without relation to mass transport is skin electroporation, where electric fields are used for breaching the impermeable stratum corneum for topical drug or gene delivery. See the literature presented already in section 2.2.3.2 and [58] in particular for a thermal study, or [59] for a more comprehensive review. Modelling thermal relations in skin electroporation is a challenging task, mainly due to highly variable properties between various layers of skin. A recent study [60] presents the development of a complex analytical bioheat model for studying temperature increases in electroporation of a subcutaneous tumour, accounting for the multi-layer heterogeneous structure of the skin.

Very different considerations and approaches as compared to the field of biomedical applications can be found in the food processing, industrial applications of electroporation. In these applications, it is not a rarity to find treatment protocols delivering high energies to target biological material, and high currents that are present in tissues during long treatment times can cause substantial rise in temperature due to ohmic heating [61]. Ohmic heating using lower voltages for longer periods of time can, with or without electroporation, also be intentionally used as mild treatment of raw material to improve mass transfer within tissue [62], [63]. Modelling with

the purpose of studying thermal effects in this field is mainly limited to various models dealing with the generation and distribution of heat in continuous-flow treatment chambers [64], [65], with the purpose of optimising their design thus avoiding hot spots that can otherwise cause electrode material degradation or treatment chamber deterioration. Theoretical studies relating thermal relations in electroporated plant tissue in industrial applications focusing on enhancing mass transport are virtually non-existent, and presently studies mainly comprise phenomenological models relating electrical or thermal damage to tissue with treatment parameters.

2.2.5 Conclusions

The modelling of mass transport in electroporation of biological cells and tissues is a complex task. For many application areas in electroporation, it is of vital importance to be able to evaluate and if possible quantify the resulting mass transport to evaluate the treatment efficacy. For this reason, a substantial body of literature exists on the subject, however, as this literature review aims to illustrate, the approaches taken are diverse and their results are difficult to compare. The experimental studies are often limited by the finite temporal and spatial resolution of measurements, difficulties in obtaining measurements in complex materials (e.g. living tissues), a large set of possible treatment parameters of high importance that vary substantially from experiment to experiment and within an experiment, and the specific responses that are obtained due to biological diversity and material inhomogeneities.

Computer simulations using mathematical models on the other hand suffer from similar deficiencies; due to the complexity of the phenomena, the models need to be kept simple (reduced and discretised space and/or time) to facilitate computation and resolving of complex sets of equations; there is a number of competing models of electroporation available; phenomena on the microscopic level can lead, due to interactions between the many influencing factors, to erroneous identification of importance of parameters (e.g. if parameters are coupled or are influencing the observed quantity in the same sense); and a lack of independent methods of measurement and available literature on anatomical, physiological, and physio-chemical properties of the material makes determining parameters in mechanistic or realistic models (as opposed to phenomenological) difficult to estimate to within even a few orders of magnitude.

For now, it remains difficult to connect individual contributions to the understanding of this subject into a unifying theory that would fit all or most of the existing applications. Solutions still largely need to be developed on a case-to-case basis. However, detailed and complex fragments do exists, but are sometimes irreconcilable due to discrepancies in their main conclusions (contradictory results) that can be (too) often observed. An additional difficulty is presented by the

enormous range of scales that we can choose to observe electroporation-related phenomena: from the level of individual components of a biological membrane (molecular level), to the level of a macroscopic sample of tissue or cell suspension, between which there is a several orders of magnitude difference. The understanding of mass transport in electroporation is an intensely developing field of science, in which the major directions are still under development.

Note that this literature review is a general introduction into a wide and diverse area of problems of mass transport in electroporation with highly specific approaches. For a review that is more detailed and pertinent to the subject of this thesis and the developed models of transport, see the introductory sections of the individual papers (II, III and IV) presented in section 4.

2.2.6 Literature

This section consists of an ordered list of references as they appear in this thesis. The bulk of the references from the list appears in the literature review chapter, however, some listed below (ref. no. above 65) are cited in the remainder of the work, particularly in chapter 5.

[1] E. Neumann and K. Rosenheck, 'Permeability changes induced by electric impulses in vesicular membranes', *J. Membr. Biol.*, vol. 10, no. 3, pp. 279–290, Dec. 1972.

[2] T. Kotnik, P. Kramar, G. Pucihar, D. Miklavcic, and M. Tarek, 'Cell Membrane Electroporation – Part 1: The Phenomenon', *IEEE Electr. Insul. Mag.*, vol. 28, no. 5, pp. 14–23, Oct. 2012.

[3] L. M. Mir, S. Orlowski, J. Belehradek, and C. Paoletti, 'Electrochemotherapy potentiation of antitumour effect of bleomycin by local electric pulses', *Eur. J. Cancer*, vol. 27, no. 1, pp. 68–72, 1991.

[4] D. Miklavčič, G. Serša, E. Brecelj, J. Gehl, D. Soden, G. Bianchi, P. Ruggieri, C. R. Rossi, L. G. Campana, and T. Jarm, 'Electrochemotherapy: technological advancements for efficient electroporation-based treatment of internal tumors', *Med Biol Eng Comput*, vol. 50, no. 12, pp. 1213–1225, Dec. 2012.

[5] R. Heller, M. Jaroszeski, A. Atkin, D. Moradpour, R. Gilbert, J. Wands, and C. Nicolau, 'In vivo gene electroinjection and expression in rat liver', *FEBS Lett.*, vol. 389, no. 3, pp. 225–228, Jul. 1996.

[6] S. Haberl, D. Miklavcic, G. Sersa, W. Frey, and B. Rubinsky, 'Cell Membrane Electroporation – Part 2: The Applications', *IEEE Electr. Insul. Mag.*, vol. 29, no. 1, pp. 29–37, Feb. 2013.

[7] S. Becker, 'Transport modeling of skin electroporation and the thermal behavior of the stratum corneum', *International Journal of Thermal Sciences*, vol. 54, pp. 48–61, Apr. 2012.

[8] B. Zorec, V. Préat, D. Miklavčič, and N. Pavšelj, 'Active enhancement methods for intra- and transdermal drug delivery: a review', *Slovenian Medical Journal*, vol. 82, no. 5, May 2013.

[9] E. Puertolas, E. Luengo, I. Alvarez, and J. Raso, 'Improving Mass Transfer to Soften Tissues by Pulsed Electric Fields: Fundamentals and Applications', in *Annual Review of Food Science and Technology, Vol 3*, vol. 3, M. P. Doyle and T. R. Klaenhammer, Eds. Palo Alto: Annual Reviews, 2012, pp. 263–282.

[10] G. Pataro, G. Ferrari, and F. Donsi, 'Mass Transfer Enhancement by Means of Electroporation', in *Mass Transfer in Chemical Engineering Processes*, J. Markoš, Ed. InTech, 2011, pp. 151–176.

[11] N. Lebovka, E. Vorobiev, and F. Chemat, *Enhancing Extraction Processes in the Food Industry*. CRC Press, 2011.

[12] J. Raso and V. Heinz, *Pulsed Electric Fields Technology for the Food Industry: Fundamentals and Applications*. Springer, 2010.

[13] T. Kotnik, W. Frey, M. Sack, S. Haberl Meglič, M. Peterka, and D. Miklavčič, 'Electroporation-based applications in biotechnology', *Trends in Biotechnology*, vol. 33, no. 8, pp. 480–488, Aug. 2015.

[14] E. Ortega-Rivas, 'Pulsed Electric Fields (PEF): Milk Pasteurization', in *Encyclopedia of Agricultural, Food, and Biological Engineering, Second Edition*, Taylor & Francis, 2010, pp. 1395–1398.

[15] K. Dymek, 'Impregnation of Leaf Tissues and its Consequences on Metabolism and Freezing; Study on Vacuum Impregnation and Pulsed Electric Field Treatment', dissertation, Lund University, 2015.

[16] O. Parniakov, O. Bals, V. Mykhailyk, N. Lebovka, and E. Vorobiev, 'Unfreezable Water in Apple Treated by Pulsed Electric Fields: Impact of Osmotic Impregnation in Glycerol Solutions', *Food Bioprocess Technol*, pp. 1–9, Oct. 2015.

[17] J. Blahovec, P. Kouřím, and M. Kindl, 'Low-Temperature Carrot Cooking Supported by Pulsed Electric Field—DMA and DETA Thermal Analysis', *Food Bioprocess Technol*, vol. 8, no. 10, pp. 2027–2035, Jul. 2015.

[18] C. Gusbeth, W. Frey, H. Volkmann, T. Schwartz, and H. Bluhm, 'Pulsed electric field treatment for bacteria reduction and its impact on hospital wastewater', *Chemosphere*, vol. 75, no. 2, pp. 228–233, Apr. 2009.

[19] M. Goettel, C. Eing, C. Gusbeth, R. Straessner, and W. Frey, 'Pulsed electric field assisted extraction of intracellular valuables from microalgae', *Algal Research*, vol. 2, no. 4, pp. 401–408, Oct. 2013.

[20] K. C. Smith and J. C. Weaver, 'Electrodiffusion of molecules in aqueous media: a robust, discretized description for electroporation and other transport phenomena', *IEEE Trans Biomed Eng*, vol. 59, no. 6, pp. 1514–1522, Jun. 2012.

[21] M. Szabo and M. I. Wallace, 'Imaging potassium-flux through individual electropores in droplet interface bilayers', *Biochim. Biophys. Acta*, Jul. 2015.

[22] M. Puc, T. Kotnik, L. M. Mir, and D. Miklavcic, 'Quantitative model of small molecules uptake after in vitro cell electropermeabilization', *Bioelectrochemistry*, vol. 60, no. 1–2, pp. 1–10, Aug. 2003.

[23] G. Pucihar, T. Kotnik, D. Miklavcic, and J. Teissié, 'Kinetics of transmembrane transport of small molecules into electropermeabilized cells', *Biophys. J.*, vol. 95, no. 6, pp. 2837–2848, Sep. 2008.

[24] J. Li and H. Lin, 'Numerical simulation of molecular uptake via electroporation', *Bioelectrochemistry*, vol. 82, no. 1, pp. 10–21, Aug. 2011.

[25] J. Li, W. Tan, M. Yu, and H. Lin, 'The effect of extracellular conductivity on electroporation-mediated molecular delivery', *Biochimica et Biophysica Acta (BBA) - Biomembranes*, vol. 1828, no. 2, pp. 461–470, Feb. 2013.

[26] S. Movahed and D. Li, 'Electrokinetic transport through the nanopores in cell membrane during electroporation', *J Colloid Interface Sci*, vol. 369, no. 1, pp. 442–452, Mar. 2012.

[27] S. Satkauskas, M. F. Bureau, M. Puc, A. Mahfoudi, D. Scherman, D. Miklavcic, and L. M. Mir, 'Mechanisms of in vivo DNA electrotransfer: respective contributions of cell electropermeabilization and DNA electrophoresis', *Mol. Ther.*, vol. 5, no. 2, pp. 133–140, Feb. 2002.

[28] B. Gabriel and J. Teissié, 'Time Courses of Mammalian Cell Electropermeabilization Observed by Millisecond Imaging of Membrane Property Changes during the Pulse', *Biophysical Journal*, vol. 76, no. 4, pp. 2158–2165, Apr. 1999.

[29] R. Bharadwaj and J. G. Santiago, ‘Dynamics of field-amplified sample stacking’, *Journal of Fluid Mechanics*, vol. 543, pp. 57–92, Oct. 2005.

[30] J. C. Neu and W. Krassowska, ‘Asymptotic model of electroporation’, *Phys. Rev. E*, vol. 59, no. 3, pp. 3471–3482, Mar. 1999.

[31] W. Krassowska and P. D. Filev, ‘Modeling Electroporation in a Single Cell’, *Biophys J*, vol. 92, no. 2, pp. 404–417, Jan. 2007.

[32] D. Miklavcic and L. Towhidi, ‘Numerical study of the electroporation pulse shape effect on molecular uptake of biological cells’, *Radiol Oncol*, vol. 44, no. 1, pp. 34–41, Mar. 2010.

[33] K. C. Smith and J. C. Weaver, ‘Transmembrane molecular transport during versus after extremely large, nanosecond electric pulses’, *Biochemical and Biophysical Research Communications*, vol. 412, no. 1, pp. 8–12, Aug. 2011.

[34] T. Kotnik, G. Pucihar, and D. Miklavcic, ‘Induced transmembrane voltage and its correlation with electroporation-mediated molecular transport’, *J. Membr. Biol.*, vol. 236, no. 1, pp. 3–13, Jul. 2010.

[35] Y. Granot and B. Rubinsky, ‘Mass Transfer Model for Drug Delivery in Tissue Cells with Reversible Electroporation’, *Int J Heat Mass Transf*, vol. 51, no. 23–24, pp. 5610–5616, Nov. 2008.

[36] B. Zorec, S. Becker, M. Reberšek, D. Miklavčič, and N. Pavšelj, ‘Skin electroporation for transdermal drug delivery: The influence of the order of different square wave electric pulses’, *International Journal of Pharmaceutics*, vol. 457, no. 1, pp. 214–223, Nov. 2013.

[37] K. Dymek, L. Rems, B. Zorec, P. Dejmek, F. G. Galindo, and D. Miklavčič, ‘Modeling electroporation of the non-treated and vacuum impregnated heterogeneous tissue of spinach leaves’, *Innovative Food Science & Emerging Technologies*, vol. 29, pp. 55–64, May 2015.

[38] H. Allali, L. Marchal, and E. Vorobiev, ‘Blanching of Strawberries by Ohmic Heating: Effects on the Kinetics of Mass Transfer during Osmotic Dehydration’, *Food Bioprocess Technol*, vol. 3, no. 3, pp. 406–414, Jul. 2008.

[39] K. El-belghiti and E. Vorobiev, ‘Modelling of Solute Aqueous Extraction from Carrots subjected to a Pulsed Electric Field Pre-treatment’, *Biosystems Engineering*, vol. 90, no. 3, pp. 289–294, Mar. 2005.

[40] E. Amami, E. Vorobiev, and N. Kechaou, ‘Modelling of mass transfer during osmotic dehydration of apple tissue pre-treated by pulsed electric field’, *LWT - Food Science and Technology*, vol. 39, no. 9, pp. 1014–1021, Nov. 2006.

[41] G. C. So and D. G. Macdonald, ‘Kinetics of oil extraction from canola (rapeseed)’, *Can. J. Chem. Eng.*, vol. 64, no. 1, pp. 80–86, Feb. 1986.

[42] G. Sersa, T. Jarm, T. Kotnik, A. Coer, M. Podkrajsek, M. Sentjurc, D. Miklavcic, M. Kadivec, S. Kranjc, A. Secerov, and M. Cemazar, ‘Vascular disrupting action of electroporation and electrochemotherapy with bleomycin in murine sarcoma’, *Br. J. Cancer*, vol. 98, no. 2, pp. 388–398, Jan. 2008.

[43] B. Markelc, G. Sersa, and M. Cemazar, ‘Differential Mechanisms Associated with Vascular Disrupting Action of Electrochemotherapy: Intravital Microscopy on the Level of Single Normal and Tumor Blood Vessels’, *PLoS One*, vol. 8, no. 3, Mar. 2013.

[44] S. Corovic, B. Markelc, M. Dolinar, M. Cemazar, and T. Jarm, ‘Modeling of Microvascular Permeability Changes after Electroporation’, *PLoS ONE*, vol. 10, no. 3, p. e0121370, Mar. 2015.

[45] M. Hjouj, D. Last, D. Guez, D. Daniels, S. Sharabi, J. Lavee, B. Rubinsky, and Y. Mardor, ‘MRI Study on Reversible and Irreversible Electroporation Induced Blood Brain Barrier Disruption’, *PLoS ONE*, vol. 7, no. 8, p. e42817, Aug. 2012.

[46] V. M. E. G. I. Barenblatt, ‘Theory of Fluid Flows Through Natural Rocks’, in *Theory and Applications of Transport in Porous Media*, 1st ed., vol. 3, Springer Science, 1990, p. 396.

[47] J. L. Lanoiselle, E. I. Vorobyov, J. M. Bouvier, and G. Piar, ‘Modeling of solid/liquid expression for cellular materials’, *AICHE J.*, vol. 42, no. 7, pp. 2057–2068, Jul. 1996.

[48] M. Petryk and E. Vorobiev, ‘Liquid flowing from porous particles during the pressing of biological materials’, *Computers & Chemical Engineering*, vol. 31, no. 10, pp. 1336–1345, Oct. 2007.

[49] M. Petryk and E. Vorobiev, ‘Numerical and Analytical Modeling of Solid-Liquid Expression from Soft Plant Materials’, *AICHE J.*, vol. 59, no. 12, pp. 4762–4771, Dec. 2013.

[50] T. Kotnik and D. Miklavcic, ‘Theoretical evaluation of the distributed power dissipation in biological cells exposed to electric fields’, *Bioelectromagnetics*, vol. 21, no. 5, pp. 385–394, Jul. 2000.

[51] A. L. Garner, M. Deminsky, V. B. Neculaes, V. Chashihin, A. Knizhnik, and B. Potapkin, ‘Cell membrane thermal gradients induced by electromagnetic fields’, *Journal of Applied Physics*, vol. 113, no. 21, p. 214701, Jun. 2013.

[52] T. Nakano, G. Kikugawa, and T. Ohara, ‘A molecular dynamics study on heat conduction characteristics in DPPC lipid bilayer’, *The Journal of Chemical Physics*, vol. 133, no. 15, p. 154705, Oct. 2010.

[53] R. V. Davalos and B. Rubinsky, ‘Temperature considerations during irreversible electroporation’, *International Journal of Heat and Mass Transfer*, vol. 51, no. 23–24, pp. 5617–5622, Nov. 2008.

[54] R. V. Davalos, B. Rubinsky, and L. M. Mir, ‘Theoretical analysis of the thermal effects during in vivo tissue electroporation’, *Bioelectrochemistry*, vol. 61, no. 1–2, pp. 99–107, Oct. 2003.

[55] A. Zupanič and D. Miklavčič, ‘Tissue heating during tumor ablation with irreversible electroporation’, *Elektrotehniški vestnik*, vol. 78, no. 1–2, pp. 42–47, 2011.

[56] K. Wang, F. Tavakkoli, S. Wang, and K. Vafai, ‘Analysis and analytical characterization of bioheat transfer during radiofrequency ablation’, *J Biomech*, vol. 48, no. 6, pp. 930–940, Apr. 2015.

[57] J. Okajima, S. Maruyama, H. Takeda, and A. Komiya, ‘Dimensionless solutions and general characteristics of bioheat transfer during thermal therapy’, *Journal of Thermal Biology*, vol. 34, no. 8, pp. 377–384, Dec. 2009.

[58] S. M. Becker and A. V. Kuznetsov, ‘Local temperature rises influence in vivo electroporation pore development: a numerical stratum corneum lipid phase transition model’, *J Biomech Eng*, vol. 129, no. 5, pp. 712–721, Oct. 2007.

[59] U. Pliquett, ‘Mechanistic studies of molecular transdermal transport due to skin electroporation’, *Advanced Drug Delivery Reviews*, vol. 35, no. 1, pp. 41–60, Jan. 1999.

[60] D. Sarkar, A. Haji-Sheikh, and A. Jain, ‘Temperature distribution in multi-layer skin tissue in presence of a tumor’, *International Journal of Heat and Mass Transfer*, vol. 91, pp. 602–610, Dec. 2015.

[61] E. Vorobiev and N. Lebovka, ‘Pulsed-Electric-Fields-Induced Effects in Plant Tissues: Fundamental Aspects and Perspectives of Applications’, in *Electrotechnologies for Extraction from Food Plants and Biomaterials*, Springer New York, 2008, pp. 39–81.

[62] N. I. Lebovka, I. Praporscic, S. Ghnimi, and E. Vorobiev, ‘Does Electroporation Occur During the Ohmic Heating of Food?’, *Journal of Food Science*, vol. 70, no. 5, pp. E308–E311, Jun. 2005.

[63] W.-C. Wang and S. K. Sastry, ‘Effects of moderate electrothermal treatments on juice yield from cellular tissue’, *Innovative Food Science & Emerging Technologies*, vol. 3, no. 4, pp. 371–377, Dec. 2002.

[64] M. Lindgren, K. Aronsson, S. Galt, and T. Ohlsson, ‘Simulation of the temperature increase in pulsed electric field (PEF) continuous flow treatment chambers’, *Innovative Food Science & Emerging Technologies*, vol. 3, no. 3, pp. 233–245, Sep. 2002.

[65] J. Krauss, Ö. Ertunç, C. Rauh, and A. Delgado, ‘Novel, Multi-Objective Optimization of Pulsed Electric Field Processing for Liquid Food Treatment’, in *Innovative Food Processing Technologies: Advances in Multiphysics Simulation*, K. Knoerzer, P. Juliano, P. Roupas, and C. Versteeg, Eds. Blackwell Publishing Ltd., 2011, pp. 209–231.

[66] J. Crank, *The Mathematics of Diffusion*. Oxford University Press, 1979.

[67] Andrei D. Polyanin, ‘Systems of Ordinary Differential Equations - EqWorld’, *Linear Systems of Two Ordinary Differential Equations*. [Online]. Available: http://eqworld.ipmnet.ru/en/solutions/sysode/sode-toc1.htm. [Accessed: 01-Dec-2015].

[68] N. B. Vargaftik, *Handbook of Thermal Conductivity of Liquids and Gases*. CRC Press, 1993.

[69] American Society of Heating, *2006 ASHRAE Handbook: Refrigeration: SI Edition*, SI Edition. ASHRAE, 2006.

[70] A. Eucken, ‘Allgemeine Gesetzmäßigkeiten für das Wärmeleitvermögen verschiedener Stoffarten und Aggregatzustände’, *Forsch Ing-Wes*, vol. 11, no. 1, pp. 6–20, Jan. 1940.

[71] J. F. V. Vincent, ‘Relationship between density and stiffness of apple flesh’, *J. Sci. Food Agric.*, vol. 47, no. 4, pp. 443–462, Jan. 1989.

[72] D. A. Stewart, I. R. Gowrishankar, and J. C. Weaver, ‘Transport lattice approach to describing cell electroporation: Use of a local asymptotic model’, *IEEE Trans. Plasma Sci.*, vol. 32, no. 4, pp. 1696–1708, Aug. 2004.

[73] I. Avramov, ‘Relationship between diffusion, self-diffusion and viscosity’, *Journal of Non-Crystalline Solids*, vol. 355, no. 10–12, pp. 745–747, May 2009.

[74] P. W. Linder, L. R. Nassimbeni, A. Polson, and A. L. Rodgers, ‘The diffusion coefficient of sucrose in water. A physical chemistry experiment’, *J. Chem. Educ.*, vol. 53, no. 5, p. 330, May 1976.

[75] J. Kestin, M. Sokolov, and W. A. Wakeham, ‘Viscosity of liquid water in the range −8 °C to 150 °C’, *Journal of Physical and Chemical Reference Data*, vol. 7, no. 3, pp. 941–948, Jul. 1978.

[76] F. R. Harker, R. J. Redgwell, I. C. Hallett, S. H. Murray, and G. Carter, ‘Texture of Fresh Fruit’, in *Horticultural Reviews*, J. Janick, Ed. John Wiley & Sons, Inc., 2010, pp. 121–224.

[77] E. A. Vyaz’mina and A. D. Polyanin, ‘New classes of exact solutions to general nonlinear diffusion-kinetic equations’, *Theor Found Chem Eng*, vol. 40, no. 6, pp. 555–563, Dec. 2006.

3 Materials and methods

3.1 Diffusion experiments

Diffusion experiments that are described in Paper II and Paper IV were conducted according to the same protocol. Paper III concerns pressing experiments only, therefore the experiments described herein do not concern it.

According to the diffusion experiments protocol, cylindrical samples (disks) of sugar beet taproot and apple fruit tissue (without skin) were obtained from 5 mm thick sugar beet taproot or apple fruit slices (in continuing text referred to as sugar beet and apple tissue respectively). All samples measured 25 mm in diameter, and each sample was first subjected to electroporation treatment by applying 150, 200, 300, or 400 V between two stainless-steel parallel plate electrodes at 5 mm inter-electrode distance (the thickness of the sample). The intent was to subject the treated tissue to field strengths of 300, 400, 600, and 800 V/cm, respectively (note the 5 mm thickness of the samples). The desired target field strength was not reached homogeneously within the tissue, as it is not homogeneous material, and since due to finite electrode dimensions the field reaches the maximum (desired) value only in the central area away from electrode edges (examine figures in Paper V for an illustration). Rectangular pulses of alternating polarity (see Figure 3.4 in section 3.3.1.2) were delivered in two trains of 8 pulses, where each pulse was of 100 μs in duration, and pulse repetition frequency within the train was 1 kHz. Two such trains were delivered with a pause of one second between the two trains. This protocol is referred to as Protocol A. The pulses were provided by a custom-built pulse generator with peak output current of 38 A at the maximum attainable voltage of 400 V, assembled by Service Electronique UTC, Compiègne, France (refer to section 3.3.1.2 below).

Figure 3.1: The electrical treatment chamber.

The samples were removed from the treatment chamber following electrical treatment. The surfaces of the sample disks were then were put into contact with absorbent paper and thus the surfaces were dried in order to remove the sugary liquid accumulated at the surfaces. This liquid is present due to cutting (in small amounts) and possibly due to electro-osmotic or pressure-change effects (turgor loss) that occur during the electroporation treatment (to a greater extent). Had the surfaces not have been dried, the juice on the surface would cause an immediate increase in the sugar concentration in the solution at the beginning of the diffusion experiment, resulting in kinetics also known as the "washing stage" of the process (refer to section 2.2.3.3 of the literature review). This effect is not captured by the model, neither is it easy to subtract it from the recorded kinetics due to differing juice sugar concentration and amount of this surface liquid that is variable between samples. The surface-dried samples were placed into a flask together with a magnetic stirrer. This sample-liquid mixture was constantly agitated and sampled at regular intervals; the total soluble solids (i.e. mostly sugar) concentration was analysed with a digital refractometer (details given in section 3.3.2.2 below). The liquid-to-solid ratio was 2:1 in all experiments.

The quantity which the digital refractometer measures is the sugar concentration (to be precise – concentration of total soluble solids) in liquid and is displayed in units degrees Brix (°Bx), where one degree Brix is 1 gram of sucrose in 100 grams of solution and represents the concentration of the solution as percentage by weight (% w/w). The initial sugar content of the aqueous solution $°\mathrm{Bx}_0$ is known and normally equal to zero, and during experiment the current sugar content $°\mathrm{Bx}(t)$ is measured. Connected measurements trace out the curve of extraction kinetics, and the final sugar concentration $°\mathrm{Bx}_\mathrm{d}$ can be determined separately. Theoretically, $°\mathrm{Bx}_\mathrm{d}$ is the total solutes concentration in solution in ideal conditions of completely permeabilized tissue and after infinite time of diffusion. In practice, it can easily be obtained by measuring the solutes concentration in pure fruit/root juice, and scaling the measurement according to the extracting liquid/juice mass ratio (also known as the solid-liquid ratio). Since initial and maximum concentrations are known, the *normalized degree Brix* at time t – i.e. $B(t)$, can be expressed and calculated as

$$B(t) = \frac{°\mathrm{Bx}(t) - °\mathrm{Bx}_0}{°\mathrm{Bx}_\mathrm{d} - °\mathrm{Bx}_0}$$

Normalized Brix is used throughout the works described in this thesis as a measure for the amount of solute (i.e. sugar) that has diffused out of the tissue sample from time t_0 to time t. It takes the values from the interval $0 \leq B(t) \leq 1$, and is dimensionless. It can be calculated according to the above equation given measurements obtained with the refractometer. The schematic illustration of the diffusion experiment is given by Figure 3.2.

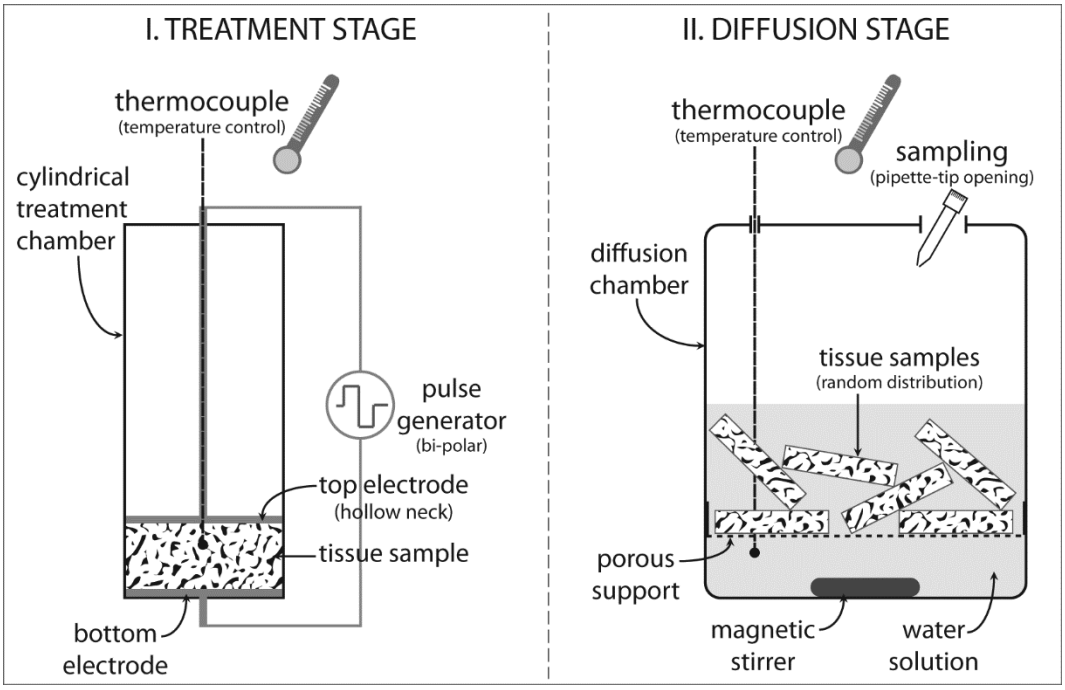

Figure 3.2: Schematic representation of the diffusion experiment setup – electroporation treatment (left) and subsequent diffusion stage (right).

3.2 Pressing experiments

The pressing experiments that are described in Paper III and Paper IV were conducted according to the same protocol. Paper II concerns diffusion experiments only, therefore the experiments described herein do not concern it.

As in the diffusion experiments, cylindrical samples of sugar beet and apple tissue were used, 25 mm in diameter, and of 5 mm thickness. The samples were placed between two parallel plate stainless-steel electrodes, and electroporation pulses were applied using three different protocols (see Figure 3.4). Protocol A: The voltage was varied, using 150 V, 200 V, 300 V, 350 V, or 400 V applied to the electrodes. Pulses of alternating polarity were delivered in two trains of 8 pulses per train, with repetition frequency of 1 kHz within the train, 1 second pause between the two trains, and 100 μs pulse duration. Protocol B: The voltage was again varied as in Protocol A, however, only two unipolar pulses were delivered of 800 μs each, and with a time delay of 1 s in between the two pulses. Protocol C: The voltage was varied as in Protocol A and Protocol B, and 8 pulses of single polarity were delivered, 100 μs in duration each second (i.e. at pulse repetition frequency of 1 Hz). This protocol is also known as one of the *standard protocols for electrochemotherapy*. Note that the total treatment time t_t (product of pulse duration t_p, number of pulses n_p and number of trains n_t) as calculated from the pulsing protocol was the same for Protocols A and B (t_t = 1.6 ms), and was 50 % lower in case of Protocol C (t_t = 0.8 ms) as compared

to the two other protocols. The delivered energy in the described setup as calculated from the measured current falls between 6 J/kg (minimum attained for sugar beet, Protocol C, 150 V) and 250 J/kg (maximum attained for apples, Protocol B, 400 V). In terms of delivered energy and treatment time, these treatment protocols are generally not encountered in food processing, where energies on the order of several kJ/kg are commonly delivered to target tissues. The maximum total delivered energy on the order of 0.25 kJ/kg results – in worst case, i.e. not accounting for any heat dissipation via electrodes or treatment chamber surfaces – in a negligible increase in sample temperature by less than 0.1 K. This estimate is based on the thermal capacity of apple tissue, and known maximum energy that was delivered. The reasons for and implications of this particular choice of low-intensity, "gentler" treatment protocols, are further given and discussed in the Results and discussion section of Paper III and Paper IV.

In all cases, regardless of the electroporation protocol, the electric treatment was followed by pressing. Electroporated samples were immediately placed into a specially fabricated treatment chamber and subjected to a load of 150 N – about 580 kPa (apple), or 300 N – about 290 kPa (sugar beet), using a texture analyser (details in section 3.3.2.1). The piston displacement was recorded by the texture analyser under constant pressure (force) application during one hour.

Piston displacement equals the sample deformation along the axis of the pressure application. This sample deformation is theoretically linked to the liquid pressure loss in tissue by the model presented first in Paper III. This enables the comparison of experimental and model results. The schematic illustration of the diffusion experiment is given by Figure 3.3.

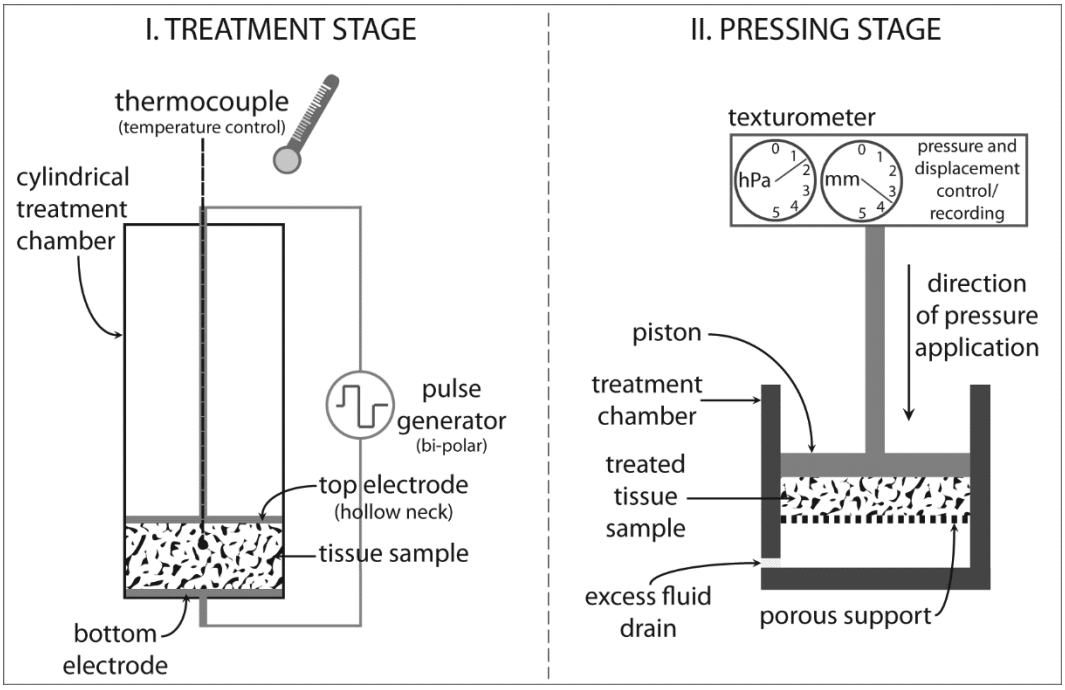

Figure 3.3: Schematic representation of the pressing experiment setup – electroporation treatment (left) and subsequent pressing (right).

3.3 Equipment and treatment/measurement protocols used

3.3.1 Pulse generation

3.3.1.1 Protocols

Three different electroporation treatment protocols were used to obtain the results presented in papers II-IV. The protocols are specified in detail in Paper IV, section 2.3, and illustrated by means of a figure given in Paper IV, Figure 3.2 (reproduced below as Figure 3.4 for reference). Three different treatment protocols were used in order to examine whether there is a detectable difference in how various treatment protocols influence the formation and evolution of pores in the cell membranes, which could be reflected in the tissue consolidation kinetics, and subsequently modelled with the dual-porosity model. Results of the comparison are given in the appropriate section of Paper IV.

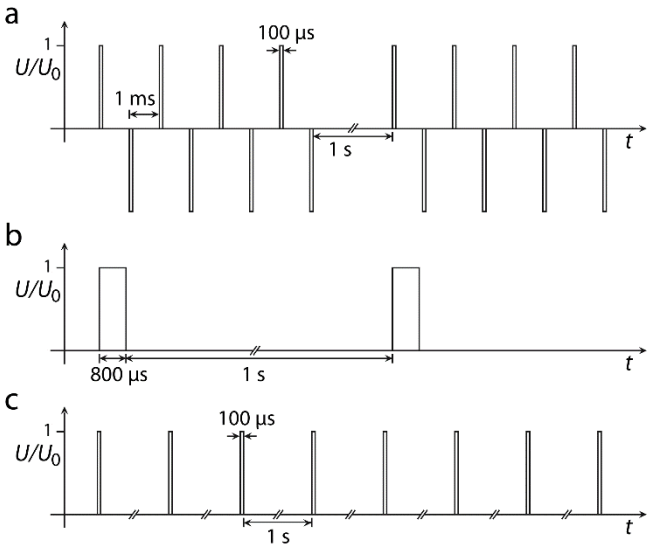

Figure 3.4: A graphic representation of the three pulse delivery protocols: Protocol A (a), Protocol B (b), and Protocol C (c). Pulse widths and distances are to scale, except where denoted otherwise – the '//' sign indicates a break in the axis (i.e. there is a one second long pause between every two pulses in between which the axis brake is indicated).

3.3.1.2 Generators

In the experiments reported on or mentioned in this thesis, three different generators were used to achieve electroporation in treated tissue; two laboratory-scale generators and one industrial / pilot-plant scale generator. However, only one generator was used to obtain results presented in Papers II-IV which form the main body of the work reported on in this thesis. The generator used to treat sugar beet taproot and apple fruit tissue used in the validation experiments for the dual-porosity model has been manufactured by the UTC Service Electronique (Electronics department of the Université de Technologie de Compiègne), and is capable of delivering a maximum voltage of 400 V and a maximum current of 38 A, and produces exclusively bipolar pulses of near-rectangular shape.

The other two generators were used in subsequent work on turgor relaxation and electroosmosis experiments that are briefly referred to in the concluding section of this thesis. Both produce exclusively unipolar pulses, and are capable of delivering rectangular electric pulses at voltages higher than 400 V. For these two reasons, the 400 V maximum voltage bipolar pulse generator was not suitable for these experiments. As no detailed discussion is given on the turgor relaxation and electroosmosis experiments and their results in this thesis, the specifications of the two unipolar pulse generators are out of scope of the thesis and are omitted from this section.

3.3.2 Other equipment

3.3.2.1 Measurements of tissue sample deformation – texture analysis

In order to obtain the expression kinetics, constant pressure was applied to tissue samples using a low-power high-precision texture analyser manufactured by Stable Micro Systems, model "TA.XT *plus*". The maximum force this texture analyser can exert on the sample is 50 kg (500 N), with a force resolution of 1 N. The texture analyser was employed in the *constant force* mode of operation, meaning that a specified force was applied to the tissue samples via the piston of the texture analyser for a specified amount of time and the displacement was measured and recorded at a high resolution of 0.001 mm with a measurement accuracy of ± 0.001 mm.

Figure 3.5: The used texture analyser TA.XT plus (image taken at the laboratory). One of the laboratory generators (an industrial-scale model, manufactured by Hazemeyer) is visible in the background.

3.3.2.2 Digital refractometry

In order to measure concentration of total soluble solutes in sugar beet taproot and apple fruit tissue experiments, two digital refractometers were used. Results reported on in Paper II were obtained using the digital refractometer ATAGO PR-32α (alpha), and new results reported on in Paper IV by using the ATAGO PR-101α (alpha) digital refractometer. Both have a resolution of 0.1 % Brix, and a measurement accuracy of 0.1 % Brix, however the measurement range of the PR-32α model is from 0.0 % Brix to 32.0 % Brix, while for the PR-101α model the respective

range is from 0.0 % Brix to 45.0 % Brix. Both refractometers were calibrated before use using distilled water and a reference solution (mixed on site) of sucrose and distilled water.

Figure 3.6: The digital refractometers ATAGO PR-32α (left) and the ATAGO PR-101α (right). Images courtesy of ATAGO CO., LTD, source: http://www.atago.net/product/?l=en&f=products_pr.html

4 Papers on the subject of mass transport by diffusion or pressing in electroporated tissue published in international scientific journals

4.1 Paper II: "Dual-porosity model of solute diffusion in biological tissue modified by electroporation"

4.1.1 Introduction

The problem of mass transfer during and after application of electroporation pulses has been treated both experimentally and theoretically, and in studies combining both approaches, but mainly employing less complex systems, e.g. cell suspensions and monolayers of cells (see the literature review section). This focus on systems of lesser complexity seems to hold particularly true for theoretical models.

The model that is presented in this paper is an attempt at advancing the basis of theoretical modelling of mass transport in electroporation applications. It has been developed in order to model experimental results in a particular case of plant tissue electroporation with purpose of solute extraction, but can, with modification, also be applied to applications in biomedicine (e.g. electrochemotherapy) and other fields of electroporation research where there is a need to model solute transport on the level of tissue. This first attempt at building a dual-porosity model is concerned only with free diffusion of small molecules (several kDa in size) post-pulse, when the effects of the electric field are either no longer present, or are negligible. It features, however, the coupling of diffusion with the effects of electroporation through its effects on membrane permeability.

4.1.2 Summary

In the model presented in this paper, tissue is modelled as a dual-porosity medium. One medium is represented by the intracellular and the other by extracellular space, with cell membrane separating the two compartments. In the model study that follows, the transport modelled is that of sucrose extracted from sugar beet tissue. A comparison is included of model results with experimental data for purposes of model validation, as well as an illustration of the model application. A parametric study is presenting the effects of various model parameters on extraction kinetics (theoretical work only). The parametrical study is also an attempt at analysing the influence of some of the electroporation parameters on model predictions, as well as gauging the sensitivity of the model to potential errors in parameter estimation. Since the model presented is a proof of concept and the interpretation of its results has illustrative value, the model has been kept

simple enough in this first account, so that an analytical solution could be readily found and discussed. A clear and complete demonstration of applying the model to problems in a different field of electroporation research, e.g. in electrochemotherapy or intra/transdermal drug transport, requires and deserves a study and paper of its own. For brevity, the paper only presents, in theory, the necessary modifications to the model, which the authors believe are necessary to adapt it to problems of drug diffusion in tissues for biomedical applications.

4.1.3 Conclusions

The model is designed as an attempt to provide a framework for future work in both computer modelling and experimental design. The paper demonstrates how it can be applied to a typical problem of solute extraction by diffusion in tissue that has been pre-treated with electroporation, and how it can be adapted to model mass transport-related phenomena in a disparate field of biomedical electroporation applications. The authors are confident that the dual-porosity model can be further improved and adapted to solve problems in mass transfer in many applications of electroporation, whether the object of interest is animal or plant tissue, whether the interest is in (selective) extraction of solute from the cells or introduction of solute into the cells, and even whether the species of interest are small ions or large organic compounds. The basic physical phenomena underlying the processes after application of electroporation treatment exhibit differences predominantly in details, which renders a general approach such as described by this paper, possible.

Biochimica et Biophysica Acta 1838 (2014) 1950–1966

Contents lists available at ScienceDirect

Biochimica et Biophysica Acta

journal homepage: www.elsevier.com/locate/bbamem

Dual-porosity model of solute diffusion in biological tissue modified by electroporation

Samo Mahnič-Kalamiza [a,b,*], Damijan Miklavčič [b], Eugène Vorobiev [a]

[a] University of Technology of Compiègne, Centre de Recherches de Royallieu, BP 20529, 60205 Compiègne Cedex, France
[b] University of Ljubljana, Faculty of Electrical Engineering, Tržaška c. 25, SI-1000 Ljubljana, Slovenia

ARTICLE INFO

Article history:
Received 10 January 2014
Received in revised form 6 March 2014
Accepted 12 March 2014
Available online 19 March 2014

Keywords:
Diffusion
Electroporation
Mass transfer
Solute extraction
Mathematical modeling
Analytical solution of PDE

ABSTRACT

In many electroporation applications mass transport in biological tissue is of primary concern. This paper presents a theoretical advancement in the field and gives some examples of model use in electroporation applications. The study focuses on post-treatment solute diffusion.

We use a dual-porosity approach to describe solute diffusion in electroporated biological tissue. The cellular membrane presents a hindrance to solute transport into the extracellular space and is modeled as electroporation-dependent porosity, assigned to the intracellular space (the finite rate of mass transfer within an individual cell is not accounted for, for reasons that we elaborate on). The second porosity is that of the extracellular space, through which solute vacates a block of tissue.

The model can be used to study extraction out of or introduction of solutes into tissue, and we give three examples of application, a full account of model construction, validation with experiments, and a parametrical analysis. To facilitate easy implementation and experimentation by the reader, the complete derivation of the analytical solution for a simplified example is presented.

Validation is done by comparing model results to experimentally-obtained data; we modeled kinetics of sucrose extraction by diffusion from sugar beet tissue in laboratory-scale experiments. The parametrical analysis demonstrates the importance of selected physicochemical and geometrical properties of the system, illustrating possible outcomes of applying the model to different electroporation applications. The proposed model is a new platform that supports rapid extension by state-of-the-art models of electroporation phenomena, developed as latest achievements in the field of electroporation.

1. Introduction

As shown by experiments on lipid bilayers, cells in suspensions, monolayers and biological tissue, electric field can, if of sufficient strength, cause a significant increase in the conductivity and permeability of the lipid membrane [1]. This effect is known as electroporation and has been attributed to creation of aqueous pathways in the lipid bilayer [2,3]. Throughout this paper we will assume that solute diffusivity in biological tissue can be enhanced by electroporation by means of applying one or a series of electroporative pulses of a particular amplitude and duration to the tissue.

Electroporation is studied in a number of diverse fields [4,5], such as in biomedicine for gene delivery [6–8], electrochemotherapy [9–12], transdermal drug delivery [13–16], or tumor ablation by irreversible electroporation [17,18]; in food engineering and chemistry for increasing extraction yield [19–21], improving the quality of extract [22–24], or food preservation [25–27]; as well as in environmental sciences for waste water treatment [28,29], lipid extraction [30], or plant growth stimulation [31,32]. In all domains we encounter the need for introducing into or extracting out of the biological cells the solutes of interest. These range from small chemical compounds such as sucrose molecules [33,34] in food processing to larger and more complex drugs for electrochemotherapy [35] and to still larger lipids [30], and finally to the very large RNA and DNA molecules in gene therapy research [36]. This variability poses a challenge when determining parameters of electroporation, and recommended treatment protocols for their respective applications [37,38], as well as protocol optimization [39], are subjects of intensive research.

The problem of mass transfer during and after application of electroporative pulses has been treated both experimentally [40–42] and theoretically [43–48], and in studies combining both approaches [49–52], but mainly employing less complex systems, e.g. cell suspensions [43] and monolayers of cells [50,53]. This reservation to systems of lesser complexity seems to hold particularly true for theoretical models.

* Corresponding authors at: Université de Technologie de Compiègne (UTC), Département de Génie des Procédés Industriels, Laboratoire Transformations Intégrées de la Matière Renouvelable, Centre de Recherches de Royallieu, BP 20529, 60205 Compiègne Cedex, France. Tel.: +33 6 52 17 30 92.
E-mail addresses: samo.mahnic@utc.fr, samo.mahnic@fe.uni-lj.si, samo.mahnic@gmail.com (S. Mahnič-Kalamiza).

http://dx.doi.org/10.1016/j.bbamem.2014.03.004
0005-2736/

In many important electroporation applications, e.g. electrochemotherapy or extraction of valuable compounds from plant tissue, the object of interest is heterogeneous tissue composed of cells in close contact that are of variable size [54], shape [55], and that may be interconnected via intercellular junctions [56]. These factors influence – to a varying extent – the electroporation process, electrotransfer and diffusion of solute, both during and after electroporation. Additionally, membrane contacts of adjacent cells in animal tissues reduce the effects of the electric field, as shown by studies on dense cell suspensions [57], while the effects of the cell wall in plant tissues and the porosity of extracellular space have not yet been evaluated in relation to electroporation. Furthermore, we often come across clearly defined sources and/or sinks of observed solute. These introduce the need for not only temporal observation and inclusion of reaction kinetics in the model [45], but also the need to determine the spatial distribution of solute concentration in tissue [46].

With respect to electroporation and its effects on cell membrane transport, we have to examine the nature of solute transported in relation to the electric pulse parameters and electrical properties of tissue [58,59], as well as the local electric field distribution [60,61]. Several mechanisms of transport were reported in addition to free diffusion, such as electrokinetic effects facilitated by the electric field. The list of these comprises electrophoresis [45], electroosmosis [47] and FASS (Field-Amplified Sample Stacking) [45,62], as well as cellular and membrane processes such as endocytosis [63]. The importance of individual mechanisms depends not only on the nature of solute, but also on the parameters of delivered electric pulses [48,64] and the time of observation of the system. The time of observation is important since it delineates two modeling paradigms — we either model periods during as well as after electric pulse application with electrokinetic effects, or we focus on the post-pulse period only, where the dominant mass transport is by diffusion through long-lived pores [50,59,65].

The model that we present in this paper is an attempt at advancing the basis of the theoretical modeling of mass transport in electroporation applications. Tissue is modeled as a dual-porosity medium. One medium is represented by the intracellular and the other by extracellular space, with cell membrane separating the two media. It has been developed in order to model experimental results in a particular case of plant tissue electroporation with purpose of solute extraction, but can, with modification, also be applied to applications in biomedicine (e.g. electrochemotherapy) and other fields of electroporation research where there is a need to model solute transport on the level of tissue. In this first attempt at building a dual-porosity model, we are concerned only with free diffusion of small molecules (several kDa) post-pulse, when the effects of the electric field are either no longer present or are negligible. We have, however, coupled diffusion with the effects of electroporation through its effects on membrane permeability.

In our model study, the transport modeled will be that of sucrose extracted from sugar beet tissue. We are including a comparison of model results with experimental data as model validation and an illustration of the model application, while also presenting a parametric study. By means of the latter we attempt to both analyze the influence of some of the electroporation parameters on model predictions as well as gauge the sensitivity of the model to potential errors in parameter estimation.

Since the model presented is a proof of concept and the interpretation of its results has illustrative value, we have kept the model in this first account simple enough, so that an analytical solution could be readily found and discussed. A clear and complete demonstration of applying the model to problems in a different field of electroporation research, e.g. in electrochemotherapy or intra/transdermal drug transport, requires and deserves a study and paper of its own. For brevity, we therefore only present, in theory, the necessary modifications to the model, which we believe are necessary to adapt it to problems of drug diffusion in tissues for biomedical applications. For a schematic representation on how the paper explores the dual-porosity modeling paradigm and how its contents are divided into subsections, see Fig. 1.

2. Theoretical formulation of the problem, model construction, and its application

2.1. System of solute diffusion equations in a dual-porosity medium

The rationale behind the use of the following model equations comes from the theory of porous media [66], more precisely from the observations of liquid flow in soils and fractured rocks. From the mathematical point of view, we exploit the analogy of fluid flow and heat transfer in porous media with problems in mass transport by diffusion [67]. The same (mathematical) treatment is thus applicable that has been thoroughly studied in problems of heat and mass transfer in porous media [68,69].

We model a block of tissue as composed of essentially two media, the extracellular and the intracellular. At their respective volume fractions, they occupy the same block of tissue, as is illustrated by Fig. 2. Tissue is modeled as comprising cells' interior volume that collectively forms the intracellular space. The intracellular space is separated by the cell membrane from the extracellular space, which comprises primarily the cell wall (in plants) or collagen (e.g. in skin tissue), as well as miscellaneous and other biomolecules in addition to the entrapped liquid (and air in plants) in the intercellular compartments. Electric field primarily acts on membranes, rendering them permeable thus effectively affecting the porosity of the intracellular space; electroporation of membranes is therefore enabling diffusive transport of solutes through the membrane.

If we imagine a sample of tissue of finite thickness (e.g. a few hundred layers of cells), we can identify two diffusive flows of solute. Assuming that initially there is a higher concentration of solute within the cells as compared to the extracellular space, first, the solute has to diffuse out of individual cells (i.e. from intracellular space) into the extracellular space. This is the transmembrane flow. Second, the solute diffuses through the block of tissue via the extracellular route; this diffusion is driven by the gradient that appears in the block of tissue due to conditions at the tissue sample boundaries. In extraction applications, the boundary condition can ideally be assumed constant and equal to zero (i.e. infinite dilution into surrounding solvent). In electrochemotherapy or transdermal drug transfer applications, the boundary condition is non-zero, i.e. constant or time-varying (depending on application), e.g. a skin reservoir of finite capacity; or a local drug plasma concentration dependent on locally (un)obstructed blood flow, etc. The extracellular path results in an extracellular flow in the presence of concentration gradients imposed by the boundary and initial conditions. Solute leaving the cells results in a decrease of intracellular concentration, and an increase in extracellular concentration. On the other hand, solute leaving the tissue sample in effect decreases extracellular concentration. This gives us, for intrinsic concentration (i.e. concentration averaged over the volume fraction of each phase) in extracellular space and intracellular space respectively, the following set of partial differential equations (PDEs):

$$\frac{\partial c_e(z,t)}{\partial t} - D_{s,e}\frac{\partial^2 c_e(z,t)}{\partial z^2} - \frac{1-\varepsilon}{\varepsilon}k\cdot[c_i(z,t)-c_e(z,t)] = 0 \tag{1}$$

$$\frac{\partial c_i(z,t)}{\partial t} + k\cdot[c_i(z,t)-c_e(z,t)] = 0. \tag{2}$$

In Eqs. (1)–(2), c_i and c_e denote intrinsic volume-averaged intracellular and extracellular (respectively) molar concentrations in units $\mathrm{mol\cdot m^{-3}}$, $D_{s,e}$ is the diffusion coefficient of solute species s in extracellular space with units $\mathrm{m^2\cdot s^{-1}}$, z is the spatial coordinate aligned with

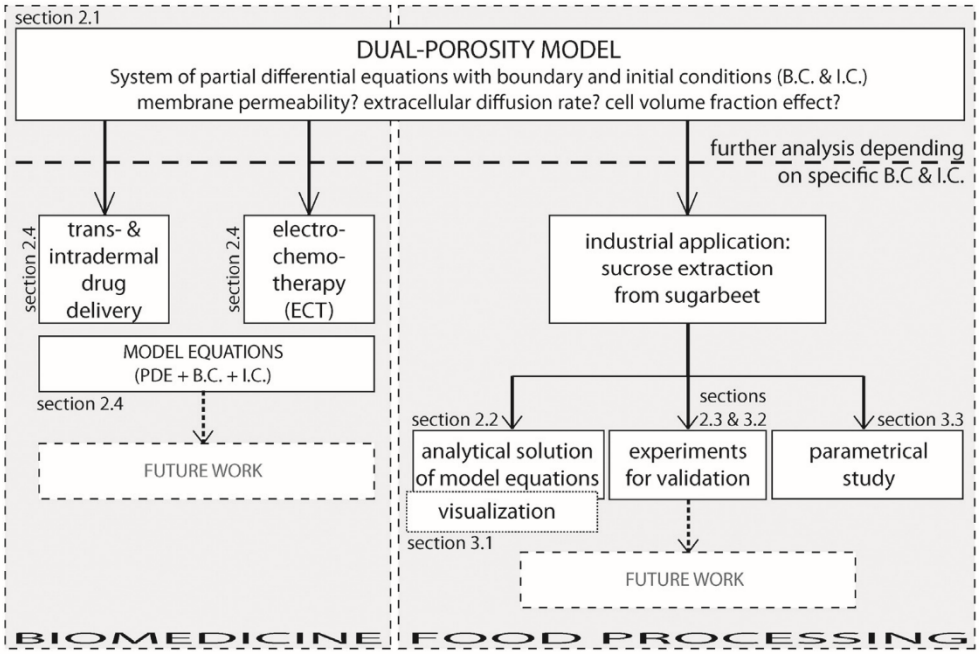

Fig. 1. The dual-porosity modeling paradigm as explored in this article.

(i.e. parallel to) the principal axis of diffusion, and $k(c_i - c_e)$ is the volume-averaged flow in units $mol \cdot m^{-3}.s^{-1}$. This member as well as the multiplicative factor $(1-\varepsilon)/\varepsilon$ will be further deconstructed and explained during the course of the following analysis. We have supposed only one principal axis of diffusion is relevant, and that is the axis perpendicular to the largest surface of the tissue sample. In other words, we have simplified the problem to one spatial dimension, our rationale supported by an assumption that the thickness of the studied block of tissue is small as compared to its largest surface. The model as given by Eqs. (1)–(2) does not account for convective flow or chemical reactions, but can readily be expanded with additional terms if necessary. The model geometry (as illustrated by Fig. 3) appears in a number of electroporation applications; in industrial extraction of solutes from plant tissues, tissue is sliced or grated into thin blocks or cossettes to facilitate faster diffusion; in transdermal drug delivery, skin patches can be modeled as thin reservoirs with large surface area in contact with the skin; while in subcutaneous tumor electrochemotherapy for example, large tumors not protruding deep into the subcutaneous tissue exhibit properties that can be, by in no means excessive stretch of imagination, approximated using the proposed model geometry.

The given system of model equations describes what is commonly referred to in the relevant established literature as a LNE (Local Non-Equilibrium) model. See e.g. [67] for a recent review of LNE models as applied in theory of mass transport in biological tissue modeled as a porous medium.

In order to support further theoretical treatment and procurement of an analytical solution, we must establish the following set of assumptions and simplifications: (i) — as indicated by Eq. (1), diffusion coefficient of solute in extracellular space is assumed to be constant. For spatial dependence, the second member in Eq. (1) has to be revised to $\partial/\partial z[D_{s,e} \cdot \partial c_e(z,t)/\partial z]$, rendering the system complex and cumbersome for analytical treatment, while for temporal dependence $D_{s,e} = f(t)$, a new timescale T has to be introduced, so that $dT = f(t)\ dt$. Fortunately, there are no strong arguments from the physics of the process point of view that would necessitate taking either spatial or temporal dependence of $D_{s,e}$ into account; (ii) — the tissue is modeled as consisting of perfectly spherical cells of radius R, collectively occupying a volume fraction F of the tissue block and forming the intracellular space. The rest of the volume is extracellular space, occupying the volume fraction $1 - F$. Thus, the porosity (ratio of void volume to total volume) denoted

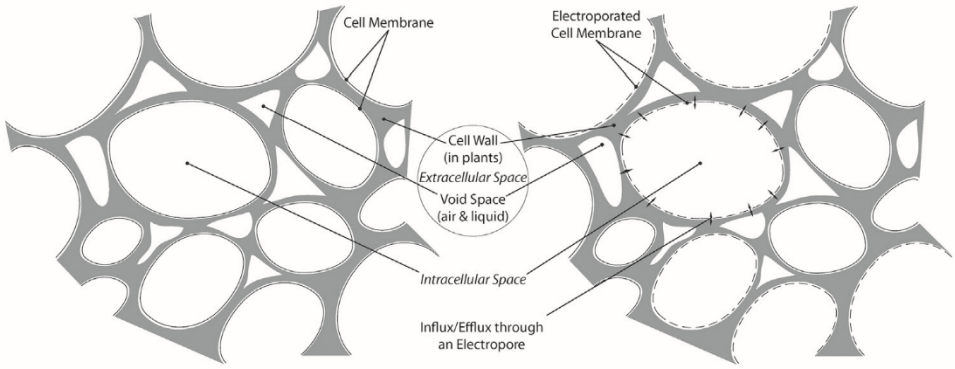

Fig. 2. Schematic representation of biological tissue, before electroporation (left) and after electroporation (right). Note that a segment (e.g. block) of modeled tissue may consist of several hundred layers of cells.

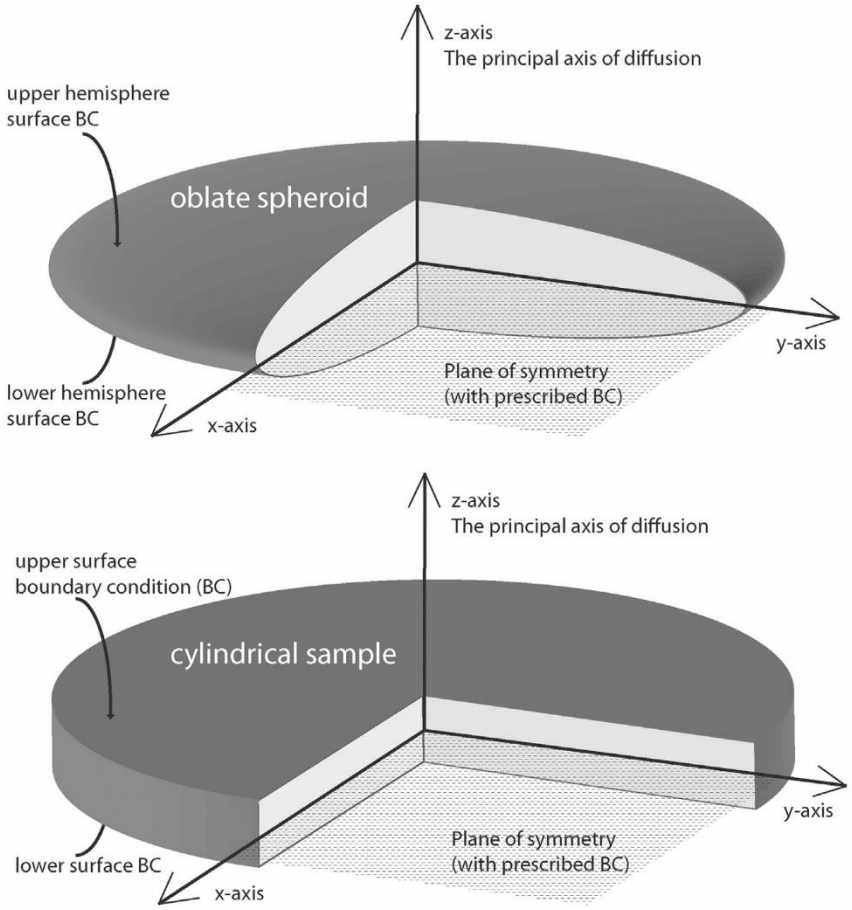

Fig. 3. Tissue sample geometry. An oblate spheroid modeling the subcutaneous tumor geometry; and a thin cylinder as a model of a sugar beet tissue sample as used in many laboratory experiments. The boundary conditions are prescribed either on the both surfaces or on one surface and at the central plane due to symmetry, depending on the modeled system.

ε is equal to $1 - F$; (iii) – the electrical field applied to the tissue during electroporation is assumed spatially homogeneous. This is a valid assumption for the bulk volume of tissue in an electroporation setup with parallel plate electrodes, or even a small block of tissue with an otherwise heterogeneous field distribution (local homogeneity); (iv) – since all cells are modeled as being of equal size and shape and the electrical field homogeneous throughout the modeled block of tissue, application of electroporating pulses to the tissue inflicts an equal distribution of pores, irrespective of the location of an individual cell in tissue; (v) – pores created by electroporation are of various sizes according to some statistical distribution. All further analysis operates with an *average size* of a pore created in the cellular membrane. The same logic of averaging applies to the *number of pores* created, which is assumed to be dependent only on electroporative pulse parameters (e.g. maximum field strength, number and duration of pulses, etc.) and not on local inhomogeneity (in either field strength, geometry or conductivity – these are considered homogeneous throughout the sample).

Returning now to the initial model Equations (1)–(2), we need to establish how volume-averaged intra-to-extracellular (i.e. transmembrane/pore) flow, denoted $k(c_i - c_e)$, depends on electroporation. We start by writing Fick's first law of diffusion for flow through pores in membrane of total (pore) area A_p in spherical geometry of an idealized spherical cell of radius R

$$j_{s,p} = -D_{s,\mathrm{eff}} A_p \frac{dc}{dr}. \tag{3}$$

Integrating across the membrane where the gradient of concentration is non-zero, we obtain

$$j_{s,p} \int_R^{R+d_m} dr = -D_{s,\mathrm{eff}} A_p \int_{c_i}^{c_e} dc$$

giving

$$j_{s,p} = \frac{D_{s,\mathrm{eff}} A_p}{d_m} (c_i - c_e) \tag{4}$$

where d_m is membrane thickness on the order of several nanometers, and $D_{s,\mathrm{eff}}$ is the effective diffusion coefficient of solute species s through a single pore in the cell membrane, which can be approximated as

$$D_{s,\mathrm{eff}} = D_{s,0} y_s \tag{5}$$

where $D_{s,0}$ is the diffusion coefficient of solute species s in water at a given temperature and y_s is the dynamic hindrance coefficient, accounting for hydrodynamic drag and steric exclusion effects.

The change in concentration of solute in intracellular space is entirely due to the trans-pore flow of solute into the extracellular space, i.e.

$$\frac{\partial c_i}{\partial t} = \frac{j_{s,p}}{V_i}. \tag{6}$$

If the pore flow $j_{s,p}$ is that across a single cell membrane, volume V_i is that of one cell and equals $V_i = 4\pi R^3/3$. Since the surface of a single cell A_0 is $4\pi R^2$, we can rewrite Eq. (6) as

$$\frac{\partial c_i}{\partial t} = \frac{3j_{s,p}}{A_0 R} = \frac{3D_{s,eff} f_p}{d_m R}(c_i - c_e) \tag{7}$$

where f_p is the pore surface fraction ratio calculated as A_p/A_0. This formulation using pore surface fraction ratio is useful, as this construct is often encountered in relevant literature (see e.g. [65]). Note that the pore area A_p is the total pore area per cell, and can be expressed as $A_p = \pi N_p r_p^2$, where N_p is the number of pores per cell and r_p the average radius of a single pore.

Comparing now Eq. (2) with Eq. (7), flow coefficient k (also termed mass transfer coefficient) can immediately be expressed as

$$k = \frac{3D_{s,eff} f_p}{d_m R} = P\frac{3}{R} \tag{8}$$

where P is the membrane permeability coefficient [70] and the term $3/R$ accounts for spatial averaging of transmembrane flow within the volume of a single cell and its exact value results from the idealized spherical geometry.

Furthermore, if the volume fraction F of cells in tissue would be exactly 0.5, the transmembrane flow would result in a change in intrinsic intracellular concentration equal to the change in intrinsic extracellular concentration. However, since in tissue in general the cells can occupy a significantly larger (e.g. in plant tissues [71]) or smaller (in e.g. tumor tissues [72]) volume fraction, as compared to extracellular space, the flow of solute out of the cells will also cause a significantly larger or smaller (but proportional) change in intrinsic extracellular concentration, as compared to the change in intrinsic intracellular concentration. Neglecting for a moment extracellular diffusion (in Eq. (1)), we write an equation analogous to Eq. (6), but for the extracellular space

$$\frac{\partial c_e}{\partial t} = \frac{j_{s,p}}{V_e} = \frac{j_{s,p} V_i}{V_e V} = \frac{V_i}{V_e} k \cdot (c_i - c_e) = \frac{1-\varepsilon}{\varepsilon} k \cdot (c_i - c_e) \tag{9}$$

where we have taken into account that in homogeneous tissue, for any arbitrarily chosen, finite and limited (i.e. on the order of comprising only several cells) volume of tissue ΔV, intracellular volume V_i to total volume ΔV ratio can be expressed as $F = 1 - \varepsilon$, and extracellular V_e to ΔV ratio as $1 - F = \varepsilon$. Note that if flow coefficient k were defined using extracellular volume as opposed to the intracellular, the factor $(1 - \varepsilon)/\varepsilon$ would not be present in Eq. (1). Instead, k would have been multiplied by $\varepsilon/(1 - \varepsilon)$ in Eq. (2), giving exactly the same model results.

What remains is to explain the behavior of the dynamic hindrance coefficient y_s. This coefficient captures the effects that hinder solute diffusion through an aqueous pore due to comparable size of the solute molecule to that of the pore as well as any effects of electrical forces due to net surface charges on pore walls and the solute. A number of models have been proposed to describe hindered diffusion through aqueous pores, and comprehensive reviews were published by Deen [73] and Dechadilok and Deen [74]. The suitability of a particular model depends on the application, due to the varying physicochemical properties of the solute of interest that are of primary importance. For the model study with sucrose that we present later on in this paper, we follow a recent study by Liesche and Shulz [75], who modeled sucrose diffusion through plasmodesmata and used a model already proposed in [74], which is based on a modified model previously described by Higdon and Muldowney [76]. According to this model, if λ_r is the solute to pore ratio, $\lambda_r = r_s/r_p$, the hindrance coefficient y_s as a function of λ_r can be given as

$$\begin{aligned} y_s(\lambda_r) = 1 + \frac{9}{8}\lambda_r \ln\lambda_r - 1.56034\lambda_r + 0.528155{\lambda_r}^2 + 1.91521{\lambda_r}^3 \\ -2.81903{\lambda_r}^4 + 0.270788{\lambda_r}^5 + 1.10115{\lambda_r}^6 - 0.435933{\lambda_r}^7. \end{aligned} \tag{10}$$

A slightly simpler but comparable alternative is the Renkin equation [77], given by

$$\begin{aligned} y_s(\lambda_r) = 1 - 4.1\lambda_r + 5.2{\lambda_r}^2 - 0.01{\lambda_r}^3 - 4.18{\lambda_r}^4 + 1.14{\lambda_r}^5 \\ + 1.9{\lambda_r}^6 - 0.95{\lambda_r}^7. \end{aligned} \tag{11}$$

Both functions, plotted for λ_r within the interval [0, 1] and within [0.5, 0.9], are presented in Fig. 4. As evident, the difference in model results for $\lambda_r \geq 0.3$ is practically insignificant.

In order to determine $D_{s,e}$, the solute diffusion coefficient in extracellular space, in general we would have to consider the tortuosity of the extracellular pathways as well as the porosity. However, since we are operating with intrinsic concentrations c_i and c_e, and not concentrations averaged to the total tissue volume (see [67], Section 3.2.1.1 for a detailed explanation of the difference), $D_{s,e}$ is not a function of porosity. It is, however, reduced considerably and to a non-negligible extent due to the tortuosity of the extracellular pathways. In our simplified model of spherical cells, the solute has to diffuse, in order to move a net distance dz along z in the extracellular space, around the model spherical cell. On the level of a single cell, to diffuse by one cell diameter

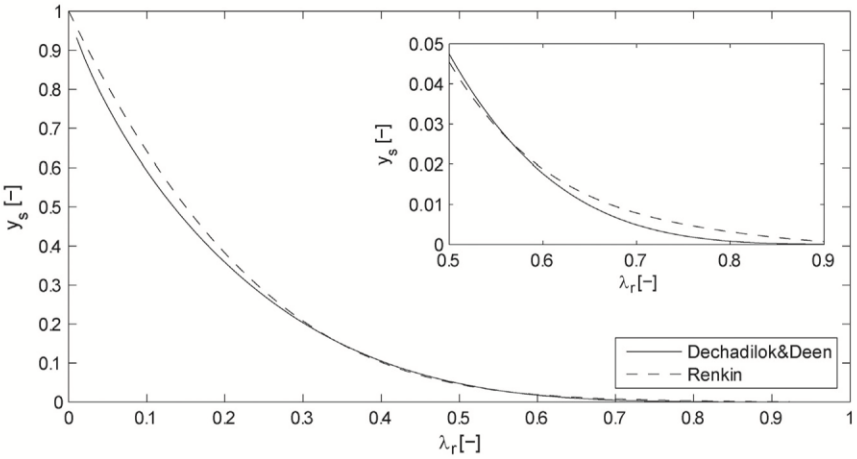

Fig. 4. Effect of steric exclusion and hydrodynamic drag on the dynamic hindrance coefficient y_s of solute through a pore in the membrane-model comparison. The insert is a closer look for λ_r within the bounds [0.5, 0.9].

$2R$ along z, it has to cover a total distance of πR along the hemi-sphere. The tortuosity τ then equals $\tau = \pi R/2R = \pi/2$. The extracellular diffusion coefficient, if intrinsic concentrations are observed, is then $D_{s,e} = D_{s,0}/\tau = D_{s,0}\cdot 2/\pi$, where $D_{s,0}$ is the diffusion coefficient of solute species s in water at a given temperature.

2.2. Analytical solution

In some, albeit few, electroporation applications we are operating with a more or less homogeneous tissue that can also be relatively homogeneously treated with electroporation due to the particular implementation of the treatment application. Such is the case in some industrial applications of electroporation (e.g. extraction, drying, impregnation). This makes coefficients $D_{s,e}$ and k constant in space and time-invariant. Under such conditions, an analytical solution of the dual-porosity model can be obtained. The complete derivation is given in Appendix A.

In order to solve the system of Eqs. (1)–(2), we need to define initial and boundary conditions. To demonstrate the use of the dual-porosity model and provide validation, we will study sucrose extraction from vegetable (sugar beet) tissue. For the purposes of this study, we will model a thin slice of tissue pretreated with electroporation and suspended into a diffusion chamber in a prescribed solid-to-liquid volume ratio, and the liquid medium well stirred. Such setups can readily be found described in the literature, e.g. in [20–22]. The geometrical data for the tissue samples can be found in the table of parameters, Table 1.

We assume that sucrose is initially homogeneously distributed within the intracellular phase and within the extracellular phase (but not necessarily equal in the two media), giving initial conditions

$$c_e(z,0) = c_{e0} \tag{12}$$

$$c_i(z,0) = c_{i0}. \tag{13}$$

During the modeled diffusion experiment, a tissue sample is submerged in distilled water which is constantly agitated. The setup allows us to model one half of a tissue sample due to symmetry. We have the following boundary conditions (BC) for extracellular concentration (l is the thickness of the tissue sample)

$$\frac{\partial c_e(t)}{\partial z}\Big|_{z=0} = 0 \tag{14}$$

$$c_e(t)|_{z=l/2} = 0. \tag{15}$$

The BC for intracellular concentration at the plane of symmetry (mid-section of tissue block at $z = 0$) also equals 0 (no-flux boundary)

$$\frac{\partial c_i(t)}{\partial z}\Big|_{z=0} = 0 \tag{16}$$

while the BC for intracellular concentration at the sample surface is not immediately apparent. It is governed by Eq. (2), and can easily be determined due to the homogeneous BC just given by Eq. (15). Writing Eq. (2) for $z = l/2$, we get an ordinary differential equation

$$\left[\frac{dc_i(t)}{dt}\right]_{z=l/2} + k[c_i(t)]_{z=l/2} = [c_e(t)]_{z=l/2} = 0 \tag{17}$$

with initial condition as already given by Eq. (13). The solution of this ordinary differential equation, as can easily be verified, is

$$c_i(t)|_{z=l/2} = c_{i0}e^{-kt}. \tag{18}$$

The system of Eqs. (1)–(2) with initial and boundary conditions as defined above represents a mathematical model of solute diffusion according to the theory of mass transfer in porous media.

The solution of the PDE system is

$$c_e(z,t) \quad \frac{4c_{i0}}{\pi}\sum_{n\ 0}^{\infty}\frac{(-1)^n}{2n+1}\cos(\lambda_n z)\left(C_{n,1}e^{\gamma_{n,1}t}\left(\frac{\gamma_{n,1}}{k}+1\right)+C_{n,2}e^{\gamma_{n,2}t}\left(\frac{\gamma_{n,2}}{k}+1\right)\right) \tag{19}$$

$$c_i(z,t) = \frac{4c_{i0}}{\pi}\sum_{n=0}^{\infty}\frac{(-1)^n}{2n+1}\cos(\lambda_n z)\left(C_{n,1}e^{\gamma_{n,1}t}+C_{n,2}e^{\gamma_{n,2}t}-e^{-kt}\right)+c_{i0}e^{-kt} \tag{20}$$

where

$$C_{n,1} = \frac{\left(\frac{c_{e0}}{c_{i0}}-1\right)k-\gamma_{n,2}}{\gamma_{n,1}-\gamma_{n,2}} \tag{21}$$

$$C_{n,2} = \frac{\left(1-\frac{c_{e0}}{c_{i0}}\right)k+\gamma_{n,1}}{\gamma_{n,1}-\gamma_{n,2}} \tag{22}$$

and

$$\gamma_{n_{1,2}} = \frac{-\left((\delta+1)k+{\lambda_n}^2 D_{s,e}\right)\pm\sqrt{\left((\delta+1)k+{\lambda_n}^2 D_{s,e}\right)^2-4k{\lambda_n}^2 D_{s,e}}}{2} \tag{23}$$

where for the sake of algebra we have set (see also Appendix A)

$$\delta = \frac{1-\varepsilon}{\varepsilon}.$$

The eigenvalues λ_n equal $\lambda_n = (2n + 1)\cdot\pi/l$.

Observing Eqs. (19) and (20) we notice that process kinetics is determined entirely by the roots of the characteristic polynomial (given by Eq. (23)) of the hyperbolic equation (see Eq. A.15). If there is no electroporation and $k \to 0$, Eq. (23) can be simplified and gives $\gamma_{n,1} \to 0$ and $\gamma_{n,2} \to -\lambda_n^2 D_{s,e}$. At these conditions, diffusion kinetics is governed entirely by the rate of diffusion in extracellular space, i.e. $D_{s,e}$, and there is no transmembrane flow (since $k \to 0$). Eq. (1) becomes an ordinary one-dimensional diffusion equation, whose solution is well-known and can be found in e.g. [69]:

$$c_e(z,t) = \frac{4c_{e0}}{\pi}\sum_{n=0}^{\infty}\frac{(-1)^n}{2n+1}\exp\left(-\frac{D_{s,e}(2n+1)^2\pi^2 t}{l^2}\right)\cos\left(\frac{(2n+1)\pi}{l}z\right). \tag{24}$$

We should point out however that the analytical solution given by Eqs. (19)–(20) becomes extremely unstable during numerical evaluation for $k \to 0$. As k decreases, numerical errors due to finite machine precision (32- or 64-bit floating point representation and operations) are amplified and the model results become unstable. For machine precision on the order of 10^{-16}, this effect becomes observable around $k = 10^{-13}$ and the results become completely unusable for $k < 10^{-14}$. At these extreme conditions however, there is no justification for use of the dual-porosity model whatsoever, and analysis of free diffusion in extracellular space is well described by a much simpler model, such as given by Eq. (24).

At the other extreme, for highly electroporated tissue ($f_p \to 1$), for f_p values above approximately 10^{-3}, the membrane appears to disintegrate, i.e. to lose its barrier function for solute diffusion. In Eq. (23) we

Table 1
Parameters used for model validation and the parametric study of the model.

Parameter	Symbol	Value
Diffusion coefficient — sucrose in water at 20 °C	$D_{s,0}$	4.5×10^{-10} m^2 s^{-1} [34]
Hydrodynamic radius of sucrose molecule	r_s	0.4 to 0.5 $\times 10^{-9}$ m [59,78]
Average stable pore radius	r_p	0.5×10^{-9} m [27,79]
Cell membrane thickness	d_m	5×10^{-9} m [80]
Long-lasting pore surface fraction ratio for one 100 μs pulse	f_p	1.4×10^{-6} [65]
Sucrose initial concentration[a]	c_{e0}, c_{i0}	1 mol m^{-3}
Volume fraction of cells	F	0.6 to 0.8 [71]
Diffusion coefficient of sucrose in extracellular space[b]	$D_{s,e}$	$D_{s,e} = D_{s,0}/\tau = D_{s,0} \cdot 2/\pi$
Average cell size (radius)	R	2.5×10^{-5} m [81]
Tissue sample size (cylinder radius)	ρ	0.0125 m
Tissue sample size (thickness)	l	0.002 m

[a] The absolute value of initial concentration is irrelevant for model analysis, since the model is linear and thus the resulting profiles of concentration kinetics are linearly scalable.
[b] Diffusion in extracellular space is assumed to occur at the rate of diffusion in water but reduced by the factor of tortuosity of the extracellular space. See the last paragraph of Subsection 2.1 for a detailed explanation.

then have $(\delta + 1)k >> \lambda_n^2 D_{s,e}$. This results in extremely fast kinetics ($|\gamma_2| \approx (\delta + 1)k >> 1$) of transmembrane transport and instantaneous diffusion of solute from the intracellular into the extracellular space, provided there is a concentration gradient. This is again unrealistic and outside the scope of the model, as the finite rate of intracellular diffusion is not captured by model equations. The other exponential however, $C_1 \exp(\gamma_1 t)$, is governed primarily by $D_{s,e}$, which limits diffusion out of the tissue block through the extracellular space. Since $C_1 >> C_2$ this results in almost identical diffusion kinetics in extracellular space as in non-electroporated tissue, but with comparatively higher concentrations at a given time. This is as expected, since the extracellular space has to facilitate vacation of not only the solute initially present in the extracellular phase, but of the solute present within the cells as well (determined by the initial condition for intracellular concentration).

As emphasized by this analysis, there are limitations of the proposed dual-porosity model and its analytical solution. These limitations must be kept in mind during experimentation with the model, and one should maintain a critical view at the results in light of these observations to avoid analysis under unrealistic or extreme conditions.

2.3. Parameters and experimental methodology for the model study of sugar extraction and the parametric study

To provide model validation, we performed diffusion experiments with sugar beet tissue pretreated with electroporation. The experimental setup was then modeled by the dual-porosity model and results were compared with experimental measurements. We also present a parametric study (see Results and discussion), by means of which we evaluate the sensitivity of the model to five parameters. Table 1 summarizes the parameters of the model that were used in the model study for validation of the model and for the (purely theoretical) parametrical study. The references are given in square brackets where applicable.

A brief note on the initial concentration; the parameters presented in Table 1 will be used for parametrical model analysis in the special case of plant tissue electroporation, and since we start observing diffusion in tissue about two to three minutes after the electric pulse application, we believe this pause is long enough to assume that initial concentrations inside and outside the cells are equal at the beginning of simulation. This initial state is supposed to result from release of intracellular fluid from electroporated cells containing solute of our interest (among other dissolved substances) into the extracellular space, a process that begins after applying electroporative pulses, presumably leading to local equilibrium in concentration before the start of the simulated diffusion experiment. Note that this supposition is only valid if treatment is applied to the sample. In a non-electroporated sample, we would have to suppose an initial imbalance between the intra- and extracellular concentration.

The details of the experimental setup have been previously described elsewhere [22], though some important differences do exist in the particularities of the geometry and experiment execution. Cylindrical samples (disks) of sugar beet tissue were obtained from 5 mm thick sugar beet slices. The samples measured 25 mm in diameter. Each individual sample was electroporated by applying 400 V between parallel plate electrodes at 5 mm distance (sample thickness). Bipolar pulses rectangular in shape, of 100 μs duration each and pulse repetition frequency of 1 kHz were delivered within each train of 8 pulses. Two such trains were delivered with a pause of one second between the two trains. The samples were removed from the treatment cell, after which the surfaces of the disks were dried with absorbent paper to remove sugary liquid on the surfaces. This liquid is present due to cutting and possibly due to electro-osmotic or pressure-change effects that occur during the electroporation treatment. Note that had this step been omitted, the surface liquid would cause an immediate increase in sucrose concentration in the solution at the beginning of the experiment, an effect which is not captured by the model. The surface-dried samples were then placed into a flask with a magnetic stirrer. The liquid was constantly agitated and sampled at regular intervals; sucrose concentration was analyzed with a digital refractometer. The liquid-to-solid ratio was 2:1.

The quantity measured by the digital refractometer is sugar concentration in liquid with unit degrees Brix (°B). One degree Brix is 1 g of sucrose in 100 g of solution and represents the concentration of the solution as percentage by weight (% w/w). If we know the initial sugar content of the aqueous solution ($^\circ Bx_0$) and the final content ($^\circ Bx_d$) – which in an ideal situation would be equal to the total sugar content in a tissue sample – we can define *normalized degree Brix* at time t — i.e. $B(t)$, as

$$B(t) = \frac{^\circ Bx(t) - ^\circ Bx_0}{^\circ Bx_d - ^\circ Bx_0}. \tag{25}$$

Normalized Brix will be our measure for the amount of solute (e.g. sugar) that has diffused out of the tissue sample in time t. It takes the values $0 \le B(t) \le 1$ and is dimensionless. It is obtained by a trivial calculation from measurements with the refractometer, according to Eq. (25). To arrive at the same quantity from the spatio-temporal intra- and extracellular concentration profiles given by the model (see Fig. 7), these profiles must be integrated on the spatial coordinate z to obtain the observable and measurable bulk concentration of sucrose in

the solvent outside the tissue samples. The total mass left in the sample equals

$$m(t) = 2\pi\rho^2\left[\varepsilon\int_0^{l/2} c_e(z,t)dz + (1-\varepsilon)\int_0^{l/2} c_i(z,t)dz\right]. \quad (26)$$

On the other hand, the total initial mass of solute is equal to

$$m_0 = m(0) = \pi\rho^2 l[\varepsilon c_{e0} + (1-\varepsilon)c_{i0}]. \quad (27)$$

Normalized Brix for the solution into which the sample is submerged is then

$$B(t) = 1-\frac{m(t)}{m_0} = 1-\frac{2\left[\varepsilon\int_0^{l/2} c_e(z,t)dz + (1-\varepsilon)\int_0^{l/2} c_i(z,t)dz\right]}{l[\varepsilon c_{e0} + (1-\varepsilon)c_{i0}]}. \quad (28)$$

A subtraction of $m(t)/m_0$ from 1 is necessary since we are interested in the extracted solute and not the amount remaining in the sample.

2.4. The dual-porosity model of tissue electroporation in biomedicine — model generalization

To demonstrate the universal applicability of the dual-porosity model in modeling tissue electroporation, we describe in this section the necessary modifications to the model that are required to study transport phenomena in two biomedical applications of electroporation: electrochemotherapy (ECT) [10], and trans- or intradermal drug transport [16].

The objective of ECT is to facilitate introduction of chemotherapeutic drugs into tumor cells by applying electroporation [82]. The two most commonly used drugs in ECT are bleomycin and cisplatin. Bleomycin is a highly potent drug that binds to DNA where it causes DNA cleavage resulting in eventual cell death at mitosis; it however poorly permeates the intact cellular membrane. Electroporation enhances the drug uptake and thus low local or systemic drug concentrations can be used for effective local chemotherapy. As a model example, we examine the situation illustrated by Fig. 5. The subcutaneous tumor is modeled as an oblate spheroid embedded into the subcutaneous tissue immediately under the skin layer. In this model configuration, the tumor is separated from the surrounding tissue by two interfaces; the tumor–subcutaneous tissue boundary surface and the tumor–skin boundary surface. For the purposes of further analysis, we establish the following set of assumptions: *a*) In our example, bleomycin is given intravenously, not intratumorally. Due to interstitial fluid pressure that is present inside the tumor before electroporation [83,84], the initial drug concentration inside the tumor region for both intra- and extracellular spaces is zero, as the drug cannot extravasate into the tumor region; *b*) If surface-applied plate electrodes are used, the skin is electropermeabilized along with the tumor, the resulting vascular lock [85,86] and damage due to irreversible electroporation in the dermis warrant the supposition that skin presents a negligible sink or source of bleomycin, i.e. from the point of view of pharmacokinetics, the skin does not represent a compartment; *c*) Provided the perfusion of subcutaneous structures remains unaffected by electroporation, it can be represented, locally, as an infinite reservoir of bleomycin, since the localized drop in concentration due to cellular uptake is immediately replenished via convective transport by the vascular system; *d*) If the drug has difficulties entering tissue (e.g. due to interstitial fluid pressure), its concentration locally may be low within the tumor region. In those areas, bleomycin that is reacting with the DNA and is getting used up decreases the drug concentration, which may be important. We thus include in the model the bleomycin reaction rate R_B, where $R_B < 0$; *e*) Achieving local tumor coverage with fields above the threshold of reversible electroporation is critical for permeabilizing the cells and facilitating bleomycin uptake. Electrode configuration, placement, pulsing protocol, and tissue electrical properties determine field distribution and the energy delivered. These factors should not be neglected as the research field is highly advanced on this subject and importance of local field distribution has been strongly emphasized in numerous works, see e.g. [87–89].

The model equations for tumor intra- and extracellular concentrations c_i and c_e, respectively, are

$$\frac{\partial c_i}{\partial t} + k(c_i - c_e) - R_B = 0 \quad (29)$$

$$\frac{\partial c_e}{\partial t} + \nabla\cdot\left(-D_{B,e}\nabla\cdot c_e\right) - \frac{1-\varepsilon_t}{\varepsilon_t}k(c_i - c_e) = 0 \quad (30)$$

where $D_{B,e}$ is the bleomycin diffusion coefficient in the extracellular space and ε_t is the porosity of tumor tissue. Note that in Eqs. (29)–(30) the concentrations are functions of all 3 spatial coordinates and time. R_B is the reaction rate of bleomycin as it binds to DNA. There is also a difference in the flow coefficient k as compared to the expression previously given by Eq. (8). In Eqs. (29)–(30) above,

$$k(t,E) = \frac{3D_{B,eff}f_p(t)}{d_m R}\cdot u(E) \quad (31)$$

where

$$u\left(\left|E\left(\vec{r}\right)\right|\right) = \begin{cases} 1 & ;\left|E\left(\vec{r}\right)\right| > E_{rev} \\ 0 & ;\left|E\left(\vec{r}\right)\right| < E_{rev} \end{cases}. \quad (32)$$

The introduced function $u(E)$ is a unit step that models the effects of the inhomogeneous electric field established in tissue and is a time-invariant function of local maximal electric field strength distribution. E_{rev} is the reversible field strength threshold (scalar value) that must be reached locally to successfully permeabilize the cells [61,90]. Additionally, the pore surface fraction f_p of long-lasting pores is now time-dependent to capture the effects of pore resealing [59]. Due to the interstitial fluid pressure within the tumor (see model assumption *a*), initial conditions are:

$$c_{i0} = c_i(t=0) = 0 \quad (33)$$

$$c_{e0} = c_e(t=0) = 0 \quad (34)$$

and boundary conditions (according to model assumptions *b* and *c*) are

$$[c_e]_{S_1} = c_e^{\,s}(t) \quad (35)$$

$$\left[\frac{\partial c_e}{\partial\,\vec{r}}\right]_{S_2} = 0 \quad (36)$$

$$\left[\frac{\partial c_i}{\partial\,\vec{r}}\right]_{S_1} = \left[\frac{\partial c_i}{\partial\,\vec{r}}\right]_{S_2} = 0 \quad (37)$$

where S_1 is the tumor–subcutaneous tissue boundary surface and S_2 the tumor–skin boundary surface (see Fig. 5). For intracellular bleomycin concentration, both boundaries are reflective (no-flux), while for the extracellular concentration the tumor–skin boundary surface is reflective and the tumor-subcutaneous tissue boundary surface has a prescribed time-dependent concentration $c_e^s(t)$. This is the extracellular concentration of bleomycin in the subcutaneous

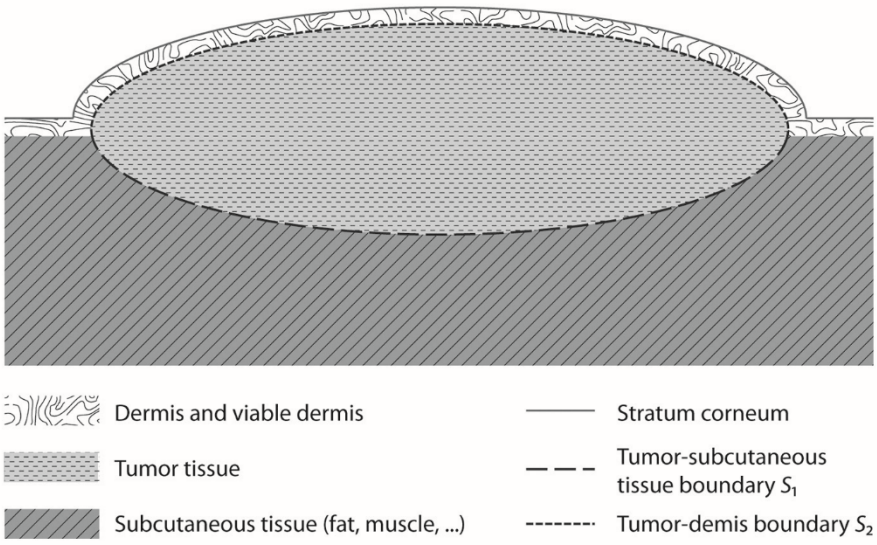

Fig. 5. Model of a subcutaneous tumor.

tissue (comprising fat and muscle tissue, and the vascular system) and is determined by the amount of drug given intravenously, the body mass of the animal and the time passed since the moment of injection. Solving the system of Eqs. (29)–(37) is out of the scope of this paper and requires a numerical approach. Finite element software supporting immediate and direct implementation and analysis of this exemplary model is readily available on the market (e.g. COMSOL Multiphysics, COMSOL AB, Sweden).

In the second example of applying the dual-porosity model in the biomedical field we examine the trans- and intradermal drug transports [16]. For transdermal drug transport, perhaps the most interesting effect of electroporation application to the skin is the disruptive effect of electric pulses to the skin's most protective barrier layer — the stratum corneum (SC). Due to formation of the so-called local transport regions (LTRs) [14,15] during electroporation, the permeability to molecules of the skin's outermost protective layer can be increased by orders of magnitude. During electroporation, this occurs rather rapidly and as subsequently the electrical resistance of the SC drops, this allows for electroporation of underlying skin layers (see Fig. 6). The disruption of the barrier function in SC facilitates diffusion of molecules with molecular weight even greater than 7 kDa, though the process is relatively nonspecific and dose control difficult [16]. To enhance the passive transport, application of low-voltage electrophoretic pulses after high-voltage electroporation has been proposed and is a subject of recent studies [91]. If the therapeutic molecules (e.g. DNA material, or fentanyl [92]) are present in the dermis, electroporation facilitates uptake of these molecules by viable electroporated cells of the dermis and/or underlying tissues [16]. This is the intradermal application, used, in example, for intradermal gene transfection for DNA vaccination [93]. Given the structure of the skin (stratum corneum, viable epidermis, dermis, follicles, etc.) there are several routes available for transport. Which route is more important depends on the treatment protocol and the properties of the drug (charge, size, partition coefficient). In example, lipophilic molecules can permeate via the transcellular route, while hydrophilic molecules generally do not. If the epidermal cells are electroporated however, the hydrophilic molecules can enter the cells of the epidermis with expressed therapeutic effect.

To model this situation with the dual-porosity model, we examine the situation conceptualized with the help of Fig. 6. A patch (reservoir) containing the therapeutic drug is placed on the electroporation-treated section of the skin, and we are interested in the amount of

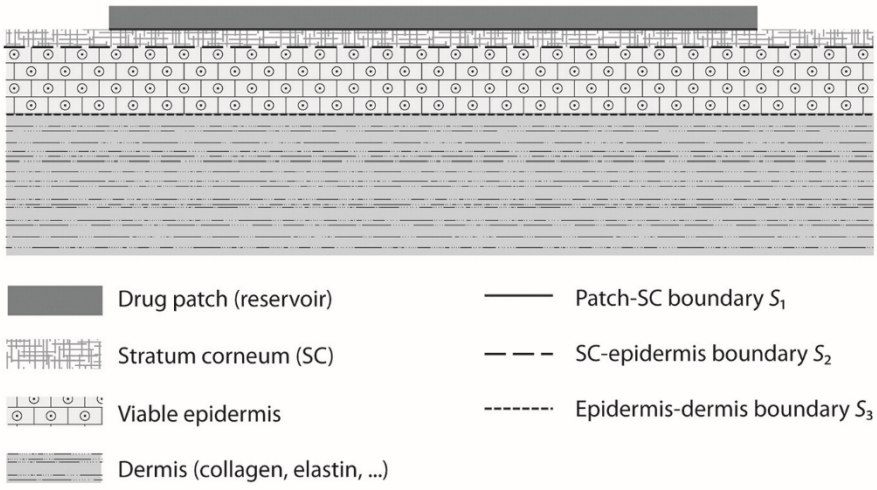

Fig. 6. The conceptual skin model for the transdermal drug delivery example.

drug reaching the bottom-most layer, i.e. the basal layer, of viable epidermis. Following the model of SC permeabilization established by Becker [15], we write, for the SC layer,

$$\frac{\partial c^{SC}}{\partial t} = \frac{1}{\tau_{SC}}\left[\nabla \cdot \left(D_L \nabla c^{SC}\right)\right] \tag{38}$$

where c^{SC} is the intrinsic (not accounting for porosity!) drug concentration in the lipid pathways between corneocytes in the SC and τ_{SC} is the tortuosity of the SC phase. D_L is the effective diffusion coefficient of the permeating drug in the porous lipid-filled spaces between the corneocytes in the SC layer. Assuming the SC layer is homogeneous and the patch containing the drug as well as the electroporated area are large as compared to the thickness of the SC layer, only the gradient along the principal axis of diffusion can be considered and diffusion coefficient moved out of the gradient operator, yielding

$$\frac{\partial c^{SC}}{\partial t} = \frac{D_L}{\tau_{SC}}\frac{\partial^2 c^{SC}}{\partial z^2} \tag{39}$$

with initial condition $c^{SC}(z, 0) = 0$, and boundary conditions

$$\left[c^{SC}\right]_{S_1} = c_R(t) \tag{40}$$

$$\left[c^{SC}\right]_{S_2} = \left[c_e^E\right]_{S_2} \tag{41}$$

$$\left[\frac{\varepsilon_{SC} D_L}{\tau_{SC}}\frac{\partial c^{SC}}{\partial z}\right]_{S_2} = \left[\frac{\varepsilon_E D_E}{\tau_E}\frac{\partial c_e^E}{\partial z}\right]_{S_2} \tag{42}$$

where ε_{SC} is the porosity of the SC layer, ε_E and D_E are the porosity and effective drug diffusion coefficient in the epidermis, respectively, c_R is the reservoir (drug patch) concentration that can be modeled as constant if the drug is poorly permeable and the reservoir volume large, c_e^E is the epidermis extracellular intrinsic concentration, and τ_E is the tortuosity of the lipid-filled pathways in the epidermal layer. If the cells of the epidermis are electroporated and this significantly influences the drug's ability to enter viable cells, we can now write the dual-porosity model equations for the epidermis

$$\frac{\partial c_e^E}{\partial t} - \frac{D_E}{\tau_E}\frac{\partial^2 c_e^E}{\partial z^2} - \frac{1-\varepsilon_E}{\varepsilon_E} k_E\left(c_i^E - c_e^E\right) = 0 \tag{43}$$

$$\frac{\partial c_i^E}{\partial t} + k_E\left(c_i^E - c_e^E\right) - R_d = 0 \tag{44}$$

where c_i^E is the epidermis intracellular intrinsic concentration, R_d the reaction rate of the drug species d as it reaches its intracellular target, and k_E the epidermis permeabilization coefficient calculated according to Eq. (8). The rest of the boundary conditions, in addition to Eqs. (41)–(42) are all homogeneous Neumann (i.e. no-flux) boundaries

$$\left[\frac{\partial c_i^E}{\partial z}\right]_{S_2} = \left[\frac{\partial c_i^E}{\partial z}\right]_{S_3} = \left[\frac{\partial c_e^E}{\partial z}\right]_{S_3} = 0 \tag{45}$$

and initial conditions are ${c_e}^E(z, 0) = {c_i}^E(z, 0) = 0$.

If the finite dimensions (capacity) of the drug patch are not negligible, i.e. the emptying of the reservoir is significantly fast due to high rate of trans- or intradermal diffusion, we have to account for the fact the patch concentration of drug c_R is time-dependent. In this case, the concentration c_R can be expressed according to the law of mass conservation as

$$c_R(t) = c_{R0} - \frac{D_{SC}}{d_R}\int_0^t \frac{\partial c^{SC}}{\partial z}\Big|_{S_1} dT \tag{46}$$

where d_R is the thickness of the patch or more precisely, the patch volume to SC-patch contact surface ratio, D_{SC} is the effective drug diffusion coefficient where the complete SC layer is taken into account ($D_{SC} = D_L \varepsilon_{SC}/\tau_{SC}$), and c_{R0} is the reservoir initial drug concentration.

The two examples given above illustrate how the dual-porosity model can be incorporated into or coupled with existing models developed within their respective fields of biomedical electroporation applications. Further development of these models, parameter estimations and validation extend beyond the scope of this paper and are the subject of our future work.

3. Results and discussion

3.1. The intra- and extracellular concentration profiles — visualization of model results

All of the following figures were made with MATLAB version 2012a (MathWorks, Massachusetts, USA), an engineering software package by means of which the analytical solution was implemented in computational terms, and built-in functions provided by this package were used to draw the calculated results. The meshing coefficient (number of vector elements for space and time) was 100 in all cases, providing good spatial and temporal resolutions. Fig. 7 presents the extracellular (Fig. 7a, c) and intracellular (Fig. 7b, d) concentrations as a function of space and time, obtained via the analytical calculation for the set of parameters presented in Table 1 (upper limit values were used where a range is given). In terms of the spatial dimension, only one half of the tissue slab is modeled since we have assumed symmetry along the central plane (see Fig. 3). We can observe (Fig. 7a, b) that while in intact tissue solute diffuses out of the extracellular space and into the space surrounding the tissue block relatively unhindered at a rate determined by $D_{s,e}$, it is mostly retained in the intracellular space. This is consistent with observation, since the surface fraction ratio of pores close to 1.4×10^{-6} corresponds to a single 100 μs pulse of amplitude that is generally considered insufficient to successfully permeabilize the membrane [49,65,94].

Fig. 7c–d shows the results for a situation very similar to that illustrated in Fig. 7a–b, but with a change in one model parameter. To obtain results given by Fig. 7c–d, we have made an increase in value of f_p from 1.4×10^{-6} to 2.5×10^{-5}, effectively increasing the pore surface fraction (and thus k) by about an order of magnitude. As a result, solute diffuses noticeably from both the intracellular space as well as the extracellular space. Notice that the extracellular concentration at the end of the simulation (7200^{th} second, Fig. 7d) is higher than the corresponding concentration in Fig. 7a due to the contribution of intracellular solute diffusing out of the cells.

Fig. 8 shows intracellular intrinsic concentration calculated analytically for $n = 0$ (Fig. 8a), $n = 0…3$ (Fig. 8b) and $n = 0…10$ (Fig. 8c) for the same set of parameters used to obtain Fig. 7d, where n is the index of the infinite series in Eqs. (19)–(20). Fig. 8 demonstrates rapid convergence of the series given by Eq. (19). If we look carefully at Fig. 8a, we may observe a slight overestimate of concentration near $z = 0$, which is almost completely gone if we account for 4 members of the series (Fig. 8b) and for even higher accuracy, becomes impossible to detect by merely examining concentration profiles, as is evident in comparing Fig. 8b and 8c. This rapid convergence makes the analytical model highly suitable for use in optimization algorithms, in which optimal values of parameters may be determined given a set of experimentally-obtained data. Note that the boundary condition for extracellular concentration in combination with constant initial condition

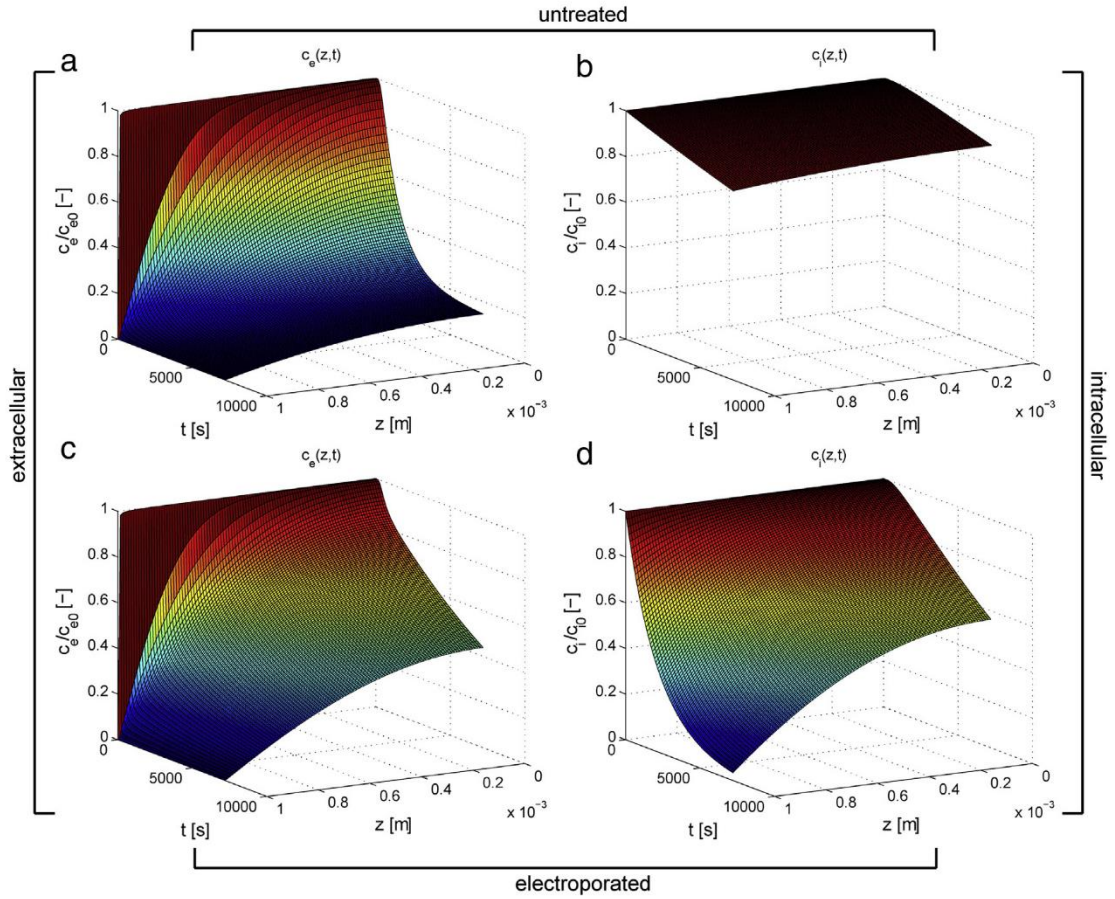

Fig. 7. Results of the calculation of concentration in our model study for parameters given in Table 1. The spatio-temporal dependence of intrinsic concentration in the extracellular (a) and in the intracellular space (b) for one 100 μs pulse (almost intact tissue). Results after increase of the pore surface fraction f_p by about one order of magnitude; extracellular (c) and intracellular (d) intrinsic concentration.

(an artifact of modeling only for the steady-state conditions) results in a sharp discontinuity at $z = l/2$. This makes the series in Eq. (20) converge rather poorly. To overcome this limitation, we calculate intracellular concentration first according to Eq. (19), then perform (numerically) differentiation, multiplication and addition according to Eq. A.1 (see Appendix A) to obtain extracellular concentration, avoiding the use of the poorly convergent infinite series (Eq. (20)) altogether.

3.2. Model study with extraction experiments — model validation

In this section we evaluate how well the described model performs at the task of modeling a particular process and explaining experimentally obtained data. The details of the experiment have been previously described in the literature [22]. Important deviations from the published setup were described in Section 2.3 of this paper. Data obtained during the course of these experiments was used for the purposes of the following analysis.

In the experiments, cylindrical blocks of sugar beet tissue were pretreated with electric field according to a protocol ensuring a low degree of membrane permeabilization (see section 2.3). Following the electroporation treatment, samples were placed into a diffusion chamber. In the literature where such or similar experiments have been described, quantitative analysis of the results is often done by fitting the experimental data to the model of diffusion kinetics in a

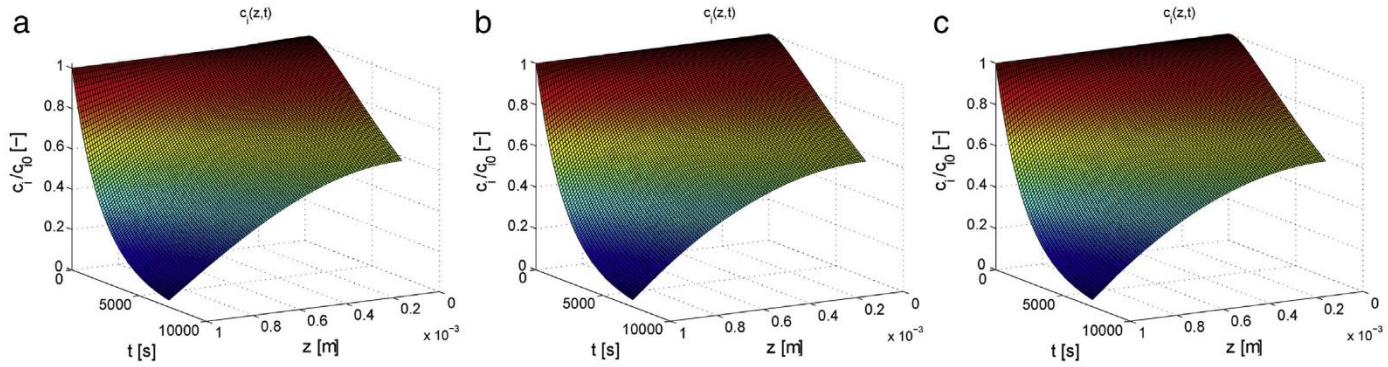

Fig. 8. Analytical solution for intracellular concentration according to the dual-porosity model. (a) For $n = 0$ (see Eq. (19)); (b) for $n = 0…3$; and (c) for $n = 0…10$.

homogeneous plane sheet of uniform thickness, found in e.g. [69] and obtainable by integration of Eq. (24) (see section 2.2). The normalized Brix according to this model is

$$B = 1 - \frac{8}{\pi^2}\sum_{n=0}^{\infty}\frac{1}{(2n+1)^2}\exp\left(\frac{-D_{\text{eff}}(2n+1)^2\pi^2 t}{l^2}\right) \quad (47)$$

where l is, contrary to the definition in [69], the total sample thickness (not half-width) as defined and used in this paper. Note that D_{eff} in Eq. (47) is the effective diffusion coefficient in the (homogeneous!) material forming the plane sheet, and must not be confused with the effective pore diffusion coefficient $D_{s,\text{eff}}$ as defined earlier in this paper. As the series in Eq. (47) converges rapidly for large values of time, about five of the first members of the series are usually accounted for to find the effective diffusion coefficient by fitting the model to the experiment with the least-square error method. In doing so however due to the nature of the one-exponential model we sacrifice a good fit for either low or for high values of time. In Fig. 9, we show experimental data and three results of modeling. Two were obtained using Eq. (47) and the third is a result of parametrical optimization on the dual-porosity model. From comparison of all three model results (RMSD equal to 0.173 and 0.092 for model in Eq. (26) using $D_{\text{eff}} = 0.15 \times 10^{-10}$ and $D_{\text{eff}} = 0.34 \times 10^{-10}$ m^2s^{-1}, respectively; and to 0.014 for the dual-porosity model) it is evident that the dual-porosity model provides for a superior fit and can explain what the one-exponential model of homogeneous material cannot; that is the approximately linear increase in sucrose concentration during the experiment (except at the very beginning), as a result of hindered diffusion of the sucrose deposited in the intracellular space leaving the tissue block via the extracellular route. The model as given by Eq. (47) is insufficient to capture this phenomenon as it has been derived for a sheet of homogeneous material with one effective and constant rate of diffusion (governed by D_{eff}). The dual-porosity model however offers this possibility since its temporal solution is based on a description of the system via a 2nd order hyperbolic differential equation (see Appendix A). This means we have, in terms of kinetics, two additive exponential members in the solution determined by the parameters of electroporation and its impact on the porosity of the membrane separating the two phases. According to the theory of electroporation and our understanding of its effects on cells in tissue, such a model is needed to capture the contribution of presumably faster extracellular diffusion and that of slower, hindered diffusion, out of electroporated cells through a semi-permeable membrane. What is even more important is that the effective diffusion coefficient as obtained from fitting experimental data by Eq. (47) has no physiological meaning. It is purely phenomenological, as it does not equal either the rate of extracellular diffusion, neither the rate of transmembrane diffusion, nor the solute diffusion coefficient in the liquid medium (i.e. water). On the contrary, all of the parameters used in the dual-porosity model reflect properties of the tissue before or after electroporation treatment. The parameter values are either obtained from or estimated based on published literature.

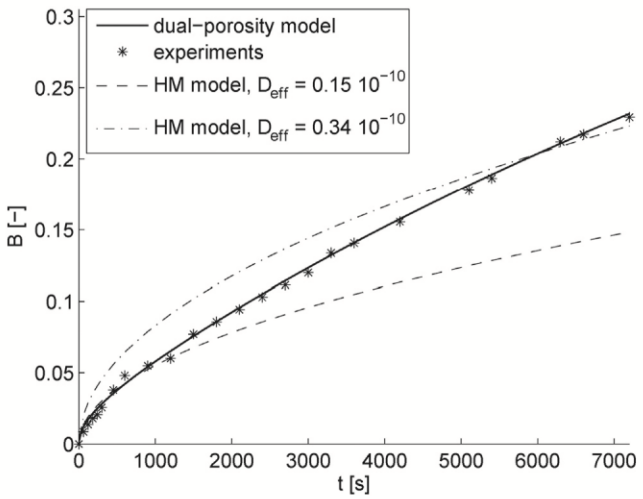

Fig. 9. Fitting the model to experimental data. The experimentally obtained data and the best-fit dual-porosity model results are given along with two plots of Eq. (47) using different value of parameter D_{eff}. The two values were selected in order to obtain a good agreement either during the initial 1000 s or towards the end of the experiment. Parameters of the dual-porosity medium used (those that differ from Table 1): $f_p = 0.9 \times 10^{-5}$, $l = 0.005$ m. HM in figure legend stands for homogeneous material.

A note about the method used for initial estimation of f_p, the fraction of long-lived pores, used to model experimental data as shown in Fig. 9. Table 1 gives f_p determined based on experiments as described in [65], where the authors give an estimation of the fraction of long-lived pores for a single 100 μs pulse of 860 V/cm, as well as a train of 2, 4 and 8 such pulses. Since we used a similar protocol, applying 800 V/cm in two trains of 8 pulses (details can be found in Section 2.3), we linearly extrapolated the results of the cited study, and we arrived to an initial estimate for pore surface fraction on the order of 10^{-5}. However, via model simulation and optimization of results to match the experimental data, we had to reduce this estimate by 10% to 0.9×10^{-5}, in order to obtain the best agreement between the model and the experimental results.

Also note that since the experimental data used to evaluate the model in this specific example was obtained at a relatively low degree of membrane electroporation (disintegration index Z [38] equal to about 0.35), the potential for quantitative analysis of this model cannot be accurately assessed from a single experimental study alone. The low degree of permeabilization also results in a higher discrepancy between the dual-porosity model results and results of the model of homogeneous material, thus demonstrating the better performance of the dual-porosity model under such conditions. During experiments at various treatment intensities (pulse number and duration) we observed that as tissue is being treated by electroporation of ever increasing intensity, it also tends to behave more and more as though it were a homogeneous material. Thus, further work is needed in order to evaluate the model in relation to experimental results, especially at higher degrees of membrane electroporation.

3.3. Parametrical study — analysis of model behavior and sensitivity

We begin by analyzing the influence of pore surface fraction, f_p. Fig. 10a gives $B(t)$ for a number of values of this parameter, equally spaced on a logarithmic scale. We observe that for very low values of pore surface fraction, B reaches the value 0.2, which is the volume fraction of extracellular space used in this model study (Table 1). This makes sense, as only the solute present in the extracellular medium is extracted. For highly porous membranes on the other hand, the final B is just below 0.7, a consequence of simulation time which is not long enough (relative to the extracellular diffusion rate and sample dimensions) to allow for all the solute to vacate the tissue sample completely (see Fig. 7). In between these two extremes, the total yield of solute at simulation end changes rapidly for pore surface fractions between 10^{-6} and 10^{-4}. This is clearly demonstrated in Fig. 10b, where the value of B at simulation end is plotted for sixteen (arbitrarily chosen number) distinct values of f_p in the range $2.5 \times 10^{-10} \le f_p \le 7.5 \times 10^{-3}$.

Next, we analyze the impact of varying λ_r, the solute to pore radius ratio. This is perhaps the most difficult and problematic of the parameters of the model we present, since it displays a strong nonlinearity (see Eqs. (10)–(11) and Fig. 4) and very rapidly approaches 0 as the radius of solute becomes comparable to the radius of an average pore, which is our case since the sucrose hydrodynamic radius of about 0.4 nm is

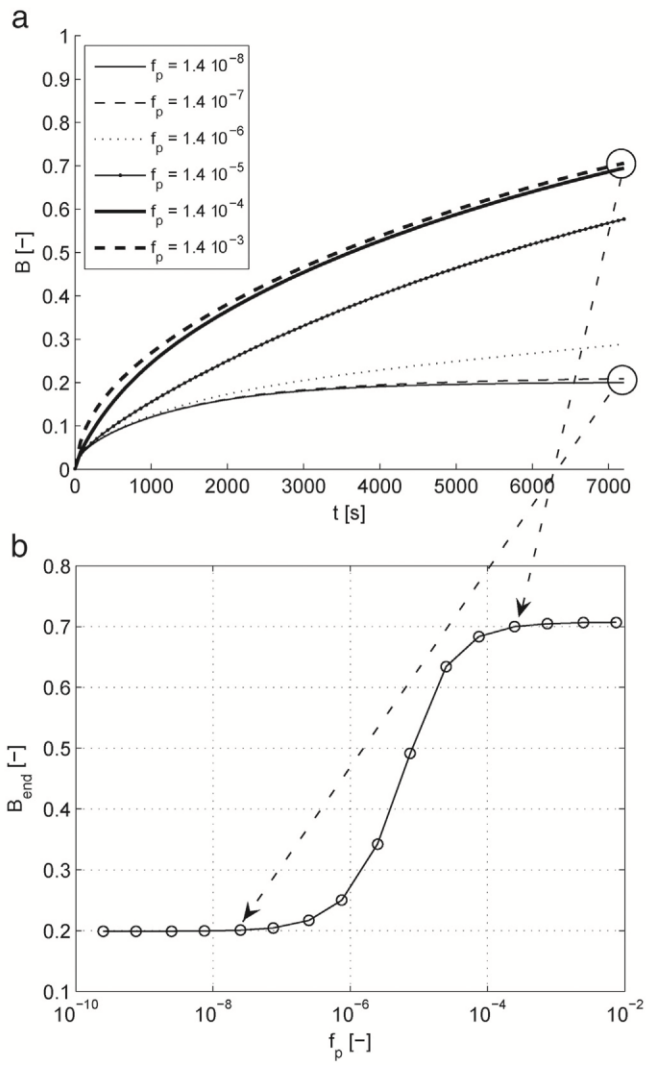

Fig. 10. (a) Normalized Brix as a function of time for six distinct values of pore surface fraction. (b) Normalized Brix at the end of simulation for sixteen values of pore surface fraction — note the sharp increase around $f_p = 10^{-6}$.

comparable to a 0.5 nm radius of a stable electro-pore. Often the solute radius is unknown and pore size is hard to determine, but even at best it is always a result of a statistical model or estimation based on particular experiments. The value used in this study ($\lambda_r = 0.85$) is based on rough estimates of both the solute and average pore size from literature and should be understood as a best guess that enables this model to present results and the parametric study consistent with literature. A detailed analysis and development of the model in this direction are matters of future research. The impact of λ_r on the effective pore diffusion coefficient is already given in Fig. 4. We varied this parameter linearly within the range $0.05 \leq \lambda_r \leq 0.95$ and the effect on normalized Brix is shown in Fig. 11a.

In Fig. 11b we examine the impact of volume fraction ratio of cells in tissue F, as defined in section 2.1 (see model assumptions). The fraction ratio is very important for extraction dynamics since it defines the porosity of tissue ε (where $\varepsilon = 1 - F$), and porosity determines the macroscopically observable rate of diffusion, as viewed within the context of the complete block of tissue. If rate of diffusion is averaged over the entire volume of the tissue sample, the extracellular diffusion coefficient is dependent on the extracellular porosity, $D_{s,e} = \varepsilon/\tau \cdot D_{s,0}$, and thus on the volume fraction of cells in tissue. However, the effects of electroporation on these parameters, or indeed on the porosity, are not well known and will have to be evaluated in the future. We have included this parameter in the analysis, since experimental and theoretical evidences exist that the cell volume fraction ratio is a function of electroporation [95,96]. The effective change (an increase) of cell volume ratio has been observed to occur in animal tissues due to colloid-osmotic swelling [95] and presumably cell shrinkage in plant tissue due to loss of turgor [96] during and after electroporation causes an effective decrease of the cell volume fraction. Moreover, with very high degrees of damage to tissues in extraction processes, a fraction of cells may be irreversibly electroporated. Irreversible electroporation leads to cell lysis, and we can reasonably assume that after the complete loss of the barrier function of the cell membrane, we can no longer consider the space previously occupied by the cell as intracellular space. We also need to consider that cell volume fraction ratio is dependent on the tissue sample and origin, as it varies between species of animal or plant whose tissue we are subjecting to the electroporation treatment. Plant tissues, in example, exhibit various volume fractions by virtue of natural diversity alone, among different species and even samples taken from a single species, depending on growing, harvest, and storage conditions [71].

Since some of the processes in electroporation-facilitated mass transfer also occur at temperatures higher than room temperature, e.g. in extraction of compounds from plant tissues, a combination of electroporation and temperature as high as 80 °C is used [22,97] and for clinical electrochemotherapy the temperature is that of the patient's body, we present model results at different temperatures by means of varying the diffusion coefficient $D_{s,0}$ (see Fig. 11c). The diffusion coefficient at various temperatures was recalculated from measurements reported in the literature [34] with the help of the Einstein–Stokes relation and data on viscosity of water as a function of temperature [98].

Fig. 11d shows the influence of the more realistic assumptions about initial extracellular concentrations for low degrees of membrane permeabilization. To obtain Fig. 10a, we assumed that initial intrinsic concentrations are equal in the extracellular space and the intracellular space, i.e. $c_{i0} = c_{e0}$. The rationale is that since some time passes between the electrical treatment of a sample and the beginning of a diffusion experiment, for high degrees of electroporation the intra- and extracellular concentrations equilibrate. At low permeability of the cell membrane however, this assumption is no longer valid. We therefore illustrate extraction kinetics if at $f_p = 1.4 \times 10^{-6}$ the c_{e0}/c_{i0} ratio varies within the range [0.2, 1].

Notice that λ_r (Fig. 11a) does not dramatically decrease the speed of diffusion at around the value of 0.20, but has a very strong impact at values of 0.45 and above, where the transmembrane through-pore flux due to constriction is brought almost to a halt. This is explained by the highly nonlinear relation between λ_r and the effective diffusion coefficient, as previously shown by the insert in Fig. 4. An interesting point is made by interpreting the results at very low values of λ_r. Under these conditions, we have low permeabilization ($f_p = 1.4 \times 10^{-6}$) but a high yield of solute that has diffused out of the tissue. We can suppose the transport modeled at these parameter values is that of small molecules (much smaller than sucrose) and that of ions.

Not surprisingly, the dependence on volume fraction of cells (Fig. 11b) shows a linear dependence on extracted solute yield due to low pore surface fraction used in simulation (see Table 1), resulting in the bulk of diffused (extracted) solute being the solute found initially in the extracellular medium.

Results in Fig. 11c quantify the effect of increasing the temperature of extraction if only the thermal effects on diffusion rate are supposed, with no influence of heat on cell or tissue structure. The values of $D_{s,0}$ used correspond to 20, 30, 40, 50, 60 and 80 °C.

The model results given by Fig. 11d confirm our expectations and are in accordance with performed diffusion experiments (as published in the literature, see e.g. [22]). If membrane permeabilization is low or nil, only extracellular sucrose diffuses and as the sucrose is primarily stored in the intracellular vacuoles, the final yield is low. Note that the range of values on the ordinate axis is [0, 0.5].

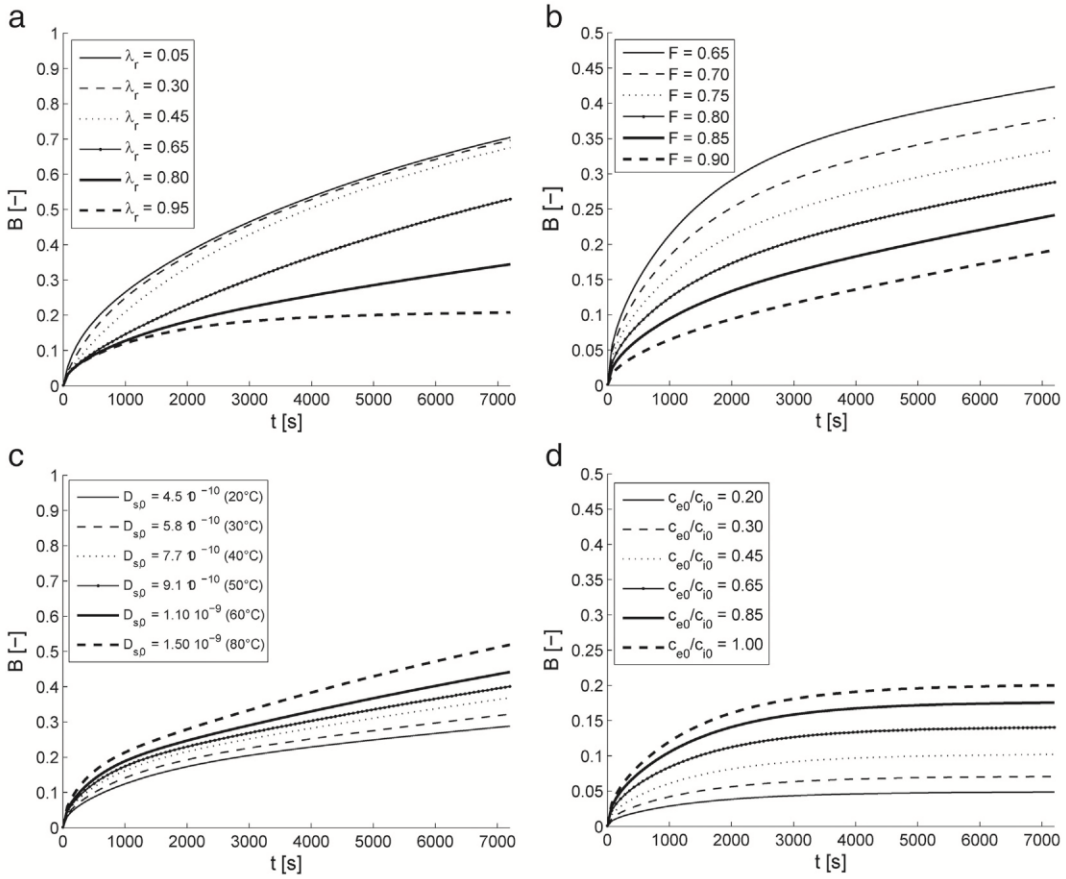

Fig. 11. Parametrical analysis of the model. (a) Varying the solute to pore radius λ_r. (b) Varying the cell volume fraction F. (c) Effect of temperature through its influence on diffusion coefficient of sucrose. (d) Varying c_{e0}/c_{i0} at no membrane permeabilization, i.e. $f_p \approx 10^{-8}$.

4. Conclusions

This paper gives an account of the development of a dual-porosity model of solute diffusion in tissue treated with electroporation. The fundamental assumptions in developing this model are based on phenomenological observations of liquid flow in porous media such as fractured rocks and soils. The model is designed as an attempt to provide a framework for future work in both computer modeling and experimental design. We demonstrated how it can be applied to a typical problem of solute extraction by diffusion in tissue that has been pretreated with electroporation, and we illustrated how it can be adapted to model mass transport phenomena in a disparate field of biomedical electroporation applications. We are confident that the dual-porosity model can be further improved and adapted to solve problems in mass transfer in many applications of electroporation, whether we are observing animal or plant tissue, whether we are interested in extraction of solute from the cells or introduction of solute into the cells, and even whether our species of interest are small ions or large organic compounds. The basic physical phenomena underlying the processes after application of electroporation treatment exhibit differences predominantly in details, which renders a general approach such as described by this paper, possible. The main focus of future work on the model will be verification by further experimentation, consolidation, as well as further inquiry designed to determine the influence of four important factors: pore evolution in number and size as a function of time; solute diffusivity through permeated membrane with pores evolving according to a model of electroporation; effect of net electric charge of solute and the effects of electroosmosis and electrophoresis; and the impact of electrical tissue damage to the effective cell volume fraction and consequent effect on the porosity of biological tissue, which influences the rate of solute diffusion within the extracellular phase. The model is easy to adapt and extend and can be thus further enhanced, albeit at the cost of losing the possibility of obtaining an analytical solution and having to solve the model numerically.

Acknowledgements

The authors appreciate the financial support from the French Ministry of Research and Higher Education (PhD scolarship grant for SMK) and the Slovenian Research Agency (projects of the research programme P2—0249: Electroporation in biology, biotechnology and medicine). This research was in part made possible due to networking activity of COST TD1104 Action (www.electroporation.net). We (DM and SMK) would also like to thank Dr. Sid Becker from the University of Canterbury, New Zealand, for the fruitful discussion on the theory of porous media as applied to problems in tissue electroporation.

Appendix A. Derivation of the analytical solution for constant coefficients k and $D_{s,e}$

In this Appendix we give a complete and detailed derivation of the analytical solution, given by Eqs. (19)–(23) in the main body of the paper, as it is derived from model Eqs. (1)–(2) taking appropriate initial and boundary conditions (Eqs. (12)–(18)) into the account.

We begin by joining the two first-order PDEs, Eq. (1)–(2), into one second-order PDE for solute concentration in intracellular space. From Eq. (2), we express c_e as

$$c_e = \frac{1}{k}\frac{\partial c_i}{\partial t} + c_i \tag{A.1}$$

and carry this into Eq. (1), obtaining

$$\frac{\partial}{\partial t}\left(\frac{1}{k}\frac{\partial c_i}{\partial t} + c_i\right) - D_{s,e}\frac{\partial}{\partial z}\left(\frac{\partial}{\partial z}\left(\frac{1}{k}\frac{\partial c_i}{\partial t} + c_i\right)\right) - \frac{1-\varepsilon}{\varepsilon}k\left(c_i - \left(\frac{1}{k}\frac{\partial c_i}{\partial t} + c_i\right)\right) = 0 \tag{A.2}$$

and after rearrangement, multiplication by k and on introducing $\delta = (1-\varepsilon)/\varepsilon$

$$\frac{\partial^2 c_i}{\partial t^2} + (\delta+1)k\frac{\partial c_i}{\partial t} - D_{s,e}\frac{\partial^3 c_i}{\partial t \partial z^2} - D_{s,e}k\frac{\partial^2 c_i}{\partial z^2} = 0. \tag{A.3}$$

To resolve the inhomogeneous boundary condition (Eq. (18)), we introduce a new function $\psi(z,t)$ as

$$\psi = c_i - c_{i0}e^{-kt} \tag{A.4}$$

with boundary conditions

$$\frac{\partial \psi}{\partial z}\Big|_{z=0} = \left(\frac{\partial}{\partial z}\left(c_i - c_{i0}e^{-kt}\right)\right)\Big|_{z=0} = \frac{\partial c_i}{\partial z}\Big|_{z=0} = 0 \tag{A.5}$$

$$\psi|_{z=l/2} = c_i|_{z=l/2} - c_{i0}e^{-kt} = c_{i0}e^{-kt} - c_{i0}e^{-kt} = 0 \tag{A.6}$$

and initial condition

$$\psi_0 = \psi_0(z,0) = \left(c_{i0} - c_{i0}e^{-kt}\right)\Big|_{t=0} = c_{i0}(z,0) - c_{i0} = 0. \tag{A.7}$$

Inserting A.4 and its temporal derivatives into A.3 following rearrangement, yields

$$\frac{\partial^2 \psi}{\partial t^2} - D_{s,e}\frac{\partial^3 \psi}{\partial t \partial z^2} - D_{s,e}k\frac{\partial^2 \psi}{\partial z^2} + (\delta+1)k\frac{\partial \psi}{\partial t} = \delta c_{i0}k^2 e^{-kt}. \tag{A.8}$$

We proceed with separation of variables on the homogeneous form of Eq. A.8, and assemble the complete solution as

$$\psi(z,t) = \psi_h(z,t) + \psi_p(t) \tag{A.9}$$

where the homogeneous solution $\psi_h(z,t)$ is a solution of

$$\frac{\partial^2 \psi}{\partial t^2} - D_{s,e}\frac{\partial^3 \psi}{\partial t \partial z^2} - D_{s,e}k\frac{\partial^2 \psi}{\partial z^2} + (\delta+1)k\frac{\partial \psi}{\partial t} = 0. \tag{A.10}$$

According to the method of separation of variables, we represent the solution of a PDE as a product of two constituents, one a function of z and the other of t

$$\psi(z,t) = Z(z)\cdot T(t). \tag{A.11}$$

We insert Eq. A.11 into Eq. A.10 and after rearrangement, separating the two functions and their derivatives, we obtain

$$\frac{Z''}{Z} = \frac{T'' + (\delta+1)kT'}{D_{s,e}T' + D_{s,e}kT}. \tag{A.12}$$

Eq. A.12 can only hold if both sides are equal to a constant. For the sake of subsequent algebra we set the constant to $-\lambda^2$. For z, we obtain

$$\frac{Z''}{Z} = -\lambda^2 \tag{A.13}$$

of which the solution is a linear combination of trigonometric functions

$$Z(z) = \sum_{m=1}^{\infty} A_m \sin(\lambda_m z) + B_m \cos(\lambda_m z) \tag{A.14}$$

while the right-hand side of A.12 can be written as

$$T'' + \left((\delta+1)k + \lambda^2 D_{s,e}\right)T' + \lambda^2 D_{s,e}kT = 0 \tag{A.15}$$

of which the characteristic polynomial is

$$\gamma_{1,2} = \frac{-\left((\delta+1)k + \lambda^2 D_{s,e}\right) \pm \sqrt{\left((\delta+1)k + \lambda^2 D_{s,e}\right)^2 - 4\lambda^2 k D_{s,e}}}{2} \tag{A.16}$$

finally giving the solution

$$T(t) = K_1 e^{\gamma_1 t} + K_2 e^{\gamma_2 t}. \tag{A.17}$$

The complete solution is thus

$$\begin{aligned}\psi_h(z,t) &= Z(z)\cdot T(t)\\ &= \sum_{m=1}^{\infty}(A_m \sin(\lambda_m z) + B_m \cos(\lambda_m z))\left(K_1 e^{\gamma_1 t} + K_2 e^{\gamma_2 t}\right).\end{aligned} \tag{A.18}$$

Note that since γ_1 and γ_2 are functions of λ_m, they get updated as well with every increment in the summation index m.

We now look for the particular solution of the inhomogeneous PDE, Eq. A.8, via the method of undetermined coefficients, of which the details we will omit. The particular solution is

$$\psi_p(t) = -c_{i0}e^{-kt}. \tag{A.19}$$

We can now complete Eq. A.9 to obtain $\psi(z,t)$

$$\psi(z,t) = \sum_{m=1}^{\infty}(A_m \sin(\lambda_m z) + B_m \cos(\lambda_m z))\left(K_1 e^{\gamma_1 t} + K_2 e^{\gamma_2 t} - c_{i0}e^{-kt}\right). \tag{A.20}$$

Next, we turn to the boundary conditions to determine coefficients A_m, B_m and eigenvalues λ_m. The following must be met

$$(A_m \sin(\lambda_m z) + B_m \cos(\lambda_m z))|_{z=l/2} = 0 \tag{A.21}$$

$$(A_m\lambda_m \cos(\lambda_m z) - B_m\lambda_m \sin(\lambda_m z))|_{z=0} = 0 \tag{A.22}$$

from Eq. A.21 follows that A_m equals 0, while from Eq. A.22 we get λ_m

$$\lambda_n = \frac{(2n+1)\pi}{l} \tag{A.23}$$

where summation index m was replaced with n, the latter running from 0 to infinity. The coefficient B_n can be calculated via the general formula for Fourier series coefficients

$$B_n = \frac{2}{l/2}\int_0^{l/2} \cos\left(\frac{(2n+1)\pi}{l}z\right)dz = \frac{4}{\pi}\frac{(-1)^n}{2n+1}. \tag{A.24}$$

Inserting B_n into Eq. A.20 and setting A_n to 0, we obtain

$$\psi(z,t)=\frac{4}{\pi}\sum_{n=0}^{\infty}\frac{(-1)^n}{2n+1}\left(K_1e^{\gamma_1 t}+K_2e^{\gamma_2 t}-c_{i0}e^{-kt}\right)\cos\left(\frac{(2n+1)\pi}{l}z\right). \tag{A.25}$$

For K_1 and K_2, we need two algebraic equations. One is immediately evident from Eq. A.7

$$\psi(z,0)=\frac{4}{\pi}\sum_{n=0}^{\infty}\frac{(-1)^n}{2n+1}\left(K_1e^{\gamma_1 0}+K_2e^{\gamma_2 0}-c_{i0}e^{-k0}\right)\cos\left(\frac{(2n+1)\pi}{l}z\right)=0 \tag{A.26}$$

resulting in

$$K_1+K_2=c_{i0} \tag{A.27}$$

while the other equation introduces the extracellular concentration initial condition into the solution for the intracellular concentration. We recall Eq. A.1, and write it by replacing c_i with the correct expression following from Eq. A.4, giving

$$c_e=\frac{1}{k}\frac{\partial}{\partial t}\left(\psi+c_{i0}e^{-kt}\right)+\left(\psi+c_{i0}e^{-kt}\right)=\frac{1}{k}\frac{\partial\psi}{\partial t}+\psi. \tag{A.28}$$

Carrying out the differentiation and writing Eq. A.28 for $t=0$ gives the second equation for K_1 and K_2

$$K_1\left(\frac{\gamma_1}{k}+1\right)+K_2\left(\frac{\gamma_2}{k}+1\right)=c_{e0}. \tag{A.29}$$

Solving the system of Eqs. A.27 and A.29 determines K_1 and K_2 as

$$K_1=c_{i0}\frac{\left(\frac{c_{i0}}{c_{e0}}-1\right)k-\gamma_2}{\gamma_1-\gamma_2} \tag{A.30}$$

$$K_2=c_{i0}\frac{\left(1-\frac{c_{i0}}{c_{e0}}\right)k+\gamma_1}{\gamma_1-\gamma_2}. \tag{A.31}$$

Taking the constant c_{i0} out of the summation and inserting the solution for ψ into Eq. A.4, we finally obtain the expression for intracellular intrinsic solute concentration $c_i(z,t)$, already given in the main body of this paper (see Eqs. (19)–(23)).

In order to obtain the extracellular intrinsic solute concentration, we must perform a time derivative on Eq. (20), multiply it by $1/k$ and add the product to Eq. (20) (in accordance with Eq. A.1). These operations yield

$$c_e(z,t)=\frac{4c_{i0}}{\pi}\frac{1}{k}\left[\sum_{n=0}^{\infty}\frac{(-1)^n}{2n+1}\cos(\lambda_n z)\left(C_{n,1}\gamma_{n,1}e^{\gamma_{n,1}t}+C_{n,2}\gamma_{n,2}e^{\gamma_{n,2}t}+ke^{-kt}\right)-c_{i0}ke^{-kt}\right]+ \\ +\frac{4c_{i0}}{\pi}\sum_{n=0}^{\infty}\frac{(-1)^n}{2n+1}\cos(\lambda_n z)\left(C_{n,1}e^{\gamma_{n,1}t}+C_{n,2}e^{\gamma_{n,2}t}-e^{-kt}\right)+c_{i0}e^{-kt}. \tag{A.32}$$

We see that the exponentials $c_{i0}\exp(-kt)$ subtract to 0. Joining the summative members with same constants together into one infinite series after dividing the first series by k, we finally obtain for extracellular intrinsic solute concentration the equation already given as Eq. (19) in the main body of this paper.

References

[1] T. Kotnik, P. Kramar, G. Pucihar, D. Miklavcic, M. Tarek, Cell membrane electroporation—part 1: the phenomenon, IEEE Electr. Insul. Mag. 28 (2012) 14–23.

[2] W. Krassowska, P.D. Filev, Modeling electroporation in a single cell, Biophys. J. 92 (2007) 404–417.

[3] W.K. Neu, J.C. Neu, Theory of electroporation, in: I.R. Efimov, M.W. Kroll, P.J. Tchou (Eds.), Cardiac Bioelectric Therapy: Mechanisms and Practical Implications, Springer, 2009.

[4] D. Miklavcic, Network for development of electroporation-based technologies and treatments: COST TD1104, J. Membr. Biol. 245 (2012) 591–598.

[5] S. Haberl, D. Miklavcic, G. Sersa, W. Frey, B. Rubinsky, Cell membrane electroporation—part 2: the applications, IEEE Electr. Insul. Mag. 29 (2013) 29–37.

[6] J. Gehl, Electroporation: theory and methods, perspectives for drug delivery, gene therapy and research, Acta Physiol. Scand. 177 (2003) 437–447.

[7] M.P. Rols, C. Delteil, M. Golzio, P. Dumond, S. Cros, J. Teissie, In vivo electrically mediated protein and gene transfer in murine melanoma, Nat. Biotechnol. 16 (1998) 168–171.

[8] A.I. Daud, R.C. DeConti, S. Andrews, P. Urbas, A.I. Riker, V.K. Sondak, et al., Phase I trial of interleukin-12 plasmid electroporation in patients with metastatic melanoma, J. Clin. Oncol. 26 (36) (2008) 5896–5903.

[9] L.M. Mir, L.F. Glass, G. Sersa, J. Teissie, C. Domenge, D. Miklavcic, et al., Effective treatment of cutaneous and subcutaneous malignant tumours by electrochemotherapy, Br. J. Cancer 77 (1998) 2336–2342.

[10] G. Sersa, D. Miklavcic, M. Cemazar, Z. Rudolf, G. Pucihar, M. Snoj, Electrochemotherapy in treatment of tumours, Eur. J. Surg. Oncol. 34 (2008) 232–240.

[11] B. Mali, T. Jarm, M. Snoj, G. Sersa, D. Miklavcic, Antitumor effectiveness of electrochemotherapy: a systematic review and meta-analysis, Eur. J. Surg. Oncol. 39 (2013) 4–16.

[12] I. Edhemovic, E.M. Gadzijev, E. Brecelj, D. Miklavcic, B. Kos, A. Zupanic, et al., Electrochemotherapy: a new technological approach in treatment of metastases in the liver, Technol. Cancer Res. Treat. 10 (2011) 475–485.

[13] A.R. Denet, R. Vanbever, V. Preat, Skin electroporation for transdermal and topical delivery, Adv. Drug Deliv. Rev. 56 (2004) 659–674.

[14] N. Pavselj, D. Miklavcic, Numerical models of skin electropermeabilization taking into account conductivity changes and the presence of local transport regions, IEEE Trans. Plasma Sci. 36 (2008) 1650–1658.

[15] S. Becker, Transport modeling of skin electroporation and the thermal behavior of the stratum corneum, Int. J. Therm. Sci. 54 (2012) 48–61.

[16] B. Zorec, V. Préat, D. Miklavčič, N. Pavšelj, Active enhancement methods for intra- and transdermal drug delivery: a review, Slov. Med. J. 82 (2013).

[17] R.V. Davalos, L.M. Mir, B. Rubinsky, Tissue ablation with irreversible electroporation, Ann. Biomed. Eng. 33 (2005) 223–231.

[18] P.A. Garcia, J.H. Rossmeisl, R.E. Neal, T.L. Ellis, R.V. Davalos, A parametric study delineating irreversible electroporation from thermal damage based on a minimally invasive intracranial procedure, Biomed. Eng. Online 10 (2011) 34.

[19] M. Fincan, F. DeVito, P. Dejmek, Pulsed electric field treatment for solid–liquid extraction of red beetroot pigment, J. Food Eng. 64 (2004) 381–388.

[20] N. López, E. Puértolas, S. Condón, J. Raso, Ignacio Álvarez, Enhancement of the solid–liquid extraction of sucrose from sugar beet (*Beta vulgaris*) by pulsed electric fields, LWT Food Sci. Technol. 42 (2009) 1674–1680.

[21] K.V. Loginova, M.V. Shynkaryk, N.I. Lebovka, E. Vorobiev, Acceleration of soluble matter extraction from chicory with pulsed electric fields, J. Food Eng. 96 (2010) 374–379.

[22] K. El-Belghiti, Z. Rabhi, E. Vorobiev, Kinetic model of sugar diffusion from sugar beet tissue treated by pulsed electric field, J. Sci. Food Agric. 85 (2005) 213–218.

[23] E. Puertolas, P. Hernandez-Orte, G. Sladana, I. Alvarez, J. Raso, Improvement of winemaking process using pulsed electric fields at pilot-plant scale. Evolution of chromatic parameters and phenolic content of Cabernet Sauvignon red wines, Food Res. Int. 43 (2010) 761–766.

[24] K. Loginova, M. Loginov, E. Vorobiev, N.I. Lebovka, Better lime purification of sugar beet juice obtained by low temperature aqueous extraction assisted by pulsed electric field, LWT-Food Sci. Technol. 46 (2012) 371–374.

[25] S. Toepfl, V. Heinz, D. Knorr, High intensity pulsed electric fields applied for food preservation, Chem. Eng. Process. 46 (2007) 537–546.

[26] P.Y. Phoon, F.G. Galindo, A. Vicente, P. Deimek, Pulsed electric field in combination with vacuum impregnation with trehalose improves the freezing tolerance of spinach leaves, J. Food Eng. 88 (2008) 144–148.

[27] G. Saulis, Electroporation of cell membranes: the fundamental effects of pulsed electric fields in food processing, Food Eng. Rev. 2 (2010) 52–73.

[28] A. Rieder, T. Schwartz, K. Schoen-Hoelz, S.-M. Marten, J. Suess, C. Gusbeth, et al., Molecular monitoring of inactivation efficiencies of bacteria during pulsed electric field treatment of clinical wastewater, J. Appl. Microbiol. 105 (2008) 2035–2045.

[29] C. Gusbeth, W. Frey, H. Volkmann, T. Schwartz, H. Bluhm, Pulsed electric field treatment for bacteria reduction and its impact on hospital wastewater, Chemosphere 75 (2009) 228–233.

[30] J. Sheng, R. Vannela, B.E. Rittmann, Disruption of *Synechocystis* PCC 6803 for lipid extraction, Water Sci. Technol. 65 (2012) 567–573.

[31] K. Dymek, P. Dejmek, V. Panarese, A.A. Vicente, L. Wadso, C. Finnie, et al., Effect of pulsed electric field on the germination of barley seeds, LWT-Food Sci. Technol. 47 (2012) 161–166.

[32] C.J. Eing, S. Bonnet, M. Pacher, H. Puchta, W. Frey, Effects of nanosecond pulsed electric field exposure on *Arabidopsis thaliana*, IEEE Trans. Dielectr. Electr. Insul. 16 (2009) 1322–1328.

[33] M. Kaszuba, D. McKnight, M.T. Connah, F.K. McNeil-Watson, U. Nobbmann, Measuring sub nanometre sizes using dynamic light scattering, J. Nanopart. Res. 10 (2008) 823–829.

[34] P.W. Linder, L.R. Nassimbeni, A. Polson, A.L. Rodgers, The diffusion coefficient of sucrose in water. A physical chemistry experiment, J. Chem. Educ. 53 (1976) 330.

[35] L.M. Mir, S. Orlowski, Mechanisms of electrochemotherapy, Adv. Drug Deliv. Rev. 35 (1999) 107–118.
[36] J.-M. Escoffre, B. Nikolova, L. Mallet, J. Henri, C. Favard, M. Golzio, et al., New insights in the gene electrotransfer process: evidence for the involvement of the plasmid DNA topology, Curr. Gene Ther. 12 (2012) 417–422.
[37] M. Marty, G. Sersa, J.R. Garbay, J. Gehl, C.G. Collins, M. Snoj, et al., Electrochemotherapy — an easy, highly effective and safe treatment of cutaneous and subcutaneous metastases: results of ESOPE (European Standard Operating Procedures of Electrochemotherapy) study, EJC Suppl. 4 (2006) 3–13.
[38] E. Vorobiev, N. Lebovka, Pulsed-electric-fields-induced effects in plant tissues: fundamental aspects and perspectives of applications, in: E. Vorobiev, N. Lebovka (Eds.), Electrotechnologies for Extraction from Plant Foods and Biomaterials, Springer, 2008.
[39] A. Zupanic, S. Corovic, D. Miklavcic, M. Pavlin, Numerical optimization of gene electrotransfer into muscle tissue, Biomed. Eng. Online 9 (2010).
[40] M. Golzio, J. Teissie, M.P. Rols, Direct visualization at the single-cell level of electrically mediated gene delivery, Proc. Natl. Acad. Sci. U. S. A. 99 (2002) 1292–1297.
[41] C.S. Djuzenova, U. Zimmermann, H. Frank, V.L. Sukhorukov, E. Richter, G. Fuhr, Effect of medium conductivity and composition on the uptake of propidium iodide into electropermeabilized myeloma cells, Biochim. Biophys. Acta, Biomembr 1284 (1996) 143–152.
[42] B. Gabriel, J. Teissie, Time courses of mammalian cell electropermeabilization observed by millisecond imaging of membrane property changes during the pulse, Biophys. J. 76 (1999) 2158–2165.
[43] K.C. Smith, J.C. Weaver, Electrodiffusion of molecules in aqueous media: a robust, discretized description for electroporation and other transport phenomena, IEEE Trans. Biomed. Eng. 59 (2012) 1514–1522.
[44] K.C. Smith, J.C. Weaver, Transmembrane molecular transport during versus after extremely large, nanosecond electric pulses, Biochem. Biophys. Res. Commun. 412 (2011) 8–12.
[45] J. Li, H. Lin, Numerical simulation of molecular uptake via electroporation, Bioelectrochemistry 82 (2011) 10–21.
[46] Y. Granot, B. Rubinsky, Mass transfer model for drug delivery in tissue cells with reversible electroporation, Int. J. Heat Mass Transf. 51 (2008) 5610–5616.
[47] S. Movahed, D. Li, Electrokinetic transport through the nanopores in cell membrane during electroporation, J. Colloid Interface Sci. 369 (2012) 442–452.
[48] D. Miklavcic, L. Towhidi, Numerical study of the electroporation pulse shape effect on molecular uptake of biological cells, Radiol. Oncol. 44 (2010) 34–41.
[49] M. Puc, T. Kotnik, L.M. Mir, D. Miklavcic, Quantitative model of small molecules uptake after in vitro cell electropermeabilization, Bioelectrochemistry 60 (2003) 1–10.
[50] G. Pucihar, T. Kotnik, D. Miklavcic, J. Teissie, Kinetics of transmembrane transport of small molecules into electropermeabilized cells, Biophys. J. 95 (2008) 2837–2848.
[51] M.M. Sadik, J. Li, J.W. Shan, D.I. Shreiber, H. Lin, Quantification of propidium iodide delivery using millisecond electric pulses: experiments, Biochim. Biophys. Acta 1828 (2013).
[52] J. Li, W. Tan, M. Yu, H. Lin, The effect of extracellular conductivity on electroporation-mediated molecular delivery, Biochim. Biophys. Acta 1828 (2013).
[53] N.E. Olesen, J.P. Hofgaard, N.-H. Holstein-Rathlou, M.S. Nielsen, J.C.B. Jacobsen, Estimation of the effective intercellular diffusion coefficient in cell monolayers coupled by gap junctions, Eur. J. Pharm. Sci. 46 (2012) 222–232.
[54] J. Ben Ammar, J.-L. Lanoiselle, N.I. Lebovka, E. Van Hecke, E. Vorobiev, Impact of a pulsed electric field on damage of plant tissues: effects of cell size and tissue electrical conductivity, J. Food Sci. 76 (2011) E90–E97.
[55] G. Pucihar, D. Miklavcic, T. Kotnik, A time-dependent numerical model of transmembrane voltage inducement and electroporation of irregularly shaped cells, IEEE Trans. Biomed. Eng. 56 (2009) 1491–1501.
[56] G. Pucihar, D. Miklavcic, The influence of intracellular connections on the electric field induced membrane voltage and electroporation of cells in clusters, in: O. Dossel, W.C. Schlegel (Eds.), World Congress on Medical Physics and Biomedical Engineering, vol. 25 Pt 13, Springer, New York, 2009, pp. 74–77.
[57] G. Pucihar, T. Kotnik, J. Teissie, D. Miklavcic, Electropermeabilization of dense cell suspensions, Eur. Biophys. J. Biophys. Lett. 36 (2007) 173–185.
[58] G. Pucihar, J. Krmelj, M. Reberšek, T. Napotnik, D. Miklavčič, Equivalent pulse parameters for electroporation, IEEE Trans. Biomed. Eng. 58 (2011) 3279–3288.
[59] G. Saulis, R. Saule, Size of the pores created by an electric pulse: microsecond vs millisecond pulses, Biochim. Biophys. Acta, Biomembr. 1818 (2012) 3032–3039.
[60] D. Miklavcic, K. Beravs, D. Semrov, M. Cemazar, F. Demsar, G. Sersa, The importance of electric field distribution for effective in vivo electroporation of tissues, Biophys. J. 74 (1998) 2152–2158.
[61] S. Corovic, L.M. Mir, D. Miklavcic, In vivo muscle electroporation threshold determination: realistic numerical models and in vivo experiments, J. Membr. Biol. 245 (2012) 509–520.
[62] R. Bharadwaj, J.G. Santiago, Dynamics of field-amplified sample stacking, J. Fluid Mech. 543 (2005) 57–92.
[63] M. Pavlin, G. Pucihar, M. Kanduser, The role of electrically stimulated endocytosis in gene electrotransfer, Bioelectrochemistry 83 (2012) 38–45.
[64] G. Pucihar, L.M. Mir, D. Miklavcic, The effect of pulse repetition frequency on the uptake into electropermeabilized cells in vitro with possible applications in electrochemotherapy, Bioelectrochemistry 57 (2002) 167–172.
[65] M. Pavlin, D. Miklavcic, Theoretical and experimental analysis of conductivity, ion diffusion and molecular transport during cell electroporation — relation between short-lived and long-lived pores, Bioelectrochemistry 74 (2008) 38–46.
[66] G.I. Barenblatt, V.M. Entov, V.M. Ryzhik, Theory of fluid flows through natural rocks, n.d.
[67] F. de Monte, G. Pontrelli, S. Becker, Chapter 3 — drug release in biological tissues, in: S.M. Becker, A.V. Kuznetsov (Eds.), Transport in Biological Media, Elsevier, Boston, 2013, pp. 59–118.
[68] H.S. Carslaw, J.J.C. Jaeger, Conduction of Heat in Solids, 2nd edition Oxford University Press, London, UK, 1959. (second).
[69] J. Crank, The Mathematics of Diffusion, Oxford University Press, 1979.
[70] E. Neumann, S. Kakorin, Physical chemistry theory of membrane electroporation and electrotransfer of biogenic agents, Advanced Electroporation Techniques in Biology and Medicine, 2010.
[71] F.R. Harker, R.J. Redgwell, I.C. Hallett, S.H. Murray, G. Carter, Texture of Fresh fruit, in: J. Janick (Ed.), Horticultural Reviews, John Wiley & Sons, Inc., 2010, pp. 121–224.
[72] J.W. Henshaw, Characterization and Enhancement of Interstitial Gene Transport During Electric Field-mediated Gene Delivery to Solid Tumor, ProQuest, 2007.
[73] W.M. Deen, Hindered transport of large molecules in liquid-filled pores, AIChE J 33 (1987) 1409–1425.
[74] P. Dechadilok, W.M. Deen, Hindrance factors for diffusion and convection in pores, Ind. Eng. Chem. Res. 45 (2006) 6953–6959.
[75] J. Liesche, A. Schulz, Modeling the parameters for plasmodesmal sugar filtering in active symplasmic phloem loaders, Front Plant Sci. 4 (2013).
[76] J.J.L. Higdon, G.P. Muldowney, Resistance functions for spherical particles, droplets and bubbles in cylindrical tubes, J. Fluid Mech. 298 (1995) 193–210.
[77] K. Sharma, Transport Phenomena in Biomedical Engineering: Artifical organ Design and Development, and Tissue Engineering, McGraw Hill Professional, 2010.
[78] R.O. Wayne, Plant Cell Biology: From Astronomy to Zoology, Academic Press, 2009.
[79] R.P. Joshi, Q. Hu, Evolution dynamics of pore sizes, cell volume, ionic concentrations following high-voltage pulsing, IEEE Trans. Plasma Sci. 40 (2012) 2355–2359.
[80] D.A. Stewart, I.R. Gowrishankar, J.C. Weaver, Transport lattice approach to describing cell electroporation: use of a local asymptotic model, IEEE Trans. Plasma Sci. 32 (2004) 1696–1708.
[81] C. Buttersack, W. Basler, Hydraulic conductivity of cell-walls in sugar-beet tissue, Plant Sci. 76 (1991) 229–237.
[82] L.M. Mir, Bases and rationale of the electrochemotherapy, EJC Suppl. 4 (2006) 38–44.
[83] J. Pusenjak, D. Miklavcic, Modeling of interstitial fluid pressure in solid tumor, Simul. Pract. Theory 8 (2000) 17–24.
[84] L.J. Liu, S.L. Brown, J.R. Ewing, M. Schlesinger, Phenomenological model of interstitial fluid pressure in a solid tumor, Phys. Rev. E. 84 (2011) 021919.
[85] E. Bellard, B. Markelc, S. Pelofy, F. Le Guerroue, G. Sersa, J. Teissie, et al., Intravital microscopy at the single vessel level brings new insights of vascular modification mechanisms induced by electropermeabilization, J. Control. Release 163 (2012) 396–403.
[86] T. Jarm, M. Cemazar, D. Miklavcic, G. Sersa, Antivascular effects of electrochemotherapy: implications in treatment of bleeding metastases, Expert. Rev. Anticancer. Ther. 10 (2010) 729–746.
[87] M. Golzio, J. Teissie, Direct assay of electropermeabilization in a 2D pseudo tissue, Phys. Chem. Chem. Phys. 12 (2010) 14670–14672.
[88] S. Corovic, I. Lackovic, P. Sustaric, T. Sustar, T. Rodic, D. Miklavcic, Modeling of electric field distribution in tissues during electroporation, Biomed. Eng. Online 12 (2013) 16.
[89] D. Pavliha, B. Kos, M. Marcan, A. Zupanic, G. Sersa, D. Miklavcic, Planning of electroporation-based treatments using web-based treatment-planning software, J. Membr. Biol. 246 (2013) 833–842.
[90] D. Miklavcic, S. Corovic, G. Pucihar, N. Pavselj, Importance of tumour coverage by sufficiently high local electric field for effective electrochemotherapy, EJC Suppl. 4 (2006) 45–51.
[91] B. Zorec, S. Becker, M. Rebersek, D. Miklavcic, N. Pavselj, Skin electroporation for transdermal drug delivery: the influence of the order of different square wave electric pulses, Int. J. Pharm. 457 (2013) 214–223.
[92] T. Blagus, B. Markelc, M. Cemazar, T. Kosjek, V. Preat, D. Miklavcic, et al., In vivo real-time monitoring system of electroporation mediated control of transdermal and topical drug delivery, J. Control. Release 172 (2013) 862–871.
[93] P. Chiarella, V.M. Fazio, E. Signori, Electroporation in DNA vaccination protocols against cancer, Curr. Drug Metab. 14 (2013) 291–299.
[94] M. Pavlin, V. Leben, D. Miklavcic, Electroporation in dense cell suspension — theoretical and experimental analysis of ion diffusion and cell permeabilization, Biochim. Biophys. Acta, Gen. Subj. 1770 (2007) 12–23.
[95] M. Pavlin, M. Kanduser, M. Rebersek, G. Pucihar, F.X. Hart, R. Magjarevic, et al., Effect of cell electroporation on the conductivity of a cell suspension, Biophys. J. 88 (2005) 4378–4390.
[96] M. Fincan, P. Dejmek, Effect of osmotic pretreatment and pulsed electric field on the viscoelastic properties of potato tissue, J. Food Eng. 59 (2003) 169–175.
[97] N.I. Lebovka, M.V. Shynkaryk, E. Vorobiev, Drying of potato tissue pretreated by ohmic heating, Dry. Technol. 24 (2006) 601–608.
[98] J. Kestin, M. Sokolov, W.A. Wakeham, Viscosity of liquid water in the range −8 °C to 150 °C, J. Phys. Chem. Ref. Data 7 (1978) 941–948

4.2 Paper III: “Dual-porosity model of liquid extraction by pressing from biological tissue modified by electroporation”

4.2.1 Introduction

Pressing is an important industrial operation for extraction of valuable liquid from biological tissue. Intact biological tissue exhibits considerable resistance to pressure, i.e. low compressibility and permeability. To alleviate this problem, a range of treatments exists in order to enhance and economise juice extraction and tissue dehydration. One amongst a plenitude of these treatments is electroporation.

The permeability of cells in intact plant tissue is about five orders of magnitude lower than permeability of the extracellular matrix. Therefore, the primary objective of pre-treatment is the permeabilization of the cellular membrane. Since different treatments influence the tissue structure differently, the resulting yield and quality of extract or degree of dehydration do not depend only on the specific amount of energy delivered to the material. They are also functions of the chosen treatment and the protocol of treatment application. An electrical treatment such as electroporation can leave the extracellular structures largely intact, while damaging or even completely destroying the cellular membrane (irreversible electroporation). This selective property of electroporation makes electroporation an interesting process for enhancing juice extraction and dehydration, while preserving quality and organoleptic properties of juice and solids.

In order to gain a better understanding of the processes governing juice extraction and material consolidation behaviour in tissue electroporation, mathematical models can be constructed. Due to the complexity and variability in properties of biological material and the many parameters and treatment effects on tissue, few complete and comprehensive models exist. Research in this direction is focused mainly on modelling the mechanism of filtration–consolidation during pressing, and less towards the electroporation-induced damage to the cell membranes.

This article aims to show how an extendable model can be constructed for describing filtration–consolidation behaviour of electroporated vegetable tissue. The model is named the *dual-porosity model of liquid expression*, and its construction is based on an analogy (follows from) the previous work (presented in Paper II).

4.2.2 Summary

The presented model has been named the "Dual-porosity" model since one porosity is that of the intercellular matrix of tissue, and the second the porosity of the plasma membrane of each individual tissue-constituting cell. The presented theory directly relates electroporation effects

with important filtration–consolidation parameters, namely hydraulic permeability. The intracellular and the extracellular space are considered separately, and a theoretical approach to describe effects of electroporation on cell membrane hydraulic permeability is provided.

Theoretical analysis and fitting of experimental data from pressing experiments are used as initial estimates for model parameter values, and optimization algorithms were employed to fine-tune some of the parameters for good agreement with experiments. Tissue and membrane hydraulic permeability are estimated based on published literature where available, while compressibility moduli were estimated from analysis of pressing experiments that was conducted. A demonstration on the use of the model for modelling experimental extraction kinetics and a brief parametrical study are given. The model can easily be extended by a theoretical model of electroporation (analogous to the diffusion model – Paper II), and invites further development. In order to keep the model comprehensive in this first account and to focus more on the concept of the dual porosity modelling paradigm in tissue electroporation, simplifications with respect to rather complex theory of porous media were made.

4.2.3 Conclusions

A fully developed and validated model based on the dual-porosity approach could in future be used for research into optimization of treatment parameters, or for simulations of system responses under treatment conditions impractical or costly for realisation. The main novelty of the model in relation to previous works is in connecting the theory of electroporation with the consolidation–filtration theory applied to study expression kinetics in biological tissues. The experiment-based estimation is necessary at this stage in model development, as biological complexity and diversity render theoretical estimations scarce and unrealistic. The authors propose means of relating the effects of electroporation on the plasma membrane with membrane hydraulic permeability. This point of model construction invites further development and verification, since theoretical models of electroporation give pore distribution (size, number) as a function of electric field application. There is also an increasing number of experimental studies available, which study pore resealing dynamics and selectivity of the permeabilized plasma membrane. The findings of these studies seem promising for model enhancement, since they describe a temporal dependence of permeability coefficients that are assumed as time-invariant in this work. Inclusion of such dynamics will, however, most likely require a numerical approach.

Journal of Food Engineering 137 (2014) 76–87

Contents lists available at ScienceDirect

Journal of Food Engineering

journal homepage: www.elsevier.com/locate/jfoodeng

Dual-porosity model of liquid extraction by pressing from biological tissue modified by electroporation

Samo Mahnič-Kalamiza [a,b,*], Eugène Vorobiev [a]

[a] University of Technology of Compiègne, Centre de Recherches de Royallieu – BP 20529, 60205 Compiègne Cedex, France
[b] University of Ljubljana, Faculty of Electrical Engineering, Tržaška c. 25, SI-1000 Ljubljana, Slovenia

ARTICLE INFO

Article history:
Received 29 November 2013
Received in revised form 8 March 2014
Accepted 31 March 2014
Available online 8 April 2014

Keywords:
Electroporation
Juice extraction
Pressing
Tissue porosity
Hydraulic permeability
Analytical process modelling

ABSTRACT

The objective of this study is to provide insight into the phenomena related with juice expression from electroporated tissue. We propose an analytical model and study consolidation behaviour of a block of tissue during pressing; before and after electroporation. By the dual-porosity approach, we treat compressibility and hydraulic permeability of intracellular and extracellular space separately. Initial parameter estimations are based on previously published studies (for hydraulic permeability), or analysis of modelled data (for compressibility moduli). Good agreement between simulations and experiments performed is then obtained by optimization (i.e. fitting). Impact of electroporation on membrane permeability is theoretically estimated and elucidated via the extraction–consolidation model; results are compared with experimental kinetics for validation and evaluation of model performance. Permeability coefficient estimates from literature proved valuable as initial approximations, and the model results were able to fit experimental data with high accuracy, clearly demonstrating the power of the proposed approach.

1. Introduction

Pressing is an important industrial operation for extraction of valuable liquid from a solid–liquid mixture that constitutes biological tissue (Schwartzberg, 1997), or tissue dewatering if the objective is material dehydration (Aguilera et al., 2003). To aid in the understanding of the governing processes, the solid–liquid expression (i.e. extraction by pressing) from vegetable tissues has been studied and modelled (Lanoiselle et al., 1996; Schwartzberg, 1997).

Intact biological tissue exhibits considerable resistance to pressure, i.e. low compressibility and permeability (Buttersack and Basler, 1991). To alleviate this problem, a range of treatments exists in order to enhance and economise juice extraction and tissue dehydration. By nature, these treatments are mechanical, chemical (Binkley and Wiley, 1981), enzymatic (Shankar et al., 1997), thermal (Poel et al., 1998; Praporscic et al., 2006), or electrical (Bazhal and Vorobiev, 2000; Knorr et al., 1994; Luengo et al., 2013; Sack et al., 2008; Vorobiev and Lebovka, 2010; Wiktor and Witrowa-Rajchert, 2012). Application of one or of a combination of several of these treatments damages cellular material, thus increasing its permeability. The treatments can be applied before or during pressing (Bazhal et al., 2001), however, simultaneous application often demands modifications of the existing industrial setup and therefore these operations are most interesting as pre-treatments, applied before the pressing stage.

The permeability of cells in intact plant tissue is at least five orders of magnitude lower than permeability of the extracellular matrix (Buttersack and Basler, 1991). Therefore, the primary objective of pre-treatment is the permeabilization of the cellular membrane. However, different treatments influence the tissue structure differently. The resulting yield and quality of extract or degree of dehydration do not depend only on the specific amount of energy delivered to the material. They are also functions of the chosen treatment and the protocol of treatment application. For example, mechanical treatment (e.g. slicing, grinding) or thermal treatment damage not only cell membranes, but also cell walls (Poel et al., 1998; Llano et al., 2003; Vicente et al., 2005). On the other hand, electrical treatment such as electroporation (also known as pulsed electric field treatment or PEF) can leave the extracellular structures largely intact (Bouzrara and Vorobiev, 2003; Fincan and Dejmek, 2002). While electroporation seems to have no profound effect on cell walls, it is inducing cell permeabilization to a varying degree, or even leading to complete destruction of cellular

* Corresponding author at: Université de Technologie de Compiègne (UTC), Département de Génie des Procédés Industriels, Laboratoire Transformations Intégrées de la Matière Renouvelable, Centre de Recherches de Royallieu – BP 20529, 60205 Compiègne Cedex, France. Tel.: +33 6 52 17 30 92.
E-mail addresses: samo.mahnic@utc.fr, samo.mahnic-kalamiza@fe.uni-lj.si, samo.mahnic@gmail.com (S. Mahnič-Kalamiza).

http://dx.doi.org/10.1016/j.jfoodeng.2014.03.035
0260-8774/

Nomenclature

A	cell average surface (also pore surface, membrane surface – see subscripts) (m^2)
e	void ratio (liquid to solid volume) (−)
G_e, G_i	compressibility moduli of extra/intracellular space as defined through void ratio e (Pa)
$G_{\varepsilon,e}$, $G_{\varepsilon,i}$	compressibility moduli of extra/intracellular space as defined through porosity ε (Pa)
f_p	average pore surface fraction per cell (−)
h	tissue sample thickness (m)
k	intrinsic hydraulic permeability (m^2)
L_p	hydraulic permeability as measured by experiments ($m\ MPa^{-1}\ s^{-1}$)
l	length of the fluid conduit (membrane thickness, pore length, tissue sample thickness in L_p measurements) (m)
m, n	summation indices (−)
P_E	externally applied pressure (via piston) (Pa)
p_e, p_i	liquid pressure in extra/intracellular space (Pa)
$p_{e,S}$, $p_{i,S}$	solid pressure in extra/intracellular space (Pa)
q	liquid flux (flow per area) velocity ($m\ s^{-1}$)
Q	liquid flow velocity ($m^3\ s^{-1}$)
R	spherical cell radius (without membrane) (m)
r	integration variable
r_p	pore radius (m)
S	tissue sample deformation (m)
s	relative (normalized) deformation (−)
t	model/experiment time (s)
V	average cell volume (m^3)
V_m	membrane volume (m^3)
z	spatial coordinate

Subscripts

c	cell
e	extracellular space (medium)
i	intracellular space (medium)
m	membrane
p	pore (except in L_p)
S	solid
∞	infinity

Greek letters

α	proportionality coefficient in υ_{i-e} (−)
Δ	finite difference (in e.g. pressure drop)
δ	short-hand for $1 + G_{\varepsilon,e}/G_{\varepsilon,i}$ (−)
ε	porosity (−)
μ	liquid viscosity (Pa s)
ν	short-hand for $k_e G_{\varepsilon,e}/\mu$ ($m^2\ s^{-1}$)
ξ	geometrical configuration constant relating α with k_i (−)
ρ	fluid density (g/m^3)
τ	characteristic time constant, short-hand for $\mu/\alpha G_{\varepsilon,i}$ (s)
υ_{i-e}	rate of intra-to-extracellular liquid flux (s^{-1})

membranes (Ersus and Barrett, 2010). This selective property of pulsed electric fields makes electroporation an interesting process for enhancing juice extraction and dehydration, while preserving quality and organoleptic properties of juice and solids (Lebovka et al., 2004; Schilling et al., 2007).

Electroporation (also termed electropermeabilization) is a process where an externally applied electric field of sufficient strength induces a transmembrane potential, causing an increase in plasma membrane permeability and conductivity. This increase has been attributed to creation of aqueous pathways (pores) in the lipid bilayer, and has been demonstrated by experiments on lipid bilayers, cells in suspension, monolayers, and biological tissues. For essential reading in fundamentals of electroporation, see e.g. (Haberl et al., 2013; Kotnik et al., 2012; Krassowska and Filev, 2007; Neu and Neu, 2009).

In order to gain better understanding of the processes governing juice extraction and material consolidation behaviour in tissue electroporation, mathematical models can be constructed. These models need to be validated, before they are used to study the phenomena. The purpose of modelling can be, for instance, to facilitate optimization of industrial processes in terms of required energy or product quality (Bazhal et al., 2003; Schilling et al., 2007). However, due to the complexity and variability in properties of biological material and the many parameters and treatment effects on tissue, few complete and comprehensive models exist. Research in this direction is focused on modelling the mechanism of filtration–consolidation during pressing (Shirato et al., 1986; Lanoiselle et al., 1996; Zhu and Melrose, 2003; Petryk and Vorobiev, 2007, 2013; Halder et al., 2011), and less towards the electroporation-induced damage to the cell membranes. Even less is known, in terms of theory, about the effect of electroporation on permeability and compressibility of treated material. For a recent review of some of the fundamental concepts of applying porous media theory to mass transport in biological systems, see (de Monte et al., 2013).

In this article we aim to show how an extendable model can be constructed for describing filtration–consolidation behaviour of electroporated vegetable tissue. We have named this model the *dual-porosity model of liquid expression*. "Dual-porosity" since one porosity is that of the intercellular matrix of tissue, and the second the porosity of the plasma membrane of each individual tissue-constituting cell. We directly relate electroporation effects with important filtration–consolidation parameters, namely hydraulic permeability. We consider the intracellular and the extracellular space separately, and provide a theoretical approach to describe effects of electroporation on cell membrane hydraulic permeability. Theoretical analysis and fitting experimental data from pressing experiments are used as initial estimates for model parameter values, and then optimization algorithms were employed to fine-tune some of the parameters to obtain good agreement with experimental data. Tissue and membrane hydraulic permeability are estimated based on published literature where available, while compressibility moduli were estimated from analysis of pressing experiments that we conducted. We demonstrate how the proposed model can be used to model experimental extraction kinetics for both intact and electroporated tissue. We also provide a brief parametrical study. The model can easily be extended by a theoretical model of electroporation, and invites further development. By constructing the dual-porosity model we attempt to advance the field of modelling transport phenomena in electroporated biological tissues of industrial importance. A fully developed and validated model based on this approach could in future be used for research into optimization of treatment parameters, or for simulations of system responses under treatment conditions impractical or costly for realisation. The main novelty of the model in relation to previous works by our group is in connecting the theory of electroporation with the consolidation–filtration theory applied to study expression kinetics in biological tissues.

2. Theoretical formulation of the problem and derivation of an analytical model

2.1. System of liquid pressure equations in a dual-porosity medium

In order to study the expression of liquid from vegetable tissue treated with electroporation, we consider tissue as comprising two media – the intracellular, and the extracellular. The cell membrane on which electric field acts during electroporation delineates these two media in every tissue sample. The effects of electroporation on tissue permeability are introduced into the model via the membrane, by representing it as a semi-permeable boundary. The model membrane has its own hydraulic permeability, which is a function of electroporation. The extracellular space, represented as consisting of an intricate structure formed by the cell wall, extracellular liquid, and air (see Fig. 1), also has its own hydraulic permeability.

According to previous works based on filtration–consolidation theory of biosolids (Lanoiselle et al., 1996; Petryk and Vorobiev, 2007, 2013), the following set of equations can be written for the extracellular and intracellular space, respectively

$$\frac{\partial(\rho\varepsilon_e)}{\partial t}+\frac{\partial(\rho q_e)}{\partial z}-\rho\upsilon_{i-e}=0 \tag{1}$$

$$\frac{\partial(\rho\varepsilon_i)}{\partial t}+\frac{\partial(\rho q_i)}{\partial z}+\rho\upsilon_{i-e}=0 \tag{2}$$

Eqs. (1) and (2) result from application of the law of mass conservation, and are presented in a form typical for non-equilibrium mass transfer processes in porous media. In Eqs. (1) and (2), ρ is the liquid medium density; ε_e and ε_i are the porosities; q_e and q_i the liquid flow velocities; and υ is the source term that represents the flow of liquid through the plasma membrane from the intracellular to the extracellular space. Indices 'i' and 'e' in Eqs. (1) and (2) correspond to the intracellular and the extracellular phase, respectively. The permeability of extracellular space is several orders of magnitude greater than that of intact cellular membrane (Buttersack and Basler, 1991; Tomos, 1988). This should still hold for tissue damaged by electroporation below the threshold that results in predominantly irreversible damage to the cell membranes. This is postulated in accordance with the theoretical derivations for permeability of electroporated cell membrane (see Section 2.5) and surface fraction of stable, long-lasting pores in the plasma membrane, as estimated in e.g. (Pavlin and Miklavcic, 2008). If treatment conditions support these assumptions, the liquid path is primarily from within the cells into the extracellular space and via compression of the extracellular space then out of the tissue block. Fig. 2 is in aid of illustrating the individual constituent

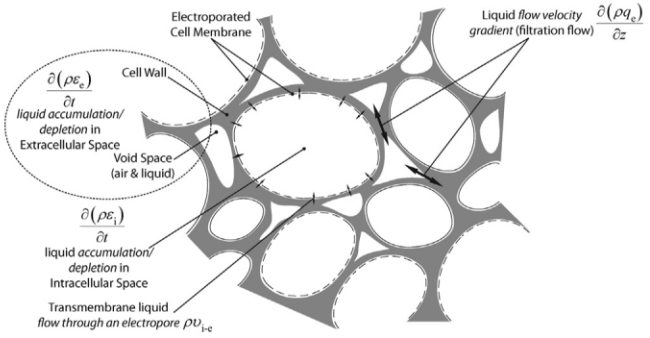

Fig. 2. A schematic representation of vegetable tissue after electroporation with identified member terms of the continuity Eqs. (1–2, also 3–4) in aid of illustrating the dual-porosity principle.

members of Eqs. (1) and (2), simplified by neglecting the filtration path through the intracellular space (see Eq. (4) below).

The experimental setup and a simplified representation of experiment physics are given in Fig. 3. The piston is applying pressure to the tissue in the $-z$ direction, and liquid is flowing out of the tissue sample at $z = 0$, where a porous support (metallic mesh or filter cloth) is placed in order to hold the block of cellular tissue in place, while allowing free flow of extracted juice. The piston displacement during experiment is recorded, and the tissue block deformation can be calculated.

Assuming constant juice density ρ, and the supposition that filtration flow inside the cells can be neglected, Eqs. (1) and (2) simplify to

$$\frac{\partial\varepsilon_e(z,t)}{\partial t}+\frac{\partial q_e(z,t)}{\partial z}-\upsilon_{i-e}(z,t)=0 \tag{3}$$

$$\frac{\partial\varepsilon_i(z,t)}{\partial t}+\upsilon_{i-e}(z,t)=0 \tag{4}$$

We reformulate the above set of equations to express the quantities in terms of the two variables of known initial and boundary conditions, i.e. liquid pressures p_i and p_e. Pressure p_i is the intracellular liquid pressure, and p_e the extracellular liquid pressure. The porosities ε_e and ε_i are related to the solid pressures $p_{e,S} = P_E - p_e$ and $p_{i,S} = P_E - p_i$ via the compressibility moduli G_e and G_i, and the void ratios e_e and e_i, where $\varepsilon_e = e_e/(1 + e_e)$ and $\varepsilon_i = e_i/(1 + e_i)$. The relationships between void ratios and solid pressures are given by (Lanoiselle et al., 1996)

$$\frac{\partial e_e}{\partial t}=\frac{\partial e_e}{\partial p_{e,S}}\cdot\frac{\partial p_{e,S}}{\partial t}=-\frac{\partial e_e}{\partial p_{e,S}}\cdot\frac{\partial p_e}{\partial t}=\frac{1}{G_e}\frac{\partial p_e}{\partial t} \tag{5}$$

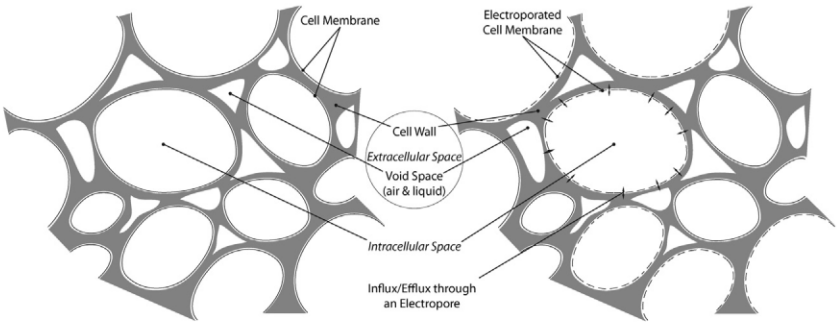

Fig. 1. A schematic representation of vegetable tissue before (left) and after (right) electroporation. The cell wall and void space, occupied by air and some liquid, are the solid and liquid phases forming the extracellular space in tissue (no external pressure applied). Redrawn based on Fig. 17 in Halder et al. (2011).

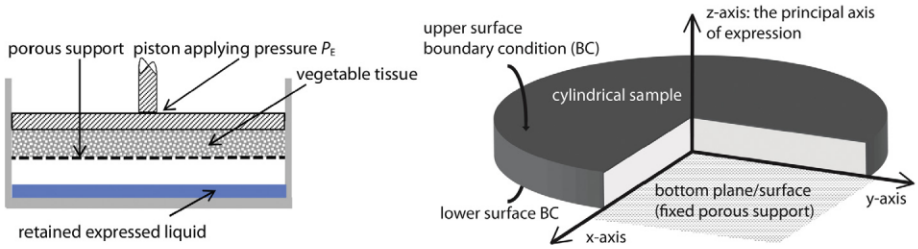

Fig. 3. A schematic representation of a typical pressing experiment (left) and a representation of the modelled block of tissue placed within a coordinate system (right).

$$\frac{\partial e_i}{\partial t} = \frac{\partial e_i}{\partial p_{i,S}} \cdot \frac{\partial p_{i,S}}{\partial t} = -\frac{\partial e_i}{\partial p_{i,S}} \cdot \frac{\partial p_i}{\partial t} = \frac{1}{G_i} \frac{\partial p_i}{\partial t} \tag{6}$$

where $p_{e,S}$ and $p_{i,S}$ are the pressures of total insoluble solids in extracellular and intracellular phase, respectively. These solid pressures increase in time proportionally to the decrease in respective liquid pressures, i.e. $\partial p_{e,S}/\partial t = -\partial p_e/\partial t$ and $\partial p_{i,S}/\partial t = -\partial p_i/\partial t$. Note that this is valid for constant-pressure expression, when $\partial P_E/\partial t = 0$. From Eqs. (5) and (6) we see that G_e and G_i, if assumed constant, can be estimated from $G_e = -\partial p_{e,S}/\partial e_e$ and $G_i = -\partial p_{i,S}/\partial e_i$, i.e. the slopes of the linear functions that relate the decrease in void ratio with an increase in solid pressure. Note that G_e and G_i are always positive-value quantities, as an increase in solid pressure is a consequence of a decrease in void ratio (expression of liquid). In experiments, we measure the changes in deformation of the tissue sample due to loss of liquid, rather than measuring the liquid pressure. Therefore, we rewrite Eqs. (5) and (6) not for the liquid-to-solid void ratio, but for porosities ε_e and ε_i, as

$$\frac{\partial \varepsilon_e}{\partial t} = \frac{\partial p_{e,S}}{\partial t} \cdot \frac{\partial \varepsilon_e}{\partial p_{e,S}} = -\frac{\partial p_e}{\partial t} \cdot \frac{\partial \varepsilon_e}{\partial p_{e,S}} = \frac{1}{G_{\varepsilon,e}} \frac{\partial p_e}{\partial t} \tag{7}$$

$$\frac{\partial \varepsilon_i}{\partial t} = \frac{\partial p_{i,S}}{\partial t} \cdot \frac{\partial \varepsilon_i}{\partial p_{i,S}} = -\frac{\partial p_i}{\partial t} \cdot \frac{\partial \varepsilon_i}{\partial p_{i,S}} = \frac{1}{G_{\varepsilon,i}} \frac{\partial p_i}{\partial t} \tag{8}$$

The compressibility moduli G_e and G_i as defined in cited literature and $G_{\varepsilon,e}$ and $G_{\varepsilon,i}$ defined in Eqs. (7) and (8) are related, as follows from the relations

$$\frac{\partial \varepsilon_e}{\partial t} = \frac{\partial p_{e,S}}{\partial t} \cdot \frac{\partial}{\partial p_{e,S}} \left(\frac{e_e}{1+e_e} \right) = -\frac{\partial p_e}{\partial t} \cdot \frac{\partial e_e}{\partial p_{e,S}} \frac{1}{(1+e_e)^2} = \frac{1}{G_e} \frac{1}{(1+e_e)^2} \frac{\partial p_e}{\partial t} = \frac{1}{G_{\varepsilon,e}} \frac{\partial p_e}{\partial t} \tag{9}$$

$$\frac{\partial \varepsilon_i}{\partial t} = \frac{\partial p_{i,S}}{\partial t} \cdot \frac{\partial}{\partial p_{i,S}} \left(\frac{e_i}{1+e_i} \right) = -\frac{\partial p_i}{\partial t} \cdot \frac{\partial e_i}{\partial p_{i,S}} \frac{1}{(1+e_i)^2} = \frac{1}{G_i} \frac{1}{(1+e_i)^2} \frac{\partial p_i}{\partial t} = \frac{1}{G_{\varepsilon,i}} \frac{\partial p_i}{\partial t} \tag{10}$$

According to the Eqs. 9–10, $G_{\varepsilon,e} = G_e \cdot (1+e_e)^2$ and $G_{\varepsilon,i} = G_i \cdot (1+e_i)^2$. By introducing compressibility moduli defined through porosity, we have made a simplification that comes at a cost. The $G_{\varepsilon,e}$ and $G_{\varepsilon,i}$ do not depend only on material properties and treatment, but also on the spatially- and temporally-dependent void ratios e_e and e_i during the pressing experiment. This is a trade-off we have opted for in order to keep the model simple and comprehensive. As a consequence, the model results are valid for small piston displacements in cases where tissue is not severely damaged. The moduli $G_{\varepsilon,e}$ and $G_{\varepsilon,i}$ that we use, should be understood as averaged values, i.e.

$$\overline{G}_{\varepsilon,e} = G_e(1+\bar{e}_e)^2 = G_e \left(1 + \frac{1}{T} \frac{1}{h} \int_0^h \int_0^T e_e(z,t) \cdot dt \cdot dz \right)^2 \tag{11}$$

$$\overline{G}_{\varepsilon,i} = G_i(1+\bar{e}_i)^2 = G_i \left(1 + \frac{1}{T} \frac{1}{h} \int_0^h \int_0^T e_i(z,t) \cdot dt \cdot dz \right)^2 \tag{12}$$

where T is the time duration of the experiment and h is the initial sample height. We omit the bar notation denoting average values in the following text. The minimum values of compressibility moduli can be directly estimated from experiments (see Section 2.4, where parameter estimation is presented), and average values as given by Eqs. (11) and (12), will be determined based on fitting of model results to experimental data. Another simplification limiting model applicability to small piston displacements is the assumption of linear elastic deformation of tissue. Compressibility moduli $G_{\varepsilon,e}$ and $G_{\varepsilon,i}$ are, more strictly following definitions of thermodynamics and stress mechanics, in fact non-normalized bulk elastic moduli. A more in-depth and rigorous treatment in filtration-consolidation theory would require introduction of material coordinates $dz_m = (1-\varepsilon)\cdot dz$ (Petryk and Vorobiev, 2013) to account for time and space-variable porosity.

The liquid flow velocity in extracellular space q_e is given by Darcy law as

$$q_e = -\frac{k_e}{\mu} \frac{\partial p_e}{\partial z}, \tag{13}$$

assuming unidirectional flow in direction of the principal axis of applied pressure (z).

The source term $v_{i-e}(z,t)$ giving liquid flow through the porous membrane can be written in terms of local pressure difference between the intracellular and extracellular liquid pressure, giving

$$v_{i-e} = \frac{\alpha}{\mu}(p_i - p_e) \tag{14}$$

wherein we notice the proportionality coefficient α, whose origin and estimation are discussed in Section 2.4.

Combining Eqs. 3–14 and dropping the notation of spatial–temporal dependency of both liquid pressures gives the following final form of the model equations:

$$\frac{1}{G_{\varepsilon,e}} \frac{\partial p_e}{\partial t} - \frac{\partial}{\partial z} \left(\frac{k_e}{\mu} \frac{\partial p_e}{\partial z} \right) - \frac{\alpha}{\mu}(p_i - p_e) = 0 \tag{15}$$

$$\frac{1}{G_{\varepsilon,i}} \frac{\partial p_i}{\partial t} + \frac{\alpha}{\mu}(p_i - p_e) = 0 \tag{16}$$

The initial and boundary conditions for Eqs. (15) and (16) are

$$p_{e0} = p_{e0}(z,0) = p_{i0} = p_{i0}(z,0) = P_E \tag{17}$$

$$p_e|_{z=0} = 0 \tag{18}$$

$$p_i|_{z=0} = p_{i0} e^{-\frac{\alpha G_i}{\mu} t} \tag{19}$$

$$\left. \frac{\partial p_e}{\partial z} \right|_{z=h} = \left. \frac{\partial p_i}{\partial z} \right|_{z=h} = 0 \tag{20}$$

The boundary condition given by Eq. (19) can be obtained by solving Eq. (16) for the boundary condition given in Eq. (18) and initial condition in Eq. (17). As the matter is trivial, we leave the details of verifying Eq. (19) to the interested reader. A note on initial condition, Eq. (17); Externally applied pressure can be assumed as equally distributed throughout the tissue sample on both the intra- and extracellular liquid phase in case the sample thickness is relatively small (in relation to the number of cell layers and piston-tissue contact surface). If the sample thickness impact to pressure distribution cannot be neglected due to sample dimensions, a more suitable approximation for pressure distribution might be linear, for details, see e.g. (Lanoiselle et al., 1996). In experiments we performed, the conditions (use of thin samples) justify applicability of this initial condition. This is consistent with consolidation theory of porous material mechanics (Šuklje, 1969). We also suppose that pressure P_E redistributes itself equally onto the liquid phase of both the extracellular (p_{e0}) as well as the intracellular space (p_{i0}) at the beginning of a pressing experiment, after the extracellular air is eliminated and replaced by liquid at the beginning of the consolidation stage (Lanoiselle et al., 1996).

2.2. Analytical solution for liquid pressure

We give the analytical solution of PDEs Eqs. (15) and (16) for initial and boundary conditions Eqs.(17)–(20). The mathematical details of the derivation can be found for the case of an analogous problem of solute diffusion in electroporated tissue, given in full details in our recent publication (Mahnič-Kalamiza et al., 2014). For brevity, we only give the solution in final form below.

The intracellular liquid pressure p_i can be expressed as

$$p_i(z,t) = \frac{4p_{i0}}{\pi}\sum_{n=0}^{\infty}\frac{1}{2n+1}\left(C_1 e^{\gamma_{n,1}t} + C_2 e^{\gamma_{n,2}t} - e^{-\tau^{-1}t}\right)\sin\left(\frac{(2n+1)\pi}{2h}z\right) + p_{i0}e^{-\tau^{-1}t} \tag{21}$$

where

$$C_1 = \frac{\left(\frac{p_{e0}}{p_{i0}} - 1\right)\tau^{-1} - \gamma_{n,2}}{\gamma_{n,1} - \gamma_{n,2}}, \tag{22}$$

$$C_2 = \frac{\left(1 - \frac{p_{e0}}{p_{i0}}\right)\tau^{-1} + \gamma_{n,1}}{\gamma_{n,1} - \gamma_{n,2}} \tag{23}$$

and

$$\gamma_{n_{1,2}} = \frac{-(\tau^{-1}\delta + \lambda_n^2 v) \pm \sqrt{(\tau^{-1}\delta + \lambda_n^2 v)^2 - 4\lambda_n^2 v\tau^{-1}}}{2}, \tag{24}$$

where for the sake of algebra we have set

$$v = \frac{k_e G_{\varepsilon,e}}{\mu}; \quad \tau^{-1} = \frac{\alpha G_{\varepsilon,i}}{\mu}; \quad \delta = \left(1 + \frac{G_{\varepsilon,e}}{G_{\varepsilon,i}}\right); \quad p_{i0} = p_i(z,0); \quad p_{e0} = p_e(z,0).$$

The eigenvalues λ_n equal $\lambda_n = (2n+1)/2\cdot\pi/h$.

For extracellular liquid pressure p_e, we have

$$p_e(z,t) \quad \frac{4p_{i0}}{\pi}\sum_{n=0}^{\infty}\frac{1}{2n+1}\left((\gamma_{n,1}\tau+1)C_1 e^{\gamma_{n,1}t} + (\gamma_{n,2}\tau+1)C_2 e^{\gamma_{n,2}t}\right)\sin\left(\frac{(2n+1)\pi}{2h}z\right) \tag{25}$$

where all coefficients are calculated according to expressions already defined for intracellular pressure.

The infinite series in Eq. (21), as can easily be verified, converges extremely rapidly, even if few members of the infinite series are taken for summation. On the contrary, the series in Eq. (25) is more demanding and converges slowly, as it has to approximate the discontinuity present at $z = 0$, where the extracellular pressure drops immediately from the constant (initial condition) value to 0. In practice though, it is far more efficient in computational terms to not use Eq. (25), but calculate $p_i(z,t)$ according to Eq. (21). As few as 3–5 members of the series suffice to achieve accuracy required by most practical applications. Once the intracellular pressure is known, we can use relation given by the following equation, which has been rewritten by expressing p_e from Eq. (16)

$$p_e = \frac{\mu}{\alpha G_{\varepsilon,i}}\frac{\partial p_i}{\partial t} + p_i \tag{26}$$

to numerically calculate the extracellular pressure $p_e(z,t)$, which is a matter of numerical derivation and some arithmetic. The calculation of both pressures on an average modern laptop computer using the software package MATLAB (MathWorks, Massachusetts, USA) and employing an algorithm based on Eqs. (21) and (26) as described above, requires between 10 and 20 ms for a spatial and temporal resolution of 100 nodes. This makes the model suitable for use in optimization algorithms, and is one of the reasons why we opted for model simplification and derivation of a relatively simple analytical solution, rather than computing liquid pressures numerically.

Another advantage of the analytical solution is it provides the possibility for analysing model behaviour. From Eqs. (21) and (25), we can determine that process kinetics is governed entirely by the roots of the characteristic polynomial (given by Eq. (24)). If there is no electroporation and $\tau^{-1} \to 0$, Eq. (24) can be simplified and gives $\gamma_{n,1} \to 0$ and $\gamma_{n,2} \to -\lambda_n^2 v$. At these conditions, expression–consolidation kinetics is governed entirely by the rate of expression through extracellular space, i.e. k_e, and there is no transmembrane flow (since $\tau^{-1} \to 0$). Eq. (1) becomes an ordinary one-dimensional filtration–consolidation equation. We should point out that the analytical solution given by Eqs. (21) and (25) becomes extremely unstable for numerical evaluation when $\tau^{-1} \to 0$. As τ^{-1} decreases, numerical errors due to finite machine precision (32- or 64-bit floating point representation and operations) are amplified and the model results become unstable. For machine precision on the order of 10^{-16}, this effect becomes observable around $\tau^{-1} = 10^{-14}$ and the results become completely unusable for $\tau^{-1} < 10^{-15}$. At these extreme conditions however, there is no justification for use of the dual-porosity model whatsoever, and analysis of filtration–consolidation behaviour in extracellular space can be better described by a simpler model.

At the other extreme, for highly electroporated tissue ($f_p \to 1$, see Section 2.5 for the definition), for f_p values above approximately 10^{-3}, the membrane appears to disintegrate, i.e. to lose its barrier function for liquid flow. In Eq. (24) we then have $\tau^{-1}\delta \gg \lambda_n^2 v$. This results in extremely rapid kinetics ($|\gamma_2| \approx \tau^{-1}\delta \gg 1$) of transmembrane filtration and instantaneous expression of liquid from the intracellular into the extracellular space, provided there is a liquid pressure gradient. This is again unrealistic and outside the scope of the model, as the intracellular filtration pathway is not captured by model equations. The other exponential however, $C_1\exp(\gamma_1 t)$, is governed primarily by k_e, which limits vacation of liquid out of the tissue block via the extracellular space. Since $C_1 \gg C_2$ this results in almost identical expression–consolidation kinetics in extracellular space as in non-electroporated tissue, but with comparatively higher extracellular liquid pressure at a given time. This is expected, since the extracellular space has to facilitate vacation of not only the liquid initially present in the extracellular phase, but of the liquid initially present within the cells as well.

As emphasized during the analysis, there are limitations of the proposed dual-porosity model and its analytical solution, in addition to those already discussed in connection with the compressibility moduli. These limitations must be kept in mind during

experimentation with the model, and one should maintain a critical outlook on the results in light of these observations to avoid analysis under unrealistic or extreme conditions. We will further comment on the issue in the Results section.

2.3. Model application – from theory to experimentally measured kinetics

In pressing experiments set up as shown schematically in Fig. 3, the quantity observed is most commonly the deformation of the sample block of tissue (Grimi et al., 2010; Mhemdi et al., 2012). Our model thus far concerns liquid pressures in the extracellular and intracellular space. In order to compare model results with experiments, we must find an expression giving deformation as a function of the cumulative change of pressure throughout the sample. The relationship between loss of liquid pressure and deformation is already given by Eqs. (5) and (6). Since total deformation is the sum of deformation of extracellular and of intracellular space, we have

$$S(t) = S_e(t) + S_i(t), \tag{27}$$

Total deformation can be expressed as a spatial integral of local infinitesimal differences in void ratio e, therefore

$$\begin{aligned} S(t) &= \int_0^h \int_{e_e(z,t)}^{e_e(z,0)} de_e \cdot dz + \int_0^h \int_{e_i(z,t)}^{e_i(z,0)} de_i \cdot dz \\ &= \frac{1}{G_e}\int_0^h \int_{p_e(z,t)}^{p_e(z,0)} dp_e \cdot dz + \frac{1}{G_i}\int_0^h \int_{p_i(z,t)}^{p_i(z,0)} dp_i \cdot dz. \end{aligned} \tag{28}$$

Since we are working with porosity ε instead of void ratio e, and for reasons of convenience, we define relative deformation s_ε

$$\begin{aligned} s_\varepsilon(t) &= \frac{S_\varepsilon(t)}{h} \\ &= \frac{1}{G_{\varepsilon,e}}\int_0^1 \int_{p_e(z,t)}^{p_e(z,0)} dp_e \cdot dz + \frac{1}{G_{\varepsilon,i}}\int_0^1 \int_{p_i(z,t)}^{p_i(z,0)} dp_i \cdot dz, \end{aligned} \tag{29}$$

where h is the tissue sample height. Eq. (29) gives relative deformation as a function of loss of liquid pressure within the tissue. We will use it to obtain model results and compare them with experimental data.

2.4. Estimation of permeability and compressibility coefficients

2.4.1. Compressibility moduli $G_{\varepsilon,e}$, $G_{\varepsilon,i}$

We imagine two experimental scenarios. In the first experiment, freshly cut intact tissue is subjected to pressing under pressure of insufficient strength to cause cell rupture. Under these conditions, when equilibrium between the pressure applied via piston and the intracellular liquid pressure is reached (neglecting the extracellular solid pressure), we will have obtained a certain measurable but small deformation. If the pressure applied is sufficient to completely express extracellular fluid while not compromising the integrity of the cell plasma membrane, this measured deformation is only due to the compression of extracellular space. We write

$$\begin{aligned} s_{e,\infty} = s_e(t\to\infty) &= \frac{1}{G_{\varepsilon,e}}\int_0^1 \int_{p_e(z,t\to\infty)}^{p_e(z,0)} dp_e \cdot dz \\ &= \frac{1}{G_{\varepsilon,e}}\int_0^1 \int_0^{P_E} dp_e \cdot dz = \frac{P_E}{G_{\varepsilon,e}} \end{aligned} \tag{30}$$

Eq. (30) provides means to estimate $G_{\varepsilon,e}$ directly from pressing experiments done on intact, untreated (non-electroporated) tissue. With known deformation at "infinite" time and known applied pressure P_E, we have

$$G_{\varepsilon,e} \cong \frac{P_E}{s_{e,\infty}}. \tag{31}$$

Since $G_{\varepsilon,e}$ is a function of void ratio, which is not constant in time (and is only approximately constant throughout the tissue block along z, provided the sample is thin), the value obtained by Eq. (31) is a rough initial estimate, and a good approximation for untreated tissue only. It is expected to decrease with increasing treatment intensity, since it is not a material property but depends on e. We will have to determine the average value (as defined by Eq. (11)) by optimization against experiments.

We propose another conceptual experiment for estimating $G_{\varepsilon,i}$. If we permeabilize the cell membranes (by e.g. electroporation), under applied pressure liquid will flow from intracellular to extracellular space and through the latter out of the tissue block. At complete equilibrium (i.e. after "infinite" time), all liquid will be expressed from the sample, and the externally applied pressure will be balanced by the sum of solid pressures of intracellular and extracellular space. We write

$$\begin{aligned} s_\infty &= s_e(t\to\infty) + s_i(t\to\infty) \\ &= \frac{1}{G_{\varepsilon,e}}\int_0^1 \int_{p_e(z,t\to\infty)}^{p_e(z,0)} \mathrm{dp_e}\cdot \mathrm{dz} + \frac{1}{G_{\varepsilon,i}}\int_0^1 \int_{p_i(z,t\to\infty)}^{p_i(z,0)} \mathrm{dp_i}\cdot \mathrm{dz} \\ &= \frac{1}{G_{\varepsilon,e}}\int_0^1 \int_0^{P_E} \mathrm{dp_e}\cdot \mathrm{dz} + \frac{1}{G_{\varepsilon,i}}\int_0^1 \int_0^{P_E} \mathrm{dp_i}\cdot \mathrm{dz} = \frac{P_E}{G_{\varepsilon,e}} + \frac{P_E}{G_{\varepsilon,i}} \\ &= \frac{P_E(G_{\varepsilon,i}+G_{\varepsilon,e})}{G_{\varepsilon,e}G_{\varepsilon,i}} \end{aligned} \tag{32}$$

If $G_{\varepsilon,e}$ is known, e.g. determined according to Eq. (31), and we measure deformation in an experiment with strongly permeabilized tissue, by expressing $G_{\varepsilon,i}$ from Eq. (32), we get

$$G_{\varepsilon,i} \cong \frac{P_E G_{\varepsilon,e}}{s_\infty G_{\varepsilon,e} - P_E}, \tag{33}$$

which is a function of either previously known or measurable parameters. This estimate gives an approximate value for $G_{\varepsilon,i}$ in case of damaged tissue. The average value (as per Eq. (12)) for untreated or only moderately electropermeabilized tissue is expected to be much higher. As with $G_{\varepsilon,e}$, the value corresponding to the particular degree of electropermeabilization will be determined by fitting model results to experimental data.

2.4.2. Intrinsic hydraulic permeabilities k_e and k_i

Hydraulic permeability of tissue is almost always measured rather than calculated (Buttersack and Basler, 1991), due to high complexity of water pathways within tissue that makes theoretical estimates hard to obtain, and the biological diversity, which renders these estimates unreliable across different plant species and across samples of a single species. Measurements on a number of plant tissues and yeast cells show a wide range of values for permeability, spanning several orders of magnitude, for both tissue as well as plasma membrane of individual cells (Buttersack and Basler, 1991; Tomos, 1988).

This paper is concerned with juice expression from untreated and electroporated sugarbeet. Since sugarbeet is of great industrial importance, it is one of the few crop species that have been more extensively studied in terms of its water transport and consolidation properties. In literature, it is possible to find several accounts of measurement of hydraulic conductivity (L_p) of sugarbeet roots and cells comprising the root tissue. Here, we demonstrate how it is possible to recalculate these measurements in order to estimate the intrinsic hydraulic permeability coefficients required by our model.

The hydraulic conductivity L_p found in literature is normally calculated based on an experiment where a tissue sample is sub-

jected to a pressure difference and liquid volume flux is measured. With known flux and pressure, the hydraulic conductivity is

$$L_p = \frac{q}{\Delta p}. \tag{34}$$

On the other hand, the Darcy law relates the pressure drop across a conduit of length l with the liquid flux q as

$$|q| = \frac{k}{\mu}\frac{\Delta p}{l}. \tag{35}$$

Note that we write the absolute value of q since we are not interested in the direction of the flow. Inserting q from Eq. (34) into Eq. (35) and expressing k gives

$$k = L_p \cdot \mu \cdot l. \tag{36}$$

Eq. (36) can be used to calculate the intrinsic hydraulic permeability of tissue from measurements obtained via experiments described above. For instance, Amodeo et al. (Amodeo et al., 1999) measured conductivity of 3 mm slices (osmotic flow length l) of untreated sugarbeet roots in the axial and radial direction, obtaining in the radial direction (perpendicular to the major water transport channels) a conductivity of $5{\cdot}10^{-6}$ m MPa^{-1} s^{-1}. Using Eq. (31) and water viscosity of 10^{-3} Pa s, we obtain (for l = 3 mm) $k = 1.5{\cdot}10^{-17}$ m^2. Assuming negligible symplastic flow (i.e. only apoplastic), this is the sought hydraulic permeability of extracellular space, k_e.

The intracellular hydraulic permeability k_i is in fact the hydraulic permeability of the plasma membrane of thickness l. This coefficient is expected to change when treatment, be it mechanical, thermal, chemical, enzymatic or electrical, is applied to the tissue. Its initial value (i.e. for untreated tissue) can be estimated from pressure-probe experiments. Tables of cell membrane hydraulic permeability are given in literature for many plant and yeast species, including sugarbeet. In (Tomos, 1988) we find for hydraulic conductivity of sugarbeet cell membrane the value of $0.2{\cdot}10^{-6}$ m MPa^{-1} s^{-1}. Given a membrane thickness of 5 nm, Eq. (36) yields membrane intrinsic hydraulic permeability $k_i = 10^{-24}$ m^2.

2.5. Electroporation effects on plasma membrane permeability – the proportionality coefficient α

The proportionality coefficient α (dimensionless) proposed in the model definition (Eq. (14)), relates the intracellular and extracellular deformation due to transmembrane flux with the pressure drop across the plasma membrane. It needs to be, according to model design and assumptions, a function of membrane permeability k_i, multiplied by a corrective geometrical factor ξ with units m^{-2}. This corrective factor ξ accounts for the geometrical configuration of the cell and its porous membrane by relating intracellular space porosity with volume-averaged transmembrane flux (further explanation can be found in the Appendix). For negligible membrane thickness as compared to the size of the cell, ξ equals the square of specific surface (surface-to-volume ratio), i.e. $\xi = (A/V)^2$. On the level of a biological cell, where transmembrane fluid transport occurs, the surface A and volume V are those of a single cell. For an idealized, average, spherical cell of sugarbeet tissue with a radius of 25 μm (Buttersack and Basler, 1991), the corrective factor ξ equals $1.44{\cdot}10^{10}$. Consequently, the proportionality coefficient α is written as $\alpha = 1.44{\cdot}10^{10}{\cdot}k_i$. For a detailed theoretical derivation which is also applicable in cases where membrane is not of negligible thickness, see the Appendix.

We now turn to the effect of electroporation treatment on the hydraulic permeability coefficient, k_i. According to the theory of electroporation (Neu and Neu, 2009; Kotnik et al., 2012; Haberl et al., 2013), electric field of sufficient strength creates pores in the plasma membrane. These pores nucleate at an initial radius of about 0.5 nm, and can expand in both number and size during the application of electric field. The effect has a transient as well as a long-lasting component, i.e. transient and long-lasting pores are created in the membrane (Pavlin and Miklavcic, 2008). It has been demonstrated by several experiments, see e.g. (Saulis and Saule, 2012), that long-lasting pores permeable to molecules of e.g. bleomycin (about 1.6 nm in diameter) or sucrose (0.44–0.52 nm diameter), can exist in an electroporated membrane for minutes after the application of electric pulses, though they are subject to resealing if physiological conditions are favourable. We can, assuming an average stable pore diameter and pore fraction ratio (i.e. the surface fraction of all pores per one cell), estimate how electroporation changes the hydraulic permeability of the cell membrane.

We start by relating membrane permeability k_i with permeability of a single aqueous pore. The absolute value of membrane flux is, according to Darcy law,

$$|Q_m| = \frac{k_i A_m}{\mu}\frac{\Delta p}{l}, \tag{37}$$

but it is also the sum of all single-pore fluxes, of which there are as many as there are pores, i.e. N_p. We write

$$|Q_m| = N_p|Q_p| = \frac{N_p k_p A_p}{\mu}\frac{\Delta p}{l}. \tag{38}$$

From equating transmembrane flux in Eqs. (37) and (38) we obtain the relation

$$k_i = \frac{N_p k_p A_p}{A_m} = f_p k_p, \tag{39}$$

where $f_p = N_p A_p / A_m$ is the pore surface fraction.

According to literature (Pavlin and Miklavčič, 2008), surface fraction of long-lasting pores in B16F1 (mouse melanoma) cells for 8 pulses of 100 μs duration and strength of 1 kV/cm is on the order of $0.5{\cdot}10^{-5}$. In experiments with electroporation treatment of vegetable tissue for enhancing liquid extraction by pressing, many more pulses are normally used (100, 1000 or more), and cells in treated tissue can measure more than 10 times the size of cells in animal cell lines used most often in electroporation studies (i.e. Chinese hamster ovary – CHO, mouse melanoma – B16F1, etc.). Therefore, the upper limit of the range into which long-lasting pore fraction is expected to fall should be generously increased. Extrapolating results published in (Pavlin and Miklavčič, 2008), where a similar treatment protocol to ours was used, places the initial estimate for f_p at around $2{\cdot}10^{-5}$. However, this value must be understood as a highly unreliable estimate, as various phenomena involved in pore formation and stabilization were not accounted for (e.g. media conductivity, cell suspension vs. biological tissue, differences in cell size, etc.). Optimization with model results to fit experimental data in our model study resulted in estimates of pore surface fraction an order of magnitude higher (see Table 2, Section 3.1) as compared to the initial estimate. One possible reason we can suggest to explain this discrepancy is the much higher induced transmembrane voltage in large plant cells (our study) as opposed to smaller animal cells (cited reference). According to electroporation theory, pore surface fraction is strongly dependent on induced transmembrane voltage. More work should be dedicated to determining the parameters that describe membrane long-term permeability with respect to the treatment protocol. More specifically, if the radius of an average stable pore is underestimated – and due to persistence of large pores several minutes after pulse application it most probably is (Saulis and Saulė, 2012) – the resulting pore surface fraction according to pressing experiments will be overestimated, as higher surface fraction will compensate for the lower single pore hydraulic permeability.

Table 1
Expressions for model parameter estimations – a summary.

Parameter	Value	Method
$G_{\varepsilon,e}$	P_E/s_∞	From experiments
$G_{\varepsilon,i}$	$\frac{P_E G_{\varepsilon,e}}{s_\infty G_{\varepsilon,e} - P_E}$	From pressing experiments
k_e	$L_p \cdot \mu \cdot l$	Osmotic flow measurements (l is tissue sample thickness)
k_i	$L_p \cdot \mu \cdot l$	Pressure probe measurements (l is membrane thickness)
k_p	$r_p^2/8$	Hagen-Poiseuille theoretical estimation
$k_{i,EP}$	$\frac{N_E k_E A_E}{A_m} = f_p k_p$	Theoretical estimation (k_p) and estimate based on fitting the model to experimental data (f_p)
α	$k_i \cdot (A/V)^2$	Theoretical estimate based on pressure probe measurements
α_{EP}	$k_{i,EP} \cdot (A/V)^2$	Theoretical estimate based on fitting the model to experimental data

Table 2
Parameters used to obtain model results, simulation results are plotted against experiments in Fig. 4.

Parameter	Value	Method/source
P_E	5.82×10^5 Pa	As used in experiments
G_{e0} (initial estimate)	129×10^5 Pa	From final deformation of intact tissue – experiments
G_{i0} (initial estimate)	8×10^5 Pa	Recalculated from final deformation of electroporated tissue given known G_{e0} – experiments
G_{e0} (optimized)	130×10^5 Pa	Optimization using experimental results
G_{i0} (optimized)	16×10^5 Pa	Optimization using experimental results
k_{e0} (initial estimate)	1.5×10^{-17} m^2	Osmotic flow measurements (Amodeo et al., 1999)
k_e (optimized)	3.75×10^{-17} m^2	Optimization using experimental results
k_{i0} (initial estimate)	10^{-24} m^2	Pressure probe measurements (Tomos, 1988)
k_i (optimized)	10^{-24} m^2	Optimization using comparison with experimental results ($k_i = f_p \cdot k_p$)
$k_{i,EP}$ (optimized, at 400 V, Protocol A)	2.8×10^{-23} m^2	Optimization using comparison with experimental results ($k_i = f_p \cdot k_p$)
k_p	1.25×10^{-19} m^2	Hagen-Poiseuille theoretical estimation based on estimated average stable pore size
f_{p0}	2.5×10^{-5}	Extrapolation of experimentally-obtained estimates (Pavlin and Miklavčič, 2008)
f_p (optimized, at 400 V, Protocol A)	2.22×10^{-4}	Optimization using comparison with experimental results
α	1.44×10^{-10} m^{-2} k_i	Theoretical estimate for $\xi = 1.44 \times 10^{-10}$ m^{-2}, k_i from pressure-probe experiments
α_{EP}	1.44×10^{-10} m^{-2} $k_{i,EP}$	Theoretical estimate for $\xi = 1.44 \times 10^{-10}$ m^{-2}, $k_{i,EP}$ from experiments and pore size/population estimates (see f_p and k_p)

The remaining parameter to be estimated is the single pore intrinsic hydraulic permeability, k_p. To that end, we use the Hagen–Poiseuille equation for cylindrical pores of length l and radius r_p in combination with Darcy law. We get

$$\Delta p = \frac{8\mu l Q_p}{\pi r_p^4} = \frac{8\mu l Q_p}{r_p^2 A_p} = \frac{\mu l Q_p}{k_p A_p}. \quad (40)$$

From Eq. (40) k_p can be expressed as $r_p^2/8$. We now assume that the average size of a stable pore can be estimated from models of pore evolution during and after treatment, such as those reviewed by Saulis (Saulis, 2010). If we remain conservative, and suppose an average pore radius of about 1 nm with lifetime of minutes up to hours after treatment, k_p equals $1.25 \cdot 10^{-19}$ m^2. This gives for membrane (and intracellular space) permeability in electroporated tissue $k_{i,EP}$ the value of $2.7 \cdot 10^{-23}$, which is about 30-times higher than what has been estimated for intact cellular membrane, and can be found in literature (Tomos, 1988). The cited estimate is based on one particular study utilising a pressure probe technique, available only to the author of the cited review as an unpublished manuscript. We are therefore unable to analyse the methodology and calculations to evaluate the reliability and accuracy of this estimate. Parameter estimations are summarized in Table 1. Note that the model tissue under consideration is sugarbeet.

3. Results and discussion

3.1. Modelling experimental extraction kinetics for model validation

In order to demonstrate how the proposed model can be used in practice to explain experimentally-obtained kinetics, we present a comparison between experimental data obtained by pressing cylindrical sugarbeet slices, and the model simulation results. All parameters were initially estimated as described in the preceding sections, and kept constant, except for the two compressibility moduli $G_{\varepsilon,e}$ and $G_{\varepsilon,i}$, the pore surface fraction of electroporated tissue f_p, and the extracellular permeability coefficient k_e. These parameters were sought for by means of optimization against the experimental data, with estimates (obtained via methods in Table 1) used as initial guesses. Using an optimization search to correct the values of these parameters is justified by the fact their estimate is prone to inaccuracy due to biological variability, and the compromises we made in theory to keep the model simple. We have however managed to remain well within one order of magnitude difference between the initial guess and the optimized value, suggesting the methods used for estimation are fairly reliable.

Fig. 4 below shows relative tissue sample deformation as a function of time. The simulated expression curves were obtained using parameters summarized in Table 2. Compressibility moduli were first estimated from modelled experiments as explained in

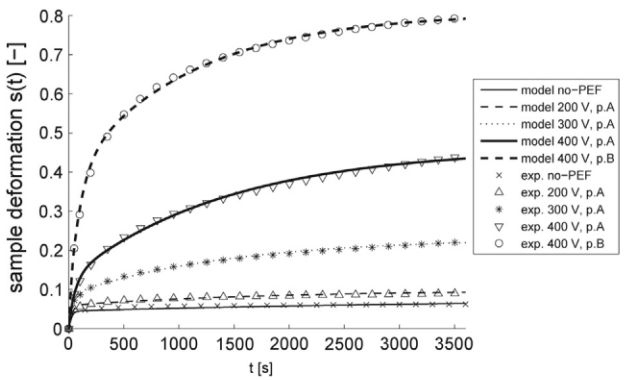

Fig. 4. Experimental data and model results. An optimization using RMSE as a criterion function was run to determine the parameters resulting in the best fit. Note that "p.A" stands for Protocol A and "p.B" for Protocol B.

Section 2.4.1, and then an optimization search for global minima of RMSE between experimental and model data was used to identify optimal values. The total relative deformation calculation follows Eq. (29) based on liquid pressures calculated using Eqs. (21) and (26). Detailed descriptions of the experimental setup used for data acquisition have previously been published in literature (Grimi et al., 2010). In short; we used cylindrical samples of sugarbeet tissue, 25 mm in diameter and 5 mm thick. The samples were placed between two parallel plate electrodes, and electroporation pulses were applied using two protocols. Protocol A: The voltage was varied, using 200 V, 300 V or 400 V applied to the electrodes. Bipolar pulses were delivered in two trains of 8 pulses per train, with repetition frequency of 1 kHz within the train, 1 s pause between the two trains, and 100 μs pulse duration. Protocol B: The voltage was fixed at 400 V, 20 unipolar pulses of 1 ms duration were applied with repetition frequency of 0.5 Hz. In all cases, regardless of the electroporation protocol, the electric treatment was followed by pressing. Electroporated samples were immediately placed into a specially fabricated treatment cell and subjected to a load of 300 N using a texturometer. The piston displacement was recorded by the texturometer under constant pressure application during one hour.

To fit experimental results, parameter f_p had to be increased from $8.0{\cdot}10^{-6}$ for untreated tissue to $2.0{\cdot}10^{-5}$ for the electrode voltage of 200 V; further to $9.5{\cdot}10^{-5}$ for 300 V; and finally to $2.2{\cdot}10^{-4}$ for 400 V (Protocol A). In case of treatment according to Protocol B at 400 V, f_p had to increase only slightly as compared to Protocol A at the same voltage, to $3.3{\cdot}10^{-4}$. This is consistent with electroporation theory and observations; pore surface fraction is a function of maximal electric field strength (Pavlin and Miklavcic, 2008). What had to be significantly altered comparing Protocol A at B at 400 V were the compressibility moduli and k_e. This was expected, as compressibility moduli reflect the extent of the bulk tissue damage (fraction of permeabilized cells), and in highly electroporated tissue, additional liquid paths (increase in k_e) should be created by vacant cell compartments of destroyed cells. One surprising and unexpected observation is the highly significant difference in compressibility modulus of the extracellular space, especially when comparing tissue treated with 400 V pulses and two different Protocols, A and B. This marked discrepancy cannot be explained as resulting from model (over)simplifications. The theory of electroporation however does offer a plausible explanation; Electroporation is a threshold phenomenon. Depending on the treatment parameters, a cell remains either undamaged, is reversibly permeabilized (and recovers if conditions are favourable), or is irreversibly electroporated. Irreversibly electroporated cells lose the ability to control transmembrane liquid and solutes flow. From the porous medium point of view, they can no longer be regarded as intracellular space. From this perspective, irreversible electroporation is responsible for transformation of the intra- to the extracellular phase; it is modifying the volumetric ratio of intra- and extracellular space, i.e. the volume fraction of cells. For field strengths and protocols that result in irreversible electroporation, we must take these effects into account, as the transmembrane filtration law (source term $v_{i-e}(z,t)$ in Eqs. (1) and (2), governed by f_p) cannot describe behaviour of irreversibly damaged membranes. This suggests that future model development should head towards coupling the filtration–consolidation model with models of field strength distribution, pore evolution, and the resulting cell damage distribution. Moreover, the effect of electrically induced damage to tissue on extracellular permeability k_e must be evaluated.

3.2. Parametrical study

To study the sensitivity of the model to parameter variations we present a parametrical study for four parameters. Note that the parameters that remain constant as each examined parameter is varied were taken from Table 2 and were estimated for sugarbeet tissue from literature or experiments. This tissue thus represents our model tissue throughout the parametrical study.

First, we varied the viscosity of the liquid medium μ (Fig. 5a) to demonstrate the effect of different temperatures of the material during pressing. If the process is not isothermal, a possibility of heat accumulation and temperature elevation exists. In industry, pressure processing is also often combined with heat processing (in oil extraction for example). The range of viscosities chosen is based on a range of temperatures between 10 and 50 °C, and given for water. If applied to material with markedly different composition of liquid media (e.g. oil), these viscosities should be adapted to the application. We limited the temperature to 50 °C as the model is no longer applicable at higher temperatures, as it does not account for temperature damage to the material. The remaining parameters were the same as determined for sugarbeet, treated according to Protocol A at 300 V pulse amplitude. Model results are also presented for several ratios of compressibility moduli in intact tissue $G_{\varepsilon,e}/G_{\varepsilon,i}$ (Fig. 5b), to demonstrate possible expression kinetics in highly porous tissues containing considerably larger fractions of extracellular space occupied predominantly by air, as in e.g. apple tissue (Harker et al., 2010). We used parameters obtained for sugarbeet in experiments (Protocol A, 300 V) and varied $G_{\varepsilon,e}$. Furthermore, Fig. 5c shows model results for varying k_i, not as a function of electroporation, but as a function of plant species, as membrane permeability seems to vary considerably between various tissues of different plant species. Modelled tissues include pea epicotyl epidermis ($k_i = 10^{-25}\ m^2$), ripe apple tissue ($k_i = 5{\cdot}10^{-25}\ m^2$), maize leaves midrib mid parenchyma ($k_i = 10^{-23}\ m^2$) and soybean hypocotyl elongating epidermis ($k_i = 3{\cdot}10^{-23}\ m^2$). All permeability coefficients were recalculated from hydraulic conductivities obtained from (Tomos, 1988), and model results calculated for the intact tissue permeability (no effects of electroporation). Finally, Fig. 5d shows deformation as a function of time for electroporated sugarbeet tissue (Protocol A, 300 V) when varying external pressure P_E. Validating all of these dependencies is out of the scope of this paper, whose purpose is to introduce the basic model by its theoretical formulation and basic proof of concept.

Results in Fig. 5a show the system is stable with regard to the temperature-dependence of viscosity. However, elevated temperatures damage biological tissues, and the model does not capture these effects. Varying the compressibility modulus of extracellular space and thus changing the $G_{\varepsilon,e}/G_{\varepsilon,i}$ ratio has, for fixed $G_{\varepsilon,i}$, f_p, and P_E, a profound effect on the compressibility of the sample during the initial compression stage (Fig. 5b). As the model does not account for the volumetric relationship between the intra- and extracellular phases and $G_{\varepsilon,e}$ in reality varies with time and treatment parameters, the effects as shown in this simulation should be viewed as overestimations. They do however demonstrate possible behaviour of expression kinetics in tissues with different textural properties. In example, apple tissue has large extracellular compartments of air, and is more compressible than sugarbeet or similar, more compact biological materials. Fig. 5c demonstrates the relative unimportance of intrinsic hydraulic permeability of intact cellular membrane (note the scale on the ordinate axis), which depends on the plant species, originating tissue (epidermal, parenchyma, etc.), moisture content at harvesting, and other conditions. We performed these simulations for an intact membrane only, using available permeability data in literature (Tomos, 1988). We chose to exclude electroporation effects since it would be difficult to reliably estimate compressibility coefficients for electroporated tissues cross-species, since they exhibit significant differences in textural properties. Finally, Fig. 5d gives filtration–consolidation kinetics for different constant external pressures.

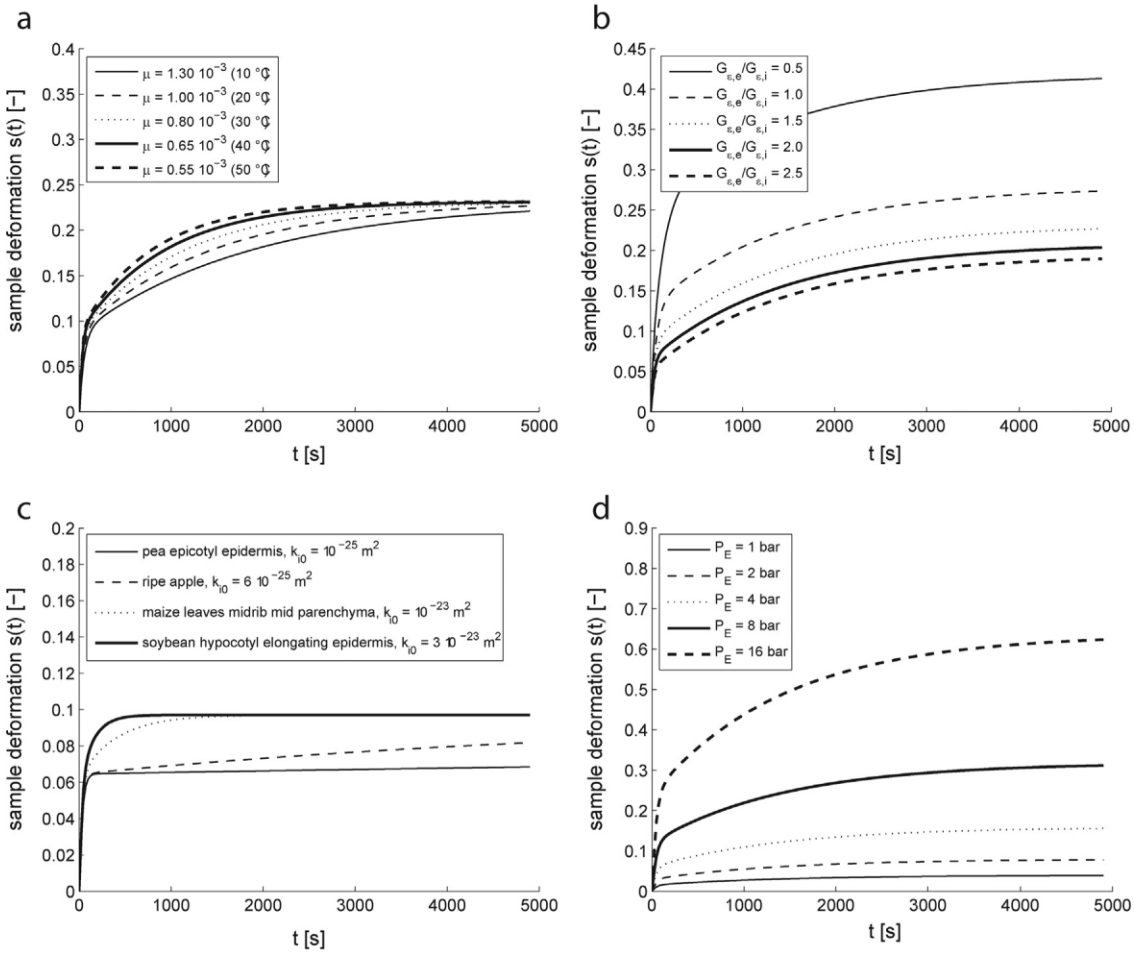

Fig. 5. Results of the parametric model study. (a) Effect of varying the viscosity of the liquid medium μ (temperature variation 10–50 °C); (b) effect of varying the compressibility moduli ratio $G_{\varepsilon,e}/G_{\varepsilon,i}$; (c) effect of varying the intracellular/membrane hydraulic permeability k_i; and (d) effect of variable external pressure P_E.

As anticipated, the resulting profiles are linearly scalable, which is also consistent with various experimental observations, see e.g. experimental results in (Grimi et al., 2010). Since compressibility moduli were determined based on a single pressing experiment at constant external pressure, slight discrepancies between simulated results and experimental data at higher pressures are expected. The compressibility G_ε based on total press-cake deformation is a nonlinear function of pressure for electroporated tissue. See e.g. Fig. 8, pp. 34 in Grimi et al. (2010) for details. Due to this nonlinearity, the compressibility modulus of intracellular space must be recalculated at high pressures.

4. Conclusions

In this work we presented a dual-porosity model for liquid expression from tissue treated by electroporation. The fundamental theory for model construction is rooted in phenomenological observations of liquid flow in porous media.

We connect experiments with the theoretical model through parameter estimation. The experiment-based estimation is necessary at this stage in model development, as biological complexity and diversity render theoretical estimations scarce and unrealistic. We propose means of relating the effects of electroporation on the plasma membrane with membrane hydraulic permeability. This point of model construction invites further development and verification, since theoretical models of electroporation give pore distribution (size, number) as a function of electric field application. There are also an increasing number of experimental studies available that study pore resealing dynamics and selectivity of the permeabilized plasma membrane. The findings of these studies seem promising for model enhancement, since they describe a temporal dependence of permeability coefficients that we assumed as time-invariable. Inclusion of such dynamics will however most likely require a numerical approach.

In order to keep the model comprehensive in this first account and to focus more on the concept of the dual porosity modelling paradigm in tissue electroporation, we made simplifications with regard to the theory of porous media, which is much more advanced. We intend to elaborate on this issue and develop a more complex model from the consolidation theory point of view in the future. A more complete and complex model is expected to have an added value of reliable predictive capabilities.

We verified the model by fitting simulated consolidation kinetics to experimental data. Based on estimated parameters, we modelled a pressing experiment. The results calculated using optimized initial parameter estimates (compressibility moduli and tissue/membrane permeability) were in good agreement with experimental data; since membrane and tissue permeability are highly variable parameters, we improved our estimates by varying the coefficients within an optimization algorithm. The optimized values were found to be within one order of magnitude from initial estimates, which is acceptable, given the wide range that these parameters normally exhibit, even for a single variety of plant species.

Further work will be dedicated to verification with additional experiments and to extension by combination with a model of

electroporation (pulse protocol effects, pore resealing, etc.). Validation by changing the model material (e.g. apple, carrot, red beet tissue) also poses a potentially interesting challenge.

Acknowledgements

The authors appreciate the financial support from the French Ministry of Research and Higher Education. This research was in part made possible due to networking activity of COST TD1104 Action (www.electroporation.net).

Appendix A

In this appendix we give a theoretical derivation of factor ξ, which is a constitutive member of the dimensionless parameter α, found in model equations (Eqs. (15) and (16)). Factor ξ relates the intrinsic hydraulic permeability of the cell membrane and the pressure drop across the membrane with the resulting decrease in intracellular porosity (related to liquid pressure via compressibility) and the increase in extracellular porosity due to expression of liquid from the intracellular to the extracellular space.

We begin the derivation by writing Darcy law for transmembrane flow for a single individual cell

$$q_m = \frac{Q_m}{4\pi r^2} = -\frac{k_m}{\mu}\frac{dp}{dr} \tag{A.1}$$

and integrate both sides across the membrane, where the pressure drop $p_i - p_e$ occurs, obtaining

$$Q_m \int_R^{R+l} \frac{dr}{4\pi r^2} = -\frac{k_m}{\mu}\int_{p_e}^{p_i} dp, \tag{A.2}$$

where l is the thickness of the membrane and R the inner cell radius (i.e. the radius of the cell without the membrane). After carrying out the integration and some rearrangement, we have

$$Q_m = \frac{k_m}{\mu}\frac{4\pi R(R+l)}{l}(p_i - p_e). \tag{A.3}$$

The intra-to-extracellular or transmembrane flow of liquid Q_m results in a change in cell porosity ε_c, which is defined as the ratio of liquid phase to total intracellular volume, thus yielding

$$\frac{Q_m}{V} = \frac{d\varepsilon_c}{dt} = \frac{k_i}{\mu}\frac{3(R+l)}{R^2 l}(p_i - p_e). \tag{A.4}$$

Eq. A.4 is not directly comparable with Eqs. (15) and (16), as A.4 gives cell porosity as a function of time only, due to the spatial integration across the domain of a single cell, while in Eqs. (15) and (16) we have both space- and time-dependent liquid pressure of extracellular and intracellular space, or rather of their respective porosities. We must therefore first obtain a volume-normalized equivalent intracellular porosity. In short,

$$v_{i-e} = \frac{V_m}{V}\frac{d\varepsilon_c}{dt}, \tag{A.5}$$

and therefore

$$\begin{aligned}\frac{k_i\xi}{\mu}(p_i - p_e) &= \frac{k_i}{\mu}\frac{(R+l)^3 - R^3}{R^3}\frac{3(R+l)}{R^2 l}(p_i - p_e)\\ &= \frac{k_i}{\mu}\frac{9R(R+l)^2 + 3l^2(R+l)}{R^5}(p_i - p_e).\end{aligned} \tag{A.6}$$

From A.6 it immediately follows

$$\xi = \frac{9R(R+l)^2 + 3l^2(R+l)}{R^5}, \tag{A.7}$$

simplifying to $\xi = 9/R^2$ for $R \gg l$, which for spherical geometry equals exactly $(A/V)^2$, the square of the surface-to-volume ratio (also termed specific surface). If the membrane thickness l is not insignificant as compared to cell radius R, the more complex form as given by Eq. A.7 should be used to calculate the geometrical factor ξ, however, in biological tissues used in electroporation experiments, this is never the case. A much greater error than neglecting the influence of finite membrane dimensions and using a simplified specific-surface-squared approximation for ξ as proposed, is already introduced several steps earlier with the assumption of spherical cell geometry, since cells in real biological tissues do not exhibit perfectly spherical geometry.

As a final note, a physical interpretation of Eq. (A.5); in the model that we propose, intracellular porosity and thus liquid pressure is modelled as a continuous differentiable function of space (coord. z) and time. In reality, it is discretized by individual biological cells, within which the liquid pressure is constant. The pressure difference exists only across the membrane and is driving the intracellular liquid into the extracellular space, as extracellular liquid pressure is always lower than intracellular (assuming external pressure initially distributes itself equally on the two phases). Thus, in order to maintain the representation of intracellular space porosity continuous on z, the transmembrane flux has to be averaged over the entire intracellular volume, replacing the local effect of variable permeability of the cell membrane with an average permeability of intracellular space. Upon integrating liquid pressure difference in this equivalent media over one layer of cells, and multiplying by $k_i\xi/\mu$, we will obtain effectively the same liquid expression (change in ε) as we would have if we were to calculate the transmembrane flow Q_m.

References

Aguilera, J.M., Chiralt, A., Fito, P., 2003. Food dehydration and product structure. Trends Food Sci. Technol. 14, 432–437.
Amodeo, G., Dorr, R., Vallejo, A., Sutka, M., Parisi, M., 1999. Radial and axial water transport in the sugar beet storage root. J. Exp. Bot. 50, 509–516.
Bazhal, M., Lebovka, N., Vorobiev, E., 2003. Optimisation of pulsed electric field strength for electroplasmolysis of vegetable tissues. Biosyst. Eng. 86, 339–345.
Bazhal, M., Vorobiev, E., 2000. Electrical treatment of apple cossettes for intensifying juice pressing. J. Sci. Food Agric. 80, 1668–1674.
Bazhal, M.I., Lebovka, N.I., Vorobiev, E., 2001. Pulsed electric field treatment of apple tissue during compression for juice extraction. J. Food Eng. 50, 129–139.
Binkley, C., Wiley, R., 1981. Chemical and physical treatment effects on solid–liquid extraction of apple tissue. J. Food Sci. 46, 729–732.
Bouzrara, H., Vorobiev, E., 2003. Solid-liquid expression of cellular materials enhanced by pulsed electric field. Chem. Eng. Process. 42, 249–257.
Buttersack, C., Basler, W., 1991. Hydraulic conductivity of cell-walls in sugar-beet tissue. Plant Sci. 76, 229–237.
De Monte, F., Pontrelli, G., Becker, S., 2013. Drug release in biological tissues. In: Becker, S.M., Kuznetsov, A.V. (Eds.), Transport in Biological Media. Elsevier, Boston, pp. 59–118 (Chapter 3).
Ersus, S., Barrett, D.M., 2010. Determination of membrane integrity in onion tissues treated by pulsed electric fields: use of microscopic images and ion leakage measurements. Innov. Food Sci. Emerg. Technol. 11, 598–603.
Fincan, M., Dejmek, P., 2002. In situ visualization of the effect of a pulsed electric field on plant tissue. J. Food Eng. 55, 223–230.
Grimi, N., Vorobiev, E., Lebovka, N., Vaxelaire, J., 2010. Solid–liquid expression from denaturated plant tissue: filtration–consolidation behaviour. J. Food Eng. 96, 29–36.
Haberl, S., Miklavcic, D., Sersa, G., Frey, W., Rubinsky, B., 2013. Cell membrane electroporation-Part 2: the applications. IEEE Electr. Insul. Mag. 29, 29–37.
Halder, A., Datta, A.K., Spanswick, R.M., 2011. Water transport in cellular tissues during thermal processing. AICHE J. 57, 2574–2588.
Harker, F.R., Redgwell, R.J., Hallett, I.C., Murray, S.H., Carter, G., 2010. Texture of Fresh Fruit. In: Janick, J. (Ed.), Horticultural Reviews. John Wiley & Sons, Inc., pp. 121–224.
Knorr, D., Geulen, M., Grahl, T., Sitzmann, W., 1994. Food application of high-electric-field pulses. Trends Food Sci. Technol. 5, 71–75.
Kotnik, T., Kramar, P., Pucihar, G., Miklavcic, D., Tarek, M., 2012. Cell membrane electroporation- Part 1: The phenomenon. IEEE Electr. Insul. Mag. 28, 14–23.
Krassowska, W., Filev, P.D., 2007. Modeling electroporation in a single cell. Biophys. J 92, 404–417.
Lanoiselle, J.L., Vorobyov, E.I., Bouvier, J.M., Piar, G., 1996. Modeling of solid/liquid expression for cellular materials. AICHE J. 42, 2057–2068.

Lebovka, N.I., Praporscic, I., Vorobiev, E., 2004. Effect of moderate thermal and pulsed electric field treatments on textural properties of carrots, potatoes and apples. Innov. Food Sci. Emerg. Technol. 5, 9–16.

Llano, K.M., Haedo, A.S., Gerschenson, L.N., Rojas, A.M., 2003. Mechanical and biochemical response of kiwifruit tissue to steam blanching. Food Res. Int. 36, 767–775.

Luengo, E., Alvarez, I., Raso, J., 2013. Improving the pressing extraction of polyphenols of orange peel by pulsed electric fields. Innov. Food Sci. Emerg. Technol. 17, 79–84.

Mahnič-Kalamiza, S., Miklavčič, D., Vorobiev, E., 2014. Dual-porosity model of solute diffusion in biological tissue modified by electroporation. Biochim. Biophys. Acta accepted for publication, n/a.

Mhemdi, H., Bals, O., Grimi, N., Vorobiev, E., 2012. Filtration diffusivity and expression behaviour of thermally and electrically pretreated sugar beet tissue and press-cake. Sep. Purif. Technol. 95, 118–125.

Neu, W.K., Neu, J.C., 2009. Theory of Electroporation. In: Efimov, I.R., Kroll, M.W., Tchou, P.J. (Eds.), Cardiac Bioelectric Therapy: Mechanisms and Practical Implications. Springer.

Pavlin, M., Miklavcic, D., 2008. Theoretical and experimental analysis of conductivity, ion diffusion and molecular transport during cell electroporation - Relation between short-lived and long-lived pores. Bioelectrochemistry 74, 38–46.

Pavlin, M., Miklavčič, D., 2008. Theoretical and experimental analysis of conductivity, ion diffusion and molecular transport during cell electroporation — relation between short-lived and long-lived pores. Bioelectrochemistry 74, 38–46.

Petryk, M., Vorobiev, E., 2007. Liquid flowing from porous particles during the pressing of biological materials. Comput. Chem. Eng. 31, 1336–1345.

Petryk, M., Vorobiev, E., 2013. Numerical and analytical modeling of solid–liquid expression from soft plant materials. AIChE J. 59, 4762–4771.

Poel, P.W. van der, Schiweck, H.M., Schwartz, T.K., 1998. Sugar Technology: Beet and Cane Sugar Manufacture. Verlag Dr Albert Bartens KG.

Praporscic, I., Lebovka, N.I., Ghnimi, S., Vorobiev, E., 2006. Ohmically heated, enhanced expression of juice from apple and potato tissues. Biosyst. Eng. 93, 199–204.

Sack, M., Eing, C., Berghoefer, T., Buth, L., Staengle, R., Frey, W., Bluhm, H., 2008. Electroporation-assisted dewatering as an alternative method for drying plants. IEEE Trans. Plasma Sci. 36, 2577–2585.

Saulis, G., 2010. Electroporation of cell membranes: the fundamental effects of pulsed electric fields in food processing. Food Eng. Rev. 2, 52–73.

Saulis, G., Saule, R., 2012. Size of the pores created by an electric pulse: Microsecond vs millisecond pulses. Biochim. Biophys. Acta-Biomembr. 1818, 3032–3039.

Saulis, G., Saulė, R., 2012. Size of the pores created by an electric pulse: microsecond vs millisecond pulses. Biochim. Biophys. Acta 1818, 3032–3039.

Schilling, S., Alber, T., Toepfl, S., Neidhart, S., Knorr, D., Schieber, A., Carle, R., 2007. Effects of pulsed electric field treatment of apple mash on juice yield and quality attributes of apple juices. Innov. Food Sci. Emerg. Technol. 8, 127–134.

Schwartzberg, H.G., 1997. Expression of fluid from biological solids. Sep. Purif. Methods 26, 1–213.

Shankar, D., Agrawal, Y.C., Sarkar, B.C., Singh, B.P.N., 1997. Enzymatic hydrolysis in conjunction with conventional pretreatments to soybean for enhanced oil availability and recovery. J. Am. Oil Chem. Soc. 74, 1543–1547.

Shirato, M., Murase, T., Iwata, M., Nakatsuka, S., 1986. The terzaghi-voigt combined model for constant-pressure consolidation of filter cakes and homogeneous semisolid materials. Chem. Eng. Sci. 41, 3213–3218.

Šuklje, L., 1969. Rheological aspects of soil mechanics. Wiley-Interscience.

Tomos, A.D., 1988. Cellular water relations of plants. In: Franks, F. (Ed.), Water Science Reviews 3, Water Science Reviews. Cambridge University Press.

Vicente, A.R., Costa, M.L., Martínez, G.A., Chaves, A.R., Civello, P.M., 2005. Effect of heat treatments on cell wall degradation and softening in strawberry fruit. Postharvest Biol. Technol. 38, 213–222.

Vorobiev, E., Lebovka, N., 2010. Enhanced extraction from solid foods and biosuspensions by pulsed electrical energy. Food Eng. Rev. 2, 95–108.

Wiktor, A., Witrowa-Rajchert, D., 2012. Applying pulsed electric field to enhance plant tissue dehydration process. ZYWN.-Nauk Technol. Jakosc 19, 22–32.

Zhu, H.X., Melrose, J.R., 2003. A mechanics model for the compression of plant and vegetative tissues. J. Theor. Biol. 221, 89–101.

4.3 Paper IV: “Dual-porosity model of mass transport in electroporated biological tissue: Simulations and experimental work for model validation”

4.3.1 Introduction

The two previous works presented in this thesis (Paper II and Paper III) on the development of a mathematical model we refer to as the dual-porosity model were conceived as basic introductory works, giving details on the theory and mathematical modelling that is the basis of the model construction and application. The first account (Paper II) presents the model as describing extraction or introduction of solute by diffusion out of or into electroporated biological tissue, where the authors used sucrose extraction from sugar beets for a simple model study aimed at illustrating via a practical example a single model application. Furthermore, the authors suggest two possible applications of the model for introduction of compounds into animal or plant cells. Since the analogy between diffusion and liquid flow laws allows for a rapid adaptation of the model for the problem of filtration–consolidation behaviour of electroporated tissue, this is the subject of the second paper (Paper III) on the dual-porosity principle.

In this, the third paper on the subject, the two analogues are brought together and the model validity as well as its performance are examined by comparing experimental data with diffusion/expression kinetics, which result from simulations done using the proposed model. Two kinds of vegetable tissue are used as model material, with markedly different properties (sugar beet taproot and apple fruit), but the same methodology is employed to determine if the postulates and simplifications during model development are justifiable, i.e. if results of model simulations can be reconciled with those obtained via experiments and with the theory of electroporation. Paper IV shows under what treatment conditions it is expected that the model will be insufficient to describe experimental kinetics, since the model has been simplified in order to preserve the ability to work with its analytical solution. This analysis is grounds for pointing the future development of the model in the right direction and towards improvements that will need to be accomplished for further model generalization and validation.

4.3.2 Summary

The Results in Paper IV are presented in three main parts: The Z-index analysis; modelling the diffusion kinetics; and modelling the expression (or filtration-consolidation) kinetics. First, the paper gives the dependence of disintegration index Z on the pulse amplitude U, since electrical treatment as applied to tissue with varying intensity. The study includes this Z-index calculation

and analysis in order to be able to later correlate its dependence on field strength with the subsequent (post-treatment) mass transport. Since three different treatment protocols were used in pressing experiments, the Z-index was measured for apples for all three protocols as well.

In the second part, the experimental data on total solute concentration were fitted with simulated kinetics obtained using the dual-porosity model. Model parameters were optimized to give the best fit to experimental data according to the criterion function, which was the least-square-difference temporal integral. A comparison of extraction kinetics and the values obtained for the pore surface fraction (a parameter describing effects of electroporation to the cell membrane) confirms expectations according to the model and the theory of electroporation; in terms of applied voltage, and significantly higher induced transmembrane voltage due to size difference, the study finds a lower permeabilization threshold for an average cell in apple tissue as compared to sugar beet. There are also indications in favour of the assumption that the volume fraction of cells in apple tissue is altered by electroporation due to irreversible damage to cells.

The pressing experiments further elucidate the behaviour of electroporated sample tissues, but more importantly, some of the assumptions about tissue structure and electroporation effects on diffusion can be confirmed by the presented results, and possible interpretations for the difference in values of corresponding parameters in the pressing and diffusion case is extensively discussed and hypothesized about. The authors conclude the presentation of results with the results of pressing experiments done for various electrical treatment protocols. These kinetics were modelled with the dual-porosity model and the optimal values of parameters used to obtain the best fit were put into perspective and critically evaluated from the point of view of the theory of electroporation.

4.3.3 Conclusions

In the previous two papers (II and III), the authors set out to describe a new framework for studying mass transport in electroporated tissue—i.e. the dual-porosity model of solute diffusion and consolidation-filtration behaviour of electroporated tissue. In this paper, experiments on two model materials, sugar beet taproot and apple fruit tissue, were used to test the model performance and verify some of the basic model assumptions. It has been demonstrated that the model is capable of accurately modelling extraction kinetics obtained by diffusion as well as by pressing experiments. During model construction, one model parameter, the pore surface fraction, was identified as the most important parameter as a function of electroporation treatment parameters. In this paper, however, additional important factors were identified (most importantly changes in permeability and compressibility of tissue due to structural modifications) that reflect the complicated nature of electric field effects on texture and mass transport in electroporated tissue.

To develop the model further, there is a need to evaluate the influence of these additional factors, and to mathematically describe these effects, arriving at a more generalized model solution capable of predicting extraction kinetics based on treatment parameters and material characteristics. The authors are confident the model can already be successfully applied to evaluate electroporation treatment efficiency with respect to mass transport, that it can be used for optimization of treatment parameters with prediction of treatment results, and that its further development will help understand the phenomena related to mass transport and textural properties of electroporated biological material.

Innovative Food Science and Emerging Technologies 29 (2015) 41–54

Contents lists available at ScienceDirect

Innovative Food Science and Emerging Technologies

journal homepage: www.elsevier.com/locate/ifset

Dual-porosity model of mass transport in electroporated biological tissue: Simulations and experimental work for model validation

Samo Mahnič-Kalamiza [a,b,*], Damijan Miklavčič [b], Eugène Vorobiev [a]

[a] Centre de Recherches de Royallieu-BP 20529, University of Technology of Compiègne, 60205 Compiègne Cedex, France
[b] Faculty of Electrical Engineering, University of Ljubljana, Tržaška c. 25, SI-1000 Ljubljana, Slovenia

ARTICLE INFO

Article history:
Received 23 June 2014
Revised 22 September 2014
Accepted 23 September 2014
Available online 30 October 2014

Editor Proof Receive Date 30 October 2014

Keywords:
Electroporation
Pulsed electric fields
Mass transfer
Diffusion
Pressing
Mathematical modeling

ABSTRACT

Electroporation or pulsed electric field treatment is an important technique for facilitating mass transport in biological tissues with proven benefits for the food processing industry. One of the challenges in understanding its basic mechanisms and effects is mass transport processes in treated tissue. We recently presented a mathematical model called dual-porosity model to describe post-electroporation diffusion in biological tissue and filtration–consolidation behavior of electroporated tissue during pressing. In this work we bring the two analogues together and study the model's applicability and performance by comparing experimental and simulated kinetics. We use two kinds of plant tissue of dissimilar properties (sugar beet taproot and apple fruit), but employ the same methodology to evaluate the validity of basic assumptions. We show that the model describes experimental data and provides more insight into the mass transport processes during post-pulse extraction/pressing. We comment on treatment conditions that expose limitations and indicate possibilities for future development.

Industrial relevance: In order to study and optimize extraction processes following treatment of biological material with electroporation (pulsed electric fields), good knowledge on mass transport processes in electroporated tissue is of essential importance. Development, final form and application of a new mathematical model are presented that will aid in understanding of mass transport by solute diffusion and filtration–consolidation behavior of electroporated tissue under external pressure. It is foreseen that such a model could be used for predictive purposes and optimization of treatment parameters in industrial applications of electroporation, where *in silico* modeling can thus help find new or improved protocols to increase efficiency and efficacy in pulsed electric field applications.

1. Introduction

The terms electroporation, electropermeabilization, and pulsed electric field treatment, are commonly used to refer to the application of short, high-intensity electrical impulses to biological material and consequences that such electric pulses have on biological material (Kotnik, Kramar, Pucihar, Miklavcic, & Tarek, 2012; Raso & Heinz, 2010; Yarmush, Golberg, Serša, Kotnik, & Miklavčič, 2014). We prefer to and will use the term electroporation throughout the remainder of this article. In electroporation, the electric pulses of specific parameters are applied to the target tissue or cell suspension, the parameters depending on the intended goal of application. Often the objectives are to induce a transient increase in cell membrane permeability (Gehl, 2003; Haberl, Miklavcic, Sersa, Frey, & Rubinsky, 2013; Marty et al., 2006; Zorec, Préat, Miklavčič, & Pavšelj, 2013), or to permanently damage and ultimately destroy the cells (Goettel, Eing, Gusbeth, Straessner, & Frey, 2013; Golberg & Yarmush, 2013; Jiang, Qin, & Bischof, 2014; Morales-de la Pena, Elez-Martinez, & Martin-Belloso, 2011; Saulis, 2010). To achieve selective extraction of bio-compounds, complete destruction of the cells is an undesirable effect leading to impure solutions.

A closer look at the electroporation processes on the biochemical level reveals that treatment outcome and efficacy are largely governed by electrical and (related) chemical properties of the treated material, and mass transport that occurs during and after application of electric pulses (Kotnik et al., 2012; Li & Lin, 2011a; Li, Tan, Yu, & Lin, 2013b; Pucihar, Kotnik, Miklavcic, & Teissie, 2008; Sel et al., 2005). These properties and transport phenomena influence the development of the electropermeabilized state of the cell membrane during electroporation, and continue to be important in the post-pulsation period of pore shrinkage, resealing, cell lysis, etc. (Reigada, 2014; Sridhara & Joshi, 2014).

* Corresponding author at: Université de Technologie de Compiègne (UTC), Département de Génie des Procédés Industriels, Laboratoire Transformations Intégrées de la Matière Renouvelable, Centre de Recherches de Royallieu-BP 20529, 60205 Compiègne Cedex, France. Tel.: +33 6 52 17 30 92.
E-mail addresses: samo.mahnic@utc.fr, samo.mahnic@fe.uni-lj.si, samo.mahnic@gmail.com (S. Mahnič-Kalamiza).

http://dx.doi.org/10.1016/j.ifset.2014.09.011
1466-8564/

Mass transport is also of significance in light of the intended purpose of electroporation treatment application. If electroporation is applied to facilitate solute extraction by diffusion (increasing rate, yield, etc.) or to change the permeability of the cell membrane and overall tissue for improving juice expression or tissue dehydration, the mass transport processes (both of solutes and liquid) are of primary importance and should be the focus of study. Moreover, since much the same processes of transport in electroporated cells and tissues are of interest in other fields of electroporation applications, such as biomedicine—in e.g. electrochemotherapy (Cadossi, Ronchetti, & Cadossi, 2014; Miklavcic, Mali, Kos, Heller, & Sersa, 2014), gene transfection (Dean, 2013), trans- and intradermal drug delivery (Becker, 2012), etc.—the study of mass transport phenomena in electroporated biological material is a trans-domain research field. Within this expanded field incorporating biology, medicine, pharmacology, electrical engineering, process and food engineering, chemistry and chemical physics, as well as several other domains, there is an abundance of published theoretical and experimental approaches employed to identify and describe the basic mechanisms of electroporation. These developments and theoretical advances add pieces to the greater puzzle that is the theory of electroporation. Mass transport phenomena represent an important integral part of this work in progress. The significance of the trans-domain span in research on electroporation is in the analogies that appear throughout the various domains of electroporation applications that can complement to form a more complete and complex picture of the effects of short-duration, high-intensity electric fields on biological material. To illustrate with a particular example; if passive diffusion of solute through an electroporated membrane is the predominant mechanism of mass transport in electroporated tissue in the post-pulse period (Pucihar et al., 2008), a study of the process is of greatest importance to biomedicine in e.g. electrochemotherapy (introduction of molecules of a chemotherapeutic drug into tumor cells—see sources on electrochemotherapy cited above), and for food processing industry in e.g. industrial extraction of valuable compounds from their primary biological sources (extraction of carbohydrates, polyphenols, lipids, etc.) (see e.g. Boussetta, Soichi, Lanoiselle, & Vorobiev, 2014; Donsi, Ferrari, & Pataro, 2010; Grimi et al., 2014; Liu, Lebovka, & Vorobiev, 2013).To give another example; liquid pressure gradients are present in many of the tissues which are of interest in electroporation. Plant cells for instance maintain their shape and plant tissue its turgidity due to turgor pressure, resulting from a solute concentration imbalance across the cell membrane that causes an osmotic pressure build-up (Campbell et al., 2008; Pereira, Galindo, Vicente, & Dejmek, 2009). In tumors, poorly formed vascular system and lacking lymphatic drainage system result in local gradients in interstitial fluid pressure, leading to a higher intratumoral pressure as compared to liquid pressure in the surrounding healthy tissue (Ariffin, Forde, Jahangeer, Soden, & Hinchion, 2014; Liu, Brown, Ewing, & Schlesinger, 2011; Pusenjak & Miklavcic, 2000; Simonsen, Gaustad, Leinaas, & Rofstad, 2012). Rendering the cell membrane semipermeable in presence of pressure gradients will, in theory, result in filtration flows in the direction opposite to that of the pressure gradient both during and after electroporation. Pressure gradients exist in untreated tissue (e.g. osmotic pressure, interstitial fluid pressure) that may be of significant importance already during application of electric pulses, and after electroporation treatment, a pressure gradient is established by the externally-applied pressure during the pressing stage. This is yet another mechanism of solid–liquid mass transport of importance in relation to electroporation in two disparate domains of electroporation application.If the same approach, from the theoretical point of view, can be used to study two very disparate goals of electroporation application, one should need to develop mathematical descriptions of the process physics (i.e. *models*) once only for the process and then apply them, with necessary modifications, to each particular application. Following this paradigm, we recently published two works on the development of a mathematical model we refer to as the dual-porosity model. The first account presents the model as describing extraction or introduction of solute by diffusion out of or into electroporated biological tissue (Mahnič-Kalamiza, Miklavčič, & Vorobiev, 2014). We used sucrose extraction from sugar beets for the model study, but also suggested two possible applications of the model for introduction of compounds into animal or plant cells. Furthermore, the analogy between diffusion and liquid flow laws allows for a rapid adaptation of the model for the problem of filtration–consolidation behavior of electroporated tissue, and is the subject of the second account (Mahnič-Kalamiza & Vorobiev, 2014). In the present work, we bring the two analogues together and examine the model validity and its performance by comparing experimental data with diffusion/expression kinetics, which result from simulations done using the model proposed. We use two kinds of vegetable tissue as model material with markedly different properties (sugar beet taproot and apple fruit), but employ the same methodology to determine if the postulates and simplifications during model development are justifiable, i.e. can results of model simulations be reconciled with those obtained via experiments. We also show under what treatment conditions it is expected the model will be insufficient to describe experimental kinetics, since the model has been simplified in order to preserve the ability to work with its analytical solution. This analysis enables us to indicate how the model needs to be expanded and to point towards the possible improvements that will need to be accomplished during future development.

2. Materials and methods

2.1. Disintegration index Z

The disintegration index Z is a conductivity-based measure that can be used to estimate the degree of tissue damage during or after treatment—in our case electrical—and is defined as $Z = (\sigma - \sigma_i)/(\sigma_d - \sigma_i)$, where σ is the material conductivity (during or at the end of treatment protocol application), σ_i is the conductivity of the intact sample tissue (prior to treatment), and σ_d corresponds to the conductivity of a tissue sample considered to be destroyed by the treatment, i.e. fully treated. The value of Z increases during electrical treatment, beginning at 0 (intact tissue) and approaches 1 (completely permeabilized cells—i.e. maximally damaged tissue) as the conductivity of the treated sample increases. Various methods can be used to determine σ_d; e.g. freezing–thawing or high-intensity long-duration electroporation have been proposed (Vorobiev & Lebovka, 2008). For the purposes of the present study, an average σ_d was obtained by averaging the measured conductivity of several tissue samples, each of which was treated with 50 trains of 10 pulses of amplitude 400 V (per 5 mm electrode distance), pulse width 100 μs and 5 s pause in between the trains to allow for cooling of the sample and thus avoiding thermal damage to the tissue.

2.2. Diffusion experiments

Cylindrical samples (disks) of sugar beet taproot and apple fruit tissue (skin removed) were obtained from 5 mm thick sugar beet taproot or apple fruit slices.[1] All samples measured 25 mm in diameter. Each sample was subjected to electroporation treatment by applying 150, 200, 300, or 400 V between two parallel plate stainless-steel electrodes at 5 mm inter-electrode distance (sample thickness). Our intent was to subject the treated tissue to field strengths of 300, 400, 600, and 800 V/cm, respectively. Note that this would hold if the tissue were electrically homogeneous material, and only in the central area away from electrode edges. Rectangular pulses of alternating polarity (see Fig. 2) of 100 μs duration each, and pulse repetition frequency of 1 kHz, were delivered within each train of eight pulses. Two such trains

[1] In the remainder of the paper, for brevity, we refer to «apple fruit tissue» and «sugar beet taproot tissue» as «apple tissue» and «sugar beet tissue», respectively.

were delivered with a pause of 1 s between the two trains. This protocol will here on be referred to as Protocol A (see Fig. 2a). The pulses were provided by a custom-built pulse generator with peak output current of 38 A at the maximum attainable voltage of 400 V, assembled by Service Electronique UTC, Compiegne, France.

The samples were then removed from the treatment chamber, after which the surfaces of the sample disks were put into contact with absorbent paper and thus the surfaces dried, in order to remove the sugary liquid. This liquid is present due to cutting and possibly due to electro-osmotic or pressure-change effects that occur during the electroporation treatment. Note that had the surfaces not been dried, the juice on the surface would cause an immediate increase in the sugar concentration in the solution at the beginning of the experiment, resulting in kinetics also known as the "washing stage" of the process (El Belghiti & Vorobiev, 2004). This effect is not captured by the model, neither is it easy to subtract it from the kinetics due to varying juice sugar concentration and amount of this surface liquid that varies per sample. The surface-dried samples were placed into a flask with a magnetic stirrer. The sample-containing liquid was constantly agitated and sampled at regular intervals; total soluble solids (i.e. predominantly sugar) concentration was analyzed with a digital refractometer. The liquid-to-solid ratio was 2:1 in all experiments.

The quantity which is measured by the digital refractometer is sugar (more precisely total soluble solids) concentration in liquid with unit degrees Brix (°Bx), where 1 °Bx is 1 g of sucrose in 100 g of solution and represents the concentration of the solution as percentage by weight (% w/w). We know the initial sugar content of the aqueous solution $^{\circ}\mathrm{Bx}_0$ (normally equal to zero), we measure and record (during experiment) the current sugar content $^{\circ}\mathrm{Bx}(t)$—i.e. the extraction kinetics, and the final sugar concentration $^{\circ}\mathrm{Bx}_d$ can be determined separately. Theoretically, $^{\circ}\mathrm{Bx}_d$ is the total solute concentration in solution in ideal conditions of completely permeabilized tissue and after infinite time of diffusion. In practice, it is easily determined by measuring the solute concentration in pure fruit/root juice, and scaling the measurement according to the extracting liquid/juice mass ratio (also known as the solid–liquid ratio). Since initial and maximum concentrations are known, we can define and calculate *normalized degree Brix* at time t—i.e. $B(t)$, as

$$B(t) = \frac{^{\circ}\mathrm{Bx}(t) - {}^{\circ}\mathrm{Bx}_0}{^{\circ}\mathrm{Bx}_d - {}^{\circ}\mathrm{Bx}_0}. \quad (1)$$

We use Normalized Brix throughout the remainder of this paper as a measure for the amount of solute (e.g. sugar) that has diffused out of the tissue sample in time t. It takes the values from the interval $0 \le B(t) \le 1$, and is dimensionless. It can be calculated from measurements with the refractometer, according to Eq. (1). The schematic illustration of the diffusion experiment is given by Fig. 1.

2.3. Pressing experiments

We used cylindrical samples of sugar beet and apple tissue, 25 mm in diameter and of 5 mm thickness. The samples were placed between two parallel plate stainless-steel electrodes, and electroporation pulses were applied using three different protocols (see Fig. 2). Protocol A: The voltage was varied, using 150 V, 200 V, 300 V, 350 V, or 400 V applied to the electrodes. Pulses of alternating polarity were delivered in two trains of eight pulses per train, with repetition frequency of 1 kHz within the train, 1 s pause between the two trains, and 100 μs pulse duration. Protocol B: The voltage was again varied as in Protocol A, however only two unipolar pulses were delivered of 800 μs each, and with a time delay of 1 s in between the two pulses. Protocol C: The voltage was varied as in Protocol A and Protocol B, and eight pulses of singular polarity were delivered, 100 μs in duration each second (i.e. at pulse repetition frequency of 1 Hz). This protocol is also known as one of the *standard protocols for electrochemotherapy* (Marty et al., 2006). Note that the total treatment time t_t (product of pulse duration t_p, number of pulses n_p and number of trains n_t) as calculated from the pulsing protocol was the same for Protocols A and B ($t_t = 1.6$ ms), and was 50% lower in case of Protocol C ($t_t = 0.8$ ms) as compared to the two other protocols. The delivered energy in our setup as calculated from the measured current falls between 6 J/kg (minimum attained for sugar beet, Protocol C, 150 V) and 250 J/kg (maximum attained for apples, Protocol B, 400 V). In terms of delivered energy and treatment time, these treatment protocols are normally not encountered in food processing, where energies on the order of several kJ/kg are commonly delivered to target tissues (Donsi et al., 2010; Turk, Vorobiev, & Baron, 2012). The maximum total delivered energy on the order of 0.25 kJ/kg results—in worst case, i.e. not accounting for any heat dissipation via electrodes or treatment chamber surfaces—in a negligible increase in sample temperature by less than 0.1 K. This estimate is based on the thermal capacity of apple tissue, found in Mykhailyk and Lebovka

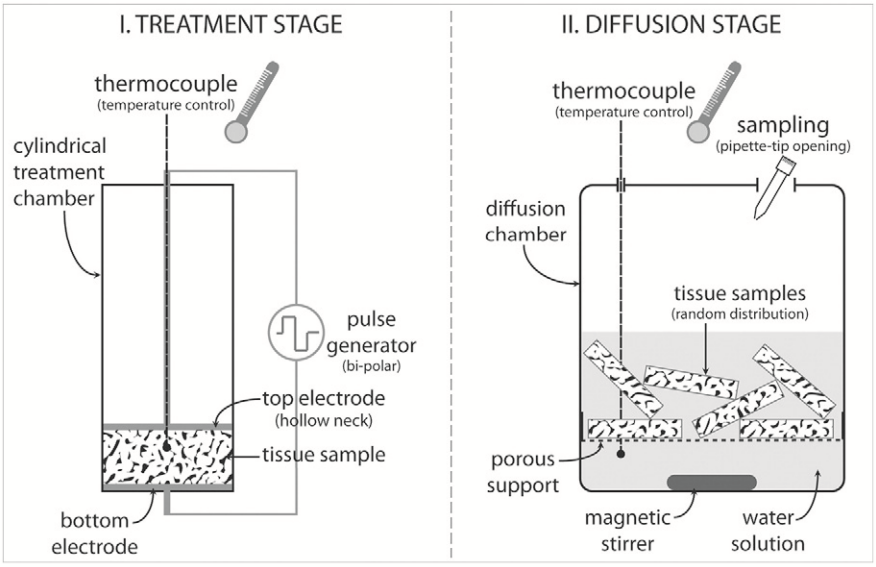

Fig. 1. Schematic representation of the diffusion experiment setup—electroporation treatment (left) and subsequent diffusion (right).

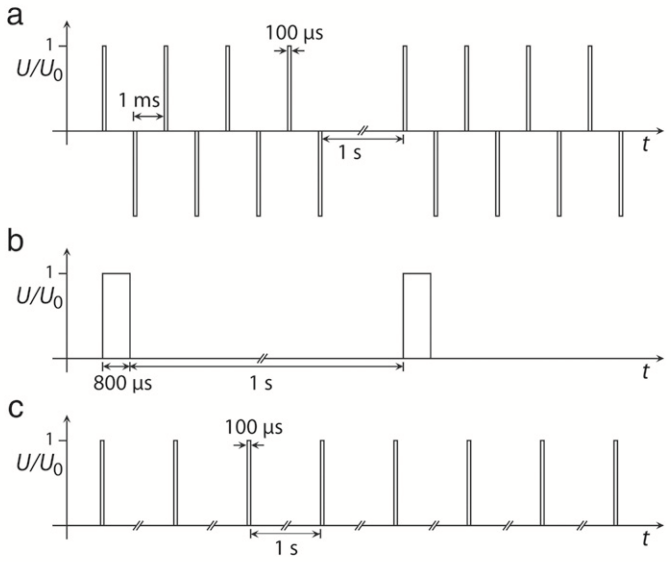

Fig. 2. Schematic representation of the three pulse delivery protocols: Protocol A (a), Protocol B (b), and Protocol C (c). Pulse widths and distances are to scale, except where denoted otherwise—the '//' sign indicates a break in the axis (i.e. there is a 1 s long pause between every two pulses in between which the axis brake is indicated).

(2014), and known maximum energy that was delivered. We further discuss the reasons for and implications of our particular choice of low-intensity, "gentler" treatment protocols in Section 3.

In all cases, regardless of the electroporation protocol, the electric treatment was followed by pressing. Electroporated samples were immediately placed into a specially fabricated treatment chamber and subjected to a load of 150 N—about 580 kPa (apple), or 300 N—about 290 kPa (sugar beet), using a texturometer. The piston displacement was recorded by the texturometer under constant pressure (force) application during 1 h.

Piston displacement equals the sample deformation along the axis of the pressure application. At the end of Section 2.5 on the dual-porosity model for filtration–consolidation, we show how the simulated pressure distribution in sample in time can be related with the measured deformation. This is necessary in order to enable comparison of experimental and model results.

2.4. The dual-porosity model of solute diffusion

The dual-porosity approach for studying diffusion of solute in electroporated tissue is presented in detail in Mahnič-Kalamiza et al. (2014). Here, we give the experimental setup geometry (Fig. 3), the partial differential equation system (Eqs. (2)–(3)) that represents the fundamental model equations for diffusion according to the dual-porosity model, the appropriate boundary and initial conditions (Eq. (4)–(9)) and the final solution (Eqs. (10)–(14)) of the system. All but Fig. 3 are reproduced from Mahnič-Kalamiza et al. (2014).

The fundamental model equations for the extracellular and the intracellular phase (space) are, respectively,

$$\frac{\partial c_e(z,t)}{\partial t} - D_{s,e}\frac{\partial^2 c_e(z,t)}{\partial z^2} - \frac{1-\varepsilon}{\varepsilon}k\cdot[c_i(z,t)-c_e(z,t)] = 0 \tag{2}$$

$$\frac{\partial c_i(z,t)}{\partial t} + k\cdot[c_i(z,t)-c_e(z,t)] = 0 \tag{3}$$

where c_e and c_i are extracellular and intracellular solute concentrations, respectively, $D_{s,e}$ is the intrinsic diffusion coefficient of solute species s in extracellular space, ε is the tissue porosity (cell-to-extracellular volume ratio, i.e. $\varepsilon = 1 - F$, where F is cell volumetric fraction), and k is the transmembrane flow coefficient defined by Eq. (15).

The boundary conditions (BC) are determined, in summary, as follows; the left BC requires the extracellular concentration of solute be 0 for all times, since we are working under the supposition of infinite dilution outside the tissue sample,

$$c_e(t)|_{z=h/2} = 0. \tag{4}$$

The intracellular concentration at that boundary is seemingly undetermined, but can be expressed by combining Eq. (3) with the left BC for extracellular space (Eq. (4)), solving the resulting ordinary differential equation yields

$$c_i(t)|_{z=h/2} = c_{i0}e^{-kt}. \tag{5}$$

The right boundary is the plane of symmetry—the central plane of the tissue sample perpendicular to the principal axis of diffusion (see Fig. 3). At this plane of symmetry, Fick's diffusive flux must equal zero

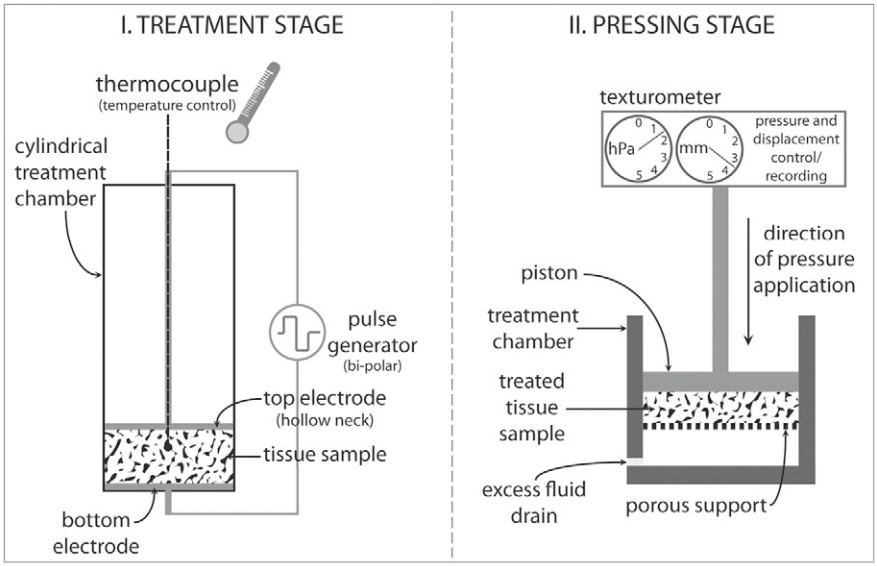

Fig. 3. Schematic representation of the pressing experiment setup—electroporation treatment (left) and subsequent pressing (right).

for both the intra- and the extracellular phase, as there are no solute sources or sinks (absence of chemical reactions). We have

$$\left.\frac{\partial c_e(t)}{\partial z}\right|_{z=0} = 0 \tag{6}$$

$$\left.\frac{\partial c_i(t)}{\partial z}\right|_{z=0} = 0. \tag{7}$$

For the initial conditions (IC) we suppose a homogeneous initial distribution of solute concentrations. The initial concentrations need not be equal in the extracellular and intracellular space, which is a valid assumption for intact or poorly permeabilized tissue where solute remains intracellular. We define constants c_{e0} and c_{i0} as

$$c_e(z,0) = c_{e0} \tag{8}$$

$$c_i(z,0) = c_{i0}. \tag{9}$$

The solution of the system of partial differential equations (Eqs. (2)–(3)) for BC and IC (Eqs. (4)–(9)) is

$$c_e(z,t) - \frac{4c_{i0}}{\pi}\sum_{n=0}^{\infty}\frac{(-1)^n}{2n+1}\cos(\lambda_n z)\left(C_{n,1}e^{\gamma_{n,1}t}\left(\frac{\gamma_{n,1}}{k}+1\right)+C_{n,2}e^{\gamma_{n,2}t}\left(\frac{\gamma_{n,2}}{k}+1\right)\right), \tag{10}$$

$$c_i(z,t) = \frac{4c_{i0}}{\pi}\sum_{n=0}^{\infty}\frac{(-1)^n}{2n+1}\cos(\lambda_n z)\left(C_{n,1}e^{\gamma_{n,1}t}+C_{n,2}e^{\gamma_{n,2}t}-e^{-kt}\right)+c_{i0}e^{-kt}, \tag{11}$$

where

$$C_{n,1} = \frac{\left(\frac{c_{e0}}{c_{i0}}-1\right)k-\gamma_{n,2}}{\gamma_{n,1}-\gamma_{n,2}}, \tag{12}$$

$$C_{n,2} = \frac{\left(1-\frac{c_{e0}}{c_{i0}}\right)k+\gamma_{n,1}}{\gamma_{n,1}-\gamma_{n,2}}, \tag{13}$$

and

$$\gamma_{n_{1,2}} = \frac{-\left((\delta+1)k+{\lambda_n}^2 D_{s,e}\right)\pm\sqrt{\left((\delta+1)k+{\lambda_n}^2 D_{s,e}\right)^2-4k{\lambda_n}^2 D_{s,e}}}{2}, \tag{14}$$

where for the sake of algebra we have set $\delta = (1-\varepsilon)/\varepsilon$. The eigenvalues λ_n equal $\lambda_n = (2n+1)\cdot\pi/h$.

The transmembrane flow coefficient (also termed mass transfer coefficient) k is the critical constituent of the model capturing the electroporation effects on the cell membrane. If cells can be modeled as perfect spheres of radius R and membrane thickness d_m, $D_{s,0}$ is the solute diffusion rate in water at a given temperature, y_s is the pore diffusion hindrance coefficient and f_p is the stable pore surface fraction ($f_p = N_p \cdot A_p/A_0$, where N_p is the number of pores per cell, A_p is the average single pore area and A_0 is the cell area equaling $4\pi R^2$), we can determine k as

$$k = \frac{3D_{s,0}y_s f_p}{d_m R} \tag{15}$$

The electroporation treatment affects the pore surface fraction f_p as well as the hindrance coefficient y_s, assuming the radius of an average stable pore is dependent on treatment parameters. For more details on the hindrance coefficient and k, see Mahnič-Kalamiza et al. (2014).

2.5. The dual-porosity model of filtration–consolidation under external pressure

There is an obvious analogy from the mathematics and physics point of view between the Fick's law of diffusion and Darcy's law of liquid flow in porous media. The dual-porosity model as given by Eqs. (2)–(3) can therefore also be written to describe filtration–consolidation behavior of tissue under applied pressure, the model formulation remaining much the same, except for some replacements, omissions and added details. Namely, the diffusion rate $D_{s,e}$ is replaced by the hydraulic permeability k_e of the tissue over viscosity μ, i.e. k_e/μ, and the mass transport coefficient k by a similar proportionality coefficient α over viscosity, i.e. α/μ. We account for the initial tissue porosity ε already by permeability k_e and compressibility modulus $G_{\varepsilon,e}$ that are not intrinsic, but rather quantities volume-averaged throughout the whole sample (for explanation see Section 3.2.1.1 in De Monte, Pontrelli, & Becker, 2013), and thus we drop the factor $(1-\varepsilon)/\varepsilon$. And finally, the concentration gradients are replaced, as the driving forces of the transport processes, by the liquid pressure gradients, and thus concentrations c_e and c_i are replaced by liquid pressures p_e and p_i. We have, as analogues to the diffusion fundamental model equations (Eqs. (2)–(3)), the following equations

$$\frac{1}{G_{\varepsilon,e}}\frac{\partial p_e}{\partial t} - \frac{\partial}{\partial z}\left(\frac{k_e}{\mu}\frac{\partial p_e}{\partial z}\right) - \frac{\alpha}{\mu}(p_i - p_e) = 0 \tag{16}$$

$$\frac{1}{G_{\varepsilon,i}}\frac{\partial p_i}{\partial t} + \frac{\alpha}{\mu}(p_i - p_e) = 0. \tag{17}$$

These equations are, as in the diffusion problem, derived from the law of mass conservation. However, as opposed to solute concentration, which is both the measured/observed quantity and (via its gradient) the originating force for the diffusive solute flow, the liquid pressure though a driving force is not itself a subject of the mass conservation law. It has to be related to the conserved density and, consequently, the porosity of the respective phases by the *compressibility moduli*. More details on this can be found in Mahnič-Kalamiza and Vorobiev (2014). Compressibility modulus or its inverse, the bulk modulus, is traditionally defined as a relative change in volume (or void ratio) in response to a given pressure change. If void ratio e denotes the ratio between the void (liquid) and solid phase within the intra- and extracellular space, compressibility moduli can be determined from

$$\frac{\partial e_e}{\partial t} = -\frac{\partial p_e}{\partial t}\cdot\frac{\partial e_e}{\partial p_{e,S}} = \frac{1}{G_e}\frac{\partial p_e}{\partial t} \tag{18}$$

$$\frac{\partial e_i}{\partial t} = -\frac{\partial p_i}{\partial t}\cdot\frac{\partial e_i}{\partial p_{i,S}} = \frac{1}{G_i}\frac{\partial p_i}{\partial t}. \tag{19}$$

The bulk moduli G_e and G_i relate the change in void ratio with the loss of liquid pressure. In experiments we measure piston displacement and thus tissue sample deformation, and this measured deformation is more closely related to porosity (void to total volume ratio) than to the void ratio itself. For this reason, we have redefined the bulk moduli via averaged porosity of each space, so that

$$\overline{G}_{\varepsilon,e} = G_e(1+\overline{e}_e)^2 \tag{20}$$

$$\overline{G}_{\varepsilon,i} = G_i(1+\overline{e}_i)^2. \tag{21}$$

Note that in all but Eqs. (20)–(21), we omit the notation for averaged values. This definition makes initial estimates for the moduli readily obtainable from total- or end-deformation points reached in experiments. However, there is a trade-off. Averaging the void ratio, a function of both space and time, and assuming it constant, narrows down the generality of the model. It is now valid for a particular segment of the parameter space that demands the piston displacement be small as compared to the thickness of the entire sample. This condition is met if the tissue is not severely damaged by the applied treatment, something we have to keep in mind when interpreting model results. A more general approach omitting these simplifications is highly demanding in mathematical terms and unwieldy for analytical treatment (Petryk & Vorobiev, 2013).

To solve the system of Eqs. (16)–(17), we need appropriate boundary and initial conditions. The initial conditions can be rewritten from Eqs. (8)–(9) by simple replacement of concentration with liquid pressure, obtaining

$$p_e(z,0) = p_{e0} \tag{22}$$

$$p_i(z,0) = p_{i0}. \tag{23}$$

On the other hand, the boundary conditions are somewhat different. There is no central plane of symmetry in the mid-section of the tissue sample (see Fig. 4). Instead, we have a no-flux boundary at the sample—piston contact surface

$$\left.\frac{\partial p_e}{\partial z}\right|_{z=h} = \left.\frac{\partial p_i}{\partial z}\right|_{z=h} = 0 \tag{24}$$

and free flow of liquid at the sample–porous support contact surface

$$p_e|_{z=0} = 0 \tag{25}$$

while the intracellular liquid pressure BC calculation at this surface follows the same logic as with the diffusion problem, giving

$$p_i|_{z=0} = p_{i0}e^{-\frac{\alpha G_{\varepsilon,i}t}{\mu}}. \tag{26}$$

The solution of Eqs. (16)–(17) under IC and BC Eqs. (22)–(26) is analogous to the one for the diffusion problem, with the sole exceptions

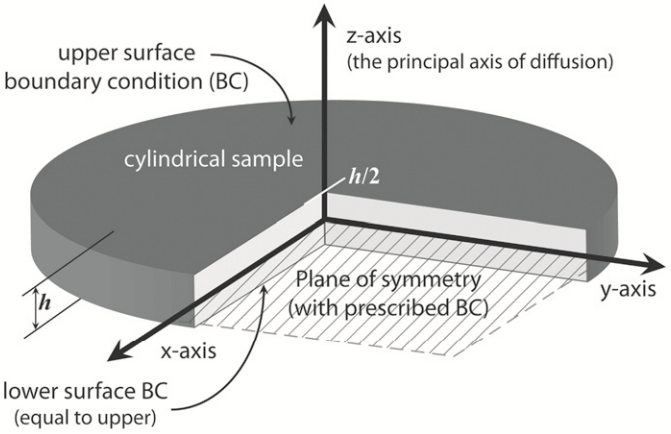

Fig. 4. Schematic representation of the tissue sample as used in the diffusion experiment—the model geometry, coordinate system and boundary conditions (BC).

of sine replacing the cosine in the Fourier series and updating the eigenvalues, due to different boundary conditions (Fig. 5)

$$p_e(z,t) = \frac{4p_{i0}}{\pi}\sum_{n=0}^{\infty}\frac{1}{2n+1}\left(\left(\gamma_{n,1}\tau+1\right)C_1e^{\gamma_{n,1}t} + \left(\gamma_{n,2}\tau+1\right)C_2e^{\gamma_{n,2}t}\right)\sin\left(\frac{(2n+1)\pi}{2h}z\right) \tag{27}$$

$$p_i(z,t) = \frac{4p_{i0}}{\pi}\sum_{n=0}^{\infty}\frac{1}{2n+1}\left(C_1e^{\gamma_{n,1}t} + C_2e^{\gamma_{n,2}t} - e^{-\tau^{-1}t}\right)\sin\left(\frac{(2n+1)\pi}{2h}z\right) + p_{i0}e^{-\tau^{-1}t} \tag{28}$$

where

$$C_1 = \frac{\left(\frac{p_{e0}}{p_{i0}}-1\right)\tau^{-1}-\gamma_{n,2}}{\gamma_{n,1}-\gamma_{n,2}} \tag{22}$$

$$C_2 = \frac{\left(1-\frac{p_{e0}}{p_{i0}}\right)\tau^{-1}+\gamma_{n,1}}{\gamma_{n,1}-\gamma_{n,2}} \tag{23}$$

and

$$\gamma_{n_{1,2}} = \frac{-\left(\tau^{-1}\delta+\lambda_n{}^2\nu\right) \pm \sqrt{\left(\tau^{-1}\delta+\lambda_n{}^2\nu\right)^2-4\lambda_n{}^2\nu\tau^{-1}}}{2}. \tag{24}$$

For the sake of algebra, we have set

$$\nu = \frac{k_eG_{\varepsilon,e}}{\mu};\ \tau^{-1} = \frac{\alpha G_{\varepsilon,i}}{\mu};\ \delta = \left(1+\frac{G_{\varepsilon,e}}{G_{\varepsilon,i}}\right) \tag{25}$$

and the eigenvalues λ_n equal $\lambda_n = (2n+1)\cdot\pi/2h$.

Once liquid pressures are known, we can use Eqs. (18)–(21) to calculate the sample deformation. If we use the dimensionless deformation $s_\varepsilon(t)$ normalized to the initial sample height, we have

$$s_\varepsilon(t) = \frac{S_\varepsilon(t)}{h} = \frac{1}{G_{\varepsilon,e}}\int_0^1\int_{p_e(z,t)}^{p_e(z,0)}dp_e\cdot dz + \frac{1}{G_{\varepsilon,i}}\int_0^1\int_{p_i(z,t)}^{p_i(z,0)}dp_i\cdot dz. \tag{26}$$

The remaining parameter in need of some explanation is the dimensionless factor α, which accounts for the influence of the electroporation treatment on hydraulic permeability of the cell membrane. According to the theory presented in Mahnič-Kalamiza and Vorobiev (2014), for a spherical cell of radius R, with a stable pore surface fraction f_p consisting of N_p pores of an average radius r_p, it can be written as

$$\alpha = \frac{9f_pr_p^2}{8R^2} \tag{27}$$

where $k_p = r_p^2/8$ is the hydraulic permeability of a single pore.

3. Results and discussion

In this section we present experimental results obtained as described in Sections 2.1–2.3 of the Materials and Methods, the results of model simulations and data fitting, and a discussion on model-experiment correspondence and significance of the necessary alterations in parameter values.

First, we present the dependence of disintegration index Z on the pulse amplitude U (Fig. 6). The bars give standard deviation. Note that the voltage was applied to the electrodes 5 mm apart. Under ideal conditions (homogeneous material, sufficient distance from electrode

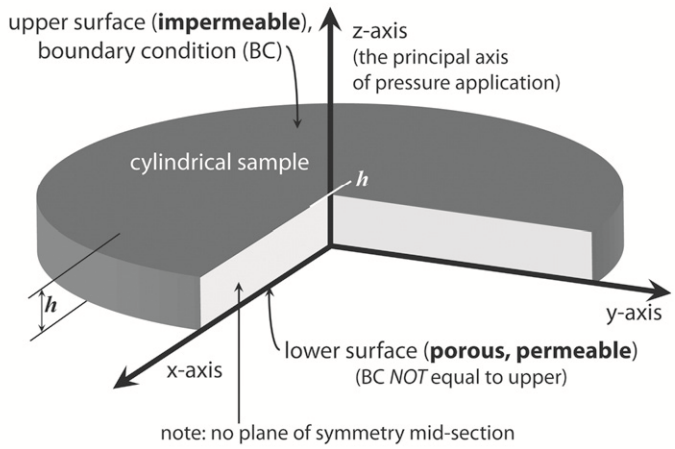

Fig. 5. Schematic representation of the tissue sample as used in the pressing experiment—the model geometry, coordinate system and boundary conditions (BC).

edges), the applied voltage would result in exposure of tissue to a homogeneous electric field of strength $E = U/d$, where U is the voltage applied and d the electrode distance ($d = 5$ mm for all samples in this study). For clarity of presentation, the insert in Fig. 6 gives the dependence for sugar beet tissue only, since the Z response for sugar beet is about an order of a magnitude lower as compared to apple.

We measured Z in order to correlate its dependence on field strength with the subsequent (post-treatment) mass transport. Since we used three different treatment protocols in pressing experiments, we measured Z for apples for all three protocols as well. The conductivity of completely damaged tissue σ_d was determined according to the method described in Section 2.1, and was equal to 20 mS for sugar beet and 10 mS for apple tissue.

The relatively low values of Z can be attributed to the particular treatment protocols used. We chose short treatment times and low voltages that should result in not only irreversible damage to the tissue, but also a significant fraction of reversibly electroporated cells. This is necessary in order to demonstrate the use of the dual-porosity model. If we would have permanently and completely damaged the tissue by irreversible electroporation, we would not have been able to show the influence of the porosity of the electroporated transport-hindering

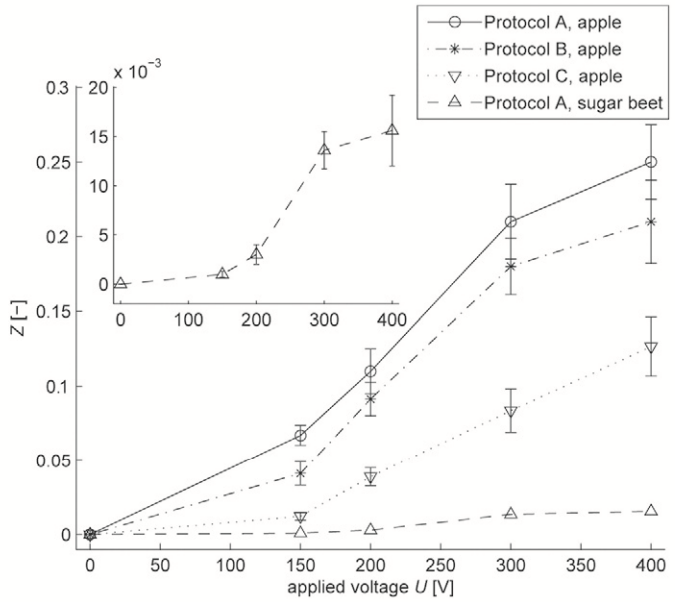

Fig. 6. Disintegration index Z as a function of voltage applied to the electrodes and treatment protocol (the latter for apples only).

membrane. The kinetics of extraction from tissue that has been electroporated to a high degree ($Z \approx 1$) can satisfactorily be represented using a much simpler model of extraction from homogeneous material (Lebovka, Shynkaryk, El-Belghiti, Benjelloun, & Vorobiev, 2007). Treatment protocols used to attain high Z values usually entail the use of hundreds of trains of several pulses or several trains of hundreds of pulses, totaling in treatment times of around 100 ms (Lebovka et al., 2007). In our experiments, the total treatment time never exceeded 1.6 ms.

Use of low-intensity electroporation of biological tissues is not without possible applications in the processing industry. It may open up new possibilities in selective extraction of intracellular compounds, further increasing the purity of juice or extract (Grimi, Praporscic, Lebovka, & Vorobiev, 2007). Or, as in the case of tissue impregnation for e.g. cryopreservation (Shayanfar, Chauhan, Toepfl, & Heinz, 2013), low permanent damage to cells still facilitating molecule uptake (reversible electroporation) is preferred over irreversible damage, as one of the objectives is to preserve the tissue textural properties.

3.1. Diffusion experiments

Fig. 7 gives extraction kinetics obtained in diffusion experiments as described in Materials and Methods (Section 2.2). Experimental data on total solute concentration were fitted with simulated kinetics obtained using the dual-porosity model. Model parameters were optimized to give the best fit to experimental data according to the criterion function, which was the least-square-difference temporal integral. Parameter values are listed in the Appendix, Table A.1, and pore fraction coefficient f_p is additionally given (for convenience) in the legend entries (Fig. 7).

First thing to note comparing Fig. 7a to b, is the comparatively higher yield of soluble solids (predominantly sucrose in sugar beet; and a mixture of sucrose, fructose, and glucose in apple—see e.g. Fuleki et al., 1994) at the end of the 2-h experiment/simulation. In 2 h and given the same applied voltage, more than twice the fractional amount of total solutes detected by the refractometer is extracted from apples as compared to sugar beet. We present two plausible explanations for this difference in final yield: *i*) that cells of apple tissue were permeabilized to a significantly higher degree when same voltage was applied to the electrodes; and/or *ii*) that extracellular space in apples is far more permeable to sugar molecules than in sugar beets. Neglecting the effects of possible differences in membrane composition and electrochemical properties of the liquid medium between the two materials, we suggest three other factors to account for this difference in yield: *i*) larger cells in apple tissue (50 μm as opposed to 200 μm in diameter for sugar beets and apples, respectively; Buttersack & Basler, 1991; Harker et al., 2010) result in a higher induced transmembrane voltage, causing more intense permeabilization, which is achieved at lower applied voltage; *ii*) apple tissue is not as compact as sugar beet, the amount of extracellular space is comparatively larger in apples than in sugar beets, leading to a higher rate of diffusion in the extracellular space—note that we suppose the extracellular air is locally replaced by intracellular liquid released from cells at the onset of electroporation or shortly thereafter; and *iii*) the high induced transmembrane voltage on large apple cellular membranes possibly results in irreversible damage to the membranes, thus increasing the intra-to-extracellular space ratio (effectively lowering the cell volume fraction F).

A comparison of extraction kinetics in Fig. 7 and the values of f_p (see Appendix, Table A.2), confirms expectations according to the model and the theory of electroporation; in terms of applied voltage, and significantly higher induced transmembrane voltage due to size difference, we find a lower permeabilization threshold for an average cell in apple tissue as compared to sugar beet. If an average sugar beet cell is much smaller than an average cell in apple tissue, electroporation occurs at correspondingly higher electric field strength, requiring higher applied voltage for a comparable effect. The pore surface fraction (f_p) is on the same order of magnitude at 150 V in apples ($f_p = 0.8 \times 10^{-6}$) as that in sugar beet, but at 300 V ($f_p = 0.9 \times 10^{-6}$). This also indicates that

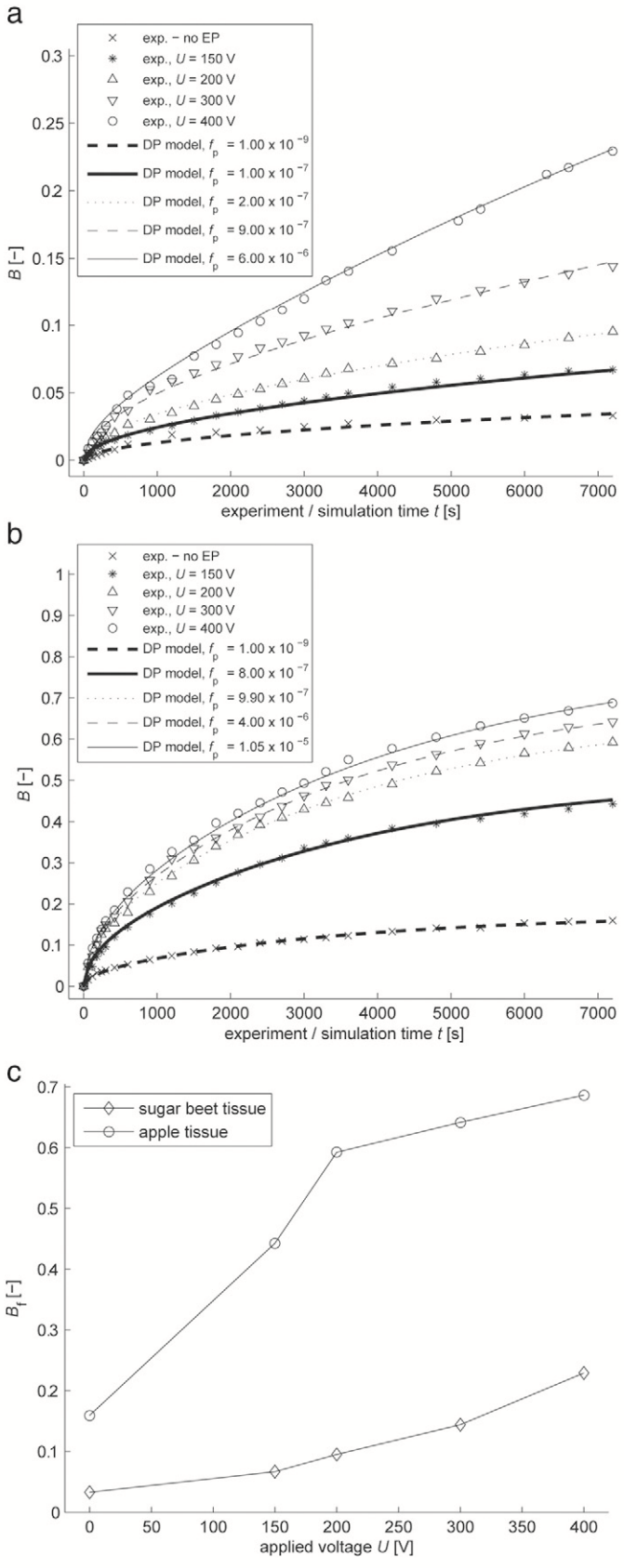

Fig. 7. Results of diffusion experiments (Protocol A) and model simulations of extraction kinetics, for sugar beet (a) and apple (b) tissue. Plot (c) gives the dependence of B at the end of the experiment (i.e. B_f) on voltage applied to the electrodes.

we are above the threshold of irreversible electroporation for a large range of cell sizes in apple tissue for voltages above about 200 V, which is reflected in practically insignificant differences in final yield of solutes from apples at 200, 300, and 400 V applied on electrodes (see Fig. 7c).

There are also indications in favor of our assumption that the volume fraction of cells in apple tissue is altered by electroporation due to irreversible damage to cells. We observe the behavior of one of the model parameters (namely F), which needs to vary in order for the simulation to be able to fit the experimental data. Not supposing serious alterations in apple tissue composition (for instance, a decrease in cell volume fraction from initial value of 0.75 for intact apple tissue to 0.265 at 400 V), the model cannot possibly describe the behavior observed in diffusion experiments (the measured yield at the end of the experiment is much too high in comparison to model results, for any value of f_p). This difference cannot be accounted for merely by assuming a higher extracellular diffusion rate (via a strong influence of convective flow for instance), as this would result in simulated extraction kinetics incompatible with experimental data. This reasoning is supported by yet another observation in diffusion kinetics; the kinetics after the first 30 min of experiment exhibits an almost linear behavior in sugar beet, whereas in apples a strong exponential nature of the process is clearly discernible. According to the theory of the dual-porosity model, the behavior as exhibited by apple tissue is expected of a homogeneous material. The lower the volume fraction of cells F, and the higher the fraction of pores on electroporated cells f_p, the more tissue behaves as homogeneous material (i.e. of singular porosity). We can conclude that irreversible electroporation is, from the dual-porosity model point of view, altering tissue composition by rendering cells or domains of cells in tissue into extracellular space, effectively lowering the cell volume fraction in tissue and increasing its bulk porosity.

To conclude the analysis of diffusion experiments, we compare the $Z(U)$ dependence (Fig. 6) with extraction kinetics (Fig. 7a,b). The value of disintegration index Z at 400 V is an order of magnitude lower for sugar beet as compared to apple. However, the resulting extraction yield after 2 h of extraction does not reflect such significant difference. Also, Z measured on apples seems to have an almost linear dependence on applied voltage after the reversible threshold is reached (around 150 V), whereas a clear sigmoid dependence was found for sugar beet tissue. If we compare this with extraction kinetics, we would expect exactly the opposite behavior as is shown in Fig. 7; apple tissue more clearly exhibits a threshold phenomenon, whereas the sucrose yield in sugar beet seems to increase almost linearly between 150 and 300 V applied to the electrodes (see Fig. 7c). In sugar beet, at about 300 V, the reversible field strength threshold of an average cell seems to be reached, and the final sucrose yield increases in disproportion to the increase in applied voltage. Increasing this voltage further above the reversible field strength threshold, we would probably have observed a similar threshold in terms of yield, as we did for apple tissue. To complement these observations, Fig. 8 shows the relationship between the final normalized degree Brix, B_f (total yield at the end of the 2-h experiment/simulation run), and the disintegration index Z. The threshold nature of the electroporation phenomenon is clearly visible; the $B_f(Z)$ linear correlation coefficient for both apple and sugar beet tissue is only around 0.91. Near the critical electric field strength, a small increase in the disintegration index does not reflect in a proportionally small increase in solute yield. The $B_f(Z)$ and $B_f(U)$ dependencies indicate that the reversible field strength threshold of an average sugar beet cell is somewhere above 600 V/cm (note the 5 mm electrode distance), while for apple, the corresponding value is estimated to be just under 300 V/cm. The conclusion is that although Z is a valuable, simple and efficient method of detecting and quantifying tissue electroporation, due to the threshold nature of electroporation, use of Z in predicting aspects of extraction behavior should be carefully (re)examined, at least for protocols resulting in more "gentle" permeabilization (i.e. at low values of Z). Measuring conductivity and

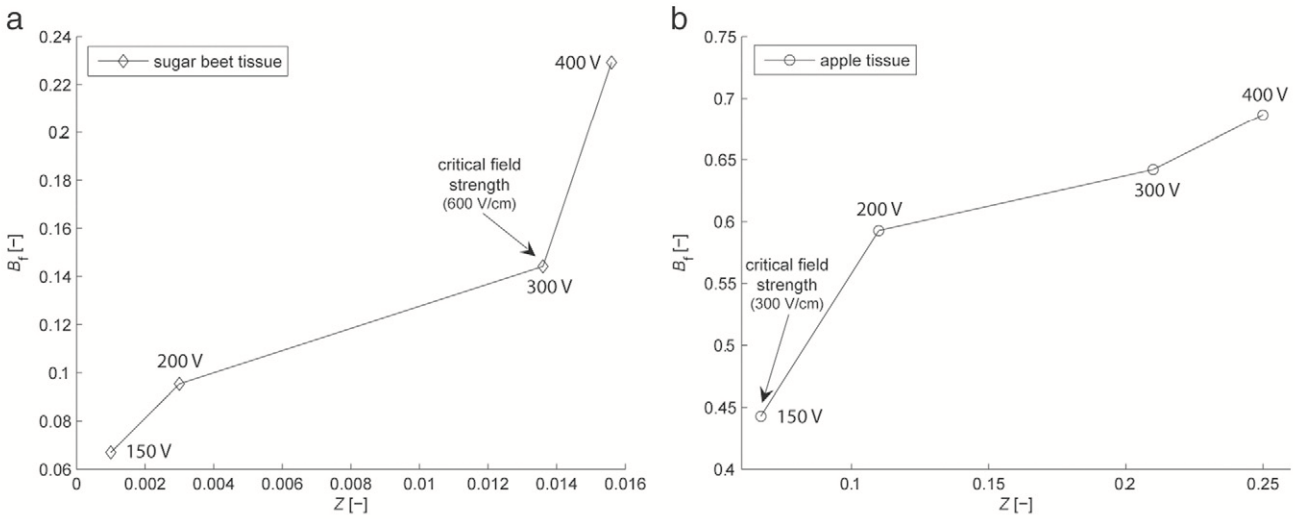

Fig. 8. The $B_f(Z)$ relationship for treatment according to Protocol A; sugar beet (a) and apple (b) tissue. Numbers next to data points indicate the corresponding electrode voltage.

conductivity-based indices are, however, valuable tools in detecting reversible electroporation (Pavlin & Miklavcic, 2008).

3.2. Pressing experiments

Figs. 9 and 10 give pressing kinetics obtained from a texturometer during constant pressure application, as described in Materials and methods (Section 2.3). Experimental data on total tissue sample deformation were fitted with simulation results using the dual-porosity model. Parameters for simulation were optimized to give the best fit with experimental data according to the same criterion function, as was used for the diffusion experiments. Parameter values are listed in the Appendix, Table A.2. Fig. 9 presents extraction kinetics for the two materials as dependent on applied field strength, while Fig. 10 gives expression kinetics for apple tissue using three different protocols (A, B, and C) at three voltages (200, 300, or 400 V).

The pressing experiments further elucidate the behavior of electroporated sample tissues, but more importantly, some of our assumptions about tissue structure and electroporation effects on diffusion can be confirmed by results presented in Fig. 9.

Analogous to the total soluble solutes yield in diffusion experiments, is the total sample deformation at the end of the 1-h pressing experiment. The filtration–consolidation kinetics at 300, 350, and 400 V voltage applied to the 5 mm tissue sample does not differ significantly for apple tissue (see Fig. 9c), while for sugar beet, the final deformation seems to exhibit a roughly quadratic dependence on electric field strength (this dependence was approximately linear in diffusion experiments). This confirms the earlier observation of the lower electroporation threshold for cells in apple tissue. We note that precise cutting and rigorous control via measurements are required to ensure that initial sample thickness is constant in all of the experiments, as an error on the order of 0.5 mm in sample thickness can result in contradictive results (higher final deformation at lower voltage, for example).

Also, the highly compressible extracellular space (about 30% of all sample volume) containing some air and extracellular liquid in intact apple tissue (Fig. 9b), results in a relatively high total sample deformation, as compared to the more densely-packed sugar beet tissue with liquid-filled extracellular space. Note that we did not model the presence of air in the extracellular space of apple tissue; we are assuming that the extracellular air is driven out of the compartments in tissue by intracellular liquid that permeates through the cell membranes at the moment of electroporation or soon thereafter. This can at times be visually observed via appearance of small bubbles of air, provided that a transparent treatment chamber is used and there is enough liquid (juice) around the sample.

Furthermore, final total sample deformation changes most dramatically when applied voltage is increased from 300 to 400 V in sugar beet and from 150 to 200 V in apple tissue (Fig. 9c). This would indicate that, for the pulsing protocols we used, the reversible threshold field strength of an average sugar beet cell is above 600 V/cm, and for the apple this threshold falls somewhere below 300 V/cm (values are estimated based on voltage applied to electrodes over a 5 mm distance). More experiments would be needed for more precise estimates, however, values obtained by analysing pressing experiments are in good agreement with earlier estimates presented in discussion of diffusion data. Also note that using a different treatment protocol (altering the duration and/or number of pulses, temperature, etc.) can result in markedly disparate estimates of the electric field strength required for electroporation, see e.g. (De Vito, Ferrari, Lebovka, Shynkaryk, & Vorobiev, 2008; Lebovka et al., 2007).

A noticeable difference in the consolidation–filtration behavior (apple vs. sugar beet) is caused by the higher extracellular hydraulic permeability of ripe apple. The factor is about 1.5, according to estimates from literature (see Table A.1). However, both the extracellular permeability of apple and of sugar beet tissue had to have been augmented by a factor of 2.5 and 1.5, respectively, in order for the model to successfully fit the experimental extraction kinetics. The extracellular space permeability is potentially a problematic parameter for evaluation; it is time-dependent (it drops in time due to compression of the sample), it cannot be reliably estimated from pressing experiments on intact tissue (only by special, pressure probe or similar experiments), and it is affected by the electroporation treatment as well as a function of ripeness and other biological variables. As discussed in the preceding section on diffusion experiments, electroporation may affect the effective cell volume fraction in tissue, thus reducing hydraulic resistance of tissue, and it may also increase permeability through release of turgor pressure in electroporated cells and consequent plasmolysis (Bazhal, Ngadi, Raghavan, & Nguyen, 2003; Fincan & Dejmek, 2003; Pereira et al., 2009).

According to the theory of electroporation, higher electric field strength results in a larger area of a cell membrane populated by pores, and thus a larger pore surface fraction per cell (Pavlin & Miklavcic, 2008). For this reason, we modeled electroporation effects on cells in tissue via the parameter f_p—the pore surface fraction. We expect that, given the same treatment conditions and raw material, the pore surface fraction will not depend on whether we are observing diffusion or liquid extraction by pressing. However, comparing values of parameter f_p in Table A.2, we notice a large discrepancy—a difference of about two orders of magnitude in values of f_p when comparing apple tissue in diffusion experiments with pressing experiments. If pore surface fraction is only a function of electroporation parameters (and

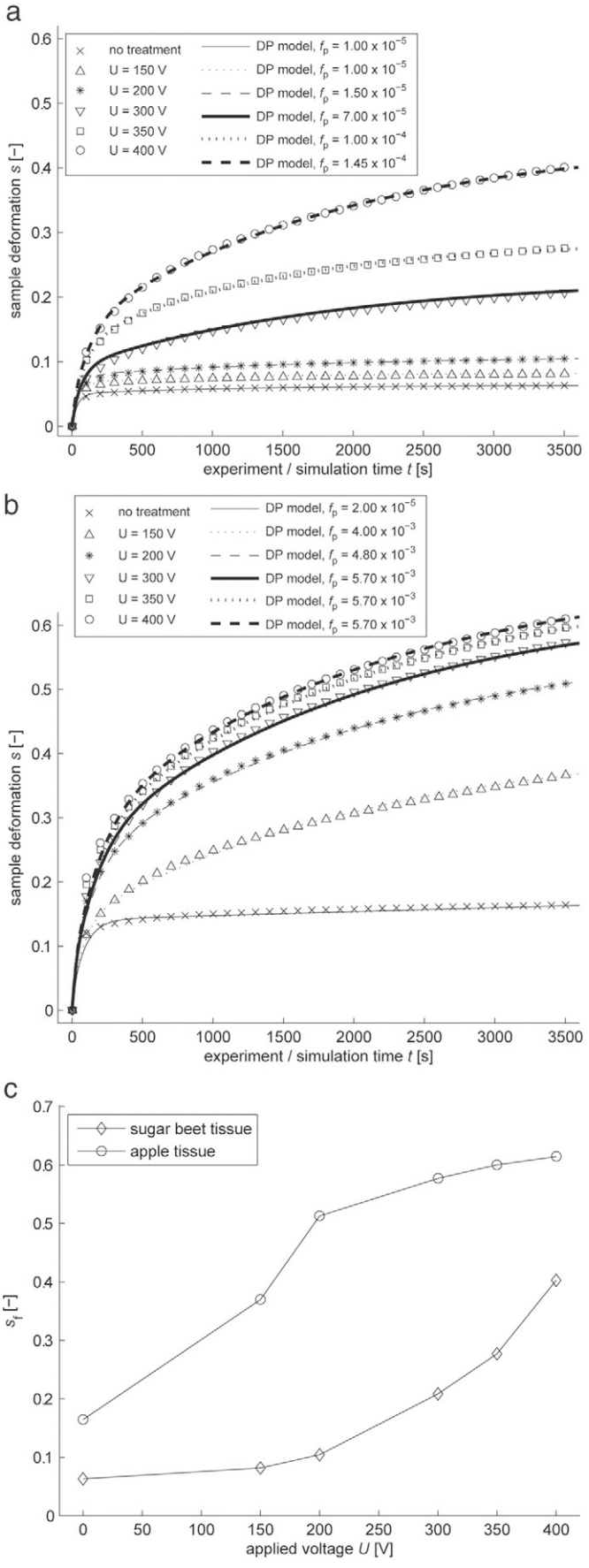

Fig. 9. Results of pressing experiments performed on the texturometer and model simulations of extraction kinetics, with sugar beet (a) and apple (b) tissue. Plot (c) shows the dependence of sample deformation s at the end of the experiment (i.e. s_f) on voltage applied to the electrodes. All samples were electroporated according to Protocol A.

according to the theory of electroporation, it is), this observed discrepancy cannot be explained. A possible non-trivial explanation (in the trivial one we conclude that one or more of the model assumptions are wrong) is in the fundamentally different methods of estimation of parameter f_p. Parameter f_p is one of the factors in a coefficient, a product of multiple parameters, which describes the state of membrane permeabilization. In the dual-porosity model equations for diffusion, pore surface fraction is multiplied with the hindrance coefficient, y_s. This parameter relates transmembrane solute diffusion rate with the solute-to-pore size ratio. The relationship is highly non-linear (see Mahnič-Kalamiza et al., 2014). In diffusion experiments with sugar beets or apples, what the pore surface fraction estimate is based on, is the amount of solute detected in the solution outside the tissue sample. The solute is predominantly sucrose (or a mix of sugars), with the hindrance coefficient around 10^{-3}, calculated based on a supposed *average* and *constant* pore size. In pressing experiments, the molecules traversing the membrane are not merely sucrose and molecules dissolved in water small enough to pass through the pores, but are primarily the molecules of solvent itself, i.e. intracellular water. Moreover, the hydraulic permeability of the membrane is a product of the pore surface fraction and the *assumed constant* radius of an *average* pore. A 10-times larger pore in diameter has a 100-times greater hydraulic permeability. This indirectly implies that in pressing experiments, what we are also measuring is the surface fraction of all pores, those permeable to sugars and those small enough to be permeable to water only. This could also explain why the initial value of f_p for intact tissue, as estimated from pressing experiments, is four orders of magnitude higher than the corresponding value as estimated from diffusion experiments; there are always water-permeable pores, aquaporins (Agre, Sasaki, & Chrispeels, 1993), present in the plasma membrane!

Fig. 10a–c shows the most effective (though not necessarily most energy efficient) treatment protocol for enhancing juice expression from apple tissue is Protocol B, in which only two unipolar pulses 1 s apart of 800 μs in duration each were applied. The reason for the difference in effectiveness of Protocols A and B might be, as already postulated by De Vito et al., in the longer membrane charging times, required for electroporation of large cells in apple tissue (De Vito et al., 2008). Another possibility is the uncharacterized effect of electrokinetic transport mechanisms (electroosmosis, electrophoresis) that may play a significant role in unipolar pulses on the order of about a millisecond.

Fig. 10a–c also illustrates that Protocol C, with half the total treatment time and carrying between 55–64% (at 400 V) and 78–85% (at 150 V) the energy of Protocols A and B (estimates based on current measurements), is most sensitive to pulse amplitude (also seen in the alternative view, Fig. 10f). Protocol A, by means of which two trains of eight bipolar pulses of 100 μs each were delivered, shows least sensitivity to pulse amplitude in tissue response (see Fig. 10d). Comparing results in Fig. 10d–f suggests an interesting conclusion; choosing the right treatment protocol (in this case either Protocol A or B, but not C) can at best result in a 40% relative increase (an extra 20% in absolute terms) in juice yield at twice the field strength (400 V as opposed to 200 V)—case of Protocol B. However, doubling the pulse amplitude (and thus, theoretically, at least quadrupling the delivered energy—in practice, the current more than doubles) can have almost negligible effects on juice yield—case of Protocol A. In summary, our results indicate that it is more energy efficient to search for the most appropriate pulsing protocol (depending on material and other treatment and/or processing parameters) and use the lowest sufficiently high voltage, rather than adapt and continue to use a particular protocol that has once proven to be effective and merely increase the voltage until reaching the desired outcome of treatment (e.g. target yield). This observation is of significant

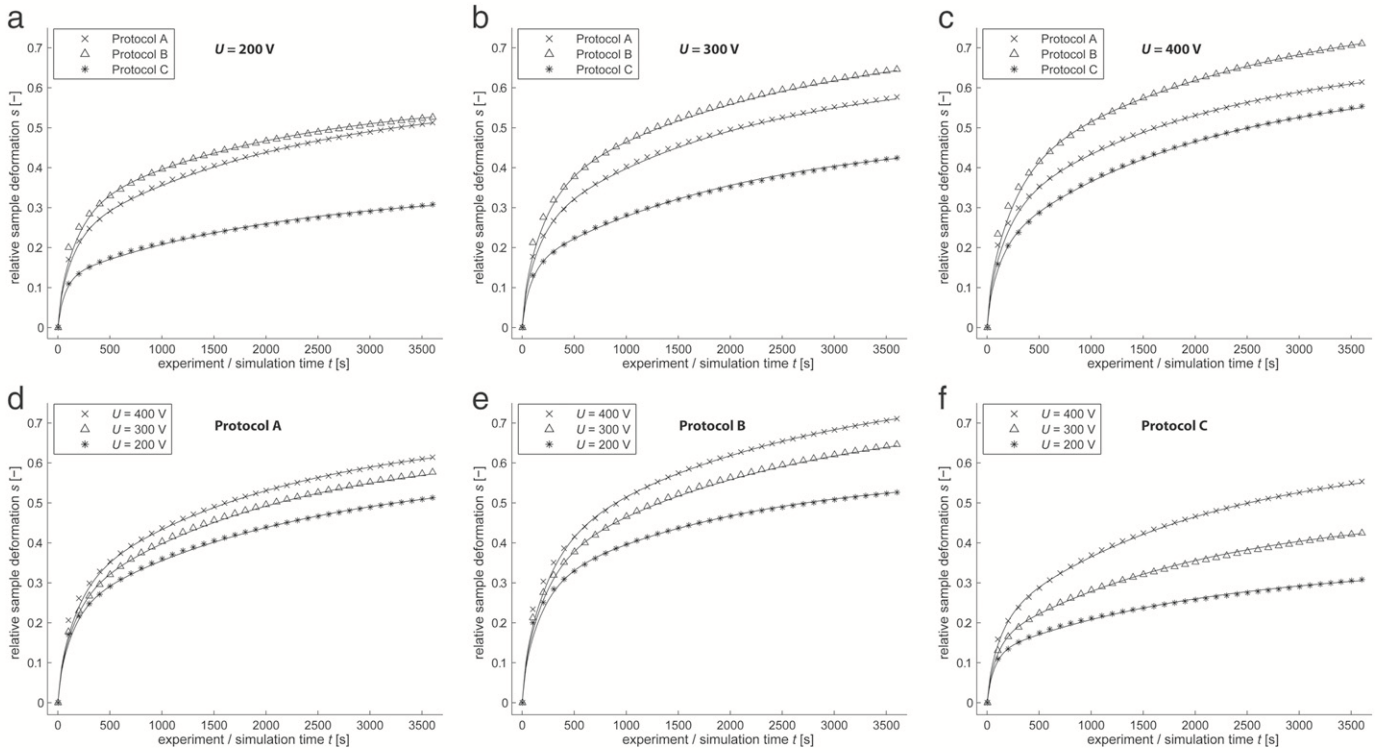

Fig. 10. Protocol comparison at fixed applied voltage during electroporation treatment—results of pressing experiments and model simulations using the dual-porosity model. For clarity, the same results are presented twice—for different voltages applied at the electrodes: 200 V (a), 300 V (b), or 400 V (c); and grouped by one of the three protocols used: Protocol A (d), Protocol B (e), and Protocol C (f).

importance if we consider the transfer from laboratory to industrial scale, as it has implications in operational cost reduction.

Results with Protocol C show that we can also design and apply treatment according to a protocol that exhibits high sensitivity to pulse amplitude. This may be due to significant effects of pore resealing during the second-long pauses between the pulses, as applied according to Protocol C; in other words, the 100 μs pulses spaced 1 s apart may not be able to stabilise a pore population at lower field strengths. This reasoning is supported by observations in animal cell electroporation (Pucihar, Krmelj, Reberšek, Napotnik, & Miklavčič, 2011). The investigation into various treatment protocols highlights the importance of choosing the optimal parameters of electroporation treatment for achieving extraction efficacy and energy efficiency, at least under conditions of low-energy, "gentle" (low Z) treatment, using few pulses of relatively short duration (on the order of about 10–100 μs, with total treatment times of 0.1 up to several milliseconds) and low field strengths (under 1 kV/cm).

If we examine the parameters of the dual-porosity model (Appendix, Table A.2) to look for indications of behavior just described, we notice that with the exception of Protocol C, there are no significant deviations from the mean value at the given pulse amplitude. This suggests that pore fraction ratio is indeed, as expected, primarily a function of pulse amplitude. What the protocol parameters seem to influence are the compressibility moduli. From the electroporation theory point of view, we postulate that what the compressibility moduli in some way reflect, are the respective fractions of reversibly and irreversibly electroporated cells. Extracellular space compressibility modulus determines the total relative deformation in the first few seconds to minutes of the pressing experiment. During this first stage, extracellular juice and juice that was or can be released from irreversibly damaged cells is expressed via the extracellular pathways, which are highly permeable. During the second, less dynamic stage, juice is first filtered through the electroporated cell membranes into the extracellular space, as described by the dual-porosity model, and then vacates the tissue sample via the extracellular route. The resulting deformation corresponds to the share of reversibly electroporated cells and is related to the applied pressure via the intracellular space compressibility modulus. The main difference between Protocol A and Protocol B is found in the values of the compressibility moduli, which indicates that different protocols affect the ratio of (ir)reversibly electroporated cells differently. This is consistent with theory of pore formation and its dependence on local electrochemical material properties. In this respect, Protocol C is particularly interesting; it exhibits the highest ratio of extra-to-intracellular compressibility modulus of all protocols, and the highest sensitivity of pore surface fraction to pulse amplitude, the latter reaching the highest value of all protocols at 400 V pulse amplitude. This is a characteristic of a protocol optimized for achieving reversible electroporation—the ratio of reversibly-to-irreversibly electroporated cells is high (low permanent damage) and reversibly electroporated cells' membranes are highly permeabilized. Not surprisingly, Protocol C is one of the standard protocols of electrochemotherapy (Lebar, Sersa, Kranjc, Groselj, & Miklavcic, 2002; Mir, Orlowski, Belehradek, & Paoletti, 1991) and gene electrotransfer (Mir et al., 1999), designed for causing minimal lasting damage to tissues and effective reversible electroporation for introducing molecules into target cells.

As the final point, we note the relatively low pressure used for juice expression in our model and experiments. The pressure was either 5.82 bar (sugar beet) or 2.91 bar (apple). This is low in comparison with similar filtration–consolidation behavior studies, where pressures from 1 bar up to 90 bars and higher are used (Grimi, Vorobiev, Lebovka, & Vaxelaire, 2010). This also significantly increased the required experiment duration in our case. We chose low external pressure in order to avoid very important mechanical damage to tissue. If we wish to experimentally observe and model filtration through an electroporated membrane, the integrity of the cell membrane should not be significantly altered due to the applied pressure. We chose the pressure for apple tissue so as to remain well under the saturation limit ($s = 1$) at the end of the 1 h experiment, and though the pressure used for sugar beet could have been further increased according to this saturation criterion, we were limited by the maximum load capabilities of the texturometer.

3.3. Problems, perspectives and directions for future development

The results presented in the preceding sections show that the dual-porosity model can be effectively used to model experimentally-obtained extraction kinetics. There remain, however, several issues that reduce the scientific rigor of the model when applied to practical problems in tissue electroporation. One of these issues concerns treatment parameters in ranges where there may be significant effects to tissue and transport that are not accounted for by the model. This can occur, for instance, under conditions that result in tissue electroporated to a high degree ($Z \approx 1$), or by using a treatment protocol where electrokinetic effects (electroosmosis, electrophoresis) are of significant importance, as these are not captured by the model equations (Li & Lin, 2011b; Li, Tan, Yu, & Lin, 2013a; Movahed & Li, 2012; Sadik, Li, Shan, Shreiber, & Lin, 2013). Electrokinetic effects may already be important under conditions used in this study (up to 800 μs pulses). High degree of electroporation causes problems to modeling of the structure and processes due to irreversible damage to tissue; the model provides parameters that can account for the transition of intracellular to extracellular phase (volume fraction of cells and compressibility moduli), however, as the fraction of irreversibly electroporated cells cannot easily be determined, this unknown variable presents a degree of freedom in the model that influences simulated kinetics much in the same way as the pore surface fraction, the only theoretically determined electroporation-dependent parameter. Recent experiments have shown that future development of the model in the direction of determining reversible/irreversible electroporation thresholds and local damage distribution is unavoidable, as these changes are as important, if not more important, than the permeabilization state of the membrane. In order to model the extent of damage and its distribution, statistical cell size and shape distributions and local inhomogeneities, tissue conductivity and its temporal evolution, and electrokinetic effects will have to be considered. Also, pores resulting from electroporation have a temporal cycle of evolution (e.g. changing size, resealing) that has not been taken into account so far. In conclusion, a more generalized form of the model is required, which entails the need to increase model complexity, and each such expansion or addition must be independently verified, followed by an evaluation of its impact and thus necessity.

4. Conclusions

In our previous papers we set out to describe a new framework for studying mass transport in electroporated tissue—i.e. the dual-porosity model of solute diffusion and consolidation-filtration behavior of electroporated tissue. In this paper we describe experiments on two model materials, sugar beet taproot and apple fruit tissue, which we used to test the model performance and verify some of the basic model assumptions. We have demonstrated the model is capable of accurately modeling extraction kinetics obtained by diffusion as well as pressing experiments. During model construction, we have identified and chose one model parameter, the pore surface fraction, as the most important parameter that is a function of electroporation treatment parameters—the local electric field strength, pulse number, and pulse duration. In this work, we have identified other important factors (most importantly changes in permeability and compressibility of tissue due to structural modifications) that reflect the complicated nature of electric field effects on texture and mass transport in electroporated tissue. To develop the model further, we need to evaluate their influence and mathematically describe these effects, to arrive at a more generalized model solution, capable of predicting extraction kinetics based on treatment parameters and material characteristics that can be obtained either from literature or estimated by independent experiments. We are confident the model can already be successfully applied to evaluate electroporation treatment efficiency with respect to mass transport, that it can be used for optimization of treatment parameters with prediction of treatment results, and that its further development will help understand the phenomena related to mass transport and textural properties of electroporated biological material.

Acknowledgments

The authors appreciate the financial support from the French Ministry of Research and Higher Education and the Slovenian Research Agency. This research was in part made possible due to networking activity of COST TD1104 Action (www.electroporation.net). We (SMK and DM) would also like to thank Dr. Sid Becker from the University of Canterbury, New Zealand, for fruitful discussion on the theory of porous media as applied to problems in tissue electroporation.

Appendix A

Table A.1
Parameters of the dual-porosity model pertaining to tissue textural, geometrical or physicochemical properties, not dependent on electroporation.

Parameter	Sugar beet	Apple	Source (if applicable)
Average cell radius, R [m]	$2.5 \cdot 10^{-5}$	$1.0 \cdot 10^{-4}$	(Buttersack & Basler, 1991; Harker, Redgwell, Hallett, Murray, & Carter, 2010)
Literature-based estimate of cell initial volume fraction, F [–]	0.97	0.75	(Richter & Ehwald, 1983; Vincent, 1989)
Sucrose diffusion constant in water at 20 °C, $D_{s,0}$ [$m^2\ s^{-1}$]	$4.5 \cdot 10^{-10}$	$4.5 \cdot 10^{-10}$	(Linder, Nassimbeni, Polson, & Rodgers, 1976; Venâncio & Teixeira, 1997)
Extracellular network tortuosity, τ_e [–]	π/2 (~1.57)	π/2 (~1.57)	n/a (approximation explained in Mahnič-Kalamiza et al., 2014)
Sucrose-to-pore hydrodynamic radius ratio, r_s/r_p	0.85	0.85	(Mahnič-Kalamiza et al., 2014)
Convection factor, f_c [–][a]	1	2.5	n/a
Membrane thickness, d_m [m]	$5 \cdot 10^{-9}$	$5 \cdot 10^{-9}$	(Stewart, Gowrishankar, & Weaver, 2004)
Single (average) pore hydraulic permeability, k_p [m^2]	$1.25 \cdot 10^{-19}$	$1.25 \cdot 10^{-19}$	(see Mahnič-Kalamiza & Vorobiev, 2014)
Solvent viscosity, μ [Pa·s]	10^{-3}	10^{-3}	dynamic viscosity of water
Extracellular hydraulic permeability, k_e [m^2]	$1.5 \cdot 10^{-17}$	$2.25 \cdot 10^{-17}$	(Tomos, 1988)
Extracellular hydraulic permeability correction factor, f_k [–][b]	1.5	2.5	n/a
Spherical cell squared surface-to-volume ratio (for α), $9/R^2$ [m^{-2}]	$1.44 \cdot 10^{10}$	$9.00 \cdot 10^{8}$	n/a
Applied (via piston) external pressure, P_E [MPa]	0.582 (5.82 bar)	0.291 (2.91 bar)	n/a

[a] The convection factor augments the extracellular diffusion rate ($D_{s,e} = D_{s,e} / \tau_e \cdot f_c$) to account for the effect of convection (washing out) of solute from the tissue samples due to solvent agitation. It was computationally determined based on comparison of model predictions and experimentally observed kinetics of solute percolating through the tissue matrix out of samples into the solvent. The effect was observed in apple tissue but not in sugar beets. The reason for this may be the relatively low packing ratio (cell-to-cell contacts, void extracellular space) of apple tissue (Harker et al., 2010). In part, the faster rate of diffusion can also be attributed to sugar composition in apple fruits; compared to sugar beet taproots, there are significant amounts of fructose and glucose present, molecules which are smaller than sucrose and with higher diffusion coefficients (Fuleki, Pelayo, & Palabay, 1994; Venâncio & Teixeira, 1997).

[b] In both sugar beet and apple tissue, the estimated extracellular space hydraulic permeability recalculated from measurements reported in literature had to have been augmented by a certain factor to account for experimentally-observed faster expression rate as opposed to the rate governed by the estimated permeability coefficient. This is most likely due to the fact the effect of electrical treatment on extracellular permeability (particularly noticeable in apple tissue) is not accounted for in the model equations.

Table A.2
Parameters of the dual-porosity model with dependence on electroporation treatment used to fit experimental data in diffusion (shown in Fig. 7) and pressing experiments (as shown in Figs. 9 and 10).

		Diffusion experiments			Pressing experiments		
Tissue	U [V]	f_p [−]	c_{e0}/c_{i0} [−]	F [−]	f_p [−]	$G_{\varepsilon,e}$ [Pa]	$G_{\varepsilon,i}$ [Pa]
Sugar beet	0	$1.0 \cdot 10^{-9}$	0.65	0.92	$1.00 \cdot 10^{-5}$	$115.0 \cdot 10^{5}$	$450.0 \cdot 10^{5}$
	150	$1.0 \cdot 10^{-7}$	1.00	0.90	$1.00 \cdot 10^{-5}$	$85.0 \cdot 10^{5}$	$400.0 \cdot 10^{5}$
	200	$2.0 \cdot 10^{-7}$	1.00	0.86	$1.50 \cdot 10^{-5}$	$73.0 \cdot 10^{5}$	$200.0 \cdot 10^{5}$
	300	$9.0 \cdot 10^{-7}$	1.00	0.80	$7.00 \cdot 10^{-5}$	$58.0 \cdot 10^{5}$	$45.0 \cdot 10^{5}$
	350	n/a	n/a	n/a	$1.00 \cdot 10^{-4}$	$39.5 \cdot 10^{5}$	$41.5 \cdot 10^{5}$
	400	$6.0 \cdot 10^{-6}$	1.00	0.77	$1.45 \cdot 10^{-4}$	$32.0 \cdot 10^{5}$	$22.0 \cdot 10^{5}$
Apple (Protocol A)	0	$1.0 \cdot 10^{-9}$	0.65	0.75	$2.00 \cdot 10^{-5}$	$20.5 \cdot 10^{5}$	$12.0 \cdot 10^{5}$
	150	$8.0 \cdot 10^{-7}$	1.00	0.50	$4.00 \cdot 10^{-3}$	$18.5 \cdot 10^{5}$	$11.0 \cdot 10^{5}$
	200	$9.9 \cdot 10^{-7}$	1.00	0.345	$4.80 \cdot 10^{-3}$	$11.0 \cdot 10^{5}$	$9.2 \cdot 10^{5}$
	300	$4.0 \cdot 10^{-6}$	1.00	0.30	$5.70 \cdot 10^{-3}$	$9.80 \cdot 10^{5}$	$8.5 \cdot 10^{5}$
	350	n/a	n/a	n/a	$5.70 \cdot 10^{-3}$	$9.00 \cdot 10^{5}$	$8.45 \cdot 10^{5}$
	400	$1.05 \cdot 10^{-5}$	1.00	0.265	$5.70 \cdot 10^{-3}$	$8.60 \cdot 10^{5}$	$8.45 \cdot 10^{5}$
Apple (Protocol B)	200	n/a			$4.20 \cdot 10^{-3}$	$9.00 \cdot 10^{5}$	$11.6 \cdot 10^{5}$
	300				$4.85 \cdot 10^{-3}$	$7.50 \cdot 10^{5}$	$8.5 \cdot 10^{5}$
	400				$5.10 \cdot 10^{-3}$	$6.55 \cdot 10^{5}$	$8.0 \cdot 10^{5}$
Apple (Protocol C)	200	n/a			$3.20 \cdot 10^{-3}$	$21.2 \cdot 10^{5}$	$14.0 \cdot 10^{5}$
	300				$4.80 \cdot 10^{-3}$	$16.3 \cdot 10^{5}$	$9.6 \cdot 10^{5}$
	400				$6.35 \cdot 10^{-3}$	$11.8 \cdot 10^{5}$	$7.8 \cdot 10^{5}$

References

Agre, P., Sasaki, S., & Chrispeels, M.J. (1993). Aquaporins: A family of water channel proteins. *American Journal of Physiology - Renal Physiology, 265*(3), F461.

Ariffin, A.B., Forde, P.F., Jahangeer, S., Soden, D.M., & Hinchion, J. (2014). Releasing pressure in tumors: What do we know so far and where do we go from here? A review. *Cancer Research, 74*(10), 2655–2662. http://dx.doi.org/10.1158/0008-5472.CAN-13-3696.

Bazhal, M.I., Ngadi, M.O., Raghavan, G.S.V., & Nguyen, D.H. (2003). Textural changes in apple tissue during pulsed electric field treatment. *Journal of Food Science, 68*(1), 249–253. http://dx.doi.org/10.1111/j.1365-2621.2003.tb14147.x.

Becker, S. (2012). Transport modeling of skin electroporation and the thermal behavior of the stratum corneum. *International Journal of Thermal Sciences, 54*, 48–61. http://dx.doi.org/10.1016/j.ijthermalsci.2011.10.022.

Boussetta, N., Soichi, E., Lanoiselle, J. -L., & Vorobiev, E. (2014). Valorization of oilseed residues: Extraction of polyphenols from flaxseed hulls by pulsed electric fields. *Industrial Crops and Products, 52*, 347–353. http://dx.doi.org/10.1016/j.indcrop.2013.10.048.

Buttersack, C., & Basler, W. (1991). Hydraulic conductivity of cell-walls in sugar-beet tissue. *Plant Science, 76*(2), 229–237. http://dx.doi.org/10.1016/0168-9452(91)90145-X.

Cadossi, R., Ronchetti, M., & Cadossi, M. (2014). Locally enhanced chemotherapy by electroporation: Clinical experiences and perspective of use of electrochemotherapy. *Future Oncology (London, England), 10*(5), 877–890. http://dx.doi.org/10.2217/fon.13.235.

Campbell, N.A., Reece, J.B., Urry, L.A., Cain, M.L., Wasserman, S.A., Minorsky, P.V., et al. (2008). *Biology*. San Francisco: Pearson, Benjamin Cummings.

De Monte, F., Pontrelli, G., & Becker, S. (2013). Chapter 3—Drug release in biological tissues. In S.M. Becker, & A.V. Kuznetsov (Eds.), *Transport in biological media* (pp. 59–118). Boston: Elsevier (Retrieved from http://www.sciencedirect.com/science/article/pii/B9780124158245000035).

De Vito, F., Ferrari, G., Lebovka, N.I., Shynkaryk, N.V., & Vorobiev, E. (2008). Pulse duration and efficiency of soft cellular tissue disintegration by pulsed electric fields. *Food and Bioprocess Technology, 1*(4), 307–313. http://dx.doi.org/10.1007/s11947-007-0017-y.

Dean, D.A. (2013). Cell-specific targeting strategies for electroporation-mediated gene delivery in cells and animals. *Journal of Membrane Biology, 246*(10), 737–744. http://dx.doi.org/10.1007/s00232-013-9534-y.

Donsi, F., Ferrari, G., & Pataro, G. (2010). Applications of pulsed electric field treatments for the enhancement of mass transfer from vegetable tissue. *Food Engineering Reviews, 2*(2), 109–130. http://dx.doi.org/10.1007/s12393-010-9015-3.

El Belghiti, K.E., & Vorobiev, E. (2004). Mass transfer of sugar from beets enhanced by pulsed electric field. *Food and Bioproducts Processing, 82*(C3), 226–230.

Fincan, M., & Dejmek, P. (2003). Effect of osmotic pretreatment and pulsed electric field on the viscoelastic properties of potato tissue. *Journal of Food Engineering, 59*(2–3), 169–175. http://dx.doi.org/10.1016/S0260-8774(02)00454-5.

Fuleki, T., Pelayo, E., & Palabay, R.B. (1994). Sugar composition of varietal juices produced from fresh and stored apples. *Journal of Agricultural and Food Chemistry, 42*(6), 1266–1275. http://dx.doi.org/10.1021/jf00042a003.

Gehl, J. (2003). Electroporation: Theory and methods, perspectives for drug delivery, gene therapy and research. *Acta Physiologica Scandinavica, 177*(4), 437–447. http://dx.doi.org/10.1046/j.1365-201X.2003.01093.x.

Goettel, M., Eing, C., Gusbeth, C., Straessner, R., & Frey, W. (2013). Pulsed electric field assisted extraction of intracellular valuables from microalgae. *Algal Research - Biomass Biofuels and Bioproducts, 2*(4), 401–408. http://dx.doi.org/10.1016/j.algal.2013.07.004.

Golberg, A., & Yarmush, M.L. (2013). Nonthermal irreversible electroporation: Fundamentals, applications, and challenges. *IEEE Transactions on Biomedical Engineering, 60*(3), 707–714. http://dx.doi.org/10.1109/TBME.2013.2238672.

Grimi, N., Dubois, A., Marchal, L., Jubeau, S., Lebovka, N.I., & Vorobiev, E. (2014). Selective extraction from microalgae Nannochloropsis sp. using different methods of cell disruption. *Bioresource Technology, 153*, 254–259. http://dx.doi.org/10.1016/j.biortech.2013.12.011.

Grimi, N., Praporscic, I., Lebovka, N., & Vorobiev, E. (2007). Selective extraction from carrot slices by pressing and washing enhanced by pulsed electric fields. *Separation and Purification Technology, 58*(2), 267–273. http://dx.doi.org/10.1016/j.seppur.2007.03.020.

Grimi, N., Vorobiev, E., Lebovka, N., & Vaxelaire, J. (2010). Solid–liquid expression from denaturated plant tissue: Filtration–consolidation behaviour. *Journal of Food Engineering, 96*(1), 29–36. http://dx.doi.org/10.1016/j.jfoodeng.2009.06.039.

Haberl, S., Miklavcic, D., Sersa, G., Frey, W., & Rubinsky, B. (2013). Cell membrane electroporation-Part 2: The applications. *IEEE Electrical Insulation Magazine, 29*(1), 29–37.

Harker, F.R., Redgwell, R.J., Hallett, I.C., Murray, S.H., & Carter, G. (2010). Texture of fresh fruit. In J. Janick (Ed.), *Horticultural reviews* (pp. 121–224). John Wiley & Sons, Inc (Retrieved from http://onlinelibrary.wiley.com/doi/10.1002/9780470650646.ch2/summary).

Jiang, C., Qin, Z., & Bischof, J. (2014). Membrane-targeting approaches for enhanced cancer cell destruction with irreversible electroporation. *Annals of Biomedical Engineering, 42*(1), 193–204. http://dx.doi.org/10.1007/s10439-013-0882-7.

Kotnik, T., Kramar, P., Pucihar, G., Miklavcic, D., & Tarek, M. (2012). Cell membrane electroporation-Part 1: The phenomenon. *IEEE Electrical Insulation Magazine, 28*(5), 14–23. http://dx.doi.org/10.1109/MEI.2012.6268438.

Lebar, A.M., Sersa, G., Kranjc, S., Groselj, A., & Miklavcic, D. (2002). Optimisation of pulse parameters in vitro for in vivo electrochemotherapy. *Anticancer Research, 22*(3), 1731–1736.

Lebovka, N.I., Shynkaryk, M.V., El-Belghiti, K., Benjelloun, H., & Vorobiev, E. (2007). Plasmolysis of sugarbeet: Pulsed electric fields and thermal treatment. *Journal of Food Engineering, 80*(2), 639–644. http://dx.doi.org/10.1016/j.jfoodeng.2006.06.020.

Li, J., & Lin, H. (2011a). Numerical simulation of molecular uptake via electroporation. *Bioelectrochemistry, 82*(1), 10–21. http://dx.doi.org/10.1016/j.bioelechem.2011.04.006.

Li, J., & Lin, H. (2011b). Numerical simulation of molecular uptake via electroporation. *Bioelectrochemistry (Amsterdam, Netherlands), 82*(1), 10–21. http://dx.doi.org/10.1016/j.bioelechem.2011.04.006.

Li, J., Tan, W., Yu, M., & Lin, H. (2013a). The effect of extracellular conductivity on electroporation-mediated molecular delivery. *Biochimica et Biophysica Acta, 1828*(2), 461–470. http://dx.doi.org/10.1016/j.bbamem.2012.08.014.

Li, J., Tan, W., Yu, M., & Lin, H. (2013b). The effect of extracellular conductivity on electroporation-mediated molecular delivery. *Biochimica et Biophysica Acta, 1828*(2). http://dx.doi.org/10.1016/j.bbamem.2012.08.014.

Linder, P.W., Nassimbeni, L.R., Polson, A., & Rodgers, A.L. (1976). The diffusion coefficient of sucrose in water. A physical chemistry experiment. *Journal of Chemical Education, 53*(5), 330. http://dx.doi.org/10.1021/ed053p330.

Liu, L.J., Brown, S.L., Ewing, J.R., & Schlesinger, M. (2011). Phenomenological model of interstitial fluid pressure in a solid tumor. *Physical Review E: Statistical, Nonlinear, and Soft Matter Physics, 84*(2 Pt 1), 021919.

Liu, D., Lebovka, N.I., & Vorobiev, E. (2013). Impact of electric pulse treatment on selective extraction of intracellular compounds from saccharomyces cerevisiae yeasts. *Food and Bioprocess Technology, 6*(2), 576–584. http://dx.doi.org/10.1007/s11947-011-0703-7.

Mahnič-Kalamiza, S., Miklavčič, D., & Vorobiev, E. (2014). Dual-porosity model of solute diffusion in biological tissue modified by electroporation. *Biochimica et Biophysica Acta, 1838*(7), 1950–1966. http://dx.doi.org/10.1016/j.bbamem.2014.03.004.

Mahnič-Kalamiza, S., & Vorobiev, E. (2014). Dual-porosity model of liquid extraction by pressing from biological tissue modified by electroporation. *Journal of Food Engineering, 137*, 76–87. http://dx.doi.org/10.1016/j.jfoodeng.2014.03.035.

Marty, M., Sersa, G., Garbay, J.R., Gehl, J., Collins, C.G., Snoj, M., et al. (2006). Electrochemotherapy—An easy, highly effective and safe treatment of cutaneous and subcutaneous metastases: Results of ESOPE (European Standard Operating Procedures of Electrochemotherapy) study. *European Journal of Cancer Supplements, 4*(11), 3–13. http://dx.doi.org/10.1016/j.ejcsup.2006.08.002.

Miklavcic, D., Mali, B., Kos, B., Heller, R., & Sersa, G. (2014). Electrochemotherapy: From the drawing board into medical practice. *Biomedical Engineering Online, 13*, 29. http://dx.doi.org/10.1186/1475-925X-13-29.

Mir, L.M., Bureau, M.F., Gehl, J., Rangara, R., Rouy, D., Caillaud, J. -M., et al. (1999). High-efficiency gene transfer into skeletal muscle mediated by electric pulses. *Proceedings of the National Academy of Sciences of the United States of America, 96*(8), 4262–4267.

Mir, L.M., Orlowski, S., Belehradek, J., Jr., & Paoletti, C. (1991). Electrochemotherapy potentiation of antitumour effect of bleomycin by local electric pulses. *European Journal of Cancer (Oxford, England : 1990), 27*(1), 68–72.

Morales-de la Pena, M., Elez-Martinez, P., & Martin-Belloso, O. (2011). Food preservation by pulsed electric fields: An engineering perspective. *Food Engineering Reviews, 3*(2), 94–107. http://dx.doi.org/10.1007/s12393-011-9035-7.

Movahed, S., & Li, D. (2012). Electrokinetic transport through the nanopores in cell membrane during electroporation. *Journal of Colloid and Interface Science, 369*, 442–452. http://dx.doi.org/10.1016/j.jcis.2011.12.039.

Mykhailyk, V., & Lebovka, N. (2014). Specific heat of apple at different moisture contents and temperatures. *Journal of Food Engineering, 123*, 32–35. http://dx.doi.org/10.1016/j.jfoodeng.2013.09.015.

Pavlin, M., & Miklavcic, D. (2008). Theoretical and experimental analysis of conductivity, ion diffusion and molecular transport during cell electroporation - Relation between short-lived and long-lived pores. *Bioelectrochemistry, 74*(1), 38–46. http://dx.doi.org/10.1016/j.bioelechem.2008.04.016.

Pereira, R.N., Galindo, F.G., Vicente, A.A., & Dejmek, P. (2009). Effects of pulsed electric field on the viscoelastic properties of potato tissue. *Food Biophysics, 4*(3), 229–239. http://dx.doi.org/10.1007/s11483-009-9120-0.

Petryk, M., & Vorobiev, E. (2013). Numerical and analytical modeling of solid–liquid expression from soft plant materials. *AIChE Journal, 59*(12), 4762–4771. http://dx.doi.org/10.1002/aic.14213.

Pucihar, G., Kotnik, T., Miklavcic, D., & Teissie, J. (2008). Kinetics of transmembrane transport of small molecules into electropermeabilized cells. *Biophysical Journal, 95*(6), 2837–2848. http://dx.doi.org/10.1529/biophysj.108.135541.

Pucihar, G., Krmelj, J., Reberšek, M., Napotnik, T.B., & Miklavčič, D. (2011). Equivalent pulse parameters for electroporation. *IEEE Transactions on Biomedical Engineering, 58*(11), 3279–3288. http://dx.doi.org/10.1109/TBME.2011.2167232.

Pusenjak, J., & Miklavcic, D. (2000). Modeling of interstitial fluid pressure in solid tumor. *Simulation Practice and Theory, 8*(1–2), 17–24. http://dx.doi.org/10.1016/S0928-4869(00)00003-3.

Raso, J., & Heinz, V. (2010). *Pulsed electric fields technology for the food industry: Fundamentals and applications*. Springer.

Reigada, R. (2014). Electroporation of heterogeneous lipid membranes. *Biochimica Et Biophysica Acta - Biomembranes, 1838*(3), 814–821. http://dx.doi.org/10.1016/j.bbamem.2013.10.008.

Richter, E., & Ehwald, R. (1983). Apoplastic mobility of sucrose in storage parenchyma of sugar beet. *Physiologia Plantarum, 58*(3), 263–268. http://dx.doi.org/10.1111/j.1399-3054.1983.tb04179.x.

Sadik, M.M., Li, J., Shan, J.W., Shreiber, D.I., & Lin, H. (2013). Quantification of propidium iodide delivery using millisecond electric pulses: Experiments. *Biochimica et Biophysica Acta, 1828*(4), 1322–1328. http://dx.doi.org/10.1016/j.bbamem.2013.01.002.

Saulis, G. (2010). Electroporation of cell membranes: The fundamental effects of pulsed electric fields in food processing. *Food Engineering Reviews, 2*(2), 52–73. http://dx.doi.org/10.1007/s12393-010-9023-3.

Sel, D., Cukjati, D., Batiuskaite, D., Slivnik, T., Mir, L.M., & Miklavcic, D. (2005). Sequential finite element model of tissue electropermeabilization. *IEEE Transactions on Biomedical Engineering, 52*(5), 816–827. http://dx.doi.org/10.1109/TBME.2005.845212.

Shayanfar, S., Chauhan, O.P., Toepfl, S., & Heinz, V. (2013). The interaction of pulsed electric fields and texturizing - antifreezing agents in quality retention of defrosted potato strips. *International Journal of Food Science and Technology, 48*(6), 1289–1295. http://dx.doi.org/10.1111/ijfs.12089.

Simonsen, T.G., Gaustad, J. -V., Leinaas, M.N., & Rofstad, E.K. (2012). High interstitial fluid pressure is associated with tumor-line specific vascular abnormalities in human melanoma xenografts. *PloS One, 7*(6), e40006. http://dx.doi.org/10.1371/journal.pone.0040006.

Sridhara, V., & Joshi, R.P. (2014). Evaluations of a mechanistic hypothesis for the influence of extracellular ions on electroporation due to high-intensity, nanosecond pulsing. *Biochimica et Biophysica Acta, 1838*(7), 1793–1800. http://dx.doi.org/10.1016/j.bbamem.2014.03.010.

Stewart, D.A., Gowrishankar, I.R., & Weaver, J.C. (2004). Transport lattice approach to describing cell electroporation: Use of a local asymptotic model. *IEEE Transactions on Plasma Science, 32*(4), 1696–1708. http://dx.doi.org/10.1109/TPS.2004.832639.

Tomos, A.D. (1988). Cellular water relations of plants. In F. Franks (Ed.), *Water Science Reviews 3 (1st ed.). Water dynamics*. Cambridge University Press (Vol.).

Turk, M.F., Vorobiev, E., & Baron, A. (2012). Improving apple juice expression and quality by pulsed electric field on an industrial scale. *LWT - Food Science and Technology, 49*(2), 245–250. http://dx.doi.org/10.1016/j.lwt.2012.07.024.

Venâncio, A., & Teixeira, J.A. (1997). Characterization of sugar diffusion coefficients in alginate membranes. *Biotechnology Techniques, 11*(3), 183–186. http://dx.doi.org/10.1023/A:1018457631368.

Vincent, J.F.V. (1989). Relationship between density and stiffness of apple flesh. *Journal of the Science of Food and Agriculture, 47*(4), 443–462. http://dx.doi.org/10.1002/jsfA.1740470406.

Vorobiev, E., & Lebovka, N. (2008). Pulsed-electric-fields-induced effects in plant tissues: Fundamental aspects and perspectives of applications. *Electrotechnologies for extraction from food plants and biomaterials* (pp. 39–81). New York: Springer (Retrieved from http://link.springer.com/chapter/10.1007/978-0-387-79374-0_2).

Yarmush, M.L., Golberg, A., Serša, G., Kotnik, T., & Miklavčič, D. (2014). Electroporation-based technologies for medicine: Principles, applications, and challenges. *Annual Review of Biomedical Engineering, 16*(1), 295–320. http://dx.doi.org/10.1146/annurev-bioeng-071813-104622.

Zorec, B., Préat, V., Miklavčič, D., & Pavšelj, N. (2013). Active enhancement methods for intra- and transdermal drug delivery: A review. *Slovenian Medical Journal, 82*(5). http://dx.doi.org/10.6016/1889.

5 Thermal effects on mass transport associated with electroporation

Electroporation is essentially the application of electric pulses of sufficient amplitude to target material. Due to the finite resistance of the material, electroporation unavoidably entails the flow of an electric current through the material, and this current through an ohmic load consequently results in heat generation and dissipation. This means that thermal effects are necessarily integrally and inseparably associated with electroporation. Noticeable rises in temperature have been noted in a number of electroporation applications (see the introductory sections of the thesis for a literature review). These temperature rises are a potential source of alteration of the thermodynamic properties of the material where mass transport is occurring. Parameters such as viscosity and diffusion rate coefficient are known to be strongly dependent on temperature, since they are related to fundamentally thermodynamic processes.

Due to the electroporation-associated heat dissipation, this thesis bears the title of "Effects of electrical *and thermal* pre-treatment on mass transport in biological tissue", emphasizing the inseparable connection between electroporation and the thermal effects that are associated with it. Furthermore, research has shown (again, the reader is referred to the literature review section) that thermal gradients across the plasma membrane can result in the differences in *electric potential* on either side of the membrane, meaning that there seems to exist an inverse connection whereby thermal gradients resulting from electroporation can alter electric relations on the membrane, thus affecting electroporation directly.

Given the considerations above, this thesis includes a complete presentation of the thermal formulation of the dual-porosity model, analogous to its mass transport formulations, and the applicability of such a model is discussed and theoretically analysed. In continuation, a suitable simplified formulation of the model is presented, which can be considered sufficiently detailed for studying thermal relations in electroporated plant tissues, but could also conceivably be extended in a suitable way (e.g. to the Pennes bioheat equation) to facilitate evaluation of thermal effects to the post-electroporation mass transport processes in perfused animal tissues. The given thermal model is coupled, via the temperature-dependent mass transport parameters, to the previously presented mass transport models of diffusion and pressing, and results are presented in the form of a parametric study. The work related to thermal relations is entirely theoretical, based on existing literature and extension of the work done on mass transport models in this thesis to the thermal problem. Validation and evaluation of suitability of these thermal formulations is a work in progress and exempted from presentation in this thesis.

All literature cited in this section can be found at the end of chapter 2 giving the literature review, i.e. in section 2.2.6.

5.1 The heat transfer model and the model of dual porosity – an extension by analogy with the Fourier law

5.1.1 The heat distribution model – fundamental model equations and its derivation by analogy

By analogy of the Fick's law of diffusion and Darcy law for liquid flow, the dual-porosity model of diffusion has been translated to the problem of filtration-consolidation of biological tissue during pressing (compare Paper II and Paper III, or refer to Paper IV). By a physically and mathematically equivalent analogy of the Fourier law, and using basic relations from non-equilibrium thermodynamics, one can postulate that a dual-porosity model can be written (in its original non-simplified form – see explanation below) also to describe thermal relations in biological tissue, and this should, in principle, be applicable whether the tissue is electroporated or not.

The equations of the thermal model for the case of thermal flux along one principal axis, for the extracellular and the intracellular space are, respectively

$$(1-F)\frac{\partial T_e}{\partial t}-(1-F)\frac{k_e}{\rho c_p}\frac{\partial^2 T_e}{\partial z^2}-F\frac{h_v}{\rho c_p}(T_i-T_e)=0 \tag{5.1.1}$$

$$F\frac{\partial T_i}{\partial t}-F\frac{k_i}{\rho c_p}\frac{\partial^2 T_i}{\partial z^2}+F\frac{h_v}{\rho c_p}(T_i-T_e)=0 \tag{5.1.2}$$

In eq. 5.1.1–5.1.2, the factors F and $1–F$ account for the specific relative volume fraction of each space in a block of tissue, where F is the volume fraction of cells. As tissue normally comprises of cells in more than half its volume, we must account for the conservation of energy in the transmembrane flux term. In order to do so, the third member in both equations must be equal, as it represents the same thermal flux. Note that temperatures T_e and T_i in all of the equations presented herein are *intrinsic* quantities, that is, they are temperatures that would actually have been measured, had a probe been inserted to measure the temperature at a given point or an infinitesimally small volume anywhere in either the extra- or intracellular space. If one, however, measures the bulk temperature in a given finite fraction of volume ΔV of tissue, which occurs in practice, the measured temperature will be, theoretically, a volume-averaged sum of the two respective space contributions. It is therefore important to distinguish between the bulk temperatures (volume-averaged) and their intrinsic definitions.

Dividing eq. 5.1.1 by $1–F$ and eq. 5.1.2 by F, one obtains

$$\frac{\partial T_e}{\partial t} - \frac{k_e}{\rho c_p}\frac{\partial^2 T_e}{\partial z^2} - \frac{f_v h_v}{\rho c_p}\left(T_i - T_e\right) = 0 \tag{5.1.3}$$

$$\frac{\partial T_i}{\partial t} - \frac{k_i}{\rho c_p}\frac{\partial^2 T_i}{\partial z^2} + \frac{h_v}{\rho c_p}\left(T_i - T_e\right) = 0 \tag{5.1.4}$$

In eq. 5.1.3, the new parameter – the volumetric ratio f_v – is a multiplicative factor accounting for the volumetric space distribution imbalance and equalling $F/(1–F)$. Other quantities are as follows: T_e and T_i the extracellular and the intracellular temperature [K], respectively; k_e and k_i are the extracellular and the intracellular tissue thermal conductivities [W/(m.K)], respectively; z is the spatial and t the temporal coordinate; c_p is the tissue heat capacity [J/(kg.K)]; ρ the tissue density [kg/m^3]; and h_v the volumetric heat transfer coefficient [W/(m^3.K)]. Coefficient h_v reflects the thermal conductivity of the plasma membrane and the particular heat exchange geometry, and a spatio-temporal dependence of the parameter as a function of electroporation can at this point be postulated to maintain complete generality. Whether such a dependence exists or not remains to be theoretically and experimentally evaluated. Subsection 5.1.4 is largely devoted to this question in theoretical terms.

A note on the difference between equations 5.1.2 or 5.1.4 and the corresponding equations for the diffusion / pressing problem. In both the diffusion problem and the consolidation-filtration version of the dual-porosity model, the intracellular porosity and associated concentration or pressure gradients were neglected, simplifying the intracellular space equation. This simplification was based on the assumption that the limiting factor in solute transport or liquid flow was the limited permeability of the cell membrane, that was assumed to be orders of magnitude lower as compared to the corresponding diffusivity or permeability in the extracellular space. However, in the thermal problem, thermal conductivities if comparing cytoplasm, plasma membrane and extracellular liquid, are not different in orders of magnitude (see references [51], [52] cited in the literature review section 2.2.4.3). Therefore, a simplification by omitting intracellular thermal flux cannot be justified, and this term has to be kept in the equation, greatly complicating the analytical solution for the general case where $k_e \neq k_i$, which admits travelling wave-type solutions. The solution of such a coupled system of second-order linear partial differential equations is out of scope of this thesis, and the reader is referred to the Appendix to this chapter, section 5.4, for a general idea towards obtaining a solution. For the special case however, where the extra- and intracellular thermal conductivities are equal (or approximately equal), i.e. $k_e \approx k_i$, the system is simplified, and it is not difficult to obtain its solution, which is presented in the following subsection 5.1.2.

The system of equations 5.1.3–5.1.4 can still be readily solved by using numerical methods and appropriate initial and boundary conditions. If studying the distribution of temperature within tissue after electroporation or ohmic heating, one can suppose that the tissue sample has been heated to a given temperature T_0 both in the extra- and the intracellular space (i.e. $T_0 = T_{e0} = T_{i0}$), and that during subsequent treatment, if no additional heat is generated, all surfaces of the sample are exposed to the ambient temperature T_{amb}, where $T_{amb} < T_0$ (cooling). In mathematical notation, and taking the symmetry on either side of the plane at $z = 0$ perpendicular to the principal axis of thermal flux into account (analogous to the diffusion problem), one can write

$$T_e\big|_{z=h/2} = T_i\big|_{z=h/2} = T_{\text{amb}} \tag{5.1.5}$$

$$\left.\frac{\partial T_e}{\partial z}\right|_{z=0} = \left.\frac{\partial T_i}{\partial z}\right|_{z=0} = 0 \tag{5.1.6}$$

$$T_e\big|_{t=0} = T_i\big|_{t=0} = T_0 \tag{5.1.7}$$

where the plane of symmetry ($z = 0$) is located exactly in the middle of the tissue sample of height h at a distance of $h/2$ from either of the sample's largest surfaces, at which the bulk of heat exchange is taking place (see Figure 5.1).

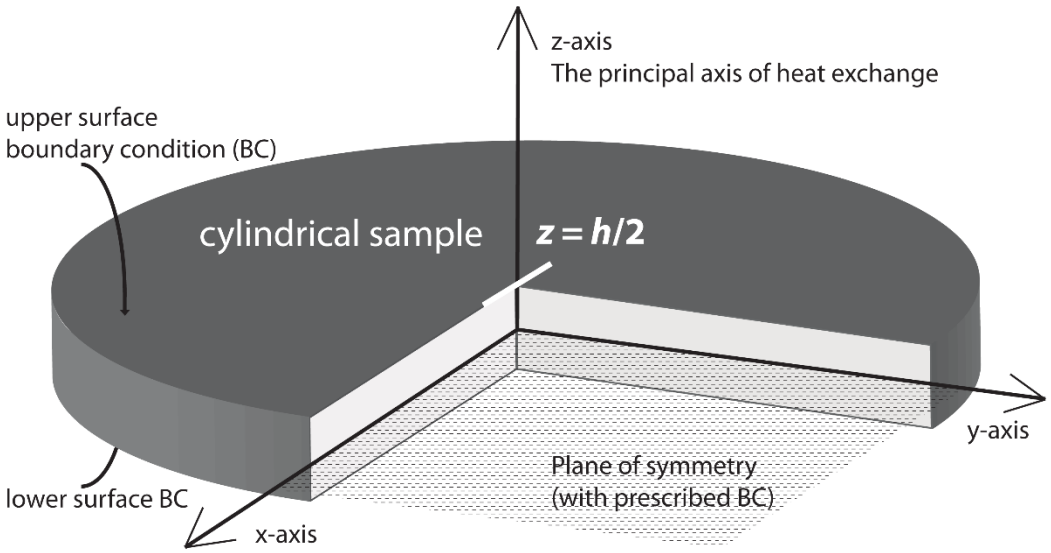

Figure 5.1: The thermal problem geometry – plane of symmetry and boundary conditions. The particular cylindrical geometry of the tissue sample is not significant, but has been used for this illustration for purposes of maintaining consistence with mass transport experiments. For the presented model to be relevant, the sample and setup geometry has to favour thermal transfer along one (principal) axis.

The set of equations 5.1.3–5.1.7 represents a complete mathematical description of thermal dissipation out of the sample block of tissue. The electroporation effects to the thermal

conductivity of the membrane, if substantial, can be accounted for by varying the transmembrane volumetric heat transfer coefficient h_v, and in case of additional thermal generation (time of observation during the electroporation application), an additional additive member accounting for heat generation can be appended to both equations 5.1.3 and 5.1.4. The system of equations could conceivably even be extended to take the form of the Pennes equation in case of studying perfused animal tissues. Anisotropy can be modelled via a spatial dependence of k_e and/or k_i, and a similar approach can be used for heat capacity and density if required. The resulting model can easily be solved via numerical integration, however, the main problem (as with the other two analogous models) remains the (un)reliable parameter estimation for realistic systems and the high number of degrees of freedom that the numerous parameters introduce to the model.

5.1.2 The thermal dual-porosity model: Analytical solution for the particular case of equal thermal conductivities ($k_e = k_i$)

In the particular case where both the intra- and the extracellular thermal conductivities are the same – a supposition realistic in exceptional cases of very homogeneous tissues – it is possible to obtain an analytical solution for the intra- and extracellular temperature profiles in space and time.

One can begin by first rewriting into a suitable form the partial differential equations of the system, taking $k = k_e = k_i$, thus obtaining

$$\frac{\partial T_e}{\partial t} = \frac{k}{\rho c_p}\frac{\partial^2 T_e}{\partial z^2} + \frac{f_v h_v}{\rho c_p}\left(T_i - T_e\right) \tag{5.1.8}$$

$$\frac{\partial T_i}{\partial t} = \frac{k}{\rho c_p}\frac{\partial^2 T_i}{\partial z^2} - \frac{h_v}{\rho c_p}\left(T_i - T_e\right) \tag{5.1.9}$$

To simplify the arithmetic in the following development of the solution, new constants α and β can be introduced, where $\alpha = k/\rho c_p$ and $\beta = h_v/\rho c_p$, and thus

$$\frac{\partial T_e}{\partial t} = \alpha\frac{\partial^2 T_e}{\partial z^2} + f_v\beta\left(T_i - T_e\right) \tag{5.1.10}$$

$$\frac{\partial T_i}{\partial t} = \alpha\frac{\partial^2 T_i}{\partial z^2} - \beta\left(T_i - T_e\right) \tag{5.1.11}$$

The last term of both eq. 5.1.10 and 5.1.11 involves only a linear combination of the unknown functions without non-linearities or appearance of the independent variables (z, t) in general, and therefore it is possible to suppose that the solution will consist of a combination (product) of a particular solution of the homogeneous equation

$$\frac{\partial \Theta}{\partial t} - \alpha \frac{\partial^2 \Theta}{\partial z^2} = 0 \tag{5.1.12}$$

satisfying the boundary conditions, and the particular solution of an autonomous system of two first-order ordinary differential equations for any plane along the z coordinate

$$\left(\frac{\partial T_e}{\partial t} \right)_z = f_v \beta \left((T_i)_z - (T_e)_z \right) \tag{5.1.13}$$

$$\left(\frac{\partial T_i}{\partial t} \right)_z = -\beta \left((T_i)_z - (T_e)_z \right) \tag{5.1.14}$$

satisfying the two initial conditions T_{e0} and T_{i0}. Note that to illustrate the effects and evaluate the dynamics of the transmembrane thermal flux, it is necessary to suppose (only in the particular case of $k_e = k_i$) that the initial temperatures in the respective spaces are not equal. If they were, and since the intra-/extracellular space thermal conductivities are supposed equal as well, it would be impossible to observe any transmembrane thermal flux due to the fact that both T_e and T_i remain perfectly equalised throughout the sample and for all times (i.e. $T_i - T_e = 0$ for all z, t). This observation should become evident upon closer examination of the final analytical solution.

In order to simplify calculations and presentation of results, it is convenient to introduce new variables to observe only temperature differences in relation to the ambient temperature instead of working with absolute values, thus

$$T_{e,\delta} = T_e - T_{amb} \tag{5.1.15}$$

$$T_{i,\delta} = T_i - T_{amb} \tag{5.1.16}$$

This results in corrections to one of the boundary conditions, which now read

$$T_{e,\delta}\big|_{z=h/2} = T_{i,\delta}\big|_{z=h/2} = T_{\text{amb}} - T_{\text{amb}} = 0 \tag{5.1.17}$$

$$\left. \frac{\partial T_{e,\delta}}{\partial z} \right|_{z=0} = \left. \frac{\partial T_{i,\delta}}{\partial z} \right|_{z=0} = 0 \tag{5.1.18}$$

and initial conditions are henceforth equal to the temperature differences between the absolute and ambient temperature

$$T_{e,\delta}\big|_{t=0} = T_e\big|_{t=0} - T_{amb} = \delta T_{e0} \tag{5.1.19}$$

$$T_{i,\delta}\big|_{t=0} = T_i\big|_{t=0} - T_{amb} = \delta T_{i0} \tag{5.1.20}$$

In the following text, the introduced δ-notation is dropped throughout for simplicity, and the reader should beware that both T_e and T_i were redefined by eq. 5.1.15–5.1.16, and these equations must be consulted in order to obtain absolute values from their relative counterparts.

To solve the eq. 5.1.12 for the boundary conditions 5.1.17–5.1.18, the classical method of separation of variables can be used [66]. At the outset, one supposes that the variables are separable and the solution is a product of two functions that are both functions of only one variable, thus

$$\Theta(z,t) = Z(z)\tau(t) \tag{5.1.21}$$

Note that the Greek letter τ is used here instead of the more conventional T for the temporal component of the solution $\tau(t)$ in order to avoid confusion with the letter designating temperature distribution $T(z, t)$. Substituting 5.1.21 into 5.1.12 yields

$$\frac{1}{\tau}\frac{d\tau}{dt} = \frac{\alpha}{Z}\frac{d^2Z}{dz^2} \tag{5.1.22}$$

Both sides of 5.1.22 must equal a constant, which is conveniently chosen to equal

$$\frac{1}{\tau}\frac{d\tau}{dt} = -\lambda^2\alpha \tag{5.1.23}$$

and

$$\frac{1}{Z}\frac{d^2Z}{dz^2} = -\lambda^2 \tag{5.1.24}$$

Solution of 5.1.23 is

$$\tau(t) = e^{-\lambda^2\alpha t} \tag{5.1.25}$$

and of 5.1.24

$$Z(z) = A\sin(\lambda z) + B\cos(\lambda z) \tag{5.1.26}$$

and therefore the solution has the form

$$\Theta(z,t) = Z(z)\tau(t) = \left[A\sin(\lambda z) + B\cos(\lambda z)\right]e^{-\lambda^2\alpha t} \tag{5.1.27}$$

The most general solution is obtained by summing the solutions of type 5.1.27, thus

$$\Theta(z,t) = \sum_{m=1}^{\infty}\left[A_m\sin(\lambda_m z) + B_m\cos(\lambda_m z)\right]e^{-\lambda_m{}^2\alpha t} \tag{5.1.28}$$

where A_m, B_m and λ_m are constants determined by boundary and initial conditions. In order to satisfy the boundary conditions eqs. 5.1.17–5.1.18, A_m must equal zero and $\lambda_m = (2m\text{-}1)\pi/l$ where l is the thickness of the tissue sample and $m = 1, 2, 3, \ldots$

Supposing the final form of the solution will be a linear combination of $\Theta(z, t)$ and additional time-dependent functions, the initial condition can be satisfied in the final step, for now, it can be demanded that it equals 1, and is not a function of the spatial coordinate (since it is supposed that initial temperature distribution is homogeneous and equal throughout the sample). Representing the constant 1 as an infinite sum of functions of the form $\cos(\lambda_m z)$, i.e. by a Fourier cosine series, determines the constants B_m to be equalling

$$B_m = \frac{4(-1)^m}{\pi(2m-1)} \tag{5.1.29}$$

Replacing *m* by the more convenient index *n* running from 0 to infinity, and assembling eqs. 5.1.28–5.1.29, one obtains

$$\Theta(z,t) = \frac{4}{\pi}\sum_{n=0}^{\infty}\frac{(-1)^n}{2n+1}\cos(\lambda_n z)e^{-\lambda_n^2 \alpha t} \tag{5.1.30}$$

where $\lambda_n = (2n+1)\pi/l$.

Turning now the attention to the system of equations 5.1.13–5.1.14, one can observe that it is fundamentally a system of two linear homogeneous first-order constant-coefficient ordinary differential equations. A reference handbook or guide on solving such systems of equations [67] states that a system of the form

$$x_t' = ax + by \tag{5.1.31}$$

$$y_t' = cx + dy \tag{5.1.32}$$

has a characteristic equation and a discriminant, written as

$$\lambda^2 - (a+d)\lambda + ad - bc = 0 \tag{5.1.33}$$

$$D = (a-d)^2 + 4bc \tag{5.1.34}$$

Rewriting the system 5.1.13–5.1.14 to the form of eqs. 5.1.31–5.1.32, thus obtaining

$$\left(\frac{\partial T_e}{\partial t}\right)_z = -f_v\beta(T_e)_z + f_v\beta(T_i)_z \tag{5.1.35}$$

$$\left(\frac{\partial T_i}{\partial t}\right)_z = \beta(T_e)_z - \beta(T_i)_z \tag{5.1.36}$$

and writing the characteristic equation for this system, one notices that $ad - bc = 0$ in this particular case, since the whole straight line $ax + by = 0$ consists of singular points. For this particular case, the system must be rewritten (note that *k* in the equations below is not of any particular quality and should not be confused with the thermal conductivity coefficient) into the form

$$x_t' = ax + by \tag{5.1.37}$$

$$y_t' = k(cx + dy) \tag{5.1.38}$$

and thus (note the change in the order of equations and variables on the right-hand side to conform to the above template)

$$\left(\frac{\partial T_i}{\partial t}\right)_z = -\beta(T_i)_z + \beta(T_e)_z \tag{5.1.39}$$

$$\left(\frac{\partial T_e}{\partial t}\right)_z = -f_v\left(-\beta\left(T_i\right)_z + \beta\left(T_e\right)_z\right) \tag{5.1.40}$$

From comparison of 5.1.39–5.1.40 to 5.1.37–5.1.38, it follows that $a = c = -\beta$, $b = d = \beta$, and $k = -f_v$. The final solution of the system 5.1.37–5.1.38 can be given as

$$x = bC_1 + C_2 e^{(a+bk)t} \tag{5.1.41}$$

$$y = -aC_1 + C_2 k e^{(a+bk)t} \tag{5.1.42}$$

and given the equalities for a, b, c, d, and k, the general solution of 5.1.39–5.1.40 is thus

$$\left(T_i\right)_z = \beta C_1 + C_2 e^{-\beta(1+f_v)t} \tag{5.1.43}$$

$$\left(T_e\right)_z = \beta C_1 - C_2 f_v e^{-\beta(1+f_v)t} \tag{5.1.44}$$

The final solution is a product of $\Theta(z, t)$ and the presently developed temporal functions

$$T_i\left(z,t\right) = \beta C_1 \Theta\left(z,t\right) + C_2 e^{-\beta(1+f_v)t}\Theta\left(z,t\right) \tag{5.1.43}$$

$$T_e\left(z,t\right) = \beta C_1 \Theta\left(z,t\right) - C_2 f_v e^{-\beta(1+f_v)t}\Theta\left(z,t\right) \tag{5.1.44}$$

yielding

$$T_i\left(z,t\right) = \frac{4\beta C_1}{\pi}\sum_{n=0}^{\infty}\frac{\left(-1\right)^n}{2n+1}\cos\left(\lambda_n z\right)e^{-\lambda_n{}^2\alpha t} + \frac{4C_2}{\pi}\sum_{n=0}^{\infty}\frac{\left(-1\right)^n}{2n+1}\cos\left(\lambda_n z\right)e^{-\lambda_n{}^2\alpha t}e^{-\beta(1+f_v)t} \tag{5.1.43}$$

$$T_e\left(z,t\right) = \frac{4\beta C_1}{\pi}\sum_{n=0}^{\infty}\frac{\left(-1\right)^n}{2n+1}\cos\left(\lambda_n z\right)e^{-\lambda_n{}^2\alpha t} - \frac{4C_2 f_v}{\pi}\sum_{n=0}^{\infty}\frac{\left(-1\right)^n}{2n+1}\cos\left(\lambda_n z\right)e^{-\lambda_n{}^2\alpha t}e^{-\beta(1+f_v)t} \tag{5.1.44}$$

Finally, initial conditions must be satisfied in order to determine the as-yet unknown constants C_1 and C_2. Writing for $t = 0$ and taking into consideration

$$\frac{4}{\pi}\sum_{n=0}^{\infty}\frac{\left(-1\right)^n}{2n+1}\cos\left(\lambda_n z\right) = 1 \tag{5.1.45}$$

one obtains two algebraic equations for the unknown constants

$$T_{i0} = \beta C_1 + C_2 \tag{5.1.46}$$

$$T_{e0} = \beta C_1 - f_v C_2 \tag{5.1.47}$$

of which the solution is

$$C_1 = \frac{f_v T_{i0} + T_{e0}}{\beta\left(f_v + 1\right)} \tag{5.1.48}$$

$$C_2 = \frac{T_{i0} - T_{e0}}{f_v + 1} \tag{5.1.49}$$

Inserting 5.1.48–5.1.49 into 5.1.43–5.1.44 and simplifying gives the final analytical solution of the thermal dual-porosity model,

$$T_i\left(z,t\right)=\frac{4}{\pi}\left(\frac{f_vT_{i0}+T_{e0}}{f_v+1}+\frac{T_{i0}-T_{e0}}{f_v+1}e^{-\beta(1+f_v)t}\right)\sum_{n=0}^{\infty}\frac{\left(-1\right)^n}{2n+1}\cos\left(\lambda_n z\right)e^{-\lambda_n{}^2\alpha t} \tag{5.1.50}$$

$$T_e\left(z,t\right)=\frac{4}{\pi}\left(\frac{f_vT_{i0}+T_{e0}}{f_v+1}-\frac{f_v\left(T_{i0}-T_{e0}\right)}{f_v+1}e^{-\beta(1+f_v)t}\right)\sum_{n=0}^{\infty}\frac{\left(-1\right)^n}{2n+1}\cos\left(\lambda_n z\right)e^{-\lambda_n{}^2\alpha t} \tag{5.1.51}$$

This solution is instructive. The expression in parentheses is particularly interesting to examine in some detail, while the Fourier cosine series member introduces the spatial dependence and has been discussed previously during the mass transport analysis (see Paper III in example). The first additive member in parentheses is a volume-weighed or averaged contribution of temperatures to the intrinsic temperature of each respective space. For the particular case of F = 0.5, f_v = 1, and this factor degenerates to an arithmetic mean. The second additive member in parentheses is the contribution of the transmembrane heat exchange to the temperature of the intra-/extracellular space. It is clearly identically equal to 0 in case $T_{i0} = T_{e0}$. As previously mentioned and foreseen, this reflects the equal rate of heat transfer in each space. In absence of any initial thermal gradient that would have resulted from non-equal initial temperatures, equal thermal conductivity cannot possibly result in a thermal gradient necessary for transmembrane heat exchange. This case has predictable results that are not of interest to further analysis.

The following Figure 5.2 gives the thermal profiles in the extracellular space for several different values of the transmembrane volumetric heat transfer coefficient h_v. To facilitate an easier comparison by display of simulated results, the following Figure 5.3 presents a plot of $T_i(z = 0, t)$ and $T_e(z = 0, t)$ for different values of h_v. The presented curves are intrinsic temperature kinetics (time profiles) taken from the centre of the tissue sample where the temperature is the highest. Parameters that were used to obtain these simulated model results with the analytical solution are collected in Table 5.1 with references.

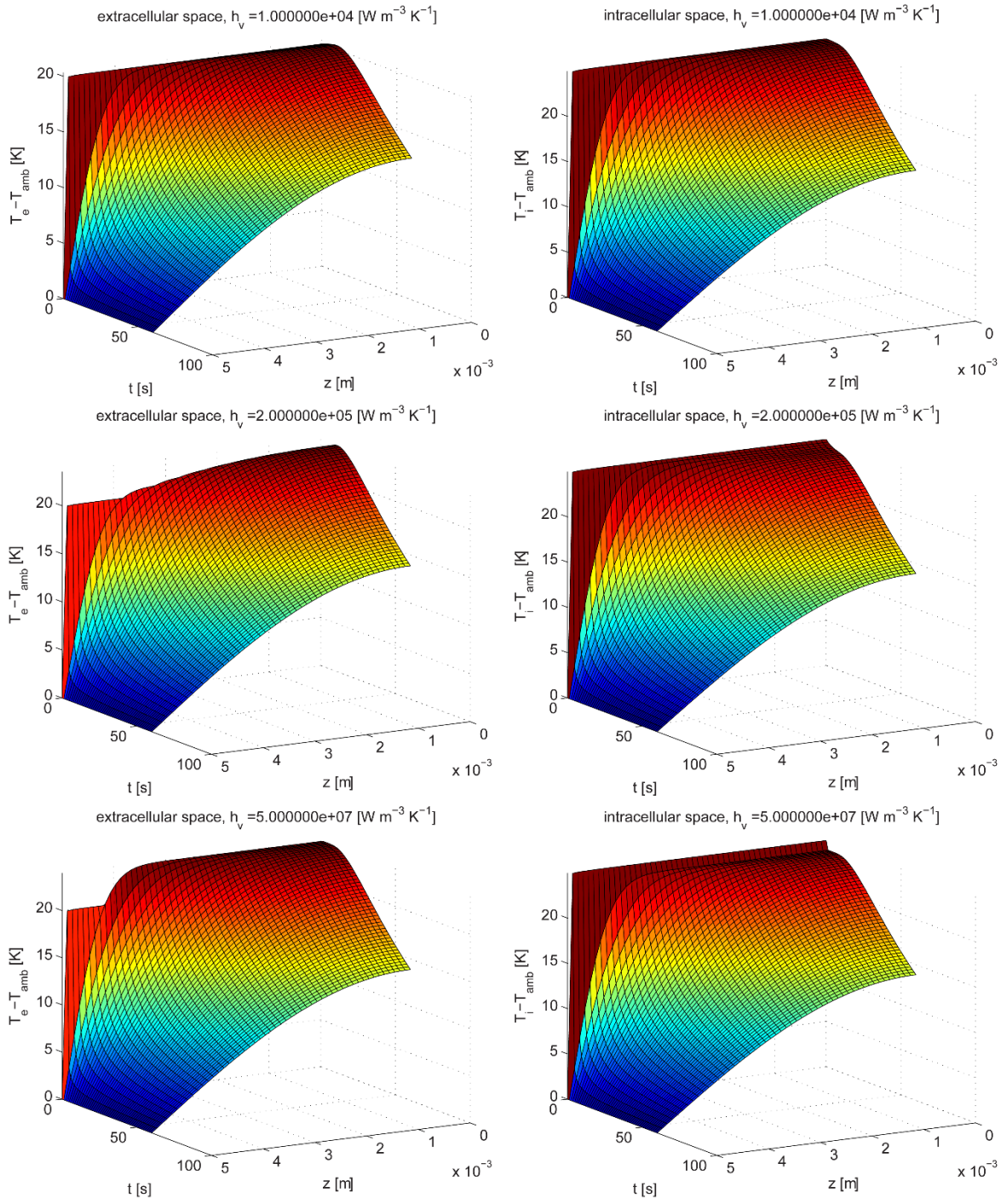

Figure 5.2: The spatio-temporal profiles of the intrinsic temperature in the intra- and extracellular space for three different values of the transmembrane volumetric heat transfer coefficient h_v. The initial temperatures above T_{amb} were T_{i0} = 25 °C and T_{e0} = 20 °C in all cases. Two thousand members of the Fourier cosine series (n = 0…1999) were computed in eqs. 5.1.50–5.1.51 to ensure the artefacts originating from the discontinuity at $z = l/2$ between the initial and the boundary condition are not visible in the surface plots.

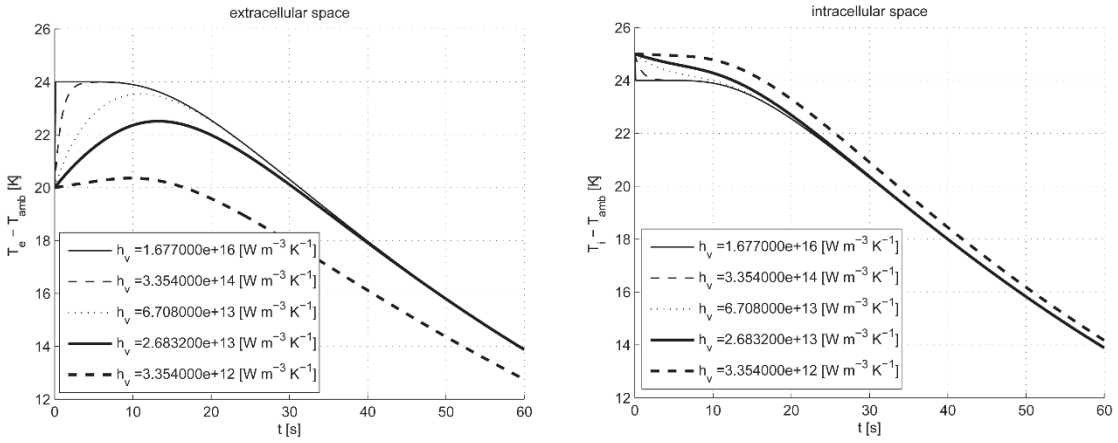

Figure 5.3: The time profiles (kinetics) of the intrinsic temperature in the intra- and extracellular space for five different values of the transmembrane volumetric heat transfer coefficient h_v.

As is shown in Figures 5.2 and 5.3, higher values of the volumetric heat transfer coefficient h_v permit heat transfer from the intracellular space into the extracellular due to the initial difference of 5 K between the two spaces. This transfer can be almost instantaneous (from the point of view of the simulation length, which is 1 minute) for very high values of h_v, or it can be delayed if h_v is not very large. See section 5.1.4 for a discussion on realistic values of this parameter in biological tissues. Note that due to a rather large volume fraction of 0.8 used for these simulated kinetics, the heat transfer from the intracellular to the extracellular space does not result in a large reduction of the intracellular temperature, however, it does result in a proportionally large increase in the extracellular temperature, where f_v is the proportionality factor.

parameter	**value**	**source**	**parameter**	**value**	**source**
l (m)	0.01	previous experiments	ρ (kg/m^3)	1000	water [68]
F (-)	0.80	arbitrarily chosen	c_p (J/kg.K)	4200	water [68], [69]
k (W/m.K)	0.559	apple juice [69]	h_v (W/m^3.K)	*varied*	n/a
t_{end} (s)	60	arbitrarily chosen	δT_{i0} (K)	25	arb. chosen
f_v (-)	4	F/(1-F)	δT_{e0} (K)	20	arb. chosen

Table 5.1: Parameters used in simulations presented in this section.

The value of k chosen to approximate both the intracellular and extracellular thermal conductivity is that of apple juice and will be used again in subsequent analysis. All other parameters were chosen to simulate a possible experimental situation with tissue, except of volume fraction F that was slightly reduced (from about 0.92 found in apples to 0.80) in order to amplify the effect of parameter f_v in figures 5.2 and 5.3. The initial temperatures were chosen arbitrarily

for demonstrative purposes and are not important in terms of kinetics, since the model is linear and the final result can be scaled.

As a final note to this subsection, consider that in the eventual presence of a transmembrane thermal gradient, i.e. a difference between the intracellular and the extracellular temperature (in case the transmembrane heat exchange would be noticeably hindered – see subsection 5.1.4 for a discussion), the bulk tissue temperature as measured in a finite volume ΔV comprising cells and extracellular space would, in relation to the intrinsic quantities worked with herein, equal

$$\left(T_{\text{bulk}}\right)_{\Delta V} = \left[\left(1-F\right)T_e + FT_i\right]_{\Delta V} \tag{5.1.52}$$

5.1.3 The thermal dual-porosity model: A numerical integration scheme for the general case where $k_e \neq k_i$

In case where the difference in thermal conductivities of the spaces comprising bulk material cannot be neglected or one considers these conductivities to differ with the purpose of evaluating and quantifying the consequences of the inhomogeneity on thermal transfer within the material, it is necessary to maintain the thermal dual-porosity model equations in their original form, which is

$$\frac{\partial T_e}{\partial t} = \frac{k_e}{\rho c_p}\frac{\partial^2 T_e}{\partial z^2} + \frac{f_v h_v}{\rho c_p}\left(T_i - T_e\right) \tag{5.1.53}$$

$$\frac{\partial T_i}{\partial t} = \frac{k_i}{\rho c_p}\frac{\partial^2 T_i}{\partial z^2} - \frac{h_v}{\rho c_p}\left(T_i - T_e\right) \tag{5.1.54}$$

As mentioned, this system is not as straightforward to solve as is the simplified system 5.1.8–5.1.9 (see the "5.4 Appendix" section of this chapter). It does, however, readily admit a numerical solution that is stable for a wide range of parameters and suitable for computer evaluation.

One of the possible methods of numerically resolving the system 5.1.53–5.1.54 is the well-known and established Crank-Nicolson implicit method. Using this method, the derivatives in the equation

$$\frac{\partial T}{\partial t} = \alpha\frac{\partial^2 T}{\partial z^2} \tag{5.1.55}$$

can be substituted with finite differences in intervals δt and δz as follows

$$\frac{T_{n,m+1} - T_{n,m}}{\delta t} = \frac{\alpha}{2}\left[\frac{T_{n-1,m+1} - 2T_{n,m+1} + T_{n+1,m+1}}{\left(\delta z\right)^2} + \frac{T_{n-1,m} - 2T_{n,m} + T_{n+1,m}}{\left(\delta z\right)^2}\right] \tag{5.1.56}$$

where index n runs along the spatial, and index m along the temporal coordinate.

Rewriting equation 5.1.53 using 5.1.55, substituting $r = \delta t / (\delta z)^2$, $\alpha_e = k_e/(\rho c_p)$, $\beta = h_v/(\rho c_p)$, and placing all unknowns on the left side while keeping the known variables on the right, one obtains

$$\begin{aligned}&\left(1+\alpha_e r\right)T_{n,m+1}^{(e)} - \frac{\alpha_e r}{2}T_{n-1,m+1}^{(e)} - \frac{\alpha_e r}{2}T_{n+1,m+1}^{(e)} = \\ &= \left(1-\alpha_e r - f_v\beta\delta t\right)T_{n,m}^{(e)} + \frac{\alpha_e r}{2}T_{n-1,m}^{(e)} + \frac{\alpha_e r}{2}T_{n+1,m}^{(e)} + f_v\beta\delta t T_{n,m}^{(i)}\end{aligned} \tag{5.1.57}$$

where indices ‘e’ or ‘i’ in brackets in superscript designate the extracellular or the intracellular temperature, respectively. Note that δt is the time step of discretization, and δz the step of discretization along the spatial coordinate. As an implicit method, the Crank-Nicolson is unconditionally stable regardless of the size of these steps or coefficient α. However, this is only valid for a homogeneous second-order diffusion/heat transfer partial differential equation, such as is given in eq. 5.1.12. Equations 5.1.53 and 5.1.54 contain the so-called *source terms*, and the method for their integration as presented is not unconditionally stable, but depends on the size of $\beta\delta t$. A detailed analysis of conditions for stability, while most suitable for a treatise on the Crank-Nicolson method, would be completely out of scope of this thesis, and is therefore omitted. Note however that a sufficiently small time step δt must be selected, particularly for “large” coefficients β (large in comparison to α) in order for the solution to converge.

Assembling the node temperatures in vectors along the spatial dimension, and writing in matrix form, this can be more conveniently represented as

$$\mathbf{P}_e\mathbf{T}_{m+1}^{(e)} = \mathbf{Q}_e\mathbf{T}_m^{(e)} + f_v\beta\delta t\mathbf{T}_m^{(i)} \tag{5.1.58}$$

where

$$\mathbf{P}_e = \begin{pmatrix} 1+\alpha_e r & -\alpha_e r & 0 & \cdots & 0 \\ -\frac{\alpha_e r}{2} & 1+\alpha_e r & -\frac{\alpha_e r}{2} & 0 & \vdots \\ 0 & \ddots & \ddots & \ddots & 0 \\ \vdots & 0 & -\frac{\alpha_e r}{2} & 1+\alpha_e r & -\frac{\alpha_e r}{2} \\ 0 & \cdots & 0 & 0 & 1 \end{pmatrix} \tag{5.1.59}$$

and

$$\mathbf{Q}_e = \begin{pmatrix} 1-\alpha_e r - f_v\beta\delta t & \alpha_e r & 0 & \cdots & 0 \\ \frac{\alpha_e r}{2} & 1-\alpha_e r - f_v\beta\delta t & \frac{\alpha_e r}{2} & 0 & \vdots \\ 0 & \ddots & \ddots & \ddots & 0 \\ \vdots & 0 & \frac{\alpha_e r}{2} & 1-\alpha_e r - f_v\beta\delta t & \frac{\alpha_e r}{2} \\ 0 & \cdots & 0 & 0 & 1 \end{pmatrix} \tag{5.1.60}$$

Note that the homogeneous Dirichlet boundary condition 5.1.17 at $z = l/2$ demands that the final element of the bottom row in matrices $\mathbf{P}_e$ and $\mathbf{Q}_e$ equals 1, while all other elements of this row are equal 0 (fixed temperature). Similarly, the homogeneous Neumann boundary condition 5.1.18 at $z = 0$ demands that the element $\mathbf{P}_e(1,2) = -\alpha_e r$ and the element $\mathbf{Q}_e(1,2) = \alpha_e r$ (reflective boundary). For the Dirichlet boundary at $z = l/2$, it is necessary to set the last element of the vector on the right-hand side of 5.1.58, i.e. of $\mathbf{Q}_e\mathbf{T}_m^{(e)} + f_v\beta\delta t\mathbf{T}_m^{(e)}$, to zero at every consecutive time step (i.e. for all $k > 0$). As mentioned, this last element corresponds to $z = l/2$ where the sample is kept at the ambient temperature and thus the relative temperature difference here is 0.

For the intracellular space, discretizing eq. 5.1.54 according to the Crank-Nicolson formula leads to slightly modified matrices and, following the same procedure as for the extracellular space, it is possible to write

$$\begin{aligned}&\left(1+\alpha_i r\right)T_{n,m+1}^{(i)} - \frac{\alpha_i r}{2}T_{n-1,m+1}^{(i)} - \frac{\alpha_i r}{2}T_{n+1,m+1}^{(i)} = \\ &= \left(1-\alpha_i r-\beta\delta t\right)T_{n,m}^{(i)} + \frac{\alpha_i r}{2}T_{n-1,m}^{(i)} + \frac{\alpha_i r}{2}T_{n+1,m}^{(i)} + \beta\delta t T_{n,m}^{(e)}\end{aligned} \tag{5.1.61}$$

where, as before, indices ‘e’ or ‘i’ in brackets in superscript designate the extracellular or the intracellular temperature, respectively, and $\alpha_i = k_i/(\rho c_p)$ was introduced for the sake of algebra.

In matrix notation, as before,

$$\mathbf{P}_i\mathbf{T}_{m+1}^{(i)} = \mathbf{Q}_i\mathbf{T}_m^{(i)} + \beta\delta t\mathbf{T}_m^{(e)} \tag{5.1.62}$$

where

$$\mathbf{P}_i = \begin{pmatrix} 1+\alpha_i r & -\alpha_i r & 0 & \cdots & 0 \\ -\frac{\alpha_i r}{2} & 1+\alpha_i r & -\frac{\alpha_i r}{2} & 0 & \vdots \\ 0 & \ddots & \ddots & \ddots & 0 \\ \vdots & 0 & -\frac{\alpha_i r}{2} & 1+\alpha_i r & -\frac{\alpha_i r}{2} \\ 0 & \cdots & 0 & 0 & 1 \end{pmatrix} \tag{5.1.63}$$

and

$$\mathbf{Q}_i = \begin{pmatrix} 1-\alpha_i r-\beta\delta t & \alpha_i r & 0 & \cdots & 0 \\ \frac{\alpha_i r}{2} & 1-\alpha_i r-\beta\delta t & \frac{\alpha_i r}{2} & 0 & \vdots \\ 0 & \ddots & \ddots & \ddots & 0 \\ \vdots & 0 & \frac{\alpha_i r}{2} & 1-\alpha_i r-\beta\delta t & \frac{\alpha_i r}{2} \\ 0 & \cdots & 0 & 0 & 1 \end{pmatrix} \tag{5.1.64}$$

The algorithm for obtaining the temperature profiles in the extracellular and intracellular space for all z in the next time step for all times t until the end of the simulation, can now be given as

1. Calculate $\mathbf{b}_{m+1}^{(e)} = \mathbf{Q}_e \mathbf{T}_m^{(e)} + f_v \beta \delta t \mathbf{T}_m^{(i)}$
2. Set $\mathbf{b}_{m+1}^{(e)}(n_{\max}) = 0$
3. Calculate $\mathbf{T}_{m+1}^{(e)} = \mathbf{P}_e^{-1} \mathbf{b}_{m+1}^{(e)}$ (by left division $\mathbf{T} = \mathbf{P} \backslash \mathbf{b}$, inverting matrix $\mathbf{P}$ is unnecessary)
4. Calculate $\mathbf{b}_{m+1}^{(i)} = \mathbf{Q}_i \mathbf{T}_m^{(i)} + \beta \delta t \mathbf{T}_m^{(e)}$
5. Set $\mathbf{b}_{m+1}^{(i)}(n_{\max}) = 0$
6. Calculate $\mathbf{T}_{m+1}^{(e)} = \mathbf{P}_e^{-1} \mathbf{b}_{m+1}^{(e)}$ (by left division $\mathbf{T} = \mathbf{P} \backslash \mathbf{b}$, inverting matrix $\mathbf{P}$ is unnecessary)

The sequence of steps 1–6 must be repeated until the spatial profiles for the unknown temperatures are obtained for all time steps m. For $m = 1$, i.e. the first step, vectors $\mathbf{T}_m$ are the respective initial conditions in the intra-/extracellular space. These can be constant as seen throughout this chapter, or arbitrary functions of the spatial coordinate to account for inhomogeneities or sources/sinks of thermal energy in the most general case. The numerical solution is therefore more general and easier to manipulate than the analytical.

Figure 5.4 below gives a comparison between model results for the extra- and intracellular space using the same parameters as used for subplots presented in Figure 5.2 (middle example), where the solution was obtained analytically. To calculate the temperature distribution Figure 5.4b with the numerical method, k_e was set to equal k_i, since the analytical solution does not admit $k_e \neq k_i$. Figure 5.4c gives the difference between the numerical and analytical solution, and can be considered to represent the error of the numerical solution. The error is the greatest near the surface of the tissue sample, and only for the initial time steps. This is due to the discontinuity at $z = l/2$ where the initial condition demands that $T = T_0$, while the boundary condition immediately sets $T = 0$. Elsewhere, the maximal error is between about 10-7 and 10-5 on most of the z-t plane.

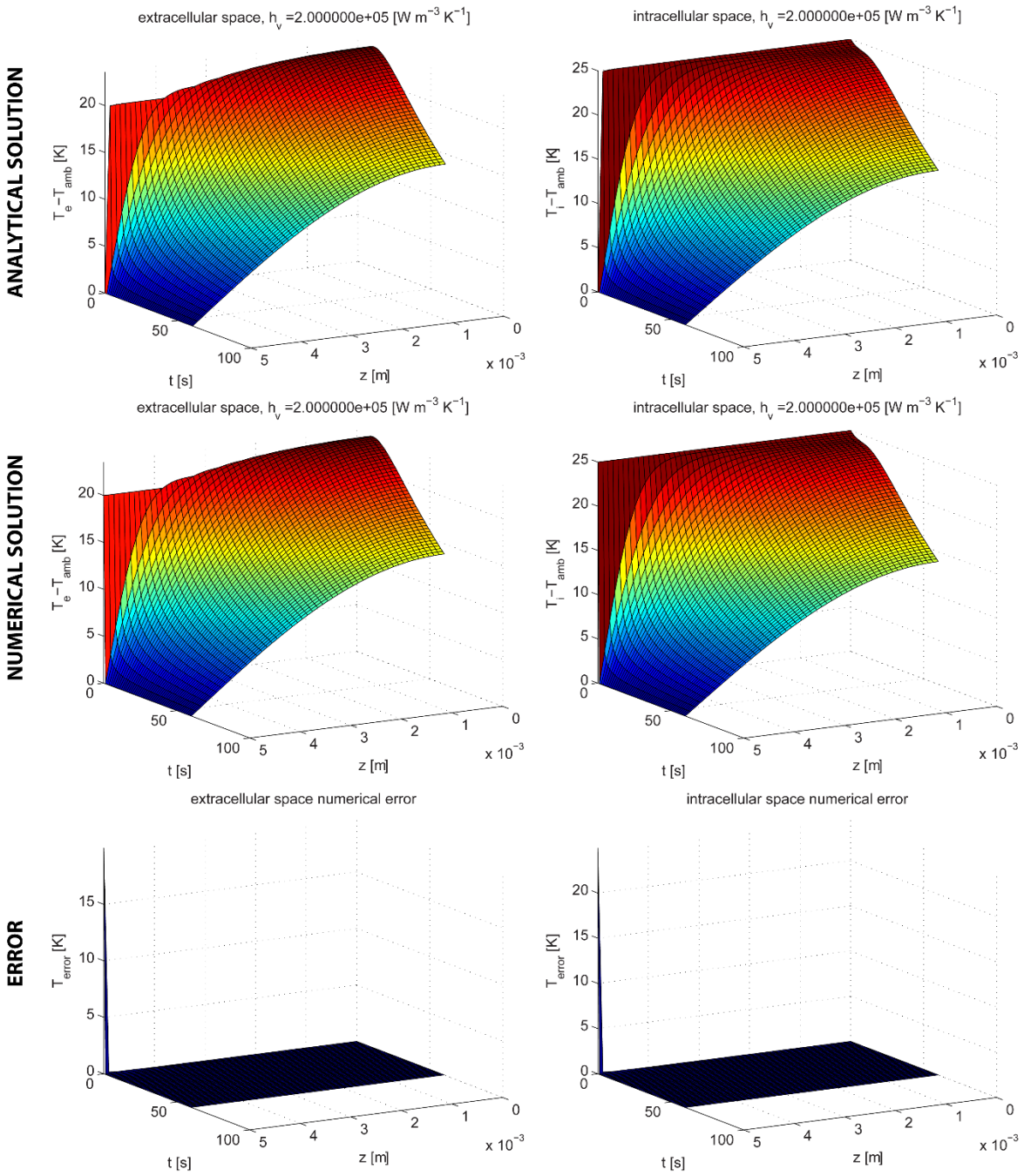

Figure 5.4: Comparison of the analytical and numerical solution for evaluation of the accuracy of the numerical solution.

The numerical solution that was just presented is a suitable method of evaluating thermal conduction in a multi-phase material (e.g. a two-component or two-space model of biological tissue) whether there is a significant influence of the interspace interface conduction hindrance or not. The importance of the latter for biological tissues will be examined in the following section on parameter estimation, shedding light on the fundamental quandary – the as yet uncertain applicability of the dual-porosity approach and its usefulness in studying thermal relations in tissues, as opposed to a much simpler homogeneous material model.

5.1.4 A theoretical estimation of the volumetric heat transfer coefficient h_v and other parameters; the relevance of the dual-porosity model for the thermal problem in electroporated tissues

The parameter h_v, called the volumetric heat transfer coefficient, relates the temperature difference across the interface (e.g. a membrane) separating the continuous phase (e.g. extracellular space) and the discontinuous phase (e.g. intracellular space), with the resulting local heat generation or dissipation in the respective phases or spaces. Given the medium density and specific heat capacity, this causes a local increase or decrease in temperature, as described by eqs. 5.1.3–5.1.4.

To arrive at an estimate for h_v in the particular case of biological tissue comprising cells with biological membranes, the following two paths leading to the same conclusion can be taken.

First, consider the Fourier law of thermal conduction in its differential form with thermal transfer occurring only along one spatial dimension. Writing for the membrane (index *m*) and in a spherical coordinate system, it reads

$$\dot{q}_m = -k_m \frac{dT}{dr} \tag{5.1.65}$$

Integrating across the membrane where the heat flux density q_m is non-zero and the temperature changes from intracellular $T_{i,m}$ to the extracellular $T_{e,m}$ in the immediate proximity to the membrane (denoted by index *m*), yields

$$\dot{q}_m \int_R^{R+d_m} dr = -k_m \int_{T_{i,m}}^{T_{e,m}} dT \tag{5.1.66}$$

Resolving the integrals results in

$$\dot{q}_m = \frac{k_m \left(T_{i,m} - T_{e,m}\right)}{d_m} \tag{5.1.67}$$

where d_m is the membrane thickness (about 4-5 nm).

The expressed heat flux density is in W m^{-2}, and the source term in the dual-porosity model fundamental equations is in W.m^{-3}. It is necessary thus to express the heat flux per unit volume, q_v, and the expression involves the particular problem geometry

$$\dot{q}_v = a_v \dot{q}_m = a_v h\left(T_{i,m} - T_{e,m}\right) = h_v \left(T_{i,m} - T_{e,m}\right) \tag{5.1.68}$$

where h is the heat transfer coefficient [W/m^2K], h_v the volumetric heat transfer coefficient [W/m^3K], and a_v the surface-to-volume ratio reflecting the particular geometry. In case of spherical cells of radius R, this coefficient equals

$$a_v = \frac{A_c}{V_c} = \frac{4\pi R^2}{\frac{4\pi R^3}{3}} = \frac{3}{R} \tag{5.1.69}$$

and therefore

$$\dot{q}_v = a_v \dot{q}_m = \frac{3k_m\left(T_{i,m} - T_{e,m}\right)}{d_m R} = h_v\left(T_{i,m} - T_{e,m}\right) \tag{5.1.70}$$

from where it immediately follows

$$h_v = \frac{3k_m}{d_m R} \tag{5.1.71}$$

Second, consider the Fourier law of thermal conduction in the differential form, but written for the amount of heat transferred across the membrane per unit time Q_m, not for flux q_m

$$\dot{Q}_m = -k_m 4\pi r^2 \frac{dT}{dr} \tag{5.1.72}$$

Separating the variables left/right and integrating as before yields, after some rearrangement

$$\dot{Q}_m = \frac{4\pi k_m\left(T_{i,m} - T_{e,m}\right)}{\frac{1}{R} - \frac{1}{R + d_m}} = \frac{4\pi k_m\left(T_{i,m} - T_{e,m}\right)}{\frac{d_m}{R\left(R + d_m\right)}} = \frac{4\pi R\left(R + d_m\right)k_m\left(T_{i,m} - T_{e,m}\right)}{d_m} \tag{5.1.73}$$

For $R >> d_m$, one can take the approximation $R + d_m \approx R$ and the equation 5.1.73 simplifies to

$$\dot{Q}_m = \frac{4\pi R^2 k_m\left(T_{i,m} - T_{e,m}\right)}{d_m} \tag{5.1.74}$$

The simplification step $R + d_m \approx R$ also exists in the first approach that was presented above, however it is implicit and hidden in the eq. 5.1.69, or more precisely, already in 5.1.68. For R approximately equal or on the same order of magnitude as d_m, a more complex expression than 5.1.69 must be used. This was already discussed in this thesis; see Paper III, Appendix A section, equation A.7 for example.

Expressing the amount of heat transferred across the membrane Q_m per unit volume, a division with the cell volume V_c is needed to arrive at

$$\dot{q}_v = \frac{\dot{Q}_m}{V_c} = \frac{4\pi R^2 k_m\left(T_{i,m} - T_{e,m}\right)}{\frac{4\pi R^3}{3} d_m} = \frac{3k_m\left(T_{i,m} - T_{e,m}\right)}{d_m R} = h_v\left(T_{i,m} - T_{e,m}\right) \tag{5.1.75}$$

which is exactly 5.1.70 and h_v can be expressed again to equal what has already been defined by eq. 5.1.71.

Given a known estimate on the cell size and membrane thickness, the parameter missing in order to obtain h_v is only the transmembrane thermal conductivity, k_m. Since the biological cell

membrane is composed of a lipid bilayer, it is expected that its thermal conductivity will be lower than that of cytoplasm and certainly lower than that of bulk water. Molecular dynamics simulations can be used to arrive at an estimate for k_m. In example, authors of [52] report the thermal resistance of the water-lipid bilayer-water system of thickness 40 Å to be 9.3 10^{-9} m^2K/W. Since the thermal resistance equals

$$R_t = \frac{x}{k} \tag{5.1.76}$$

where x is the thickness of the resistive layer, k can be recovered from 5.1.76, and for the reported thermal resistance value of 9.3 10^{-9} m^2K/W, k_m is estimated to equal 0.430 W/m.K. This is about 71 % of the thermal conductivity of bulk water, which is indeed higher, as assumed.

For the volumetric heat transfer coefficient of a biological cell of radius 100 μm (e.g. apple fruit cells) and membrane thickness of 5 nm, this yields

$$h_v = \frac{3k_m}{d_m R} = \frac{3 \cdot 0.430}{5 \cdot 10^{-9} \cdot 100 \cdot 10^{-6}} = 2.58 \cdot 10^{12} \frac{\mathrm{W}}{\mathrm{m}^3\mathrm{K}} \tag{5.1.77}$$

The value thus obtained is extremely high, however, this is to be expected. The entire cell area is available for thermal exchange, as opposed to the opposite seen in the mass transfer problems, where only a small fraction on the order of about 10^{-7} to 10^{-4} of the cell membrane area was available for diffusion or liquid flow. Regardless of this consideration, the volumetric heat transfer coefficient is still unrealistically high, since it has been derived for an idealized system of cell-membrane-extracellular space, where the finite thermal resistances of the intracellular and extracellular media do not play any significant role. This was a valid assumption in case of mass transport across a permeabilized membrane (Papers II – IV), since there, the membrane was the single most important component of the system greatly hindering the transport of mass between the two spaces. In the thermal problem, the thermal conductivity of the membrane is within the same order of magnitude as that of bulk water and thus the cytoplasm, probably also of the extracellular space (the permeability of which will be evaluated in the following text). Moreover, the thickness of the plasma membrane is several orders of magnitude (3 to 4) lower than the cell radius.

Before the finite thermal conductivity of the cell membrane and its influence are wholly discarded as unimportant, a more realistic estimate of h_v can be obtained and re-evaluated in relation to the intra-/extracellular thermal conductivities and its influence simulated using the dual-porosity model. Only then should any final conclusions be drawn.

Given a finite thermal conductivity/resistance of both the intra- and the extracellular space, the amount of heat transferred across the membrane will be much lower than what would be calculated according to eq. 5.1.74. This equation would hold in the particular case where the membrane

thermal resistance would be so high so as to render the finite conductivities on either side of the membrane apparently infinite. This can be further illustrated by noting an apparent absence of any thermal gradients on either side of the membrane, which would mean that $T_i = T_{i,m}$ and $T_e = T_{e,m}$ anywhere in tissue, a situation schematically presented in Figure 5.5-left, where the temperature profile at the plasma membrane is drawn in idealised conditions where $k_m << k_i$ and $k_m << k_e$. A more realistic situation ($k_m \approx k_i \approx k_e$) is illustrated by Figure 5.5-right.

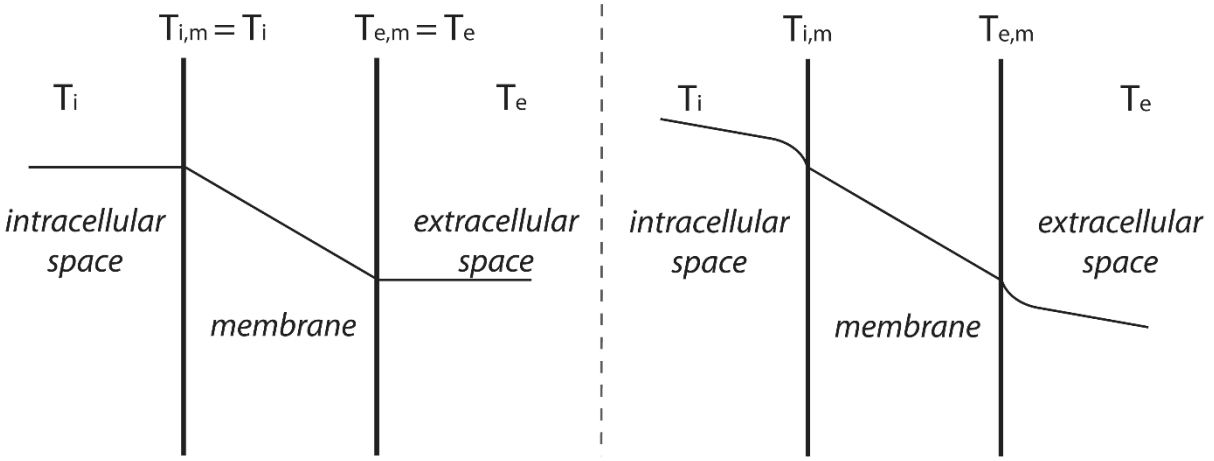

Figure 5.5: A schematic illustration of the thermal situation near the membrane for the idealised situation (left) and a more realistic situation reflecting the influence of finite thermal conductivities of the spaces on either side of the membrane (right).

The amount of heat transferred across the membrane per unit time is, considering that $k_m \approx k_i \approx k_e$,

$$\dot{Q}_m = \frac{A_c\left(T_i - T_e\right)}{\left(\frac{1}{h_i} + \frac{d_m}{k_m} + \frac{1}{h_e}\right)} \tag{5.1.78}$$

since thermal resistances are additive. In eq. 5.1.78, $1/h_i$ is the intracellular and $1/h_e$ the extracellular thermal resistance. Following a similar logic as employed during the derivation of the membrane heat transfer coefficient h, one can estimate that h_i equals approximately k_i/R, where R is the radius of an average cell in tissue, and k_i the intracellular thermal conductivity. It is difficult to arrive similarly at a theoretical estimate for h_e, but as a first approximation, it can be considered equal to the intracellular, in particular in systems where $k_i \approx k_e$, which should be a reasonable assumption for biological tissues (this will be re-examined in continuation). This results in

$$\dot{Q}_m = \frac{A_c\left(T_i - T_e\right)}{\left(2\frac{R}{k_i} + \frac{d_m}{k_m}\right)} \cong \frac{A_c k_i\left(T_i - T_e\right)}{2R} \tag{5.1.79}$$

which is an approximation, since for $k_m \approx k_i$ the term d_m/k_m is insignificant in comparison to R/k_i. From eq. 5.1.79 it is evident that the influence of the membrane on the transmembrane transport has completely vanished, and according to the assumptions made, the transmembrane heat transfer rate will be governed by the intra- and/or extracellular thermal conductivity (depending on which of these is lower) and the geometric relations of the system, and not by the membrane.

Dividing Q_m with volume of a cell gives the new heat flux per unit volume

$$\dot{q}_m = \frac{\dot{Q}_m}{V_c} = \frac{A_c k_i \left(T_i - T_e\right)}{2RV_c} = \frac{3k_i \left(T_i - T_e\right)}{2R^2} \tag{5.1.80}$$

and the new volumetric heat transfer coefficient equals

$$h_v = \frac{3k_i}{2R^2} = \frac{3 \cdot 0.559}{2\left(100 \cdot 10^{-6}\right)^2} = 8.385 \cdot 10^7 \, \frac{\mathrm{W}}{\mathrm{m^3 K}} \tag{5.1.81}$$

which is more realistic, however, still larger than the largest value used in simulations using the analytical solution (see Figure 5.2 and Figure 5.3). The conclusion that can be drawn from this, based on the observed behaviour of the temperatures in Figure 5.3 for values of h_v greater than 10^6, is that any cross-membrane thermal gradient that would result from inhomogeneities in local electric field or current distribution, would be instantaneously (i.e. on a sub-second timescale) annihilated due to the rapid thermal transfer across the membrane.

This finding should not lead to the conclusion that the dual-porosity thermal model is unnecessarily complicated with the source term, since in this most general form the analysis is instructive, and all the mathematical derivations and analysis presented herein can be used to further advance the state of the art of the mass transport analogues of the dual-porosity model. Moreover, the numerical solution allowing the thermal conductivities intra- and extracellularly to differ might still be relevant for studying thermal relations in tissue, whether electroporated or not, if the thermal conductivities differ significantly. The extremely fast transmembrane thermal transfer does however mean that the analytical solution which does not admit $k_i \neq k_e$ is of limited use, at least in the thermal dual-porosity model, since if no intra-to-extracellular thermal gradients can be observed on the timescale of seconds, initial differences in temperature cannot come into existence ($T_{i0} = T_{e0}$ for all t) resulting in exactly equal thermal kinetics in both spaces according to the model.

In order to evaluate whether the general formulation of the model can still be useful in cases where $k_i \neq k_e$ and there is a marked difference in these conductivities, a sample study with estimated realistic values of parameters is presented for the case of apple tissue, using the numerical solution as presented in subsection 5.1.3 to obtain the results.

For apple tissue, tabulated data can be found in literature [69], giving the bulk tissue thermal conductivity at room temperature of about 0.418 W/m.K, and that of apple juice is 0.559 W/m.K (this value was already used in the sample study in subsections 5.1.2–5.1.3 as the intracellular thermal conductivity). There is no reliable data on estimates for the extracellular thermal conductivity, however, using a model of bulk properties of equivalent media such as follow from the modified Maxwell's equivalent medium theory [70], one can suppose that the unknown thermal conductivity can be obtained from the known bulk thermal conductivity and the supposedly known thermal conductivity of the intracellular space, assuming that the latter comprises primarily intracellular juice that can be extracted from the cells and its thermal conductivity independently measured. The extracellular thermal conductivity in apples is presumably much lower than that of the cells, since the juice thermal conductivity is relatively high as compared to apple tissue bulk conductivity. Note that at a higher than 0.5 fraction of cell volume (about 0.75 in apples, see e.g. Paper IV), according to the equivalent medium model, the extracellular thermal conductivity must be considerably lower to result in a difference of 0.141 W/m.K (25 % relative to juice) between the bulk and juice thermal conductivities.

The equivalent medium model for a packed bed of spherical particles constituting the *discontinuous* phase embedded in a matrix (i.e. the *continuous* phase) states [69] that

$$k = k_c \frac{1-\left[1-a\left(k_d / k_c\right)\right]b}{1+\left(a-1\right)b} \tag{5.1.82}$$

where k is the bulk thermal conductivity, k_c the thermal conductivity of the continuous and k_d that of the discontinuous phase, b equals V_d / (V_c + V_d) where V_d and V_c are the volume shares of the discontinuous and the continuous phase, respectively, and a equals $3k_c$ / ($2k_c$ + k_d). Cells in tissue (modelled as perfect spheres) form the discontinuous phase, while the extracellular space is the continuous phase in eq. 5.1.82. Setting k = 0.418 W/m.K, k_d = 0.559 W/m.K, V_d = 0.92, and V_c = 0.08, the unknown that can be expressed from 5.1.82 is k_c, which is determined by the following expression (the expression following from 5.1.82 for k_c is a quadratic function, of its two roots, only the one yielding a positive k_c is relevant)

$$k_c = -\frac{2k+bk-kd-2bkd+\sqrt{8\left(b-1\right)^2 kkd+\left(\left(b+2\right)k-\left(2b+1\right)kd\right)^2}}{4\left(b-1\right)} \tag{5.1.83}$$

with the solution k_c = k_e = 0.174 W/m.K, which is indeed much lower than either the bulk k or k_d (i.e. k_i). The thusly calculated value of k_e is still however almost an order of magnitude greater than thermal conductivity of air, which is (at 20 °C and 1 atm) 0.0257 W/m.K [68]. This is expected, since in intact apple fruit tissue the extracellular space comprises, besides the extracellular matrix structure, pockets of air [71]. These are causing the apple fruit to float rather

than sink in water. The extracellular air, however, is not homogeneously distributed in the continuous phase, and therefore is not predominantly determining its thermal conductivity.

The Table 5.2 below can now be filled with all the necessary data allowing for the numerical study with the dual-porosity model to be carried out and presented. The results (spatio-temporal distribution of temperature) for the two spaces (i.e. intra- and extracellular space) are given in Figure 5.6.

parameter	**value**	**source**	**parameter**	**value**	**source**
l (m)	0.01	previous experiments	ρ (kg/m)	1000	water [68]
F (-)	0.92	previous works (see P. IV)	c_p (J/kg.K)	4200	water [68, 69]
k_i (W/m.K)	0.559	apple juice [69]	k_m (W/m.K)	0.430	[52]
k_e (W/m.K)	0.174	estimated based on [69]	h_v (W/m^3.K)	$8.385 \cdot 10^7$	n/a
t_{end} (s)	60	arbitrarily chosen	δT_{i0} (K)	20	arb. chosen
f_v (-)	11.5	$F/(1-F)$	δT_{e0} (K)	20	arb. chosen
R (μm)	100	previous works (see P. IV)	d_m (nm)	5	[72]

Table 5.2: Parameters used in simulations presented in this section and in some of the theoretical derivations.

The theoretical experiment (simulation) whose results are given in Figure 5.6 represents a simulation whereby an apple fruit sample of 1 cm thickness and much larger in the other two dimensions (to assure that the bulk of the thermal flow is only along one axis) is heated (by the electric current during electroporation or otherwise) for 20 °C and then left to rapidly cool (via the electrodes at the boundary surfaces, for example). As the given figure illustrates (Figure 5.6-left column), there is no detectable difference between the intra- and the extracellular temperature for such high values of h_v as realistically calculated for apple fruit cells. The theoretical simulated cell would have to be about 20-times larger (see Figure 5.6-right column) in order for a considerable temperature gradient to be established across the cell membrane due to the finite membrane thermal conductivity.

All of the preceding theoretical analysis and simulations using realistic model tissue seem to indicate that there is no noticeable influence of the plasma membrane to the heat transfer in tissue *directly* as a result of the membrane's intrinsic thermal permeability. The membrane is simply too thin and the cells too small for the membrane to present a significant thermal insulation boundary between the intra- and the extracellular space. Therefore, electroporation and its effects to the membrane can be safely assumed to have no *direct* consequences to heat (re)distribution in tissue,

at least not on the timescale of seconds following electroporation. However, there still might be undetected effects at the nano level in terms of space and on the micro- to milliseconds timescale during pulse application that the presented study does not explore.

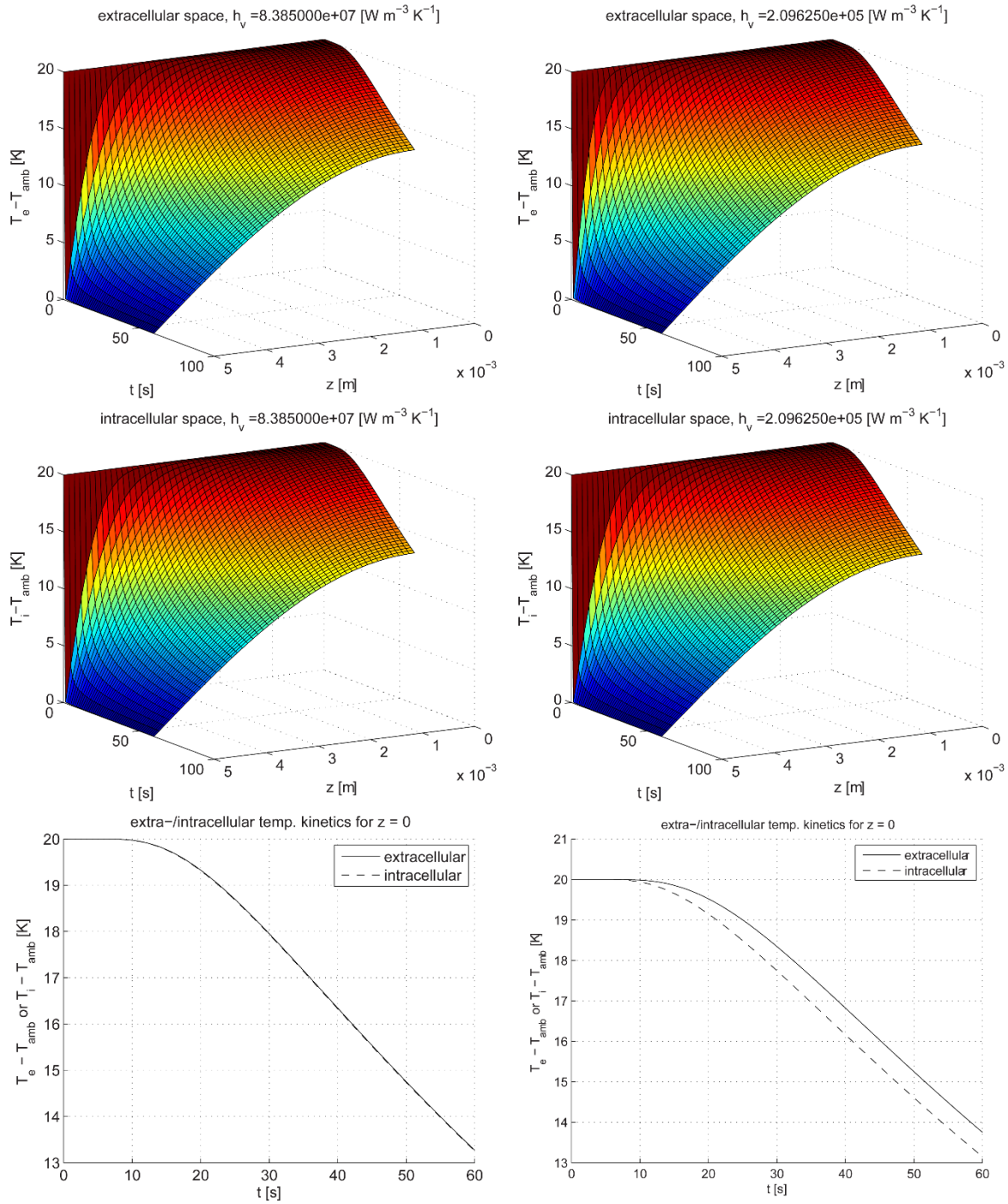

Figure 5.6: The results of the numerical study using the dual-porosity model and parameters as given in Table 5.2. Left column: The volumetric heat transfer coefficient was equal to value given in Table 5.2 (realistic). Right column: The volumetric heat transfer coefficient was reduced by a factor of 400, corresponding to cells 20-times as large as an average apple fruit cell (exaggerated and unrealistic).

It would also be incorrect to assume that electroporation has no effects on thermal relations in electroporated tissue whatsoever, as it is certainly plausible it has at least some *indirect* effects, e.g. via its effect of tissue homogenization, whereby insulated domains (cells) within the connective matrix of low thermal conductivity (air pockets) may become connected due to the release of intracellular liquid. In this respect, it might be interesting to re-examine the dual-porosity model again in more detail to evaluate whether its basic premise of heat being primarily transferred via the intracellular space needs revisi(ti)ng. This may as well be the case, especially in light of the considerably lower thermal conductivity of extracellular space, which is both insulating the cells from one another as well as connecting the individual cells together in a matrix.

5.2 Effects on mass transport: the relation between tissue temperature, diffusion coefficient, and viscosity

The temperature as calculated according to the heat distribution model can be used to calculate the local diffusion coefficient of a solute species and of the liquid viscosity, and thus parameters that figure in the dual-porosity model of mass transfer gain a temporal dependency that can be considered during a simulated mass transport experiment, and the effect of increased temperature to these transport coefficients can by these means be evaluated. This section of chapter 5 is thus dedicated to first finding an appropriate numerical formulation of the mass transport models that will admit spatially and temporally variable temperature-dependent coefficients to be incorporated into the solution. Then, these models are used in combination with the thermal dissipation model (in its classical, not dual-porosity form) to evaluate the influence of a temperature increase on mass transport dynamics.

5.2.1 The dual-porosity model of mass transport and its suitable numerical integration scheme admitting non-constant coefficients

This subsection presents the already reported on in detail and thoroughly discussed models of dual-porosity for the diffusion and pressing problem, the full accounts of which are given in Paper II – Paper IV, however here these models are given in their numerical form. These forms are necessary in order to facilitate coupling of the theoretical heat distribution model with the mass transport models via temperature-dependent coefficients in order to theoretically evaluate the influence of raised temperature in tissue to mass transport for various temperatures in a parametric simulation study to follow.

5.2.1.1 The diffusion problem

The slightly rearranged fundamental equations of the dual-porosity model for the diffusion problem read

$$\frac{\partial c_e(z,t)}{\partial t} = D_{s,e}\frac{\partial^2 c_e(z,t)}{\partial z^2} + f_v k_m\left(c_i(z,t) - c_e(z,t)\right) \tag{5.2.1}$$

$$\frac{\partial c_i(z,t)}{\partial t} = -k_m\left(c_i(z,t) - c_e(z,t)\right) \tag{5.2.2}$$

where k_m here is the transmembrane diffusive flow coefficient, not to be confused with k_m as used throughout the remainder of this chapter to refer to the membrane thermal conductivity coefficient. The appropriate boundary and initial conditions are

$$c_e(t)\big|_{z=l/2} = 0 \tag{5.2.3}$$

$$c_i(t)\big|_{z=l/2} = c_{i0}e^{-k_m t} \tag{5.2.4}$$

$$\left.\frac{\partial c_e(t)}{\partial z}\right|_{z=0} = 0 \tag{5.2.5}$$

$$\left.\frac{\partial c_i(t)}{\partial z}\right|_{z=0} = 0 \tag{5.2.6}$$

$$c_e(z,0) = c_{e0} \tag{5.2.7}$$

$$c_i(z,0) = c_{i0} \tag{5.2.8}$$

Strictly adhering to the fundamental physics background of eq. 5.2.1, if the diffusion coefficient $D_{s,e}$ is not space-invariant, eq. 5.2.1 must be rewritten into

$$\frac{\partial c_e(z,t)}{\partial t} = \frac{\partial}{\partial z}\left(D_{s,e}(z,t)\frac{\partial c_e(z,t)}{\partial z}\right) + f_v k_m\left(c_i(z,t) - c_e(z,t)\right) \tag{5.2.9}$$

which complicates the numerical integration scheme used to calculate c_e.

Using the finite difference approximations of $\partial c/\partial t$ and $\partial c/\partial z$ and the Crank-Nicolson approximation of the temporal derivative by an arithmetic mean of its finite difference representations at the j-th and the (j+1)-th node, it is relatively straightforward (and thus the details are omitted from presentation) to arrive at the finite difference scheme for the extracellular concentration

$$\begin{aligned} &c_{i,j+1}^{(e)} - \frac{r}{4}\left[p_{j+1}c_{i+1,j+1}^{(e)} - q_{j+1}c_{i,j+1}^{(e)} + s_{j+1}c_{i-1,j+1}^{(e)}\right] = \\ &= c_{i,j}^{(e)} + \frac{r}{4}\left[p_j c_{i+1,j}^{(e)} - q_j c_{i,j}^{(e)} + s_j c_{i-1,j}^{(e)}\right] - f_v k_m \delta t c_{i,j}^{(e)} + f_v k_m \delta t c_{i,j}^{(i)} \end{aligned} \tag{5.2.10}$$

where

$$p_j = D_{i,j}^{(s,e)} + D_{i+1,j}^{(s,e)} \tag{5.2.11}$$

$$q_j = D_{i+1,j}^{(s,e)} + 2D_{i,j}^{(s,e)} + D_{i-1,j}^{(s,e)} \tag{5.2.12}$$

$$s_j = D_{i,j}^{(s,e)} + D_{i-1,j}^{(s,e)} \tag{5.2.13}$$

and similarly

$$p_{j+1} = D_{i,j+1}^{(s,e)} + D_{i+1,j+1}^{(s,e)} \tag{5.2.14}$$

$$q_{j+1} = D_{i+1,j+1}^{(s,e)} + 2D_{i,j+1}^{(s,e)} + D_{i-1,j+1}^{(s,e)} \tag{5.2.15}$$

$$s_{j+1} = D_{i,j+1}^{(s,e)} + D_{i-1,j+1}^{(s,e)} \tag{5.2.16}$$

As in subsection 5.1.3 on the numerical solution of the thermal model, this set of eqs. 5.2.10–5.2.16 can be written in matrix form with the appropriate initial and boundary conditions taken into the account. A similar finite differencing scheme can be written for the intracellular concentration, except that in this case due to absence of a spatial derivative from eq. 5.2.2, this scheme is reduced to a simple integration on time and does not necessitate the use of the Crank-Nicolson scheme.

Eqs. 5.2.11–5.2.16 show that the diffusion coefficient must be known in all spatial and temporal nodes from the plane of independent variables (the *z-t* plane), and since the diffusion coefficient is dependent on temperature, the following functional dependence must be known

$$D_{s,\mathrm{e}}\left(z,t\right)=\frac{f_c}{\tau}D_{s,0}\left(T_{e,\delta}\left(z,t\right)+T_{amb}\right) \tag{5.2.17}$$

where f_c is the convection correction factor and τ_e the extracellular matrix pathway tortuosity (temperature independent factors) – for details on these parameters, see Paper II and Paper IV. $D_{\mathrm{s},0}$ is the diffusion coefficient of solute species '*s*' in bulk water.

According to the famous Einstein-Stokes relation [73], the diffusion coefficient in bulk solvent can be (re)calculated from temperature given a known dependence of the solvent viscosity η on temperature

$$D_0\left(T\right)=\frac{kT}{6\pi r\eta\left(T\right)}=C_0\frac{T}{\eta\left(T\right)} \tag{5.2.18}$$

Rather than estimating the diffusion coefficient from solute effective dimensions etc. as demanded by 5.2.18, the diffusion coefficient is normally given in form of tabulated data for various solutes at a given temperature. In example, sucrose at 20°C in water has the diffusion coefficient of about 4.5 10^{-10} m^2/s [74]. This holds for 20 °C i.e. at 293 K, and the viscosity of water at this temperature is 1.002 10^{-3} Pa.s [75]. This permits the determination of constant C_0 from 5.2.18, which equals $C_0 = D_0(293\ \mathrm{K}) \cdot \eta(293\ \mathrm{K}) / 293\ \mathrm{K} = 1.54\ 10^{-15}\ \mathrm{m}^2\mathrm{Pa/K}$. This allows for an immediate recalculation of the diffusion coefficient according to eq. 5.2.18, and several representative values are collected in Table 5.3 below.

T (°C)	10	20	30	40	50	60	70
$D_{\mathrm{s},0}(T)$ ($\mu\mathrm{m}^2/\mathrm{s}$)	333.7	450.3	584.7	737.0	909.4	1100.5	1310.7
η (μPa.s)	1306.9	1002.0	797.5	653.5	547.1	466.6	403.9

Table 5.3: Values of the diffusion coefficient of sucrose in an aqueous solution for different temperatures. Recalculated using relation 5.2.18 and constant $C_0 = 1.54\ 10^{-15}\ \mathrm{m}^2\mathrm{Pa/K}$. The corresponding values of viscosity are given alongside for reference, taken from [75].

From values in Table 5.3 one can calculate that from 10 °C to 70 °C, the diffusion coefficient of sucrose in water increases 4-fold. While this is less than an order of magnitude difference, the diffusion phenomenon is strongly dependent on temperature, since the rate of diffusion $D_{s,e}$ is the most important parameter governing solute extraction kinetics in eq. 5.2.9 if the cellular membranes have been permeabilized to a sufficient degree. The values given in Table 5.3 are used as initial temperatures and the corresponding diffusion coefficients in the parametric study presented in subsection 5.2.2, where the numerical approach to the dual-porosity model of solute diffusion as given in this subsection is used to calculate the $B(t)$ (i.e. normalized Brix) dependence for various initial temperatures of tissue.

Note that the parameter $D_{s,0}$ is also one of the multiplicative factors determining the transmembrane diffusive flow coefficient k_m, according to eq. 15 presented in Paper IV. Since this parameter is not subject to the spatial derivative, it is much easier to incorporate it into the numerical solution than is the term $D_{s,e}$, and the issue is not considered further, although the temperature dependence of k_m was taken into the account during the parametric study as presented in continuation (see Figure 5.7).

In order to calculate $D_0(T)$, which is a spatio-temporal function, i.e. $D_0(T(z, t))$, according to eq. 5.2.18 the temperature-dependant viscosity $\eta(T(z, t))$ needs to be determined first. Tabulated data for viscosity such as given in Table 5.3 can be used in order to obtain a polynomial that can aid in obtaining a high fidelity estimate of viscosity for any temperature within the range of temperatures for which the polynomial fit was calculated. Using the MATLAB (MathWorks, Inc.) function *polyval* and the data in Table 5.3, one can obtain a fifth-degree polynomial in the form

$$\eta(T) = -1.129\hat{T}^5 - 3.528\hat{T}^4 + 13.006\hat{T}^3 - 23.943\hat{T}^2 + 83.598\hat{T} - 265.818\hat{T} + 654.000 \qquad (5.2.19)$$

where $\hat{T}$ is the scaled and centered temperature. Scaling and centering transformation improves the numerical properties of the polynomial and the fitting algorithm. For the above eq. 5.2.19, the transformed temperature that can be used to calculate an arbitrary viscosity of water in range of 10 °C to 70 °C is obtained according to the following formula

$$\hat{T} = \frac{T - 313.0000}{21.6025} \qquad (5.2.20)$$

An additional note on the use of the numerical solution 5.2.10–5.2.16. Given a known temperature distribution in the extracellular space, which is equal to the general distribution of temperature in tissue since both the intra- and the extracellular temperatures were previously shown not to differ significantly, this temperature distribution can be expressed analytically and is equal to

$$T_{e,\delta}(z,t) = \frac{4\delta T_{e0}}{\pi} \sum_{n=0}^{\infty} \frac{(-1)^n}{2n+1} \cos\left(\frac{2n+1}{l} z\right) \exp\left(-\left(\frac{2n+1}{l}\right)^2 \frac{k_e}{\rho c_p} t\right) \tag{5.2.21}$$

which can be directly inserted into eq. 5.2.18 and then $D_{s,0}$ into 5.2.17 to obtain values for the diffusion coefficient $D_{s,e}(z, t)$. These values can then immediately be used in the numerical integration scheme 5.2.10–5.2.16. Note that in eqs. 5.2.17 and 5.2.21, the δ-notation was reintroduced into the equations, which was omitted throughout model derivations, in order to emphasize that for determining the diffusion coefficient, absolute values and not only relative increases/decreases are necessary. In example, for a δT_{e0} of 15 °C, the diffusion coefficient that is sought is the coefficient calculated for 35 °C, given the ambient temperature of 20 °C.

5.2.1.2 The pressing problem

The slightly rearranged fundamental equations of the dual-porosity model for the pressing problem read

$$\frac{\partial p_e(z,t)}{\partial t} = \frac{k_e G_{\varepsilon,e}}{\mu} \frac{\partial^2 p_e(z,t)}{\partial z^2} + \frac{\alpha G_{\varepsilon,e}}{\mu} \left(p_i(z,t) - p_e(z,t)\right) \tag{5.2.22}$$

$$\frac{\partial p_i(z,t)}{\partial t} = -\frac{\alpha G_{\varepsilon,i}}{\mu} \left(p_i(z,t) - p_e(z,t)\right) \tag{5.2.23}$$

The appropriate boundary and initial conditions are

$$p_e(t)\big|_{z=0} = 0 \tag{5.2.24}$$

$$p_i(t)\big|_{z=0} = p_{i0} e^{-\frac{\alpha G_{\varepsilon,e}}{\mu} t} \tag{5.2.25}$$

$$\left.\frac{\partial p_e(t)}{\partial z}\right|_{z=l} = 0 \tag{5.2.26}$$

$$\left.\frac{\partial p_i(t)}{\partial z}\right|_{z=l} = 0 \tag{5.2.27}$$

$$p_e(z,0) = p_{e0} \tag{5.2.28}$$

$$p_i(z,0) = p_{i0} \tag{5.2.29}$$

Strictly adhering to the fundamental physics background of eq. 5.2.22, if the viscosity of liquid η is not space-invariant, eq. 5.2.22 must be rewritten into

$$\frac{\partial p_e(z,t)}{\partial t} = \frac{\partial}{\partial z}\left(\frac{k_e G_{\varepsilon,e}}{\mu} \frac{\partial p_e(z,t)}{\partial z}\right) + \frac{\alpha G_{\varepsilon,e}}{\mu} \left(p_i(z,t) - p_e(z,t)\right) \tag{5.2.30}$$

Using exactly the same approach as with the diffusion problem described in subsection 5.2.1.1, and introducing the following replacements for the sake of algebra

$$\kappa = \frac{k_e G_{\varepsilon,e}}{\mu} \tag{5.2.31}$$

$$\upsilon_e = \frac{\alpha G_{\varepsilon,e}}{\mu} \tag{5.2.32}$$

$$\upsilon_i = \frac{\alpha G_{\varepsilon,i}}{\mu} \tag{5.2.33}$$

leads to the following finite difference Crank-Nicolson scheme for extracellular liquid pressure

$$\begin{aligned} & p_{i,j+1}^{(e)} - \frac{r}{4}\left[\chi_{j+1} p_{i+1,j+1}^{(e)} - \varphi_{j+1} p_{i,j+1}^{(e)} + \vartheta_{j+1} p_{i-1,j+1}^{(e)}\right] = \\ & = p_{i,j}^{(e)} + \frac{r}{4}\left[\chi_j p_{i+1,j}^{(e)} - \varphi_j p_{i,j}^{(e)} + \vartheta_j p_{i-1,j}^{(e)}\right] - \upsilon_e \delta t p_{i,j}^{(e)} + \upsilon_e \delta t p_{i,j}^{(i)} \end{aligned} \tag{5.2.34}$$

where

$$\chi_j = \kappa_{i,j} + \kappa_{i+1,j} \tag{5.2.35}$$

$$\varphi_j = \kappa_{i+1,j} + 2\kappa_{i,j} + \kappa_{i-1,j} \tag{5.2.36}$$

$$\vartheta_j = \kappa_{i,j} + \kappa_{i-1,j} \tag{5.2.37}$$

and similarly

$$\chi_{j+1} = \kappa_{i,j+1} + \kappa_{i+1,j+1} \tag{5.2.38}$$

$$\varphi_{j+1} = \kappa_{i+1,j+1} + 2\kappa_{i,j+1} + \kappa_{i-1,j+1} \tag{5.2.39}$$

$$\vartheta_{j+1} = \kappa_{i,j+1} + \kappa_{i-1,j+1} \tag{5.2.40}$$

As in the case of the diffusion problem, the system of equations 5.2.34–5.2.40 can be written in matrix form with the appropriate initial and boundary conditions taken into the account. A similar finite differencing scheme can also be written for the intracellular liquid pressure, except that in this case due to absence of a spatial derivative from eq. 5.2.23, this scheme is reduced to a simple integration on time and does not necessitate the use of the Crank-Nicolson scheme.

Since the dependence of viscosity on temperature has been treated in full detail in subsection 5.2.1.1 with the diffusion problem, it is omitted from repetition at this point. If temperature and therefore viscosity is known for all *z*, coefficients 5.2.35–5.2.40 can be determined and the finite difference scheme applied successively for all *t* to determine the extra- and intracellular liquid pressure profiles. Integration and scaling to obtain the sample deformation from liquid pressure loss is thereafter a trivial matter, as already presented in detail in Paper III and Paper IV.

5.2.2 Relation between tissue temperature, diffusion coefficient, and viscosity – a parametric simulation study

Using the relation 5.2.19 presented in subsection 5.2.1.1, the thermal distribution in a tissue sample can be estimated for the entire duration of a diffusion or pressing experiment. In this parametric study, the time of observation is limited to the first few minutes of the experiment (in contrast to an hour in diffusion and/or pressing experiments – see Paper II/III/IV). This is due to the rapidly dissipating thermal energy, assuming the tissue sample is heated (by the electric current of electroporation or otherwise) to a temperature above that of the ambient or that of the solution prior to the start of the mass transport experiment/simulation. This thermal energy is rather rapidly dissipated out of the sample tissue block and thus its effects cannot be examined at the same timescales as those of the much slower processes of mass transport. Such an initial temperature increase may however have an important role in mass transport processes immediately after the pre-treatment, i.e. during the first few seconds to minutes. The following parametric study is an attempt at quantifying this influence.

Using the parameters collected in Table 5.4 that follow directly from findings presented in Paper II and Paper IV, simulations using the numerical dual-porosity model for solute diffusion yield results shown in Figure 5.7a, calculated for a range of tissue temperatures between 10 °C and 70 °C. These simulated kinetics take into the account the reduced (for 10 °C) or increased (for all temperatures > 20 °C, absolute ambient temperature was fixed to 20 °C) diffusion coefficient in electroporated tissue. This increase/decrease is relative to the diffusion coefficient value at the temperature of the ambient, which was the value used in all previous works (i.e. 20 °C).

Figure 5.7b on the other hand presents simulation results based on the variable viscosity depending on temperature as evaluated by eq. 5.2.21, and dual-porosity pressing model results were obtained using the numerical solution from subsection 5.2.1.2. The range of temperatures in this case was the same, and parameters are collected in Table 5.5.

parameter	value	source	parameter	value	source
l (m)	0.005	previous experiments	ρ (kg/m^3)	1000	water [68]
F (-)	0.345	Paper IV (apple tissue)	c_p (J/kg.K)	4200	water [68], [69]
k_i (W/m.K)	0.559	apple juice [69]	h_v (W/m^3.K)	-	not used
k_e (W/m.K)	0.174	estimated by eq. 5.1.83	k_m* (1/s)	-	see P. IV, eq. 15
t_{end} (s)	120	arbitrarily chosen	δT_{i0} (K)	*var.*	arb. chosen
f_v (-)	0.527	F/(1-F)	δT_{e0} (K)	*var.*	arb. chosen
d_m (nm)	5	Paper II	f_c (-)	2.5	Paper IV

τ_e (-)	$\pi/2$	Paper II	f_{por} (-)	10^{-6}	Paper IV
r_s/r_p (-)	0.80	Paper II / IV	R_{cell} (μm)	100	[76]

Table 5.4: Parameters used for the parametric study with the dual-porosity model of solute diffusion in an electroporated sample of apple tissue, accounting for variable tissue temperature. Note the lower cell volume fraction F due to electroporation. The simulated experiment is for tissue treated according to Protocol A, with 200 V applied to the electrodes. Full details can be found in Paper IV. *k_m with units 1/s is not thermal conductivity, but the transmembrane diffusive flow coefficient as defined in Paper II/IV.

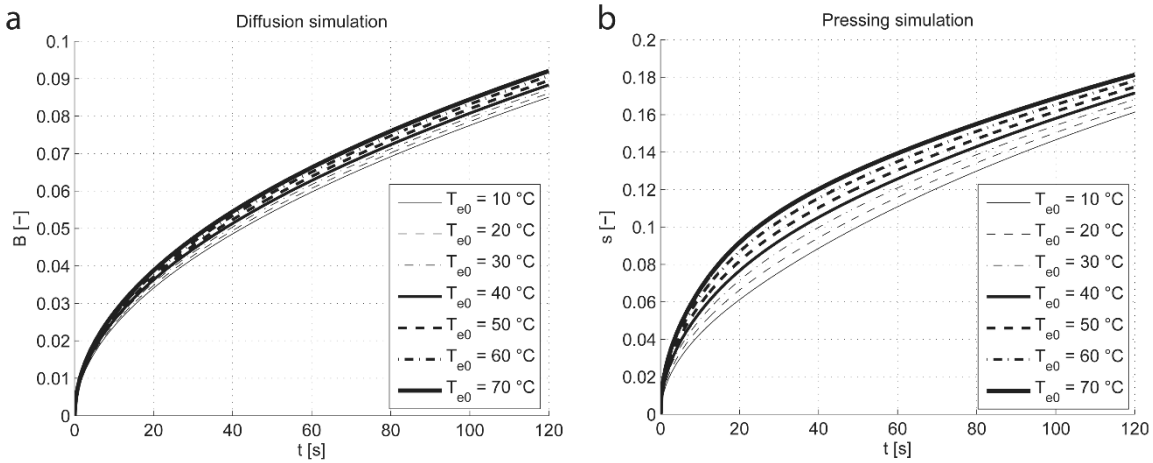

Figure 5.7: The parametric study for electroporated tissue with the dual-porosity models of solute diffusion (a) and pressing (b) illustrating the effect of temperature-dependent parameters of these models (diffusion coefficient, viscosity). Only the diffusion coefficient and/or viscosity were varied to obtain the different kinetics, and these were dependent on the initial temperature increase (the varied parameter). All constant parameters can be found in Table 5.4 and Table 5.5.

parameter	**value**	**source**	**parameter**	**value**	**source**
l (m)	0.005	previous experiments	ρ (kg/m^3)	1000	water [68]
F (-)	0.345	Paper IV (apple tissue)	c_p (J/kg.K)	4200	water [68], [69]
k_i (W/m.K)	0.559	apple juice [69]	h_v (W/m^3.K)	-	not used
k_e (W/m.K)	0.174	estimated by eq. 5.1.83	k_m (1/s)	-	see P. IV eq. 15
t_{end} (s)	120	arbitrarily chosen	δT_{i0} (K)	*var.*	arb. chosen
f_v **(-)	0.527	$F/(1-F)$	δT_{e0} (K)	*var.*	arb. chosen
k_p (m)	$1.25\ 10^{-19}$	Paper III / IV	f_k (-)	2.5	Paper IV
μ (Pa.s)	$f(T_e)$	Function of T_e	f_{por} (-)	$4.8\ 10^{-3}$	Paper IV
P_E (MPa)	0.291	Paper III/IV	R_{cell} (μm)	100	[76]

G_e (Pa)	$11.0\ 10^5$	Paper IV	G_i (Pa)	$9.2\ 10^5$	Paper IV
k_e* (m^2)	$2.25\ 10^{-17}$	Paper IV	α (-)	-	see P. IV eq. 27

Table 5.5: Parameters used for the parametric study with the dual-porosity model of filtration-consolidation (pressing) accounting for variable tissue temperature. Note the lower cell volume fraction F due to electroporation. The simulated experiment is for tissue treated according to Protocol A, with 200 V applied to the electrodes. Full details can be found in Paper IV. *k_e in m^2 is the extracellular hydraulic permeability, not to be confused with k_e in W/m.K, the thermal conductivity of extracellular space. **f_v is not a parameter in the version of the dual-porosity model for pressing as presented in Paper III and Paper IV, and therefore for this parametric study, f_v is only used in temperature distribution calculation.

The results in figure 5.7b clearly demonstrate that during the first two minutes of the simulated pressing experiment, the influence of temperature-dependent viscosity is initially substantial. However, the effect of decreased viscosity subsides rather rapidly as temperature drops and viscosity increases, and the end result after two minutes is a discrepancy of only about 10-15 % as compared to ambient temperature even for the largest initial increase in temperature that was modelled.

Examining the results in Figure 5.7a – the diffusion case – one could conclude that the increased or decreased temperature of the tissue does not have any substantial effect on the rate of diffusion. Nevertheless, it would be too early to dismiss the influence of a temperature increase based only on this particular case. The temperature in the simulation drops rapidly due to the small sample thickness and the model representation of an infinitely powerful heat sink/source that is supposed to surround the sample (either liquid solution or electrodes). In case of pressing experiments where metal electrodes are in contact with the tissue sample at all times, this may be a valid approximation, but in case of the liquid solution in the diffusion example, the finite thermal conductivity of water and its finite quantity cannot be neglected, especially since the tissue bulk thermal conductivity is only slightly below that of bulk water.

For the reasons mentioned above, an important change has to be introduced into the model to account for the finite thermal conductivity in the region exterior to the tissue sample(s). Reconsidering the boundary condition for $z = l/2$, instead of enforcing this boundary condition to 0, one can postulate that the thermal flux entering the interface is equal to the thermal flux exiting the interface (conservation of energy), and is proportional to the temperature difference between tissue and surrounding material (water). The proportionality constant h_s (the tissue-environment

heat transfer coefficient) relates this difference in temperatures with the resulting thermal flux, according to the heat exchange properties of the contact tissue-environment.

The boundary condition defined above can be written as

$$\left.\frac{\partial T_e}{\partial z}\right|_{z=l/2^-} = \left.\frac{\partial T_{amb}}{\partial z}\right|_{z=l/2^+} \cong -h_s\left(T_e - T_{amb}\right) \tag{5.2.41}$$

and indicates that a positive difference $T_e - T_{amb}$, i.e. a higher tissue sample temperature as compared to that of the ambient, will lead to a negative thermal gradient along the normal vector to the sample surface and in direction of increasing z. The thermal gradient depends on the geometrical properties of the system, which is captured by the heat transfer coefficient h_s. The use of eq. 5.2.41 is problematic however, if the surrounding medium is agitated, when there is no thermal gradient in the space outside of the tissue sample. This renders the derivative in eq. 5.2.41 identical to zero at $z = l/2^+$, and the derivative (Neumann) boundary condition degenerates to the condition $T_e = T_{amb}$, which is the original Dirichlet boundary condition one was trying to avoid at the outset.

The above dilemma can easily be resolved by ignoring the flux altogether and considering the energy balance. If one accounts for the finite thermal capacity of the sample-surrounding medium, which is a valid assumption when the tissue/solution mass ratio is low (valid for laboratory and industrial-scale applications where just enough water is added to grated material to make it pumpable through the treatment chamber), the ambient temperature T_{amb} should also be allowed to increase due to heat leaving the tissue particles and heating the surrounding medium. This renders the ambient temperature T_{amb} a function of time, however this is not a problem, since the known thermal distribution in tissue enables precise calculation of the thermal energy dissipated from the sample that was used to heat the environment. One possible approach is thus to determine the total amount of thermal energy leaving the tissue sample by integration, and recalculating (for every time step) the resulting increase in ambient temperature due to this energy. In case the sample and medium density and thermal capacity are assumed identical, the ambient temperature is the following function of tissue temperature

$$T_{amb}(t) = \frac{r_m}{l}\int_0^l \left(T_e(z,t) - T_{e0}\right) dz \tag{5.2.42}$$

where r_m is the solid-to-liquid mass ratio, the mass ratio of tissue to the surrounding medium, and l is the sample thickness (along z). Since in all of the analysis thus far, only half of the tissue sample was modelled due to symmetry, the integration boundary has to be corrected, and for hypothetical solid-to-liquid ratio of 1:2 (see diffusion experiments Paper II, Paper IV), the ambient temperature changes according to

$$T_{amb}(t)=\frac{2}{2l}\int_0^{l/2}\left(T_e(z,t)-T_{e0}\right)dz=\frac{1}{l}\int_0^{l/2}\left(T_e(z,t)-T_{e0}\right)dz \tag{5.2.43}$$

Note that temperatures in eqs. 5.2.42–5.2.43 should all be understood as relative and not absolute quantities (see subsection 5.1.2). Using the ambient temperature dependence 5.2.43 into the account in the boundary condition, and simulating using the same system and range of temperatures as used to produce Figure 5.7, one obtains results as shown in Figure 5.8b. Results from Figure 5.7a were reproduced here as Figure 5.8a but at the same scale along the ordinate axis for easier comparison.

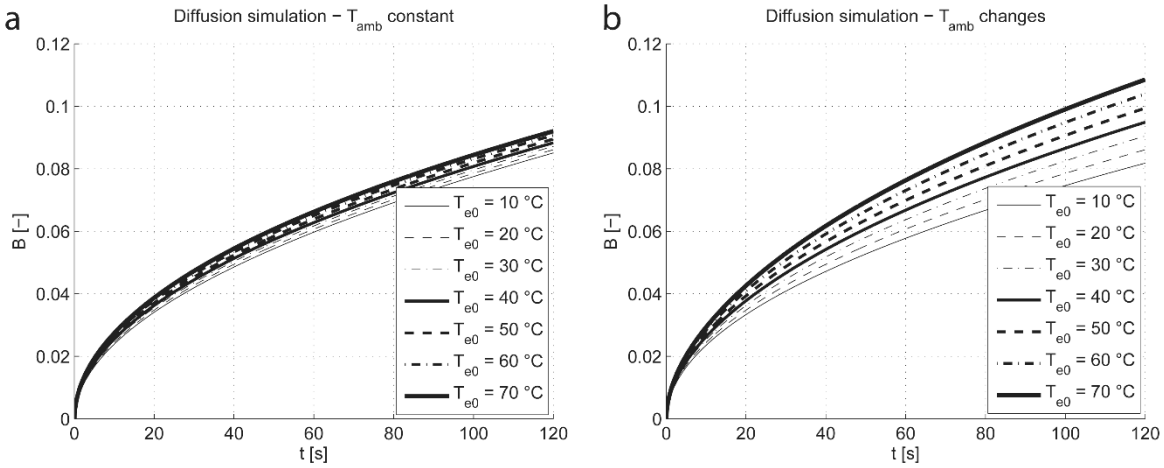

Figure 5.8: The parametric study for electroporated tissue with the dual-porosity models of solute diffusion taking the temperature-dependent diffusion coefficient into account. Without accounting for the surrounding medium heating (or cooling) due to thermal exchange between the medium and the tissue (a) and with the medium temperature (T_{amb}) re-calculated at every time step and diffusion coefficient modified accordingly.

In order to calculate results in Figure 5.8b, a numerical method of calculating the temperature profile in tissue was used. Note that this causes slight artefacts for small values of *t* if the timescale is divided into equidistant nodes. In this case, a more accurate solution with limited numerical artefacts would have been obtained by use of a logarithmic or otherwise non-linear non-equidistant meshing along the temporal coordinate with finer gradation for small values of *t*. Work concerning this issue extending beyond the basic identification of the problem and illustration by simple simulation as just described, is at this point relegated to future work, and is therefore not further discussed within the scope of the present thesis.

The simulated extraction kinetics shown in Figure 5.8b indicate that in case the more realistic case is modelled where tissue heats (or cools) the medium, the rate of diffusion is more extensively altered as compared to the simulation study where the ambient (medium) is modelled as an ideal

sink (or source) of heat. However, since the system of the tissue particles and surrounding medium is not thermally insulated (e.g. in a treatment chamber), the ambient/medium temperature will drop nonetheless and the effect of tissue initial temperature will diminish in time. Also note that only a very substantial increase in tissue initial temperature (e.g. by 20 °C to 50 °C – note that the given temperatures in the legend are absolute initial tissue temperatures) is needed to produce a noteworthy increase in the diffusion rate.

5.3 Concluding remarks to the chapter on thermal relations in electroporated tissue and their effects to mass transport

This chapter of the thesis presents work performed within the scope of this thesis dedicated to the thermal relations in biological tissues, predominantly of plant origin. The first section is dedicated to the analogy between the dual-porosity models of mass transport and its thermal equivalent formulation, and gives a detailed analysis of the model from its formulation to development of an analytical and a numerical solution, as well as providing theoretical grounds for estimating all of the required model parameters. This is followed by an adaptation of the previously presented mass transport models into a form suitable for combining them with the thermal distribution model, leading to a parametric study that attempts to answer the question of how important are temperature increases during or after electroporation for mass transport in pre-treated tissue.

The conclusion that can be drawn from the analysis of thermal relations in tissue with the use of the dual-porosity thermal model (section 5.1) is that, from the thermal point of view, tissue (electroporated tissue in particular) is too homogeneous to necessitate the study of its thermal properties with a complex model of dual porosity. The thermal properties of the extracellular and the intracellular space can, for all ordinary purposes of industrial applications of electroporation of plant tissue at the very least, be considered approximately equal and bulk properties of tissue can be used in a simple model of heat transfer in homogeneous material to study heat relations in tissue with adequate accuracy.

The same however cannot be said or claimed for very short timescales and events on the nano scale that were not considered. The dual-porosity model might present an interesting starting point for modelling thermal relations on the level of cells and on very short timescales, something that has been shown as being important not in the seconds after electroporation, but rather during the pulse application.

Section 5.2 of this chapter examines the relation between tissue temperature, diffusion coefficient and viscosity in two parametric studies where temperature is varied and the effect simulated using the dual-porosity model and its calculated diffusion/expression kinetics. The effect of *constant* raised temperature was already studied in a similar way in Paper II, therefore, in section 5.2, the approach is taken a step further by considering the influence of temperature if heat is *dissipated* out of tissue during the diffusion stage. The main conclusion of this section with relevance to electroporation of tissues is that, given moderate increases in tissue temperature and thermally non-insulated systems permitting sufficiently rapid cooling, the temperature increase itself via augmented diffusion coefficient and reduced viscosity will not have a noteworthy effect

on the rate of mass transport. A more important effect to mass transport in the case of elevated temperature is probably the structural alterations in tissue due to increased temperature. These findings should not be misconstrued by concluding that elevated temperature does not have a strong and direct effect on transport kinetics, but that in most practical cases, thermal dissipation due to electroporation will most likely not be sufficient to noticeably alter mass transport kinetics, simply because the electroporation-generated heat dissipates too quickly, and the system returns to ambient temperature within seconds or minutes following the treatment.

5.4 Appendix: The form of the analytical solution for the dual-porosity thermal model in the general case of $k_e \neq k_i$

The subsection 5.1.2 contains a complete analytical solution for the thermal analogue of the mass transport dual-porosity model that was written for the particular case where the thermal conductivities of the intra- and extracellular spaces are the same ($k_e = k_i$). However, the contrary (i.e. $k_e \neq k_i$) is a valid assumption corroborated by studies reported on in literature, and an analytical solution for this general case can theoretically be obtained. The entire process is outside the scope of this thesis, however, for completeness, a general form of the solution for the interested reader is presented here, which could serve as a starting point in finding the particular solution.

According to [77], a system of the form

$$\frac{\partial u}{\partial t} = a_1 \frac{\partial^2 u}{\partial x^2} + f\left(bu + cw\right) \tag{5.4.1}$$

$$\frac{\partial w}{\partial t} = a_2 \frac{\partial^2 w}{\partial x^2} + g\left(bu + cw\right) \tag{5.4.2}$$

has, for any a_1 and a_2, the solution

$$u = c\left(\alpha x^2 + \beta x + \gamma t\right) + y\left(\xi\right) \tag{5.4.3}$$

$$w = -b\left(\alpha x^2 + \beta x + \gamma t\right) + z\left(\xi\right) \tag{5.4.4}$$

$$\xi = kx - \lambda t \tag{5.4.5}$$

where k, α, β, γ, and λ are arbitrary constants, and the functions $y(\xi)$ and $z(\xi)$ are described by an autonomous system of ordinary differential equations

$$a_1 k^2 y''_{\xi\xi} + \lambda y'_\xi + 2a_1 c\alpha - c\gamma + f\left(by + cz\right) = 0 \tag{5.4.6}$$

$$a_2 k^2 z''_{\xi\xi} + \lambda z'_\xi - 2a_2 b\alpha + b\gamma + g\left(by + cz\right) = 0 \tag{5.4.7}$$

By comparing systems 5.1.1–5.1.2 and 5.4.1–5.4.2, we see that $u = T_e$, $w = T_i$, $f = -f_v$, and $g = 1$, while the constants equal

$$a_1 = \frac{k_e}{\rho c_v} \tag{5.4.8}$$

$$a_2 = \frac{k_i}{\rho c_v} \tag{5.4.9}$$

$$b = -c = \frac{h_v}{\rho c_v} \tag{5.4.10}$$

Determining the arbitrary constants in the system described by eqs. 5.4.1–5.4.10 for the particular initial and boundary conditions of the thermal dual-porosity model is not a trivial task and is at this point deferred as future work.

6 Concluding remarks and suggestions for future work

6.1 Future work

This section gives the author's opinion on possible future directions for the further development of the main work presented in this dissertation, the dual-porosity model. For a better understanding of the proposed approach, a previously published article is appended to this section and its significance is put into perspective in the discussion on future work directions.

6.1.1 Directions for further development and improvements

The dual-porosity model which constitutes the main scientific advance described in this dissertation is a model describing a fundamental framework for theoretically coupling electroporation effects and treated biological tissue. Regardless of whether the principle process governing mass transport in electroporated tissue after applying the treatment is diffusion or liquid flow, the model provides means of theoretically describing the permeability of the cell membrane of cells in tissue and relating this permeability with the resulting mass transport, quantifying the latter. Therefore, the principal focus for further model improvements should be in coupling a model of pore formation and resealing (i.e. pore evolution) on to the model, thus giving the parameter describing the transmembrane mass transport a temporal component. In order to determine pore evolution locally, the local electric field strength during electroporation must be known. The paper given in the following subsection describes an application for calculating the electric field distribution in tissue. The model presented therein has been kept simple, not taking into the account the local inhomogeneities in tissue electrical properties (e.g. conductivity), since it was designed to be used in an educational application where speed of calculation is more important than accuracy. Nevertheless, it illustrates one possible approach to calculating the local electric field distribution in tissue, which could, if known (calculated), facilitate the characterization of local electroporation effects with respect to tissue material and electrical properties. This would lead to a known pore size, number, and local distribution function, a spatio-temporal function that would replace the (thus far) constant coefficient that relates transmembrane mass transport with the concentration/pressure difference across the membrane. This means that tissue inhomogeneities could be accounted for, and furthermore, the parameters in the dual-porosity model would more closely reflect true material properties rather than describe averaged effects resulting from the assumptions about tissue homogeneity and temporal invariability that can at the moment be considered as unrealistic assumptions in the model.

Other possible improvements that are foreseen (and experimental work has already been undertaken to this effect) are related with further model upgrades necessary to provide the model the ability to describe other influences on mass transport; the two effects that have been determined to be important are turgor pressure loss and electroosmosis. Figure 6.1 below gives an illustration of the effect of these two phenomena; in Figure 6.1a, we see the effects on tissue volume loss (and concurrent liquid expression) due to release of turgor pressure at the onset of electroporation and immediately afterwards, while Figure 6.1b shows consolidation kinetics for two tissue samples where one has only been electroporated using high-voltage electrical impulses, and the other has been electroporated according to the same protocol, but also additionally exposed to long impulses of much lower amplitude as compared to electroporation pulses. The difference between the two consolidation kinetics is indicating what might be the net contribution to liquid expression due to electroosmosis. The turgor pressure loss can be considered and modelled (paper in preparation) as additional external compressive pressure that is only present for a limited duration of the experiment (initial few seconds) and whose effects become negligible once the elastic tension in the cell wall has been depleted.

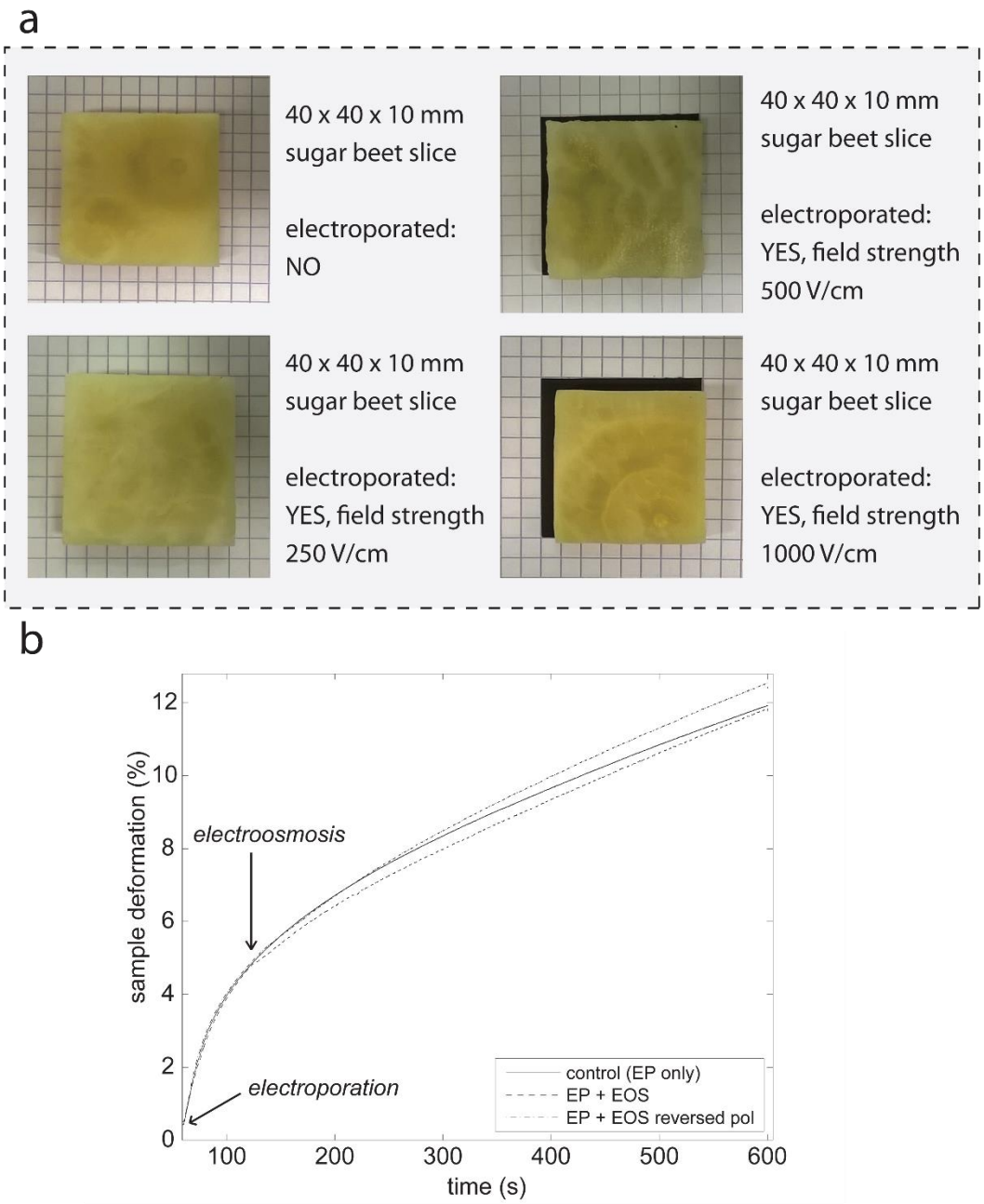

Figure 6.1: (a) A set of photographs illustrating the effects of internal turgor pressure loss in tissue due to electroporation (the samples observably shrink); and (b) Kinetics of tissue (potato tuber) deformation in time due to constant external low pressure application – with and without low-voltage millisecond-scale pulses ("EOS protocol", i.e. electroosmosis protocol) following the initial electroporation treatment. In the second "electroosmosis" example, the polarity on the electrodes was reversed during the "electroosmosis" period, thus presumably reversing the direction of the electroosmotic current, resulting in what appears to be a counterforce opposing the externally applied pressure.

6.1.2 Appendix to this section – Paper V: "Educational application for visualization and analysis of electric field strength in multiple electrode electroporation"

As shown in Figure 1 of the following article, electric field distribution in biological tissue is strongly dependent on the problem geometry. Important factors include, but are not limited to; electrode type (plate, needle, etc.), electrode size/length and orientation, number of electrodes, and tissue electrical conductivity distribution. These factors influence the inhomogeneous distribution of the electric field in tissue, and consequently, electroporation effects in tissue will be expressed to a varying degree, leading to inhomogeneous treatment effects. The local electric field distribution can exhibit marked differences according to the given condition of its application, and so any rigorous theoretical treatment of problems related to mass transport in electroporated tissue should begin by first examining the effects of the electric field and its homogeneity in target tissue. This is especially true in cases where it is of great importance that tissue is not too extensively damaged (applications on living tissue, animals, applications in selective extraction, etc.).

What is presented in the following article is an account of creation and development of an educational software solution intended for education of medical personnel working in the field of electrochemotherapy, however, it also highlights the importance of the local electric field distribution and gives an analytical method of calculating the electric field distribution in homogeneous tissue, created by two parallel needle electrodes.

It is the author's vision that such calculations will in future represent the starting point in the theoretical studies of the mass transport in electroporated tissue, and will constitute an integral part of a comprehensive and rigorous treatment of the problem.

BMC Medical Education

SOFTWARE Open Access

Educational application for visualization and analysis of electric field strength in multiple electrode electroporation

Samo Mahnič-Kalamiza, Tadej Kotnik and Damijan Miklavčič*

Abstract

Background: Electrochemotherapy is a local treatment that utilizes electric pulses in order to achieve local increase in cytotoxicity of some anticancer drugs. The success of this treatment is highly dependent on parameters such as tissue electrical properties, applied voltages and spatial relations in placement of electrodes that are used to establish a cell-permeabilizing electric field in target tissue. Non-thermal irreversible electroporation techniques for ablation of tissue depend similarly on these parameters. In the treatment planning stage, if oversimplified approximations for evaluation of electric field are used, such as U/d (voltage-to-distance ratio), sufficient field strength may not be reached within the entire target (tumor) area, potentially resulting in treatment failure.

Results: In order to provide an aid in education of medical personnel performing electrochemotherapy and non-thermal irreversible electroporation for tissue ablation, assist in visualizing the electric field in needle electrode electroporation and the effects of changes in electrode placement, an application has been developed both as a desktop- and a web-based solution. It enables users to position up to twelve electrodes in a plane of adjustable dimensions representing a two-dimensional slice of tissue. By means of manipulation of electrode placement, i.e. repositioning, and the changes in electrical parameters, the users interact with the system and observe the resulting electrical field strength established by the inserted electrodes in real time. The field strength is calculated and visualized online and instantaneously reflects the desired changes, dramatically improving the user friendliness and educational value, especially compared to approaches utilizing general-purpose numerical modeling software, such as finite element modeling packages.

Conclusion: In this paper we outline the need and offer a solution in medical education in the field of electroporation-based treatments, e.g. primarily electrochemotherapy and non-thermal irreversible tissue ablation. We present the background, the means of implementation and the fully functional application, which is the first of its kind. While the initial feedback from students that have evaluated this application as part of an e-learning course is positive, a formal study is planned to thoroughly evaluate the current version and identify possible future improvements and modifications.

Keywords: Education on electroporation, Electromagnetic field visualization, Applications in subject areas, Interdisciplinary projects, Interactive learning environments

* Correspondence: damijan.miklavcic@fe.uni-lj.si
Faculty of Electrical Engineering, University of Ljubljana, Tržaška 25, Ljubljana SI-1000, Slovenia

Background

Electroporation

Electroporation is a term coined in the early 1980's [1] for phenomena already described more than a decade earlier [2], when an interesting property of biological membranes has been observed. Electroporation mainly results in transient increase in membrane permeability when these membranes – which are mainly composed of lipid bilayers – are exposed to very short and intense electric fields. The physical mechanism responsible for increased permeability is thought to be the formation of nano-scale defects termed *pores* (thus electro*poration*) in the lipid structure [3,4]. This allows molecules that usually do not cross the membrane to cross it with relative ease, though the exact mechanism of this transport remains a subject of scientific debate [5]. In case the electric field strength is too high, changes to membrane structures and consequently to the cell are not temporary, but instead result in cell death, a phenomenon known as irreversible electroporation. On the other hand, if the cells survive, increased permeability of membrane is only temporary and the phenomenon is termed reversible electroporation. This observed transient increase in permeability of electroporated membranes of biological cells has offered opportunities for extensive research and development resulting in a number of applications of electroporation, such as gene (DNA) delivery, introduction of drugs into cells, fusion of cells, electrochemotherapy for treatment of cancer, gene delivery in tissue and transdermal delivery of drugs and genes as well as a number of other applications, see for instance [6,7] for an overview. In these applications viability of the porated cells is important and thus irreversible electroporation is consciously avoided and generally considered to be an undesired side effect. However, there are also interesting medical applications of irreversible electroporation [8], such as non-thermal irreversible electroporation for tissue ablation. Irreversible electroporation is also rapidly entering the domains of industrial [9,10] and environmental [11] applications.

Electrochemotherapy

Electrochemotherapy (ECT) is a local treatment that successfully combines application of cell-membrane-permeabilizing electric pulses and chemotherapeutic drugs. For successful ECT, the pulses must be of adequate amplitude, duration, number, repetition frequency and shape [12], in order to achieve local increase in uptake and hence cytotoxicity of otherwise non-permeant or poorly permeant anticancer drugs. Two drugs have been identified as candidates for ECT: bleomycin and cisplatin [13,14]. The transport of bleomycin across the nonpermeabilized plasma membrane is highly limited [15]. Using electroporation to increase membrane permeability provides bleomycin with access to cytosol and DNA, where it causes DNA breakdown. The cytotoxicity of bleomycin is thereby increased by a factor of several thousand [16]. In short, the main mechanism of ECT is the electroporation of cells in tumors and consequent increase in drug effectiveness by enabling the drug to reach intracellular targets. For other supporting mechanisms, see [17,18].

Since all clonogenic cells in the tumor need to be eradicated for effective treatment, all cells have to be permeabilized, i.e. all cells in the tumor have to be exposed to appropriate electric pulses. This means that the effectiveness of electrochemotherapy depends on both the drug availability in the tumor and coverage of the whole target area by a sufficiently high electric field [19].

There are several factors in ECT of tumors that we must consider before we can confidently assume we have successfully electroporated the entire tumor area. First, there is the issue of tumor and surrounding tissue electrical properties that may exhibit considerable inhomogeneity. Conductivity is of particularly high importance for example, since higher tumor conductivity compared to surrounding tissue results in lower electric field strength in the tumor and undesirably high fields in the surrounding healthy area that may cause irreversible electroporation [20]. Second, there is the issue of electrodes used to apply the pulses, mainly of their shape, size and position. In general, there are two types of electrodes – plate and needle electrodes. Plate electrodes are non-invasive, usually parallel and with either a fixed or adjustable distance in between the two plates, whereas needle electrodes are used invasively, which ensures good electrical contact, but has other drawbacks. In using plate electrodes, we must ensure good electrical contact and optimal distance between electrodes to fit the tumor [21,22] and with needle electrodes – since electric field distribution is more inhomogeneous and dependent on their diameter, distance between them and depth of insertion [23] – the task of ensuring entire tumor area coverage is even more arduous [19].

Several papers have been published based on numerical modeling, e.g. [19,24] and in vivo studies [25] on importance of tumor coverage by sufficiently high electric fields for successful ECT, demonstrating the need for careful consideration and control of variables. Effectiveness of ECT has been confirmed in a study conducted by a consortium of four medical institutions gathered in the ESOPE (European Standard Operating Procedures of Electrochemotherapy) project, in the scope of which standard operating procedures for ECT were published

[26]. However, in advanced cases such as intracranial [27] or liver metastasis tumor treatment [28], the need for patient-specific treatment planning has been highlighted and is being developed [29,30].

Non-thermal irreversible electroporation for tissue ablation and other techniques

Irreversible electroporation has been studied extensively in recent years as a method of tissue ablation. While the high number of applied pulses used to achieve classical irreversible electroporation may also cause thermal damages due to Joule heating of the current-conducting tissue, non-thermal irreversible electroporation (NTIRE) is of particular interest since it results in well-defined areas of tissue ablation and no protein coagulation [31]. The potential clinical applications of NTIRE are therefore numerous. It is technically a simple procedure, requiring only the insertion of electrode needles without any addition of chemotherapeutic as with ECT; it is fast in comparison to other ablation methods such as RF ablation or cryoablation; can be monitored with ultrasound; produces a sharp delineation between treated and untreated regions; and affects only cells while sparing the connective structure [8,32]. Since it has been observed that NTIRE spares the vascular structure and nerves, there is hope of using this technique in treatment of tumors abutting large blood vessels [33]. Promising as this treatment is, we are faced with similar considerations as with reversible electroporation in the case of ECT or its many other applications, namely to ensure adequate local electric field strength, sufficient for irreversible, yet non-thermal electroporation.

In addition to NTIRE and ECT, a number of other minimally invasive therapies for treatment of deep-seated tumors (particularly those of the liver) exist, e.g. high intensity focused ultrasound, microwave ablation and radiofrequency ablation. The latter is a minimally invasive procedure where a needle electrode is inserted percutaneously into a tumor, much as in ECT or NTIRE. The electrode acts as an antenna for electromagnetic waves emitted by a generator; the tumor is heated up and thereby destroyed [34]. As with NTIRE or ECT, the need for accurate needle placement exists and its importance has been evaluated. Success, i.e. improved treatment, has been proven to be correlated to the experience of the operator [34].

The need for education on electroporation

As outlined in the paragraphs above, both reversible and irreversible electroporation are promising approaches in treating solid tumors, however their success is highly dependent on local field strength. Poorly defined or unknown properties such as tissue conductivities and inhomogeneities in addition to our choice of electrode type, positions and pulse amplitudes, affect the electric field distribution. With many factors to take into consideration, we may dismiss important uncontrolled variables or use a well-studied but irrelevant model that cannot be applied to a specific situation. An example of this is the persistent use of a very simple approximation for electric field strength that holds only under very particular conditions. This frequently used approximation equates the electric field strength E to the voltage U applied on the electrodes divided by the distance d between the electrodes, i.e. $E \approx U/d$. Since the local electric field strength has been identified as the key factor in achieving both reversible and irreversible electroporation (see [19] for details), i.e. local E has to reach a certain threshold value E_{rev} or E_{irrev}, it is the parameter we most often optimize our electrode configuration for. There is a problem, however, since this simple relation is strictly valid only in an isotropic homogeneous medium between two infinitely large parallel plate electrodes. When using parallel plate electrodes in ECT or NTIRE, this simple model best approximates the actual field strength far from the electrode edges, provided the electrode width is sufficiently large compared to the electrode distance. In any case, the approximate model fails completely as we approach the edges (see Figure 1a). Results are even worse in the case of needle electrodes, where of course there are no parallel plates to speak of (see Figure 1b and [35] for further elucidation). Therefore, using the simple parallel plate approximation for E in individual cases of tumor treatment could possibly result in significant reduction of response in treatment for which the complete response rate has been shown to be as high as 74% [17].

As ECT and NTIRE are steadily finding their way into more and more clinics worldwide [36-39] and establishing themselves as safe and effective treatments of cancer, it is becoming more and more important that medical personnel performing and planning ECT (or NTIRE) is aware of their mechanisms of action, the underlying physics and possible pitfalls. This paper presents an application for visualization and analysis of the electric field strength in multiple-needle-electrode electroporation aimed at users with basic knowledge of the principles of electroporation, but lack of education in physics and engineering who may therefore need visual, interactive and didactic instruments to gain a deeper understanding of the principles necessary for effective use of these promising treatments. Since educational applications of the sort are scarce and research is focused primarily on advancing the field rather than educating, the need to explore options and applications in this area of engineering education seems pressing and applicative

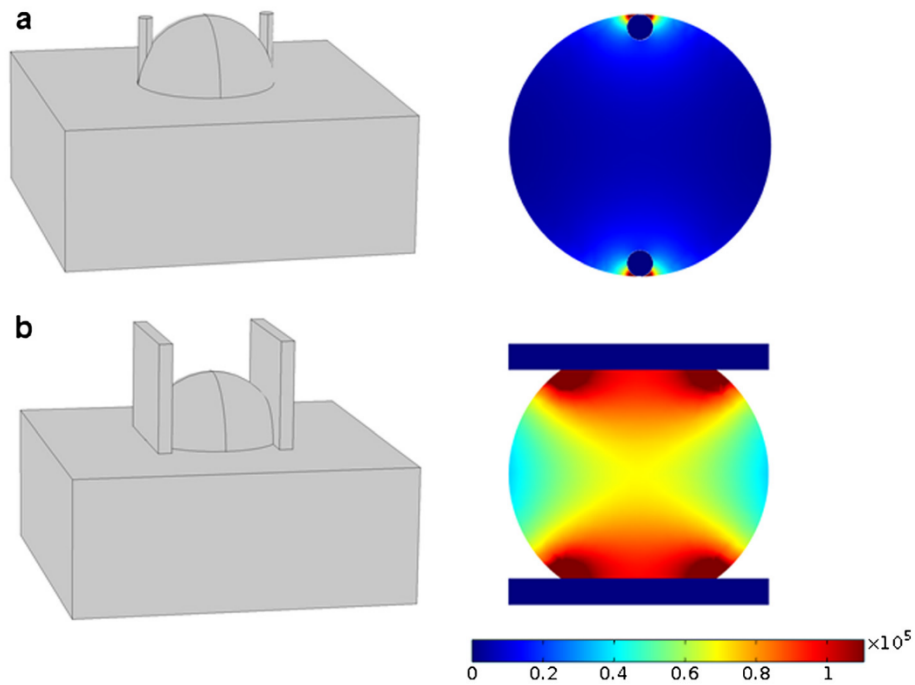

Figure 1 Electric field distribution for plate electrodes in a cutaneous tumor electroporation (a) and parallel needle electrodes in cutaneous tumor electroporation (b). Geometry is shown on the left hand side and resulting field strength on the right. Tumor diameter in both instances is 2 cm, electrode thickness 0.2 cm and electrode distance 1.6 cm. The applied voltage was 1300 V. Resulting field strength on the color scale is in volts per meter.

results should be welcome. The application is part of a now firmly established annual course Electroporation Based Technologies and Treatments, EBTT (http://www.ebtt.org). The e-learning laboratory exercise into which the presented application has been incorporated, has been developed and described previously [40].

Implementation

Theoretical background

The theoretical background for the mathematical engine that is at the heart of our application has been derived from the electrostatic field theory, more specifically, extended from a solution for electrostatic potential generated by two long parallel charged conductors given in [41]. We have omitted the detailed mathematical derivations here as they are outside the scope of this paper; however, we have included a derivation of the equations below in the Appendix for those readers that may be interested in further development or modifications to our model. Below, we specify only the final formulation of the mathematical model and the method of application of this analytical solution into the field-calculating engine that represents the core of Application for Visualization of Target Tissue in Electroporation (ApiVizTEP), since this is the only essential part of the application around which the user interface is built. Similarly to the approach that we present in this paper, other analytical models have been developed previously using complex analysis. For a six-needle array, one may find a first-order analytical approximation for the electric field strength in [42]. Other authors have expanded on this approach further, see e.g. [43] and [44]; however, these solutions do not give an accurate analytical expression for the electric field strength since quite possibly such a solution cannot be obtained for three or more electrodes active concurrently at a given time. Since currently electroporation devices mostly power only one pair of electrodes at a time [45], we have not pursued a solution with more than two concurrently active electrodes, thus avoiding the derivation of an approximate solution. Instead, we give an accurate solution for a two needle electrode system that is not based (mathematically) on previously published work.

The accurate analytical solution for electric field strength of two long parallel cylindrical conductors (needle electrodes) on a plane perpendicular to the conductor longitudinal axis (2-D solution), is given by the following equation

$$|E(x,y)| = C \cdot \sqrt{\left(\frac{x'_A - x}{(x'_A - x)^2 + (y'_A - y)^2} - \frac{x'_B - x}{(x'_B - x)^2 + (y'_B - y)^2}\right)^2 + \left(\frac{y'_A - y}{(x'_A - x)^2 + (y'_A - y)^2} - \frac{y'_B - y}{(x'_B - x)^2 + (y'_B - y)^2}\right)^2}$$

$$\text{where} \quad C = \frac{V_{AB}}{2 \cdot \log \frac{d_{AB} + \sqrt{{d_{AB}}^2 - 4 \cdot {\rho_0}^2}}{2 \cdot \rho_0}}$$

$$\text{and} \quad \begin{array}{ll} x'_A = x_A + |e| \cdot \cos\Theta_1, & \Theta_1 = \arctan\frac{y_B - y_A}{x_B - x_A} \\ x'_B = x_B + |e| \cdot \cos\Theta_2, & \Theta_2 = \arctan\frac{y_A - y_B}{x_A - x_B} \\ y'_A = y_A + |e| \cdot \sin\Theta_1, & e = d_{AB}/2 - \sqrt{(d_{AB}/2)^2 - {\rho_0}^2} \\ y'_B = y_B + |e| \cdot \sin\Theta_2 & \end{array}$$

V_{AB} is the voltage on an electrode pair (anode–cathode), d_{AB} is the distance between the electrodes, ρ_0 is the electrode diameter, while x'_A, y'_A and x'_B, y'_B are coordinates of the center of the electrode mathematical equivalents (the electrical center x'_A, y'_A and x'_B, y'_B of the electrodes is eccentric to the actual geometrical center x_A, y_A and x_B, y_B due to finite i.e. non-zero electrode diameter).

Our application employs a mesh of 400 × 400 points and the electric field strength E is calculated for each of the 160.000 points using the expression above. The time needed to perform the necessary calculations and display the results is practically negligible, ranging from a few hundred milliseconds for two active electrodes up to one and a half seconds for twelve active electrodes using an average modern personal computer, i.e. at least a dual core 2 GHz processor equipped with 2 GB of memory or more. It needs to be emphasized that while the application allows for inclusion of up to twelve electrodes distributed into one to six groups with variable voltages, the application fundamentally breaks down these groups into anode–cathode pairs and calculates the electric field strength by means of the equations above for every pair. It then searches this set of results to obtain the maximum value of the electric field in each of the 160.000 points. This value represents the final solution in that point, since what we are interested in is determining the maximum value for the local field strength. In this way we have eliminated the need for a solution for the electric field of more than two concurrently active electrodes. Such an approach is justified by the fact that we have already mentioned – i.e. currently electroporation devices only power two electrodes at the same time.

Tools and platforms

The application has been written in C# programming language in the Microsoft® Visual Studio 2010 integrated development environment. The library used was the Microsoft® .NET Framework version 4. The development environment and base library have both been selected based on personal preference and possibilities that are enabled by the enhancements in these tools concerning ease of graphical user interface (GUI) development by separating the markup that describes the GUI elements from programming logic that provides the functionality.

The internet version of the application is hosted on a semi-open platform, since a Microsoft® Windows operating system is hosting an Apache™ HTTP Server web server with installed PHP support and a free edition of Oracle® MySQL, providing a web interface to basically the same, though slightly modified and recompiled, engine as in the desktop version.

Results

The application that we developed has been named Application for Visualization of Target Tissue in Electroporation, or ApiVizTEP in short. It is a Microsoft .NET application bundled into an installation package together with the .NET Framework version 4 Client Profile redistributable installation, which enables the user to install the application locally, provided the machine hardware and operating system support this prerequisite framework, as do most modern Windows operating systems installed on compatible hardware.

At the start the application presents itself with a navigational panel on the left-hand side of the window and a help panel to the right (see Figure 2).

The help panel contains instructions on locating the configuration of the system, i.e. directs to the *config* and *settings* panels. These contain various model and system settings that we describe here briefly: It is possible to include from two up to twelve needle electrodes in the model that may be distributed into one, two, or more (up to six) groups. One cathode and one or more anodes or vice versa (one anode and one or more cathodes) form such a group. These are defined in electroporation studies in situations where applied voltages are different for different pairs (or groups in general) of electrodes, as currently electroporation devices mostly power only one pair of electrodes at the same time [45]. The applied voltages are configurable per group (see Figure 3). The reversible electroporation threshold E_{rev} as well as irreversible electroporation threshold E_{irrev} may also be set (default settings 300 V/cm and 800 V/cm, respectively), as these thresholds are highly dependent on the modeled tissue (e.g. bone vs. muscle vs. liver etc.) as well as on treatment parameters, e.g. number and duration of pulses [46]. These thresholds may be set in three different units:

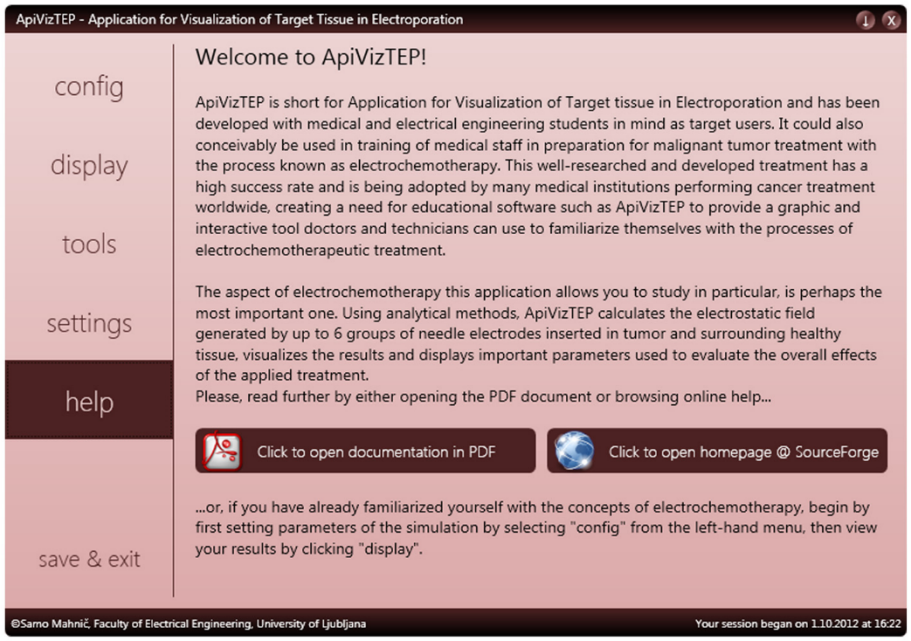

Figure 2 The help panel of ApiVizTEP with introduction and brief instructions.

V/cm, V/mm, or V/in. There are also interface elements for changing the ratio of tumor size to healthy tissue area, and for modifying the conductivity ratio of tumor to healthy tissue, but these options are not, at present, taken into account in calculations of the field strength, although the effects of inhomogeneous conductivities can be significant (see Discussion, Evaluation of accuracy and usefulness of obtained solution).

An electroporation model studied in ApiVizTEP is flexible in terms of adjustable tissue area (1.61 mm^2 to 16129.00 mm^2) and electrode diameter (0.10 mm to 2.00 mm, see Figure 4). The user interface for configuring has also been designed with extensive error-checking capabilities to prevent users from misconfiguring the model.

Once satisfied with the configuration, the user may switch to the *display* panel, which contains the results

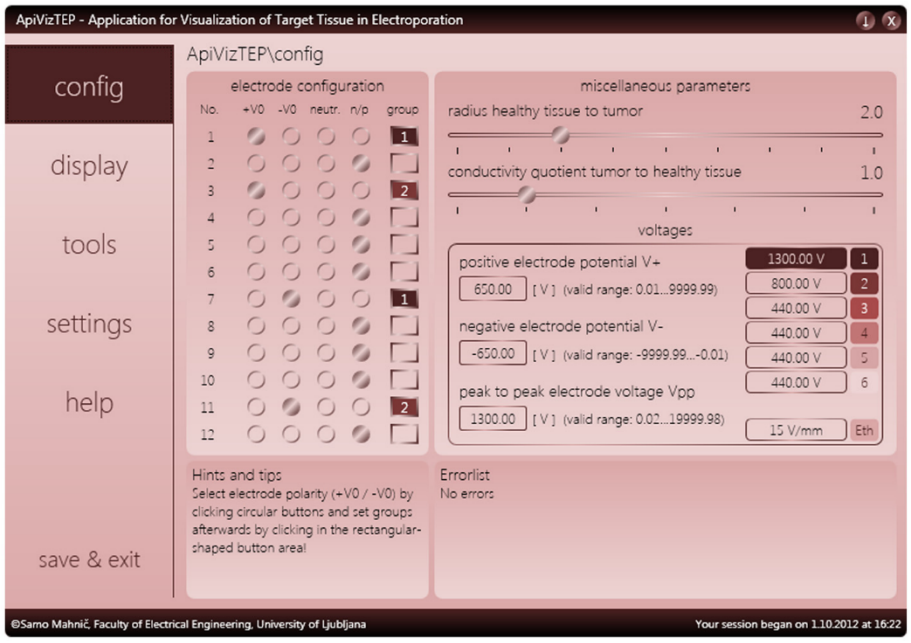

Figure 3 The configuration panel of ApiVizTEP with various options.

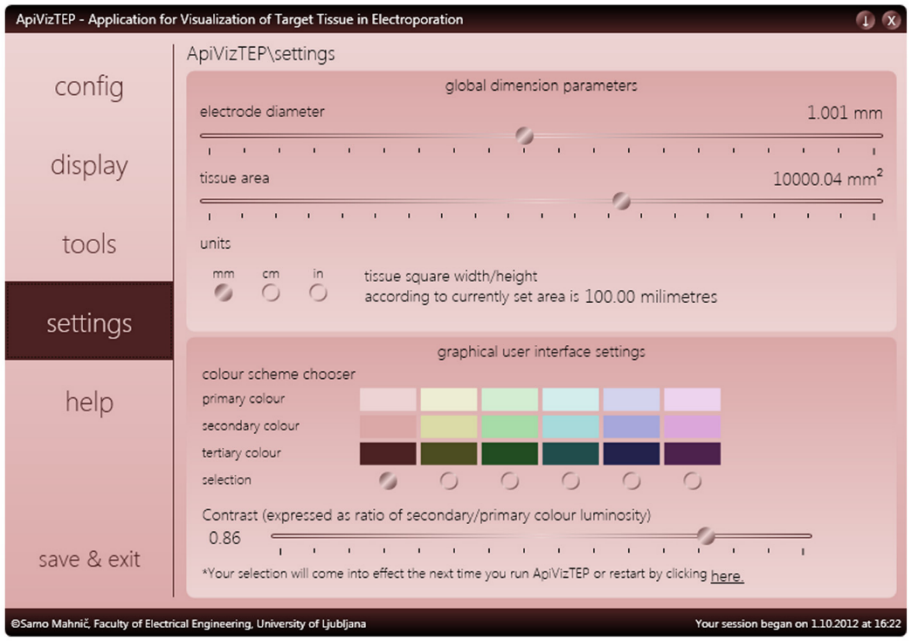

Figure 4 The settings panel of ApiVizTEP with various options.

part of the application (see Figure 5). This display panel is divided into five areas; (1) the tissue area with color-coded display of calculated electric field strength, electrode positions and miniature color bar (legend); (2) the large color bar and controls area (accessible via the *color controls* button, see Figure 6); (3) the position fine-tuning, coordinates and units panel; (4) the selected electrode position and mouse cursor position bar; and (5) the position and display settings reset bar. The tissue area, measuring 400 × 400 picture elements (pixels), is displaying the results of our model. There are also the X and Y axes and a circle representing the boundary between the tumor and the surrounding tissue. Currently, this boundary serves no particular function other than representing a target for our modeled ECT or NTIRE efforts, a point on which we will elaborate later. What we

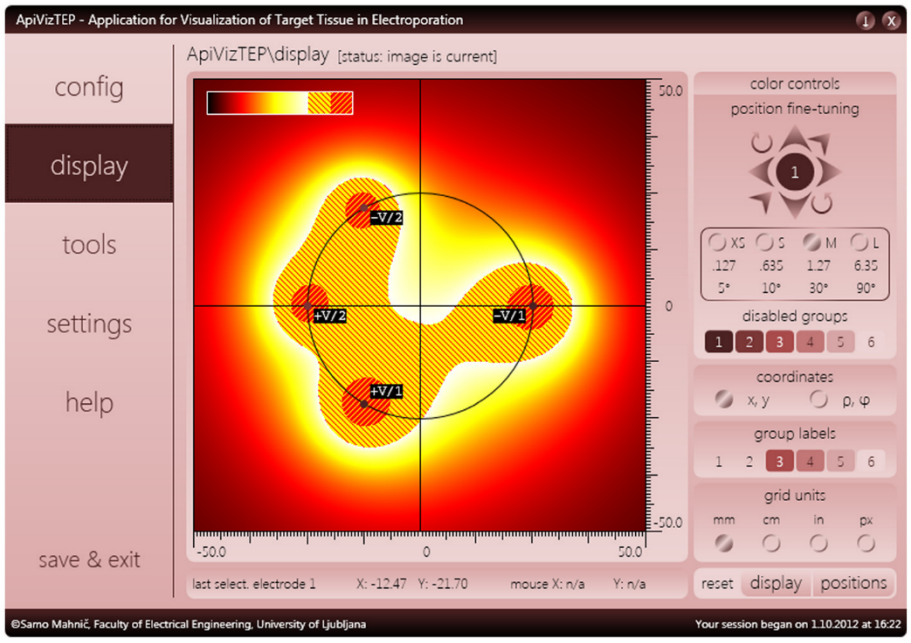

Figure 5 The display panel of ApiVizTEP with its 5 sub-sections.

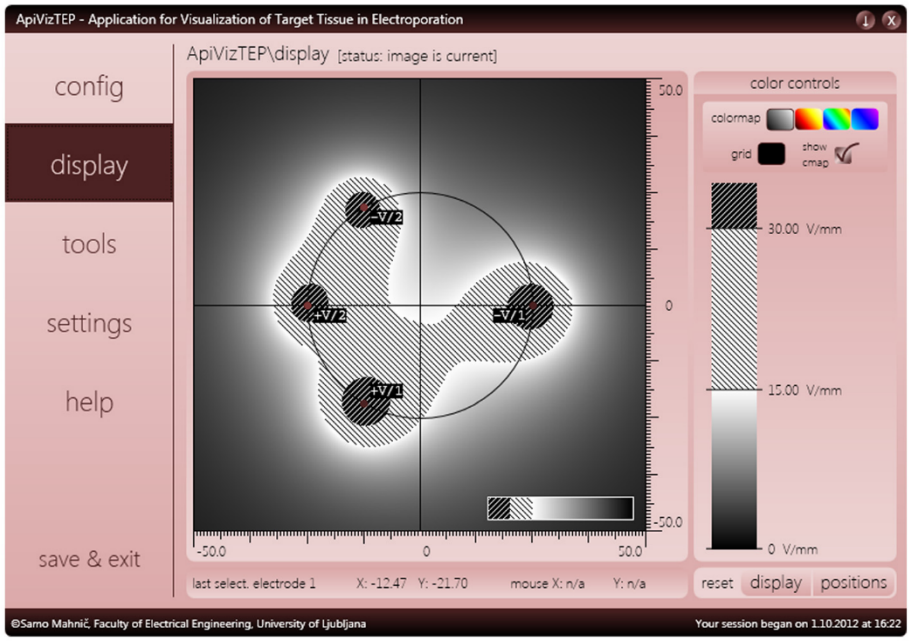

Figure 6 The display panel of ApiVizTEP with the color controls sub-section of the display panel visible. The color bar is annotated with important field strength values (thresholds) and a gray color scheme has been selected to illustrate the results display adaptability (see for comparison the same results displayed in "hot" color scheme in Figure 5).

are seeing in this area is color-coded electric field strength, of which the values are encoded into color based on the chosen palette (color bar), shown in Figure 6.

As described in the Background, coverage of the entire target area with fields above reversible threshold is very important for successful ECT, and above irreversible threshold for ablation of tissue by NTIRE. Thus, the learning experience for the user is in the experimentation with the chosen setup, by one or more of the following methods of interaction: (1) repositioning of electrodes via mouse (drag and drop) or eight buttons by a defined increment (up, down, left, right, rotation around center point, towards or away from the center point); (2) adjusting the number of electrodes or the applied voltages (*configuration* panel); or (3) varying tissue and electrode dimensions (*settings* panel).

The *tools* panel of the application contains two useful analysis tools, one already developed (*data collector*) and the other currently under development (*data analyzer*). Data collector (as shown in Figure 7) is capable of maintaining a record of our selected configurations that we wish to analyze. An individual record holds information about the electrode and voltage settings as well as analysis performed at the instance of record creation; the maximum and minimum field strength, as well as percentage of tumor and surrounding tissue subjected to irreversible or reversible electric field strengths (see Figure 7).

ApiVizTEP also allows the user to save data via the *save & exit* panel. An option is available to either save configuration to a file that can be loaded at any time via a key combination, or automatically at the next startup of the application. Additionally, there is an option to retain the data collected in the data collector.

For platform cross-compatibility and accessibility, a web interface has been developed (Figure 8) that uses the same engine as the standalone application; in other words, the application has been recompiled without the graphical interface and the interface built as a web application. This is now part of an online e-learning course presented at the EBTT International Workshop [40].

Discussion

The main result of the work presented in this paper is the educational application that calculates and provides visualization of the electric field in multiple needle electrode electroporation, such as is commonly used in electrochemotherapy [28] or tissue ablation by non-thermal irreversible electroporation [39]. It has been developed both as an installable desktop application and a web service with a graphical interface.

ApiVizTEP from the user's point of view

From the perspective of a potential user, the application has been designed in an attempt to be both easy to use and work with, and aesthetically pleasing. It is important for a modern educational piece of software to be not only functional in the educational sense, but also designed in a way that is inviting the user to "play" with the various features and modes of use, thus provoking a motivated self-

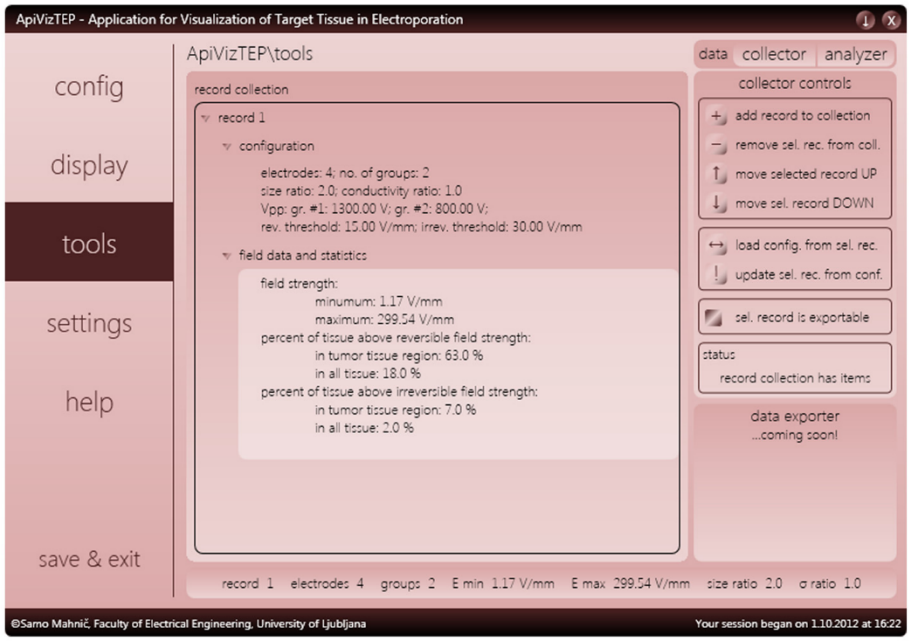

Figure 7 The tools panel of ApiVizTEP with data collector showing analysis of results obtained with configuration and settings shown in Figures 3 and 4, respectively.

paced learning experience [47]. We believe the design of our application has successfully incorporated these principles in the following sense; the amount of textual information related to the understanding of user interface functionality is minimal, the help section of the application is mainly concerned with bridging the gap in knowledge of the electroporation background and need not be focused on the interface as it is minimalistic in design; since we also aimed at flexibility in customizing and individualizing the interface by the users themselves, we offer several different color options and palettes for visualizing the data as well as six selectable color schemes of the graphical interface (see Figure 3 – graphical user interface settings); and finally, intelligent programming logic of error reporting and warnings prevents the user from misconfiguring or misusing the system and therefore failing to produce or obtain erroneous results. Thus far feedback from users, i.e. students at a workshop on electroporation, has been positive. While no formal study on the usability and user-friendliness has been performed, based on individual oral accounts of the learning experience, we can conclude that the application is easy to use and the graphical interface is intuitive; there have been no requests for clarification from users during courses that incorporated ApiVizTEP, while all participants successfully completed their assignments that were based on work with the application.

Evaluation of accuracy and usefulness of obtained solution

With respect to the accuracy and reliability of the results in light of present knowledge on mechanisms of ECT and NTIRE, there are a couple of points to consider. First, it needs to be emphasized that due to optimization of speed with which we obtain our results within ApiVizTEP and our desire to enhance user experience – consequently using an analytical model – we are limited by the need for a low-complexity model of electroporation. The reason for this is that an analytical model may be described and solved without utilization of numerical methods which come with high computational costs. Of main concern in this regard are differences in electrical properties of tumor and surrounding tissue. Since tumors normally exhibit higher conductivity compared to the surrounding area [48], local electric field strength inside the tumor can be only a fraction of the field strength of the surrounding tissue [20]. This inhomogeneity in tissue conductivity is at the time of writing of this article incorporated into the graphical user interface of ApiVizTEP, i.e. the user may set tumor conductivity to surrounding tissue conductivity ratio, but our mathematical model and therefore the field-calculating engine do not take this ratio into account. We therefore treat the entire area as homogeneous in conductivity. The functionality of varying the tumor tissue to surrounding tissue conductivity ratio is built into the graphical user interface in anticipation of future work on developing the analytical model still further. If possible, the conductivity inhomogeneity will be accounted for in a future model, i.e. a future version of the application. If it is, however, impossible to obtain such a solution analytically, the application will be extended with a numerical engine.

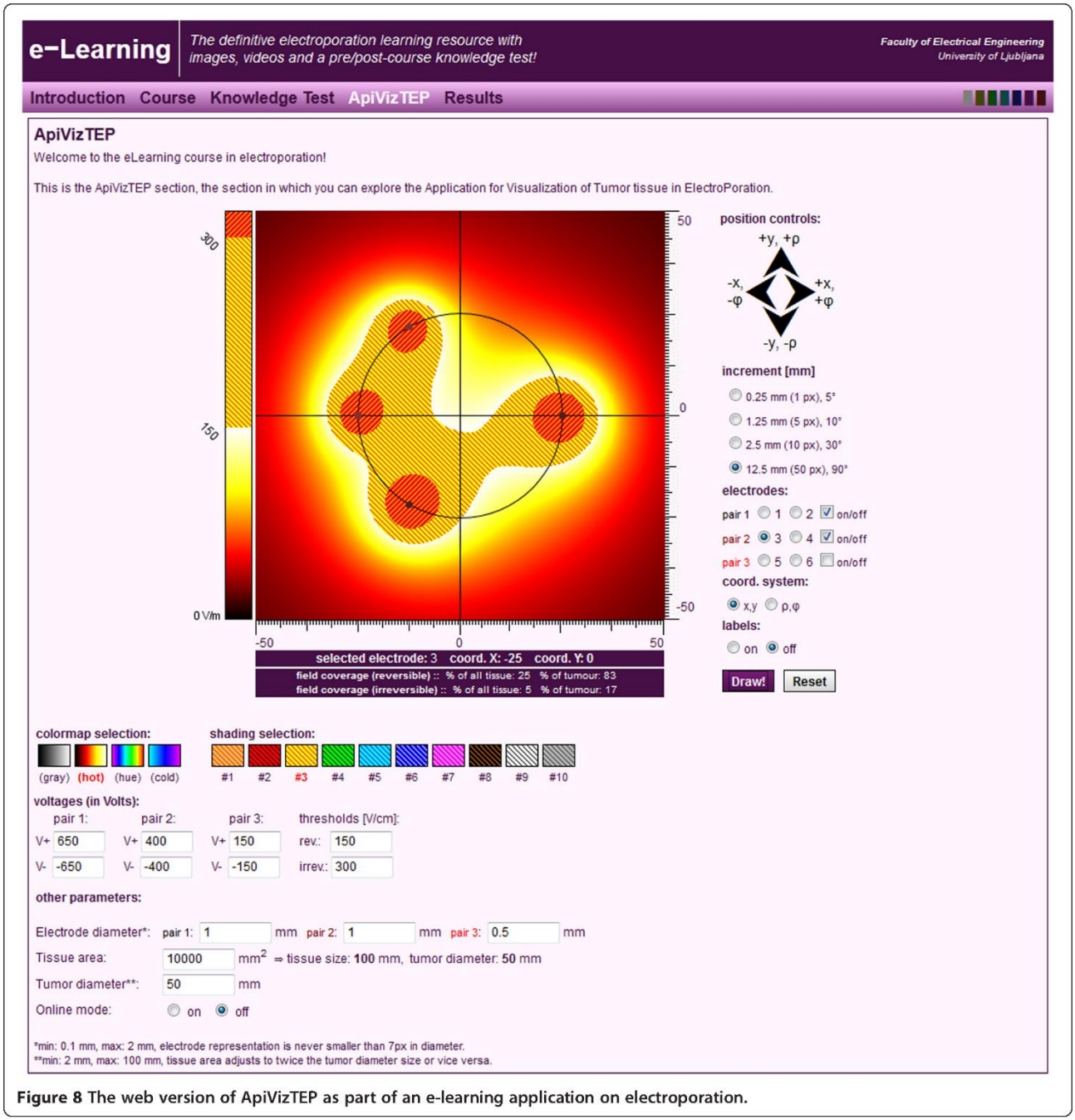

Figure 8 The web version of ApiVizTEP as part of an e-learning application on electroporation.

Secondly, we would like to point out that our model is two-dimensional, as we have imagined our area of interest to be a slice of three-dimensional space. This simplification is made under the assumption that the generated field is homogeneous along the electrode insertion axis if we observe a plane that is distant from electrode end points. Since currently in ECT [28,29] and NTIRE [49-52] of deep-seated tumors the electrodes are normally inserted into tissue parallel to each other, the fact that we do not consider the third spatial dimension is not of particular concern.

Conclusions

The research and development presented in this paper is grounded in decades of studying the phenomenon of electroporation and the development of electroporation-based technologies and treatments. It has resulted in a software product aimed at educating a relatively small but rapidly growing population of researchers and medical staff in fields where applications utilizing electroporation are growing in numbers, such as cancer treatment, food processing and the environment (e.g. waste water treatment, biofuel, etc.). As these applications mature

into standard practices, a further increase in need for educational solutions of this kind will become a necessity, especially in the field of health care provision, since ECT and NTIRE are highly successful modalities for treatment of malignant tumors and tissue ablation, respectively. The application presented here is portable and accessible, as it can be distributed either as a standalone software package that can be downloaded and installed, or as an online web application that is easily accessed from any computer possessing browsing capabilities. Feedback from students that have had an educational course of which ApiVizTEP is a part of, have provided feedback that confirms the usefulness and ease of use of the educational solution presented.

Availability and requirements

Project name: ApiVizTEP

Project home page: e.g. http://sourceforge.net/projects/apiviztep/

Operating system(s): Web version: Platform independent, Desktop version: Microsoft Windows XP and above

Programming language: Web version: PHP (GUI) and C# (service), Desktop version: C#

Other requirements: Web version: Apache Server, MySQL, XHTML, CSS, CodeIgniter library, IIS 7 Web Server, .NET Framework v4, Desktop version: .NET Framework v4

License: GNU General Public License v3

Any restrictions to use by non-academics: Desktop version is subject to GNU GPL v3 license. Web-based version is closed to all public access, due to it being part of a wider educational framework that is not in public domain.

Appendix

This appendix provides a detailed mathematical derivation for electric field strength of two long thin parallel cylindrical conductors. The basic theory of electric field supporting this derivation may be found in [40] or derived by means of almost any comprehensive treatment of electrostatic field theory that is found in literature, e.g. [53].

The general situation is illustrated by Figure 9 below. We are looking for an analytical expression for the electric field of two long parallel cylindrical conductors of diameter ρ_0 distance d_{AB} apart that carry electrical charges $+q$ and $-q$. Charges $+q$ and $-q$ are the actual charges on the surface of the conductors, while charges $(+q)$ and $(-q)$ are their mathematical equivalents, which is why they are given in parentheses. These charges are located eccentrically to the geometrical axes of the conductors. The axes of the equivalent charges are also known as the *electrical axes* and the distance between these electrical axes and the geometrical axes is known as *eccentricity,* denoted *e.* Via means of the geometrical parameters of equipotential curves we determine the distance between the electrical axes, denoted by *s*, which we find is related to the existing system parameters as shown by the following equation:

$$s = \sqrt{\left(\frac{d_{AB}}{2}\right)^2 - {\rho_0}^2}.$$

From Figure 9 it also follows:

$$e = \frac{d_{AB}}{2} - s = \frac{d_{AB}}{2} - \sqrt{\left(\frac{d_{AB}}{2}\right)^2 - {\rho_0}^2}.$$

The electric potential in the area outside the conductors is defined by the equivalent charges:

$$V(T) = \frac{q}{2\pi\varepsilon_0} \log\frac{\rho_B}{\rho_A},$$

and the voltage between the two conductors is the difference in potentials:

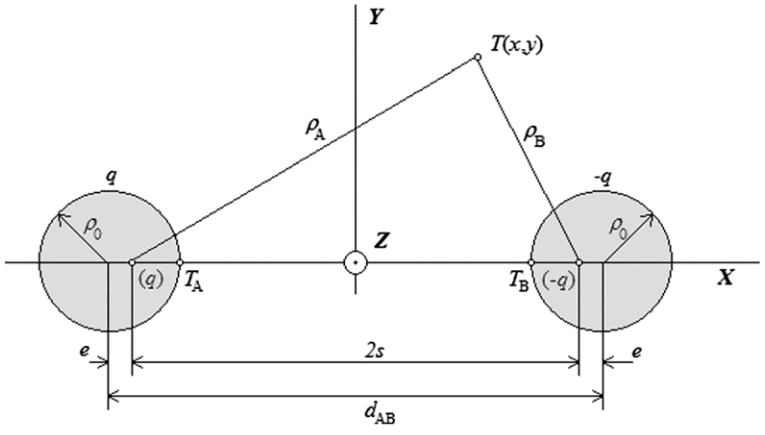

Figure 9 Two long parallel cylindrical electrical conductors.

$$V_{AB}(T) = V(T_A) - V(T_B) = 2\,V(T_A) = \frac{q}{\pi\varepsilon_0}\log\frac{d_{AB}+\sqrt{{d_{AB}}^2-4{\rho_0}^2}}{2\rho_0}.$$

If the voltage $V_{AB}(T)$ is known, the expression for the unknown potential $V(T)$ is given by:

$$V(T) = \frac{V_{AB}\log\frac{\rho_B}{\rho_A}}{2\log\frac{d_{AB}+\sqrt{{d_{AB}}^2-4{\rho_0}^2}}{2\rho_0}}. \quad (A.1)$$

The electric field strength $E(T)$ is the absolute value (length) of the vector $\boldsymbol{E}(T)$, obtained by means of the gradient function of the scalar potential $V(T)$:

$$E(T) = |-grad\,V(T)| = |-\nabla V(T)|. \quad (A.2)$$

The gradient in two-dimensional space described using Cartesian coordinates x and y is:

$$-grad\,V(x,y) = -\left(\frac{\delta V}{\delta x}+\frac{\delta V}{\delta y}\right). \quad (A.3)$$

The gradient operation applies to the expression $\log(\rho_B/\rho_A)$ contained in A.1, where ρ_A and ρ_B are expressed as (see Figure 9):

$$\rho_A = \sqrt{(x_A+|e|-x)^2+(y_A-y)^2} = \sqrt{(x_A{}'-x)^2+(y_A-y)^2}$$
$$\rho_B = \sqrt{(x_B-|e|-x)^2+(y_B-y)^2} = \sqrt{(x_B{}'-x)^2+(y_B-y)^2}, \quad (A.4)$$

for the particular case where the y coordinates of the conductors' geometrical axes are identical (and happen to be equal to 0, see Figure 9). If this is not the case – i.e. the coordinates of the geometrical centers are completely arbitrary – we need to determine the coordinates of the electrical axes via a rotational transformation (i.e. trigonometrically). For this general case, combining equations A.1 – A.4 and accounting for the rotational transformation to generalize eq. A.4, we get the following set of expressions that represent the final and general solution to our problem:

$$|E(x,y)| = C\cdot\sqrt{\left(\frac{x'_A-x}{(x'_A-x)^2+(y'_A-y)^2}-\frac{x'_B-x}{(x'_B-x)^2+(y'_B-y)^2}\right)^2+\left(\frac{y'_A-y}{(x'_A-x)^2+(y'_A-y)^2}-\frac{y'_B-y}{(x'_B-x)^2+(y'_B-y)^2}\right)^2}$$

$$\text{where}\quad C = \frac{V_{AB}}{2\cdot\log\frac{d_{AB}+\sqrt{{d_{AB}}^2-4\cdot{\rho_0}^2}}{2\cdot\rho_0}}$$

$$x'_A = x_A+|e|\cdot\cos\Theta_1,\quad \Theta_1 = \arctan\frac{y_B-y_A}{x_B-x_A}$$
$$\text{and}\quad x'_B = x_B+|e|\cdot\cos\Theta_2,\quad \Theta_2 = \arctan\frac{y_A-y_B}{x_A-x_B}$$
$$y'_A = y_A+|e|\cdot\sin\Theta_1,\quad e = d_{AB}/2-\sqrt{(d_{AB}/2)^2-{\rho_0}^2}$$
$$y'_B = y_B+|e|\cdot\sin\Theta_2$$

In eq. A.5 – A.7, V_{AB} is the voltage on an electrode pair (anode–cathode), d_{AB} is the distance between the electrodes, ρ_0 is the electrode diameter, while x'_A, y'_A and x'_B, y'_B are coordinates of the center of the electrode mathematical equivalents (the electrical center x'_A, y'_A and x'_B, y'_B of the electrodes is eccentric to the actual geometrical center x_A, y_A and x_B, y_B due to finite i.e. non-zero electrode diameter).

Abbreviations

ECT: ElectroChemoTherapy; NTIRE: Non-Thermal IRreversible Electroporation; EBTT: Electroporation-Based Technologies and Treatments.

Competing interests

The authors declare they have no competing interests.

Authors' contributions

SMK developed and tested the application and wrote the manuscript. TK contributed to the design of the application, tested the application and reviewed the manuscript. DM contributed to the design of the application, tested the application and reviewed the manuscript. All authors have read and approved the final manuscript.

Acknowledgements

Research conducted in the scope of the EBAM European Associated Laboratory (LEA) and in part financially supported by the Slovenian Research Agency (ARRS).

Received: 23 June 2012 Accepted: 25 October 2012
Published: 30 October 2012

References

1. Neumann E, Schaeferridder M, Wang Y, Hofschneider P: **Gene-transfer into mouse lyoma cells by electroporation in high electric-fields.** *EMBO J* 1982, 1:841–845.
2. Neumann E, Rosenheck K: **Permeability changes induced by electric impulses in vesicular membranes.** *J Membr Biol* 1972, 10:279–290.
3. Kinosita K, Tsong T: **Formation and resealing of pores of controlled sizes in human erythrocyte membrane.** *Nature* 1977, 268:438–441.
4. Gurtovenko A, Anwar J, Vattulainen I: **Defect-mediated trafficking across cell membranes: Insights from in silico modeling.** *Chem Rev* 2010, 110:6077–6103.
5. Rols M: **Electropermeabilization, a physical method for the delivery of therapeutic molecules into cells.** *Biochim Biophys Acta-Biomembr* 2006, 1758:423–428.
6. Kanduser M, Miklavcic D: **Electroporation in Biological Cell and Tissue: An Overview.** In *Electrotechnologies for Extraction from Food Plants and*

Biomaterials. Edited by Vorobiev E, Lebovka N. New York: Springer Science +Business Media; 2008:1–37.
7. Weaver J: **Electroporation: A general phenomenon for manipulating cells and tissues.** *J Cell Biochem* 1993, **51**:426–435.
8. Rubinsky B, Onik G, Mikus P: **Irreversible electroporation: A new ablation modality - clinical implications.** *Technol Cancer Res Treat* 2007, **6**:37–48.
9. Bouzrara H, Vorobiev E: **Beet juice extraction by pressing and pulsed electric fields.** *Int Sugar J* 2000, **102**:194–200.
10. Sack M, Sigler J, Frenzel D, Eing C, Arnold J, Michelberger T, Frey W, Attmann F, Stukenbrock L, Mueller G: **Research on industrial-scale electroporation devices fostering the extraction of substances from biological tissue.** *Food Eng Rev* 2010, **2**:147–156.
11. Castro A, Barbosacanovas G, Swanson B: **Microbial inactivation of foods by pulsed electric-fields.** *J Food Process Preserv* 1993, **17**:47–73.
12. Miklavcic D, Towhidi L: **Numerical study of the electroporation pulse shape effect on molecular uptake of biological cells.** *Radiol Oncol* 2010, **44**:34–41.
13. Orlowski S, Belehradek J, Paoletti C, Mir L: **Transient electropermeabilization of cells in culture - increase of the cyto-toxicity of anticancer drugs.** *Biochem Pharmacol* 1988, **37**:4727–4733.
14. Sersa G, Cemazar M, Miklavcic D: **Antitumor effectiveness of electrochemotherapy with cis-diamminedichloroplatinum(ii) in mice.** *Cancer Res* 1995, **55**:3450–3455.
15. Tounekti O, Pron G, Belehradek J, Mir L: **Bleomycin, an apoptosis-mimetic drug that induces 2 types of cell-death depending on the number of molecules internalized.** *Cancer Res* 1993, **53**:5462–5469.
16. Mir L, Orlowski S, Belehradek J, Paoletti C: **Electrochemotherapy potentiation of antitumor effect of bleomycin by local electric pulses.** *Eur J Cancer* 1991, **27**:68–72.
17. Sersa G, Cemazar M, Snoj M: **Electrochemotherapy of tumours.** *Curr Oncol* 2009, **16**:118–119.
18. Jarm T, Cemazar M, Miklavcic D, Sersa G: **Antivascular effects of electrochemotherapy: Implications in treatment of bleeding metastases.** *Expert Rev Anticancer Ther* 2010, **10**:729–746.
19. Miklavcic D, Corovic S, Pucihar G, Pavselj N: **Importance of tumour coverage by sufficiently high local electric field for effective electrochemotherapy.** *EJC Suppl* 2006, **4**:45–51.
20. Kos B, Zupanic A, Kotnik T, Snoj M, Sersa G, Miklavcic D: **Robustness of Treatment Planning for Electrochemotherapy of Deep-Seated Tumors.** *J Membr Biol* 2010, **236**:147–153.
21. Corovic S, Al Sakere B, Haddad V, Miklavcic D, Mir L: **Importance of contact surface between electrodes and treated tissue in electrochemotherapy.** *Technol Cancer Res Treat* 2008, **7**:393–399.
22. Ivorra A, Al-Sakere B, Rubinsky B, Mir L: **Use of conductive gels for electric field homogenization increases the antitumor efficacy of electroporation therapies.** *Phys Med Biol* 2008, **53**:6605–6618.
23. Miklavcic D, Semrov D, Mekid H, Mir L: **A validated model of in vivo electric field distribution in tissues for electrochemotherapy and for DNA electrotransfer for gene therapy.** *Biochim Biophys Acta-Gen Subj* 2000, **1523**:73–83.
24. Zupanic A, Corovic S, Miklavcic D: **Optimization of electrode position and electric pulse amplitude in electrochemotherapy.** *Radiol Oncol* 2008, **42**:93–101.
25. Miklavcic D, Beravs K, Semrov D, Cemazar M, Demsar F, Sersa G: **The importance of electric field distribution for effective in vivo electroporation of tissues.** *Biophys J* 1998, **74**:2152–2158.
26. Mir L, Gehl J, Sersa G, Collins C, Garbay J-R, Billard V, Geertsen P, Rudolf Z, O'Sullivan G, Marty M: **Standard operating procedures of the electrochemotherapy: Instructions for the use of bleomycin or cisplatin administered either systemically or locally and electric pulses delivered by the Cliniporator (TM) by means of invasive or non-invasive electrodes.** *EJC Suppl* 2006, **4**:14–25.
27. Mahmood F, Gehl J: **Optimizing clinical performance and geometrical robustness of a new electrode device for intracranial tumor electroporation.** *Bioelectrochemistry* 2011, **81**:10–16.
28. Edhemovic I, Gadzijev EM, Brecelj E, Miklavcic D, Kos B, Zupanic A, Mali B, Jarm T, Pavliha D, Marcan M, Gasljevic G, Gorjup V, Music M, Vavpotic TP, Cemazar M, Snoj M, Sersa G: **Electrochemotherapy: A New Technological Approach in Treatment of Metastases in the Liver RID B-9396-2008.** *Technol Cancer Res Treat* 2011, **10**:475–485.
29. Miklavcic D, Snoj M, Zupanic A, Kos B, Cemazar M, Kropivnik M, Bracko M, Pecnik T, Gadzijev E, Sersa G: **Towards treatment planning and treatment of deep-seated solid tumors by electrochemotherapy.** *Biomed Eng Online* 2010, **9**:10.
30. Pavliha D, Kos B, Zupanic A, Marčan M, Serša G, Miklavčič D: **Patient-specific treatment planning of electrochemotherapy: Procedure design and possible pitfalls.** *Bioelectrochemistry* 2012, **87**:265–273.
31. Sano M, Neal R, Garcia P, Gerber D, Robertson J, Davalos R: **Towards the creation of decellularized organ constructs using irreversible electroporation and active mechanical perfusion.** *Biomed Eng Online* 2010, **9**:31.
32. Edd J, Horowitz L, Davalos R, Mir L, Rubinsky B: **In vivo results of a new focal tissue ablation technique: Irreversible electroporation.** *IEEE Trans Biomed Eng* 2006, **53**:1409–1415.
33. Rubinsky B: **Irreversible electroporation in medicine.** *Tech Canc Res Treat* 2007, **6**:255–259.
34. Rempp H, Boss A, Helmberger T, Pereira P: **The current role of minimally invasive therapies in the management of liver tumors.** *Abdom Imaging* 2011, **36**:635–647.
35. Sel D, Mazeres S, Teissie J, Miklavcic D: **Finite-element modeling of needle electrodes in tissue from the perspective of frequent model computation.** *IEEE Trans Biomed Eng* 2003, **50**:1221–1232.
36. Sersa G, Gehl J, Garbay J-R, Soden D, O'Sullivan G, Matthiessen L, Snoj M, Mir L: *Electrochemotherapy of small tumors: the experience from the ESOPE (European Standard Operating Procedures for Electrochemotherapy) group*, Clinical aspects of electroporation. New York: Springer; 2011:93–102.
37. Magjarevic R, Lackovic I, Miklavcic D: **Pet godina šire primjene elektrokemoterapije u klinici.** *Liječničke novine* 2011, **97**:36–39.
38. Pech M, Janitzky A, Wendler J, Strang C, Blaschke S, Dudeck O, Ricke J, Liehr U-B: **Irreversible electroporation of renal cell carcinoma: A first-in-man phase I clinical study.** *Cardiovasc Interv Radiol* 2011, **34**:132–138.
39. Onik G, Rubinsky B: **Irreversible Electroporation: First Patient Experience Focal Therapy of Prostate Cancer.** In *Irreversible Electroporation*. Edited by Rubinsky B. Berlin Heidelberg: Springer; 2010:235–247.
40. Corovic S, Bester J, Miklavcic D: **An e-learning application on electrochemotherapy.** *Biomed Eng Online* 2009, **8**:26.
41. Sinigoj A: *Osnove elektromagnetike*. Ljubljana: Fakulteta za elektrotehniko; 2002.
42. Dev S, Dhar D, Krassowska W: **Electric field of a six-needle array electrode used in drug and DNA delivery in vivo: Analytical versus numerical solution.** *IEEE Trans Biomed Eng* 2003, **50**:1296–1300.
43. Corovic S, Pavlin M, Miklavcic D: **Analytical and numerical quantification and comparison of the local electric field in the tissue for different electrode configurations.** *Biomed Eng Online* 2007, **6**:23.
44. Bergues Pupo AE, Bory Reyes J, Bergues Cabrales LE, Bergues Cabrales JM: **Analytical and numerical solutions of the potential and electric field generated by different electrode arrays in a tumor tissue under electrotherapy.** *Biomed Eng Online* 2011, **10**:85.
45. Rebersek M, Miklavcic D: **Advantages and disadvantages of different concepts of electroporation pulse generation.** *Automatika* 2011, **52**:12–19.
46. Pucihar G, Krmelj J, Rebersek M, Napotnik T, Miklavcic D: **Equivalent pulse parameters for electroporation.** *IEEE Trans Biomed Eng* 2011, **58**:3279–3288.
47. Sun P-C, Tsai R, Finger G, Chen Y, Yeh D: **What drives a successful e-Learning? An empirical investigation of the critical factors influencing learner satisfaction.** *Comput Educ* 2008, **50**:1183–1202.
48. Haemmerich D, Staelin S, Tsai J, Tungjitkusolmun S, Mahvi D, Webster J: **In vivo electrical conductivity of hepatic tumours.** *Physiol Meas* 2003, **24**:251–260.
49. Adeyanaju OO, Al-Angari HM, Sahakian AV: **The optimization of needle electrode number and placement for irreversible electroporation of hepatocellular carcinoma.** *Radiol Oncol* 2012, **46**:126–135.
50. Lee E, Loh C, Kee S: **Imaging guided percutaneous irreversible electroporation: Ultrasound and immunohistological correlation.** *Technol Cancer Res Treat* 2007, **6**:287–293.
51. Edd J, Davalos R: **Mathematical modeling of irreversible electroporation for treatment planning.** *Technol Cancer Res Treat* 2007, **6**:275–286.
52. Zupanic A, Miklavcic D: **Tissue heating during tumor ablation with irreversible electroporation.** *Elektrotehniški vestnik* 2011, **78**:42–47.
53. Stratton JA: *Electromagnetic Theory*. New Jersey: John Wiley & Sons; 2007.

doi:10.1186/1472-6920-12-102
Cite this article as: Mahnic-Kalamiza *et al.*: Educational application for visualization and analysis of electric field strength in multiple electrode electroporation. *BMC Medical Education* 2012 **12**:102.

6.2 Concluding remarks

The effects of electroporation on mass transport within electroporated tissue continue to remain insufficiently understood and are particularly difficult to quantify. The reasons for this stem predominantly from three factors: the complexity and diversity of target material (biological tissue); a multitude of possibilities in designing and applying the electroporation treatment protocol (pulse amplitude, duration, repetition frequency, etc.); and the lack of comprehensive theoretical models describing the complex relationships between electric field effects on tissue and the subsequent processes of mass transport that the electrical treatment facilitates.

This dissertation represents a detailed account of an attempt at constructing a theoretical mathematical model, with the aim of bridging the gap between existing (or new and future) models of electroporation effects on cells, and models of mass transport in biological materials. The presented approach has proved to be useful for purposes of modelling experimentally obtained data, but it is the author's firm belief that its true potential is in providing a platform for future work. This work should be directed towards further improvements and validated additions to the model in the direction of coupling electroporation effects on cells described by realistic mechanistic models, thus enabling better model generalization, increasing its applicability and usefulness.

Such a generalized and detailed theoretical model would not only help elucidate and quantify the effects of electroporation on mass transport in a particular case of electroporation application, but is envisioned to also provide predictive capabilities as well as solutions to unanswered questions in the field during the process of its creation and development. It is the author's belief that the work collectively described in this dissertation represents the first necessary (three little) steps in the creation of such a model.